

Alma Mater Studiorum - Università di Bologna

DOTTORATO DI RICERCA IN
CHIMICA

Ciclo 34

Settore Concorsuale: 03/C1 - CHIMICA ORGANICA

Settore Scientifico Disciplinare: CHIM/06 - CHIMICA ORGANICA

PHOTOREDOX CATALYSIS AND NUCLEOPHILIC ORGANOMETALLIC
REAGENTS – APPLICATION IN ORGANIC SYNTHESIS

Presentata da: Francesco Calogero

Coordinatore Dottorato

Luca Prodi

Supervisore

Pier Giorgio Cozzi

Co-supervisore

Andrea Gualandi

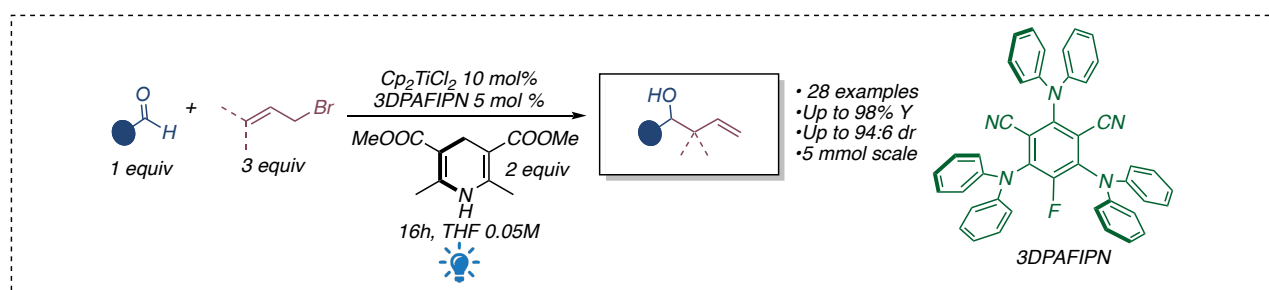
Esame finale anno 2022

Abstract

The main purpose of my PhD was the combination of the well-established principles of transition metal catalysis with photoredox catalysis and reductive radical polar cross-over catalysis (RRPCO). After the seminal works reported by Sanford, Doyle – MacMillan and Molander, an extraordinary number of new synthetic methodologies in these fields have been presented in literature involving also the use of non-toxic and hearth abundant transition metals. In the last three years we have focused our attention on the development of novel dual photoredox and transition metal-promoted protocols for the functionalization of carbonyl compounds, a largely underdeveloped topic. In the methodologies developed, a transient nucleophilic organometallic species, able to react in the presence of a carbonyl group, was generated by the merging photoredox and metal catalysis. In this scenario new visible light-promoted functionalizations of carbonyl compounds enabled by the presence of catalytic amount of transition metals in a milder and greener way, also in stereoselective fashion, were presented.

Specifically, we focused on the development of new methodologies combining photoredox catalysis with titanium and nickel chemistry in low oxidation state.

In the field of C-C or C-heteroatom bond forming reactions enabled by the generation of transient nucleophilic organometallic species, low oxidation state titanocene complexes have occupied a privileged position over the years. The simplest member of this family is the Nugent–RajanBabu reagent, $[\text{Cp}_2\text{Ti(III)Cl}]$. The main properties of titanocene monochloride are: (i) simply obtainable from the bench stable $[\text{Cp}_2\text{Ti(IV)Cl}_2]$ upon easily achievable single electron reduction ($\text{ETi}^{\text{IV}}/\text{Ti}^{\text{III}} = -0.63 \text{ V vs. SCE}$); (ii) high tolerance to different functional groups; (iii) enhanced reactivity in performing single-electron-transfer processes. In light of these properties, this class of complexes are particularly suitable for the combination with photoredox processes. In this context, during my PhD we developed different powerful methodologies by exploiting the reactivity of titanium in low oxidation state under photoredox conditions for the functionalization of carbonyl compounds. Firstly, a Barbier-type allylation of aromatic and aliphatic aldehydes –catalytic in titanium– in the presence of a blue photon-absorbing organic dye was developed.

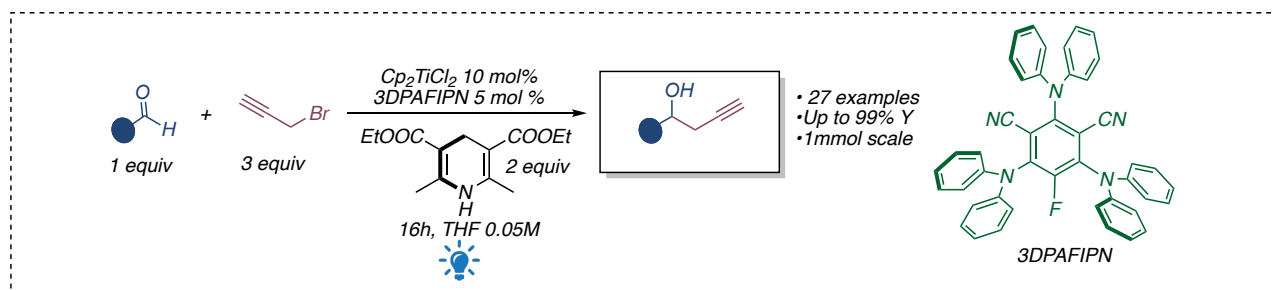


The reaction uses 3DPAFIPN as cheap and easily prepared organic photocatalyst. Under visible light irradiation *3DPAFIPN can reduce $[\text{Cp}_2\text{Ti(IV)Cl}_2]$ to $[\text{Cp}_2\text{Ti(III)Cl}]$ allowing the generation of the allyltitanium(IV) species in the presence of allyl bromide. The readily available Hantzsch's ester used as organic reductant allowed the reaction with satisfying results avoiding the use of overstoichiometric quantity of metal reductant and scavengers.

The wide applicability of our optimized finding was confirmed with a variety of aromatic and aliphatic aldehydes. The reaction is quite tolerant to various functional groups including halides, CF_3 , esters, nitriles, and ethers, leading the formation of the desired homoallylic alcohols in yields from good to moderate.

To obtain a clear picture of the reaction mechanism, thanks to the collaboration with Prof. Bergamini's Group of our department we investigated the quenching of the photocatalyst's luminescence by each of the components of the reaction. The photophysical evidence disclosed that the introduced photoredox system could efficiently promote the reduction of the titanium complex allowing the formation of the transient nucleophilic allyl titanium species.

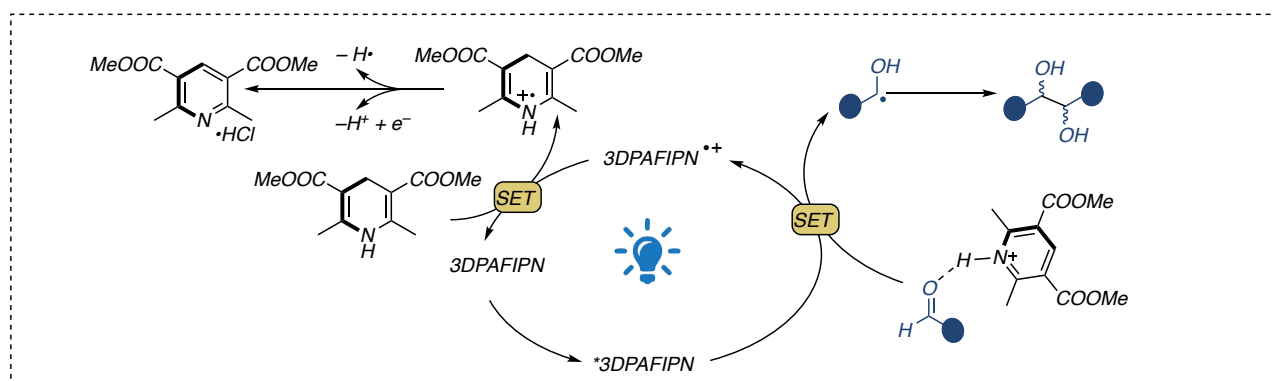
Following a parallel route, we were pleased to observe that the developed methodology could also be extended to the propargylation of aldehydes under analogous conditions.



The reaction displayed a broad scope, and no traces of allenyl-isomers were detected in presence of the simple propargyl bromide. Aliphatic, aromatic and heteroaromatic aldehydes were found suitable substrates for the reaction. Yields are, in general, from good to moderate, but comparing the presented protocol with the allylation reaction, it is noticeable that the yields in the case of aromatic aldehydes are lower in the case of propargylation.

Although the reaction conditions are comparable for the allylation and propargylation of aldehydes, it was observed that in the case of propargylations a non-negligible amount of starting material converted into an undesired and unavoidable pinacol coupling product. Due to fact that in every case the ratio between the *d/l* and *meso* isomer of the pinacol byproduct was close to 1:1, to the best of our knowledge, we believe that the formation of this byproduct results from the direct reduction of starting material by the photoredox system. Probably this unwanted pathway is favored by the acidic activation of the carbonyl group promoted by the pyridinium salt deriving from the oxidation of the

Hantzsch's ester. This interaction probably, allows the direct single electron reduction of the substrates and consequent formation of a ketyl radical.



Due to the significant difference concerning their reduction potential, this parasite reaction route is never observed when aliphatic substrates are taken into account.

After having successfully developed two methodologies to efficiently functionalize both aromatic and aliphatic aldehydes by exploiting the possibility of catalytically generating titanium in a low oxidation state, we focused on a further methodology .

Even if photoredox promoted pinacol coupling reaction of ketyl radicals is induced by many organic dyes or photoactive metal complexes, normally, this radical-radical coupling is neither diastereo- nor enatio- selective.

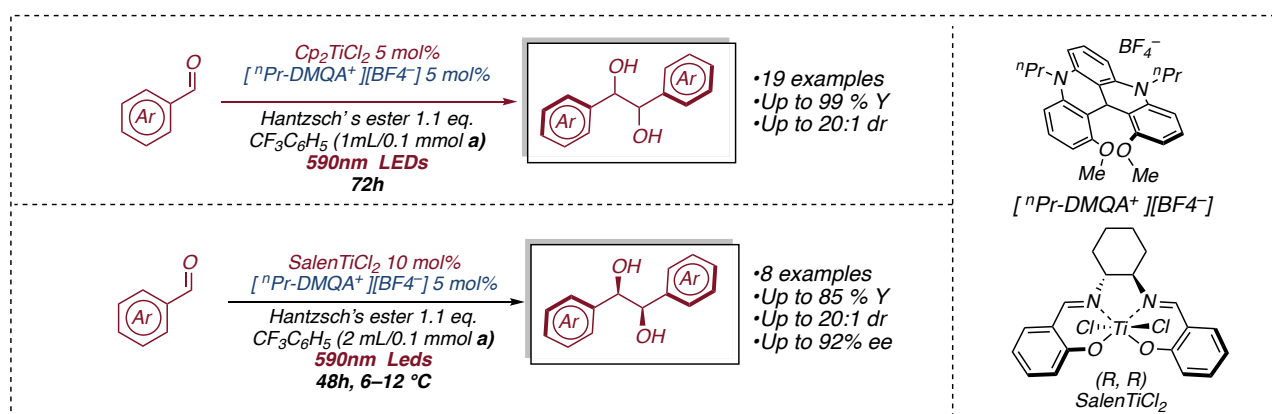
First of all, we tried to optimize the reaction conditions for a dual photoredox/titanium-mediated pinacol coupling of aldehydes using as starting point the condition that were optimized in the previous methodologies. It was possible to observe that the reaction was promoted by different organic dyes absorbing in the blue region, giving complete conversions of the aldehyde but a 1:1 ratio of the isolated diastereoisomers.

After an extensive re-optimization of all the reaction parameters, we developed a highly diastereoselective pinacol coupling of aromatic aldehydes promoted by 5 mol% of the non-toxic, cheap and available $[\text{Cp}_2\text{TiCl}_2]$ complex. The key feature, that allows the complete diastereocontrol played by titanium, is the employment of a red-absorbing organic dye. The tailored (photo)redox properties of the red-absorbing organic dye $[\text{Pr-DMQA}^+][\text{BF}_4^-]$ promote the selective reduction of Ti(IV) to Ti(III).

This latter is able to engage a single electron transfer in the presence of aromatic aldehydes leading the formation of the corresponding ketyl radical.

We were pleased to observe that these new reaction conditions allowed the formation of the desired product with good tolerance for different functional groups, good yields and with high diastereoselectivity in favor of *d/l* (*syn*) diastereoisomer (d.r. > 20:1 in most of the cases).

Moreover, by employing a simply prepared chiral SalenTi complex, the new photoredox reaction gave a complete diastereoselection for the *d,l* diastereoisomer, and high enantiocontrol (up to 92% of enantiomeric excess). Even in this case, a clear picture of the reaction mechanism has been furnished. The photophysical and electrochemical evidence disclosed both for the diastereo- and enantioselective protocol the crucial role played by the red photon-absorbing organic dye and the necessity of its use for a stereocontrolled process.



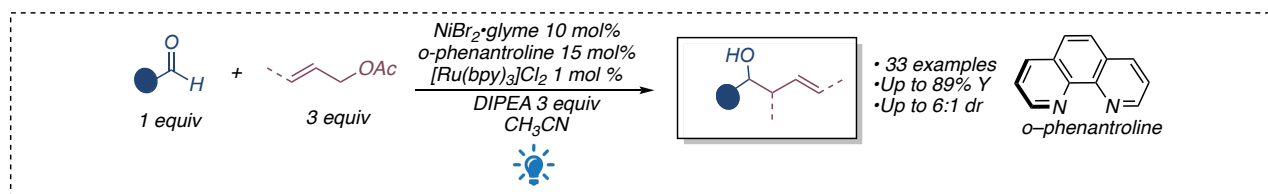
While the use of titanium catalysis in photoredox environment, although presenting unique potential, is a relatively less explored field, the use of nickel catalysis is certainly the most powerful contributor to the success of metallaphotoredox catalysis.

Remarkably, even if the major contribution in dual photoredox and nickel catalysis is devoted to the realization of cross-coupling-type reactions, we wanted to evaluate different possible scenarios. Our focus was on the possibility of exploiting intermediates arising from the oxidative addition of nickel complexes as transient nucleophilic species.

The first topic taken into account regarded the possibility to perform allylation of aldehydes by dual photoredox and nickel catalysis. In the first instance, a non-stereocontrolled version of the reaction was presented.

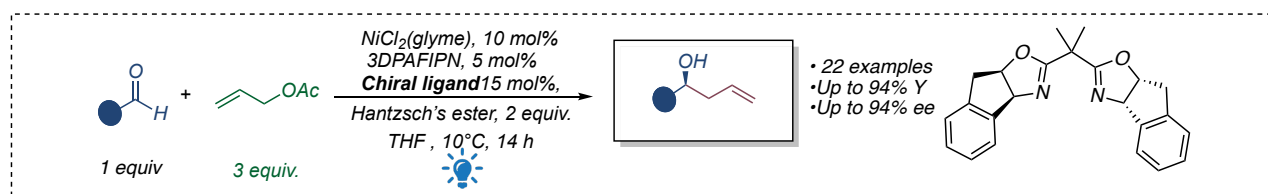
We began our investigations by studying the allylation of 2-naphthaldehyde, as model substrate, in the presence of different allylating reagents, nickel sources, photocatalysts, reaction solvents, and additives. The systematic evaluation of all reaction parameters enabled us to optimize the reaction conditions, obtaining the corresponding homoallylic alcohol in 75% isolated yield after 48 h of irradiation employing [NiBr₂(glyme)] (10 mol%), allylacetate (3 equiv.), diisopropylethylamine (DIPEA, 3 equiv.), [Ru(bpy)₃]Cl₂ (1 mol%), o-phenanthroline (15 mol%) as ligand for nickel(II), under blue LEDs irradiation centered at 450 nm. The optimized reaction conditions allowed the preparation of a wide library of homoallylic derivatives in good yields with a good tolerance to different functional groups. Careful photophysical investigation, performed in collaboration with Prof. Ceroni's group of our department, highlighted the mechanism of the reaction, analyzing the

quenching of the excited state of the photocatalyst by each of the components of the reaction (Stern-Volmer experiment).



Having in hand a powerful non-asymmetric methodology for the synthesis of homoallylic alcohols under dual nickel/photoredox conditions we were curious to highlight a possible enantioselective variant. Firstly, a wide library of chiral ligands was screened maintaining unchanged the reaction conditions but unfortunately, these attempts resulted ineffective.

After a long and unsuccessful journey, and only through a series of drastic modification of the reaction conditions, we managed to obtain satisfying results. The optimized methodology allows the clean stereoselective allylation both of aromatic and aliphatic aldehydes in good to excellent yields and up to 94% ee. The reaction is performed under visible-light radiation (centred at 456 nm) employing the commercially available allyl acetate and a catalytic amount of $[\text{NiCl}_2(\text{glyme})]$ (10 mol%) combined with a chiral aminoindanol-derived bis(oxazoline) (15 mol %), the organic dye 3DPAFIPN, and Hantzsch's ester as sacrificial reductant. The best results in terms of enantioselectivity are obtained performing the reaction at 8-12 °C.



Accurate DFT calculations, performed thanks to the collaboration of Prof. L. Cavallo's group from the King Abdullah University of Science and Technology (KAUST), and photophysical experiments, carried out by Prof. P. Ceroni's group, have clarified the mechanistic picture of the reaction, showing the key role played by Hantzsch's ester in the turnover of the catalyst.

Table of Contents

Chapter 1. Introduction.....	5
1.1 Photochemical Background: The Absorption.....	6
1.2 The Reactivity of The Excited State.....	10
• Energy Transfer (EnT).....	12
• Atom Transfer (AT).....	14
• Electron Transfer (ET).....	16
1.3 Metal-based Photocatalysts.....	26
1.4 Organic Dyes.....	34
•Acridinium–based photocatalysts.....	35
•Cyanoarenes–based photocatalysts.....	39
1.5 Visible Light–Promoted Photoredox Catalysis: The State of Art.....	46
• Different molecule activations promoted by single electron transfer.....	52
1.6 Dual Catalysis: Combination of Different Molecule Activation.....	58
•Dual photoredox and organocatalytic processes.....	60
•The merger of photoredox and transition metal catalysis.....	64
•Palladium meets photoredox catalysis.....	65
•Nickel meets photoredox catalysis.....	68
•Heart-abundant metals meet photoredox catalysis: chromium and titanium.....	75
Chapter 2. Aim of the Project.....	83
Chapter 3. Functionalization of Carbonyl Compounds Enabled by Merging Photoredox and Titanium Catalysis.....	87
3.1 Photoredox Allylation of Aldehydes Catalytic in Titanium.....	89
• Titanium-catalyzed Barbier-type allylation.....	89
• Presented work.....	91
• Optimization of the reaction conditions.....	92
• Scope evaluation.....	98

• Photophysical studies and reaction mechanism	103
• Conclusions	106
• Supplementary data	107
3.2 Photoredox Propargylation of Aldehydes Catalytic in Titanium	132
• Metal-catalyzed propargylation reaction.....	133
• Presented work	137
• Optimization of the reaction conditions	138
• Scope evaluation	140
• Photophysical studies and reaction mechanism	145
• Conclusions	147
• Supplementary data	148
3.3 Diastereoselective and Enantioselective Pinacol Coupling of Aromatic Aldehydes Promoted by Titanium and a Red-Adsorbing Organic Dye	161
• Transition metal mediated pinacol coupling reactions.....	161
• Ketyl radical generation under photoredox conditions	165
• Presented work	167
• Optimization of the reaction conditions	168
• Scope evaluation	174
• Enantioselective variant.....	176
• Mechanistic details	180
• Conclusions	190
• Supplementary data	191
Chapter 4. Visible Light-Driven Formation of Transient Nucleophilic Organonickel Species for Functionalization of Carbonyl Compounds	218
• Nickel-promoted allylation of aldehydes.....	225
4.1 Photoredox Allylation of Aldehydes Catalytic in Nickel.....	230
• Presented work	230
• Optimization of the reaction conditions	232
• Scope evaluation	239
• Mechanistic investigation	245
• Supplementary data	252
4.2 Enantioselective Photoredox Allylation of Aldehydes Catalytic in Nickel.....	275

• Optimization of the reaction conditions	275
• Scope Evaluation	283
• Photophysical and computational studies	286
• Conclusions	299
• Supplementary data	300

Chapter 1. Introduction

The main goal for the research in the field of catalysis is the development of new methodologies for the formation of carbon-carbon or carbon-heteroatom bonds in small non-activated molecules. The domain of catalysis is in continuous great foresight development, triggering the most varied techniques of organic chemistry. Nevertheless, visible photoredox processes and visible light-mediated catalysis in the last decade represented an unrestrainable, fast-growing field. The reason for this outbreak is related to the high variety of transformations that are allowed by the effect of light. In a general sense, this approach can be resumed as the possibility to convert electromagnetic energy, deriving from a visible radiation, into chemical energy in order to promote a transformation in a catalytic way. However, this definition offers a too wide framework to be effective, and a more in-depth analysis is necessary to understand the fundamentals, the characteristics, and the potentialities of photoredox catalysis.

1.1 Photochemical Background: The Absorption.

Photochemistry represents the branch of chemistry concerned with the chemical effects of light. Therefore, the chemical processes caused by absorption of light radiation are addressed as photochemical reactions.¹

If in a reaction mixture a molecule can absorb the light radiation and convert it into chemical energy this is commonly called photosensitizer.

A molecule after the absorption of light can be considered as a new chemical entity obtained after an external energy input (represented by the radiation). The effect of light determines the evolution from its lowest energy electronic state (called ground state) to a higher energy state identified as electronically excited state.

The first necessary condition for this kind of transition to happen is that the energy associated to the light radiation is at least equal to the energy difference between the two electronic states.²

This consideration can be simplified approximating the absorption as promotion of one electron of the photosensitizer from a lower to a higher energy orbital with a consequent modification of the electronic configuration.

The description of electronic transitions that can occur upon absorption is a crucial aspect for the explanation of a photochemical process. Without going into the details of the quantum-mechanical treatment of the phenomenon, the moment of the transition depends on an integral expressed as a product of three factors. (i) Momentum of the electronic transition depending on the symmetry and superposition of the initial and final orbitals; (ii) Spin superposition integral, which depends on the initial and final spin states; (iii) vibrational wavefunction superposition integral of the initial and final states.³ When even one of these components is zero, the integral results in null and the transition is addressed as *forbidden*. On the other hand, if none of the components is zero the transition is said to be *allowed*. However, since such considerations occur only with a high set of approximations and theoretically forbidden transitions are still observable experimentally.

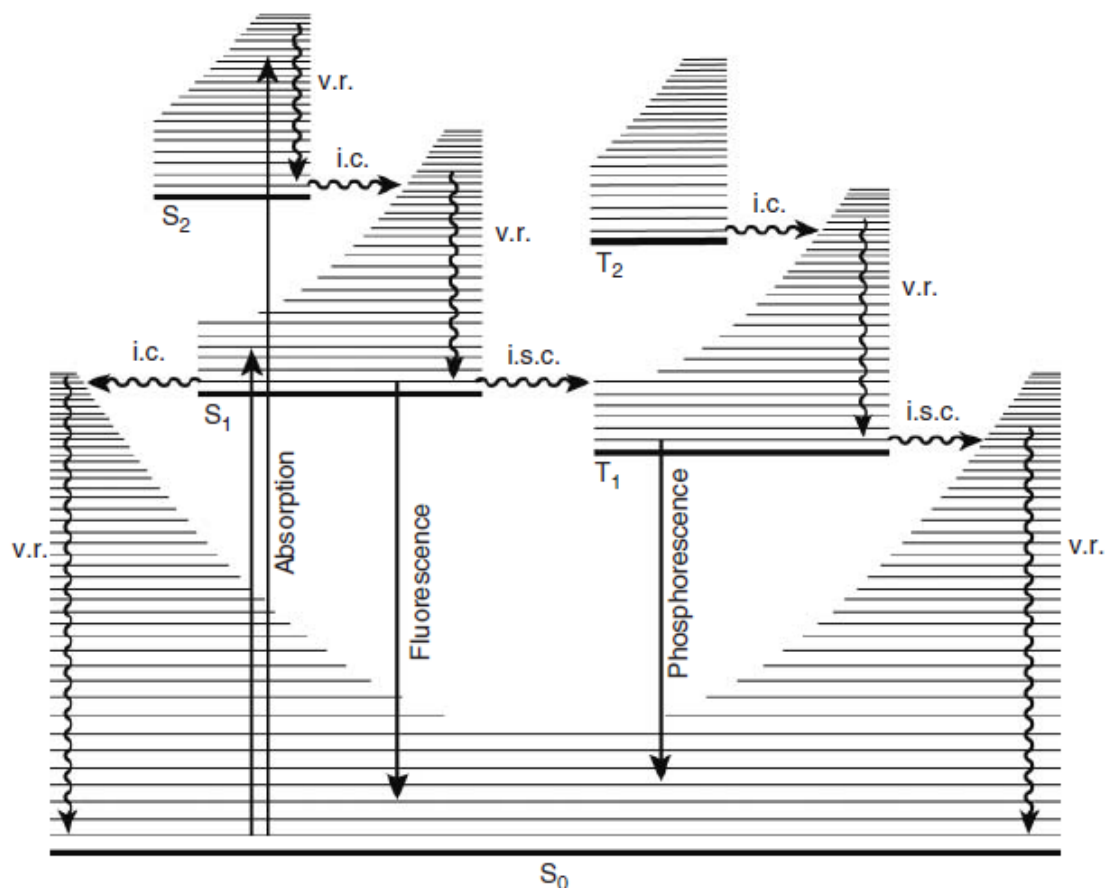
Only transitions that occur towards an excited state bearing the same spin value of the ground state are allowed. On the contrary transitions leading to excited states with different spin value are forbidden. Commonly the ground state of a molecule is a singlet (S_0), and the lowest excited state is a triplet (T_1), consequently it cannot be directly populated by light absorption. On the contrary, it can be obtained from the deactivation of higher energy excited states.

¹ Buzzetti, L.; Crisenza, G. E. M.; Melchiorre, P. Mechanistic Studies in Photocatalysis. *Angew. Chem. Int. Ed.* **2019**, 58 (12), 3730–3747. <https://doi.org/10.1002/anie.201809984>.

² Balzani, V.; Ceroni, P.; Juris, A. *Photochemistry and photophysics*; Wiley-VCH: Weinheim, **2014**.

³ Hollas, J.M. *Modern Spectroscopy, 4th edn*, John Wiley & Sons, Ltd, Chichester, **2004**

The pathway that allows the formation of an electronically excited state of a molecule and its deactivation for the restoration of the original ground state are commonly analyzed considering the Perrin-Jablonski diagrams. (**Figure 1**)



Chapter 1. Figure 1 Perrin-Jablonski diagram.

The absorption of a species with a singlet ground state S_0 determines a higher electronic excited state of singlet S_1 that is characterized with a certain vibrational energy. Upon absorption of light, when the S_1 excited state is reached, the first phenomenon occurring is a vibrational decay of the electron to a lower vibrational energy level. If the lower vibrational state reached belongs to the ground state S_0 , the electronic configuration of the ground state will be reformed without emission of light. This event is called internal conversion (IC).

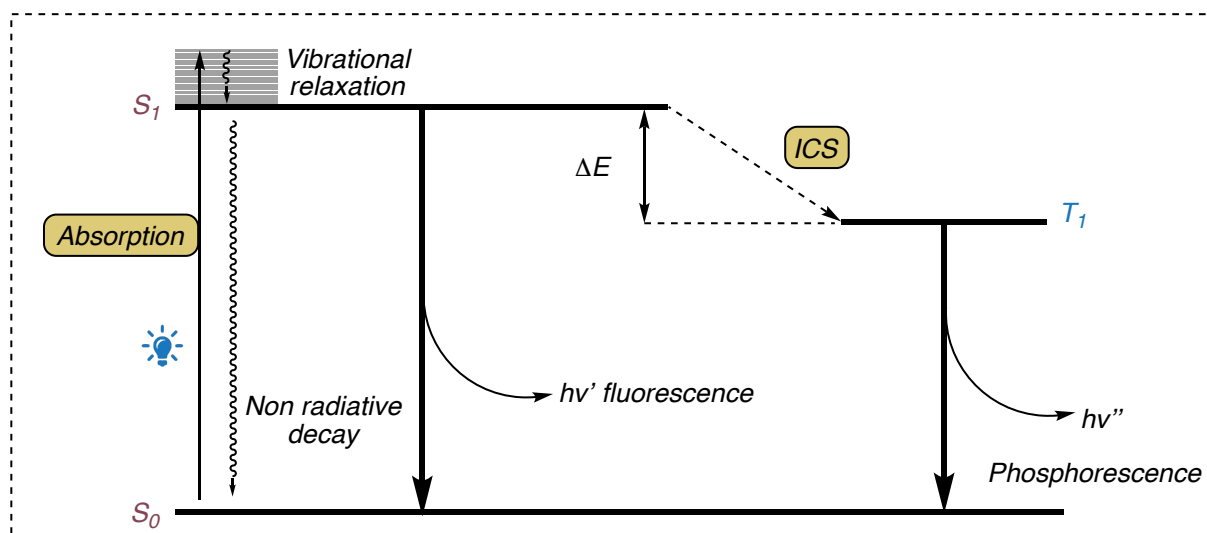
In a second case, if the vibrational decay determines a relaxation within the electronic state S_1 . This event is called vibrational relaxation (v.r.) and if it arises, the molecule can return to the ground singlet S_0 electronic state through re-emission of a photon. This phenomenon of luminescence is known as fluorescence. The re-emitted photon will present a lower energy compared with the incident one. The reason of this difference is related to the vibrational relaxation event.

The interconversion to a lower vibrational level determines a loss of energy under form of heat. Comparing the absorption and the emission spectra, the emission spectrum will be shifted to lower

8
 frequencies and is called “Stoke shift”.⁴ The frequencies that the emission and absorption spectra have in common corresponds to the difference of energy between the lower vibrational level ν_0 of the S_1 state and the lower vibrational level of the ground state. This energy value is called E_{00} .

Only in particular situations, dictated by the geometry of the molecular orbitals, a third scenario can arise. Indeed, if exists an overlap between the potential energy curves of the S_1 state with the lower-energy triplet state T_1 an inter system crossing (ICS) event can arise. In a similar manner as the internal conversion, the electronic configuration moves to lower-energy triplet state T_1 in a non-radiative way, with a consequent loss of energy. From this point, the comeback to the S_0 can be radiative or non-radiative. In the first case the re-emission is called phosphorescence. The emitted photon will be characterized by lower frequencies than the exciting photon and the fluorescence-emitted photon, due to loss of energy during the ISC event. The phenomenon of inter system crossing shows important characteristics, indeed due to the higher stability compared with the singlet S_1 ; it presents a longer lifetime than fluorescence.

(Figure 2)



Chapter 1. Figure 2 Possible events involving the excited state.

Alongside these above-mentioned phenomena, which can be identified as decay pathways, whether it is thermal decay or luminescent decay, it is possible that an excited molecule is involved in processes of different nature. Especially in the case of molecules capable of reaching the excited state of triplet T_1 . The long lifetime associated to this electronic configuration allows these molecules to be involved in unimolecular photochemical reaction. The possibility of modifying their structure by starting decomposition, isomerization or bond cleavage processes can concurrently happen together with the phosphorescence. At the same way, in a complex reaction mixture, an excited molecule with a long

⁴ G. Stokes, *On the change in Refrangibility of Light*, Philosophical Transactions of the Royal Society: London, 1852.

lifetime state like T_1 can engage bimolecular processes with other molecules that are not in the excited state.⁵

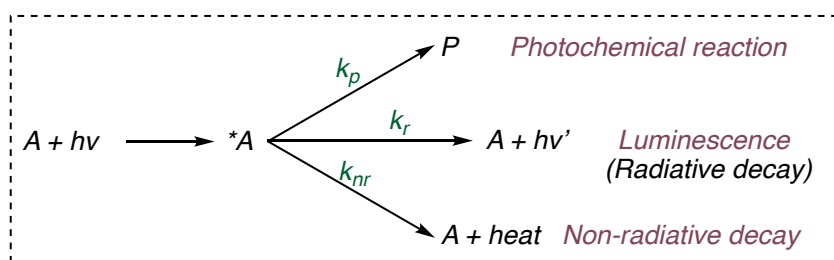
The latter scenario represents the most common condition under which photochemical reactions are carried out. The photochemical reactions can be classified into two different classes: the direct photochemical reactions and the photocatalysis. In the first case it is necessary that one or more reactants or one or more intermediates, contributes to the formation the desired product, reaching the excited state. In the second case, instead, the molecule that reaches the excited state, is not involved in the formation of the final product but, acting as a photosensitizer, it promotes the reaction between one or more reactants furnishing the chemical energy that is necessary to allow the reaction. If the photosensitizer does not modify itself and it is restored at the end of the reaction it is addressed as photocatalyst (PC) and it can be used in catalytic amount in the reaction mixture.^{1,6}

⁵ Kavarnos, G. J. *Fundamentals of Photoinduced Electron Transfer*, John Wiley & Sons Australia, **1993**.

⁶ Arias-Rotondo, D. M.; McCusker, J. K. The Photophysics of Photoredox Catalysis: A Roadmap for Catalyst Design. *Chem. Soc. Rev.* **2016**, *45* (21), 5803–5820. <https://doi.org/10.1039/C6CS00526H>.

1.2 The Reactivity of The Excited State.

As introduced in the previous section it is possible to envision that in a photoreaction there is usually competition among several processes that can simultaneously occur. Considering a quantitative analysis, A photochemical process, a radiative physical process and non-radiative physical process are always competitively happening in a reaction mixture after the absorption of light. Each process can be associated to a different rate constant, respectively: k_p , k_r and k_{nr}



Chapter 1. Figure 3 Possible deactivation pathways.

Moving from the fundamental assumption that one photon ($h\nu$) is absorbed by one molecule (A) with a consequent formation of its excited state (A^*). It is possible to estimate the lifetime of the excited species considering the equation:

Equation 1

$$\tau(*A) = \frac{1}{k_p + k_r + k_{nr}} = \frac{1}{\sum_j k_j}$$

In order to evaluate the probability of each deactivation process it is possible to introduce efficiency η of each i - event according to the relation:

Equation 2

$$\eta_i(*A) = \frac{k_i}{\sum_j k_j} = k_i \tau(*A)$$

Each physical event described by the rate constants characterizing a photoreaction is named as “primary process”. These processes are responsible of the disappearance of the molecule A^* or its deactivation to the ground state. Each event is associated to a parameter, identified as quantum yield that is expressed as:

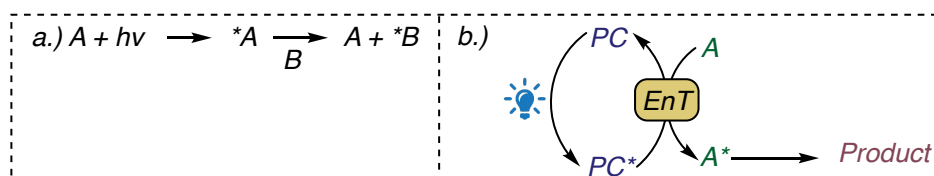
Equation 3

$$\Phi_i = \frac{\text{Number of molecules undergoing that process}}{\text{Number of photons absorbed by the reactant}}$$

In a photochemical reaction it is necessary that the rate constant k_p , and its related value of efficiency (η_p) are as high as possible or, at list, higher than the parameters referred to the radiative e non-radiative decay. When an excited molecule presents a lifetime long enough to allow the interaction with another molecule in the ground state, it is possible to describe a bimolecular process either from a qualitative or a quantitative point of view. There are three different main events that can be involved. The events, caused by the interaction between the excited molecule with another species are said “to quench” the excited state PC* and can be classified in: (i) energy transfer, (ii) atom transfer and (iii) electron transfer.²

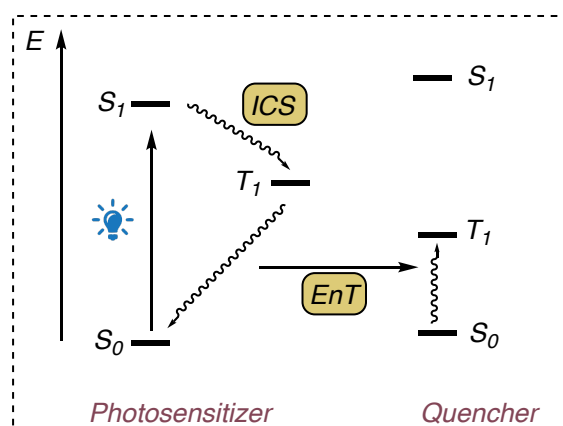
• **Energy Transfer (EnT).**

The energy transfer (EnT) deactivation pathway is linked to the energy of the excited state of a photosensitizer or of a photocatalyst compared with energy of the excited state of a quencher (B) in the reaction mixture. In the presence of a quencher (B), the EnT processes will determine the decay of A^* leading the formation of excited state of the quencher (B^*) that will be involved in its own deactivation. **(Scheme 1)**



Chapter 1. Scheme 1 General energy transfer process.

In this case the quencher acts as acceptor of energy from the photocatalyst. Hence, to perform an energy transfer, it is required that the energy associated to the excited state of the quencher is lower in energy than the excited state associated to the photocatalyst.⁷ **(Figure 4)**



Chapter 1. Figure 4 Energetic profile for energy transfer processes.

It is possible to distinguish two different types of energy transfer processes. The first one is known as radiative transfer. In this case, the excited A^* emits a photon that is reabsorbed by B forming $*B$. This case represents a peculiar type of quenching because the lifetime associated to a A^* will not be affected by B. The driving force that allows this type of process resides in the superposition between the emission spectrum of A^* and the absorption spectrum of B

⁷ Zhou, Q.; Zou, Y.; Lu, L.; Xiao, W. Visible-Light-Induced Organic Photochemical Reactions through Energy-Transfer Pathways. *Angew. Chem. Int. Ed.* **2019**, 58 (6), 1586–1604. <https://doi.org/10.1002/anie.201803102>.

The second type is defined as a non-radiative energy transfer and can formally be treated using a Marcus-type kinetic approach.⁸ A detailed treatment of this type of quenching would be far from the results that will be discussed in the following sections. Briefly, a nonradiative energy transfer process occurs without the emission of a photon by the electronically excited molecule. This quenching depends on the distance at which A* and B are during the process. For the description of a nonradiative EnT it is possible to establish two factors which can play the main role: (i) coulombic or resonance factor and (ii) exchange factor.⁹ According to the different cases, it is possible that one of the two components is preponderant compared to the other in the description of a process. If the coulombic term is preponderant the quenching will be addressed as Förster-type energy transfer,¹⁰ while if the term of exchange has the major contribute, the so-called Dexter-type energy transfer will arise.¹¹

⁸ Balzani, V.; Bolletta, F.; Scandola, F. Vertical and “Nonvertical” Energy Transfer Processes. A General Classical Treatment. *Journal of the American Chemical Society* **1980**, *102*, 2152–2163 <https://doi.org/10.1021/ja00527a002>.

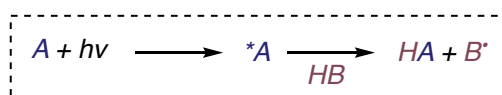
⁹ Skourtis, S. S.; Liu, C.; Antoniou, P.; Virshup, A. M.; Beratan, D. N. Dexter Energy transfer pathways. *Proc. Natl. Acad. Sci.* **2016**, *113*, 8115–8120.

¹⁰ Förster, T. Transfer mechanisms of electronic excitation. *Discuss. Faraday Soc.*, **1959**, *27*, 7–17. <https://doi.org/10.1039/DF9592700007>

¹¹ Dexter, D. L. A theory of sensitized luminescence in solids. *J. Chem. Phys.* **1953**, *21*, 836–850 <https://doi.org/10.1063/1.1699044>

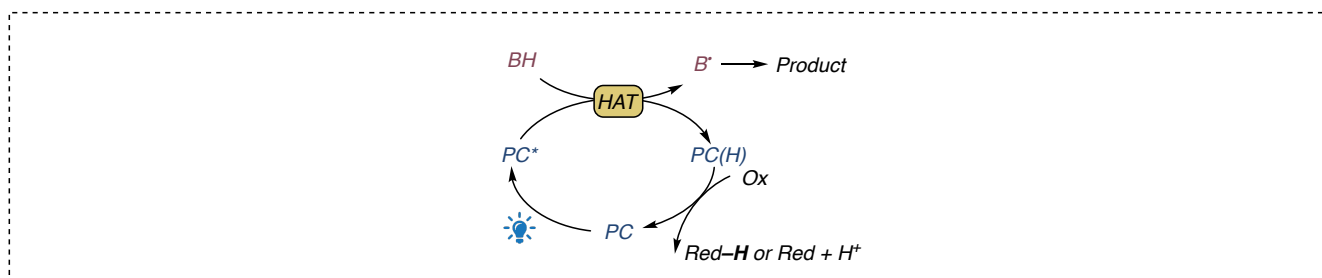
• **Atom Transfer (AT).**

The Atom Transfer (AT) deactivation pathway is a bimolecular process that is based on the ability of the excited state of certain photosensitizers or photocatalysts to abstract an atom from the quencher (BH) that act as a donor. In most cases the abstracted atom is a hydrogen atom, indeed this type of quenching is often indicated as Hydrogen Atom Transfer (HAT).



Chapter 1. Scheme 2 Hydrogen abstraction promoted by absorption of light.

A theoretical rationalization of this quenching has been described even following the Marcus kinetic approach,¹² but also by the valence bond (VB) diagram model.¹³ The main noticeable distinction between HAT and EnT is linked to the different intermediate that are generated upon the quenching event. Hence, when an energy transfer occurs, the quencher reaches its excited state restoring the photocatalyst in its ground state. Without further implications the photocatalyst can absorb again the radiation promoting another photoreaction. Differently, if an HAT-type quenching occurs, a new species is formed. Therefore, to perform an HAT-type photoreaction employing a catalytic amount of photosensitizer, the restoration of the photocatalyst is necessary in order to close the catalytic cycle.



Chapter 1. Scheme 3 General Hydrogen transfer process.

According to the nature of the photocatalyst employed to promote the reaction, the restoration of the photocatalyst can occur following different pathways.¹⁴

¹² Mayer, J. M. Understanding Hydrogen Atom Transfer: From Bond Strengths to Marcus Theory. *Acc. Chem. Res.* **2011**, *44* (1), 36–46. <https://doi.org/10.1021/ar100093z>.

¹³ Lai, W.; Li, C.; Chen, H.; Shaik, S. Hydrogen Abstraction Reactivity Patterns from A to Y: The Valence Bond Way. *Angew. Chem. Int. Ed.* **2012**, *24*. <https://doi.org/10.1002/anie.201108398>

¹⁴ For selected examples: a) Murphy, J. J.; Bastida, D.; Paria, S.; Fagnoni, M.; Melchiorre, P. Asymmetric Catalytic Formation of Quaternary Carbons by Iminium Ion Trapping of Radicals. *Nature* **2016**, *532* (7598), 218–222. <https://doi.org/10.1038/nature17438>. b) Perry, I. B.; Brewer, T. F.; Sarver, P. J.; Schultz, D. M.; DiRocco, D. A.; MacMillan, D. W. C. Direct Arylation of Strong Aliphatic C–H Bonds. *Nature* **2018**, *560* (7716), 70–75. <https://doi.org/10.1038/s41586-018-0366-x>. c) Shen, Y.; Gu, Y.; Martin, R. *Sp³ C–H Arylation and Alkylation Enabled by the Synergy of Triplet Excited Ketones and Nickel Catalysts.* *J. Am. Chem. Soc.* **2018**, *140* (38), 12200–12209. <https://doi.org/10.1021/jacs.8b07405>.

Not only a quencher, but also a sacrificial agent, an additive or a precursor of a reactive intermediate that takes part in the formation of the final product results mandatory.

Formally, the action of this second species results in the oxidation of PC-H. The photocatalyst during the HAT process, extracting a hydrogen atom (H[•]) from the substrate is converted into an electron rich species. The latter must be oxidized and, even in the presence of a base, release the proton to restore the photocatalyst in its original form.

Even if HAT-photocatalysis represents a powerful technique for organic synthesis, allowing the straightforward selective activation of aromatic and aliphatic unactivated C–H bonds,¹⁵ the limitation of available photocatalysts represents the main barrier.¹⁶ Aromatic ketones,¹⁷ and polyoxometalates (the decatungstate anion [W₁₀O₃₂]⁴⁻),^{18,19} are the most investigated classes of suitable photocatalysts for this type of reactions.

¹⁵ Capaldo, L.; Ravelli, D. Hydrogen Atom Transfer (HAT): A Versatile Strategy for Substrate Activation in Photocatalyzed Organic Synthesis *Eur. J. Org. Chem.* **2017**, 2017 (15), 2056–2071. <https://doi.org/10.1002/ejoc.201601485>.

¹⁶ Protti, S.; Fagnoni, M.; Ravelli, D. Photocatalytic C–H Activation by Hydrogen-Atom Transfer in Synthesis. *ChemCatChem* **2015**, 7 (10), 1516–1523. <https://doi.org/10.1002/cctc.201500125>.

¹⁷ a) Ravelli, D.; Fagnoni, M.; Albini, A. Photoorganocatalysis. What For? *Chem. Soc. Rev.* **2013**, 42 (1), 97–113. <https://doi.org/10.1039/C2CS35250H>.; b) Hoffmann, N. Photochemical Electron and Hydrogen Transfer in Organic Synthesis: The Control of Selectivity. *Synth.* **2016**, 48, 1782–1802. 10.1055/s-0035-1561425.; c) Oelgemöller, M.; Hoffmann, N. Photochemically Induced Radical Reactions with Furanones. *Pure and Applied Chemistry* **2015**, 87 (6), 569–582. <https://doi.org/10.1515/pac-2014-0902>.

¹⁸ a) Ravelli, D.; Protti, S.; Fagnoni, M. Decatungstate Anion for Photocatalyzed “Window Ledge” Reactions. *Acc. Chem. Res.* **2016**, 49 (10), 2232–2242. <https://doi.org/10.1021/acs.accounts.6b00339>.; b) Tzirakis, M. D.; Lykakis, I. N.; Orfanopoulos, M. Decatungstate as an Efficient Photocatalyst in Organic Chemistry. *Chem. Soc. Rev.* **2009**, 38 (9), 2609. <https://doi.org/10.1039/b812100c>.

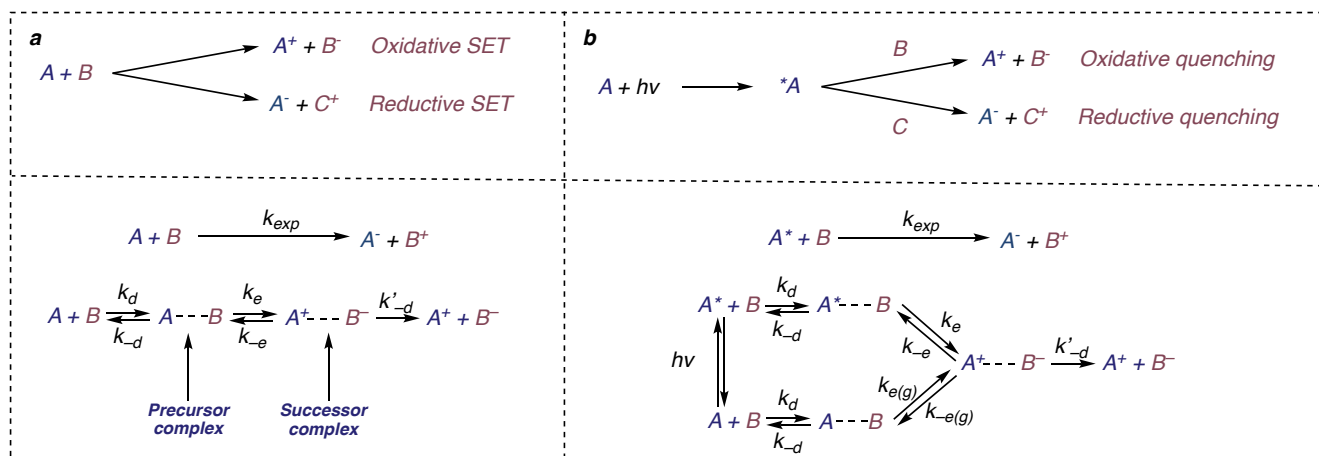
• Electron Transfer (ET).

The class of reactions that mostly represents the connection point between chemical processes and light are the electron transfer–promoted photochemical reactions.

Having envisioned the basic elements that characterize a bimolecular quenching of an excited state in the case of the energy and the atom transfer, a more rigorous treatment from a kinetic point of view is mandatory to fully understand the mechanism that allows the electron transfer process and to elucidate the factors that role the reaction rates. These events, in most of the cases, determine the exchange of only one electron, and for this reason this type of transformation is named as Single Electron Transfer (SET).²⁰

In a first assumption, a bimolecular single electron transfer, takes place thanks a weak noncovalent interaction between a species able to accept an electron and a species able to donate an electron. In a common approach, weak-interaction mediated electron-transfer processes are outer-sphere electron-transfer reactions.²¹ Remarkably, this consideration is not related to the nature of the electronic configuration of the reactants²²

As shown in **Scheme 4**, in a single electron transfer–promoted reaction it is possible to identify analogous rate constants to describe the process, notwithstanding the fact the reactants are described by a ground or an excited electronic configuration. In other words, the treatment for a light-promoted single electron transfer can be elucidated starting or as a parallel with the thermal-promoted single electron transfer.



Chapter 1. Scheme 4 a) Oxidative and reductive single electron transfer and corresponding rate constants at the ground state. b) Oxidative and reductive single electron transfer and corresponding rate constants upon absorption of visible light.

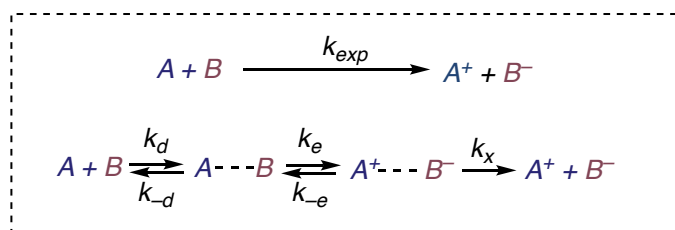
²⁰ Juris, A.; Balzani, V.; Barigelli, F.; Campagna, S.; Belser, P.; von Zelewsky, A. Ru(II) Polypyridine Complexes: Photophysics, Photochemistry, Electrochemistry, and Chemiluminescence. *radiation Chemistry Reviews* **1988**, *84*, 85–277. [https://doi.org/10.1016/0010-8545\(88\)80032-8](https://doi.org/10.1016/0010-8545(88)80032-8).

²¹ Taube, H. *Electron Transfer Reactions of Complex Ions in Solution*. Academic Press, New York, **1970**.

²² (a) Sutin, N. Nuclear, Electronic, and Frequency Factors in Electron Transfer Reactions. *Acc. Chem. Res.* **1982**, *15* (9), 275–282. <https://doi.org/10.1021/ar00081a002>. (b) Kavarnos, G. J.; Turro, N. J. Photosensitization by Reversible Electron Transfer: Theories, Experimental Evidence, and Examples. *Chem. Rev.* **1986**, *86* (2), 401–449. (c) Sutin, N. Theory of Electron Transfer Reactions: Insights and Hintsights. In *Progress in Inorganic Chemistry*; Lippard, S. J., Ed.; John Wiley & Sons, Inc.: Hoboken, NJ, USA, 2007; pp 441–498. <https://doi.org/10.1002/9780470166314.ch9>.

k_d , k_{-d} , and k'_{-d} are diffusion or dissociation rate constants; k_e and k_{-e} the unimolecular rate constants for the forward and back electron transfer in the encounter. Commonly $[A-B]$ and $[A^+-B^-]$ are often called *precursor* and *successor* complex, respectively.²³

Remarkably, considering that the *successor* complex $[A^+-B^-]$ can undergo different deactivation or disappearance pathways a more rigorous approach results necessary.²⁴ In this scenario, the kinetic observations presented above can be extended considering k_x as the sum of the rate constants of the various deactivation channels of the *successor* complex instead of k'_{-d} .²⁵



Chapter 1. Scheme 5 Rate constants for single electron transfer process.

A steady-state treatment shows that the overall rate constant for the disappearance of the reactants can be expressed as a function of the rate constants of the various steps.

Equation 4

$$k_{exp} = \frac{k_d}{1 + \frac{k_{-d}}{k_e} + \frac{k_{-d}}{k_x} \frac{k_{-e}}{k_e}}$$

Combining the above-reported equation with the work presented by Sutin²⁶ in 1968, k_{-e}/k_e can be expressed as $\exp(\Delta G/RT)$. ΔG represent the free energy change of an electron transfer process that can be estimated as:

Equation 5

$$\Delta G = \Delta G_{exp} - w_r + w_p = E(A^+/A) - E(B/B^-) - w_r + w_p$$

ΔG_{exp} is the free energy change for the reaction reported in **Scheme 4**, which can be obtained from the standard redox potentials, while w_r and w_p are the work terms related to the formation of the precursor and successor complexes, respectively.²⁷

²³ Hush, N. S. Adiabatic Theory of Outer Sphere Electron-Transfer Reactions in Solution. *Trans. Faraday Soc.* **1961**, *57*, 557. <https://doi.org/10.1039/tf9615700557>.

²⁴ Sutin, N. *Inorganic Biochemistry*, Elsevier, New York, **1973**.

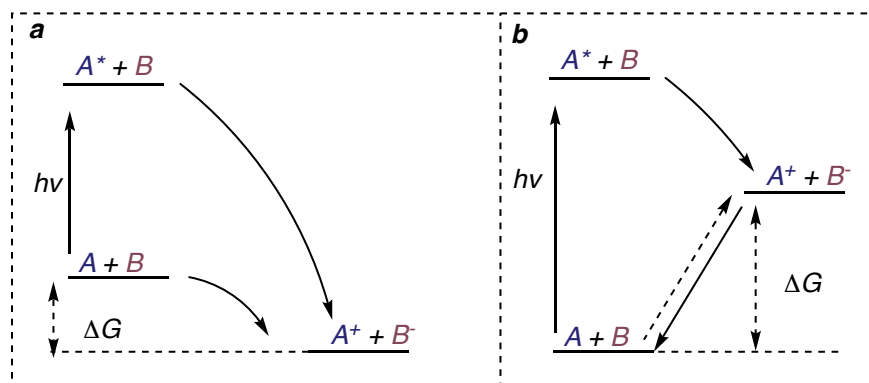
²⁵ Grätzel, M. *Energy Resources through Photochemistry and Catalysis*; Academic Press: New York, **1983**.

²⁶ Sutin, N. Free Energies, Barriers, and Reactivity Patterns in Oxidation-Reduction Reactions. *Acc. Chem. Res.* **1968**, *1* (8), 225–231. <https://doi.org/10.1021/ar50008a001>.

²⁷ Marcus, R. A. Chemical and Electrochemical Electron-Transfer Theory. *Annu. Rev. Phys. Chem.* **1964**, *15* (1), 155–196. <https://doi.org/10.1146/annurev.pc.15.100164.001103>.

From the above introduced situation, it appears that the key steps in an electron transfer process are the formation of the precursor and its conversion into the successor complex during the reaction.

Schematically, there are two possible energetic situations in which the light radiation can play a positive role in single electron transfer-promoted reaction (**Figure 5**).



Chapter 1. Figure 5 Possible effects of light, promoting single electron transfer.

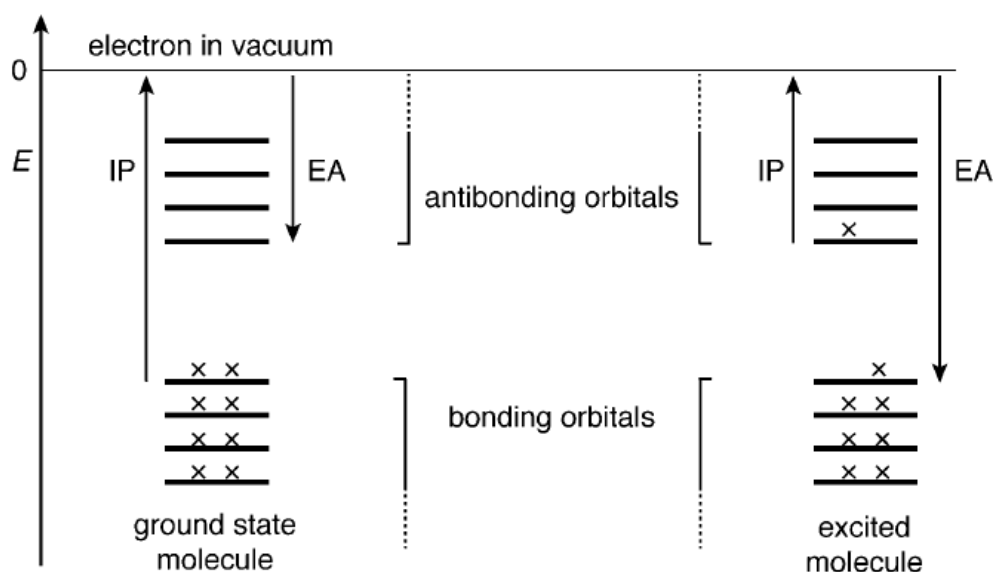
The first condition, depicted in **Figure 5a**, represents the case in which light acts as a catalyst for a reaction that is thermodynamically allowed even in dark conditions. The occurring absorption of one of the species involved in the reaction is used to increase the overall energy of the reactants. Therefore, upon absorption of light, the reaction between A^* and B results more exergonic and the effect of the light radiation contributes to overcome a kinetic barrier.

In the second, more interesting scenario (**Figure 5b**), the radiation plays a more effective role in single electron transfer-promoted reactions. When the SET between A and B is forbidden for thermodynamic issues, the occurring absorption by one of the two species is compulsory to promote the desired transformation. The effect of light allows the transformation of A and B into A^+ and B^- through the excitation of A to A^* . The transition of one of the reactants to an energetically higher electronic configuration determines that the reaction results thermodynamically allowed.

This condition is the pivotal starting point for the development of photochemical reaction and, particularly for photoredox catalysis. The main feature to underline is that in this type of reactions the energy deriving from light is directly converted into chemical energy, allowing transformation that are not permitted on the ground state.

As mentioned in the previous sections, the absorption of light determines a change in the electronic configuration of the molecule with the promotion of one electron from a lower occupied molecular orbital

of the molecule to a higher unoccupied one. The energy associated to this configuration is higher compared to the ground state and causes a strong modification on the redox reactivity of the molecule.⁶



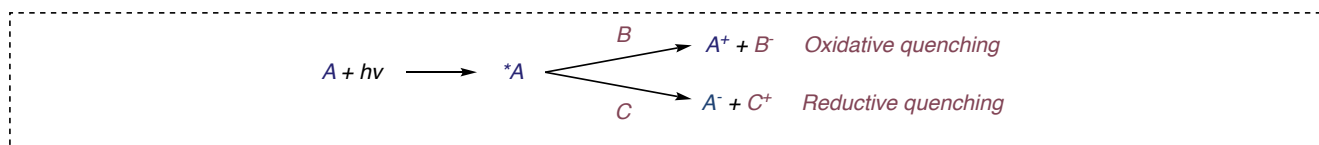
Chapter 1. Figure 6 Different electronic configuration before and after the absorption of light.

From a qualitative analysis of **Figure 6** reported above, it is easy to understand that an electronically excited photosensitizer is a better electron donor and a better electron acceptor with respect to corresponding ground state. Comparing the different configurations, it is possible to envision that in the excited state, the molecule presents at the same time, a smaller ionization potential and a higher electron affinity. This means that the “promoted” electron can be more easily removed from a species able to accept electrons. Concurrently, the promotion of an electron to the higher energy orbital determines the presence of vacancy in a less energetic molecular orbital. This scenario opens the possibility for an electron-donating species to fulfil it donating an electron.²⁸

Unlike the most common organic transformations, single electron transfer does not result in the making or breaking of bonds,²⁹ but according to the different redox reactions that can arise from the interaction of an excited molecule with a quencher it is possible to distinguish a reductive and an oxidative quenching. In the first case the excited molecule abstracts an electron from an electron donating species and the luminescence of the species *A is quenched leading the formation of the corresponding A⁻. In the second case the electron is abstracted from the excited photosensitizer by the quencher leading the formation of A⁺.

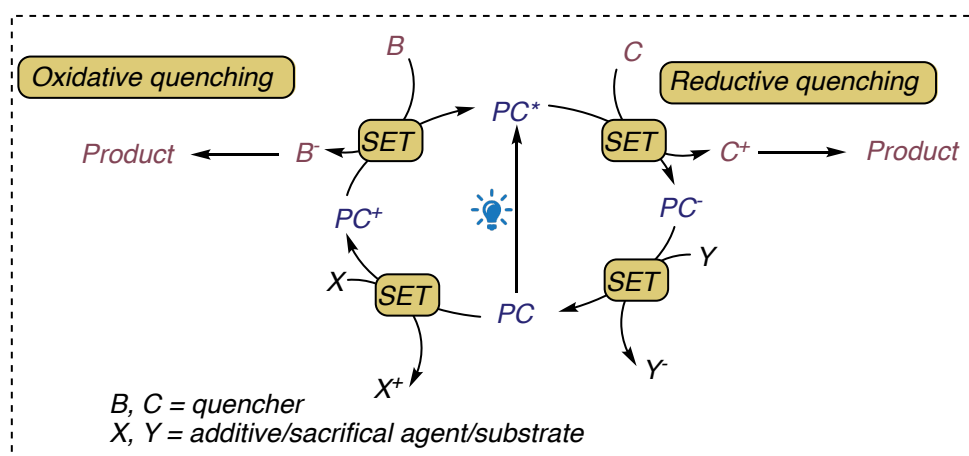
²⁸ Balzani, V.; Bergamini, G.; Ceroni, P. Light: A Very Peculiar Reactant and Product. *Angew. Chem. Int. Ed.* **2015**, *54* (39), 11320–11337. <https://doi.org/10.1002/anie.201502325>.

²⁹ Narayanam, J. M. R.; Stephenson, C. R. J. Visible Light Photoredox Catalysis: Applications in Organic Synthesis. *Chem. Soc. Rev.*, **2011**, *40*, 102-113 <https://doi.org/10.1039/B913880N>



Chapter 1. Scheme 6 Oxidative and reductive bimolecular quenching.

As in the case of an HAT-type quenching, the presence of a stoichiometric additional species (even transiently generated) able to restore the photosensitizer, is compulsory to perform a transformation with a catalytic amount of the photoactive species. In this scenario, the additive should be able to engage a redox reaction with the quenched species restoring the photocatalyst. In other words, for any closed photoredox catalytic cycle there are at least two outer-sphere electron transfer processes occurring. The first one is the quenching of the excited state, and the second leads the re-generation of the ground-state catalyst. A photocatalysis performed through SET quenching events, formally takes the name of photoredox-catalysis.



Chapter 1. Figure 7 Possible photoredox catalytic cycles.

To completely exploit all the potential of this technique, a quantitative treatment about the redox activity of the excited state of a molecule results compulsory. The Rehn-Weller equation³⁰ allows to approximate quantitatively the new potentials associated to the excited state in a thermally equilibrated excited state in a reversible redox process:

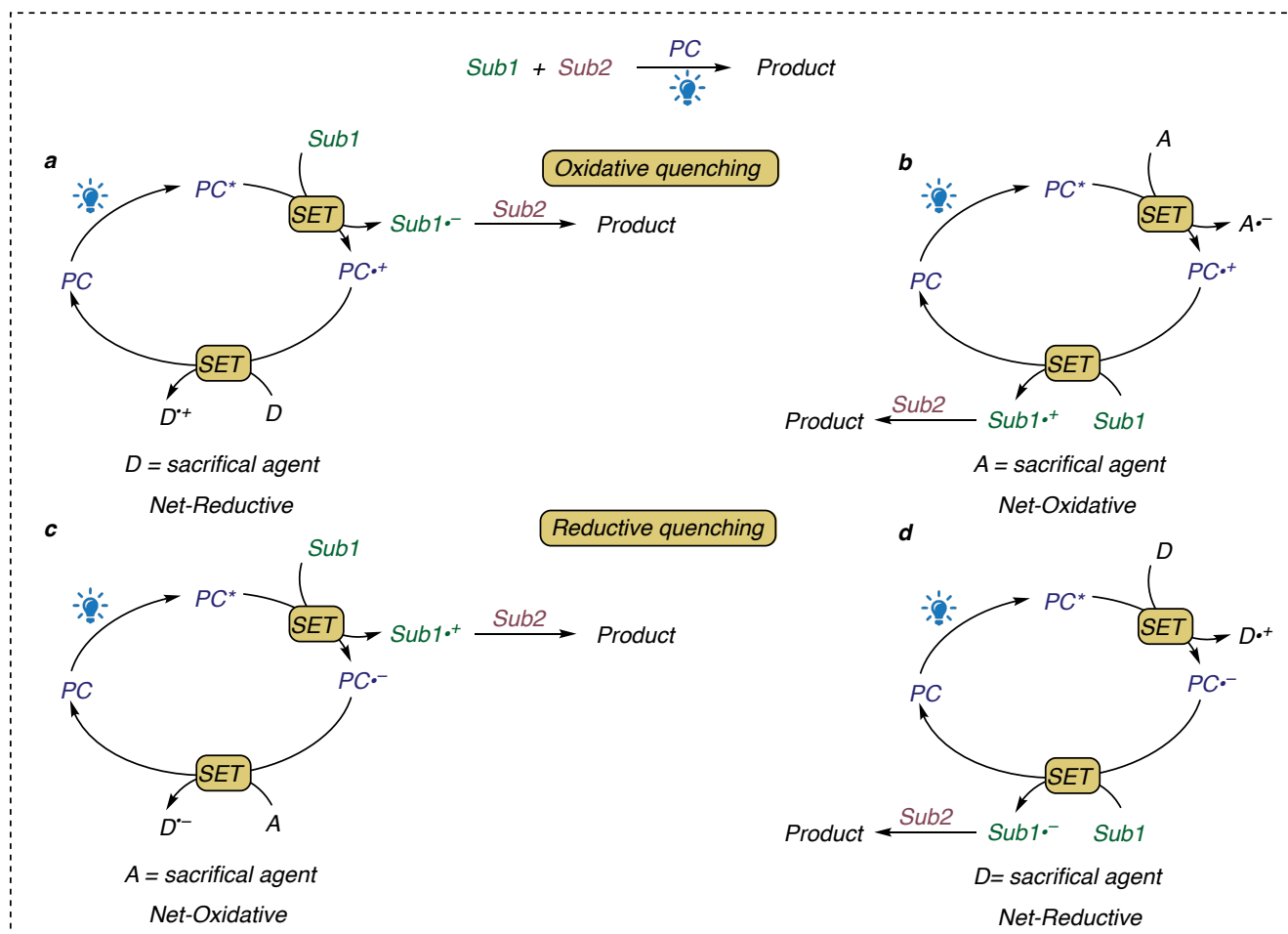
- $E_0(A^+/A^*) = E_0(A^+/A) - E_{00}({}^*A/A)$ for the oxidation of the excited state
- $E_0(A^*/A^-) = E_0(A/A^-) + E_{00}({}^*A/A)$ for the reduction of the excited state

³⁰ Lakowicz, J. R. *Principles of Fluorescence Spectroscopy*, Springer: New York, 2006.

$E_{00}(*A/A)$, as above mentioned, is the value that derives from the difference between the zero vibrational levels of the ground and excited states. The excited state considered is the one that describes the molecule when the SET event takes place (*e. g.*, if an inter system crossing from the S_1 to the long lifetime T_1 arises, the $E_{00}(*A/A)$ is not related to S_1).²⁸

Whit the purpose of summarize the different processes that can be engaged performing a photoredox catalysis, it is possible to scheme different types of catalytic cycles as a function of the different type of quenching and the role of the molecules that are involved in the single electron transfer process.

As reported in **Figure 8**, whether an oxidative quenching or a reductive quenching takes place, the catalytic cycle will be considered non-redox neutral if only one substrate interacts with the photocatalyst either in the excited state or in the ground state. In this case the presence of a sacrificial agent that does not participate in the formation of the product is compulsory in stoichiometric amount. Considering an oxidative quenching process two different scenarios are allowed. In the first one, as represented in the **Figure 8a**, the quenching occurs by the interaction between the excited photocatalyst and the substrate (Sub1). The reduced molecule $Sub1^-$ can interact with a molecule of Sub2 leading the formation of the desired product. In order to restore the photocatalyst in its in early oxidation state, an electron-donating sacrificial agent is needed. The whole catalytic cycle will be a net-reductive process since the photocatalyst only provides electrons to the substrates. The second scenario (**Figure 8b**) occurs when the oxidative quenching involves the reduction of the sacrificial agent. The photocatalyst will be restored thanks to the interaction between the substrate (Sub1), able to reduce the species PC^{*+} . The oxidized intermediate $Sub1^{*+}$ will engage a reaction with the other substrates in the reaction mixture, leading the formation of the desired product. Therefore, analogously to what previously mentioned the whole the whole catalytic cycle will be a net-oxidative process. In a similar manner, it is possible to identify net-oxidative and net-reductive catalytic cycles even if the excited state of the photocatalyst is quenched in a reductive way, as reported in **Figure 8c** and **8d**



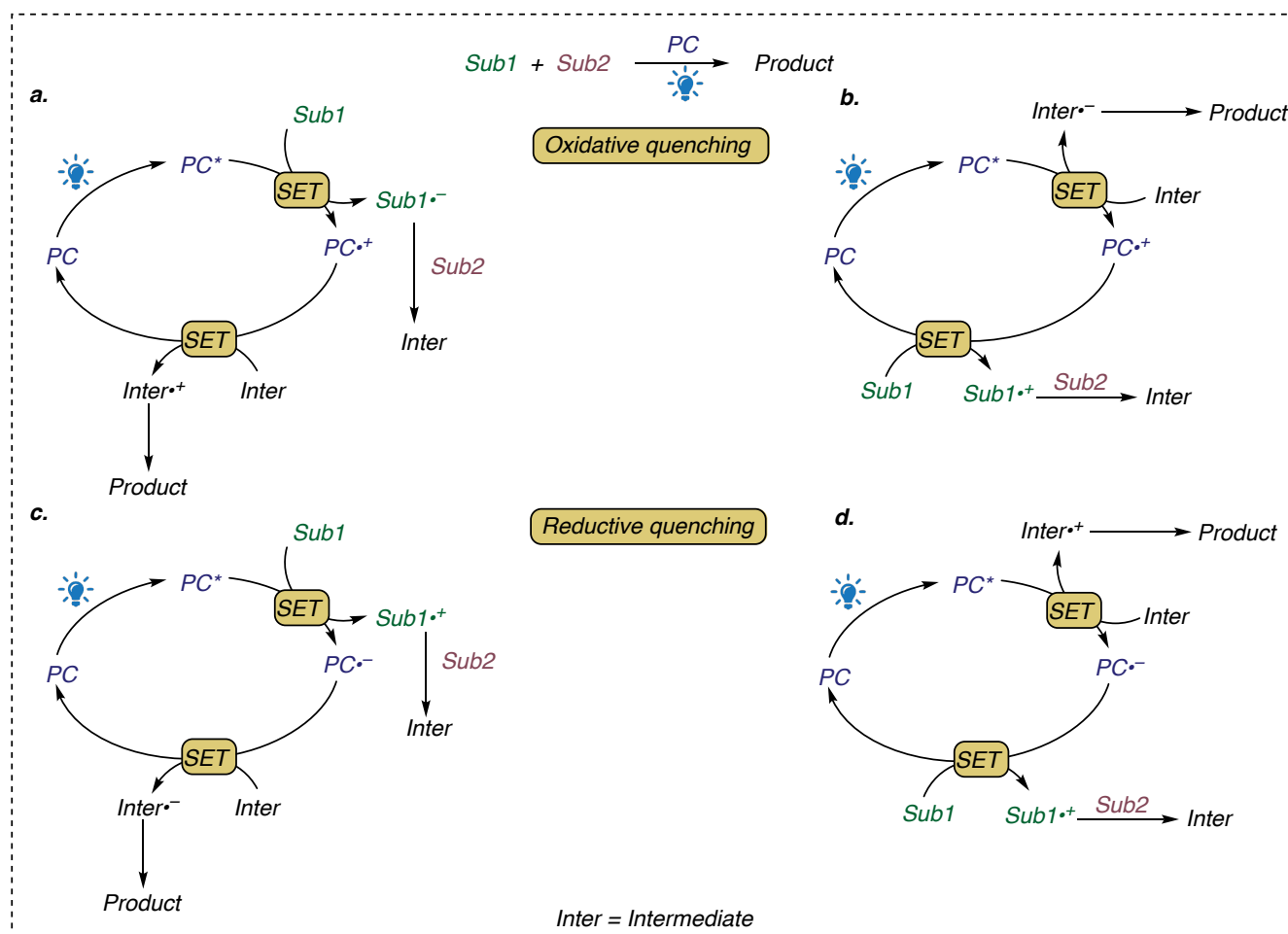
Chapter 1. Figure 8 Possible net-reductive and net-oxidative photoredox catalytic cycles.

If the catalytic cycle can be closed without the use of a sacrificial agent not taking part in the formation of the final product, the process will be described as redox-neutral. The photocatalyst in the reaction mixture will interact, both oxidizing and reducing the substrates or the intermediates that can be formed during the reaction. Even for this type of photoredox catalysis two different scenarios can occur either for oxidative quenching or for reductive quenching (**Figure 9**). The first possibility is represented in **Figure 9a** for the oxidative quenching and in **Figure 9c** for the reductive quenching. Herein, the excited state of the photocatalyst is quenched in an oxidative or reductive way by the substrate, leading the formation of the corresponding radical anion or cation (represented respectively as $Sub1^{\bullet-}$ and $Sub1^{\bullet+}$). The so formed reactive species can interact with the second substrate ($Sub2$) forming a redox active intermediate (indicated as Inter).

In order to form the desired product and allow the redox neutrality of the catalytic cycle, it is necessary for the intermediate to engage a redox reaction with oxidized or reduced photocatalyst, restoring it in its early oxidation state. This second SET allows the evolution of the reactive intermediate into the desired product.

Considering the second possibility, (**Figure 9b** and **9d**) it can occur that the substrates do not interact with the photocatalyst in the excited state but only with its reduced or oxidized form. In this case the active quencher of the excited state of the photocatalyst will be an intermediate formed during to reaction.

Remarkably, when this particular scenario takes place, it is compulsory that a small amount of a chemical species present since the beginning in the reaction mixture, acts as a sacrificial agent, quenching the excited state, starting the catalytic reaction.



Chapter 1. Figure 9 Possible redox neutral photoredox catalytic cycles.

In the light of what has been presented so far, a careful photophysical evaluation of any photocatalytic process is necessary to identify if the mechanism can be attributed to one of those previously schematized. Especially in the case of photoredox catalysis, where two consecutive and opposite redox processes are required to complete the catalytic cycle, it is essential to determine whether the reaction proceeds by reductive or oxidative quenching. Clearly, the first aspect to be taken into account is the potential associated with the species in solution. The match between the (photo)redox potentials of the photosensitizer and the substrates represents the initial point of the analysis. However, for undoubted description of the process a quantitative approach must be introduced.

As already introduced, an excited species in solution can be involved in four main deactivation pathways (radiative decay, nonradiative decay, intramolecular deactivation, intermolecular deactivation in presence of a quencher [Q]) each of which is described by a kinetic constant k_i (k_r , k_{nr} , k_p and k_{inter} also called constant of quenching k_q). Such competing processes can be kinetically described by considering the decrease in the concentration of the excited species $[PC^*]$ over time. Since only the constant related to bimolecular deactivation depends on the concentration of other species in solution, it is possible to express the relationship as:

Equation 6

$$-\frac{d[PC^*]}{dt} = (k_r + k_p + k_{nr} + k_q[Q])[PC^*]$$

Increasing the concentration of the quencher it is possible to punctually determine the concentration of excited molecule compared to the concentration in absence of quencher ($[PC^*]_0$) through:

Equation 7

$$[PC^*] = [PC^*]_0 \exp[-(k_r + k_p + k_{nr} + k_q[Q])t]$$

Similarly, it will be possible to determine the lifetime of PC^* as a function of quencher concentration.

Equation 8

$$\tau = \frac{1}{(k_r + k_p + k_{nr} + k_q[Q])}$$

Correlating the lifetime of the excited state in the absence and in the presence of quencher we obtain the so-called Stern-Volmer equation:

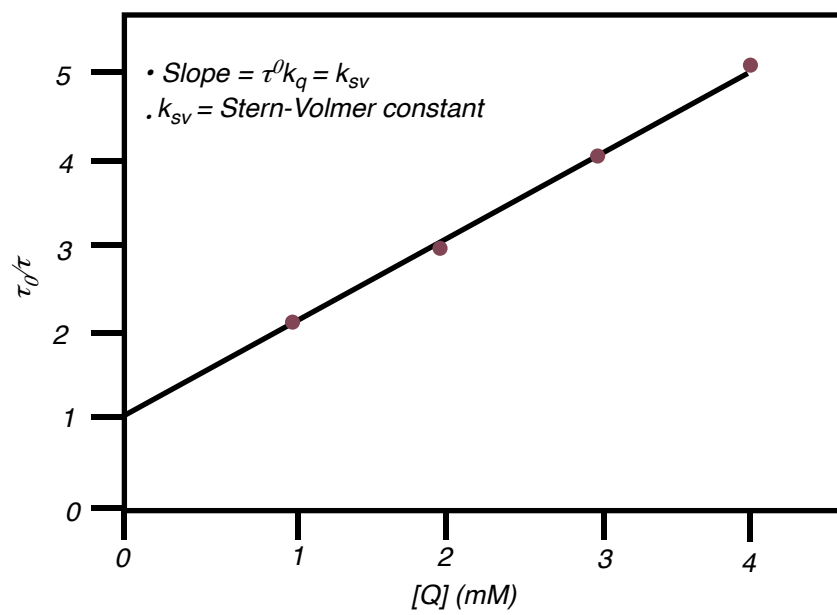
Equation 9

$$\frac{\tau^0}{\tau} = 1 + \tau^0 k_q [Q]$$

This relationship is essential for the determination of a photochemical mechanism, as it provides a linear relationship between the concentration of quencher and the ratio between τ^0 and τ (respectively, the lifetime of the excited state in the absence and presence of quencher).

By measuring the lifetime of the light-sensitive species at increasing concentrations of quencher, the Stern-Volmer plot can be obtained.

The slope of the obtained straight line provides the quenching constant for the considered species. The higher is the slope of the line, the greater is the ability of the quencher to hamper the luminescence of the excited state.



Chapter 1. Figure 10 Explicative Stern-Volmer plot

1.3 Metal-based Photocatalysts.

Even if photochemistry has been a deeply investigated area,^{2,31} both from a theoretical³² and a practical³³ point of view, before the last decade photochemistry applied to organic reactions has been mainly limited to direct excitation of one of the reactants by UV light. The use of photosensitizers, capable of absorbing visible light and promoting photoinduced electron or energy transfer processes, led to a revolution in the field for two main reasons: (i) less expensive light sources, particularly LEDs, or even sunlight can be employed and (ii) visible light can be selectively absorbed by the photosensitizers, avoiding photodegradation reactions of the organic substrates. The role model for the use of a photosensitizer is related to the properties of its excited state, as described in the previous chapters. Considering the chronological order, metal complexes, such as Ru(II) and Ir(III) complexes, had dominated the field of photoredox catalysis from the early stage of its development.³⁴ Until now, thanks to their long lifetimes of the excited states (nanosecond to microsecond range); the possibility to absorb in the visible region and the relatively high chemical stability of the oxidized and reduced forms,³⁵ these molecules are considered exceptional photosensitizers in photoredox catalysis.³⁶

In spite of the fact that late transition metal based photocatalysts have been presented in chemical literature with the purpose to expand the range of visible light-promoted transformations, for clarity this section will focus about the four more studied Ru(II) and Ir(III) complexes (**Figure 11**). The employment of these molecules, indeed, can be recognized in the greatest part of the carbon-carbon bond-forming transformations promoted by visible light radiation. In addition, the introduction to the properties of these compounds represents an explicative test case for measuring how far photoredox-mediated processes can be employed for molecular activation.

³¹ Turro, N. J.; Ramurthy, V.; Scaiano, J. C. *Modern Molecular Photochemistry of Organic Molecules*, University Science Books, Sausalito, California, **2010**

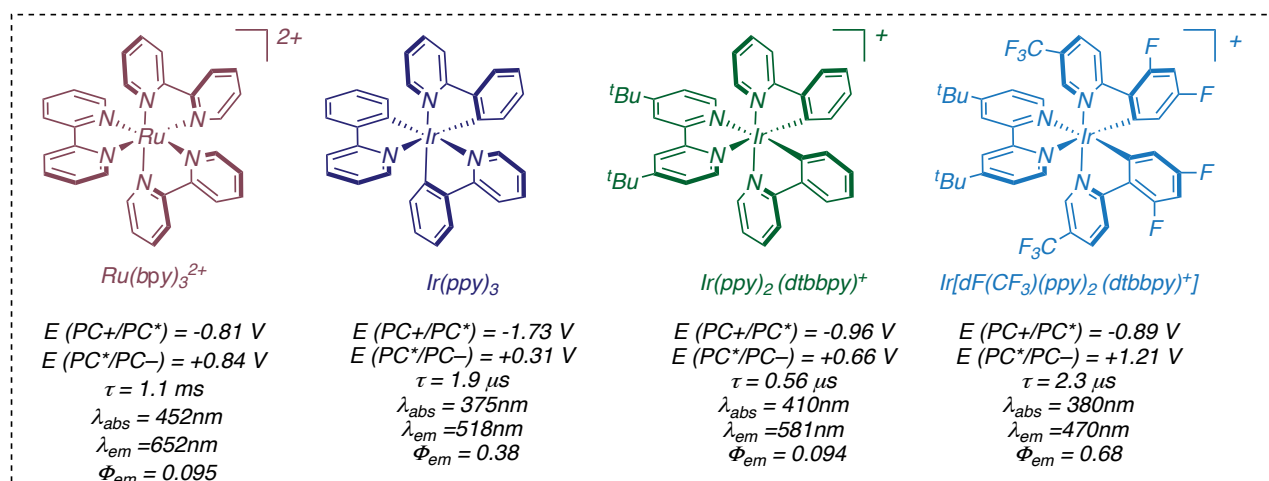
³² Mai, S.; González, L. Molecular Photochemistry: Recent Developments in Theory. *Angew. Chem. Int. Ed.* **2020**, *59* (39), 16832–16846. <https://doi.org/10.1002/anie.201916381>.

³³ *Photochemistry and Photophysics of Coordination Compounds I*; Balzani, V., Campagna, S., Eds.; Topics in Current Chemistry; Springer Berlin Heidelberg: Berlin, Heidelberg, 2007; Vol. 280. <https://doi.org/10.1007/978-3-540-73347-8>.

³⁴ Koike, T.; Akita, M. Visible-Light Radical Reaction Designed by Ru- and Ir-Based Photoredox Catalysis. *Inorg. Chem. Front.*, **2014**, *1*, 562-576 <https://doi.org/10.1039/C4QI00053F>

³⁵ Connell, T. U.; Fraser, C. L.; Czyn, M. L.; Smith, Z. M.; Hayne, D. J.; Doeven, E. H.; Agugiaro, J.; Wilson, D. J. D.; Adcock, J. L.; Scully, A. D.; Gómez, D. E.; Barnett, N. W.; Polyzos, A.; Francis, P. S. The Tandem Photoredox Catalysis Mechanism of [Ir(Ppy)₂(Dtb-Bpy)]⁺ Enabling Access to Energy Demanding Organic Substrates. *J. Am. Chem. Soc.* **2019**, *141* (44), 17646–17658. <https://doi.org/10.1021/jacs.9b07370>.

³⁶ Okada, K.; Okamoto, K.; Morita, N.; Okubo, K.; Oda, M. Photosensitized Decarboxylative Michael Addition through N-(Acyloxy)Phthalimides via an Electron-Transfer Mechanism. *J. Am. Chem. Soc.* **1991**, *113* (24), 9401–9402. <https://doi.org/10.1021/ja00024a074>.



Chapter 1. Figure 11 Most common ruthenium- and iridium-based photocatalysts and their related photochemical properties.

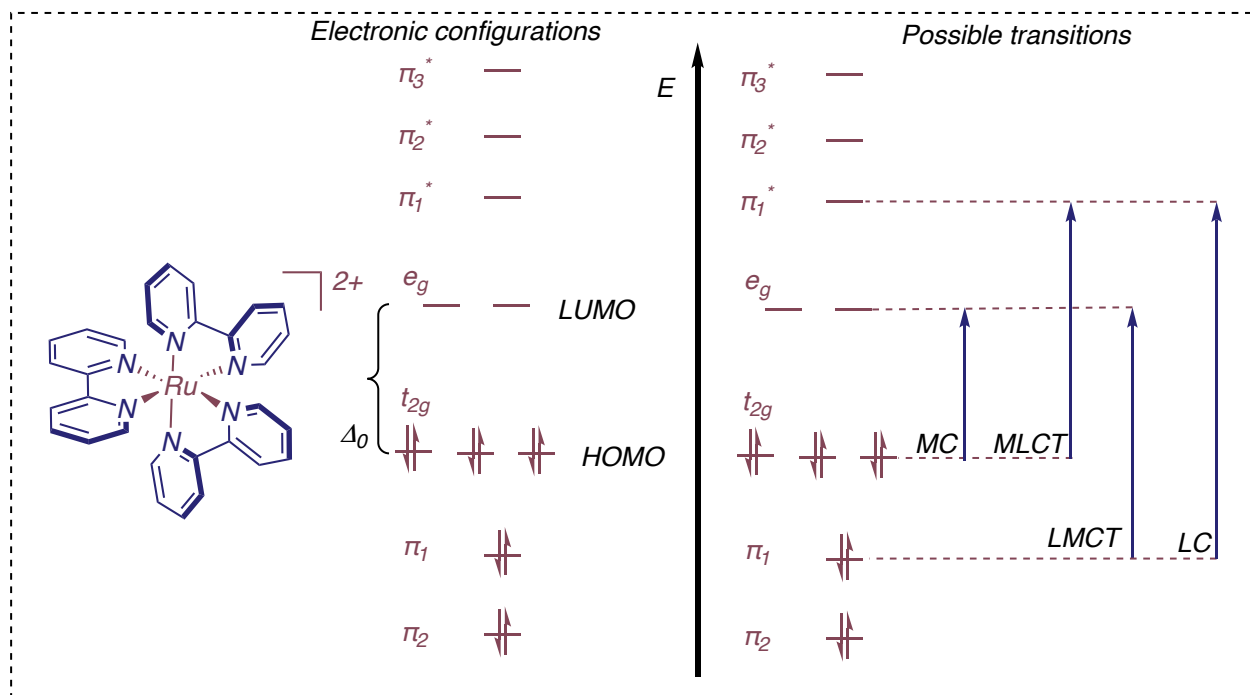
$[Ru(bpy)_3]^{2+}$ represents, undoubtedly, the prototype compound of the most investigated class of transition metal complexes from a photochemical point of view (Ru(II) polypyridine complexes).³⁷ The investigation related to its chemical and photochemical properties had tremendously contributed in the last thirty years to the development of different and diversified research topics.^{20,38}

$[Ru(bpy)_3]Cl_2$ is an octahedral transition metal complex, exhibiting a D_3 symmetry and characterized by a low-spin electronic configuration.³⁹ Thanks to the configuration of the ruthenium 2^+ ion ($[Kr]3f^{14}4d^6$) and thanks to the effect of the bipyridine ligands bearing σ -donor orbitals localized on the nitrogen atoms, π donor and π^* acceptor localized mainly on the aromatic moiety, the complex results substitutionally inert. Thanks to the octahedral coordination, according to the MO model, the electronic configuration of the ruthenium complex in its ground state is $(t_{1u})^6(a_{1g})^2(e_g)^4(t_{2g})^6$ leading to a closed shell state $^1A_{1g}$. In other words, the t_{2g} non-bonding molecular orbitals results totally occupied by the six electrons, while the e_g antibonding molecular orbitals result unoccupied. (Figure 12).

³⁷ Campagna, S.; Puntoriero, F.; Nastasi, F.; Bergamini, G.; Balzani, V. Photochemistry and Photophysics of Coordination Compounds: Ruthenium. In *Photochemistry and Photophysics of Coordination Compounds I*; Balzani, V., Campagna, S., Eds.; Topics in Current Chemistry; Springer Berlin Heidelberg: Berlin, Heidelberg, 2007; Vol. 280, pp 117–214. https://doi.org/10.1007/128_2007_133.

³⁸ Balzani, V.; Juris, A.; Venturi, M.; Campagna, S.; Serroni, S. Luminescent and Redox-Active Polynuclear Transition Metal Complexes. *Chem. Rev.* **1996**, *96* (2), 759–834. <https://doi.org/10.1021/cr941154y>.

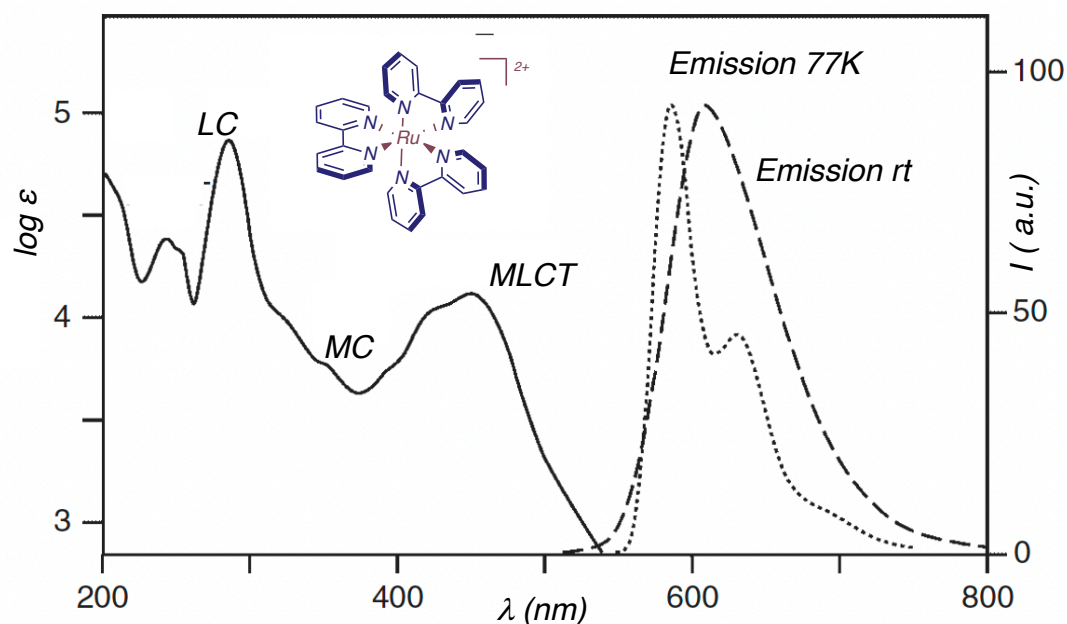
³⁹ Rillema, D.P.; Jones, D.S.; Levy, H-A. Structure of Tris(2,2'-bipyridyl)ruthenium(II)Hexafluorophosphate, $[Ru(bipy)_3][PF_6]_2$; X-Ray Crystallographic Determination *J. Chem. Soc., Chem. Commun.*, **1979**, 849–851. <https://doi.org/10.1039/C39790000849>



Chapter 1. Figure 12 Electronic configuration of ruthenium-based photosensitizer according to the MO theory and possible transitions.

Considering the simplified model of localized molecular orbitals,⁴⁰ four possible types of transition can be distinguished upon absorption of light for $[\text{Ru}(\text{bpy})_3]\text{Cl}_2$. Transitions involving molecular bonding and nonbonding orbitals that are localized on the ligand are called ligand centered (LC). In the case of $[\text{Ru}(\text{bpy})_3]\text{Cl}_2$ these transitions mainly involve the π and π^* orbitals. Comparing the absorption spectrum of the ruthenium complex (**Figure 13**) with the spectrum of bipyridine, this transition is detected by a band in the UV.

⁴⁰ Edmiston, C.; Ruedenberg, K. Localized Atomic and Molecular Orbitals. *Rev. Mod. Phys.* **1963**, 35 (3), 457–464. <https://doi.org/10.1103/RevModPhys.35.457>.



Chapter 1. Figure 13 Absorption and emission spectrum in MeOH of $[\text{Ru}(\text{bpy})_3]\text{Cl}_2$

Transitions involving $t_{2g} \rightarrow e_g$ orbitals are referred as metal centered (MC) due to the strong contribution in these orbitals from the ruthenium atom. The last two possible types of transition involve the promotion of an electron from an orbital mainly localized on the metal center to one mainly localized on the ligand or vice versa. The excited state corresponding to one of these transitions is characterized by a charge separation between the metal center and the ligand. Depending on the "direction" through which the electronic promotion takes place, the transitions are addressed as metal to ligand charge transfer (MLCT) or ligand to metal charge transfer (LMCT). In the spectrum of $[\text{Ru}(\text{bpy})_3]\text{Cl}_2$ the absorption band associated with the lowest energy transition (*i.e.*, centered at higher wavelengths, 452 nm in MeOH) is attributed to the MLCT transition. This phenomenon is attributable to the fact that the metal center can be easily oxidized while the ligand is able to delocalize the promoted electron on the aromatic scaffold.

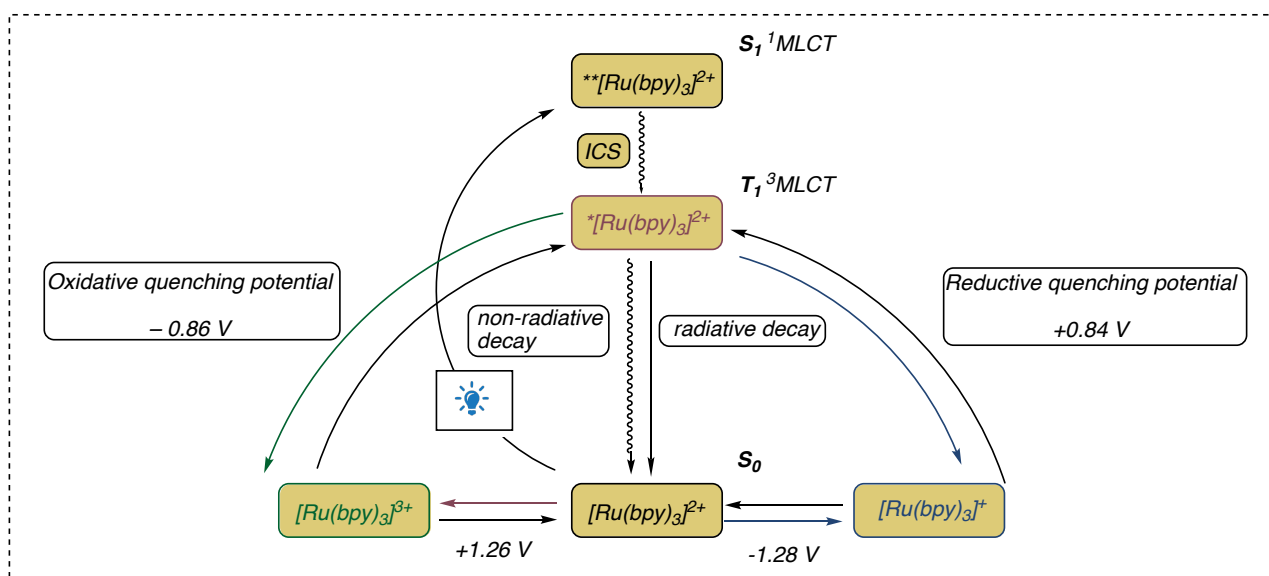
The reason why $[\text{Ru}(\text{bpy})_3]\text{Cl}_2$ has been the starting point for the development of visible light promoted reactions depends precisely on the fact that the lowest energy electronic transition determines an absorption band in the visible region of the spectrum.

According to the so-called Kasha's rule,⁴¹ the emission of a photon by a molecule in one electronically excited state will always happen from the lowest excited state of a given multiplicity. In other words, a low-energy visible radiation is sufficient for the ruthenium complex to enable its photosensitizer activity.

⁴¹ Kasha, M. Characterization of Electronic Transitions in Complex Molecules. *Discuss. Faraday Soc.* **1950**, 9, 14. <https://doi.org/10.1039/d9500900014>.

However, the excited state $^1\text{MLCT}$ presents a lifetime (τ) of 100-300 fs that is not enough long to allow the interaction with another solute species. It is in this context that the inter system crossing occurs, determining the generation of a triplet state ($^3\text{MLCT}$). Due to the heavy atom effect attributed to ruthenium, the efficiency of the inter system crossing is unitary.³⁸ The excited state from which it is possible to observe the emission of the complex corresponds to $^3\text{MLCT}$, with an associated E_{00} of 2.12 eV. The so-formed excited state is characterized by a lifetime (τ) of 1100 ns that allows its interaction with other species able to play the role of energy donor, electron acceptor, or electron donor.²⁰

With the intention to highlight the treatment presented in this and in the previous section, in **Scheme 7** a general summary of the photochemical properties of $[\text{Ru}(\text{bpy})_3]^{2+}$ and the effect of light in its redox potentials are reported.



Chapter 1. Scheme 7 The photoredox reactivity of $[\text{Ru}(\text{bpy})_3]^{2+}$.

While Ru(II) polypyridine complexes represent a class of compounds deeply investigated from the chemical community since many years, remarkably the investigation of the photophysical and photochemical properties of Ir(III) complexes before the last century remained an almost uninvestigated field.⁴²

⁴²a) Flamigni, L.; Barbieri, A.; Sabatini, C.; Ventura, B.; Barigelletti, F. Photochemistry and Photophysics of Coordination Compounds: Iridium. In *Photochemistry and Photophysics of Coordination Compounds II*; Balzani, V., Campagna, S., Eds.; Topics in Current Chemistry; Springer Berlin Heidelberg: Berlin, Heidelberg, 2007; Vol. 281, pp 143–203. https://doi.org/10.1007/128_2007_131; b) Roundhill, D. M. *Photochemistry and Photophysics of Metal Complexes*. Plenum Press, New York 1994; c) Maestri, M.; Balzani, V.; Deuschel-Cornioley, C.; Zelewsky, A. V. Photochemistry and Luminescence of Cyclometallated Complexes. In *Advances in Photochemistry*; Volman, D. H., Hammond, G. S., Neckers, D. C., Eds.; John Wiley & Sons, Inc.: Hoboken, NJ, USA, 2007; pp 1–68. <https://doi.org/10.1002/9780470133484>.

The main issue which led a non-parallel development of the two different classes of coordination complexes results from the difficulty to transpose the collected knowledge of the $[\text{Ru}(\text{bpy})_3]^{2+}$ to the corresponding $[\text{Ir}(\text{bpy})_3]^{3+}$.⁴³

The exponential growth of literature on the use iridium to convert the light radiation into chemical energy occurred with the exploitation of a wide class of coordination complexes, bearing cyclometalated ligands, whose prototype is the neutral *fac*- $\text{Ir}(\text{ppy})_3$.⁴⁴

Anionic ligands, like substituted phenyl pyridines, increase tremendously the electron density and allow the stabilization of the highly positive charged Ir(III).

Cyclometalated ligands surrounding the metal center strongly influence the redox and photochemical properties of these photosensitizers. Ir (III) shows a $[\text{Xe}]4f^{14}5d^6$ electronic configuration, isoelectric with the above-described Ru(II). Due to the different spatial extension of the two cations, the degenerate Ir(III) *d* orbitals split in an octahedral ligand field, by an amount Δ greater compared with Ru(II). Concurrently, the presence of cyclometalated ligands, according to the spectroscopical series, contributes to increase the separation. As a consequence, the energetic gap between the HOMO and the LUMO orbitals of substitutionally inert Ir(III) complexes will be greater compared to the $[\text{Ru}(\text{bpy})_3]^{2+}$.

Analogously, the difference in energy between the ground and the electronically excited state will be higher.

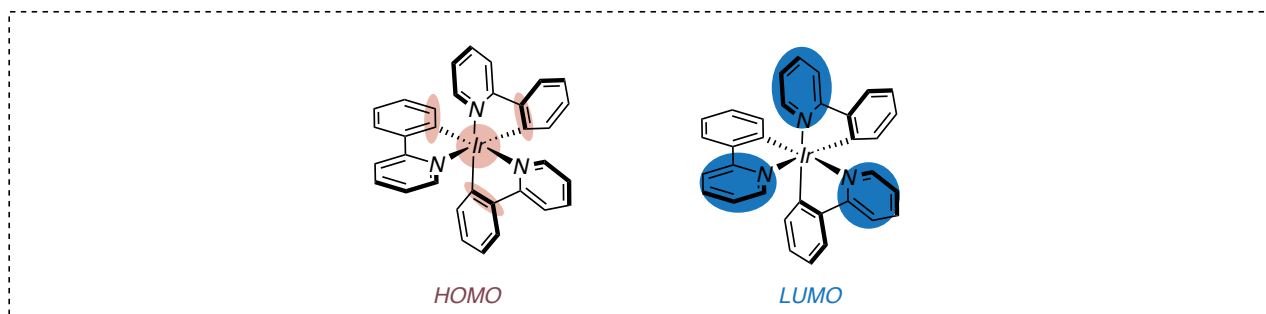
Noteworthy, the position of the iridium atom in the periodic table empowers the spin-orbit interaction. For this reason, cyclometalated iridium (III) complexes present an enhanced MLCT efficiency, forming the excited state. At the same time, a higher spin-orbit coupling favors the intersystem crossing from $^1\text{MLCT}$ to $^3\text{MLCT}$.⁴⁵

In addition, the negative charged ppy ligands, causes a strong σ -donation, heavily influencing the ground-state redox potentials. An electrochemical analysis of *fac*- $\text{Ir}(\text{ppy})_3$ shows a facile oxidation (+ 0.77 V vs. SCE), for the electrons mainly localized on the metal center, despite the high ionic charge on the metal center. On the other hand, the reduction results extremely more difficult (-2.19 V vs. SCE).⁴²

⁴³ Watts, R. J. Comments on Inorganic Chemistry. In *Comments on modern chemistry. Part A*; Watts, R. J., Gordon and Breach, London pp. 303–337

⁴⁴ a) Dixon, I. M.; Collin, J.-P.; Sauvage, J.-P.; Flamigni, L.; Encinas, S.; Barigelletti, F. A Family of Luminescent Coordination Compounds: Iridium(III) Polyimine Complexes. *Chem. Soc. Rev.* **2000**, 29 (6), 385–391. <https://doi.org/10.1039/b000704h>. 2 b) King, K. A.; Spellane, P. J.; Watts, R. J. Excited-State Properties of a Triply Ortho-Metalated Iridium(III) Complex. *J. Am. Chem. Soc.* **1985**, 107 (5), 1431–1432. <https://doi.org/10.1021/ja00291a064>.

⁴⁵ Montalti M, Credi A, Prodi L, Gandolfi M. *Handbook of Photochemistry*. Taylor and Francis, Boca Raton, Fl **2006**



Chapter 1. Figure 14 Graphical depiction of HOMO and LUMO for *fac*-Ir(ppy)₃.

Moreover, envisioning the excited state of Ir(ppy)₃,⁴⁶ it is remarkable that the combination of the metal center and of the anionic ligands' properties is reflected in the photoredox behavior of the complex. The enhanced energetic gap between the ground and the excited state determines that the maximum of the absorption peak for the MLCT transition, does not exceed 400 nm, while for [Ru(bpy)₃]²⁺ is around 450 nm.²⁰ Moreover, considering the excited state redox potentials. Ir(ppy)₃ shows lower reductive quenching potential than [Ru(bpy)₃]²⁺ (0.33 V vs. 0.84 V vs. SCE) and a much higher oxidative quenching potential (– 1.73 V vs. – 0.86 V vs. SCE).

A final consideration to underline regarding the photochemical properties of Ir(III) coordination complexes is the possibility to obtain in quite high yields heteroleptic complexes.⁴⁷

Noteworthy, this point cannot be extended to the corresponding ruthenium complexes since a non-symmetric ligand field can interrupt the spin-orbit coupling, making MLCT and the intersystem crossing less efficient.⁴⁸

The incorporation of different neutral or anionic ligands on the iridium (III) center can strongly influence the photochemical properties of the photosensitizers.⁴⁹

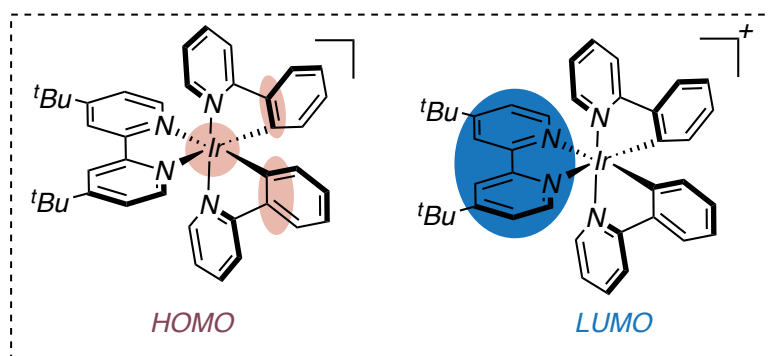
Tuning the electronic properties of the ligand gives the possibility to modulate and predict the characteristics of the resulting Ir(III) complex. Neutral ligands like in the case of [Ir(ppy)₂(dtbbpy)]⁺, as well as determining the formation of a cationic complex, allow the tuning of the HOMO–LUMO energy gap, promoting also the spatial separation of the orbitals.

⁴⁶ Lowry, M. S.; Goldsmith, J. I.; Slinker, J. D.; Rohl, R.; Pascal, R. A.; Malliaras, G. G.; Bernhard, S. Single-Layer Electroluminescent Devices and Photoinduced Hydrogen Production from an Ionic Iridium(III) Complex. *Chem. Mater.*, **2005**, *17*, 5712–5719. <https://doi.org/10.1021/cm051312+>

⁴⁷ Kelly, C. B.; Patel, N. R.; Primer, D. N.; Jouffroy, M.; Tellis, J. C.; Molander, G. A. Preparation of Visible-Light-Activated Metal Complexes and Their Use in Photoredox/Nickel Dual Catalysis. *Nat Protoc* **2017**, *12* (3), 472–492. <https://doi.org/10.1038/nprot.2016.176>.

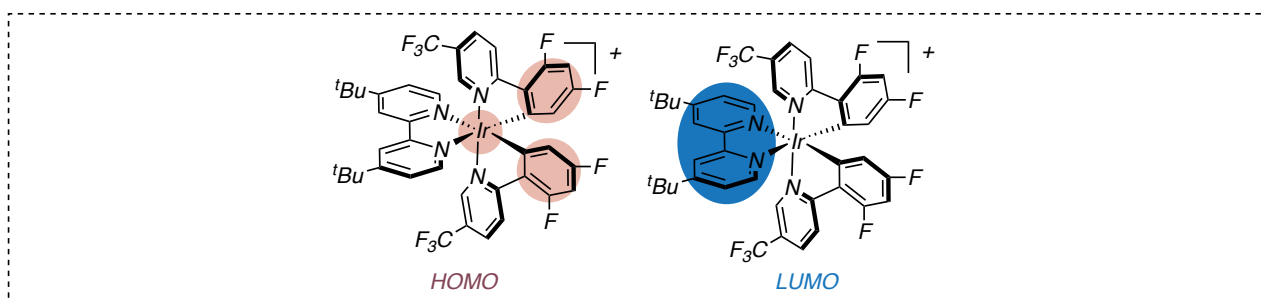
⁴⁸ a) Li, E. Y.; Cheng, Y.-M.; Hsu, C.-C.; Chou, P.-T.; Lee, G.-H.; Lin, I.-H.; Chi, Y.; Liu, C.-S. Neutral RuII-Based Emitting Materials: A Prototypical Study on Factors Governing Radiationless Transition in Phosphorescent Metal Complexes. *Inorg. Chem.* **2006**, *45*, 8041–8051. <https://doi.org/10.1021/ic060066g>;
b) Bomben, P. G.; Robson, K. C. D.; Sedach, P. A.; Berlinguette, C. P. On the Viability of Cyclometalated Ru(II) Complexes for Light-Harvesting Applications. *Inorg. Chem.* **2009**, *48* (20), 9631–9643. <https://doi.org/10.1021/ic900653q>.

⁴⁹ Lamansky, S.; Djurovich, P.; Murphy, D.; Abdel-Razzaq, F.; Lee, H.-E.; Adachi, C.; Burrows, P. E.; Forrest, S. R.; Thompson, M. E. Highly Phosphorescent Bis-Cyclometalated Iridium Complexes: Synthesis, Photophysical Characterization, and Use in Organic Light Emitting Diodes. *J. Am. Chem. Soc.* **2001**, *123* (18), 4304–4312. <https://doi.org/10.1021/ja003693s>.



Chapter 1. Figure 15 Graphical depiction of HOMO and LUMO for $[\text{Ir}(\text{ppy})(\text{dtbbpy})]^+$.

Considering, for instance, the above-introduced $(\text{Ir}[\text{dF}(\text{CF}_3)\text{ppy}]_2(\text{dtbbpy}))^+$, electron-withdrawing anionic ligands, such as fluorine or trifluoromethyl groups determine a strong stabilization of the HOMO, not affecting the LUMO level.⁵⁰ The MLCT moves to higher energy, while the photoredox potential of the excited state are strongly modified. The complex, when employed as photosensitizer, will present an enhanced ability to engage a reductive quenching, while the oxidative quenching will be less favored compared with the $\text{Ir}(\text{ppy})_3$.



Chapter 1. Figure 16 Graphical depiction of HOMO and LUMO for $(\text{Ir}[\text{dF}(\text{CF}_3)\text{ppy}]_2(\text{dtbbpy}))^+$.

⁵⁰ Dedeian, K.; Djurovich, P. I.; Garces, F. O.; Carlson, G.; Watts, R. J. A New Synthetic Route to the Preparation of a Series of Strong Photoreducing Agents: Fac-Tris-Ortho-Metalated Complexes of Iridium(III) with Substituted 2-Phenylpyridines. *Inorg. Chem.* **1991**, *30* (8), 1685–1687. <https://doi.org/10.1021/ic00008a003>.

1.4 Organic Dyes.

Ruthenium- and iridium-based photosensitizers, thanks to the specifications highlighted in the previous section, represent a fundamental tool in photoredox catalysis. The more than thirty year-lasting investigation related to their photochemical properties, combined with the possibility to tune the chemical environment around the metal centers, influencing their excited states makes them a pivotal instrument for the development of this technique.

Nevertheless, some drawbacks associated to these compounds cannot be excluded from the treatment.

First, the elevated cost of ruthenium and iridium still represent the greatest obstacle. Secondly, the reduced availability in combination with the environmental impact related to their exploitation still limits the use of these tools.⁵¹

In order to overcome the limitations associated to the employment of ruthenium and iridium complexes to perform photoredox mediated transformations, it is possible to find in literature two possible solutions. The first is represented by the employment of earth abundant metal centers (e.g., iron,⁵² copper⁵³ or chromium⁵⁴). The second occurs with the development of environmental-friendly, metal-free and cheap organic photocatalysts.

The combination of organic molecules with light to promote organic transformation represents a well-established technique since the beginning of the last century.⁵⁵ However, the range of possible allowed transformation remained tight until the last decade; especially if the UV light promoted reaction are excluded from the treatment. An impressive review about organic molecules used as photocatalysts was reported by Nicewicz and co-workers.⁵⁶

Because of the enormous number of different molecules employed as organic photosensitizers, a comprehensive and exhaustive overview is impossible.

In the following chapters two of the most investigated classes of purely organic visible light absorbing photocatalysts will be presented.

The first part will cover the photochemical properties of acridinium based photocatalysts and the features that made this class of compounds a pivotal tool for the development of photoredox catalysis. Subsequently cyanoarenes based photocatalysts will be discussed in the same manner.

⁵¹ Volz, D.; Wallesch, M.; Fléchon, C.; Danz, M.; Verma, A.; Navarro, J. M.; Zink, D. M.; Bräse, S.; Baumann, T. From Iridium and Platinum to Copper and Carbon: New Avenues for More Sustainability in Organic Light-Emitting Diodes. *Green Chem.* **2015**, *17* (4), 1988–2011. <https://doi.org/10.1039/C4GC02195A>.

⁵² Larsen, C. B.; Wenger, O. S. Photoredox Catalysis with Metal Complexes Made from Earth-Abundant Elements. *Chem. Eur. J.* **2018**, *24* (9), 2039–2058. <https://doi.org/10.1002/chem.201703602>.

⁵³ Reiser, O. Shining Light on Copper: Unique Opportunities for Visible-Light-Catalyzed Atom Transfer Radical Addition Reactions and Related Processes. *Acc. Chem. Res.* **2016**, *49* (9), 1990–1996. <https://doi.org/10.1021/acs.accounts.6b00296>.

⁵⁴ Gualandi, A.; Marchini, M.; Mengozzi, L.; Natali, M.; Lucarini, M.; Ceroni, P.; Cozzi, P. G. Organocatalytic Enantioselective Alkylation of Aldehydes with [Fe(Bpy)₃]Br₂ Catalyst and Visible Light. *ACS Catal.* **2015**, *5* (10), 5927–5931. <https://doi.org/10.1021/acscatal.5b01573>.

⁵⁵ Ciamician, G. The Photochemistry of the Future *Science*, **1912**, *36*, 385–394. [10.1126/science.36.926.385](https://doi.org/10.1126/science.36.926.385)

⁵⁶ Romero, N. A.; Nicewicz, D. A. Organic Photoredox Catalysis. *Chem. Rev.* **2016**, *116* (17), 10075–10166. <https://doi.org/10.1021/acs.chemrev.6b00057>.

•Acridinium–based photocatalysts

Acridinium–based photosensitizers represent one of the most investigated class of purely organic photocatalysts. The common feature of these molecules is characterized the *N*-methyl substituted acridinium scaffold which confers the most important photophysical properties of these molecules. The extensive conjugated π -system determines the absorption in the visible region, while the substituent, working as a protecting group on the nitrogen atom provides the required chemical stability.

Reaching the excited state, acridinium–based photocatalyst, are usually characterized by an enhanced oxidative power with a reduction potential of the excited state that can overcome 2.0 V (vs. SCE) in the singlet state. The main drawback associated to this class of photocatalyst regards the corresponding acridinyl radical formed after the reductive quenching of the acridinium excited state. Usually, the reducing power of these species is weak, and the redox potential associated to the restoration of the photocatalysts is around -0.5 V (vs. SCE). Therefore, the transformations allowed by the employment of acridinium–based photocatalysts remain relatively narrow.

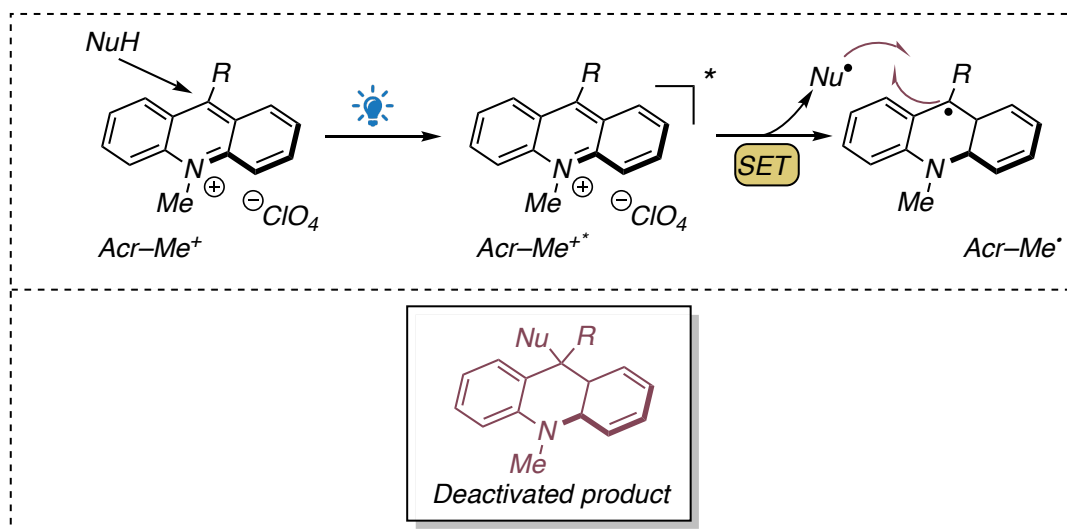
In a chronological order, one of the first examples in literature, presenting an acridinium–based photosensitizer was reported in 2001 by Fukuzumi and co-workers.⁵⁷

In the work, the photoredox and electrochemical properties of *N*-Methyl Acridinium (Acr-Me⁺) were investigated. Under visible light irradiation ($\lambda_{\text{max}} \approx 430$ nm) the photocatalyst reaches the single excited state exhibiting an extremely long lifetime for the fluorescence (31ns), a unitary quantum yield⁵⁸ and a powerful absorption–induced potential of $E(\text{Acr-Me}^{+*}/\text{Acr-Me}^{\bullet}) = +2.32$ V (vs. SCE).

At the same time, however, the photocatalyst displayed a low chemical stability in the presence of a nucleophile. Even at the ground state, through an aromatic nucleophilic substitution, or at excited state, through a radical addition, the position 9- of the acridinium scaffold resulted reactive, causing a deactivation of the photocatalyst. (**Scheme 8**).

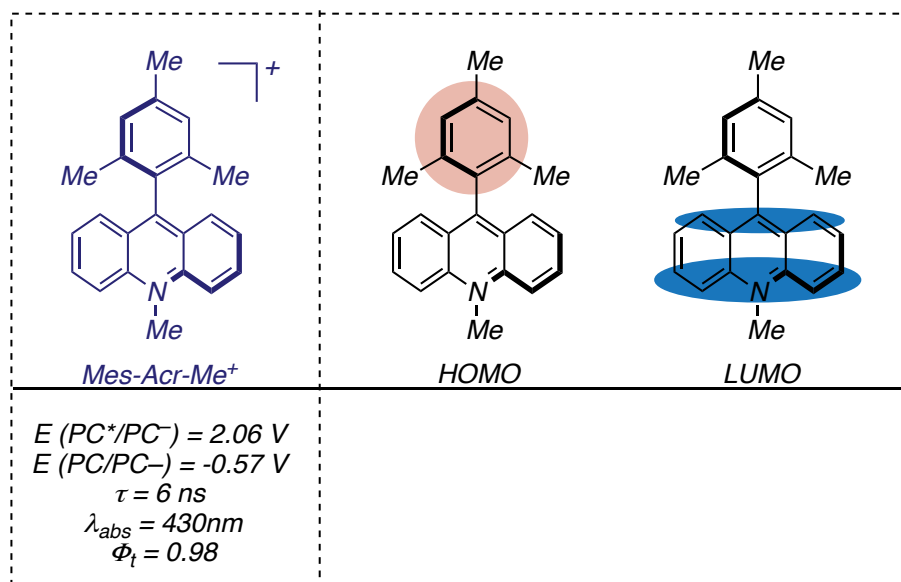
⁵⁷ Fukuzumi, S.; Ohkubo, K.; Suenobu, T.; Kato, K.; Fujitsuka, M.; Ito, O. Photoalkylation of 10-Alkylacridinium Ion via a Charge-Shift Type of Photoinduced Electron Transfer Controlled by Solvent Polarity. *J. Am. Chem. Soc.* **2001**, *123* (35), 8459–8467. <https://doi.org/10.1021/ja0043111>.

⁵⁸ Weber, G.; Teale, F. W. J. Determination of the Absolute Quantum Yield of Fluorescent Solutions. *Trans. Faraday Soc.* **1957**, *53*, 646–655. <https://doi.org/10.1039/tf9575300646>.



Chapter 1 Scheme 8: By processes causing deactivation of Acr-Me^+ .

In order to overcome these limitations and to extend the use of acridinium-based molecules as effective photoredox catalysts, the presence of an aryl substituent on position 9– resulted compulsory. The introduction of the simple phenyl ring resulted an ineffective solution since the rotational flexibility of the phenyl ring determined a drop both of the lifetime and of the quantum yield.⁵⁹ Only through the introduction of the bulky, electron-rich and rotationally rigid mesityl group, the broad use of acridinium photocatalysts was accessible.⁶⁰



Chapter 1. Figure 17 Photochemical properties of Mes-Acr-Me^+ and graphical depiction of its HOMO and LUMO.

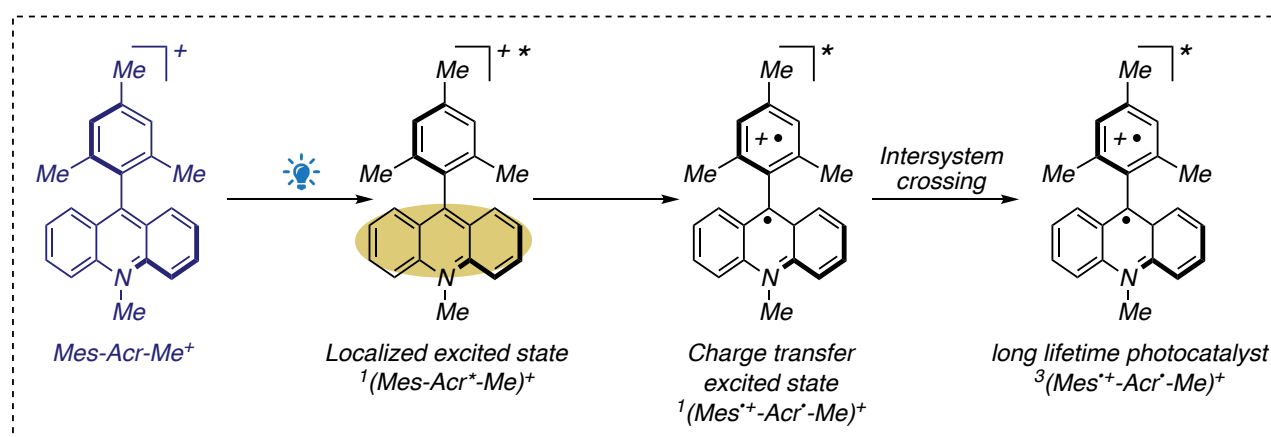
⁵⁹ a) Suga, K.; Ohkubo, K.; Fukuzumi, S. Photocatalytic Oxygenation of Pivalic Acid with Molecular Oxygen via Photoinduced Electron Transfer Using 10-Methylacridinium Ions. *J. Phys. Chem. A*, **2006**, *110*, 3860–3867. 10.1021/jp056637s. b) Zhou, D.; Khatmullin, R.; Walpita, J.; Miller, N. A.; Luk, H. L.; Vyas, S.; Hadad, C. M.; Glusac, K. D. Mechanistic Study of the Photochemical Hydroxide Ion Release from 9-Hydroxy-10-Methyl-9-Phenyl-9,10-Dihydroacridine. *J. Am. Chem. Soc.*, **2012**, *134*, 11301–11303. <https://doi.org/10.1021/ja3031888>.

⁶⁰ Fukuzumi, S.; Kotani, H.; Ohkubo, K.; Ogo, S.; Tkachenko, N. V.; Lemmetyinen, H. Electron-Transfer State of 9-Mesityl-10-Methylacridinium Ion with a Much Longer Lifetime and Higher Energy Than That of the Natural Photosynthetic Reaction Center. *J. Am. Chem. Soc.*, **2004**, *126*, 1600–1601. 10.1021/ja038656q.

The introduction of Mes-Acr-Me⁺ (also known as Fukuzumi's catalyst) paved the way to the exploitation of these class of photocatalyst for the development of fundamental synthetic applications.⁶¹

Remarkably, after the introduction in literature by Fukuzumi and co-workers, the detailed description of the behavior of its excited state resulted non-trivial.⁶²

Due to the marked differences of the two moieties of the molecule –the electron-rich mesityl and the electron-poor acridinium–, after excitation through a visible light irradiation, the excited state results extremely localized on the acridinium moiety. These kinds of excited states are commonly addressed as localized excited states (LE).⁶³ Subsequently, an internal single electron transfer occurs determining the formal motion of an electron localized on the mesityl ring to the acridinium moiety. The so formed state is called charge-separated singlet state ¹(Acr•–Mes•+)*. Only at this stage, as reported in 2008 by Fukuzumi and co-workers⁶⁴ an intersystem crossing takes place leading the formation of a triplet charge-transfer excited state ³(Acr•–Mes•+)*, exhibiting high quantum yield of 0.98 and enhanced lifetime (6.0 ns vs. 2.0 ns measured for Ph-Acr-Me⁺). In addition, the photoredox properties of the catalyst resulted maintained, with a photoredox reduction potential of the triplet state ³(Acr•–Mes•+)* of 2.06V (vs. SCE)⁶⁵ (Scheme 9)



Chapter 1. Scheme 9 description of the behavior of the excited state of Mes-Acr-Me⁺.

Although, the introduction of the mesityl group, preventing the nucleophilic attack on the acridinium moiety allowed an intensive exploitation of photoredox processes promoted by the Fukuzumi's catalyst,⁶¹ under specific reaction condition a lack of chemical stability has been highlighted.⁶⁶

⁶¹ Tlilis, A.; Lakhdar, S.; Acridinium Salts and Cyanoarenes as Powerful Photocatalysts: Opportunities in Organic Synthesis *Angew. Chem. Int.*, **2021**, *60*, 19526-19549. <https://doi.org/10.1002/anie.202102262> and the references therein.

⁶² M. M. Brasholz, Acridinium Dyes and Quinones in Photocatalysis in *Science of Synthesis* König, B. Georg Thieme Verlag, Stuttgart, **2019**. 10.1055/sos-SD-229-00224

⁶³ van Willigen, H. Time-Resolved EPR Study of Photoexcited Triplet-State Formation in Electron-Donor-Substituted Acridinium Ions. *J. Phys. Chem.*, **1996**, *100*, 3312-3316. <https://doi.org/10.1021/jp953176+>

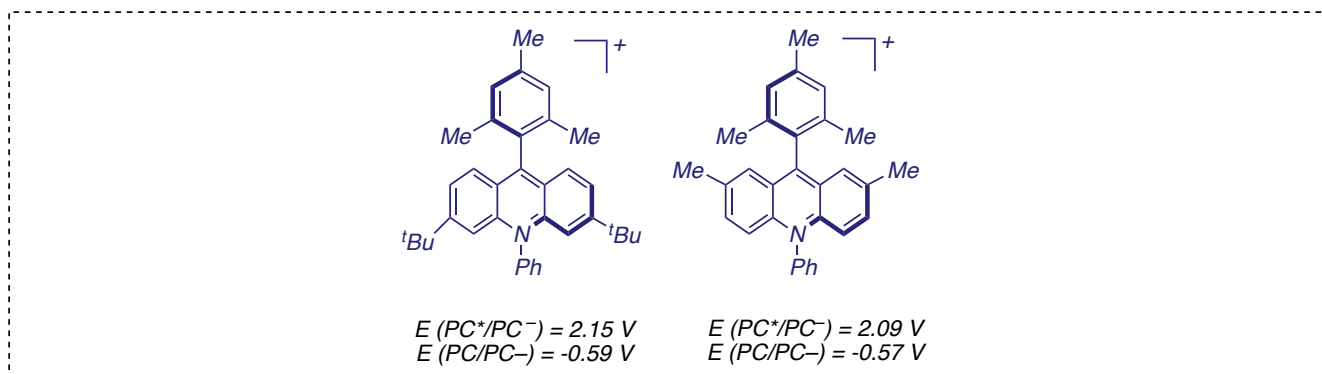
⁶⁴ Fukuzumi, S.; Kotani, H.; Ohkubo, K. Response: Why Had Long-Lived Electron-Transfer States of Donor-Substituted 10-Methylacridinium Ions Been Overlooked? Formation of the Dimer Radical Cations Detected in the near-IR Region. *Phys. Chem. Chem. Phys.*, **2008**, *10*, 5159-5162. <https://doi.org/10.1039/B809264H>

⁶⁵ Fukuzumi, S.; Ohkubo, K.; Suenobu, T. Long-Lived Charge Separation and Applications in Artificial Photosynthesis. *Acc. Chem. Res.* **2014**, *47*, 1455-1464. <https://doi.org/10.1021/ar400200u>

⁶⁶ a) Wilger, D. J.; Grandjean, J.-M. M.; Lammert, T. R.; Nicewicz, D. A. The Direct Anti-Markovnikov Addition of Mineral Acids to Styrenes. *Nature Chem* **2014**, *6* (8), 720-726. <https://doi.org/10.1038/nchem.2000>. b) J.-M. Grandjean, Anti-Markovnikov Hydrofluorination, Hydroxysulfonation and Hydration

The greatest contribution to overcome the problems related to the *N*-demethylation and the radical addition at the 2,7- or 3,6-positions of the Mes–Acr–Me⁺ was reported by Nicewicz and co-workers.⁶⁷

The substitution of the methyl group with a less reactive phenyl group and introduction of bulky group on the susceptible positions of the acridinium moiety enhanced the robustness of the photocatalyst, almost unwavering its photochemical and photophysical properties. (**Figure 18**)

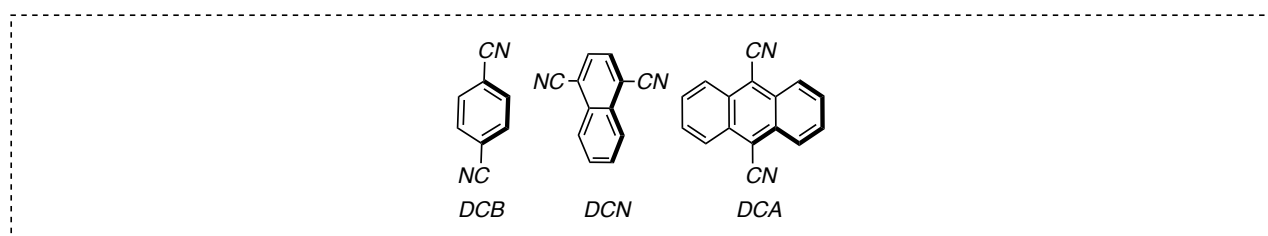


Chapter 1. Figure 18 New generation of acridinium-based photosensitizer and their related photoredox potentials (vs. SCE).

•Cyanoarenes–based photocatalysts

Among the various classes of organic dyes developed for synthetic application in photoredox catalysis, cyanoarenes derivatives occupy a privileged position.

The first reported examples in literature regarded the use of simple and unsubstituted derivatives.⁶⁸ The photochemical features of small molecules such as 1,4-dicyanobenzene (*p*-DCB), 1,4-dicyanonaphthalene (DCN) and 9,10-anthracenedicarbonitrile (DCA) were investigated. (**Figure 19**) Cyanoarenes derivatives, upon near-UV irradiation, exhibit a high energy singlet excited state that allows the oxidations of compounds with potentials exceeding +2.0 V vs. SCE. The corresponding radical anions formed upon the single electron transfer are moderate reductants, engaging a second electron transfer and restoring the original photocatalyst.



Chapter 1. Figure 19 First reported cyanoarene-based photosensitizers.

Even if these molecules have been employed in interesting transformations both for the development of new methodologies⁵⁶ and for natural product synthesis⁶⁹ The lack of absorption in the visible region, and the resulting lack of selectivity did not allow a widespread development of these molecules as affective photocatalysts.

The publication in literature of two papers; the first by Zhang *et al.* in 2016,⁷⁰ the second by Zeitler and co-workers in 2018⁷¹ represented turning point for this class of photocatalysts. Basing their treatment on the recent development of molecular dyads for optoelectronic and photovoltaic systems,⁷² a rational approach for the design of new photocatalysts, capable to absorb in the visible region, with tunable

⁶⁸ Pandey, G.; Karthikeyan, M.; Murugan, A. New Intramolecular α -Arylation Strategy of Ketones by the Reaction of Silyl Enol Ethers to Photosensitized Electron Transfer Generated Arene Radical Cations: Construction of Benzannulated and Benzospiroannulated Compounds. *J. Org. Chem.* **1998**, *63*, 2867–2872. <https://doi.org/10.1021/jo9718612>.

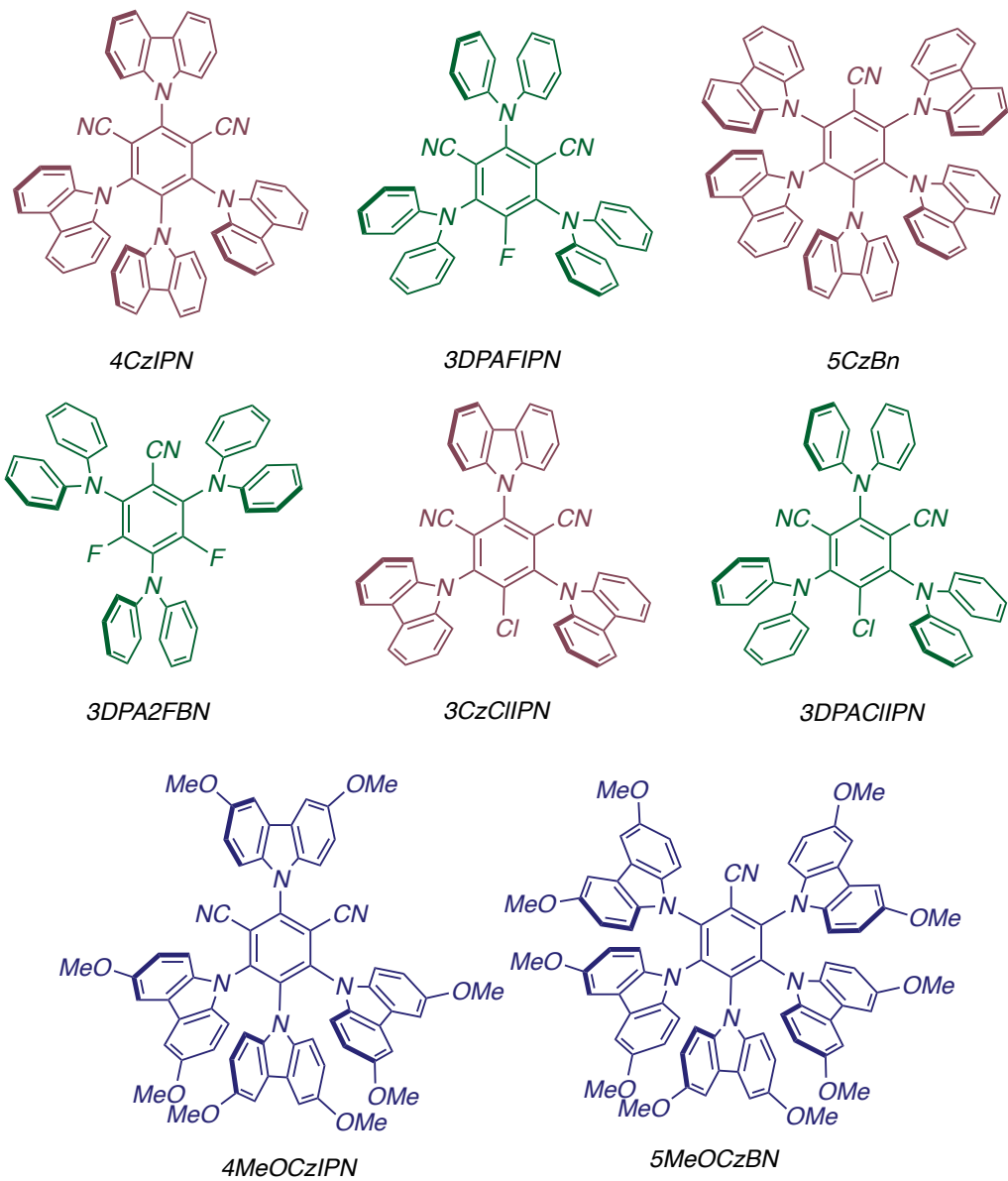
⁶⁹ Pandey, G.; Murugan, A.; Balakrishnan, M. A New Strategy towards the Total Synthesis of Phenanthridone Alkaloids: Synthesis of (+)-2,7-Dideoxypancratistatin as a Model Study. *Chem. Commun.*, **2002**, *6*, 624–625. <https://doi.org/10.1039/B200624C>

⁷⁰ Luo, J.; Zhang, J. Donor–Acceptor Fluorophores for Visible-Light-Promoted Organic Synthesis: Photoredox/Ni Dual Catalytic C(Sp³)–C(Sp²) Cross-Coupling. *ACS Catal.* **2016**, *6* (2), 873–877. <https://doi.org/10.1021/acscatal.5b02204>.

⁷¹ Speckmeier, E.; Fischer, T.; Zeitler, K. A Toolbox Approach to Construct Broadly Applicable Metal-Free Catalysts for Photoredox Chemistry – Deliberate Tuning of Redox Potentials and Importance of Halogens in Donor–Acceptor Cyanoarenes. *J. Am. Chem. Soc.*, **2018**, *140*, 15353–15365. <https://doi.org/10.1021/jacs.8b08933>

⁷² a) Saeed, M. A.; Le, H. T.; Miljanic, O. Š. Benzobisoxazole Cruciforms as Fluorescent Sensors *Acc. Chem. Res.* **2014**, *47*, 2074–2083. <https://doi.org/10.1021/ar500099z>; b) Li, Y.; Liu, T.; Liu, H.; Tian, M. Z.; Li, Y. Aggregate Nanostructures of Organic Molecular Materials *Acc. Chem. Res.* **2014**, *47*, 1186–1198. <https://doi.org/10.1021/ar100084y> c) Bergkamp, J. J.; Decurtins, S.; Liu, S. X. Current advances in fused tetrathiafulvalene donor–acceptor systems *Chem. Soc. Rev.* **2015**, *44*, 863–874. <https://doi.org/10.1039/C4CS00255E> d) D’Souza, F.; Ito, O. Supramolecular donor–acceptor hybrids of porphyrins/phthalocyanines with fullerenes/carbon nanotubes: electron transfer, sensing, switching, and catalytic applications *Chem. Commun.* **2009**, 4913–4928. <https://doi.org/10.1039/B905753F> e) Espíldora, E.; Delgado, J. L.; Martín, N. Donor–Acceptor Hybrids for Organic Electronics *Isr. J. Chem.* **2014**, *54*, 429–439. <https://doi.org/10.1002/ijch.201400007> f) Imahori, H. Porphyrin–fullerene linked systems as artificial photosynthetic mimics *Org. Biomol. Chem.* **2004**, *2*, 1425–1433. <https://doi.org/10.1039/B403024A> g) Ohkubo, K.; Fukuzumi, S. Rational Design and Functions of Electron Donor–Acceptor Dyads with Much Longer Charge-Separated Lifetimes than Natural Photosynthetic Reaction Centers *Bull. Chem. Soc. Jpn.* **2009**, *82*, 303–315. <https://doi.org/10.1246/bcsj.82.303>

features was presented. The reported polysubstituted cyanoarenes derivatives show a versatile photoredox catalytic activities, providing the possibility to obtain organic photocatalyst characterized by both an enhanced reducing power and a strong oxidative behavior in their excited states. (**Figure 20**)

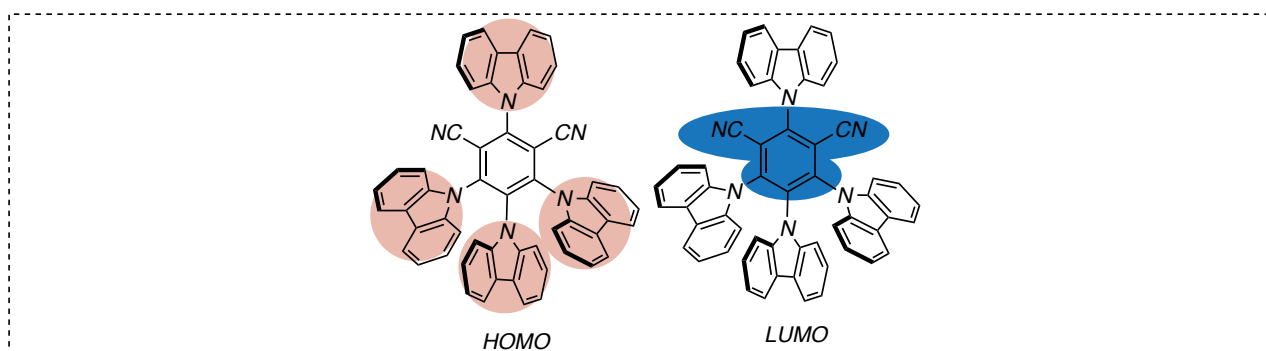


photosensitizer	$E_{1/2}(PC^{•+}/PC^*)$ [V]	$E_{1/2}(PC^*/PC^{•-})$ [V]	$E_{1/2}(PC^{•+}/PC)$ [V]	$E_{1/2}(PC/PC^{•-})$ [V]	$E_{0,0}$ [eV]
4CzIPN	-1.18	+1.43	+1.49	-1.24	2.67
3DPAFIPN	-1.38	+1.09	+1.30	-1.59	2.68
5CzBN	-1.42	+1.31	+1.41	-1.52	2.83
3DPA2FBN	-1.60	+0.92	+1.24	-1.92	2.84
3CzCIIPN	-0.93	+1.56	+1.79	-1.16	2.72
3DPACIIPN	-1.34	+1.24	+1.31	-1.41	2.65
4MeOCzIPN	-1.50	+1.27	+1.11	-1.34	2.61
5MeOCzBN	-1.79	+1.15	+1.02	-1.66	2.81

Chapter 1. Figure 20 New generation of cyanoarene-based photosensitizers and their related photoredox and redox potentials calculated vs. SCE.

The presented molecules share common structural characteristics that determine their photoredox and electrochemical properties. The high conjugation determined by the carbazolyl- and by the diphenyl

amine substituents makes these molecules strongly absorbing in the blue region of the spectrum. The electron donating nature of the substituents on the mono- or di-cyanoarenes moiety, in additions, determines a spatial separation for the level of acceptor's LUMO and donor's HOMO. (**Figure 21**)



Chapter 1. Figure 21 Graphical depiction of HOMO and LUMO for 4CzIPN.

Furthermore, considering that most of these molecules were originally introduced for the development of optical materials (e.g., OLEDs),⁷³ it is important to underline that this class of compounds expresses a thermally activated delayed fluorescence (TADF) phenomenon.⁷⁴ For sake of clarity, a TADF molecule shows highly coupled S_1 and T_1 excited state levels, strongly allowing the intersystem crossing. In addition, the difference in terms of energy between S_1 and T_1 is much smaller than in typical organic molecules (formally, less than 100 meV)⁷⁵.

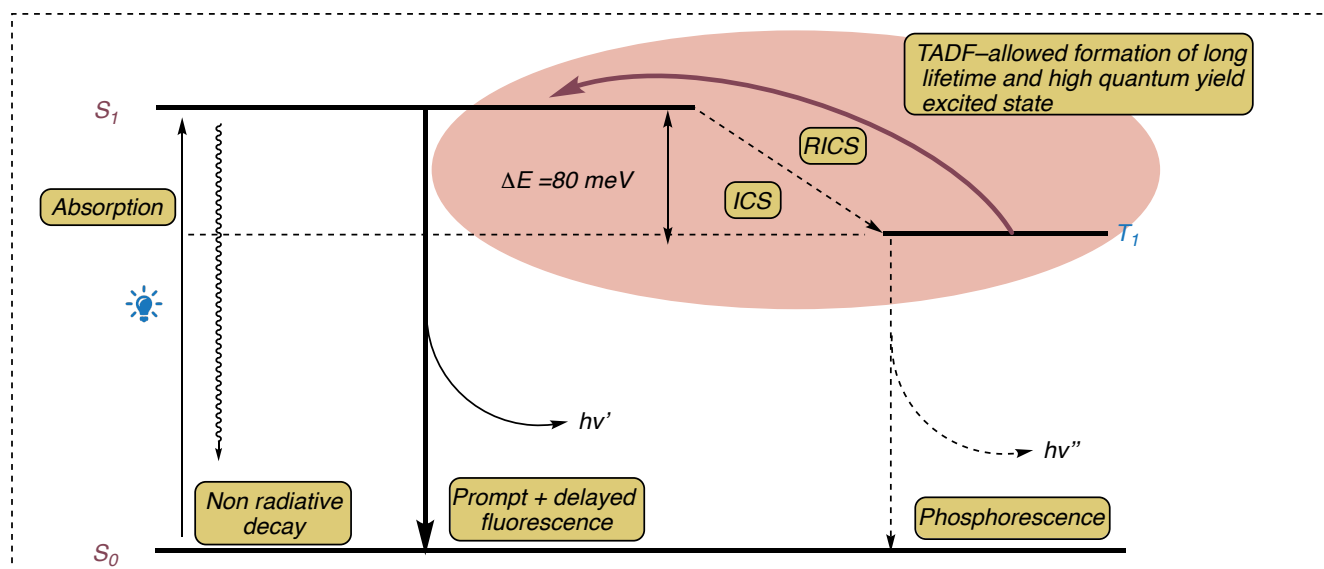
Thanks to the small energetic gap, through a thermal input, a reverse inter system crossing can occur (RISC). In other words, thanks to a thermal effect, the excited state T_1 can interconvert in a higher excited state S_1 . Noteworthy, the molecules exhibiting this feature are characterized by a first *prompt* fluorescence because of the radiative decay occurring after the visible light excitation, and a second *delayed* fluorescence occurring after the reverse intersystem crossing event. By extension of the above-mentioned phenomenon, the thermally activated delayed fluorescence allows lifetimes in the range of microseconds and quantum yields extremely enhanced with respect to other commonly used organic dyes, comparable with the ones observed for iridium- and ruthenium-based transition metal complexes. (**Figure 22**)

Moreover, an additional advantage on using TADF-displaying photosensitizers is that these molecules exhibit photoredox activity from the singlet excited state. The loss of energy associated to the active excited state is, therefore, minimized. For example, for 4CzIPN $E(4CzIPN^+/4CzIPN)$ is +1.49 V and $E(4CzIPN/4CzIPN^{\cdot-})$ is -1.24 V, considering $E_{00} = 2.67$ eV, $E(4CzIPN^{\cdot+}/^*4CzIPN) = -1.18$ V and $E(^*4CzIPN/4CzIPN^{\cdot-}) = +1.43$ V (vs. SCE).

⁷³ Penfold, T. J.; Dias, F. B.; Monkman, A. P. The Theory of Thermally Activated Delayed Fluorescence for Organic Light Emitting Diodes. *Chem. Commun.* **2018**, 54 (32), 3926–3935. <https://doi.org/10.1039/C7CC09612G>.

⁷⁴ Delorme, R.; Perrin, F. Durées de fluorescence des sels d'uranyle solides et de leurs solutions. *J. Phys. Radium* **1929**, 10 (5), 177–186. <https://doi.org/10.1051/jphysrad:01929001005017700>.

⁷⁵ Uoyama, H.; Goushi, K.; Shizu, K.; Nomura, H.; Adachi, C. Highly efficient organic light-emitting diodes from delayed fluorescence. *Nature* **2012**, 492, 234–238. [10.1038/nature11687](https://doi.org/10.1038/nature11687)

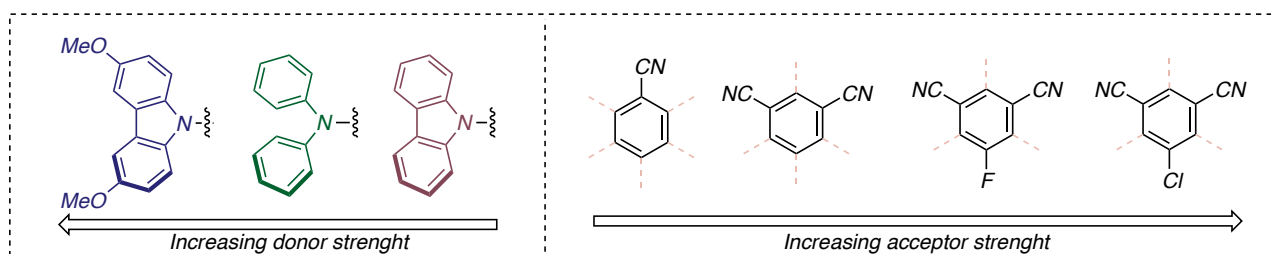


Chapter 1. Figure 22 Mechanism of thermally activated delayed fluorescence.

As introduced in the works by Zeitler and Zhang, the facile preparation of these compounds from inexpensive precursors,⁷⁶ combined with the spatial separation of the electron withdrawing and electron donating moieties of the molecule, furnish a high degree of tunability.

The modification both of the core and of the periphery of these molecules strongly influences their photoredox and electrochemical characteristics without affecting their chemical stability.

As simplified in **Figure 23**, the modification of the structure of the molecule could strongly influence the reduction and oxidation potentials both in the excited than in the ground state.



Chapter 1. Figure 23 :Effects of structural modification on the donor-acceptor properties.

Starting with a rational approach related to the electronic configuration of the molecule, it is possible to identify the LUMO localized on the electron-withdrawing cyanoarene moiety, while the HOMO can be localized on the electron donating portions of the molecule. In a first instance, hence, a structural modification of the core of the photocatalyst could produce a lowering of the LUMO energy enhancing the oxidation potential of the ground state $E(PC^{*+}/PC)$. At the same time the introduction of more or different electron donating substituents should determine a raising of the HOMO with a consequent increment of the ground state reduction potential $E(PC/PC^{*-})$

⁷⁶ Engle, S. Preparation of 2,4,5,6-Tetra(9H-Carbazol-9-Yl)Isophthalonitrile. *Org. Synth.* **2019**, 96, 455–473. <https://doi.org/10.15227/orgsyn.096.0455>.

Another important consideration highlighted from the authors accounts the presence of halogen atoms on the core of the photocatalyst. Since these groups present either a σ -acceptor or a π -donor nature,⁷⁷ the presence of one or more halogen atoms contributes to a further smooth-tuning of the photoredox properties of the presented cyanoarenes derivatives.

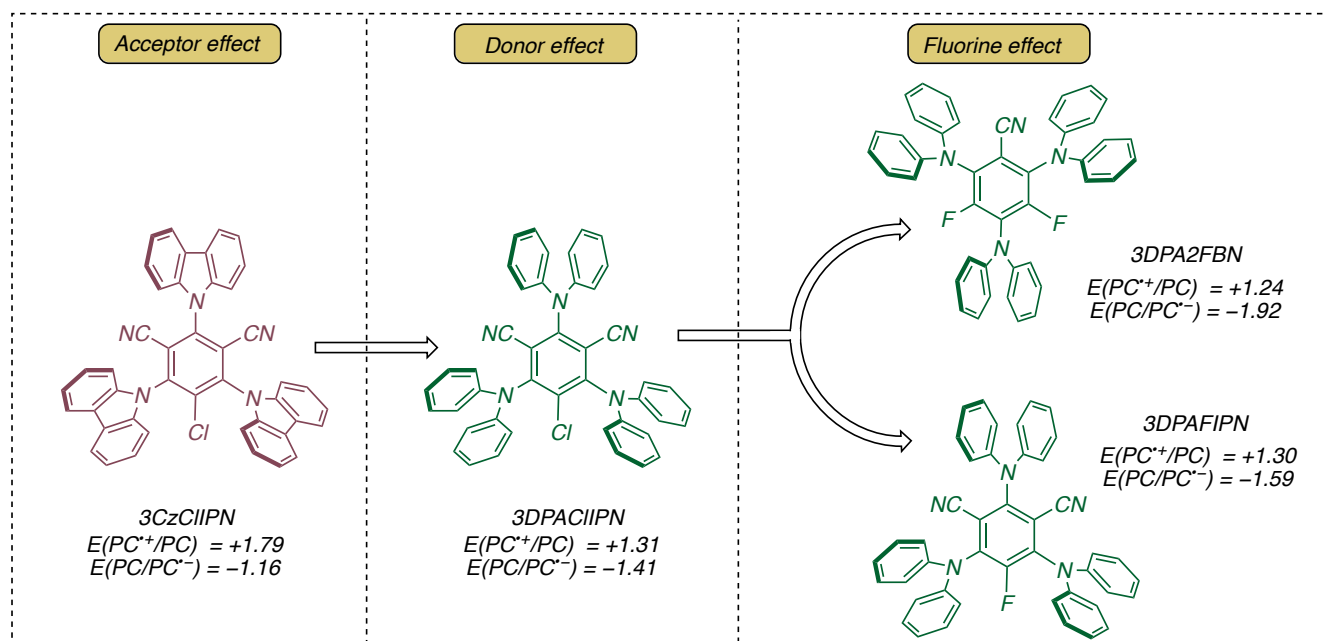
In summarizing the different possibilities opened from the modification of the core and of the periphery of these molecules, it is possible to distinguish a *donor-based* and a *core-based effect*. In the first case the increasing or decreasing of the donor strength will determine a deep modification on the reducing power of the molecule. The alteration of the core, on the other hand, will be reflected on its oxidative power. The resulting redox potentials will be determined by a combination of both effects.

For the sake of clarity, As reported in **Scheme 10**, 3CzCIIPN is characterized by the highest ground state oxidation potential ($E(3CzCIIPN^{*+}/3CzCIIPN) = 1.79$ V vs SCE). This value is justified by the fact the molecule presents as a donor-moiety, the unsubstituted carbazole while the core displays two electron-withdrawing nitril groups and a chlorine atom. This last, among the possible halogen atoms shows the more pronounced acceptor behavior.

Remarkably, replacing the carbazolyl moieties of 3CzCIIPN with the stronger electron-donating diphenyl amine, the oxidation potential drops. 3DPACIIPN, on the other hand, results a better reductant ($E(3DPACIIPN^{*+}/3DPACIIPN) = -1.34$ V vs. SCE in its excited state and $E(3DPACIIPN^{*+}/3DPACIIPN) = +1.31$ V vs SCE) than the corresponding carbazolyl-derivative.

Following the same route, replacing the chlorine group with fluorine, as in the case of 3DPAFIPN and 3DPA2FBN the reduction potentials of the two photocatalysts results tremendously effected ($E(3DPAFIPN/3DPAFIPN^{\bullet-}) = -1.59$ V vs. SCE and $E(3DPA2FBN/3DPA2FBN^{\bullet-}) = -1.92$ V vs. SCE). This feature derives from the peculiar properties of the fluorine group, that cannot be described as π -donor for mesomeric effect, but only as a σ -acceptor.

⁷⁷ Hansch, Corwin.; Leo, A.; Taft, R. W. A Survey of Hammett Substituent Constants and Resonance and Field Parameters. *Chem. Rev.* **1991**, *91* (2), 165–195. <https://doi.org/10.1021/cr00002a004>.



Chapter 1. Scheme 10 Effects of the structural modification on the redox potentials.

In conclusion, in contrast with other photosensitizers, the possibility, allowed by rationalizable and predictable structural modifications of polysubstituted cyanoarenes photosensitizers, to fine-tune their photoredox activity either under oxidative or reductive quenching conditions, determined in few years a widespread use of these class of compounds.⁷⁸

In particular, the enhanced chemical stability, the high tolerance to different functional groups and the comparable photoredox properties to the ones exhibited by the most investigated iridium- and ruthenium-based complexes made 4CzIPN the standard bearer of this class of compounds an essential equipment in the development toolbox of photoredox catalysis⁷⁹

⁷⁸ Gualandi, A.; Anselmi, M.; Calogero, F.; Potenti, S.; Bassan, E.; Ceroni, P.; Cozzi, P. G. Metallaphotoredox Catalysis with Organic Dyes. *Org. Biomol. Chem.* **2021**, *19* (16), 3527–3550. <https://doi.org/10.1039/D1OB00196E>.

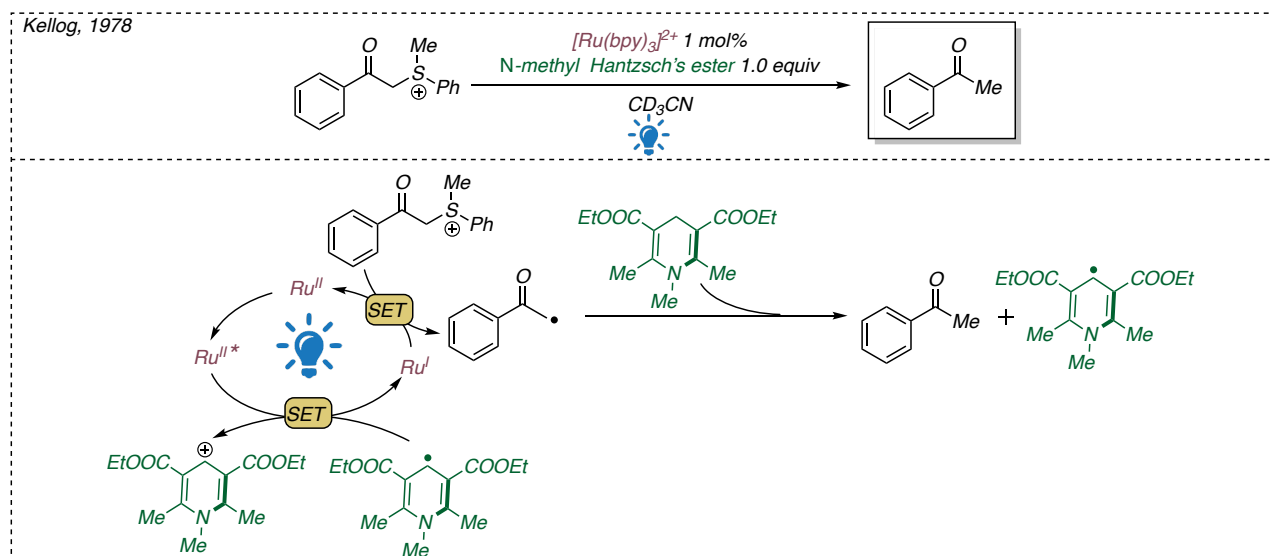
⁷⁹ Shang, T.-Y.; Lu, L.-H.; Cao, Z.; Liu, Y.; He, W.-M.; Yu, B. Recent Advances of 1,2,3,5-Tetrakis(Carbazol-9-Yl)-4,6-Dicyanobenzene (4CzIPN) in Photocatalytic Transformations. *Chem. Commun.* **2019**, *55* (38), 5408–5419. <https://doi.org/10.1039/C9CC01047E>.

1.5 Visible Light–Promoted Photoredox Catalysis: The State of Art.

Once having envisioned the main physical aspects and described the most important tools to understand the fundamentals of photoredox catalysis, in the following chapter the cornerstones of application for the development of new synthetic methodologies promoted by visible light irradiation will be described.

The first examples regarding the use of visible–light radiation to promote small molecules activation have been reported in literature about fifty years ago.

In 1978, Kellogg and co–workers, investigating possible reductions of phenacylonium salts by 1,4-dihydropyridines, noticed that the presence of catalytic amounts of $[\text{Ru}(\text{bpy})_3]^{2+}$ (or eosin Y) under visible light irradiation tremendously effected the rate of the reaction.⁸⁰ In order to understand the possible mechanism of the reaction, it has been disclosed that neither the *N*-methyl Hantzsch's ester, nor the starting material are able to quench the excited state of the ruthenium complex. According to the authors, the reaction is initiated by a hydrogen abstraction performed by a ground–state generated α -carbonyl radical leading the formation of a 1,4-dihydropyridyl radical that acts as the effective quencher of $[\text{Ru}(\text{bpy})_3]^{2+}$.⁸¹ The so-formed $[\text{Ru}(\text{bpy})_3]^+$ is supposed to engage a single electron transfer reducing the phenacylonium salt, restoring the photocatalyst. The single electron reduction of the phenacylonium salts probably leads to the initial formation of the corresponding ketyl radical that evolves forming again an α -carbonyl radical. (**Scheme 11**)



Chapter 1. Scheme 11 Photoredox reduction of phenacylonium salts reported by Kellogg.

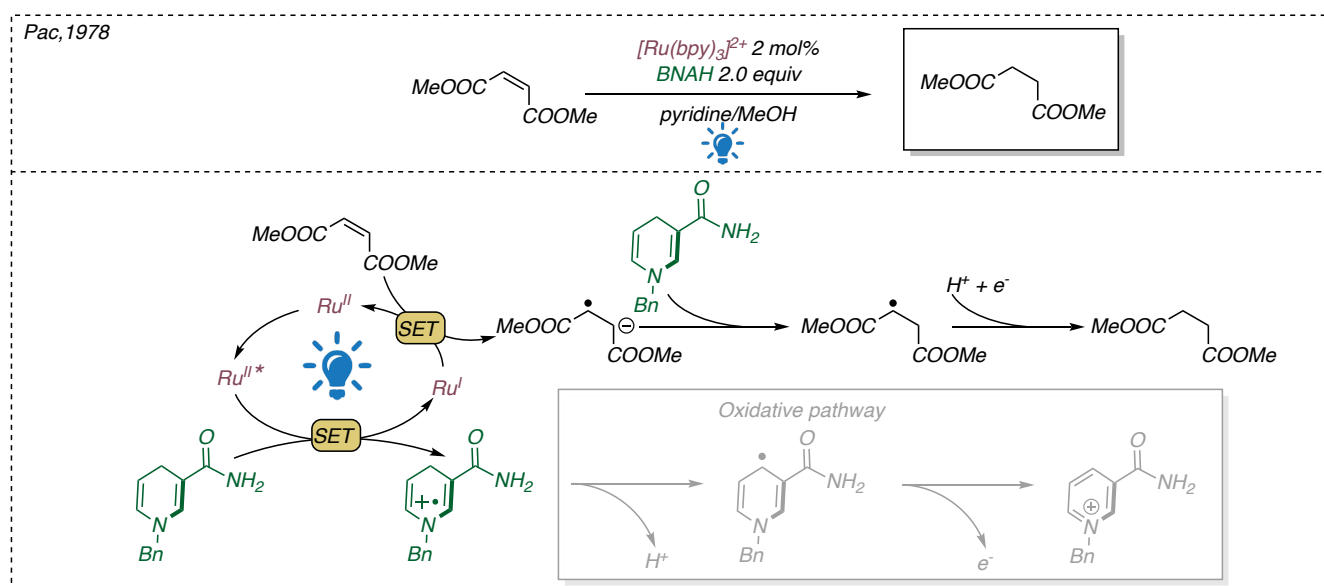
Few years later,⁸² in an analogous way, Pac proposed a visible light-promoted methodology to perform the hydrogenation of activated olefins using catalytic amounts of $[\text{Ru}(\text{bpy})_3]^{2+}$, in presence of 1-benzyl-

⁸⁰ Hedstrand, D. M.; Kruizinga, W. H.; Kellogg, R. M. Light Induced and Dye Accelerated Reductions of Phenacyl Onium Salts by 1,4-Dihydropyridines. *Tetrahedron Letters* **1978**, *19* (14), 1255–1258. [https://doi.org/10.1016/S0040-4039\(01\)94515-0](https://doi.org/10.1016/S0040-4039(01)94515-0).

⁸¹ Zhu, X.-Q.; Li, H.-R.; Li, Q.; Ai, T.; Lu, J.-Y.; Yang, Y.; Cheng, J.-P. Determination of the C4–H Bond Dissociation Energies of NADH Models and Their Radical Cations in Acetonitrile. *Chem. Eur. J.* **2003**, *9* (4), 871–880. <https://doi.org/10.1002/chem.200390108>.

⁸² Pac, C.; Ihama, M.; Yasuda, M.; Miyauchi, Y.; Sakurai, H. Tris(2,2'-bipyridine)ruthenium(2+)-mediated photoreduction of olefins with 1-benzyl-1,4-dihydropyridine: a mechanistic probe for electron-transfer reactions of NAD(P)H-model compounds *J. Am. Chem. Soc.*, **1981**, *103*, 6495–6497. <https://doi.org/10.1021/ja00411a040>

1,4-dihydronicotinamide (BNAH). According to the proposed mechanism BNAH resulted an effective quencher of the excited $[\text{Ru}(\text{bpy})_3]^+$. Remarkably, nicotinamide shows a suitable oxidation potential ($E(\text{BNAH}^{+•}/\text{BNAH}) = 0.76\text{ V vs. SCE}$) to reductively quench the excited state of the ruthenium complex ($E(^*\text{Ru}^{\text{II}}/\text{Ru}^{\text{I}}) = 0.84\text{ V vs. SCE}$). In addition, the so formed $[\text{Ru}(\text{bpy})_3]^+$ is supposed to engage a single electron transfer with the activated olefin, closing the catalytic cycle. ($E(\text{Ru}^{\text{II}}/\text{Ru}^{\text{I}}) = -1.28\text{ V vs. SCE}$ while, $E(\text{maleate}/\text{maleate}^{•-}) = -0.7\text{ V vs. SCE}$) The desired product should arise after a protonation of the generated radical anion and a consequent single electron transfer and protonation of the α -carbonyl radical.

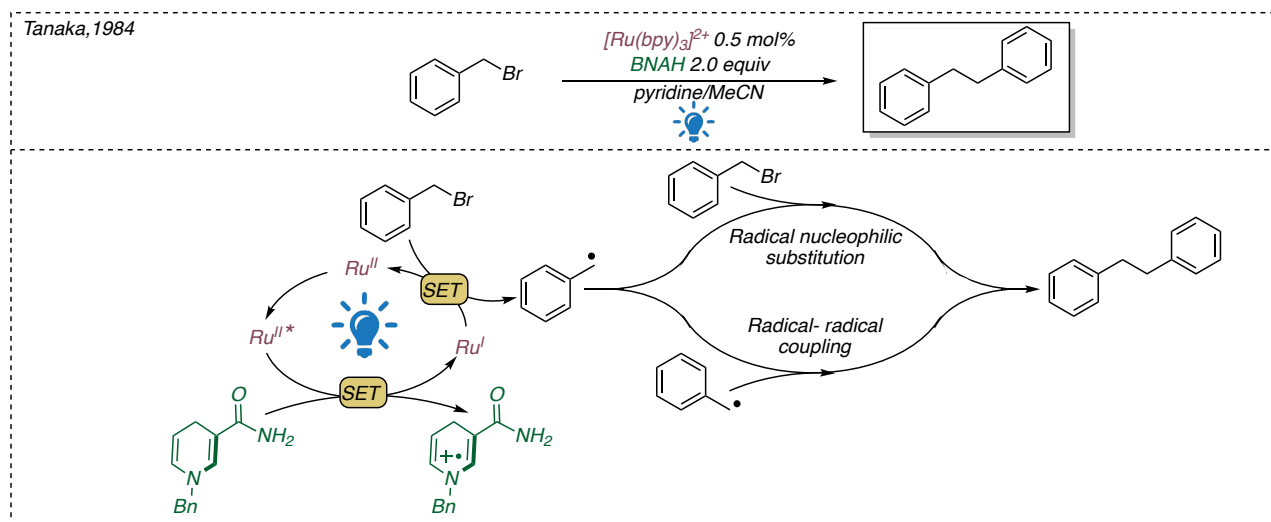


Chapter 1. Scheme 12 Photoredox reduction of olefines reported by Pac.

The third contribute to lay the foundations of photoredox catalysis was reported by Tanaka and co-workers in 1984,⁸³ even in this case a net-reductive cycle, employing a catalytic amount of $[\text{Ru}(\text{bpy})_3]^{2+}$ and an over stoichiometric amount of functionalized dihydropyridines, was reported to perform the reduction of benzyl bromide to form toluene. Noteworthy, under the presented reaction conditions the authors reported the formation of 1,2-diphenyl-ethane as major product. A rational justification for this outcome derives from the dimerization of the benzyl radical upon single electron reduction of the corresponding bromide. Another concurrent hypothesis of dimerization proposed by the authors regards a

⁸³ Hironaka, K.; Fukuzumi, S.; Tanaka, T. Tris(Bipyridyl)Ruthenium(II)-Photosensitized Reaction of 1-Benzyl-1,4-Dihydronicotinamide with Benzyl Bromide. *J. Chem. Soc., Perkin Trans. 2* **1984**, No. 10, 1705. <https://doi.org/10.1039/p29840001705>.

possible radical nucleophilic substitution occurring towards a unreacted benzyl bromide by a transient tolyl radical.



Chapter 1. Scheme 13 Photoredox synthesis of dibenzyl reported by Tanaka.

Despite these and others seminal works published starting from the 1980s,⁸⁴ the application of photoredox processes for small molecule activation remained relatively out of the spotlight of the synthetic community. The rediscovery of the visible light as a chemical energy source for catalytic processes occurred only in the late 2000s.

The beginning of modern photoredox catalysis and its concurring rise in popularity coincides with the literature report of two fundamental works.

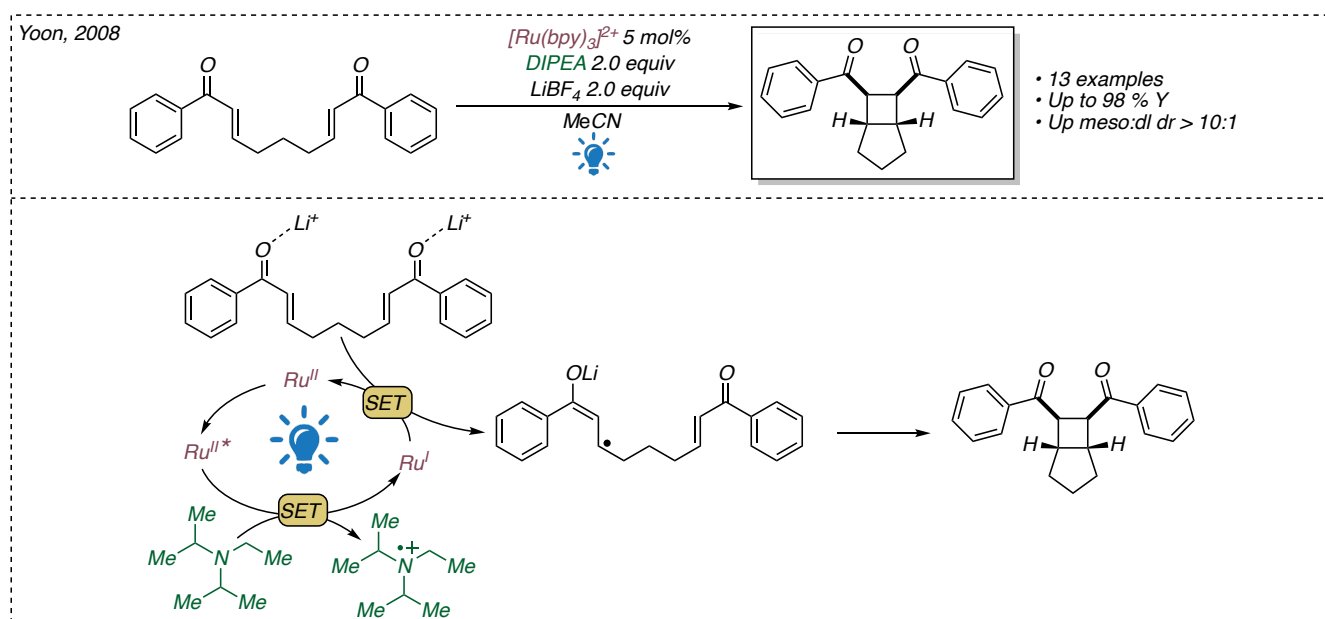
In 2008, an efficient visible light promoted [2+2] cycloaddition of bis(enones) was reported by Yoon and co-corkers.⁸⁵ Using (2E,7E)-1,9-diphenylnona-2,7-diene-1,9-dione as model substrate the desired product of intramolecular cyclization was achieved in good yield and moderate diastereoselectivity (up to d.r. > 10:1 in favor of the *meso*-isomer). The photochemical properties of $[Ru(bpy)_3]^{2+*}$ were employed to perform a single electron oxidation in the presence of a stoichiometric amount of iPr_2Net ($E(DIPEA^+/DIPEA) = 0.86V$ vs. SCE) employed as sacrificial reductant. The so-formed $[Ru(bpy)_3]^+$ thanks to its enhanced reducing power ($E(Ru^{II}/Ru^I) = -1.28$ V vs. SCE) was shown able to promote the single electron reduction of a quite broad variety of substrates. 275 W CFL lamp was found to be the best

⁸⁴ a) Kern, J.-M.; Sauvageb, J.-P. Photoassisted G C Coupling via Electron Transfer to Benzylic Halides by a Bis(Di-Imine) Copper(I) Complex. *Chem. Soc., Chem. Commun.*, **1987**, 546–548. <https://doi.org/10.1039/C39870000546>; b) Cano-Yelo, H.; Deronzier, A. Photocatalysis of the Pischorr Reaction by Tris-(2,2'-Bipyridyl) Ruthenium(II) in the Phenanthrene Series. *J. Chem. Soc., Perkin Trans. 2*, **1984**, 1093-1098/1984, 25, 5517– 5520. <https://doi.org/10.1039/P29840001093>; c) Pac, C.; Miyauchi, Y.; Ishitani, O.; Ihama, M.; Yasuda, M.; Sakurai, H. Redox-photosensitized reactions. 11. $Ru(bpy)_3^{2+}$ -photosensitized reactions of 1-benzyl-1,4-dihydronicotinamide with aryl-substituted enones, derivatives of methyl cinnamate, and substituted cinnamionitriles: electron-transfer mechanism and structure-reactivity relationships *J. Org. Chem.*, **1984**, *49*, 26–34. <https://doi.org/10.1021/jo00175a006> d) Ishitani, O.; Ihama, M.; Miyauchi, Y.; Pac, C. Redox-photosensitized reactions. Part 12. Effects of magnesium(II) ion on the $[Ru(bpy)_3]^{2+}$ -photomediated reduction of olefins by 1-benzyl-1,4-dihydronicotinamide: metal-ion catalysis of electron transfer processes involving an NADH mode *J. Chem. Soc., Perkin Trans. 1* **1985**, 1527–1531. <https://doi.org/10.1039/P19850001527> e) Ishitani, O.; Yanagida, S.; Takamuku, S.; Pac, C. *J. Org. Chem.*, **1987**, *52*, 2790–2796. <https://doi.org/10.1021/jo00389a027>

⁸⁵ Ischay, M. A.; Anzovino, M. E.; Du, J.; Yoon, T. P. Efficient Visible Light Photocatalysis of [2+2] Enone Cycloadditions *J. Am. Chem. Soc.* **2008**, *130*, 39, 12886–12887 <https://doi.org/10.1021/ja805387f>

light source for the photoexcitation of the ruthenium complex. Remarkably, the presence in the reaction mixture of a Lewis acid resulted crucial. Further work has shown that the reduction potential of the substrates used for the realization of the protocol are too negative to be compatible with the use of ruthenium complex.⁸⁶ ($E(\text{bisenone}/\text{bisenone}^{\bullet-}) = -1.4 \text{ V vs. SCE}$) The positive result of the reaction is allowed thanks to the presence of Lewis acid lithium cation that activates the bisenone towards one electron reduction.

The interaction between the LiBF_4 and the carbonyls of the bis(enones), indeed, favored the single electron transfer step facilitating the formation of the γ -carbonyl radical.

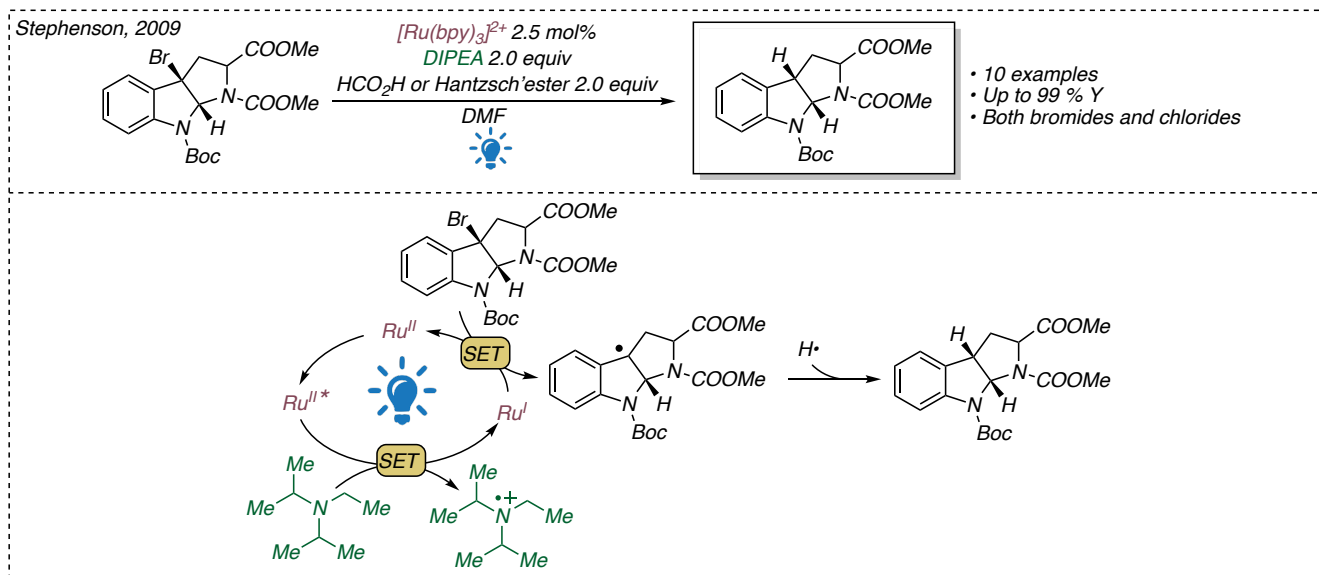


Chapter 1. Scheme 14 Photoredox radical cyclization reported by Yoon.

The next year Stephenson and co-workers reported the first tin-free reductive dehalogenation employing visible light photocatalysis.⁸⁷ Even in this case the well-known tris(2,2'-bipyridyl)ruthenium(II) chloride was employed as the photocatalyst. $i\text{Pr}_2\text{NEt}$ (2 equiv.) and Hantzsch's ester (2 equiv) were used as additives for the reaction. The first acts as the effective quencher of the excited $[\text{Ru}(\text{bpy})_3]^{2+*}$, leading the formation of $[\text{Ru}(\text{bpy})_3]^+$ that is able to reduce the substrates through a single electron reduction. The Hantzsch's ester, instead, contributes to the formation of the final products as hydrogen source.

⁸⁶ Yoon, T. P. Visible Light Photocatalysis: The Development of Photocatalytic Radical Ion Cycloadditions. *ACS Catal.* **2013**, 3 (5), 895–902. <https://doi.org/10.1021/cs400088e>.

⁸⁷ Narayanam, M. R. J.; Tucker, W.; Stephenson, C. R. J. Electron-Transfer Photoredox Catalysis: Development of a Tin-Free Reductive Dehalogenation Reaction *J. Am. Chem. Soc.* **2009**, 131, 25, 8756–8757 <https://doi.org/10.1021/ja9033582>

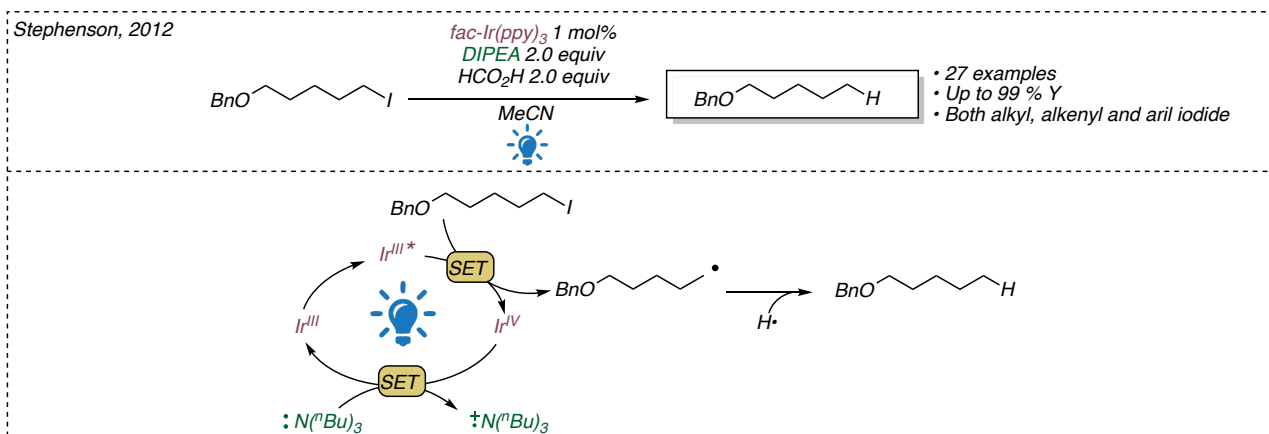


Chapter 1. Scheme 15 Photoredox reductive dehalogenation of activated halides reported by Stephenson.

The reported dehalogenation methodology, however presented a reduced applicability. The scope was limited to strongly activated benzyl halides. The reason for this limitation stems from the redox potential associated with the photocatalyst. As a result of the SET in the presence of the reducing agent, the so-formed Ru^I complex exhibits an associated redox potential of power -1.28 V vs. SCE. This determines that the system is effective in the presence of differently substituted benzyl bromides, which exhibit a potential of approximately -0.7 V vs SCE. Attempting to translate the same conditions for the reduction of less activated halides is unsuccessful because their associated potential is drastically more negative, beyond the compatibility range of the ruthenium catalyst.

The overcome of the limitation was presented by the same research group few years later.⁸⁸ The dehalogenation of non-activated alkyl, alkenyl and aryl iodides was achieved employing *fac*- $Ir(ppy)_3$ as the photocatalyst of the reaction. Noteworthy, the excited state of cyclometalated iridium-complexes show a sufficient reducing power to be directly quenched by these substrates through a single electron transfer. ($E(Ir^{IV}/Ir^{*III}) = -1.73$ V vs SCE for the photocatalyst while $E(\text{Alkyl iodide/alkyl}^\bullet) \approx -1.6$ V vs. SCE)).

⁸⁸ Nguyen, J. D.; D'Amato, E. M.; Narayanam, J. M. R.; Stephenson, C. R. J. Engaging Unactivated Alkyl, Alkenyl and Aryl Iodides in Visible-Light-Mediated Free Radical Reactions. *Nature Chem* **2012**, *4* (10), 854–859. <https://doi.org/10.1038/nchem.1452>.



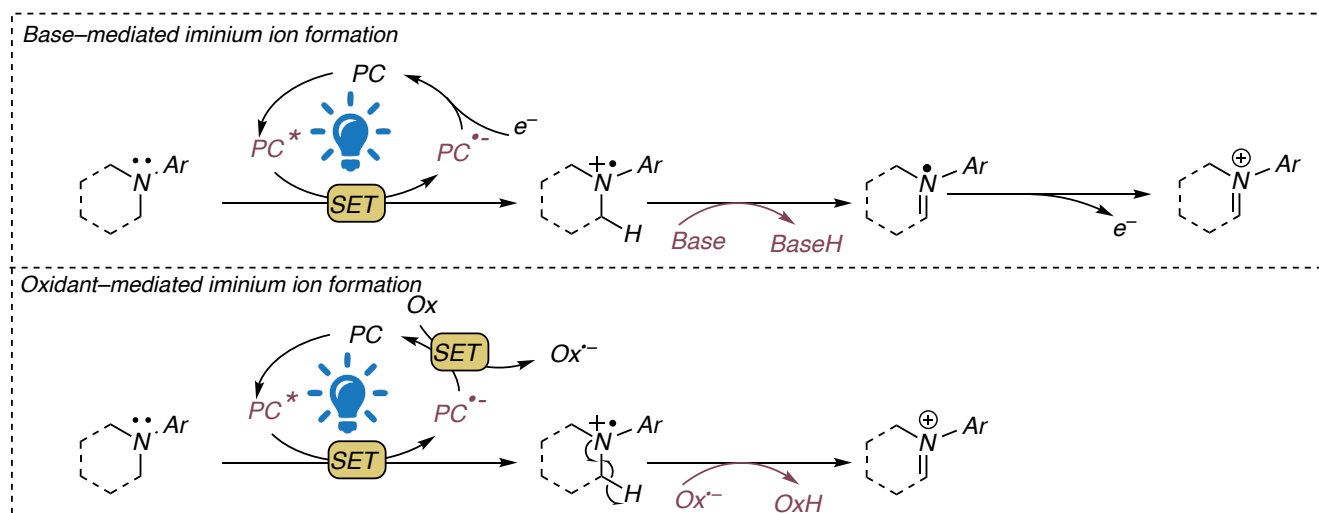
Chapter 1. Scheme 16 Photoredox reductive dehalogenation of non-activated iodides reported by Stephenson.

• Different molecule activations promoted by single electron transfer.

The publication of the above-mentioned works represented the cornerstone for the modern photoredox catalysis.

Since then, thanks to a derived mutual interest from the scientific community, different and exciting reactions had been presented showing new and unprecedented reactivities. The reason why this technique exhibited an exponential growth lies in the ability of visible photosensitizers to engage single electron processes with different redox active species. In this way the formation of crucial intermediates is allowed. Among the various offered possibilities, the formation of carbon-centered radical species in surprisingly mild conditions resulted the most attractive.⁸⁹ The extremely selective generation of both nucleophilic and electrophilic⁹⁰ alkyl radicals promoted the achievement of challenging carbon-carbon or carbon-heteroatom bond formation reactions.

In this scenario, the functionalization of the α -position of cyclic amines occupies a fortunate position. As already noticed in the early works of Yoon and Stephenson about the nature of the nitrogen-based additives used to close the photocatalyst's cycles, a nitrogen-centered radical cation is formed upon single electron oxidation of a tertiary amine. The generated electronic deficiency strongly modifies the reactivity of the molecule, enhancing the acidity of the hydrogen in its α -position. Through two possible oxidative pathways (reported in **Scheme 17**) the formation of a reactive iminium ion can be obtained.



Chapter 1. Scheme 17: Generation of transient iminium ion enabled by single electron transfer.

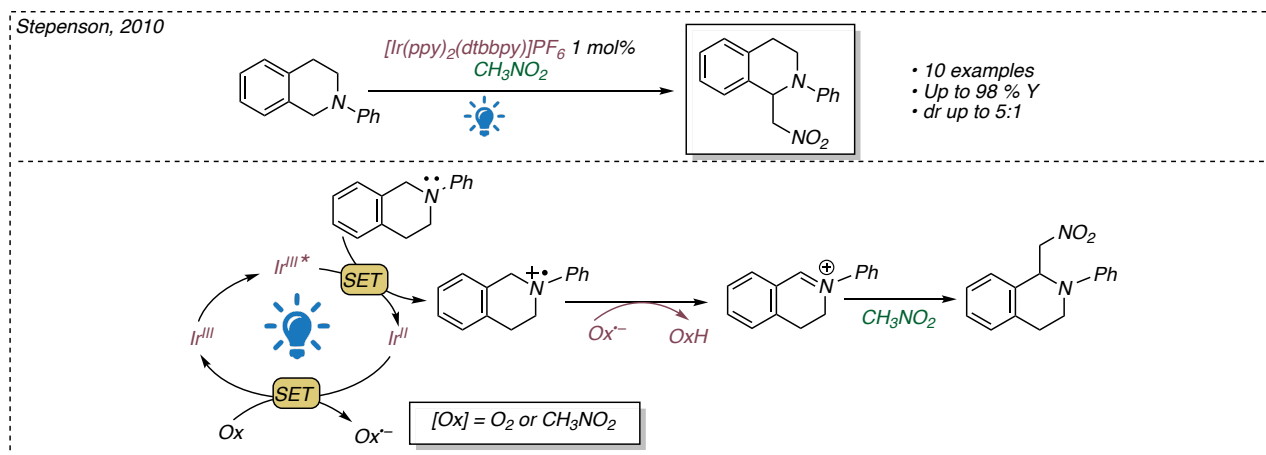
The first foresightful example reporting the use of this peculiar oxidative pathway of tertiary amines under photoredox conditions was presented by Stephenson and co-workers in 2010.⁹¹ Performing a formal C-H

⁸⁹ Matsui, J. K.; Lang, S. B.; Heitz, D. R.; Molander, G. A. Photoredox-Mediated Routes to Radicals: The Value of Catalytic Radical Generation in Synthetic Methods Development. *ACS Catal.* **2017**, *7* (4), 2563–2575. <https://doi.org/10.1021/acscatal.7b00094>.

⁹⁰ Parsaee, F.; Senarathna, M. C.; Kannangara, P. B.; Alexander, S. N.; Arche, P. D. E.; Welin, E. R. Radical Philicity and Its Role in Selective Organic Transformations. *Nat Rev Chem* **2021**, *5* (7), 486–499. <https://doi.org/10.1038/s41570-021-00284-3>.

⁹¹ Condie, A. G.; González-Gómez, J. C.; Stephenson, C. R. J. Visible-Light Photoredox Catalysis: Aza-Henry Reactions via C–H Functionalization. *J. Am. Chem. Soc.* **2010**, *132* (5), 1464–1465. <https://doi.org/10.1021/ja909145y>.

activation in the α -position of cyclic aryl amines through a transiently generated iminium ion, the first photoredox-catalyzed Aza Henry reaction was disclosed. Under visible light irradiation, in the presence of an Ir-based photosensitizer, it is possible to transiently generate an electrophilic iminium ion that can trap the nitroalkane derivatives, delivering the corresponding α -functionalized products.



Chapter 1. Scheme 18 Photoredox-catalyzed Aza Henry reaction reported by Stephenson.

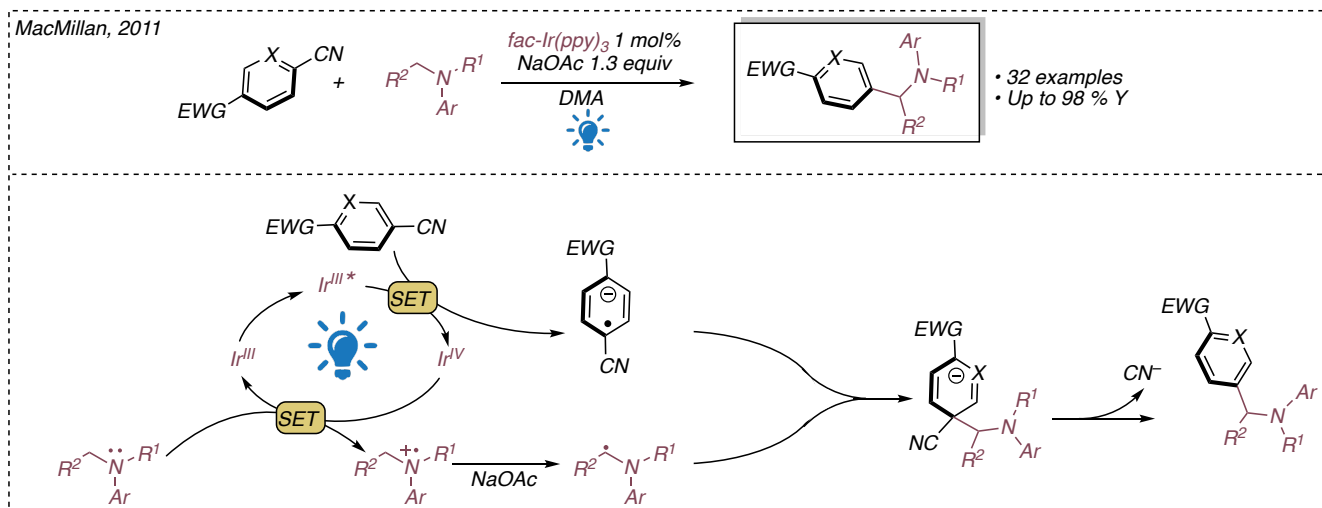
With the Stern-Volmer experiment it was possible to demonstrate that the excited state of the photocatalyst is quenched in the presence of N-phenyl tetrahydroisoquinoline. Although the nitroderivative used to promote the reaction has the compatible potentials to restore the photocatalyst in its early oxidation state, it is not possible to exclude by the authors the role of oxygen for the positive outcome of the reaction. Performing the reaction in strict inert atmosphere, it is possible to observe the formation of the product of interest, however the time required to obtain a total conversion is drastically increased.

The unveiling of this type of activation, was, later, employed furnishing a broad variety of coupling products with different nucleophiles.⁹²

In 2011 the MacMillan group reported the first strategy for photocatalyzed α -amino C–H arylation under redox neutral condition. In this work the terminal oxidant was replaced with a cyanoarene bearing electron-withdrawing substituents on the aromatic moiety.⁹³

⁹² a) Pan, Y.; Kee, C. W.; Chen, L.; Tan, C.-H. Dehydrogenative Coupling Reactions Catalysed by Rose Bengal Using Visible Light Irradiation. *Green Chem.* **2011**, *13* (10), 2682. <https://doi.org/10.1039/c1gc15489c>. b) Wang, Z.-Q.; Hu, M.; Huang, X.-C.; Gong, L.-B.; Xie, Y.-X.; Li, J.-H. Direct α -Arylation of α -Amino Carbonyl Compounds with Indoles Using Visible Light Photoredox Catalysis. *J. Org. Chem.* **2012**, *77* (19), 8705–8711. <https://doi.org/10.1021/jo301691h>. c) Rueping, M.; Zhu, S.; Koenigs, R. M. Photoredox Catalyzed C–P Bond Forming Reactions—Visible Light Mediated Oxidative Phosphonylations of Amines. *Chem. Commun.* **2011**, *47* (30), 8679. <https://doi.org/10.1039/c1cc12907d>.

⁹³ McNally, A.; Prier, C. K.; MacMillan, D. W. C. Discovery of an α -Amino C–H Arylation Reaction Using the Strategy of Accelerated Serendipity. *Science* **2011**, *334* (6059), 1114–1117. <https://doi.org/10.1126/science.1213920>.



Chapter 1. Scheme 19 Redox neutral photoredox catalyzed α -amino arylation reported by MacMillan.

According to the photophysical studies, the cyanoarenes ($E(\text{Cyanoarene}/\text{Cyanoarene}^{\bullet-}) = -1.61 \text{ V vs. SCE}$) derivatives are able to oxidatively quench the of $\text{fac-Ir}(\text{ppy})_3^*$ ($E(\text{Ir}^{\text{IV}}/\text{Ir}^{\text{III}}) = -1.73 \text{ V vs SCE}$) leading the formation of a persistent radical anion. This latter thanks to the electron withdrawing groups on the aromatic ring, presents an electrophilic character. The arylation products are obtained after a radical-radical coupling between the aryl radical and the transient nucleophilic α -amino radical formed after the single electron oxidation of arylamines. ($E(\text{Ir}^{\text{IV}}/\text{Ir}^{\text{III}}) = 0.77 \text{ V vs SCE}$, while $\text{arylamine}^{\bullet+}/\text{arylamine} \approx 0.4\text{--}0.7 \text{ V vs. SCE}$)

Even if the compulsory electron-deficient nature of the aryl moiety represents the main limitation, the methodology presents a quite elevated tolerance to different substituents on the amine and the coupling product is obtained generally yields from good to excellent.

It was, again, thanks to the work of MacMillan and co-workers that in 2014 the introduction of decarboxylative transformations under visible photoredox condition was reported for the first time.⁹⁴

Owing to the enhanced chemical stability and abundance, the conversion of readily available alkyl carboxylic acids through decarboxylative protocols has been a broad investigated research field.⁹⁵

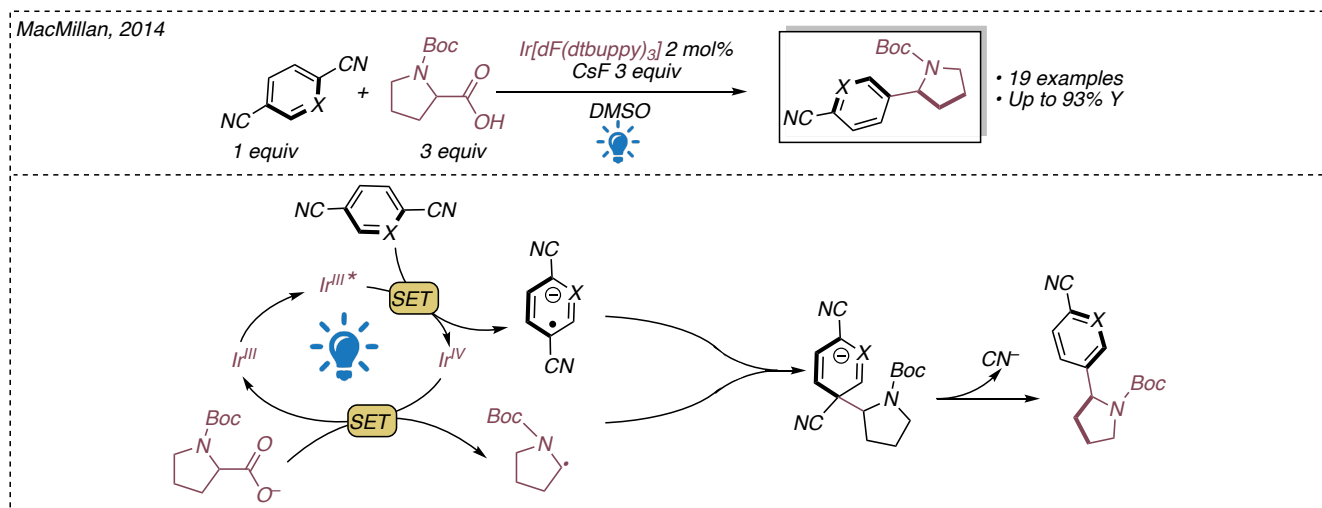
The authors demonstrated that in the presence of a base and a suitable photoredox catalyst a single electron oxidation of an aliphatic carboxylate could take place. The originally formed O-centered radicals rapidly undergo through an intramolecular rearrangement releasing a molecule of carbon dioxide forming the attractive C-centered radical.

⁹⁴ Zuo, Z.; MacMillan, D. W. C. Decarboxylative Arylation of α -Amino Acids via Photoredox Catalysis: A One-Step Conversion of Biomass to Drug Pharmacophore. *J. Am. Chem. Soc.* **2014**, *136* (14), 5257–5260. <https://doi.org/10.1021/ja501621q>.

⁹⁵ a) Johnson, R. G.; Ingham, R. K. The Degradation of Carboxylic Acid Salts by Means of Halogen The Hunsdiecker Reaction, *Chem. Rev.*, **1956**, *56*, 219–269. <https://doi.org/10.1021/cr50008a002>; b) Kolbe, H. Untersuchungen über die Elektrolyse organischer Verbindungen *Liebigs Ann. Chem.* **1849**, *69*, 257–294. <https://doi.org/10.1002/jlac.18490690302>

The first application of this process was reported in a metal-free sp^3 - sp^2 cross-coupling between electron-poor cyanoarenes and aliphatic α -amino or α -hydroxy acids leading the formation of a quite broad library of polysubstituted benzylic amines and benzylic ethers.

Remarkably, an electronically fine-tuned iridium-based complex $\text{Ir}[p\text{-F}(t\text{-Bu})\text{-ppy}]_3$ was used as photocatalyst to allow the reaction. The presence of fluorine groups on the cyclometalated ligands determined a strong modification of the redox and photoredox properties of the photosensitizer.



Chapter 1. Scheme 20 Decarboxylative α -amino arylation reported by MacMillan.

According to the photophysical investigations, $\text{Ir}[p\text{-F}(t\text{-Bu})\text{-ppy}]_3^*$ shows a reducing power strong enough to be oxidatively quenched by electron-poor cyanoarenes. ($E(\text{Cyanoarene}/\text{Cyanoarene}^{\cdot-}) = -1.61$ V vs. SCE and $E(\text{Ir}^{\text{IV}}/\text{Ir}^{*\text{III}}) = -1.67$ V vs SCE)

At the same time, the effect of the fluorine substituents determines a significant increase of the ground state reduction potential $\text{Ir}^{\text{IV}}/\text{Ir}^{\text{III}}$ compared to the most common, *fac*- $\text{Ir}(\text{ppy})_3$. ($E(\text{Ir}^{\text{IV}}/\text{Ir}^{\text{III}}) = 0.97$ V vs SCE for $\text{Ir}[p\text{-F}(t\text{-Bu})\text{-ppy}]_3$ while, $E(\text{Ir}^{\text{IV}}/\text{Ir}^{\text{III}}) = 0.77$ V for *fac*- $\text{Ir}(\text{ppy})_3$).

This latter property resulted crucial for the proceeding of the reaction. Electrochemical investigation, indeed, disclosed that aliphatic carboxylates exhibit a redox potential between 1.0 V and 0.8 V vs SCE. As a consequence, the employment of *fac*- $\text{Ir}(\text{ppy})_3$ as photoredox catalyst for the reaction resulted ineffective.

This new activation that allows the use of readily available substrates for the mild generation of C-centered nucleophilic radicals has found applications in myriad transformations since this work.⁹⁶

⁹⁶ For selected examples: a) Chu, L.; Ohta, C.; Zuo, Z.; MacMillan, D. W. C. Carboxylic Acids as A Traceless Activation Group for Conjugate Additions: A Three-Step Synthesis of (\pm)-Pregabalin. *J. Am. Chem. Soc.* **2014**, *136* (31), 10886–10889. <https://doi.org/10.1021/ja505964r>; b) Rueda-Becerril, M.; Mahe, O.; Drouin, M.; Majewski, M. B.; West, J. G.; Wolf, M. O.; Sammis, G. M. Direct C–F Bond Formation Using Photoredox Catalysis. *J. Am. Chem. Soc.* **2014**, *136*, 2637–264. <https://doi.org/10.1021/ja412083f>; c) Le Vaillant, F.; Courant, T.; Waser, J. Room-Temperature Decarboxylative Alkynylation of Carboxylic Acids Using Photoredox Catalysis and EBX Reagents. *Angew. Chem. Int. Ed.* **2015**, *54* (38), 11200–11204. <https://doi.org/10.1002/anie.201505111>; d) Gualandi, A.; Matteucci, E.; Monti, F.; Baschieri, A.; Armaroli, N.; Sambri L.; Cozzi P.G. Photoredox radical conjugate addition of dithiane-2-carboxylate promoted by an iridium(III) phenyl-tetrazole complex: a formal radical methylation of Michael acceptors *Chem. Sci.*, **2017**, *8*, 1613-1620. <https://doi.org/10.1039/C6SC03374A>

However, the employment of this class of compounds goes together with the main drawback of the relatively high single electron oxidation potential characterizing the carboxylate derivatives.

In order to overcome this main limitation, it is possible to find in literature important examples reporting the use of sulfinates derivatives as analogous sulfur-based molecules as radical source. Sulfinates derivatives are commonly used compounds in organic synthesis, known since the beginning of the last century.⁹⁷ The main feature that aroused the interest for this molecule for photoredox-mediated processes is the relatively low oxidation potential through which is possible to have an easy access to C-centered alkyl radical. If an alkyl carboxylate shows an oxidation potential $E(\text{alkyl}\cdot/\text{alkylcarboxylate}) \approx 0.8\text{--}1.2$ V vs SCE; the corresponding sulfinate derivative shows an oxidation potential $E(\text{alkyl}\cdot/\text{alkylsulfinate}) \approx 0.4\text{--}0.6$ V vs SCE. After the single electron oxidation, the oxidative pathway of sulfinates is analogous to the one exhibited by carboxylates. The O-centered radical undergoes to an intramolecular radical rearrangement determining the extrusion of SO₂ and the formation of the desired C-centered radical.⁹⁸

The very first example of utilization on sulfinates in photoredox mediated processes was presented by Nicewicz and co-workers in 2013.⁹⁹

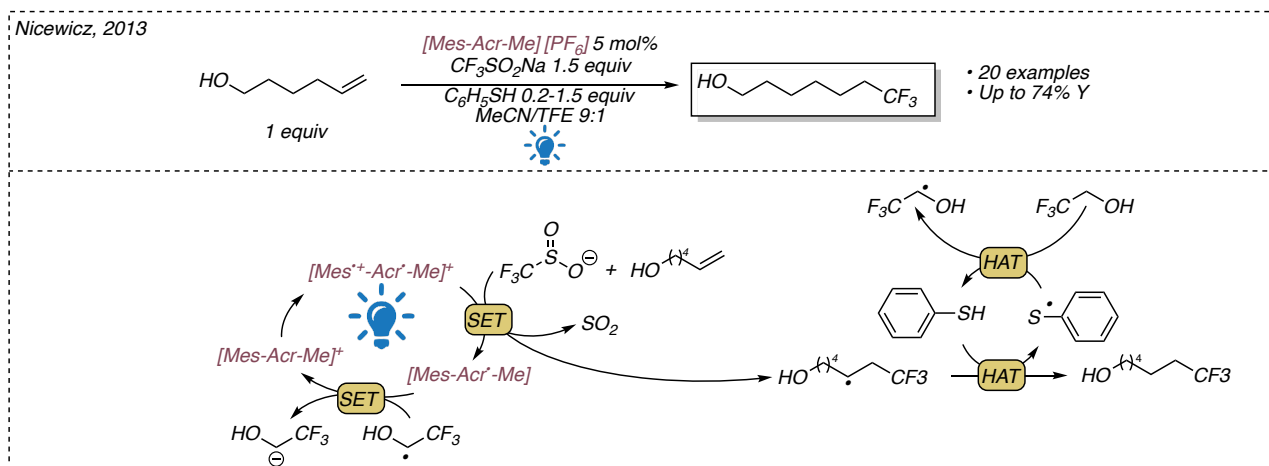
A trifluoromethylation of styrene-derivatives and unactivated aliphatic alkenes was reported employing the strong oxidant Fukuzumi's catalyst as visible organic dye and sodium trifluoromethanesulfonate (CF₃SO₂Na, Langlois reagent (CF₃•/CF₃SO₂Na)=1.05 V vs SCE) as trifluoromethyl radical source. Even if the attempts to highlight unambiguously the mechanism resulted ineffective the authors believe that the reaction proceed thanks a single electron transfer between the excited state of the acridinium-based photocatalyst and the Langlois reagent leading the formation of a trifluoromethyl radical. The addition of the radical to the alkene proceeded with anti-Markovnikov selectivity, producing the corresponding carbon-centered radical. At this point, the authors highlighted that the presence of trifluoroethanol (TFE) as co-solvent is compulsory for the reaction. The transformation, indeed, required the presence of a stoichiometric amount of a hydrogen donor species for the formation of the desired product. Moreover, in the paper it was presented that to restore the photocatalyst a suitable stoichiometric oxidant could be the carbon-centered radical formed from trifluoroethanol after the hydrogen abstraction.

A deeper investigation showed that the reaction rate could be increased introducing in the reaction mixture a sub-stoichiometric amount of an *ortho*-substituted thiol acting as HAT mediator.

⁹⁷ Smiles, S.; Le Rossignol, R. LXX.—The sulphination of phenolic ethers and the influence of substituents *J. Chem. Soc., Trans.* **1908**, 93, 745–762. <https://doi.org/10.1039/CT9089300745>

⁹⁸ (a) Galicia, M.; González, F. J. Electrochemical Oxidation of Tetrabutylammonium Salts of Aliphatic Carboxylic Acids in Acetonitrile. *J. Electrochem. Soc.* **2002**, 149 (3), D46. <https://doi.org/10.1149/1.1450616>. (b) Meyer, A. U.; Strakovska, K.; Slanina, T.; König, B. Eosin Y (EY) Photoredox-Catalyzed Sulfonylation of Alkenes: Scope and Mechanism. *Chem. Eur. J.* **2016**, 22, 8694–8699. <https://doi.org/10.1002/chem.201601000>.

⁹⁹ Wilger, D. J.; Gesmundo, N. J.; Nicewicz, D. A. Catalytic Hydrotrifluoromethylation of Styrenes and Unactivated Aliphatic Alkenes via an Organic Photoredox System. *Chem. Sci.* **2013**, 4 (8), 3160. <https://doi.org/10.1039/c3sc51209f>.



Chapter 1. Scheme 21 Photoredox trifluoromethylation reported by Nicewicz.

Another important photoredox process enabled by the activation of sulfonates to generate alkyl radicals was reported by Cozzi and Gualandi in 2017.¹⁰⁰ Thanks to the utilization of readily prepared or commercially available zinc sulfonates a useful benzylation and alkylation of a variety of electron-poor olefins triggered by the excitation of iridium (III) complex ($\text{Ir}[\text{dF}(\text{CF}_3)\text{-ppy}]_2(\text{dtbbpy})\text{PF}_6$) was described. In conclusion it is noteworthy that the use of sulfonate derivatives in photoredox-mediated processes not only was employed for the formation of C-centered radicals. Under certain reaction conditions, indeed, it is possible to stabilize the O-centered radical avoiding the SO_2 extrusion. The desulfonylation process, indeed is reversible and the equilibrium between the O-centered and the C-centered radical can be tuned enhancing or lowering the stability of the C-centered radical. Following this route powerful sulfonylation strategies have also been reported in literature.¹⁰¹

¹⁰⁰ Gualandi, A.; Mazzarella, D.; Ortega-Martinez, A.; Mengozzi, L.; Calcinelli, F.; Matteucci, E.; Monti, F.; Armaroli, N.; Sambri, L.; Cozzi, P. G. Photocatalytic Radical Alkylation of Electrophilic Olefins by Benzylic and Alkyl Zinc-Sulfonates. *ACS Catal.* **2017**, *7* (8), 5357–5362. <https://doi.org/10.1021/acscatal.7b01669>.

¹⁰¹ (a) Meyer, A. U.; Jäger, S.; Prasad Hari, D.; König, B. Visible Light-Mediated Metal-Free Synthesis of Vinyl Sulfones from Aryl Sulfonates. *Adv. Synth. Catal.* **2015**, *357* (9), 2050–2054. <https://doi.org/10.1002/adsc.201500142>. (b) Meyer, A. U.; Lau, V. W. H.; König, B.; Lotsch, B. V. Photocatalytic Oxidation of Sulfonates to Vinyl Sulfones with Cyanamide-Functionalised Carbon Nitride. *Eur. J. Org. Chem.*, **2017**, *2017*, 2179–2185. <https://doi.org/10.1002/ejoc.201601637> (c) Hering, T.; Meyer, A. U.; König, B. Photocatalytic Anion Oxidation and Applications in Organic Synthesis. *J. Org. Chem.* **2016**, *81* (16), 6927–6936. <https://doi.org/10.1021/acs.joc.6b01050>.

1.6 Dual Catalysis: Combination of Different Molecule Activation.

Even if photoredox mediated processes present the unique properties to generate ionic or open-shell intermediates from commonly unreactive substrates, the application of this peculiar type of activation displays a fundamental limitation.

The control on the formation of the products of interest depends mainly on the characteristics of the radicals that are generated.¹⁰² The reactions that can be allowed through the use of photoredox systems are essentially limited to:

(i) Radical trapping reactions in which, however, it is necessary that the trapping substrates exhibit the appropriate electronic characteristics for the generated radical (*e. g.*, nucleophilic radical combined with electrophilic substrates or vice-versa). Moreover, trapping of radicals with a neutral species leads to the formation of a new radical species. Again, it will be necessary that the new reactive intermediate has suitable properties for the reaction environment (*e.g.*, suitable redox electrochemical potential for the photosensitizer to engage single electron reduction or oxidation).

(ii) Development of radical homo- and cross-coupling reactions. However, radical cross-coupling reactions are strongly influenced by the nature of the radicals that are generated. According to the persistent radical effect (PRE) theory, the only radical cross-coupling products that can be obtained are those resulting from the encounter of two radical species formed at equal rates in the reaction mixture, but which are described by different self-reaction rate constants.¹⁰³

In addition, the possibility to perform enantioselective photoredox transformation is difficult to achieve since the photocatalyst in most of the cases only generates the reactive intermediates but does not cooperate in its reactivity when the new bond is formed.

To extend the variety of catalytic visible light-mediated processes, another type of molecule activation should be combined to the monocatalytic photoredox systems. The merger of a photoredox process with one or more catalytic systems acting synergistically could provide the reaction control that photocatalysis alone cannot furnish.¹⁰⁴

The extremely mild conditions in which photoredox processes are commonly performed, the enhanced chemical stability of the photocatalysts and the additional possibility to activate inert functional groups on redox active species further favor the combination with a different catalytic system. Moreover, the synergistic action of a catalyst on a photoredox-generated intermediate opens the way to stereoselective carbon-carbon bond formation reactions.

¹⁰² Leifert, D.; Studer, A. The Persistent Radical Effect in Organic Synthesis. *Angew. Chem. Int. Ed.* **2020**, *59* (1), 74–108. <https://doi.org/10.1002/anie.201903726>.

¹⁰³ Fischer, H. The Persistent Radical Effect: A Principle for Selective Radical Reactions and Living Radical Polymerizations. *Chem. Rev.* **2001**, *101* (12), 3581–3610. <https://doi.org/10.1021/cr990124y>.

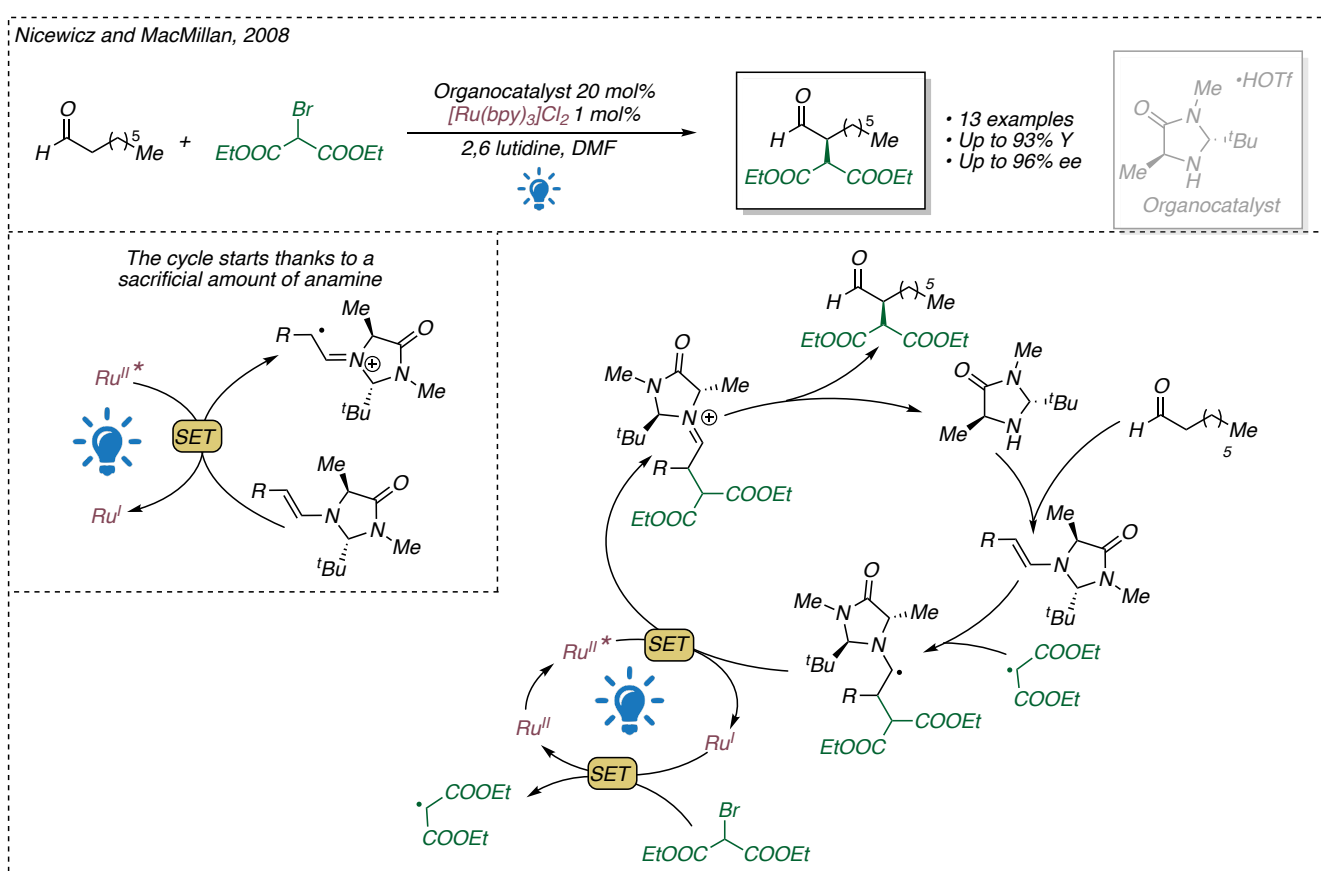
¹⁰⁴ Prier, C. K.; MacMillan, D. W. C. Dual Photoredox Catalysis: The Merger of Photoredox Catalysis with Other Catalytic Activation Modes. In *Visible Light Photocatalysis in Organic Chemistry*; Wiley-VCH Verlag GmbH & Co. KGaA: Weinheim, Germany, 2018; pp 299–333. <https://doi.org/10.1002/9783527674145.ch10>.

It is worth noticing that the development of modern photoredox catalysis is strictly related with the development of dual synergistic processes. In the last decade all the most common class of catalytic systems have been combined with light-promoted reactions.

•Dual photoredox and organocatalytic processes

Chronologically, the first reported combinations described the merging of photoredox with enamine organocatalytic processes. In 2008 MacMillan and Nicewicz developed a dual photoredox organocatalytic protocol for the enantioselective α -alkylation of aldehydes.¹⁰⁵

Combining the photochemical properties of $[\text{Ru}(\text{bpy})_3\text{Cl}_2]$ in photoredox catalysis with the ability of imidazolidinone catalysts to promote enantioselective α -functionalization of carbonyl compounds through the formation of transient enamines,¹⁰⁶ a wide library of enantioenriched highly functionalized α -substituted aldehydes was presented in high yields and enantiomeric excesses. The proposed mechanism involves both the photocatalytic and the organocatalytic cycle acting cooperatively.



Chapter 1. Scheme 22 Dual photoredox and organocatalytic α -alkylation of aldehydes reported by Nicewicz and MacMillan.

Originally, based on the emission quenching experiments performed, the $[\text{Ru}(\text{bpy})_3\text{Cl}_2]^*$ was believed to be reduced by a sacrificial amount of transient enamine formed upon interaction between the organocatalyst and the aldehyde.

¹⁰⁵ Nicewicz, D. A.; MacMillan, D. W. C. Merging Photoredox Catalysis with Organocatalysis: The Direct Asymmetric Alkylation of Aldehydes. *Science* **2008**, 322 (5898), 77–80. <https://doi.org/10.1126/science.1161976>.

¹⁰⁶ Han, B.; He, X. H.; Liu, Y.-A.; He, G.; Peng C.; Li J.-L. Asymmetric Organocatalysis: Enabling Technology for Medicinal Chemistry *Chem. Soc. Rev.*, **2021**, 50, 1522–1586. <https://doi.org/10.1039/D0CS00196A>

The so-formed $[\text{Ru}(\text{bpy})_3]^+$ is able to trigger the reduction of a quite broad library of α -bromomalonates, α -bromoketones, and α -bromoesters, restoring the original photocatalyst ($E(\text{Ru}^{\text{II}}/\text{Ru}^{\text{I}}) = -1.28$ vs SCE, while $E(\text{phenacylbromide}/\text{phenacyl}\cdot) = -0.49$ V versus SCE).

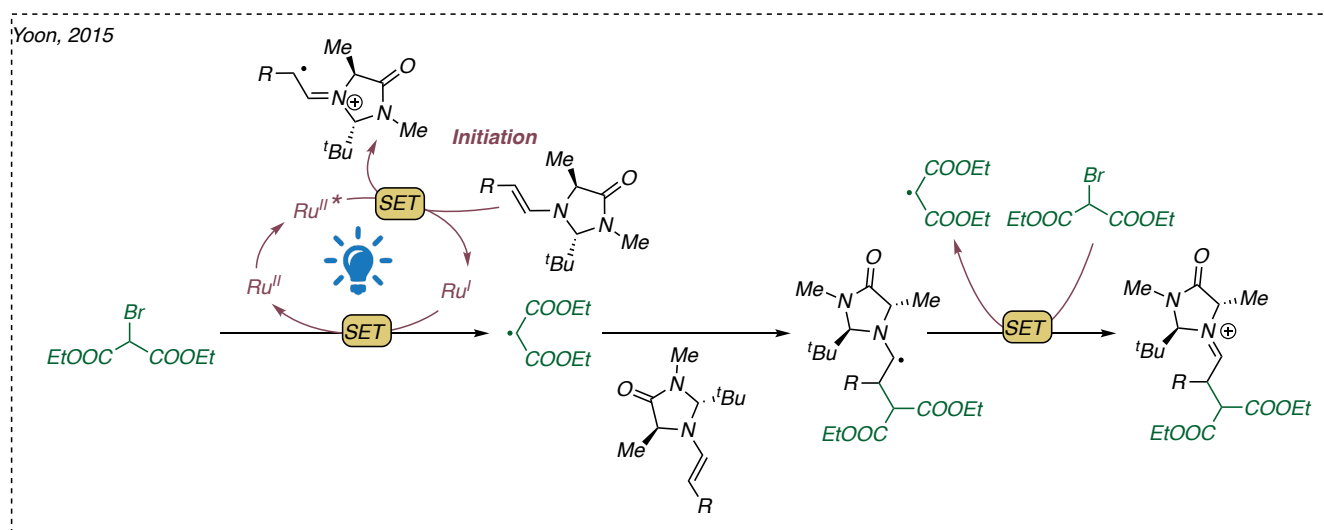
Once formed, the C-centered radicals, thanks to the presence of electron withdrawing groups, exhibits an electrophilic character that allow the selective interaction with the chiral enamine.

The radical trapping occurs in an enantioselective fashion. Thanks to the substituents on the imidazolidinone moiety, the enamine exposes only the *Si*-face for the formation of the new carbon-carbon bond during the radical addition.

The so-generated α -amino radical, presents an oxidation potential (≈ -0.9 V versus SCE) low enough to trigger the reductive quenching of ruthenium catalyst allowing the next catalytic cycle.

The desired enantioenriched α -alkylated products are obtained after the hydrolysis of the formed iminium ion, restoring also the organocatalyst.

The publication of this work and its related mechanism represented a cornerstone for the dual photoredox processes. Seven years later it was demonstrated by Yoon and co-workers that the actual mechanism of the reaction proceeded through an autonomous radical chain mechanism. The photoredox catalytic cycle was only required as initiator of the radical generation.¹⁰⁷



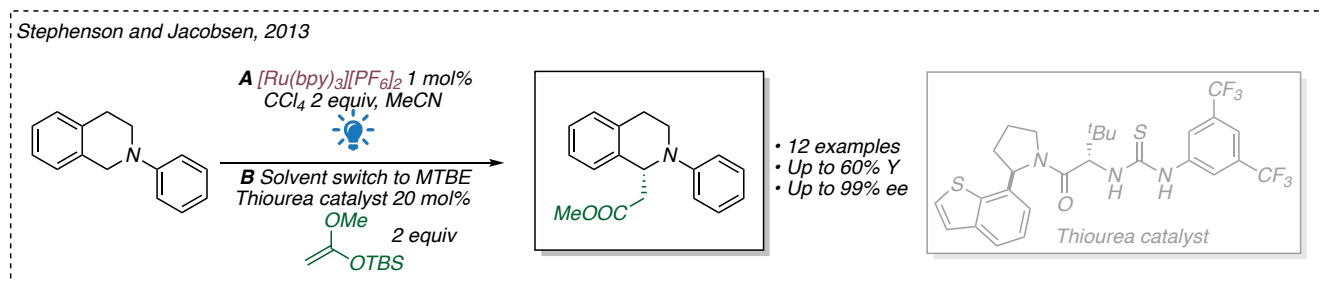
Chapter 1. Scheme 23 Radical chain mechanism proposed by Yoon in 2015

Rapidly after the presentation of the first work, however, the merging of these two catalytic techniques was reported in a several variants introducing new methodologies in organic chemistry.¹⁰⁸

¹⁰⁷ Yoon, T. P.; Cismesia, M. A. Characterizing Chain Processes in Visible Light Photoredox Catalysis *Chem. Sci.* **2015**, *6*, 5426–5434. <https://doi.org/10.1039/C5SC02185E>

¹⁰⁸ a) Rueping, M.; Vila, C.; Koenigs, R. M.; Poschary, K.; Fabry, D. C. Dual Catalysis: Combining Photoredox and Lewis Base Catalysis for Direct Mannich Reactions. *Chem. Commun.* **2011**, *47* (8), 2360–2362. <https://doi.org/10.1039/C0CC04539>; b) DiRocco, D. A.; Rovis, T. Catalytic Asymmetric α -Acylation of Tertiary Amines Mediated by a Dual Catalysis Mode: N-Heterocyclic Carbene and Photoredox Catalysis. *J. Am. Chem. Soc.* **2012**, *134* (19), 8094–8097. <https://doi.org/10.1021/ja3030164>; c) Nagib, D. A.; Scott, M. E.; MacMillan, D. W. C. Enantioselective α -Trifluoromethylation of Aldehydes via Photoredox Organocatalysis. *J. Am. Chem. Soc.* **2009**, *131* (31), 10875–10877. <https://doi.org/10.1021/ja9053338>; d) Shih, H.-W.; Vander Wal, M. N.; Grange, R. L.; MacMillan, D. W. C. Enantioselective α -Benzoylation of Aldehydes via Photoredox Organocatalysis. *J. Am. Chem. Soc.* **2010**, *132* (39), 13600–13603. <https://doi.org/10.1021/ja106593m>; e) Welin, E. R.; Warkentin, A. A.; Conrad, J. C.; MacMillan, D. W. C. Enantioselective α -Alkylation of Aldehydes by Photoredox Organocatalysis: Rapid Access to Pharmacophore Fragments from β -Cyanoaldehydes. *Angew. Chem. Int. Ed.* **2015**, *54* (33), 9668–9672.

Remarkably, not only covalent organocatalytic strategies have been combined with photoredox processes. The first example of noncovalent organocatalyst introduced under photoredox conditions was reported by Stephenson and Jacobsen.¹⁰⁹ The authors reported a stepwise enantioselective Mannich reaction starting from tetrahydroisoquinoline derivatives under visible-light irradiation using silyl ketene acetals as pre-formed nucleophiles.

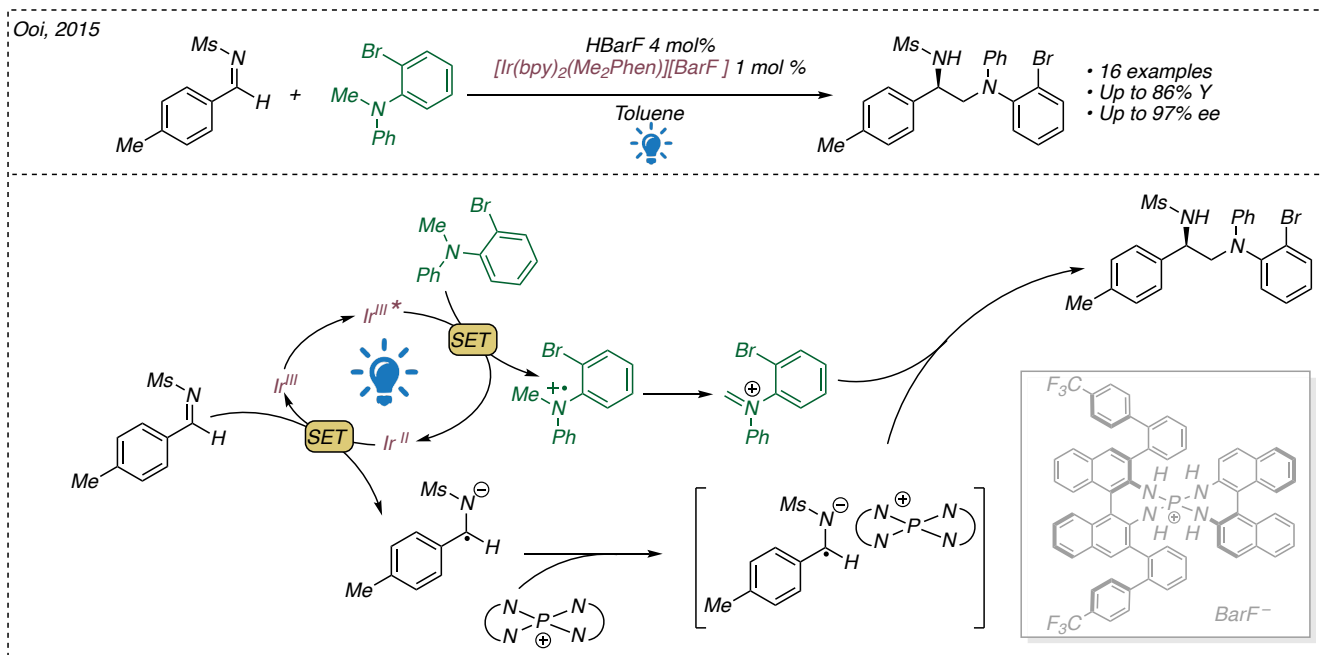


Chapter 1. Scheme 24 Stepwise enantioselective Mannich reaction reported by Stephenson and Jacobsen.

The mechanism of the reaction merges the well-known generation of transient iminium anion through a photoredox single electron oxidation of cyclic aryl amines with chiral thiourea anion-binding catalysis. The chiral thiourea noncovalently binds the chlorine of the photo-generated α -halo intermediate, allowing the stereochemical control of the nucleophilic attack enabling the stereoselective synthesis of β -amino esters in good yields and enantiomeric access up to 99%.

In a similar manner, an elegant work was reported by Ooi and co-workers. The authors introduced the possibility to control the radical intermediates formed in a photoredox-promoted process through noncovalent interaction in the presence of a chiral Brønsted acid catalyst. A highly enantioselective synthesis of diamines from *N*-sulfonylimines and di-substituted methylamines was presented.¹¹⁰ In this scenario, the photosensitizer is reductively quenched in the presence of the methylamines generating the corresponding radical cation, at the same time the Iridium (III) complex is restored after single electron oxidation of the *N*-sulfonylimines leading the formation of the corresponding radical anion. The radical-radical coupling step, leading the formation of the desired product, is mediated by the interaction of the Brønsted acid HBarF with the radical anion deriving from the *N*-sulfonylimines. In this way one of the possible sides of the coupling results shielded, allowing the induction of enantioselectivity.

<https://doi.org/10.1002/anie.201503789>; f) Cecere, G.; Ko, C. M. Enantioselective Direct α -Amination of Aldehydes via a Photoredox Mechanism: A Strategy for Asymmetric Amine Fragment Coupling. *J. Am. Chem. Soc.* **2013**, *135*, 11521–11524. <https://dx.doi.org/10.1021/ja406181e>; f) Zhu, Y.; Zhang, L.; Luo, S. Asymmetric α -Photoalkylation of β -Ketocarboxyls by Primary Amine Catalysis: Facile Access to Acyclic All-Carbon Quaternary Stereocenters. *J. Am. Chem. Soc.* **2014**, *136* (42), 14642–14645. <https://doi.org/10.1021/ja508605a>; g) Gualandi, A.; Calogero, F.; Martinelli, A.; Quintavalla, A.; Marchini, M.; Ceroni, P.; Lombardo, M.; Cozzi, P. G. A Supramolecular Bifunctional Iridium Photoaminocatalyst for the Enantioselective Alkylation of Aldehydes. *Dalton Trans.* **2020**, *49* (41), 14497–14505. <https://doi.org/10.1039/D0DT02587A>; h) Rigotti, T.; Casado-Sánchez, A.; Cabrera, S.; Pérez-Ruiz, R.; Liras, M.; de la Peña O'Shea, V. A.; Alemán, J. A Bifunctional Photoaminocatalyst for the Alkylation of Aldehydes: Design, Analysis, and Mechanistic Studies. *ACS Catal.* **2018**, *8* (7), 5928–5940. <https://doi.org/10.1021/acscatal.8b01331>; i) Murphy, J. J.; Bastida, D.; Paria, S.; Fagnoni, M.; Melchiorre, P. Asymmetric Catalytic Formation of Quaternary Carbons by Iminium Ion Trapping of Radicals. *Nature* **2016**, *532* (7598), 218–222. <https://doi.org/10.1038/nature17438>.
¹⁰⁹ Bergonzini, G.; Schindler, C. S.; Wallentin, C.-J.; Jacobsen, E. N.; Stephenson, C. R. J. Photoredox Activation and Anion Binding Catalysis in the Dual Catalytic Enantioselective Synthesis of β -Amino Esters. *Chem. Sci.* **2014**, *5* (1), 112–116. <https://doi.org/10.1039/C3SC52265B>.
¹¹⁰ Uraguchi, D.; Kinoshita, N.; Kizu, T.; Ooi, T. Synergistic Catalysis of Ionic Brønsted Acid and Photosensitizer for a Redox Neutral Asymmetric α -Coupling of *N*-Arylaminoethanes with Aldimines. *J. Am. Chem. Soc.* **2015**, *137* (43), 13768–13771. <https://doi.org/10.1021/jacs.5b09329>.



Chapter 1. Scheme 25 Enantioselective synthesis of diamines combining photoredox catalysis and noncovalent organocatalysis reported by Ooi.

•The merger of photoredox and transition metal catalysis.

Organocatalysis is not the only catalytic technique that can be combined with visible light mediated processes. The introduction of transition metal catalysis in photoredox environments offers the possibility to apply an extraordinary reaction control for new and interesting synthetic transformations. Commonly, the catalytic processes deriving by the combination of these two paradigms are known as metallaphotoredox catalysis.

Since the early works reported by Sanford,¹¹¹ Doyle and MacMillan¹¹² and Molander,¹¹³ it is possible to understand why this combination resulted extremely fruitful and has been largely explored in the last years. While the majority or purely organocatalytic processes rarely involves a change of the oxidation state of the substrates, in transition metal catalyzed transformations the modulation of the oxidation state of the metal centers is one of the crucial features to consider for the development of new transformations.¹¹⁴ In this scenario, the capability of the excited state of the photosensitizers to promote the single electron oxidation and the single electron reduction can perfectly fit the requirement for the development of new transition metal-mediated transformations. Given both the exponential growth of dual photoredox and transition metal catalyzed processes in recent years and the variety of different transition metals that have been used under photoredox conditions (*e.g.*, the use copper,¹¹⁵ gold,¹¹⁶ rhodium,¹¹⁷ cobalt,¹¹⁸ iron,¹¹⁹ bismuth¹²⁰ and zirconium¹²¹ has been recently reported), a complete overview would be impossible. For chronological reasons and relevance, in the next section the transformations in the presence of palladium and nickel will be highlighted. Subsequently, the methodologies concerning the processes enabled by the earth-abundant metals chromium and titanium will be taken as example.

¹¹¹ Kalyani, D.; McMurtrey, K. B.; Neufeldt, S. R.; Sanford, M. S. Room-Temperature C–H Arylation: Merger of Pd-Catalyzed C–H Functionalization and Visible-Light Photocatalysis. *J. Am. Chem. Soc.* **2011**, *133* (46), 18566–18569. <https://doi.org/10.1021/ja208068w>.

¹¹² Zuo, Z.; Ahneman, D. T.; Chu, L.; Terrett, J. A.; Doyle, A. G.; MacMillan, D. W. C. Merging Photoredox with Nickel Catalysis: Coupling of α -Carboxyl Sp³-Carbons with Aryl Halides. *Science*, **2014**, *345*, 437–440. [10.1126/science.1255525](https://doi.org/10.1126/science.1255525)

¹¹³ Tellis, J. C.; Primer, D. N.; Molander, G. A. Single-Electron Transmetalation in Organoboron Cross-Coupling by Photoredox/Nickel Dual Catalysis. *Science* **2014**, *345* (6195), 433–436. <https://doi.org/10.1126/science.1253647>.

¹¹⁴ R Twilton, J.; Le, C.; Zhang, P.; Shaw, M. H.; Evans, R. W.; MacMillan, D. W. C. The Merger of Transition Metal and Photocatalysis. *Nat Rev Chem* **2017**, *1* (7), 0052. <https://doi.org/10.1038/s41570-017-0052..>

¹¹⁵ Hossain, A.; Bhattacharyya, A.; Reiser, O. Copper's Rapid Ascent in Visible-Light Photoredox Catalysis. *Science* **2019**, *364* (6439), eaav9713. <https://doi.org/10.1126/science.aav9713>.

¹¹⁶ Hopkinson, M. N.; Tlahuext-Aca, A.; Glorius, F. Merging Visible Light Photoredox and Gold Catalysis. *Acc. Chem. Res.* **2016**, *49* (10), 2261–2272. <https://doi.org/10.1021/acs.accounts.6b00351>.

¹¹⁷ Fabry, D. C.; Rueping, M. Merging Visible Light Photoredox Catalysis with Metal Catalyzed C–H Activations: On the Role of Oxygen and Superoxide Ions as Oxidants. *Acc. Chem. Res.* **2016**, *49* (9), 1969–1979. <https://doi.org/10.1021/acs.accounts.6b00275>.

¹¹⁸ Gualandi, A.; Rodeghiero, G.; Perciaccante, R.; Jansen, T. P.; Moreno-Cabrerizo, C.; Foucher, C.; Marchini, M.; Ceroni, P.; Cozzi, P. G. Catalytic Photoredox Allylation of Aldehydes Promoted by a Cobalt Complex. *Adv. Synth. Catal.* **2021**, *363* (4), 1105–1111. <https://doi.org/10.1002/adsc.202001250>.

¹¹⁹ Zhang, J.; Campolo, D.; Dumur, F.; Xiao, P.; Fouassier, J. P.; Gimes, D.; LalevOe, J. Iron Complexes in Visible-Light-Sensitive Photoredox Catalysis: Effect of Ligands on Their Photoinitiation Efficiencies. **2016**, *8*, 2227– 2233.

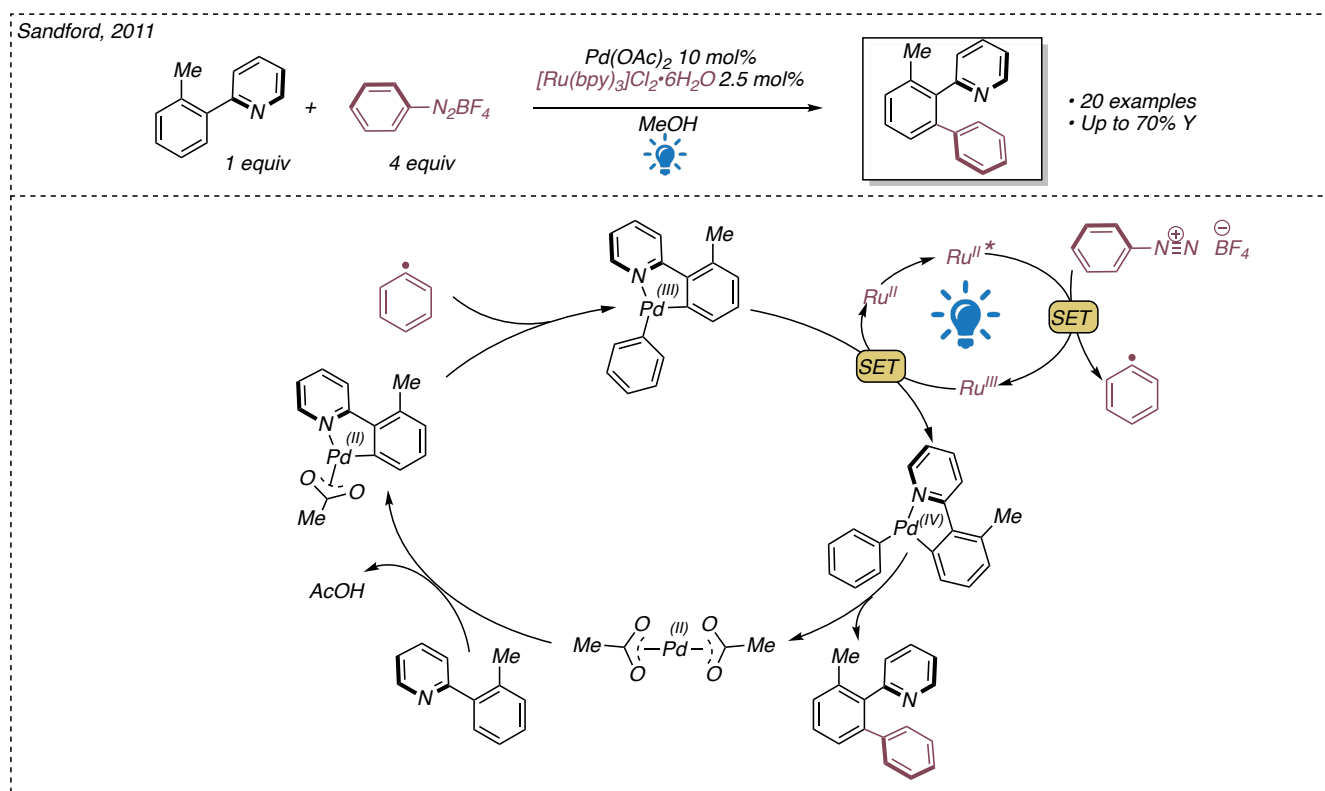
¹²⁰ Potenti, S.; Gualandi, A.; Puggioli, A.; Fermi, A.; Bergamini, G.; Cozzi, P. G. Photoredox Allylation Reactions Mediated by Bismuth in Aqueous Conditions. *Eur. J. Org. Chem.* **2021**, *2021* (11), 1624–1627. <https://doi.org/10.1002/ejoc.202001640>.

¹²¹ Aida, K.; Hirao, M.; Funabashi, A.; Sugimura, N.; Ota, E.; Yamaguchi, J. *ChemRxiv*. **2021**, preprint DOI 10.26434/chemrxiv.14605392.v1

•Palladium meets photoredox catalysis.

Apart from the work reported in 2007 by Osawa and co-workers,¹²² in which the introduction of a photoredox system into a Sonogashira protocol was shown to increase the reaction rate, the first forward-looking work reporting this synergistic combination was presented by the Sanford Group.¹¹¹

The authors reported the design of a dual photoredox and palladium catalyzed system, allowing the direct C-H arylation of a quite broad library of functionalized 2-arylpyridines.



Chapter 1. Scheme 26 Dual C-H arylation of 2-arylpyridines reported by Sanford

Although the work does not report a photophysical study for the accurate elucidation of the reaction mechanism, it has been proposed from the authors that the catalytic Pd(OAc)₂ reacts in the presence of 2-arylpyridines leading to the formation of a Pd(II) cyclometalated complex.

Concurrently, the excited state of [Ru(bpy)₃]²⁺ undergoes with an oxidative quenching in the presence of the aryl diazonium salt leading to the formation of the corresponding Ru(III) complex and an aryl radical (E(ArN₂BF₄/Ar•) = 0.2 V vs. SCE).¹²³ The radical is intercepted by the palladium II cyclometalated complex determining the formation of a Pd(III) complex. The active Pd(IV) species was firstly supposed to be enabled thanks to a single electron transfer occurring in the presence of [Ru(bpy)₃]³⁺, restoring the

¹²² Osawa, M.; Nagai, H. & Akita, M. Photo-activation of Pd-catalyzed Sonogashira coupling using a Ru/ bipyridine complex as energy transfer agent. *Dalton Trans.* 8, 827–829 (2007).

¹²³ Allongue, P.; Delamar, M.; Desbat, B.; Fagebaume, O.; Hitmi, R.; Pinson, J.; Savéant, J.-M. Covalent Modification of Carbon Surfaces by Aryl Radicals Generated from the Electrochemical Reduction of Diazonium Salts. *J. Am. Chem. Soc.* **1997**, *119* (1), 201–207. <https://doi.org/10.1021/ja963354s>.

photocatalyst. The reductive elimination restoring the original Pd(OAc)₂ leads, finally, to the formation of the desired product.

A clear picture of the reaction mechanism instead, has been provided later by computational methods.¹²⁴ Interestingly, from the modeling results, besides a more conventional Pd(II)/Pd(IV) cycle initially proposed by Sanford and co-workers, the possibility of a Pd(I)/Pd(III) cycle.

In this scenario, the Pd(III) species would lead to the formation of product after reductive elimination with consequent formation of the Pd(I) intermediate. This latter species, according to the authors of the work, is then converted into the initial Pd(OAc)₂ through a single electron transfer with the photocatalyst. There are two reasons why the work reported by Sanford and co-workers represents a groundbreaking example for the development of dual transition metal and photoredox catalysis. First, thanks to the introduction of a photoredox catalyst, under visible light irradiation, it was demonstrated the possibility to obtain transition metal-mediated C-H arylation reactions avoiding the use of strong oxidants in over-stoichiometric amount at room temperature. Moreover, the fact that C-centered radicals can be generated by a photocatalyst and then be trapped in the transition-metal cycle further shows how convenient the combination of these two catalytic techniques is for the development of new methodologies.

The opportunity provided by visible light to allow direct access to the various oxidation states of a transition metal catalyst through the utilization of the redox properties of a photocatalyst has been widely exploited after the publication by the Sanford group.¹²⁵

In 2014,¹²⁶ for instance, Rueping and co-workers reported an aerobic dual photoredox and palladium catalyzed intramolecular C-H activation of *N,N*- aryl, vinyl amines in order to obtain a library of differently substituted indoles in good yields.

¹²⁴ M Maestri, G.; Malacria, M.; Derat, E. Radical Pd(III)/Pd(I) Reductive Elimination in Palladium Sequences. *Chem. Commun.* **2013**, 49 (88), 10424–10426. <https://doi.org/10.1039/C3CC46355A>.

¹²⁵ Chen, Y.; Lin, J.; Chen, X.; Fan, S.; Zheng, Y. Engineering Multicomponent Metal-Oxide Units for Efficient Methane Combustion over Palladium-Based Catalysts. *Catal. Sci. Technol.* **2021**, 11 (1), 152–161. <https://doi.org/10.1039/D0CY01742F>.

¹²⁶ Zoller, J.; Fabry, D. C.; Ronge, M. A.; Rueping, M. Synthesis of Indoles Using Visible Light: Photoredox Catalysis for Palladium-Catalyzed C-H Activation. *Angew. Chem. Int. Ed.* **2014**, 53 (48), 13264–13268. <https://doi.org/10.1002/anie.201405478>.

•Nickel meets photoredox catalysis.

The use of nickel catalysis under photoredox conditions is certainly the most powerful contributor to the success of metallaphotoredox catalysis.^{89,127} The well-known ability of nickel, compared to palladium, to have an easier access to different oxidation states within the same catalytic cycle together with the possibility to catalyze processes through radical mechanisms are the main elements that have determined this winning combination.

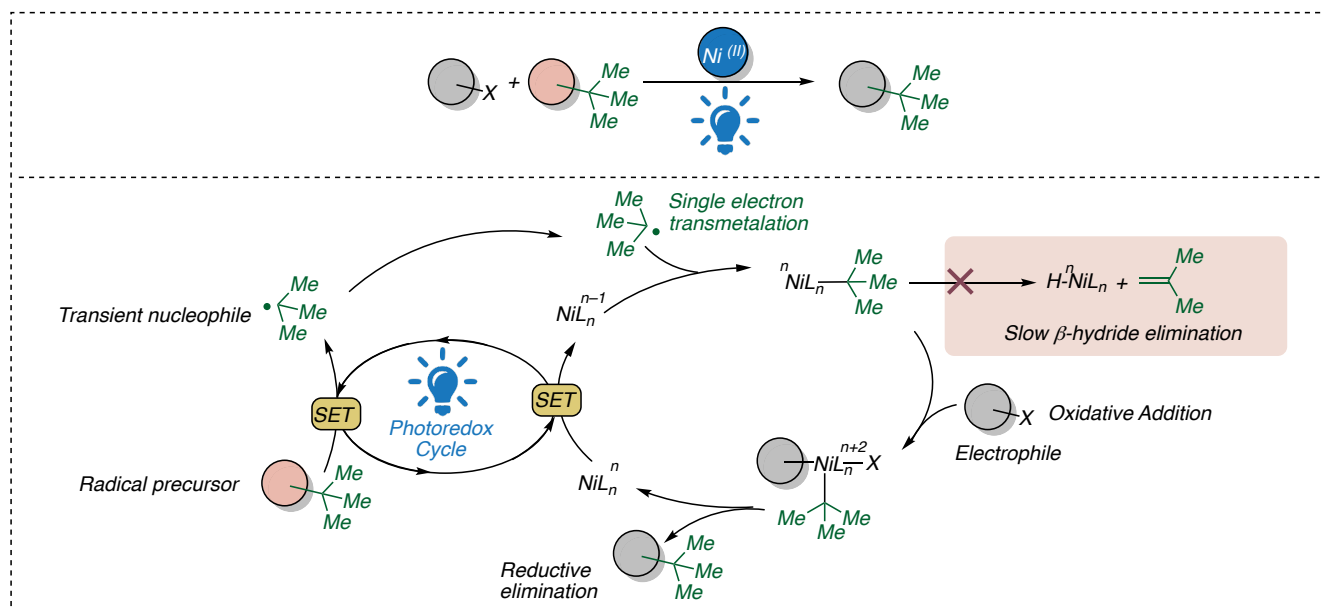
A further advantage is the particular property of nickel to hardly face by-processes of β -hydride elimination when employed in cross-coupling transformations that involve the generation of alkyl organonickel intermediates. Given the smaller atomic radius of nickel compared to palladium, the energy barriers for the rotation of C-Ni bonds are higher than Pd-C bonds, as a result the elimination with consequent formation of nickel hydride will be a relatively slow process.¹²⁸ This aspect perfectly matches the ability of photoredox systems to generate alkyl radicals that can be quickly captured by nickel evolving towards synthetically crucial transformations otherwise difficult to achieve.

C(sp³)-C(sp²) reductive cross-coupling has been the most investigated methodology in nickelaphotoredox catalysis. In this sense, several classes of organic molecules with the appropriate redox properties have been presented in the literature as radical precursors.¹²⁹ The photoredox generated radicals, therefore, replace the nucleophiles of conventional cross-coupling reactions allowing different types of C-C and C-heteroatom bond-forming reactions. In the general paradigm of these transformation, the electrophilic partner of the reaction is usually converted into the desired product taking part into the nickel catalytic cycle. (**Figure 24**) The formation of the nickel in low oxidation state is achieved upon single electron oxidation of the photocatalyst. The formation of the final product normally arises three steps after the formation of the active catalytic nickel species: (i) radical trapping, (ii) oxidative addition onto the electrophile; (iii) reductive elimination.

¹²⁷ a) Milligan, J. A.; Phelan, J. P.; Badir, S. O.; Molander, G. A. Alkyl Carbon–Carbon Bond Formation by Nickel/Photoredox Cross-Coupling. *Angew. Chem. Int. Ed.* **2019**, *58* (19), 6152–6163. <https://doi.org/10.1002/anie.201809431>.

¹²⁸ Tasker, S. Z.; Standley, E. A.; Jamison, T. F. Recent Advances in Homogeneous Nickel Catalysis. *Nature* **2014**, *509* (7500), 299–309. <https://doi.org/10.1038/nature13274>. b) Diccianni, J. B.; Diao, T. Mechanisms of Nickel-Catalyzed Cross-Coupling Reactions. *Trends in Chemistry* **2019**, *1* (9), 830–844. <https://doi.org/10.1016/j.trechm.2019.08.004>.

¹²⁹ Tellis, J. C.; Kelly, C. B.; Primer, D. N.; Jouffroy, M.; Patel, N. R.; Molander, G. A. Single-Electron Transmetalation via Photoredox/Nickel Dual Catalysis: Unlocking a New Paradigm for Sp³–Sp² Cross-Coupling. *Acc. Chem. Res.* **2016**, *49* (7), 1429–1439. <https://doi.org/10.1021/acs.accounts.6b00214>.



Chapter 1. Figure 24 Fruitful combination of photoredox catalysis and nickel catalysis in reductive cross-coupling

In recognition of what has already been discussed, it is important to make a further clarification to comprehensively describe nickel-catalyzed reductive cross couplings performed under photoredox regimes. Indeed, the mechanism of a dual Ni/photoredox transformation can start either with the reductive quenching of the excited state of the photocatalyst for the formation of the radicals, or with the corresponding oxidative quenching leading the formation of the nickel complex in low oxidation state. Depending on the case, it is required, that the chosen photosensitizer has the appropriate (photo)redox potentials to ensure an efficient formation of nickel in a low oxidation state engaging a SET.

The potential value required to allow this reduction is closely related to the nature of the ligands surrounding the metal that have a strong effect on its chemical and electrochemical properties.¹³⁰

In addition, since nickel can better access different oxidation states compared to other metals, it is often difficult to undoubtedly prove which is the oxidation state of the catalytically active species.¹³¹

Trying to extend the concept in general terms; the nickel complex reduction can occur in the presence of a photosensitizer that presents redox potentials (*either* $E(PC^+/PC^*)$ *or* $E(PC/PC^{\bullet-})$) below -1.3 V. vs SCE.

This is the key reason why the photocatalysts used for dual photoredox/nickel catalyzed processes have been performed, at least for the first developments of this technique, with rare metal-based coordination complexes like $Ir(ppy)_3$, $(Ir[dF(CF_3)ppy]_2(dtbbpy))^+$, or $[Ru(bpy)_3]^{2+}$. The use of cheaper, easily accessible, and sustainable organic dyes like *e.g.*, Eosin Y, Rose Bengal, and Mes-Acr⁺ showed no activity due to the lack of appropriate potentials to perform the reduction of nickel complexes.

¹³⁰ Lin, Q.; Dawson, G.; Diao, T. Experimental Electrochemical Potentials of Nickel Complexes. *Synlett* **2021**, 32 (16), 1606–1620. <https://doi.org/10.1055/s-0040-1719829>.

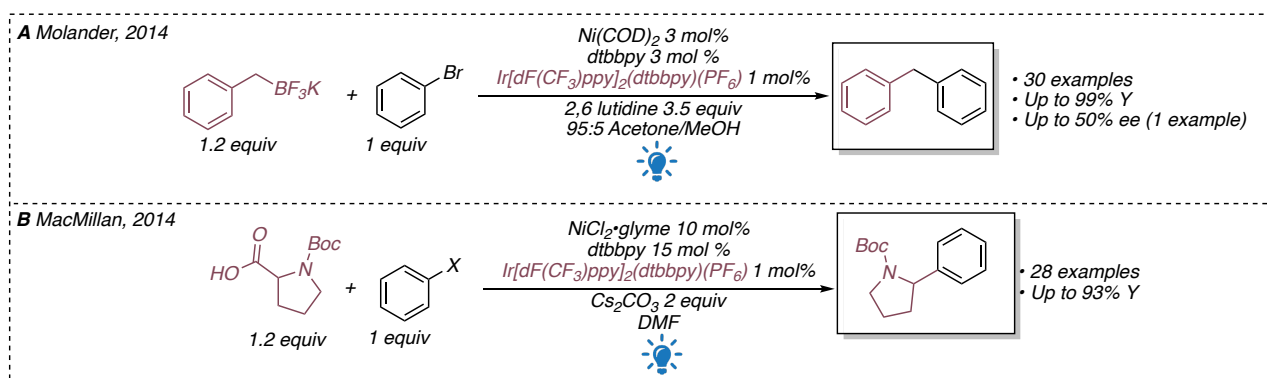
¹³¹ Sun, R.; Qin, Y.; Ruccolo, S.; Schnedermann, C.; Costentin, C.; Nocera, D. G. Elucidation of a Redox-Mediated Reaction Cycle for Nickel-Catalyzed Cross Coupling. *J. Am. Chem. Soc.* **2019**, 141 (1), 89–93. <https://doi.org/10.1021/jacs.8b11262>. Ting, S.; Williams, W.; Doyle, A. Oxidative Addition of Aryl Halides to a Ni(I)-Bipyridine Complex *ChemRxiv* **2022**. This content is a preprint and has not been peer-reviewed.

It was only after the introduction by Zhang⁷⁰ and Zeitler⁷¹ of the new generation of cyanoarenes-based photocatalysts - *whose photophysical properties have been introduced in the previous sections* - that it was possible to realize dual transformation in the presence of organic dyes. As in the case of the Ir(III)-mediated process, 4CzIPN, for instance, presents a sufficient reduction potential in its excited state to generate the C(sp³) radicals from organic precursors ($E(*4CzIPN / 4CzIPN^{\bullet-}) = +1.43$ V vs. SCE). Along with the electron transfer, the excited state of the photocatalyst is reductively quenched generating the corresponding radical anion. The so-formed species can reduce the nickel catalyst, forming a complex in a low oxidation state. ($E(4CzIPN / 4CzIPN^{\bullet-}) = -1.24$ V vs. SCE)

The first papers introducing this technique were published almost simultaneously by Molander¹¹³ and co-workers and by the collaboration of Doyle and Macmillan group in 2014.¹¹² In both cases a C(sp³)-C(sp²) visible light promoted cross coupling was presented. Both reactions proceed following the general protocol of dual nickel/photoredox processes. In the two methodologies, two different radical sources were presented as nucleophilic partner for the reaction. MacMillan and co-workers reported a decarboxylative cross-coupling in which the well-known photophysical properties of the $(Ir[dF(CF_3)ppy]_2(dtbbpy))^{*+}$ were exploited in the presence of α -amino, α -oxo and aliphatic carboxylates for the generation of alkyl radicals. (**Scheme 28b**)

On the other hand, the Molander group introduced benzyltrifluoroborates as a new class of benzyl radical sources. Alkyltrifluoroborates, in fact exhibit an electrochemical oxidation potential ($E(\text{benzyl}\bullet / \text{benzyltrifluoroborates}) = 1.2$ V vs. SCE)¹³² which allows these compounds to be engaged in a reductive quenching of the excited state of the same iridium complex. (**Scheme 28a**) Remarkably, although in the case of the decarboxylative cross coupling the nickel precatalyst used is a Ni(II) species ($[NiCl_2(\text{glyme})]$), while in the Molander's work the preferred nickel source is the highly reactive and air-sensitive Ni(0)(COD)₂ (COD = 1,5-cyclooctadiene) in both reactions a bipyridine-based ligand with bulky substituents protecting position 4 and 4' was found to be the most suitable. This feature is common for many processes occurring through a combined mechanism of photoredox and nickel catalysis. The resulting active catalytic species, in fact, very often has proven suitable both to accept a transient radical species and to engage oxidative addition processes.

¹³² Yasu, Y.; Koike, T.; Akita, M. Visible Light-Induced Selective Generation of Radicals from Organoborates by Photoredox Catalysis. *Adv. Synth. Catal.* **2012**, *354* (18), 3414–3420. <https://doi.org/10.1002/adsc.201200588>.



Chapter 1. Scheme 28 First two reported protocols involving dual nickel and photoredox catalysis

The leap forward demonstrated in these works has meant that dual nickel and photocatalytic methodologies have rapidly gained a foothold in the scientific community. The improvement of this technique has developed mainly along three interconnected lines of research: (i) the development of unique synthons from precursors whose photophysical properties were known and suitable, (ii) the presentation of new radical precursor able to react with the excited state of photosensitizers, (iii) the design of new, more accessible, and cheaper photocatalysts to replace the rare metal-based photocatalysts commonly employed.

Trifluoroborate derivatives, both for the ease with which they can be prepared and for their privileged redox properties are the class of compounds most employed in reductive cross coupling under dual nickel/photoredox conditions. In this scenario, since the first work, the Molander group ruled the scene of these transformations. Following comparable procedures, a large diversity of unique functionalization of aryl and heteroaryl halides was reported using different trifluoroborate derivatives. In the presence of the appropriate trifluoroborate derivative in the opportune reaction conditions the main reported works have concerned: synthesis of benzylic ethers;¹³³ α -arylation and heteroarylation of tertiary amines;¹³⁴ synthesis of diaryltrifluoroethane derivatives;¹³⁵ cross-coupling of acyl chlorides;¹³⁶ β -arylation of ketones;¹³⁷ cross-couplings for the synthesis of quaternary centers;¹³⁸ direct synthesis of secondary benzylic alcohols.¹³⁹ (**Figure 25**)

¹³³ Karakaya, I.; Primer, D. N.; Molander, G. A. Photoredox Cross-Coupling: Ir/Ni Dual Catalysis for the Synthesis of Benzylic Ethers. *Org. Lett.* **2015**, *17* (13), 3294–3297. <https://doi.org/10.1021/acs.orglett.5b01463>.

¹³⁴ El Khatib, M.; Serafim, R. A. M.; Molander, G. A. α -Arylation/Heteroarylation of Chiral α -Aminomethyltrifluoroborates by Synergistic Iridium Photoredox/Nickel Cross-Coupling Catalysis. *Angew. Chem. Int. Ed.* **2016**, *55* (1), 254–258. <https://doi.org/10.1002/anie.201506147>.

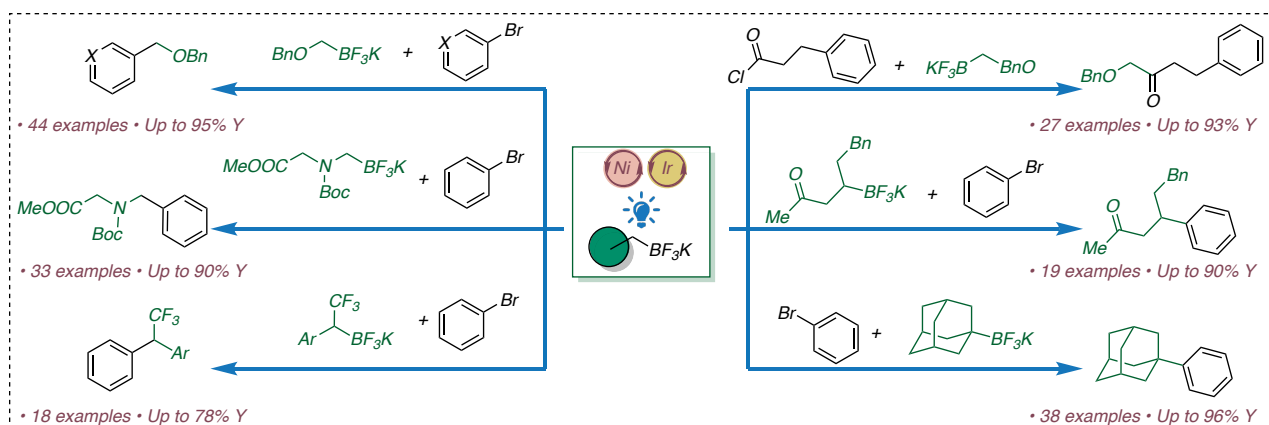
¹³⁵ Ryu, D.; Primer, D. N.; Tellis, J. C.; Molander, G. A. Single-Electron Transmetalation: Synthesis of 1,1-Diaryl-2,2,2-Trifluoroethanes by Photoredox/Nickel Dual Catalytic Cross-Coupling. *Chem. Eur. J.* **2016**, *22* (1), 120–123. <https://doi.org/10.1002/chem.201504079>.

¹³⁶ Amani, J.; Sodagar, E.; Molander, G. A. Visible Light Photoredox Cross-Coupling of Acyl Chlorides with Potassium Alkoxyethyltrifluoroborates: Synthesis of α -Alkoxyketones. *Org. Lett.* **2016**, *18* (4), 732–735. <https://doi.org/10.1021/acs.orglett.5b03705>.

¹³⁷ Tellis, J. C.; Amani, J.; Molander, G. A. Single-Electron Transmetalation: Photoredox/Nickel Dual Catalytic Cross-Coupling of Secondary Alkyl β -Trifluoroborateketones and -Esters with Aryl Bromides. *Org. Lett.* **2016**, *18* (12), 2994–2997. <https://doi.org/10.1021/acs.orglett.6b01357>.

¹³⁸ Primer, D. N.; Molander, G. A. Enabling the Cross-Coupling of Tertiary Organoboron Nucleophiles through Radical-Mediated Alkyl Transfer. *J. Am. Chem. Soc.* **2017**, *139* (29), 9847–9850. <https://doi.org/10.1021/jacs.7b06288>.

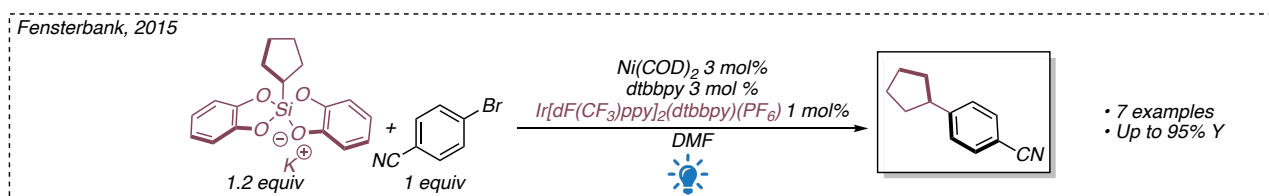
¹³⁹ Alam, R.; Molander, G. A. Direct Synthesis of Secondary Benzylic Alcohols Enabled by Photoredox/Ni Dual-Catalyzed Cross-Coupling. *J. Org. Chem.* **2017**, *82* (24), 13728–13734. <https://doi.org/10.1021/acs.joc.7b02589>.



Chapter 1. Figure 25 Application of trifluoroborate derivatives in dual Ni/photoredox processes

Alkyl trifluoroborates, however, do not represent the *paspartout* to perform all the cross-coupling methodologies. The partial solubility in organic solvents, together with the fact that all the reported methodologies require an excess of organic base to neutralize the BF_3 formed during the reaction, limit their use.

In this perspective, indeed, Goddard, Ollivier, and Fensterbank in 2015 demonstrated for the first time how silicate derivatives could be used as latent alkyl radical precursors in a comparable fashion to BF_3K derivatives.¹⁴⁰ By exploiting the already known¹⁴¹ redox properties of these compounds under photoredox conditions ($E(\text{alkyl}^\bullet/\text{alkyl-bis}(\text{catecholato})\text{silicates}) \approx 0.75 \text{ V vs SCE}$), indeed, good examples of $\text{C}(\text{sp}^3)\text{-C}(\text{sp}^2)$ visible light promoted cross couplings have been reported.



Chapter 1. Scheme 29 Application of silicate derivatives in dual Ni/photoredox processes

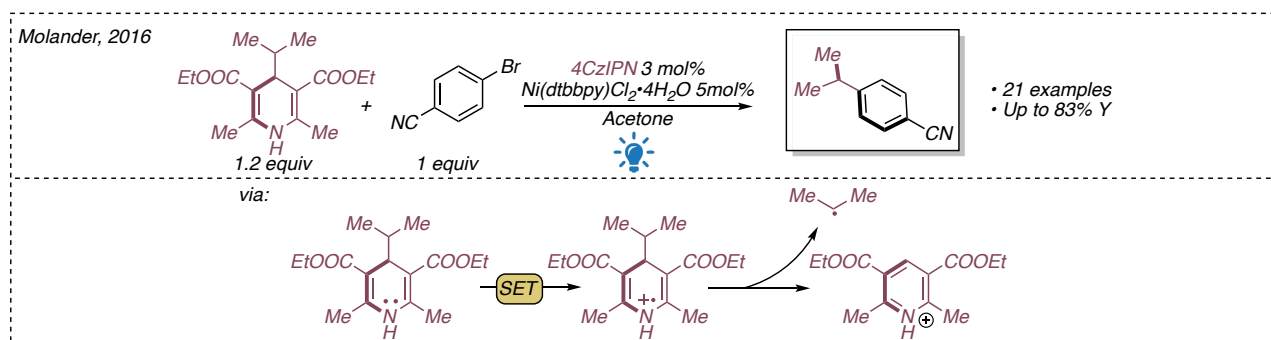
Molander and co-workers¹⁴² reported in 2016 a Ni/photoredox dual catalytic cross-coupling employing 4CzIPN, (hetero)aryl bromides as electrophilic partner and 1,4-dihydropyridines (DHP) as source of C-centered radicals ($E(\text{alkyl}^\bullet/\text{alkyl-DHP}) \approx 1.0 \text{ V vs SCE}$).¹⁴³ (**Scheme 30**). The methodology presents a quite high tolerance for different functional groups but is not suitable for primary alkyl or cyclopropyl derivatives. The process is promoted by a reductive quenching of the excited state of the photocatalyst. ($E(4\text{CzIPN}^*/4\text{CzIPN}^{\bullet-}) = 1.43 \text{ V vs. SCE}$) This event determines the formation of the corresponding strong reductant $4\text{CzIPN}^{\bullet-}$ ($E(4\text{CzIPN}/4\text{CzIPN}^{\bullet-}) = -1.24 \text{ V vs. SCE}$) that can reduce the nickel complex.

¹⁴⁰ Corcé, V.; Chamoreau, L.; Derat, E.; Goddard, J.; Ollivier, C.; Fensterbank, L. Silicates as Latent Alkyl Radical Precursors: Visible-Light Photocatalytic Oxidation of Hypervalent Bis-Catecholato Silicon Compounds. *Angew. Chem. Int. Ed.* **2015**, *54* (39), 11414–11418. <https://doi.org/10.1002/anie.201504963>.

¹⁴¹ (a) Nishigaichi, Y.; Suzuki, A.; Takawa, A. Remarkable Enhancement of Photo-Allylation of Aromatic Carbonyl Compounds with a Hypervalent Allylsilicon Reagent by Donor Molecules. *Tetrahedron Letters* **2007**, *48* (2), 211–214. <https://doi.org/10.1016/j.tetlet.2006.11.057>.

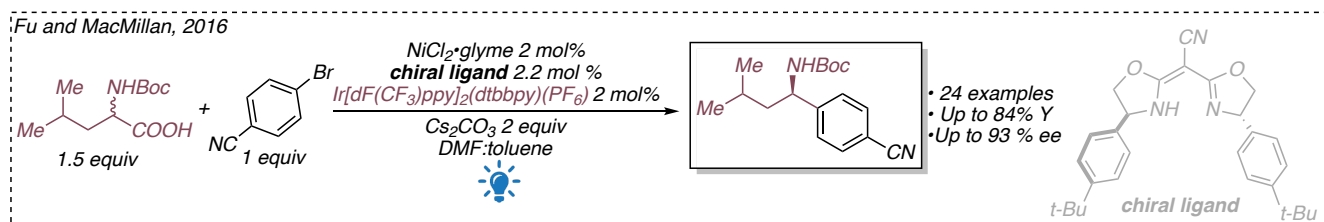
¹⁴² Gutiérrez-Bonet, Á.; Tellis, J. C.; Matsui, J. K.; Vara, B. A.; Molander, G. A. 1,4-Dihydropyridines as Alkyl Radical Precursors: Introducing the Aldehyde Feedstock to Nickel/Photoredox Dual Catalysis. *ACS Catal.* **2016**, *6* (12), 8004–8008. <https://doi.org/10.1021/acscatal.6b02786>.

¹⁴³ Nakajima, K.; Nojima, S.; Sakata, K.; Nishibayashi, Y. Visible-Light-Mediated Aromatic Substitution Reactions of Cyanoarenes with 4-Alkyl-1,4-dihydropyridines through Double Carbon–Carbon Bond Cleavage. *ChemCatChem* **2016**, *8* (6), 1028–1032. <https://doi.org/10.1002/cctc.201600037>.



Chapter 1. Scheme 30 Ni/photoredox dual catalytic cross-coupling employing 4CzIPN

To conclude this section about the exploitation of this dual catalytic technique, although it represents a challenging field, pioneering highly enantioselective transformation have been reported.¹⁴⁴ The first example was reported by Fu and MacMillan in 2016.¹⁴⁵ The authors presented a highly enantioselective decarboxylative C(sp³)-C(sp²) cross-coupling between diversely substituted aryl bromides in presence of Boc-protected amino acids. A semicorrin-based¹⁴⁶ chiral ligand combined with a commercially available Ni(II) precatalyst was found to be the best combination to promote the reaction in an enantioselective fashion.



Chapter 1. Scheme 31 Enantioselective Ni/photoredox dual catalytic decarboxylative cross-coupling reported by Fu and MacMillan

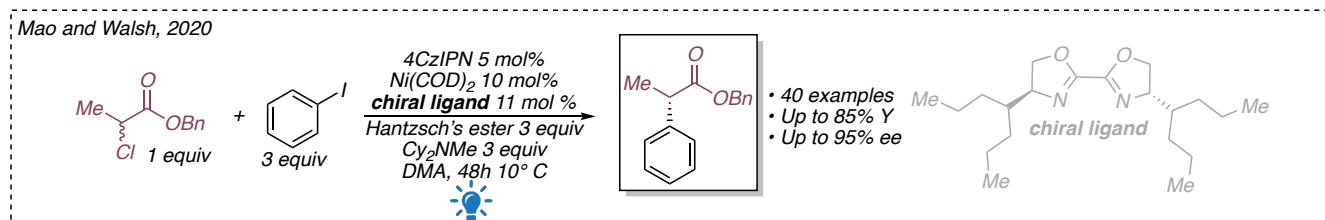
The reaction was found robust and tolerant to both electron withdrawing and electron donating functional groups (*e.g.*, carbamates, ethers, esters, alkyl chlorides, carbonates, indole, and thiophene) and a good library of differently functionalized benzyl amines was reported with excellent yields and high enantiomeric excesses. Cs₂CO₃ was selected as the most appropriate base to deprotonate carboxylic acids and allow their oxidation in the presence of photocatalyst (Ir[dF(CF₃)ppy]₂(dtbbpy))⁺. The optimized reaction conditions were shown suitable not only for *N*-Boc-protected α -amino acids, but they can also be applied to a *N*-Cbz-protected substrate, albeit in more modest yield. To further demonstrate the strength of the presented protocol, the authors applied the enantioselective decarboxylative C(sp³)-C(sp²) cross-coupling to the synthesis of two pharmacologically active molecules (a glucagon receptor antagonist and a PEG₂ receptor antagonist, respectively).

¹⁴⁴ Zhang, H.-H.; Chen, H.; Zhu, C.; Yu, S. A Review of Enantioselective Dual Transition Metal/Photoredox Catalysis. *Sci. China Chem.* **2020**, *63* (5), 637–647. <https://doi.org/10.1007/s11426-019-9701-5>.

¹⁴⁵ Zuo, Z.; Cong, H.; Li, W.; Choi, J.; Fu, G. C.; MacMillan, D. W. C. Enantioselective Decarboxylative Arylation of α -Amino Acids via the Merger of Photoredox and Nickel Catalysis. *J. Am. Chem. Soc.* **2016**, *138* (6), 1832–1835. <https://doi.org/10.1021/jacs.5b13211>.

¹⁴⁶ Fritsch, H.; Leutenegger, U.; Pfaltz, A. Chiral Copper-Semicorrin Complexes as Enantioselective Catalysts for the Cyclopropanation of Olefins by Diazo Compounds. *Angew. Chem. Int. Ed. Engl.* **1986**, *25* (11), 1005–1006. <https://doi.org/10.1002/anie.198610051>.

Very recently, Walsh and Mao¹⁴⁷ employed 4CzIPN as the photocatalyst, in the presence of Hantzsch's (HE) as the terminal reductant for a catalyzed asymmetric reductive cross-coupling of α -chloro esters with aryl iodides for the effective preparation of highly enantioenriched α -aryl esters. (**Scheme 32**) The chiral ligand used for the transformation is a quite simple and readily available modified bis-oxazoline (BiOX).



Chapter 1. Scheme 32 Enantioselective Ni/photoredox dual catalytic arylation of α -chloro esters reported by Mao and Walsh

According to the mechanistic proposal, the *in situ* formed Ni(II) complex, is reduced to Ni(0) by the 4CzIPN^{•-} which derives from the reductive quenching of the 4CzIPN in presence of the Hantzsch's ester. On the other hand, the tertiary amine, largely acted as a base in the reaction. The reduction of the α -chloro esters and the concomitant formation of the corresponding nucleophilic α -radical can be carried out by different transient reductants (the oxidized HE, the Ni(I) complex or the 4CzIPN^{•-}). The authors could not distinguish or have evidence for concluding unambiguously which process is favored.

¹⁴⁷ Walsh, P. J.; Guan, H.; Zhang, Q.; Mao, J. Nickel/Photoredox-Catalyzed Asymmetric Reductive Cross-Coupling of Racemic α -Chloro Esters with Aryl Iodides. *Angew. Chem. Int. Ed.* **2020**, 59 (13), 5172–5177. <https://doi.org/10.1002/anie.201914175>.

•Heart-abundant metals meet photoredox catalysis: chromium and titanium

Complexes of chromium and titanium have a well-known and widespread use in transition metal catalysis.¹⁴⁸ Exploiting the characteristics of both metals finds attractive applications of both academic and industrial interest.¹⁴⁹ However, the catalytic exploitation of these metals to promote synthetic transformations is only allowed in the presence of species able to single electron reduce the transition metal catalyst (commonly the reducing agents involved in Cr(III)/Cr(II) and Ti(IV)/Ti(III) reductions are metals *e.g.*, Zn or Mn). In addition, when these complexes are used, the presence of an overstoichiometric amount of scavenger (*e.g.*, proton sources, TMSCl, Ac₂O or Cp₂ZrCl₂) is required to release the product and restore the catalyst.

It is clearly understandable that although excellent methodologies have been reported using chromium and titanium coordination complexes, the main limitation is the large amount of byproducts that results from their employment. In analogy to what has been introduced in the case of nickel and palladium, the combination of these metals with photoredox-promoted processes brings two main advantages: (i) The photocatalyst either in the excited state or after a reductive quenching can reduce the titanium or chromium complex under much milder conditions and in a much more sustainable way, replacing the metal reductant. (ii) In order for the photocatalyst to work under redox neutral conditions it is possible to introduce redox active species as reaction partners which can lead to the formation of C-centered radicals after single electron oxidation.¹⁵⁰ In this scenario, the capture of C-centered radicals by the low valent metal complex leads to the formation of transient nucleophilic organometallic species that are capable to react with electrophilic species. In this sense, the behavior of the radical generated by visible radiation is particularly interesting. The conversion of a radical into a “classical” polar nucleophilic species either through reduction or capture by a transition metal complex is addressed as reductive radical-polar crossover (RRPC) and represent valuable and powerful tool to overcome limitations of both radical and traditional polar chemistry.¹⁵¹

This first protocol reported by the combination of photoredox and chromium catalysis was reported by Glorius and co-workers.¹⁵² The authors disclosed a highly diastereoselective redox-neutral allylation of aldehydes presenting the first example of Nozaki–Hiyama–Kishi (NHK) reaction in a RRPC environment. The reaction is based on the direct formation of allyl radicals from alkenes. These radicals

¹⁴⁸ a) Manßen, M.; Schafer, L. L. Titanium Catalysis for the Synthesis of Fine Chemicals – Development and Trends. *Chem. Soc. Rev.* **2020**, *49* (19), 6947–6994. <https://doi.org/10.1039/D0CS00229A>; b) Cong, X.; Zeng, X. Mechanistic Diversity of Low-Valent Chromium Catalysis: Cross-Coupling and Hydrofunctionalization *Acc. Chem. Res.*, **2021**, *54* (8), 2014–2026. <https://doi.org/10.1021/acs.accounts.1c00096>

¹⁴⁹ a) Fürstner, A. Carbon–Carbon Bond Formations Involving Organochromium(III) Reagents. *Chem. Rev.* **1999**, *99* (4), 991–1046. <https://doi.org/10.1021/cr9703360>; b) McCallum, T.; Wu, X.; Lin, S. Recent Advances in Titanium Radical Redox Catalysis. *J. Org. Chem.* **2019**, *84* (22), 14369–14380. <https://doi.org/10.1021/acs.joc.9b02465>.

¹⁵⁰ Fermi, A.; Gualandi, A.; Bergamini, G.; Cozzi, P. G. Shining Light on Ti^{IV} Complexes: Exceptional Tools for Metallaphotoredox Catalysis. *Eur. J. Org. Chem.* **2020**, *2020* (45), 6955–6965. <https://doi.org/10.1002/ejoc.202000966>.

¹⁵¹ Pitzer, L.; Schwarz, J. L.; Glorius, F. Reductive radical-polar crossover: traditional electrophiles in modern radical reactions *Chem. Sci.*, **2019**, *10*, 8285–8291. [10.1039/C9SC03359A](https://doi.org/10.1039/C9SC03359A)

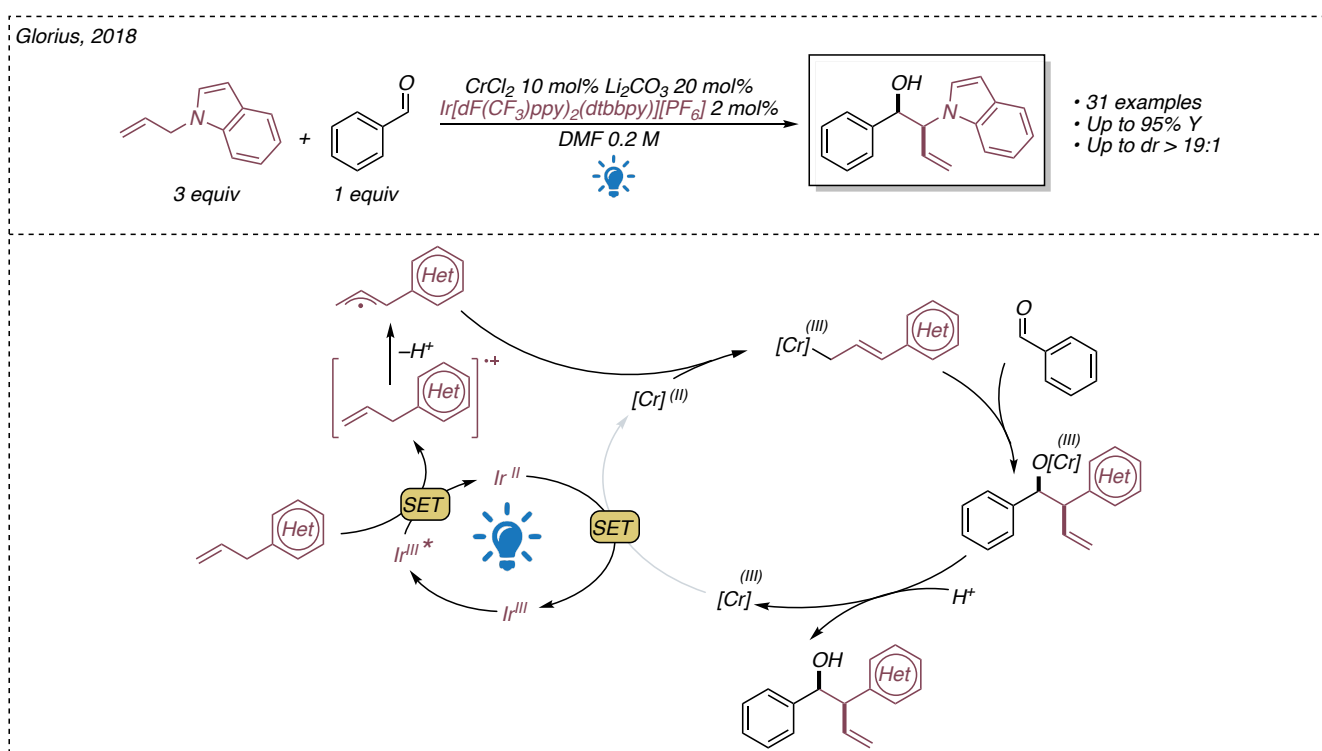
¹⁵² Schwarz, J. L.; Schäfers, F.; Tlahuext-Aca, A.; Lückemeier, L.; Glorius, F. Diastereoselective Allylation of Aldehydes by Dual Photoredox and Chromium Catalysis. *J. Am. Chem. Soc.* **2018**, *140* (40), 12705–12709. <https://doi.org/10.1021/jacs.8b08052>.

can be trapped by the air-sensitive Cr(II) employed in the reaction generating nucleophilic allylating Cr(III) species. According to the photophysical investigation, a reductive quenching of the excited state of $[\text{Ir}(\text{dF}(\text{CF}_3)\text{ppy})_2(\text{dtbbpy})][\text{PF}_6]$ in presence of the allyl radical source starts the reaction. ($E(\text{Ir}^{\text{III}*}/\text{Ir}^{\text{II}}) = 1.2 \text{ V vs. SCE}$). Remarkably, allyl(hetero)arenes were selected as substrates for the reaction thanks to their suitable oxidation potential.

Once formed, the C-centered radical cation can be rapidly deprotonated by the catalytic amount of base present in the reaction mixture. The allyl radical, according to the mechanism proposed is trapped by the chromium II species leading the formation of the transient nucleophilic allyl chromium III. This latter can perform a 1,2 nucleophilic addition in the presence of both aromatic and aliphatic aldehydes.

Subsequent chromium alkoxide hydrolysis would generate the desired unprotected homoallylic alcohol product and high-valent chromium III. This latter is supposed to restore the iridium catalytic cycle engaging a single electron transfer with the Ir II complex. ($E(\text{Cr}^{\text{III}}/\text{Cr}^{\text{II}}) = -0.51 \text{ V vs. SCE}$ while $E(\text{Ir}^{\text{III}}/\text{Ir}^{\text{II}}) = -1.37 \text{ V vs SCE}$)).

The good diastereoselectivity of the reaction can be described by a Zimmerman-Traxler transition state-controlled mechanism.

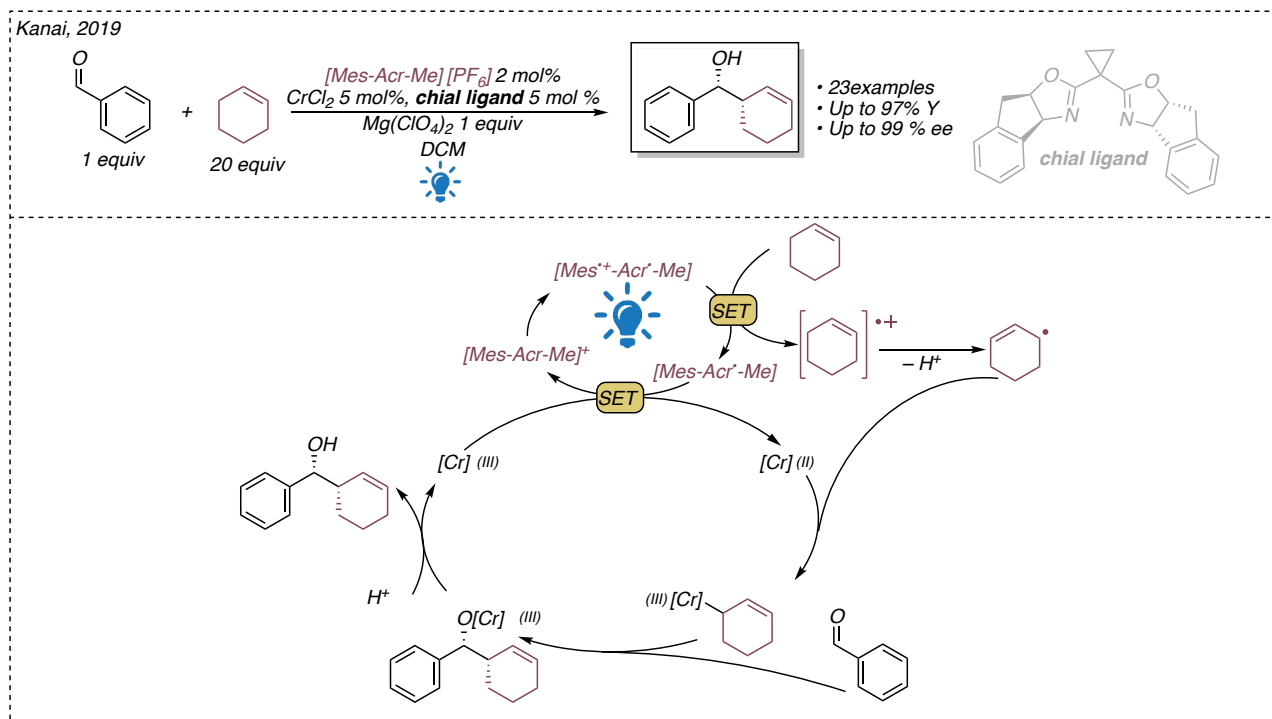


Chapter 1. Scheme 33 Cr/photoredox dual catalytic allylation of aldehydes reported by Glorius

The first enantioselective version of the same transformation was presented by Kanai and co-workers.¹⁵³ Remarkably, an amino-indanol- derived bis(oxazoline) was shown suitable to promote the reaction with

¹⁵³ Mitsunuma, H.; Tanabe, S.; Fuse, H.; Ohkubo, K.; Kanai, M. Catalytic Asymmetric Allylation of Aldehydes with Alkenes through Allylic C(Sp³)-H Functionalization Mediated by Organophotoredox and Chiral Chromium Hybrid Catalysis. *Chem. Sci.*, **2019**, *10*, 3459–3465. <https://doi.org/10.1039/C8SC05677C>

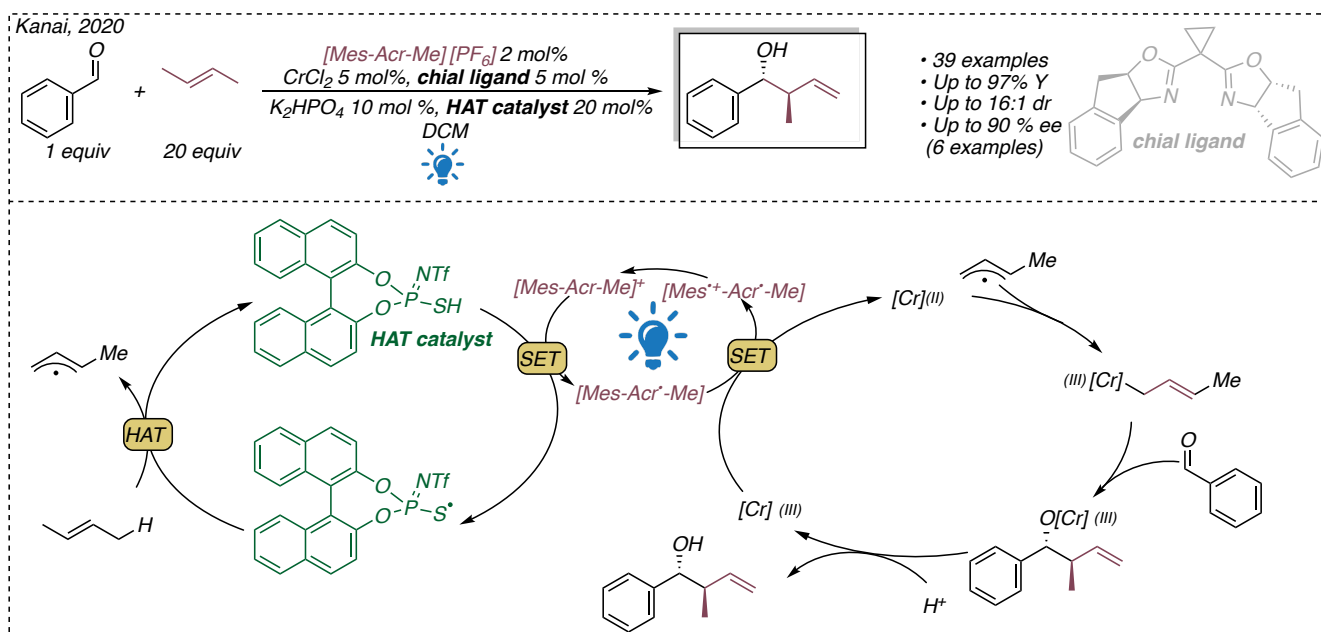
enantiomeric excesses up to 99%. Similarly, to the reaction conditions reported by Glorius, the use of $\text{CrCl}_2(\text{II})$ was preferred. In addition, selecting the Fukuzumi's acridinium salt as photocatalyst, the use of unactivated alkenes as pronucleophiles was allowed. ($E(\text{PC}^*/\text{PC}^{\bullet-}) = 2.06 \text{ V vs. SCE}$) A quite wide library of enantiomerically and diastereomerically enriched homoallylic alcohols, starting from readily available and stable substrates was achieved.



Chapter 1. Scheme 34 Enantioselective Cr/photoredox dual catalytic allylation of aldehydes reported by Kanai

Using an analogous photoredox cycle in the presence of a hydrogen-atom-transfer catalyst Kanai and co-workers were also able to extend the applicability of the protocol to various unactivated alkenes. Noteworthy, 1-butene, 2-butene and 3-methyl-1-butene were successfully employed as allylic precursors.¹⁵⁴ However, through these two methodologies, as well as in the protocol reported by Glorius, is still impossible to introduce the unsubstituted allyl moiety. The presence of a substituent on the sidechain still limits the scope of the reaction.

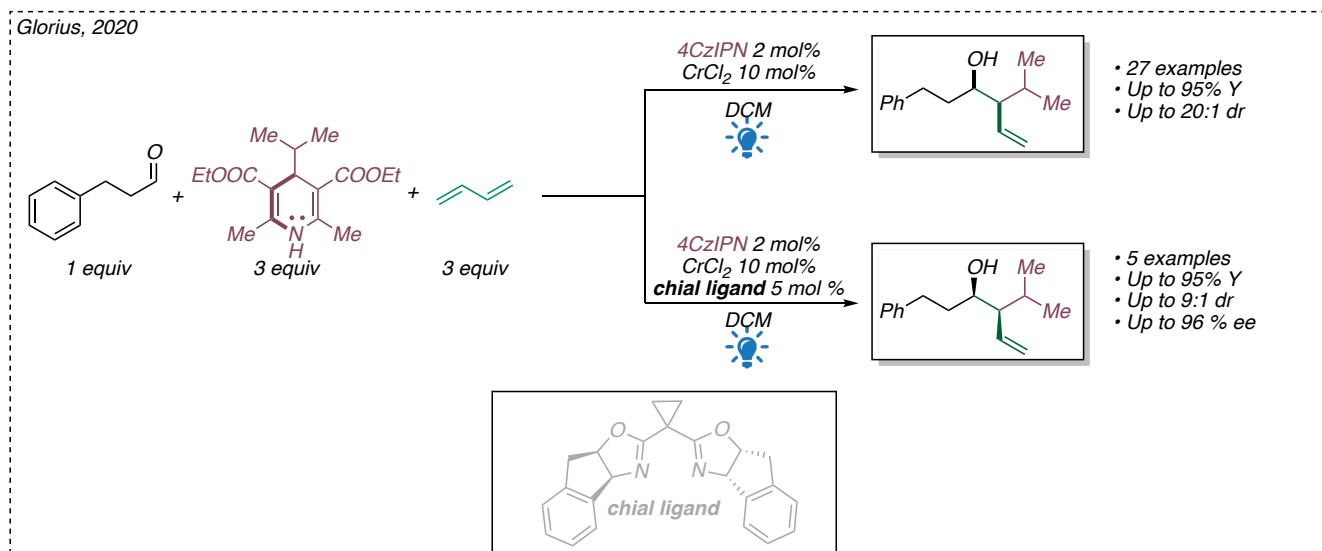
¹⁵⁴ Tanabe, S.; Mitsunuma, H.; Kanai, M. Catalytic Allylation of Aldehydes Using Unactivated Alkenes. *J. Am. Chem. Soc.* **2020**, *142* (28), 12374–12381. <https://doi.org/10.1021/jacs.0c04735>.



Chapter 1. Scheme 35 Enantioselective Cr/photoredox dual catalytic allylation of aldehydes reported by Kanai enabled by an HAT catalytic cycle

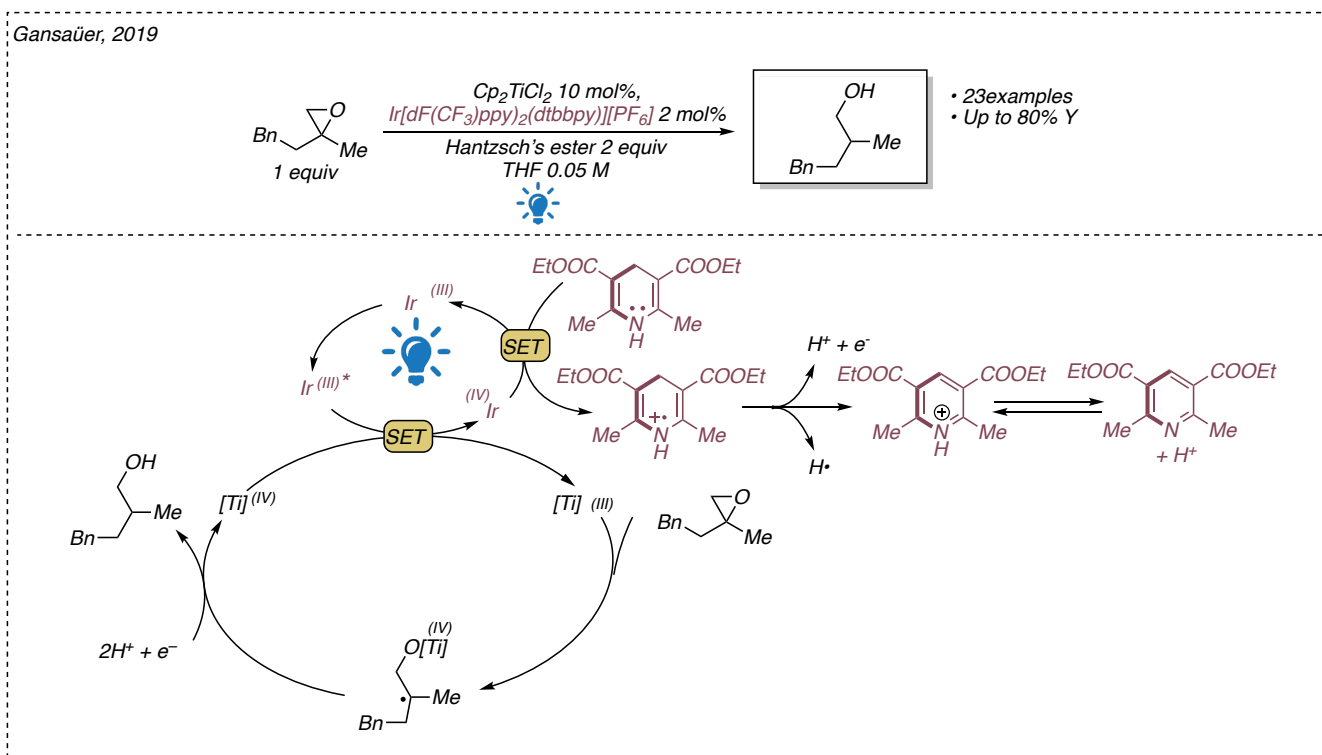
Quite recently, additional work was published in this area of research. Glorius reported a regioselective, diastereoselective, and enantioselective three-component dialkylation of substituted dienes with 4-alkyl-1,4-dihydropyridines and aldehydes, for the synthesis of homoallylic alcohols (**Scheme 36**). The organic photocatalyst employed in the reaction is 4CzIPN which, once in its excited state, is reduced by the dihydropyridine derivatives ($E(^*4CzIPN/4CzIPN^{\bullet-}) = +1.43$ V vs. SCE while $E(DHP^{\bullet+}/DHP) = +1.10$ V vs. SCE). 4CzIPN $^{\bullet-}$ is then able to reduce the chromium complex ($E(Cr^{III}/Cr^{II}) = -0.51$ V vs. SCE, while $E(4CzIPN/4CzIPN^{\bullet-}) = -1.21$ V vs. SCE). The addition of radicals formed by fragmentation of oxidized dihydropyridine derivatives occurred to the diene, and the so-formed allyl radical is trapped by Cr(II), giving the corresponding allylCr(III) chromium reagent. As in the previously described reactions, the steric induction is carried out by an amino-indanol-derived bis(oxazoline).¹⁵⁵

¹⁵⁵ Schwarz, J. L.; Huang, H.-M.; Paulisch, T. O.; Glorius, F. Dialkylation of 1,3-Dienes by Dual Photoredox and Chromium Catalysis. *ACS Catal.* **2020**, *10* (2), 1621–1627. <https://doi.org/10.1021/acscatal.9b04222>.



Chapter 1. Scheme 36 and enantioselective three-component dialkylation of substituted dienes with 4-alkyl-1,4-dihydropyridines and aldehydes, for the synthesis of homoallylic alcohols

Although recent publications remarked the low toxicity of chromium (II) and (III),¹⁵⁶ the synthetic exploitation of this metal in catalytic transformations remains doubtful. On the contrary titanium represents one of the most abundant and environmentally friendly metals. The first leading catalytic example of titanium in low oxidation state under photoredox conditions, was reported by Gansäuer and co-workers.



Chapter 1. Scheme 37 Epoxide ring opening allowed by Ti/photoredox dual catalysis reported by Gansäuer.

¹⁵⁶ Egorova, K. S.; Ananikov, V. P. Toxicity of Metal Compounds: Knowledge and Myths. *Organometallics* **2017**, *36* (21), 4071–4090. <https://doi.org/10.1021/acs.organomet.7b00605>.

In the presence of a quite broad variety of epoxides the metal-mediated ring-opening reaction was explored.¹⁵⁷

The generation of [Cp₂Ti(III)Cl] from [Cp₂Ti(IV)Cl₂] was shown to occur after oxidative quenching of the excited state of the photocatalyst (either Ir(III) or Ru(II)), employing a sacrificial hydrogen-atom donor (Hantzsch's ester HE; E(HE•+/ HE) = +1.0 V vs. SCE).

Using the same reaction mechanism and concept, Shi and coworkers reported the synthesis of spirocyclic compounds in the presence of 4CzIPN under visible light radiation.¹⁵⁸ Even if a proper photophysical investigation about the behavior of 4CzIPN in presence of the titanocene complex was not reported, the reaction is supposed to occur by the direct reduction of [Cp₂Ti(IV)Cl₂] and concurrent oxidative quenching of the photosensitizer. The titanium complex in low oxidation state, as previously reported by Gansäuer, reacts with the epoxides forming a nucleophilic C-centered radical, that is trapped by the π-system on the sidechain of the substrates triggering the cyclization.

Remarkably the Gansäuer Group expanded the combination of visible light and titanium chemistry exploiting the photochemical properties of titanocene complexes. Under green light irradiation [Cp₂TiCl₂] evolves into the electronically excited [Cp₂TiCl₂]*. This complex was shown able to promote an efficient photoredox reduction of epoxides and 5-exo cyclizations of suitably unsaturated epoxides in the presence of an organic reductant (DIPEA) employed as quencher of the reaction. The reductive quenching of the excited state of the titanocene dichloride leads to the transient formation of the titanocene monochloride in absence of external metal reductants.¹⁵⁹

To conclude, recently the Doyle group reported a thrilling example in which photoredox catalysis is combined with both a titanium and a nickel catalytic cycle.¹⁶⁰ A cross-coupling reaction between epoxides and (hetero)aryl iodides merging these three catalytic cycles has been developed.

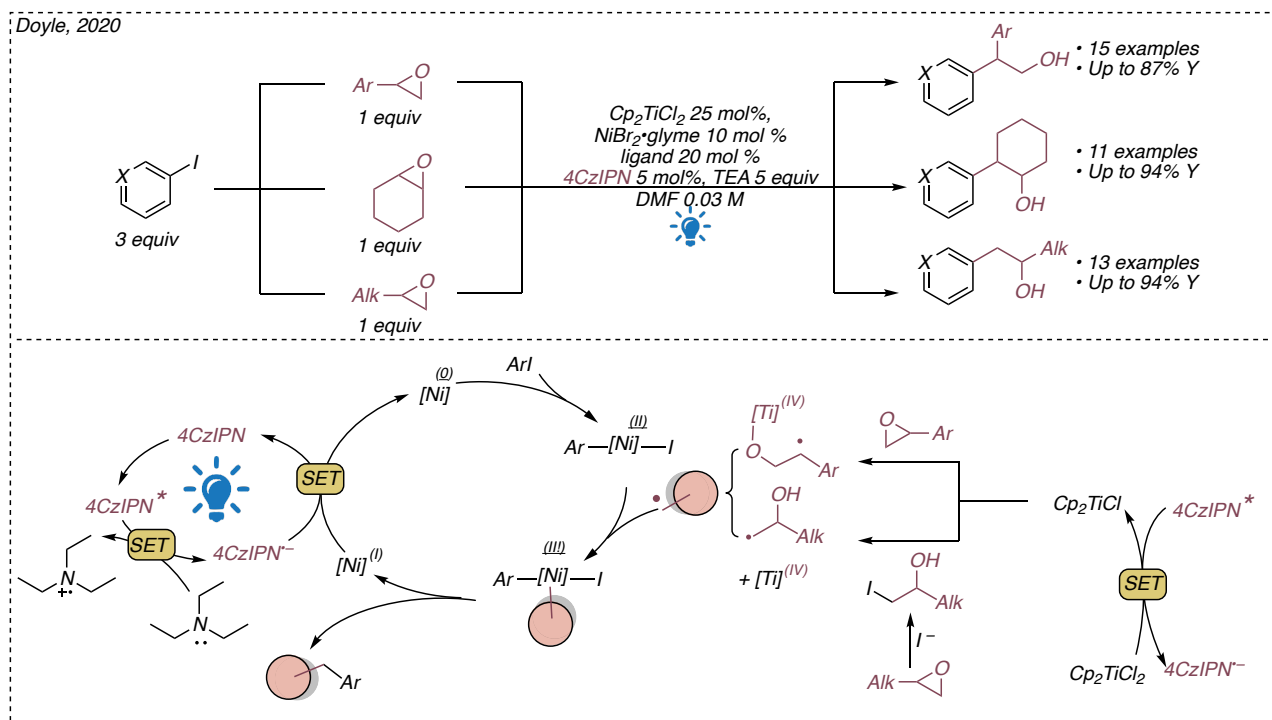
The reaction resulted suitable in presence of styrene oxides, cyclic epoxides, and terminal aliphatic epoxides and the desired product are isolated in moderate to good yields and high regioselectivity. Remarkably, the functionalization of the different classes of epoxides has been performed by appropriate modification of the selected ligand for the nickel precatalyst.

¹⁵⁷ Zhang, Z.; Richrath, R. B.; Gansäuer, A. Merging Catalysis in Single Electron Steps with Photoredox Catalysis—Efficient and Sustainable Radical Chemistry. *ACS Catal.* **2019**, *9* (4), 3208–3212. <https://doi.org/10.1021/acscatal.9b00787>.

¹⁵⁸ Lin, S.; Chen, Y.; Li, F.; Shi, C.; Shi, L. Visible-Light-Driven Spirocyclization of Epoxides *via* Dual Titanocene and Photoredox Catalysis. *Chem. Sci.* **2020**, *11* (3), 839–844. <https://doi.org/10.1039/C9SC05601G>

¹⁵⁹ Zhang, Z.; Hilche, T.; Slak, D.; Rietdijk, N. R.; Oloyede, U. N.; Flowers, R. A.; Gansäuer, A. Titanocenes as Photoredox Catalysts Using Green-Light Irradiation. *Angew. Chem. Int. Ed.* **2020**, *59* (24), 9355–9359. <https://doi.org/10.1002/anie.202001508>.

¹⁶⁰ Parasram, M.; Shields, B. J.; Ahmad, O.; Knauber, T.; Doyle, A. G. Regioselective Cross-Electrophile Coupling of Epoxides and (Hetero)Aryl Iodides *via* Ni/Ti/Photoredox Catalysis. *ACS Catal.* **2020**, *10* (10), 5821–5827. <https://doi.org/10.1021/acscatal.0c01199>.



Chapter 1. Scheme 38 Trial Ni/Ti/photoredox arylation of epoxide reported by Doyle

The optimized reaction conditions required 5 mol % 4CzIPN as organic photocatalyst, 10 mol % $[\text{NiBr}_2(\text{diglyme})]$ as precatalyst, 20 mol % of nitrogen-based ligand, 5 equivalents Et_3N as sacrificial reductant, and 25 mol % $[\text{Cp}_2\text{TiCl}_2]$ as a co-catalyst. After an extensive mechanistic investigation, two different reaction pathways are supposed to occur depending on the nature of the substrate involved. Supported by Stern–Volmer quenching studies, in both cases the excited state of 4CzIPN is oxidatively quenched by the titanocene complex (with a constant of quenching of $5.4 \times 10^8 \text{ M}^{-1}\text{s}^{-1}$). The so-formed $[\text{Cp}_2\text{Ti}(\text{III})\text{Cl}]$ in the presence of styrene oxide derivatives is able to perform a well-known ring-opening reaction. The radical intermediate reacts with the $\text{Ni}(\text{II})$ complex to form $\text{Ni}(\text{III})$ intermediate that releases the branched product after reductive elimination. The $\text{Ni}(\text{I})$ complex is reduced by $4\text{CzIPN}^{\bullet-}$ ($E(4\text{CzIPN}/4\text{CzIPN}^{\bullet-}) = -1.24 \text{ V vs SCE}$, while $E(\text{Ni}^{\text{I}}/\text{Ni}^0) = -1.17 \text{ V vs SCE}$), restoring both the nickel and the photoredox catalyst.

On the contrary, when terminal aliphatic epoxides are employed, the formation of a transient iodohydrin intermediate is supposed to occur. In this case, $[\text{Cp}_2\text{Ti}(\text{III})\text{Cl}]$ acts as a halogen atom abstractor, restoring the transition metal catalyst in the original oxidation state and leading the formation of a nucleophilic C-centered radical that is trapped into the nickel catalytic cycle.

Chapter 2. Aim of the Project

During my PhD course, the main purpose was the combination of the well-established principles of transition metal catalysis with photoredox and reductive radical polar cross-over catalysis. Albeit a tremendous number of synthetic methodologies have been presented in the literature over the past decade, a specific class of transformations has been identified for our investigation.

With the purpose of unveiling an area that until now has been almost unexplored, we have focused our attention on novel dual photoredox and transition metal-promoted protocols that involved the generation of transient nucleophilic organometallic species.

The generation of these species and their reactivity towards appropriate electrophiles were investigated. Catalytic nonvisible light driven methodologies that allow this kind of transformation also in enantioselective fashion are consolidated features in the carbon-carbon formation toolbox. However, Barbier-type transformations and analogous reactions are often accompanied by several problems which can be hardly overcome. The production of both toxic and metallic overstoichiometric wastes, the compulsory utilization of scavengers and the need to perform the reactions under harsh conditions represent the main issues.

Our main hypothesis envisaged that new dual transition metal and photoredox catalyzed protocols forming transient nucleophiles, could be the solution.

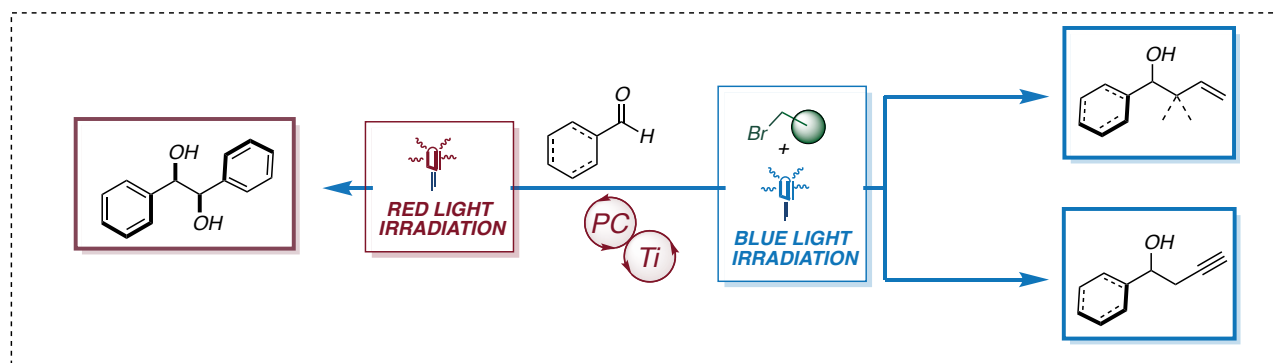
In order to develop methodologies that were as much as possible in accordance with the intrinsic principles of sustainability of photoredox catalysis, we tried to develop techniques that would involve the use of cheap and easy to synthesize organic dyes avoiding the use of rare metal-based complexes.

For the same reason, our aim was to use transition metal complexes that were earth-abundant, easy to handle, bench stable and, when possible, with a limited toxicity.

In the following chapters all the developed methodologies will be described in detail. The optimization process that led to maximize the efficiency of both the photoredox and the transition metal catalytic cycles; the range of applicability of the methodologies and the mechanistic investigations will be discussed for each case.

For the sake of clarity, the obtained results have been schematized in two chapters depending on the metal used to promote the transformations.

Chapter 3 is focused on the combination of photoredox and titanium catalysis for the functionalization of carbonyl compounds.

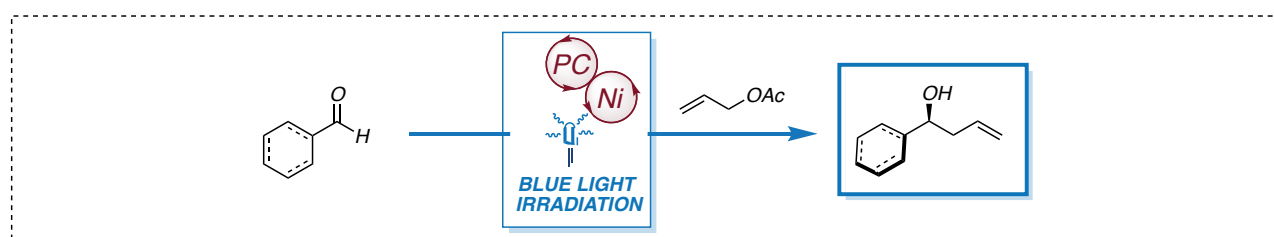


Chapter 2. Figure 1 Developed methodologies involving titanium and photoredox catalysis

In this case, during my PhD it was possible to develop three different powerful methodologies by exploiting the well-known activity of titanium in low oxidation state for the formation of transient nucleophilic species.

First, a Barbier-type allylation of aromatic and aliphatic aldehydes –catalytic in titanium– in the presence of a blue photon-absorbing organic dye will be presented. Following a parallel route, we were pleased to observe that the developed methodology could also be extended for the propargylation of aldehydes under analogous conditions. Finally, we were able to optimize a highly diastereoselective titanocene-catalyzed protocol for the pinacol coupling reaction of aromatic aldehydes promoted by a red-light absorbing organic dye. Remarkably, in relation to the latter methodology, preliminary results related to a highly enantioselective variant, developed employing a chiral Ti(Salen) complex will be discussed.

Moreover, **Chapter 4**, is dedicated to the exploitation of nickel catalytic protocols in a photoredox environment. Even if the major contribution in dual photoredox and nickel catalysis is devoted to the realization of cross-coupling-type reactions, we wanted to evaluate different possible scenarios. Our focus was on the possibility of exploiting intermediates arising from the oxidative addition of nickel complexes as transient nucleophilic species. After an extensive series of tests and a careful optimization of the reaction conditions, during my PhD one methodology was developed. The reported protocol involves, again, an allylation of aromatic and aliphatic aldehydes in the presence of a ruthenium-based photocatalyst and a nickel(II) complex with *o*-phenanthroline as a ligand. We were pleased to note that the reaction is suitable for promoting the formation of homoallylic alcohols with gratifying results.



Chapter 2. Figure 2 Developed methodologies involving nickel and photoredox catalysis

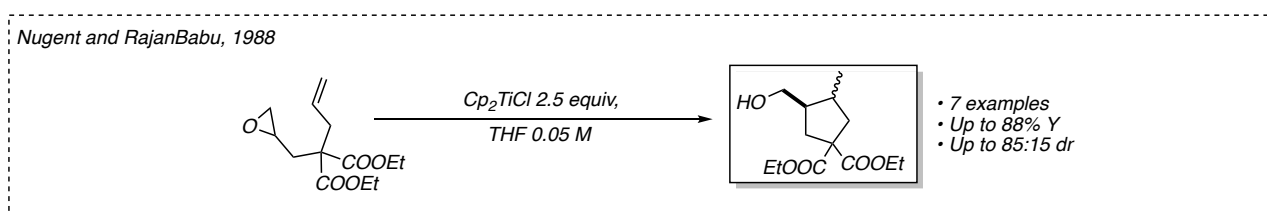
To our delight, after a radical modification of the previously proposed reaction conditions, it was possible to realize a highly enantioselective version of the reaction. Employing a bench stable nickel (II)

precatalyst, a chiral aminoindanol-derived bis(oxazoline) ligand and an organic dye, it was possible to obtain a wide gallery of homoallylic alcohols with high yields and enantiomeric excesses up to 94%.

Chapter 3. Functionalization of Carbonyl Compounds Enabled by Merging Photoredox and Titanium Catalysis

In the scenario of metal-mediated carbon-carbon or carbon-heteroatom bond forming reactions, the titanocene complexes in low oxidation state have occupied a privileged position over the years.¹⁶¹

The simplest member of this family is $[\text{Cp}_2\text{Ti}(\text{III})\text{Cl}]$ - also known as the Nugent-RajanBabu reagent. Although its structure and preparation had been known since the 1950s,¹⁶² the first landmark example of its utilization in a synthetic application was reported only in the late 80s.¹⁶³ An overstoichiometric amount of the transition metal complex was used to achieve a metal-induced radical cyclization of epoxyolefins.



Chapter 3. Scheme 1 Titanocene monochloride-induced radical cyclization of epoxyolefins by Nugent and RajanBabu

More than for the reported transformation, the work of Nugent and RajanBabu turned out to be a fundamental proof of concept explicating the main properties of titanocene monochloride: (i) obtainable from the bench stable $[\text{Cp}_2\text{TiCl}_2]$ upon single electron reduction ($E(\text{Ti}^{\text{IV}}/\text{Ti}^{\text{III}}) = -0.63 \text{ V vs. SCE}$);¹⁶⁴ (ii) high tolerance to different functional groups; (iii) enhanced reactivity in performing single-electron-transfer (SET) processes.

Considering the electronic configuration of the Nugent reagent, its highest occupied molecular orbital shows an unpaired *d* electron, that determines the chemical behavior of the transition metal complex.

Titanocene monochloride, indeed, exhibits a boosted reducing character.¹⁶⁵

This behavior together with the presence of a vacant site in the HOMO allows the coordination of a heteroatom with free valence electrons, enhancing the ability in promoting the single electron transfer event.

¹⁶¹ Rosales, A.; Rodríguez-García, I.; Muñoz-Bascón, J.; Roldan-Molina, E.; Padial, N. M.; Morales, L. P.; García-Ocaña, M.; Oltra, J. E. The Nugent Reagent: A Formidable Tool in Contemporary Radical and Organometallic Chemistry: The Nugent Reagent in Contemporary Chemistry. *Eur. J. Org. Chem.* **2015**, 2015 (21), 4567–4591. <https://doi.org/10.1002/ejoc.201500292>.

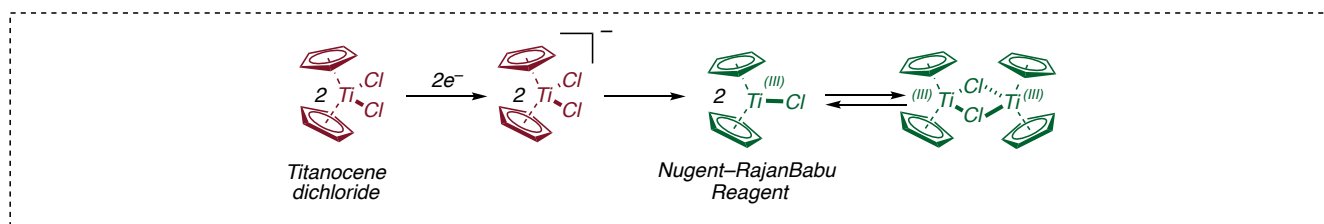
¹⁶² Birmingham, J. M.; Fischer, A. K.; Wilkinson, G. The Reduction of Bis-Cyclopentadienyl Compounds. *Naturwissenschaften* **1955**, 42 (4), 96–96. <https://doi.org/10.1007/BF00617242>.

¹⁶³ Nugent, W. A.; RajanBabu, T. V. Transition-Metal-Centered Radicals in Organic Synthesis. Titanium(III)-Induced Cyclization of Epoxy Olefins. *J. Am. Chem. Soc.* **1988**, 110 (25), 8561–8562. <https://doi.org/10.1021/ja00233a051>.

¹⁶⁴ Mugnier, Y.; Moise, C.; Laviron, E. Electrochemical Studies of Organometallic Compounds. *Journal of Organometallic Chemistry*, **1988**, 204, 61–66. [https://doi.org/10.1016/S0022-328X\(00\)82472-9](https://doi.org/10.1016/S0022-328X(00)82472-9)

¹⁶⁵ a) Enemaerke, R. J.; Larsen, J.; Skrydstrup, T.; Daasbjerg, K. Mechanistic Investigation of the Electrochemical Reduction of Cp_2TiX_2 . *Organometallics* **2004**, 23 (8), 1866–1874. <https://doi.org/10.1021/om034360h>. b) Daasbjerg, K.; Svith, H.; Grimme, S.; Gerenkamp, M.; Mück-Lichtenfeld, C.; Gansäuer, A.; Barchuk, A.; Keller, F. Mechanism of Titanocene Mediated Epoxide Opening: Experiment and Theory in Concert. *Angew. Chem. Int. Ed.* **2006**, 45, 2041–2044.

Remarkably, although the chemical and electrochemical properties of titanocene dichloride and monochloride have been highly exploited for synthetic applications, only recently it has been possible to provide quantitative data regarding the mechanism of the reduction of titanocene dichloride.¹⁶⁶



Chapter 3. Figure 1 Dimeric behavior of Nugent-reagent in organic solvent.

The maximization of the benefits of the Nugent-RajanBabu reagent has been achieved in the development of methodologies in which it is used in a catalytic fashion. In this context, the cornerstone was presented by Gansäuer and co-workers in 1997.¹⁶⁷

A titanocene-catalyzed pinacol coupling of aromatic aldehydes was reported employing a catalytic amount of $[\text{Cp}_2\text{Ti(IV)Cl}_2]$. The presence of an overstoichiometric amount of zinc as a terminal reductant leads the formation of transient Nugent-RajanBabu reagent that can promote the reaction. Henceforth, a tremendous number of protocols involving the catalytic use of titanocene dichloride to promote metal-mediated radical transformations in a reducing environment have been presented.¹⁶⁸

An exhaustive presentation of all the transformations accessible with these tools would be complex and beyond the scope of this discussion. In the next sections some pivotal examples will be described as a starting point for the development of protocols of our interest.

¹⁶⁶ Hilche, T.; Reinsberg, P. H.; Klare, S.; Liedtke, T.; Schäfer, L.; Gansäuer, A. Design Platform for Sustainable Catalysis with Radicals: Electrochemical Activation of Cp_2TiCl_2 for Catalysis Unveiled. *Chem. Eur. J.* **2021**, *27* (15), 4903–4912. <https://doi.org/10.1002/chem.202004519>.

¹⁶⁷ Gansäuer, A. Pinacol Coupling of Aromatic Aldehydes Catalysed by a Titanocene Complex: A Transition Metal Catalysed Radical Reaction. *Chem. Commun.* **1997**, *5*, 457–458. <https://doi.org/10.1039/a608438i>.

¹⁶⁸ Castro Rodríguez, M.; Rodríguez García, I.; Rodríguez Maecker, R. N.; Pozo Morales, L.; Oltra, J. E.; Rosales Martínez, A. Cp_2TiCl : An Ideal Reagent for Green Chemistry? *Org. Process Res. Dev.* **2017**, *21* (7), 911–923. <https://doi.org/10.1021/acs.oprd.7b00098>.

3.1 Photoredox Allylation of Aldehydes Catalytic in Titanium¹⁶⁹

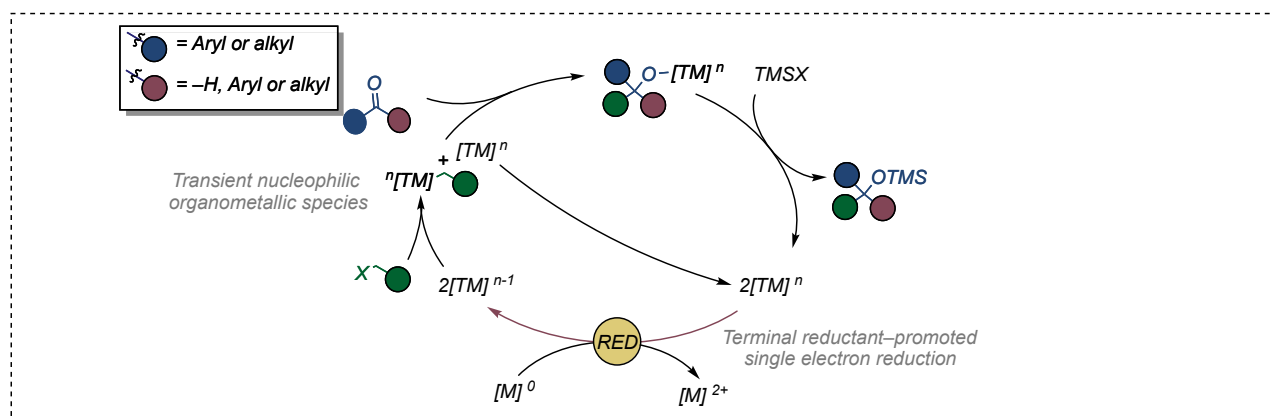
• Titanium-catalyzed Barbier-type allylation.

Allylation of aromatic and aliphatic aldehydes for the realization of libraries of homoallylic alcohols is a key strategy for the preparation of functionalized building blocks in the total synthesis of natural products.¹⁷⁰

The Barbier reaction, known since the end of the nineteenth century,¹⁷¹ is an organometallic reaction between an organohalide (chloride, bromide, iodide), a carbonyl group and a metal. Due to the crucial synthetic importance of this transformation, several metals have been demonstrated suitable to promote the reaction (*e.g.*, Bi, Pb, Zn, Cr and Sm).

Even if the reaction pathway can follow different routes,¹⁷² it is believed that the formation of the desired product is achieved by a transient organometallic species resulting from the interaction between the metal – acting as reducing agent – and the halide.

Formally, the generation of the active species requires two molecules of the metal complex in low oxidation state. The first molecule reduces the halide leading the formation of the C-centered radical that is, thus, trapped by the second molecule of transition metal complex forming the transient nucleophilic organometallic species. In presence of the suitable terminal reductant, it is possible to use catalytic amount of Barbier-active transition metal complexes.



Chapter 3. Figure 2 Catalytic transition-metal catalyzed Barbier-type reaction

¹⁶⁹ The results and the procedures described in this section are part of a published work:

Gualandi, A.; Calogero, F.; Mazzarini, M.; Guazzi, S.; Fermi, A.; Bergamini, G.; Cozzi, P. G. Cp₂TiCl₂-Catalyzed Photoredox Allylation of Aldehydes with Visible Light. *ACS Catal.* **2020**, *10* (6), 3857–3863. <https://doi.org/10.1021/acscatal.0c00348>.

S.G. and A.F. carried out the photophysical investigations, supervised by G.B.

The complete characterization of the products introduced hereafter and discussed in the section “Supplementary Data” can be found in the Supporting Information of the above-mentioned work

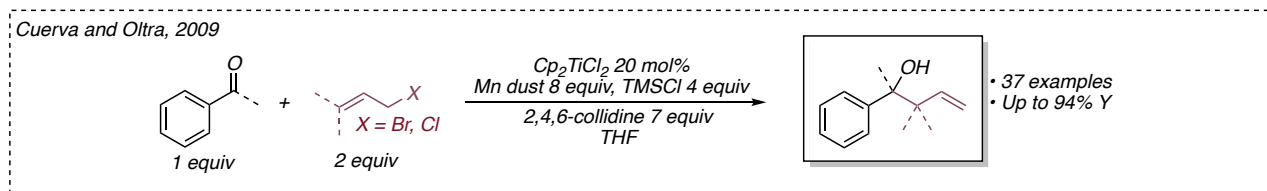
¹⁷⁰ (a) Yus, M.; Gonzalez-Gomez, J. C.; Foubelo, F. Diastereoselective Allylation of Carbonyl Compounds and Imines: Application to the Synthesis of Natural Products. *Chem. Rev.* **2013**, *113*, 5595–5698. <https://doi.org/10.1021/cr400008h> (b) Wang, P.-S.; Shen, M.-L.; Gong, L.-Z. Transition-Metal-Catalyzed Asymmetric Allylation of Carbonyl Compounds with Unsaturated Hydrocarbons. *Synthesis* **2018**, *50*, 956–967. DOI: 10.1055/s-0036-1590986 (c) Spielmann, K.; Niel, G.; de Figueiredo, R. M.; Campagne, J.-M. Catalytic Nucleophilic ‘Umpoled’ π-Allyl Reagents. *Chem. Soc. Rev.* **2018**, *47*, 1159–1173. <https://doi.org/10.1039/C7CS00449D> (d) Huo, H.-X.; Duvall, J. R.; Huang, M.-Y.; Hong, R. Catalytic Asymmetric Allylation of Carbonyl Compounds and Imines with Allylic Boronates. *Org. Chem. Front.* **2014**, *1*, 303–320 <https://doi.org/10.1039/C3QO00081H>.

¹⁷¹ Barbier, P. Synthesis of dimethylheptenol *C. R. Hebd. Seances Acad. Sci.* **1899**, *128*, 110

¹⁷² Moyano, A.; Perica's, M. A.; Riera, A.; Luche, J.-L. A Theoretical Study of the Barbier Reaction. *Tetrahedron Letters* **1990**, *31* (52), 7619–7622. [https://doi.org/10.1016/S0040-4039\(00\)97314-3](https://doi.org/10.1016/S0040-4039(00)97314-3).

Given the characteristics outlined above, titanocene complexes are particularly convenient for these transformations.

The first titanocene-catalyzed Barbier-type allylation was reported by Oltra and co-workers in 2009.¹⁷³ The authors disclosed that titanocene(III) complexes can catalyze both allylations, intramolecular crotylations and prenylations in the presence of wide range of aldehydes and ketones.



Chapter 3. Scheme 2 Titanocene-catalyzed Barbier-type allylation reported by Cuerva and Oltra in 2009

The reactions take place under mild conditions, providing good yields for linear and cyclic homoallylic alcohols, including heterocyclic derivatives. Although it certainly represents a noteworthy and powerful example, the reaction is accompanied by a tremendous production of hardly disposable wastes that are in deep contrast with the non-toxic nature of titanium complexes. To ensure good performances of the reaction, the Mn(0), employed as external reducing agent, must be at least forty times more than the titanium catalyst. Moreover, because titanium complexes are markedly oxyphilic, it is necessary that seven equivalents of collidine (35 times more than the catalyst) and four equivalents of TMSCl (20 times more than the catalyst) are present in the reaction mixture to release the product at the end of the catalytic cycle restoring the titanium (IV). These above presented issues, as well as being a problem for an eventual large-scale implementation, reduce the range of substrates compatible with the reported protocol.

¹⁷³ Estévez, R. E.; Justicia, J.; Bazdi, B.; Fuentes, N.; Paradas, M.; Choquesillo-Lazarte, D.; García-Ruiz, J. M.; Robles, R.; Gansäuer, A.; Cuerva, J. M.; Oltra, J. E. Ti-Catalyzed Barbier-Type Allylations and Related Reactions. *Chem. Eur. J.* **2009**, *15* (12), 2774–2791. <https://doi.org/10.1002/chem.200802180>.

• Presented work

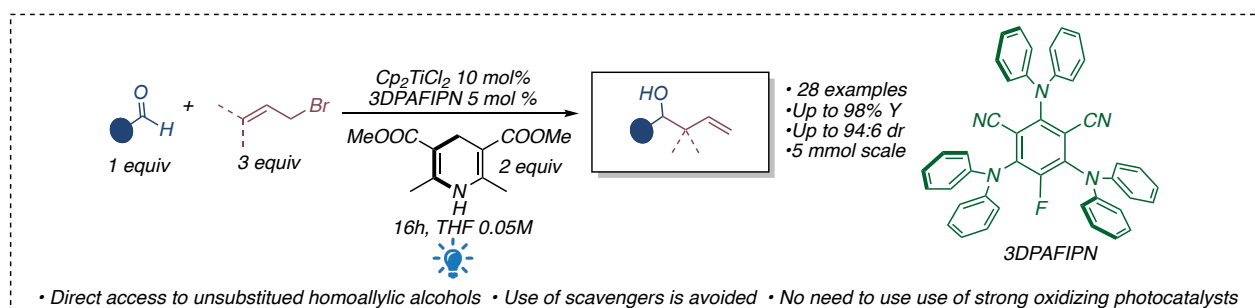
With the aim of overcoming the above-introduced limitations, during my PhD we focused on the development of a methodology merging photoredox and titanium catalysis for the generation of transient nucleophilic organometallic species.

We believed that the introduction of a photoredox system, replacing both the overstoichiometric external metal reductants and scavenger could represent an important breakthrough for the selective functionalization of aldehydes.

After a long and difficult optimization of the reaction conditions, *which will be discussed in detail in the next section*, it was possible to develop a practical and straightforward radical-polar crossover photoredox allylation of aldehydes mediated by titanium complexes.

The reaction uses 1,3-dicyano-5-fluoro-2,4,6-tris(diphenylamino)-benzene (3DPAFIPN) as organic photocatalyst. Careful photochemical investigations showed that under visible light irradiation 3DPAFIPN can reduce the titanocene complex promoting the reaction. The presence of a stoichiometric amount of Hantzsch's ester as the sacrificial reductant allows the access to a wide range of homoallylic alcohols in high yields. (**Scheme 3**)

In addition, the development of this new dual Ti/photoredox protocol also allows a further advancement over the previously reported aldehyde allylation methodologies promoted by the combination of a chromium and photoredox catalyst. Firstly, the unprecedented access to the synthesis of substituent-free homoallylic alcohols is permitted. Furthermore, the generation of the transient nucleophilic organotitanium reactant occurs through the interaction of titanium in a low oxidation state with a pronucleophile and not through radical trapping process. Thus, it was not necessary to use a photocatalyst that in its excited state behaves as a strong oxidant (*e.g.*, the Fukuzumi catalyst $E(PC^*/PC^{\cdot-})$ is +2.06 vs. SCE)). This made it possible to extend the generality of the process beyond the aryl substituted allylic precursors and to pave the way to the functionalization of oxidation-sensitive substrates.



Chapter 3. Scheme 3 Photoredox allylation of aldehydes catalytic in titanium

• Optimization of the reaction conditions

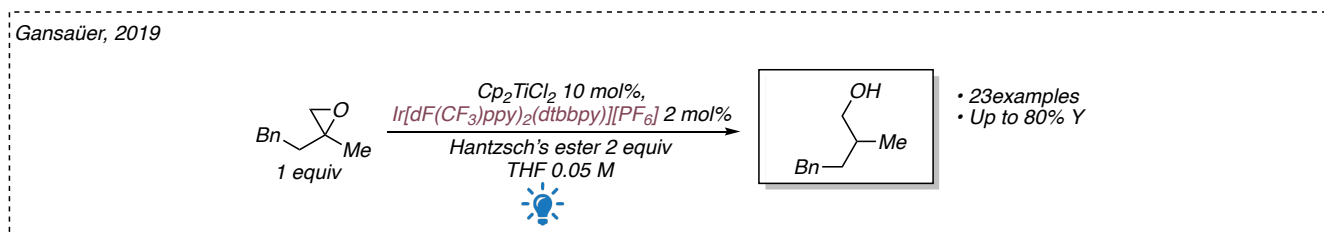
The access to the optimized reaction conditions was achieved only after a long and careful series of studies. To begin the reaction optimization and evaluate the feasibility of the project, dihydrocinnamic aldehyde (**1a**) was selected as model substrate, an excess of allyl bromide (**2a**) was chosen as pronucleophile and, in analogy with work reported by Oltra and Cuerva, titanocene dichloride was employed as catalyst to promote the reaction.

Considering the reduction potential of the titanium complex ($E(\text{Ti}^{\text{IV}}/\text{Ti}^{\text{III}}) = -0.63 \text{ V vs. SCE}$), this should allow the formation of the Nugent reagent in the presence of the most common photoredox systems. However, screening many combinations of photocatalysts and sacrificial agents, the translation of the allylation protocol into a dual photoredox fashion resulted difficult to achieve. At the beginning of our study, in all the conditions tested, it was never possible to obtain any trace of the formation of the desired product.

In the absence of positive results, we concluded that the fundamental problem was related to the titanium catalyst employed. $[\text{Cp}_2\text{TiCl}_2]$ is a deep red complex and can absorb the light radiation used to promote the reaction.

This characteristic, probably interfering with ability of the photocatalyst of absorbing the visible light, dramatically influenced all the preliminary experiments performed.

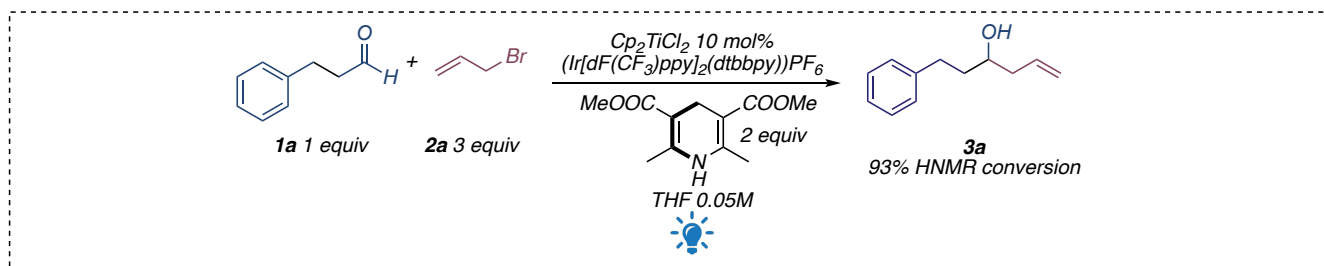
While we were trying to find a solution to avoid the deactivation of the photocatalyst during the reaction, Gansäuer and co-workers presented the previously introduced dual photoredox and titanium-mediated ring-opening reaction of epoxides, opening the way to the development of this technique.¹⁵⁷



Inspired by this work, we realized that some of the presented elements could be exploited to develop the first dual photoredox and titanium catalyzed allylation of aldehydes.

In line with our assumptions, in the work reported by Gansäuer, the catalytic loading of the titanium complex was reduced compared to non-visible light driven protocols (from 20% mol to 10% mol), in addition, to ensure a positive outcome of the reaction extremely diluted conditions were necessary.

Keeping this in mind, we decided to try to introduce the new reaction condition for the development of the protocol of our interest.



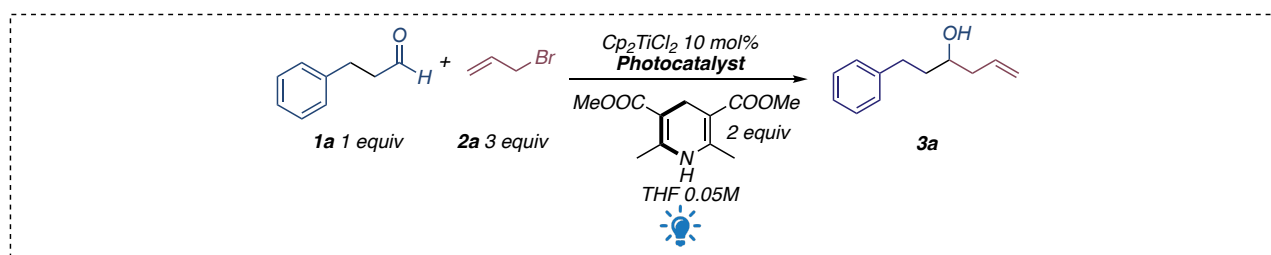
Fortunately, our evaluations proved to be correct and the allylation product of hydrocinnamic aldehyde **3a** could be obtained with satisfactory results.

Thanks to the fruitful collaboration with Prof. G. Bergamini's group of our department, the experimental evidence supporting our concentration-related hypothesis finds agreement with the photophysical data. $[\text{TiCp}_2\text{Cl}_2]$ presents an absorption band in the blue region of the spectrum ($\epsilon_{455\text{nm}} \approx 250 \text{ M}^{-1} \text{ cm}^{-1}$), thus high concentration of the red titanium complex, can prevent the photoinduced electron transfer absorbing a significant amount of the blue photons (*See the supplementary data of this section for the recorded absorption spectra of the reaction components*).

Having finally obtained satisfactory results, we continued the study of the reaction, trying to evaluate if it was possible to increase even more the reaction outcome.

Searching for the most appropriate reaction conditions, we were pleased to observe that, performing the reaction with a $[\text{TiCp}_2\text{Cl}_2]$ concentration of 0.005 M, different photocatalysts were able to promote the desired transformation (**Table 3.1.1**). This data are consistent with the reported redox properties of titanocene dichloride, and further demonstrate the effect of the concentration for the reaction outcome.

Even if the iridium-based photosensitizers was found efficient in promoting the transformation, we were pleased to observe that the employment of 5 mol % of 3DPAFIPN afforded total conversion and an extremely clean reaction.



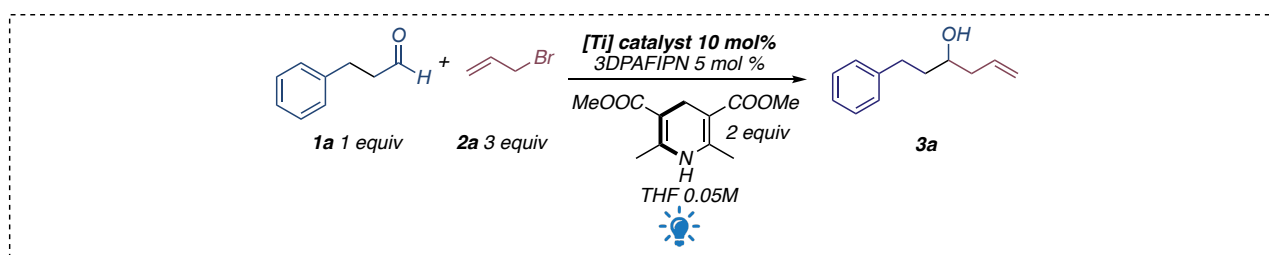
Entry ^[a]	Photocatalyst	Yield (%) ^[b]
1	-	0
2	3DPAFIPN	>99 (98) ^[c]
3 ^[d]	$(\text{Ir}[\text{dF}(\text{CF}_3)\text{ppy}]_2(\text{dtbbpy}))(\text{PF}_6)$	93
4	4CzIPN	45
5	$[\text{Ru}(\text{bpy})_3]\text{Cl}_2 \cdot 6\text{H}_2\text{O}$	0

Table 3.1.1: Screening of photocatalysts.

[a] Reaction conditions reported in the above figure on 0.1 mmol scale. [b] Determined by $^1\text{H-NMR}$ analysis. [c] Isolated yield after chromatographic purification, reaction performed on 0.2 mmol scale. [d] 1 mol% of the photocatalyst was used.

Since the organic dye has a maximum of absorption shifted towards higher wavelengths than the iridium complex, its use further minimizes the competition in absorption between the titanium catalyst and the photosensitizer.

These results allowed us to develop a methodology in which all the reagents could be obtained quickly, with a reduced overall cost and leading to the formation of the desired product in nearly quantitative yield. Pursuing the investigation of the reaction, different titanium complexes and salts were tested (**Table 3.1.2**) showing, in line with the work reported by Oltra, a lower efficiency compared to the cheap and available $[\text{Cp}_2\text{TiCl}_2]$.

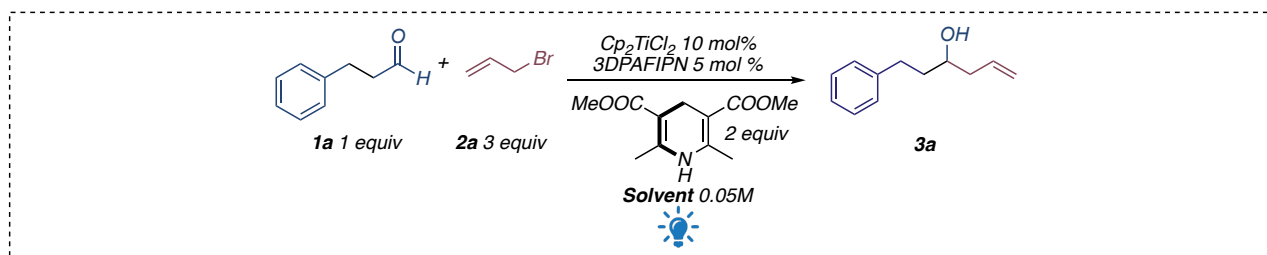


Entry ^[a]	Titanium source	Yield (%) ^[b]
1	$[\text{Cp}_2\text{TiCl}_2]$	>99 (98) ^[c]
2	$[\text{TiCl}_4]$	24
3	$[\text{CpTiCl}_3]$	15

Table 3.1.2 Screening of titanium sources.

[a] Reaction conditions reported in the above figure on 0.1 mmol scale. [b] Determined by ¹H-NMR analysis. [c] No *o*-phenanthroline was added. [c] Isolated yield after chromatographic purification, reaction performed on 0.2 mmol scale.

The screening of different organic solvent underlined the importance of THF in the reaction mixture, since many of the most commonly employed high polar solvents known to favor single electron transfer were found incompatible with our protocol.



Entry ^[a]	Solvent	Yield (%) ^[b]
1	THF	>99 (98) ^[c]
2	Toluene	60
3	MeCN	55
4	2MeTHF	39
5	DMF	0
6	DCM	0
7	MeOH	0
8	DMSO	0
9 ^[d]	THF	14
10 ^[e]	THF	0

Table 3.1.3 Screening of reaction solvent

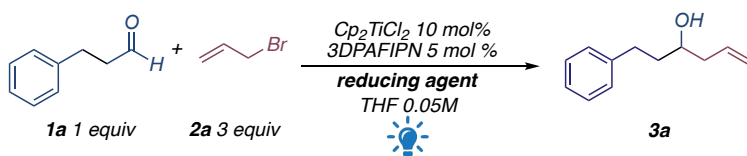
[a] Reaction conditions reported in the above figure on 0.1 mmol scale. [b] Determined by ¹H-NMR analysis. [c] Isolated yield after chromatographic purification, reaction performed on 0.2 mmol scale. [d] reaction performed with commercially available dry THF containing 250 ppm of BHT. [e] pump-freeze-thaw not performed.

Remarkably, the search for the most appropriate reaction solvent gave us the opportunity to appreciate the sensitivity of the protocol we were developing. It was also possible to find some insight on the mechanism through which the reaction proceeded.

Performing the reaction using dry THF commercially available containing 250 ppm of BHT (2,6-di-tert-butyl-4-methylphenol) to avoid the formation of peroxides a clear lowering of the yield has been observed. BHT, in fact, avoids the formation of peroxides by inhibiting the formation of radical species. Probably, the detrimental effect observed depends on the fact that the formation of the transient nucleophilic organometallic species, as usually happens for the reductive Barbier-type reaction, occurs through the formation of radical intermediates (*i.e.*, C-centered allyl radical that is intercepted by the titanium in the low oxidation state).

Similarly, performing the reaction without degassing the solvent, results in total deactivation of the system. This datum should be interpreted considering that molecular oxygen can behave as a highly efficient quencher of the excited state of the photosensitizer.

In light of these results, each reaction was carried out under both extremely anhydrous conditions and strictly inert atmosphere employing freshly distilled THF (each successful reaction was performed in oven-dried Schlenk tubes and subjected to three 30-second freeze-pump-thaw cycles before irradiation). Moreover, the role played by the Hantzsch's ester revealed crucial since the utilization of other tertiary amines as sacrificial reductants was found deleterious, giving practically no conversion. (**Table 3.1.4**).

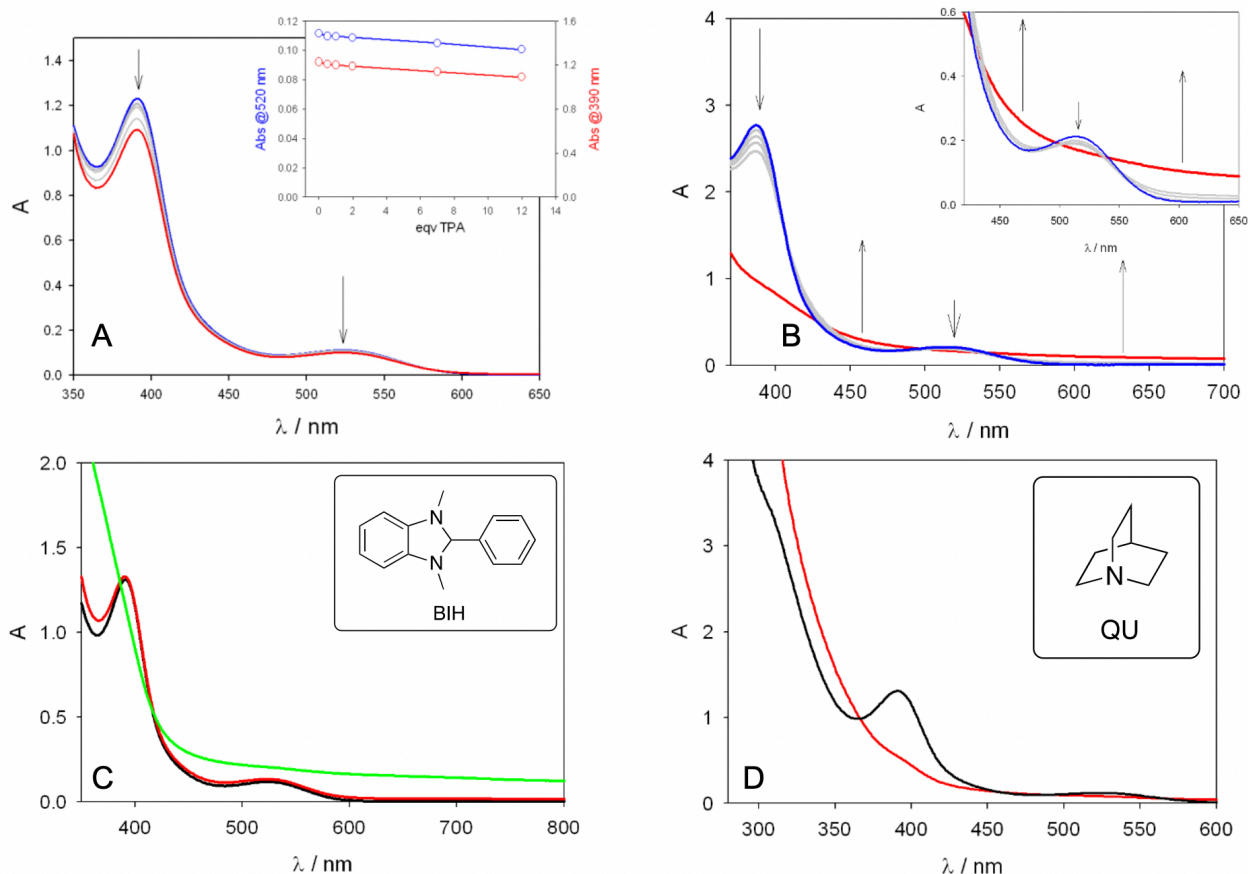


Entry ^[a]	Reducing agent	Yield (%) ^[b]
1	-	0
2	Triphenylamine	
3	BIH	0
4	DIPEA	
5	HE 1.2 equivalents	45
6	HE 2 equivalents	>99 (98) ^[c]

Table 3.1.4 Screening of reducing agents

[a] Reaction conditions reported in the above figure on 0.1 mmol scale. [b] Determined by ¹H-NMR analysis. [c] Isolated yield after chromatographic purification, reaction performed on 0.2 mmol scale.

In this regard, the stability of [Cp₂TiCl₂] in the presence of different amines was investigated.

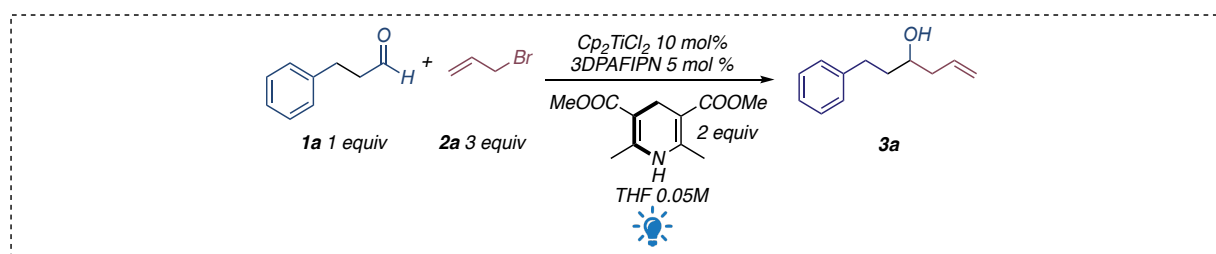


Chapter 3. Figure 3 A absorption spectra of a solution of [Cp₂TiCl₂] (ca. 0.72 mM, blue line) in air equilibrated CH₃CN recorded upon addition of increasing amounts of triphenylamine (TPA, from a 6.6 mM solution in CH₃CN. B: Evolution of absorption spectra recorded from a solution containing [Cp₂TiCl₂] and TPA (ca. 0.96 mM and 10 mM, respectively; blue line) in air-equilibrated CH₃CN at room temperature, upon irradiation with a blue-emitting LED strip (λ ≈ 460 nm). Total irradiation time ≈ 18 hours (red line). C: Absorption spectra of a solution of [Cp₂TiCl₂] (ca. 0.72 mM, black line) in air-equilibrated CH₃CN at r.t recorded upon additions of 1,3-dimethyl-2-phenyl-2,3-dihydro-1H-benzo[d]imidazole (BIH, 1.52 mM and 4.29 mM, red and green line, respectively). D: Absorption spectra of a solution of [Cp₂TiCl₂] (ca. 0.72 mM, black line) in air-equilibrated CH₃CN at r.t recorded upon addition of quinuclidine (QU, ca. 14.0 mM, red line).

As reported in figure, the bulky triphenylamine (TPA) does not interact with the titanium complex without irradiation, but absorption changes have been observed under visible light irradiation.

In a similar way, the addition of 1,3-dimethyl-2-phenyl-2,3-dihydro-1H-benzo[d]imidazole (BIH) and quinuclidine to a millimolar solution of $[\text{Cp}_2\text{TiCl}_2]$ even in absence of visible light irradiation caused changes in the absorption spectrum. We believed that these observed modifications can be attributable to ligand exchange between the titanium complex and the strongly coordinating nitrogen atom of the amines. From a practical point of view, (Table 3.1.5), the photocatalyst does not decompose and can be easily recovered at the end of the photoreaction by flash chromatography.

In conclusion, to our delight, replacing the previously employed 22W blue led strip with a more powerful 40W Kessil LED lamp¹⁷⁴ centered at 456 nm, it was possible to considerably reduce the reaction time and to scale the reaction up to 5 mmol without observing a decrease of the yield.



Entry ^[a]	Deviations from standard conditions	Yield (%) ^[b]
1	40 W Kessil® lamp 456 nm, 6 h	>99 (98) ^[c]
2	40 W Kessil® lamp 456 nm, 5 mmol scale	>99 (97) ^[c]
3	Allylchloride instead of allyl bromide	92
4	No $[\text{Cp}_2\text{TiCl}_2]$	0
5	No light	0
6	No degassed solvent	0
7	No photocatalyst, with irradiation at 380 nm	0
8	1 equivalent of TEMPO	0

Table 3.1.5 Salient aspect of optimization of the reaction conditions

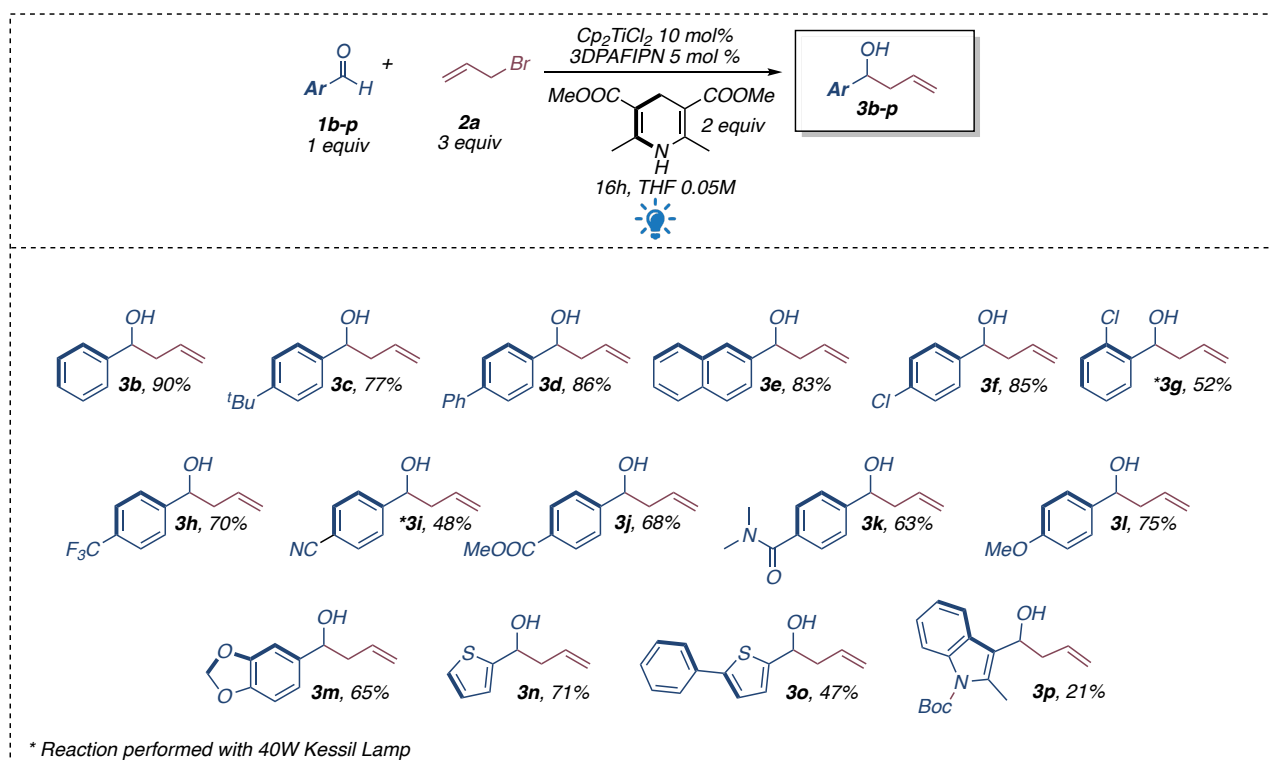
[a] Reactions performed on 0.1 mmol scale. [b] Determined by ¹H-NMR analysis. [c] Isolated yield after chromatographic purification, reaction performed on 0.2 mmol scale.

¹⁷⁴ <https://kessil.com/photoreaction/PR160L.php>

• Scope evaluation

After successfully optimizing the reaction conditions obtaining the allylation product of the model substrate **1a** in quantitative yields, we moved our attention to assess how tolerant the newly developed protocol was toward differently decorated substrates.

Aromatic aldehydes were the first class of molecules taken into analysis. Surveying the range of substrates, we were pleased to note that the dual photoredox/Ti protocol resulted widely applicable in the presence of several functional groups and the corresponding homoallylic alcohols could be obtained with yields from good to excellent. Interestingly, acidic NH groups were also tolerated although aliphatic or aromatic amines have been shown detrimental when employed as terminal reductant.



Chapter 3. Scheme 4 Allylation of aromatic aldehydes

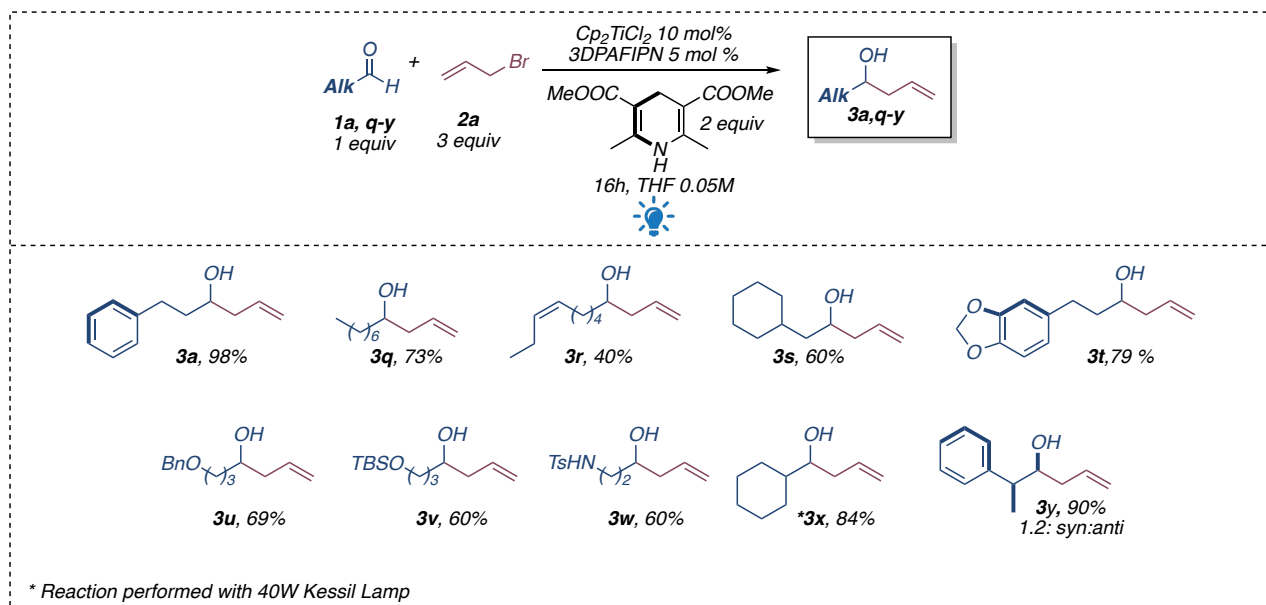
Even if the presence of electron-withdrawing groups slightly impacts on the isolated yields, commonly unreactive 4-(trifluoromethyl)benzaldehyde **1h** and 4-cyanobenzaldehyde **1i** can be employed in our protocol with a positive outcome. Remarkably, steric hindrance deriving from substituents in position 2-of the aromatic core hampers the reactivity of the reaction. To obtain the desired product from the 2-chlorobenzaldehyde (**1g**) in satisfactory yields the employment of the more powerful 40W 456nm centered Kessil lamp as light source was mandatory.

Moving our attention on aliphatic substrates, we noticed that differently substituted linear aldehydes are quite suitable and can be applied to the presented protocol.

In general, it was possible to appreciate that the reactivity of the new protocol towards aliphatic substrates is reduced and isolated yields for allylation products turned out to be slightly lower than for aromatic

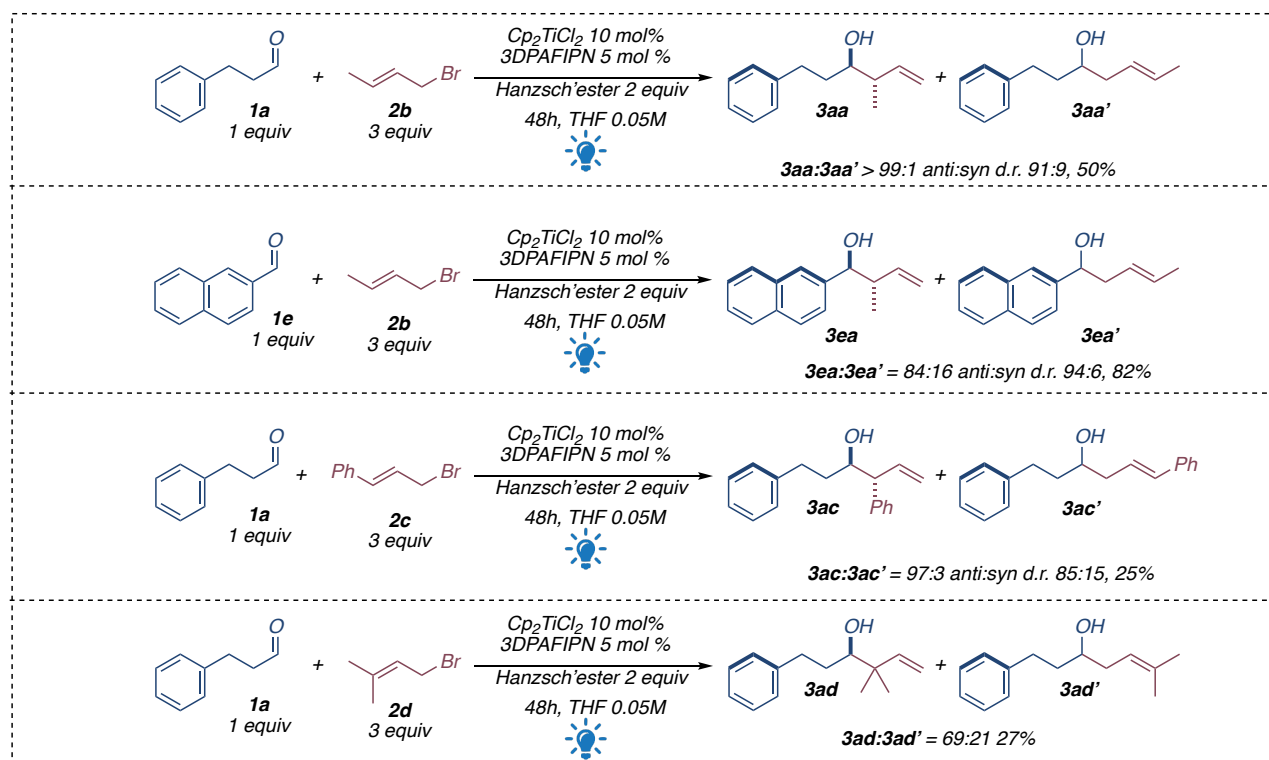
substrates. Interestingly, the best results were obtained when an aromatic ring was present on the aliphatic pendant, (**3a**, **3t**, **3y**) probably due to a possible noncovalent interaction with the metal center of the transient nucleophile.

However, even in this case, a good tolerance to different functional and protecting group is observed. Reaction with chiral aldehydes **1y** gave quite a moderate diastereoisomeric ratio, in favor of a Felkin-controlled allylation product. Interestingly, when branched aliphatic substrates, like cyclohexane carboxaldehyde (**1x**), were considered, irradiation with powerful Kessil lamp resulted mandatory.



Chapter 3. Scheme 5 Allylation of aliphatic aldehydes

After having envisioned the applicability of our protocol employing the simple and unsubstituted allyl bromide, we were curious to understand if allylating species bearing substituents in 3- position could be employed affording the desired product with good regioselectivity. As indicated by the preliminary results obtained, employing crotyl (**2b**), cinnamyl (**2c**) and prenyl bromide (**2d**), substituted pronucleophiles are in general less reactive under our dual photoredox condition. For this reason, an extension of the irradiation time was required.



Chapter 3. Scheme 6 Synergistic allylation reaction with substituted allyl Bromo derivatives

By selecting two aldehydes - one aromatic and one aliphatic - as model substrates, it was possible to observe the formation of the desired products with a marked branched selectivity and a satisfactory diastereomeric control. The predominant γ -regioselectivity observed is in line with the well-known crotyl-Ti(IV) and prenyl-Ti(IV) reactivity in non-light driven protocols.¹⁷⁵

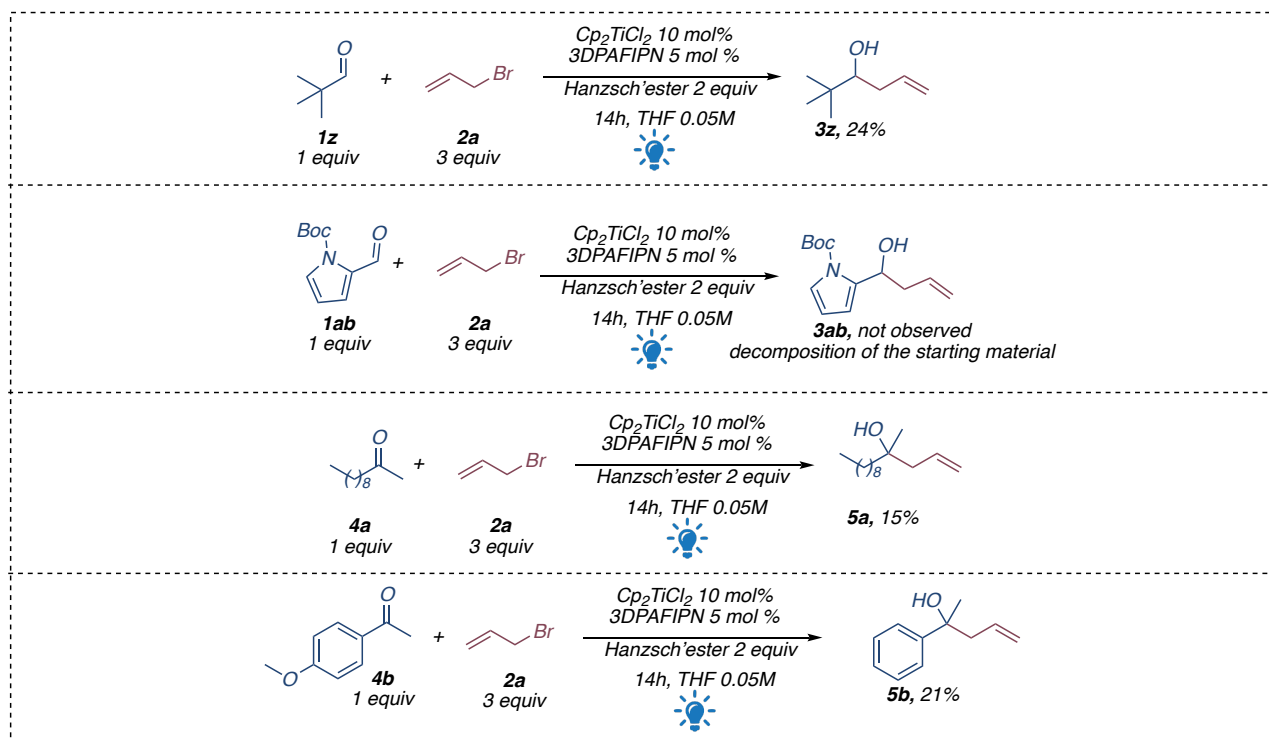
In addition, as the steric hindrance in γ -position of the chosen pronucleophilic species increased, it was possible to appreciate a clear decrease in reactivity. For this reason, using **2b** both in the presence of an aromatic and an aliphatic aldehyde it was possible to obtain the desired product with good yields, while introducing **2c** and **2d** in the reaction mixture, an effective drop in yield was appreciated. Interestingly, the introduction of more bulky allyl derivatives has an important effect also on the regioselectivity of the process.

Probably, as the size of the pronucleophilic species increases, the formation of the nucleophilic organotitanium species becomes less favored. This scenario would also justify parasitic processes that hampered the yield of the reaction.

During the overall exploration of the reaction scope, we also encountered some limitations. In the case of pivalic aldehyde, probably due to the steric hindrance adjacent to the carbonyl group, the reaction gave unsatisfactory results in terms of yield. Also ketones showed a quite reduced reactivity in this reaction

¹⁷⁵ Kasatkin, A.; Nakagawa, T.; Okamoto, S.; Sato, F. New, Efficient Method for the Synthesis of Allyltitanium Compounds from Allyl Halides or Allyl Alcohol Derivatives via Oxidative Addition. A Highly Efficient and Practical Synthesis of Homoallyl Alcohols. *J. Am. Chem. Soc.* **1995**, *117*, 3881–3882. <https://doi.org/10.1021/ja00118a030>

compared to aldehydes, the corresponding products were obtained in low yields, even using 40W Kessil lamp.



Chapter 3. Scheme 7 Poor reacting substrates

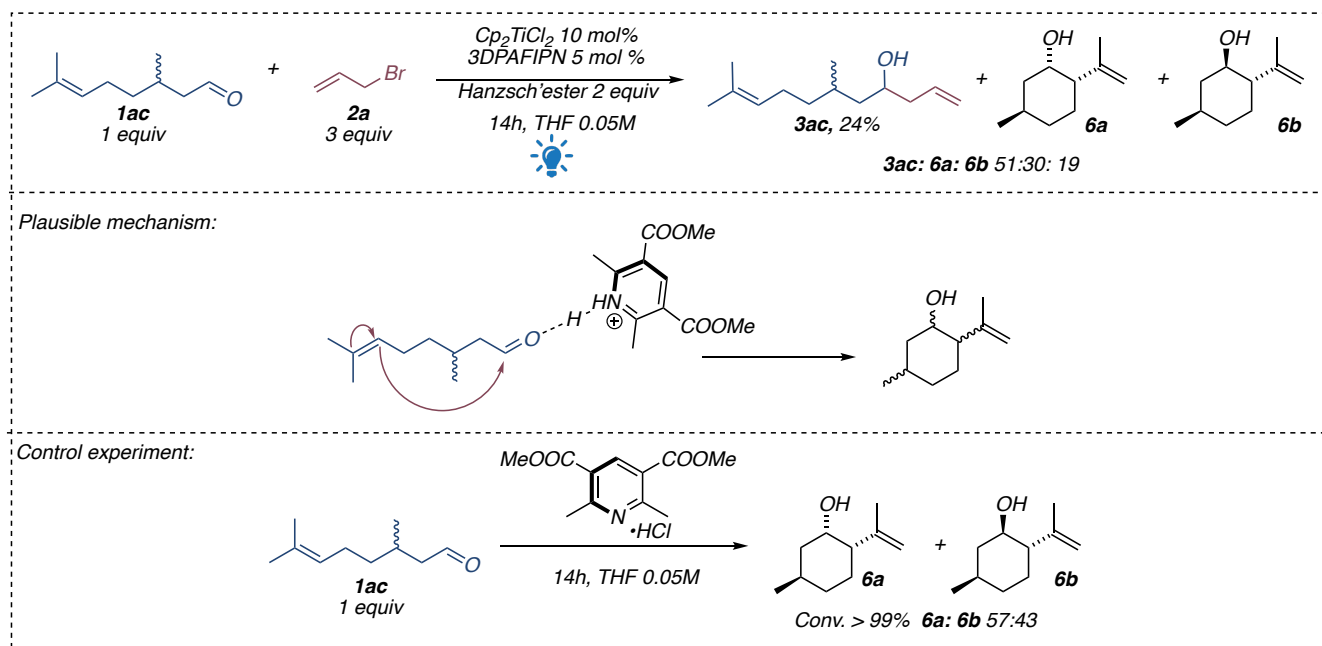
Moreover, since the Hantzsch's ester during the reaction is oxidized to the corresponding protonated pyridinium salt, the concomitant formation of H^+ forbids the use of acid sensitive substrates. Aldehydes bearing a pyrrole or indole cores, indeed, gave poor results due to decomposition promoted by the presence of Brønsted acids.

For the same reason, under the standard reaction condition *rac*-citronellal (**rac-1ac**) gave an inseparable mixture of desired product (**3ac**) and *rac*-neoisopulegol (**6a**) and *rac*-isopulegol (**6b**).

We assumed that cyclization occurred due to the presence in the reaction mixture of pyridinium salt derived from the oxidation of Hantzsch's ester favoring the activation of the double bond of the aldehyde. Our hypothesis was confirmed treating *rac*-**1ac** in the presence of one equivalent of pyridinium salt in THF for 14h. As expected, the reaction gave a mixture of *rac*-Isopulegol and *rac*-Neoisopulegol.

The acid catalyzed cyclization of citronellal to pulegol isomers, in addition, is a reported in literature and can be promoted by different catalysts.¹⁷⁶

¹⁷⁶ a) Vajglová, Z.; Kumar, N.; Mäki-Arvela, P.; Eränen, K.; Peurla, M.; Hupa, L.; Murzin, D. Y., Effect of Binders on the Physicochemical and Catalytic Properties of Extrudate Shaped Beta Zeolite Catalysts for Cyclization of Citronellal. *Organic Process Research & Development* **2019**, *23*, 2456-2463 <https://doi.org/10.1021/acs.oprd.9b00346>; b) Mikami, K.; Shimizu, M., Asymmetric ene reactions in organic synthesis. *Chem. Rev.* **1992**, *92*, 1021-1050; <https://doi.org/10.1021/cr00013a014> c) Lenardão, E. J.; Botteselle, G. V.; de Azambuja, F.; Perin, G.; Jacob, R. G., Citronellal as key compound in organic synthesis. *Tetrahedron* **2007**, *63*, 6671-6712. [10.1016/j.tet.2007.03.159](https://doi.org/10.1016/j.tet.2007.03.159)

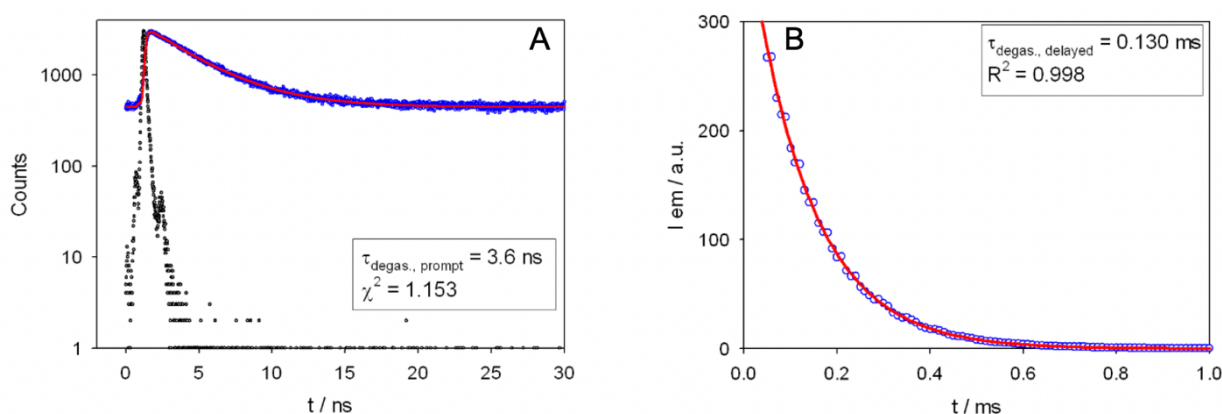


Chapter 3. Scheme 8 Reaction with citronellal

• Photophysical studies and reaction mechanism

In collaboration with the research group supervised by Prof. G. Bergamini, to evaluate the photoinduced mechanism of the reaction, we investigated the quenching of the photocatalyst's excited state in the presence of each of the components of the reaction. As reported for other cyanoarene-based photosensitizers,^{71,177} 3DPAFIPN possesses a very long emission lifetime in degassed solutions at room temperature (0.130 ms in THF at λ_{em} 520 nm).

Performing the Stern Volmer experiments, as assumed, the intensity of 3DPAFIPN emission do not change upon the addition – at the same concentrations used to perform the reaction – of allyl bromide and hydrocinnamic aldehyde. On the other hand, the addition of both Hantzsch's ester and $[Cp_2TiCl_2]$ induces strong changes in the emission intensity of the photocatalyst.

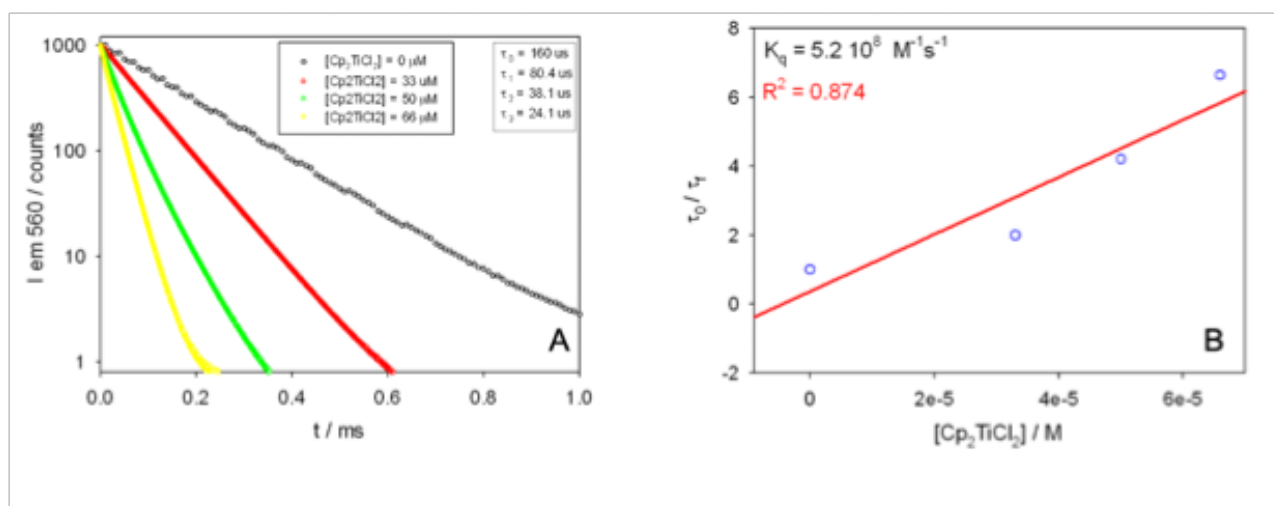


Chapter 3. Figure 4 A: prompt fluorescence decay of 3DPAFIPN in degassed THF (pump-freeze-thaw, 3 cycles; blue dots). The decay is fitted with a monoexponential function (red line); the instrument response function is also shown (black dots). $\lambda_{ex}=405$ nm, $\lambda_{em}=520$ nm. B: emission decay of 3DPAFIPN in degassed THF (pump-freeze-thaw, 3 cycles; blue dots). The decay is fitted with a monoexponential function (red line). $\lambda_{ex}=410$ nm, $\lambda_{em}=520$ nm; delay = 0.05 ms.

In particular, the quenching constants, determined from Stern–Volmer experiments, are 1.5×10^7 M⁻¹ s⁻¹ for the Hantzsch's ester and 5.2×10^8 M⁻¹ s⁻¹ for the titanium complex in degassed solutions.

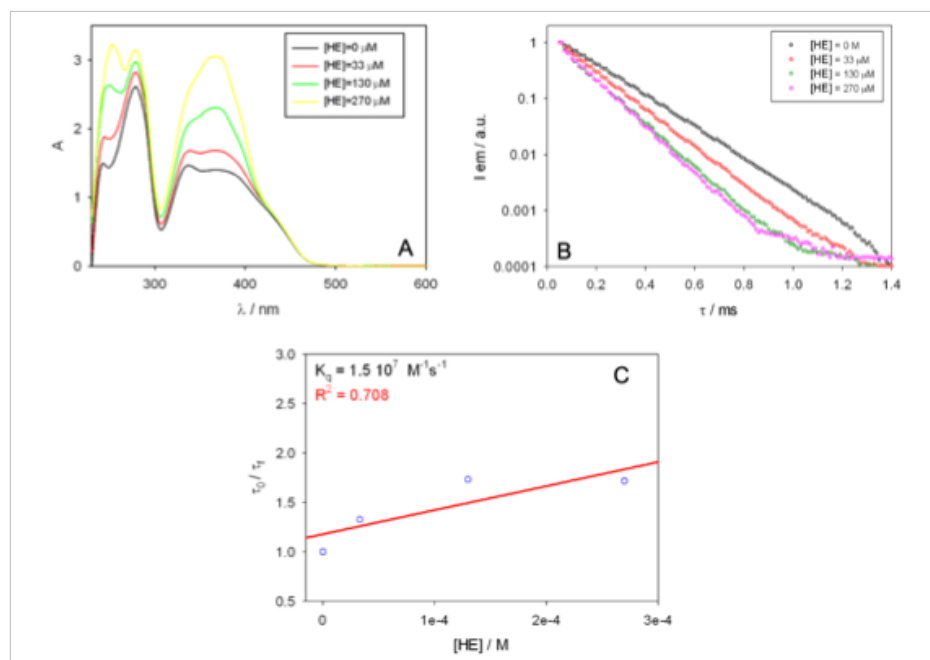
It is worth noting that, from a practical point of view, the Stern–Volmer plots deriving from the two redox active species of the reaction have been obtained evaluating different parameters. For the quenching experiments in presence of the titanium complex the variation of the lifetime (τ_0/τ) was monitored. $[Cp_2TiCl_2]$, indeed, due to its photophysical properties, can reabsorb the light emitted by 3DPAFIPN.

¹⁷⁷ (a) Wex, B.; Kaafarani, B. R. Perspective on Carbazole-Based Organic Compounds As Emitters And Hosts In TADF Applications. *J. Mater. Chem. C* **2017**, *5*, 8622–8653. DOI <https://doi.org/10.1039/C7TC02156A> (b) Berger, A. L.; Donabauer, K.; König, B. Photocatalytic Carbanion Generation From C–H Bonds – Reductant Free Barbier/Grignard-Type Reactions. *Chem. Sci.* **2019**, *10*, 10991–10996. DOI <https://doi.org/10.1039/C9SC04987H> (c) Meng, Q.-Y.; Schirmer, T. E.; Berger, A. L.; Donabauer, K.; König, B. Photocarboxylation of Benzylic C–H Bonds. *J. Am. Chem. Soc.* **2019**, *141*, 11393–11397. <https://doi.org/10.1021/jacs.9b05360>



Chapter 3. Figure 5 A: normalized emission decays of 3DPAFIPN in degassed THF (black dots) obtained upon addition of increasing amounts of [Cp₂TiCl₂] (up to ca. 65 M, yellow line). λ_{em} = 560 nm (λ_{ex} = 410 nm). B: Stern-Volmer plot relative to the emission lifetimes

On the other hand, in the case of Hantzsch's ester – due to the superposition of its emission with a pulsed laser source at 405 nm the emission intensity decay (I₀/I) was monitored.



Chapter 3. Figure 6 A: absorption spectra of solutions at r.t. of 3DPAFIPN in deoxygenated THF obtained upon addition of increasing amounts of Hantzsch's ester (up to ca. 0.27 mM, yellow line). B: normalized emission decays of 3DPAFIPN obtained from the same solutions at λ_{em} = 520 nm (λ_{ex} = 430 nm). C: Stern-Volmer diagram relative to the emission decays

To fully evaluate all the possible scenarios occurring during the reaction, we wanted to understand a possible role of the pyridine produced after the oxidation of the Hantzsch's ester in the photoinduced processes.¹⁷⁸ For this reason we also tested the quenching of 3DPAFIPN emission by this compound. To our delight, no quenching of the excited state of 3DPAFIPN was measured at any concentration of

¹⁷⁸ Bieszczad, B.; Perego, L. A.; Melchiorre, P. Photochemical C-H Hydroxyalkylation of Quinolines and Isoquinolines. *Angew. Chem., Int. Ed.* **2019**, *58*, 16878–16883. <https://doi.org/10.1002/anie.201910641>

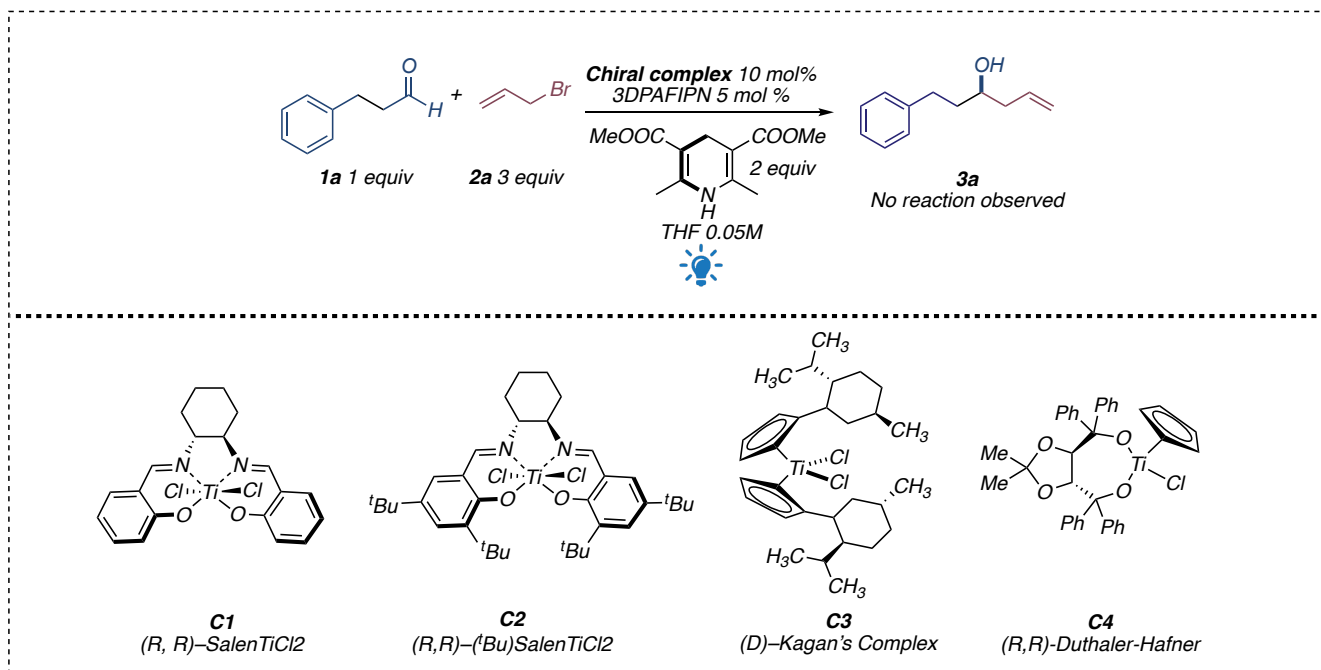
• Conclusions

In summary, a novel allylation photoredox methodology based on the use of the $[\text{Cp}_2\text{TiCl}_2]$ complex was optimized.

The reaction is extremely compatible with both aromatic and aliphatic substrates. The use of dilute conditions ($[\text{Ti}]$ 0.005 M) allowed the development of dual photoredox and titanium catalyzed reactions for the generation of transient nucleophilic organometallic species. From the point of view of a green chemistry perspective, the abundance and low toxicity of titanium make the procedure attractive for organic synthesis. Careful mechanistic studies have shed light on the application of 3DPAFIPN in accessing $[\text{Cp}_2\text{Ti(III)Cl}]$ reagent, avoiding the use of stoichiometric metal, such as Mn or Zn.

In comparison to the published titanium mediated allylation reaction, a minor percentage of titanium (10 vs 20 mol %) is necessary. No further scavengers or bases are necessary for the titanium complex since the proton derived from the oxidation of the Hantzsch's ester is able to restore the catalytic cycle acting as a scavenger.

The development of this new methodology also paves the way for a possible enantioselective variant. The investigation for its development was unfortunately only partially investigated during my PhD. Attempts to introduce chiral titanium complexes replacing titanocene dichloride have so far not led to any kind of results. Future studies within the research group will be devoted to such an ongoing exploration.



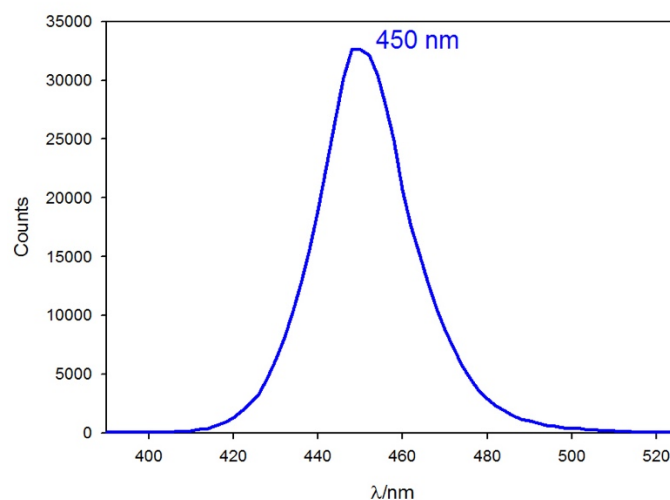
• Supplementary data

General methods and materials

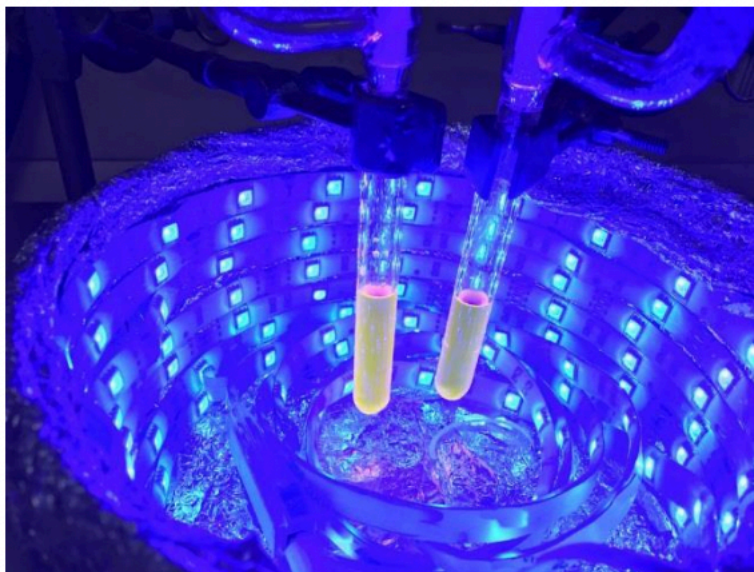
^1H -NMR spectra were recorded on Varian Mercury 400 spectrometer. Chemical shifts are reported in ppm from TMS with the solvent resonance as the internal standard (CDCl_3 ; $\delta = 7.27$ ppm). Data are reported as follows: chemical shift, multiplicity (s = singlet, d = duplet, t = triplet, q = quartet, dd = double duplet, dt = double triplet, bs = broad signal, m = multiplet), coupling constants (Hz). ^{13}C -NMR spectra were recorded on Varian MR400 spectrometer. Chemical shifts are reported in ppm from TMS with the solvent as the internal standard (CDCl_3 ; $\delta = 77.0$ ppm). GC-MS spectra were taken by EI ionization at 70 eV on a Hewlett-Packard 5971 with GC injection. LC-electrospray ionization mass spectra (ESI-MS) were obtained with Agilent Technologies MSD1100 single-quadrupole mass spectrometer. Chromatographic purification was done with 240-400 mesh silica gel. All reactions were set up under an argon atmosphere in oven-dried glassware using standard Schlenk techniques.

Anhydrous solvents were supplied by Aldrich in Sureseal® bottles and were used, unless otherwise noted, without further purification. All the reagents were purchased from commercial sources (Sigma-Aldrich, Alfa Aesar, Fluorochem, Strem Chemicals, TCI) and used without further purification unless specified.

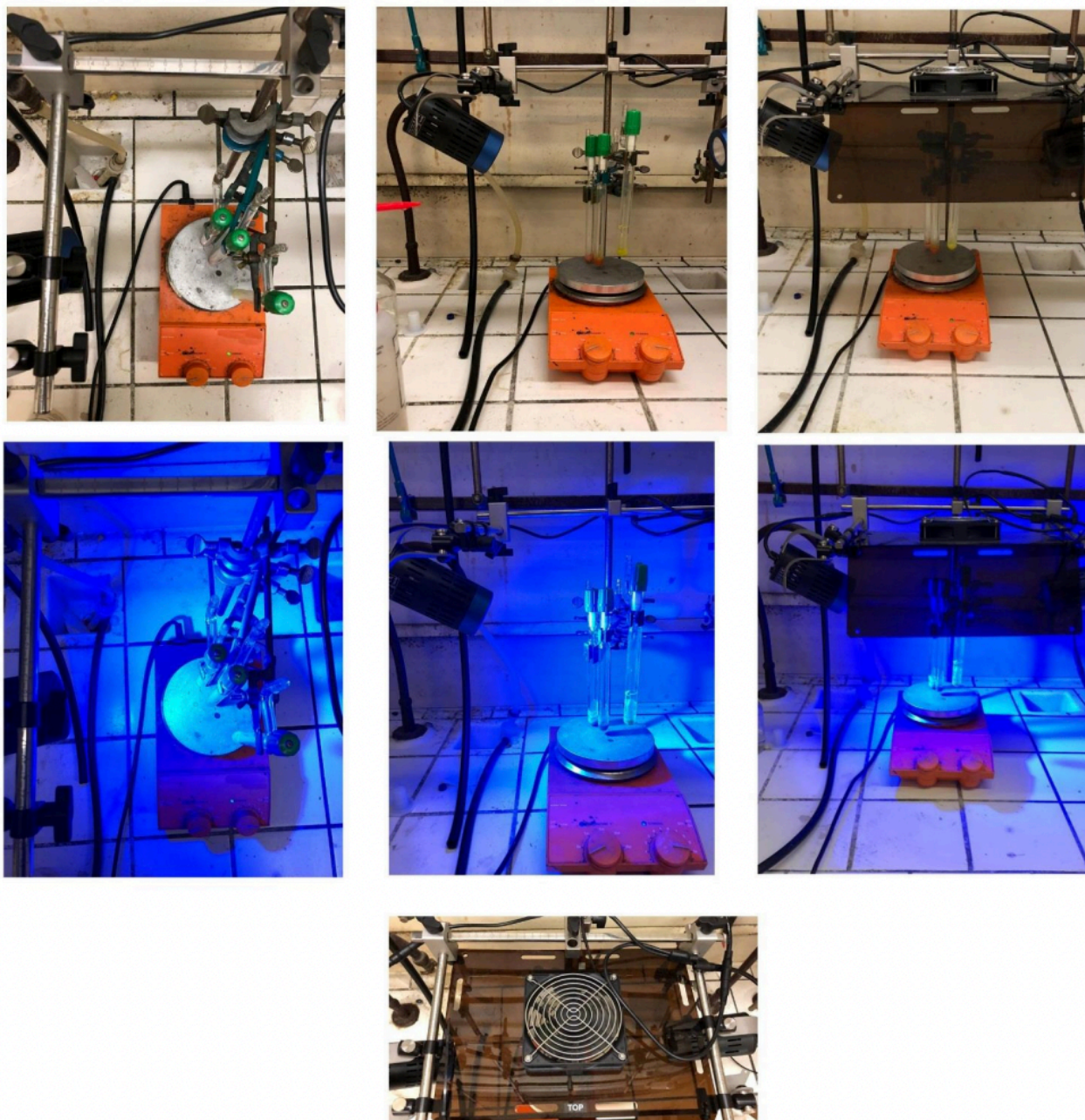
Reaction mixture was irradiated with 16 W blue LEDs strip or Kessil® PR160L@456 nm.



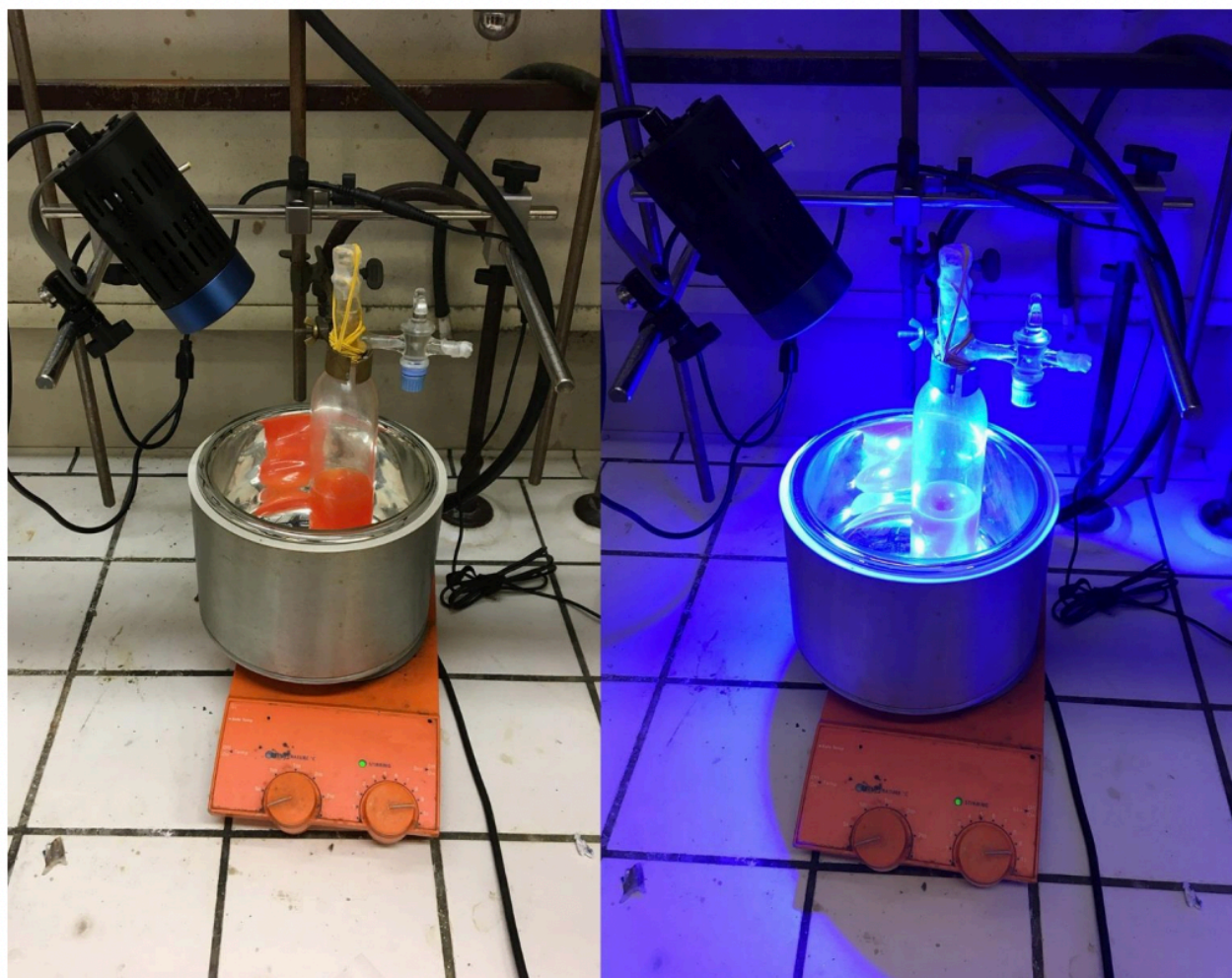
Chapter 3. Supplementary 1 Emission profile of the 16w blue led strip used to irradiate the solutions.



Chapter 3. Supplementary 2 The reaction temperature was close to room temperature during the irradiation as measured with a thermometer at 2 cm from reaction flask



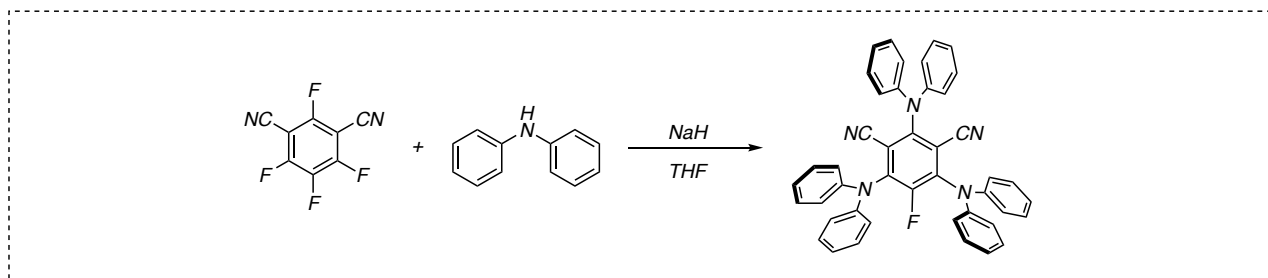
Chapter 3. Supplementary 3 Reaction set-up with Kessil® PR160L@456 nm lamp. The reaction flasks were positioned approximately at 18 cm from the light source and Kessil® PR160 Rig with Fan Kit1 was used to control the temperature. The reaction temperature was close to room temperature



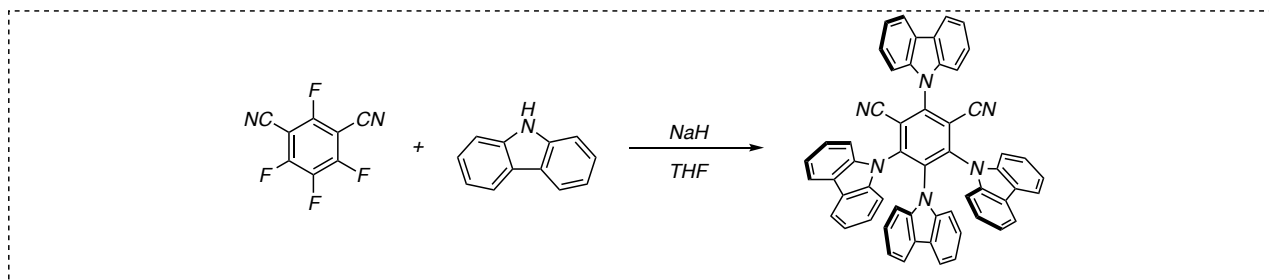
Chapter 3. Supplementary 4 Reaction set-up with Kessil® PR160L@456 nm lamp for 5 mmol scale.

Synthesis and characterization of the photocatalysts

Synthesis of 1,3-dicyano-2,4,5,6-tetrakis(diphenylamino)-benzene (3DPAFIPN)



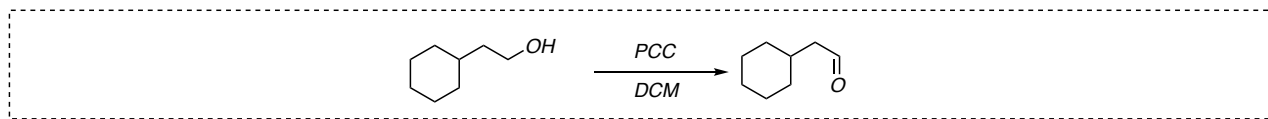
To a 50 mL round-bottom-flask was added diphenylamine (5.0 eq., 10 mmol, 1.69 g) and dry THF (20 mL). The solution was cooled down to 0 °C and NaH (60% in mineral oil) (7.5 eq., 15 mmol, 600 mg) was slowly added under vigorous stirring. After 2 hours tetrafluoroisophthalonitrile (1.0 eq., 2 mmol, 400 mg) was added and the mixture was stirred at room temperature. The solution slowly turned from colorless to dark brown. When the TLC showed a complete consumption of the starting material (usually 2 days are needed), water (1 mL) was added to neutralize the excess of NaH and the mixture was evaporated to give a yellow solid. The residue was purified by flash chromatography (cHex/AcOEt 2/1) to obtain 3DPAFIPN as bright yellow solid 80% yield. Spectroscopic data are in agreement with those reported in the literature.⁷¹

Synthesis of 2,4,5,6-tetrakis(carbazol-9-yl)-4,6-dicyanobenzene (4CzIPN)

To a 50 mL round-bottom-flask was added carbazole (5.0 eq., 10 mmol, 1.67 g) and dry THF (20 mL). The solution was cooled down to 0 °C and NaH (60% in mineral oil) (7.5 eq., 15 mmol, 600 mg) was slowly added under vigorous stirring. After 2 hours tetrafluoroisophthalonitrile (1.0 eq., 2 mmol, 400 mg) was added and the mixture was stirred at room temperature overnight. A yellow precipitate progressively appeared. When the TLC showed a complete consumption of the starting material water (1 mL) was added to neutralize the excess of NaH and the mixture was evaporated to give a yellow solid. The solid was successively washed with water and ethanol to afford the product in 69% yield. The spectroscopic data are in agreement with those reported in the literature.⁷¹

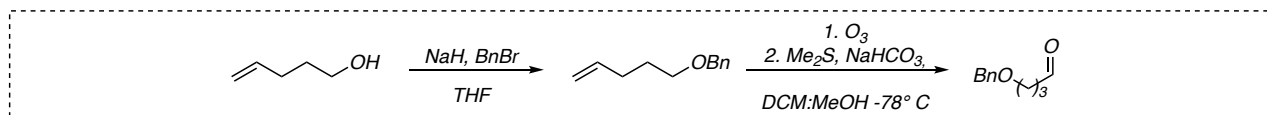
Synthesis and characterization of the substrates

Synthesis of aldehyde 1s



To a solution of cyclohexylethanol (0.300 g, 2.34 mmol) in CH₂Cl₂ (60 mL) was added pyridinium chlorochromate (0.774 g, 3.56 mmol) and stirred at room temperature overnight. The reaction mixture was diluted with diethyl ether (50 mL) and stirred at room temperature for 1 h. The mixture was filtered through a pad of Celite® and silica gel more times until the solution became colorless. The filtrate was carefully concentrated to dryness to give 2-cyclohexylacetaldehyde in quantitative yield. Spectroscopic data are in agreement with those reported in the literature.¹⁸¹

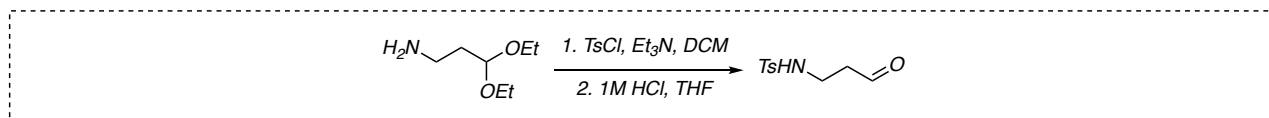
¹⁸¹ Babu, Y. S.; Kotian, P. L.; Kumar, V. S.; Wu, M.; Lin, T. BIOCRYST PHARMACEUTICALS, INC. WO2011/31554, 2011, A2.

Synthesis of aldehyde **1u**

To a suspension of NaH (60% in mineral oil, 426 mg, 10.7 mmol, 1.1 equiv.) in dry THF (10 mL), 4-penten-1-ol (1 mL, 9.7 mmol) was slowly added at 0°C. The mixture was left stirring at room temperature for 2 hours. Benzyl bromide (1.27 mL, 10.6 mmol, 1.1 equiv.) was added at 0°C and the reaction mixture was stirred at room temperature overnight. After the consumption of the starting material, the mixture was quenched with H₂O (5 mL) and the aqueous phase extracted with Et₂O (3 x 10 mL). The combined organic phase dried over Na₂SO₄ and concentrated to obtain a yellow oil. The residue was dissolved in a mixture of DCM/MeOH 3/1 (40 mL), cooled down to -78°C and ozone was bubbled until the mixture turned blue. Oxygen was then bubbled for few minutes and dimethyl sulfide (2.3 mL, 31 mmol, 3.2 equiv.) and sodium bicarbonate (2.44 g, 30 mmol, 3 equiv.) were added. The suspension was warmed to room temperature overnight, then filtered on Celite® and the solvents removed under reduced pressure. The crude was purified by flash column chromatography (cHex/AcOEt 10/1) to obtain **1u** as colorless oil 68% yield (6.6 mmol, 1.2 g).¹⁸²

¹⁸² Koyanagi, T.; Leriche, G.; Onofrei, D.; Holland, G. P.; Mayer, M.; Yang, J. Cyclohexane Rings Reduce Membrane Permeability to Small Ions in Archaeal-Inspired Tetraether Lipids *Angew. Chem. Int. Ed.* **2016**, *55*, 1890-1893. <https://doi.org/10.1002/anie.201510445>

Synthesis of aldehyde 1w



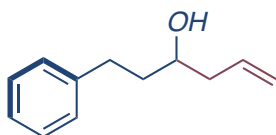
To a solution of 3,3-diethoxy-1-aminopropane (300 μL , 1.85 mmol) in DCM (8 mL) was added Et_3N (310 μL , 2.22 mmol, 1.2 equiv.). The solution was cooled to 0°C and *p*-toluenesulfonyl chloride (389 mg, 2.04 mmol, 1.1 equiv.) was carefully added. The resulting mixture was allowed to stir overnight at room temperature. The mixture was quenched with NH_4Cl sat. acq. (10 mL), the layers separated, and the aqueous phase was extracted with DCM (3 x 10 mL), dried over Na_2SO_4 , and concentrated to a brownish oil. Intermediate tosyl amide (255 mg, 0.85 mmol) was dissolved in THF (2 mL), treated with 1M HCl (850 μL , 1 equiv.) and stirred at room temperature for 2.5 hours. After that the reaction mixture was extracted with AcOEt (3 x 10 mL), the combined organic phases were washed with brine (5 mL), dried over Na_2SO_4 and concentrated to obtain a brownish oil. The crude was further purified by flash column chromatography (cHex/AcOEt 8/2). **1w** was obtained as brown oil, 51% yield (0.44 mmol, 99 mg). Spectroscopic data are in agreement with those reported in the literature.¹⁸³

¹⁸³ Jui, N. T.; Garber, J. A. O.; Finelli, F. G.; MacMillan, D. W. C. Enantioselective Organo-SOMO Cycloadditions: A Catalytic Approach to Complex Pyrrolidines from Olefins and Aldehydes. *J. Am. Chem. Soc.* **2012**, *134* (28), 11400–11403. <https://doi.org/10.1021/ja305076b>.

General procedure for photoredox titanium-catalyzed allylation of aldehydes

Standard procedure: All the reactions were performed in duplicate on 0.1 mmol scale of aldehyde. A dry 10 mL Schlenk tube, equipped with a Rotaflo stopcock, magnetic stirring bar and an argon supply tube, was first charged under argon with the organic photocatalyst 3DPAFIPN (5 mol%, 0.005 mmol, 3.2 mg), [Cp₂TiCl₂] catalyst (10 mol%, 0.01 mmol, 2.5 mg), dimethyl 1,4-dihydro-2,6-dimethyl-3,5-pyridinedicarboxylate Hantzsch's ester (2 equivalents, 0.2 mmol, 45 mg). Inhibitor-free dry THF (2 mL in order to obtain a 0.05 M substrate solution) was then added and the reaction mixture was further subjected to a freeze-pump-thaw procedure (three cycles) and the vessel refilled with argon. Then, allyl bromide **2** (0.3 mmol, 3 equiv.) and the substrate **1** (0.1 mmol) were added. The reaction was irradiated under vigorous stirring for the desired time. After that the two reaction mixtures were quenched with aqueous HCl 0.5 M (approx. 4 mL), combined together and extracted with AcOEt (4 x 3 mL). The combined organic layers were dried over anhydrous Na₂SO₄ and the solvent was removed under reduced pressure. The crude was subject of flash column chromatography (SiO₂) to afford the products **3** in the stated yields.

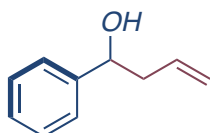
Procedure for 5 mmol scale: A dry 250 mL Schlenk tube, equipped with magnetic stirring bar and an argon supply tube, was first charged under argon with the organic photocatalyst 3DPAFIPN (3 mol%, 0.15 mmol, 95 mg), [Cp₂TiCl₂] catalyst (8 mol%, 0.4 mmol, 0.100 g), dimethyl 1,4-dihydro-2,6-dimethyl-3,5-pyridinedicarboxylate Hantzsch's ester (2 equivalents, 10 mmol, 2.25 g). Inhibitor-free dry THF (100 mL in order to obtain a 0.05 M substrate solution) was then added and the reaction mixture was further subjected to a freeze-pump-thaw procedure (four cycles) and the vessel refilled with argon. Then, allyl bromide **2a** (15 mmol, 3 equiv., 1.8 g, 1.29 mL) and the substrate **1a** (5 mmol, 0.67 g, 0.66 mL) were added. The reaction was irradiated under vigorous stirring for 48 hours. After that the solvent was removed under reduced pressure. The crude was subject of flash column chromatography (SiO₂) to afford the products **3a** in 95% yield (4.75 mmol, 0.836 g).



(3a): brown oil, 98% (0.195 mmol, 34 mg). The general procedure was applied using **1a** (0.1 mmol, 13 μ L) previously distilled and **2a** (0.3 mmol, 28 μ L, 3 equiv.) and performed in duplicate. The title compound was isolated by flash column chromatography (100% DCM).

$^1\text{H-NMR}$ (400 MHz, CDCl_3 , 25 $^\circ\text{C}$): δ = 7.29 – 7.14 (m, 5H), 5.86 – 5.76 (m, 1H), 5.16 – 5.10 (m, 2H), 3.67 (ddd, J = 12.2, 7.6, 4.7 Hz, 1H), 2.84 – 2.75 (m, 1H), 2.72 – 2.64 (m, 1H), 2.35 – 2.28 (m, J = 12.2, 6.9, 4.3, 1.3 Hz, 1H), 2.24 – 2.12 (m, 1H), 1.81 – 1.75 (m, 2H), 1.61 (br s, 1H).

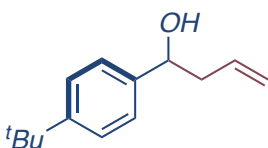
$^{13}\text{C-NMR}$ (100 MHz, CDCl_3 , 25 $^\circ\text{C}$): δ = 142.0, 134.6, 128.4 (2C), 128.4 (2C), 125.8, 118.3, 69.9, 42.0, 38.4, 32.0.



(3b): brown oil, 90% (0.18 mmol, 26 mg). The general procedure was applied using **1b** (0.1 mmol, 10.2 μ L) previously distilled and **2a** (0.3 mmol, 28 μ L, 3 equiv.) and performed in duplicate. The title compound was isolated by flash column chromatography (100% DCM).

$^1\text{H-NMR}$ (400 MHz, CDCl_3 , 25 $^\circ\text{C}$): δ = 7.36 – 7.12 (m, 5H), 5.86 – 5.74 (m, 1H), 5.18 – 5.11 (m, 2H), 4.72 (dd, J = 7.6, 5.4 Hz, 1H), 2.56 – 2.44 (m, 2H), 2.06 (br s, 1H)

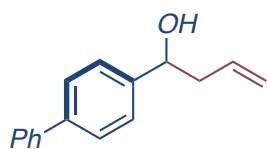
$^{13}\text{C-NMR}$ (100 MHz, CDCl_3 , 25 $^\circ\text{C}$): δ = 143.8, 134.4, 128.4 (2C), 127.5, 125.8 (2C), 118.4, 73.3, 43.8.



(3c): brown oil, 77% (0.15 mmol, 31.4 mg). The general procedure was applied using **1c** (0.1 mmol, 16 μ L) previously distilled and **2a** (0.3 mmol, 28 μ L, 3 equiv.) and performed in duplicate. The title compound was isolated by flash column chromatography (100% DCM).

$^1\text{H-NMR}$ (400 MHz, CDCl_3 , 25 $^\circ\text{C}$): δ = 7.37 (d, J = 8.3 Hz, 2H), 7.28 (d, J = 8.4 Hz, 2H), 5.82 (ddt, J = 17.1, 10.1, 7.1 Hz, 1H), 5.20 – 5.10 (m, 2H), 4.70 (t, J = 6.5 Hz, 1H), 2.57 – 2.44 (m, 2H), 1.32 (s, 9H).

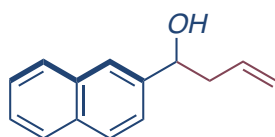
$^{13}\text{C-NMR}$ (100 MHz, CDCl_3 , 25 $^\circ\text{C}$): δ = 150.4, 140.9, 134.7, 125.5 (2C), 125.3 (2C), 118.1, 73.1, 43.6, 34.5, 31.3 (3C).⁺



(3d): brown oil, 86% (0.17 mmol, 38.5 mg). The general procedure was applied using **1d** (0.1 mmol, 18 mg) and **2a** (0.6 mmol, 64 μ L, 3 equiv.) and performed in duplicate. The title compound was isolated by flash column chromatography (100% DCM).

$^1\text{H-NMR}$ (400 MHz, CDCl_3 , 25°C): δ = 7.60 – 7.56 (m, 4H), 7.45 – 7.41 (m, 4H), 7.36 – 7.30 (m, 1H), 5.89 – 5.79 (m, 1H), 5.22 – 5.15 (m, 2H), 4.78 (t, J = 5.4 Hz, 1H), 2.62 – 2.48 (m, 2H).

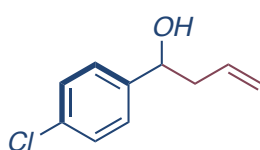
$^{13}\text{C-NMR}$ (100 MHz, CDCl_3 , 25°C): δ = 142.9, 140.8, 140.5, 134.4, 128.7 (2C), 127.2, 127.1 (2C), 127.0 (2C), 126.2 (2C), 118.5, 73.02, 43.8.



(3e): brown oil, 83% (0.17 mmol, 26 mg). The general procedure was applied using **1e** (0.1 mmol, 16 mg) and **2a** (0.3 mmol, 28 μ L, 3 equiv.) and performed in duplicate. The title compound was isolated by flash column chromatography (100% DCM).

$^1\text{H NMR}$ (400 MHz, CDCl_3 , 25°C): δ = 7.85 – 7.78 (m, 4H), 7.51 – 7.42 (m, 3H), 5.88 – 5.77 (m, 1H), 5.21 – 5.12 (m, 2H), 4.89 (dd, J = 7.2, 5.9 Hz, 1H), 2.66 – 2.52 (m, 2H);

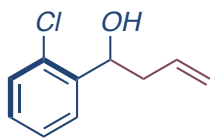
$^{13}\text{C NMR}$ (100 MHz, CDCl_3 , 25°C): δ = 141.2, 134.3, 133.2, 132.9, 128.2, 127.9, 127.6, 126.1, 125.8, 124.4, 124.0, 118.5, 73.3, 43.7.



(3f): brown oil, 85% (0.17 mmol, 31 mg). The general procedure was applied using **1f** (0.1 mmol, 14 mg) and **2a** (0.3 mmol, 28 μ L, 3 equiv.) and performed in duplicate. The title compound was isolated by flash column chromatography (100% DCM).

$^1\text{H-NMR}$ (400 MHz, CDCl_3 , 25°C): δ = 7.32 – 7.25 (m, 4H), 5.82 – 5.71 (m, 1H), 5.17 – 5.14 (m, 1H), 5.12 (m, 1H), 4.70 (dd, J = 7.8, 5.1 Hz, 1H), 2.53 – 2.39 (m, 2H).

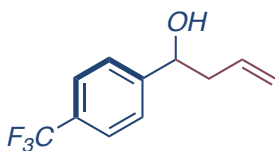
$^{13}\text{C-NMR}$ (100 MHz, CDCl_3 , 25°C): δ = 142.2, 133.9, 133.1, 128.5 (2C), 127.2 (2C), 118.8, 72.5, 43.8.



(3g): brown oil, 41% (0.08 mmol, 12 mg). The general procedure was applied using **1g** (0.1 mmol, 11.2 μ L) previously distilled and **2a** (0.3 mmol, 28 μ L, 3 equiv.) and performed in duplicate. The title compound was isolated by flash column chromatography (100% DCM).

$^1\text{H-NMR}$ (400 MHz, CDCl_3 , 25 $^\circ\text{C}$): δ = 7.55 (dd, J = 7.7, 1.3 Hz, 1H), 7.34 – 7.16 (m, 3H), 5.91 – 5.80 (m, 1H), 5.20 – 5.13 (m, 3H), 2.66 – 2.59 (m, 1H), 2.42 – 2.32 (m, 1H)

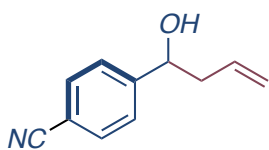
$^{13}\text{C-NMR}$ (100 MHz, CDCl_3 , 25 $^\circ\text{C}$): δ = 141.1, 134.2, 131.7, 129.4, 128.4, 127.04, 126.99, 118.7, 69.6, 42.0.



(3h): brown oil, 70% (0.14 mmol, 30 mg). The general procedure was applied using **1h** (0.1 mmol, 14 μ L) previously distilled and **2a** (0.3 mmol, 28 μ L, 3 equiv.) and performed in duplicate. The title compound was isolated by flash column chromatography (100% DCM).

$^1\text{H-NMR}$ (400 MHz, CDCl_3 , 25 $^\circ\text{C}$): δ = 7.59 (d, J = 8.2 Hz, 2H), 7.46 (d, J = 8.1 Hz, 2H), 5.83 – 5.71 (m, 1H), 5.18 (m, 1H), 5.16 – 5.13 (m, 1H), 4.78 (dd, J = 7.9, 4.8 Hz, 1H), 2.57 – 2.40 (m, 2H), 2.19 (br s, 1H)

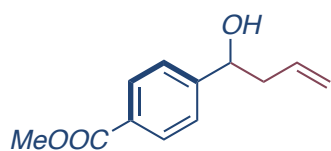
$^{13}\text{C-NMR}$ (100 MHz, CDCl_3 , 25 $^\circ\text{C}$): δ = 147.7, 133.7, 129.7 (q, J = 32.4 Hz), 126.1 (2C), 125.3 (q, J = 3.6 Hz), 124.3 (q, J = 272.1 Hz), 119.2 (2C), 72.5, 43.9; $^{19}\text{F-NMR}$ (377 MHz, CDCl_3 , 25 $^\circ\text{C}$): δ = -61.28.



(3i): brown oil, 49% (0.1 mmol, 19 mg). The general procedure was applied using **1i** (0.1 mmol, 19 mg) and **2a** (0.3 mmol, 28 μ L, 3 equiv.) and performed in duplicate. The title compound was isolated by flash column chromatography (100% DCM).

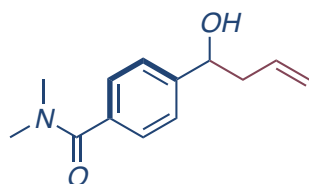
$^1\text{H-NMR}$ (400 MHz, CDCl_3 , 25 $^\circ\text{C}$): δ = 7.60 – 7.56 (m, 4H), 5.89 – 5.79 (m, 1H), 5.22 – 5.15 (m, 2H), 4.78 (t, J = 5.4 Hz, 1H), 2.62 – 2.48 (m, 2H).

$^{13}\text{C-NMR}$ (100 MHz, CDCl_3 , 25 $^\circ\text{C}$): δ = 142.9, 140.8, 140.5, 134.4, 128.7 (2C), 127.2, 127.1 (2C), 127.0 (2C), 126.2 (2C), 118.5, 73.02, 43.8.



(3j): brown oil, 68% (0.13 mmol, 28 mg). The general procedure was applied using **1j** (0.1 mmol, 17 mg) and **2a** (0.3 mmol, 28 μ L, 3 equiv.) and performed in duplicate. The title compound was isolated by flash column chromatography (gradient to 100% DCM to 99.5/0.5 DCM/MeOH). $^1\text{H-NMR}$ (400 MHz, CDCl_3 , 25 $^\circ\text{C}$): δ = 8.00 (dt, J = 8.4, 1.9 Hz, 1H), 7.44 – 7.40 (m, 3H), 5.83 – 5.71 (m, 1H), 5.19 – 5.15 (m, 2H), 5.15 – 5.12 (m, 1H), 4.80 (ddd, J = 8.0, 4.8, 3.6 Hz, 1H), 3.90 (s, 3H), 2.58 – 2.40 (m, 2H).

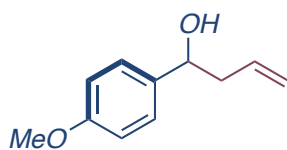
$^{13}\text{C-NMR}$ (100 MHz, CDCl_3 , 25 $^\circ\text{C}$): δ = 166.8, 148.9, 133.8, 129.7 (2C), 129.3, 125.7 (2C), 119.0, 72.7, 52.0, 43.8.



(3k): brown oil, 63% (0.13 mmol, 28 mg). The general procedure was applied using **1k** (0.1 mmol, 17 mg) and **2a** (0.3 mmol, 28 μ L, 3 equiv.) and performed in duplicate. The title compound was isolated by flash column chromatography (gradient to 100% DCM to 99.5/0.5 DCM/MeOH).

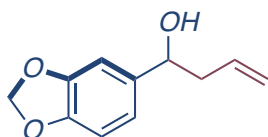
$^1\text{H-NMR}$ (400 MHz, CDCl_3 , 25 $^\circ\text{C}$): δ = 7.39 – 7.34 (m, 4H), 5.77 (dddd, J = 17.0, 10.3, 7.6, 6.6 Hz, 1H), 5.17 – 5.11 (m, 2H), 4.74 (dd, J = 7.7, 5.0 Hz, 1H), 3.08 (s, 3H), 2.95 (s, 3H), 2.55 – 2.40 (m, 2H).

$^{13}\text{C-NMR}$ (100 MHz, CDCl_3 , 25 $^\circ\text{C}$): δ = 171.4, 145.3, 135.4, 134.0, 127.2 (2C), 125.7 (2C), 118.7, 72.8, 43.8, 39.6, 39.5.



(3l): brown oil, 75% (0.15 mmol, 27 mg). The general procedure was applied using **1l** (0.1 mmol, 13 μ L) and **2a** (0.3 mmol, 28 μ L, 3 equiv.) and performed in duplicate. The title compound was isolated by flash column chromatography (100% DCM). Spectroscopic data were in agreement with those reported in the literature.

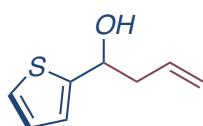
$^1\text{H-NMR}$ (400 MHz, CDCl_3 , 25 $^\circ\text{C}$): δ = 7.30 – 7.23 (m, 2H), 6.90 – 6.84 (m, 2H), 5.78 (ddt, J = 17.2, 10.2, 7.1 Hz, 1H), 5.17 – 5.08 (m, 2H), 4.67 (t, J = 6.5 Hz, 1H), 3.79 (s, 3H), 2.51 – 2.46 (m, 2H); $^{13}\text{C-NMR}$ (100 MHz, CDCl_3 , 25 $^\circ\text{C}$): δ = 159.0, 136.0, 134.6, 127.0 (2C), 118.2, 113.8 (2C), 73.0, 55.2, 43.7.



(3m): brown oil, 65% (0.13 mmol, 25 mg). The general procedure was applied using **1m** (0.1 mmol, 19 mg) and **2m** (0.3 mmol, 28 μ L, 3 equiv.) and performed in duplicate. The title compound was isolated by flash column chromatography (100% DCM).

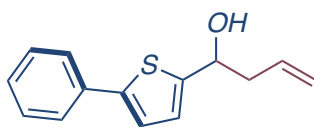
$^1\text{H-NMR}$ (400 MHz, CDCl_3 , 25 $^\circ\text{C}$): δ = 6.85 (d, J = 1.5 Hz, 1H), 6.80 – 6.72 (m, 2H), 5.92 (s, 2H), 5.82 – 5.70 (m, 1H), 5.16 – 5.09 (m, 2H), 4.62 (t, J = 6.5 Hz, 1H), 2.48 – 2.42 (m, 2H).

$^{13}\text{C-NMR}$ (100 MHz, CDCl_3 , 25 $^\circ\text{C}$): δ = 147.7, 146.8, 138.0, 134.4, 119.2, 118.3, 108.0, 106.4, 100.9, 73.2, 43.8.



(3n): brown oil, 63% (0.13 mmol, 20 mg). The general procedure was applied using **1n** (0.1 mmol, 15.4 mg) and **2a** (0.3 mmol, 28 μ L, 3 equiv.) and performed in duplicate. The title compound was isolated by flash column chromatography (100% DCM). Spectroscopic data are in agreement with those reported in the literature. $^1\text{H-NMR}$ (400 MHz, CDCl_3 , 25 $^\circ\text{C}$): δ = 7.29 (dd, J = 5.0, 3.0 Hz, 1H), 7.19 (d, J = 2.9 Hz, 1H), 7.07 (dd, J = 5.0, 1.2 Hz, 1H), 5.86 – 5.73 (m, 1H), 5.22 – 5.10 (m, 2H), 4.83 (dt, J = 8.0, 4.2 Hz, 1H), 2.61 – 2.46 (m, 2H)

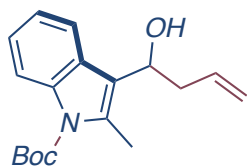
$^{13}\text{C-NMR}$ (100 MHz, CDCl_3 , 25 $^\circ\text{C}$): δ = 145.3, 134.2, 126.0, 125.6, 120.7, 118.5, 69.5, 43.0.



(3o): brown oil, 47% (0.09 mmol, 22 mg). The general procedure was applied using **1o** (0.2 mmol, 23 mg) and **2a** (0.3 mmol, 28 μ L, 3 equiv.) and performed in duplicate. The title compound was isolated by flash column chromatography (100% DCM).

$^1\text{H-NMR}$ (400 MHz, CDCl_3 , 25 $^\circ\text{C}$): δ = 7.57 (d, J = 8.1, 2H), 7.38 – 7.33 (m, 2H), 7.27 (d, J = 7.2 Hz, 1H), 7.15 (d, J = 3.6 Hz, 1H), 6.93 (d, J = 3.6 Hz, 1H), 5.85 (ddt, J = 17.2, 10.2, 7.1 Hz, 1H), 5.25 – 5.15 (m, 2H), 4.96 (t, J = 6.3 Hz, 1H), 2.70 – 2.58 (m, 2H), 2.20 (br s, 1H)

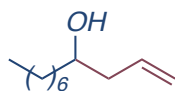
$^{13}\text{C-NMR}$ (100 MHz, CDCl_3 , 25 $^\circ\text{C}$): δ = 147.2, 143.5, 134.4, 133.7, 128.8 (2C), 127.4, 125.7 (2C), 124.6, 122.5, 118.9, 69.5, 43.6.



(3p): brown oil, 21% (0.04 mmol, 13 mg). The general procedure was applied using **1p** (0.1 mmol, 30 μ L) and **2a** (0.6 mmol, 64 μ L, 3 equiv.) and performed in duplicate. The title compound was isolated by flash column chromatography (100% DCM). Spectroscopic data are in agreement with those reported in the literature.

$^1\text{H-NMR}$ (400 MHz, CDCl_3 , 25°C): δ = 8.10 – 8.07 (m, 1H), 7.80 – 7.75 (m, 1H), 7.27 – 7.15 (m, 2H), 5.84 – 5.71 (m, 1H), 5.18 – 5.06 (m, 2H), 5.04 (dd, J = 7.9, 6.3 Hz, 1H), 2.86 – 2.57 (m, 2H), 2.55 (s, 3H), 1.67 (s, 9H)

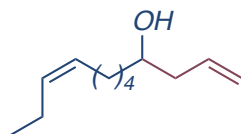
$^{13}\text{C-NMR}$ (100 MHz, CDCl_3 , 25°C): δ = 150.7, 136.0, 134.6, 133.6, 127.7, 123.4, 122.3, 119.7, 119.6, 117.9, 115.4, 83.8, 67.8, 41.6, 28.2 (3C), 14.1.



(3q): brown oil, 73% (0.14 mmol, 24 mg). The general procedure was applied using **1q** (0.1 mmol, 16 μ L) freshly distilled at $59^\circ\text{C}/21$ mbar and **2a** (0.3 mmol, 28 μ L, 3 equiv.) and performed in duplicate. The title compound was isolated by flash column chromatography (100% DCM). Spectroscopic data are in agreement with those reported in the literature.

$^1\text{H-NMR}$ (400 MHz, CDCl_3 , 25°C): δ = 5.86 – 5.75 (m, 1H), 5.13 – 5.08 (m, 2H), 3.63 (ddt, J = 9.7, 7.8, 4.9 Hz, 1H), 2.36 – 2.24 (m, 2H), 2.16 – 2.08 (m, 2H), 2.03 (br s, 1H), 1.63 – 1.20 (m, 10H), 0.85 (dd, J = 6.8, 5.9 Hz, 3H).

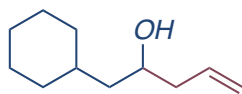
$^{13}\text{C-NMR}$ (100 MHz, CDCl_3 , 25°C): δ = 134.9, 118.0, 70.7, 41.9, 36.8, 31.8, 29.6, 29.3, 25.7, 22.6, 14.1.



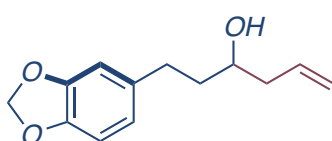
(3r): yellow oil, 40%. (0.08 mmol, 14 mg). The general procedure was applied using **1r** (0.1 mmol, 17 μ L) freshly distilled at $68^\circ\text{C}/13$ mbar and **2a** (0.3 mmol, 28 μ L, 3 equiv.) and performed in duplicate. The title compound was isolated by flash column chromatography (100% DCM).

$^1\text{H-NMR}$ (400 MHz, CDCl_3 , 25°C): δ = 5.81 (dddd, J = 12.5, 9.6, 7.6, 6.4 Hz, 1H), 5.38-5.26 (m, 2H), 5.14-5.08 (m, 2H), 3.66-3.60 (m, 1H), 2.32-2.24 (m, 1H), 2.16-2.10 (m, 1H), 1.98 (m, 5H), 1.56 (br s, 1H), 1.49-1.29 (m, 7H), 0.94 (t, J = 7.5 Hz, 3H).

^{13}C -NMR (100 MHz, CDCl_3 , 25°C): $\delta = 134.8, 131.7, 128.9, 118.0, 70.6, 41.9, 36.7, 29.7, 27.0, 25.2, 20.5, 14.3$.



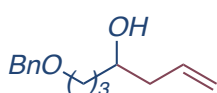
(3s): yellow oil, 60%. (0.12 mmol, 20 mg). The general procedure was applied using **1s** (0.1 mmol, 13 mg) at $68^\circ\text{C}/13$ mbar and **2a** (0.3 mmol, $28\ \mu\text{L}$, 3 equiv.) and performed in duplicate. The title compound was isolated by flash column chromatography (100% DCM). Spectroscopic data are in agreement with those reported in the literature.¹⁸⁴



(3t): brown oil, 79% (0.16 mmol, 34.7 mg). The general procedure was applied using **1u** (0.1 mmol, 18 mg) previously synthesized and **2a** (0.6 mmol, $64\ \mu\text{L}$, 3 equiv.) and performed in duplicate. The title compound was isolated by flash column chromatography (100% DCM).

^1H -NMR (400 MHz, CDCl_3 , 25°C): $\delta = 6.72$ (s, 1H), 6.69 (d, $J = 7.8$ Hz, 1H), 6.63 (d, $J = 7.9$ Hz, 1H), 5.90 (s, 2H), 5.85 – 5.74 (m, 1H), 5.15 – 5.10 (m, 2H), 3.67 – 3.61 (m, 1H), 2.65 (ddt, $J = 30.1, 13.9, 7.9$ Hz, 2H), 2.33 – 2.26 (m, 1H), 2.15 (dt, $J = 7.9, 4.3$ Hz, 1H), 1.75 – 1.69 (m, 2H), 1.59 (br s, 1H).

^{13}C -NMR (100 MHz, CDCl_3 , 25°C): $\delta = 147.5, 145.6, 135.8, 134.5, 121.1, 118.3, 108.9, 108.1, 100.7, 69.7, 42.1, 38.6, 31.7$.

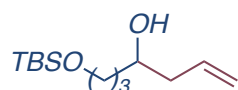


(3u): brown oil, 69% (0.14 mmol 27 mg). The general procedure was applied using **1v** (0.1 mmol, 15 mg) previously synthesized and **2a** (0.3 mmol, $28\ \mu\text{L}$, 3 equiv.) and performed in duplicate. The title compound was isolated by flash column chromatography (100% DCM).

^1H -NMR (400 MHz, CDCl_3 , 25°C): $\delta = 7.35 - 7.25$ (m, 5H), 5.87 – 5.76 (m, 1H), 5.13 – 5.08 (m, 2H), 4.50 (s, 2H), 3.68 – 3.62 (m, 1H), 3.50 (t, $J = 6.0$ Hz, 2H), 2.35 (br s, 1H), 2.30 – 2.11 (m, 2H), 1.81 – 1.59 (m, 3H), 1.48 (ddd, $J = 14.3, 11.1, 7.2$ Hz, 1H);

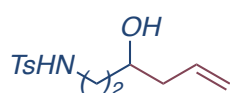
^{13}C -NMR (100 MHz, CDCl_3 , 25°C): $\delta = 138.2, 135.0, 128.4$ (2C), 127.7 (2C), 127.6, 117.7, 73.0, 70.5, 70.4, 42.0, 34.0, 26.2.

¹⁸⁴ K. Tamao, T. Iwahara, R. Kanatani, M. Kumada, Some new aspects of conjugate addition of grignard and alkylolithium reagents to vinylsilanes *Tetrahedron Lett.* **1984**, 25, 1909-1912. [https://doi.org/10.1016/S0040-4039\(01\)90072-3](https://doi.org/10.1016/S0040-4039(01)90072-3)



(3v): brown oil, 69% (0.14 mmol 27 mg). The general procedure was applied using **1w** (0.1 mmol, 15 mg) previously synthesized and **2a** (0.3 mmol, 28 μ L, 3 equiv.) and performed in duplicate. The title compound was isolated by flash column chromatography (100% DCM). ^1H NMR (401 MHz, CDCl_3) δ 5.84 (m, $J = 17.4, 10.3, 7.2$ Hz, 1H), 5.17 – 5.01 (m, 1H), 3.66 (m, $J = 5.0$ Hz, 3H), 2.32 – 2.16 (m, 2H), 1.70 – 1.39 (m, 4H), 0.90 (s, 9H), 0.06 (s, 6H).

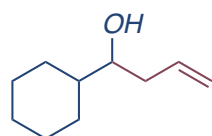
^{13}C NMR (101 MHz, CDCl_3) δ 135.11, 117.53, 70.58, 64.90, 63.44, 56.25, 41.90, 40.54, 33.94, 29.13, 25.89.



(3w): brown oil, 60% (0.12 mmol, 32 mg). The general procedure was applied using **1x** (0.1 mmol, 22 mg) previously synthesized and **2a** (0.3 mmol, 28 μ L, 3 equiv.) and performed in duplicate. The title compound was isolated by flash column chromatography (gradient to 100% DCM to 99.5/0.5 DCM/MeOH).

^1H -NMR (400 MHz, CDCl_3 , 25 $^\circ\text{C}$): $\delta = 7.72$ (d, $J = 8.3$ Hz, 2H), 7.32 – 7.25 (m, 2H), 5.71 (dddd, $J = 16.9, 10.3, 7.9, 6.5$ Hz, 1H), 5.22 (br s, 1H), 5.13 – 5.05 (m, 2H), 3.72 (ddd, $J = 12.3, 7.8, 4.4$ Hz, 1H), 3.16 (dtd, $J = 12.5, 7.5, 4.9$ Hz, 1H), 3.00 (ddt, $J = 12.2, 7.1, 4.9$ Hz, 1H), 2.40 (s, 3H), 2.25 – 2.16 (m, 1H), 2.13 – 2.05 (m, 1H), 2.01 (br s, 1H), 1.66 (dddd, $J = 14.4, 7.8, 5.0, 3.0$ Hz, 1H), 1.52 (dddd, $J = 14.3, 9.3, 7.1, 4.9$ Hz, 1H).

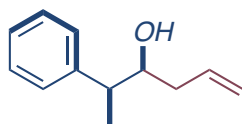
^{13}C -NMR (100 MHz, CDCl_3 , 25 $^\circ\text{C}$): $\delta = 143.3, 136.9, 133.9, 129.6$ (2C), 127.1 (2C), 118.8, 69.5, 42.0, 41.0, 35.2, 21.5.



(3x): brown oil, 84% (0.12 mmol, 26 mg). The general procedure was applied using **1y** (0.1 mmol, 11 mg) freshly distilled at 68 $^\circ\text{C}$ /13 mbar and **2a** (0.3 mmol, 28 μ L, 3 equiv.) and performed in duplicate. The title compound was isolated by flash column chromatography (gradient to 100% DCM to 99.5/0.5 DCM/MeOH).

^1H -NMR (400 MHz, CDCl_3 , 25 $^\circ\text{C}$): $\delta = 5.82$ (dddd, $J = 12.5, 9.2, 8.0, 6.4$ Hz, 1H), 5.15 – 5.09 (m, 2H), 3.39-3.35 (m, 1H), 2.35-2.28 (m, 1H), 2.11 (dt, $J = 14, 8.4$ Hz, 1H), 1.84 (d, $J = 12.6$ Hz, 1H), 1.77-1.63 (m, 4H), 1.54 (d, $J = 16$ Hz, 1H), 1.38-0.95 (m, 6H).

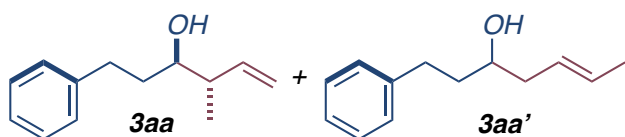
^{13}C -NMR (100 MHz, CDCl_3 , 25 $^\circ\text{C}$): $\delta = 135.4, 117.9, 74.7, 43.0, 38.8, 29.1, 28.1, 26.5, 26.2, 26.1$.



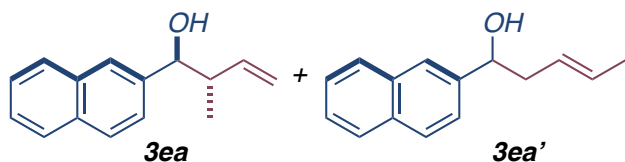
(3y): yellow oil, 90% (0.18 mmol, 32 mg) as *syn:anti* mixture dr of 1.2:1. The general procedure was applied using **1z** (0.1 mmol 13 μ L) freshly distilled at 52°C/3 mbar and **2a** (0.3 mmol, 28 μ L, 3 equiv.) and performed in duplicate. The title compound was isolated by flash column chromatography (100% DCM).

$^1\text{H-NMR}$ (400 MHz, CDCl_3 , 25°C): δ = 7.38 – 7.18 (m, 5H), 5.93 – 5.83 (m, 1H *anti*), 5.84 – 5.73 (m, 1H), 5.14 – 5.06 (m, 2H), 3.76 – 3.68 (m, 1H), 2.83 – 2.73 (m, 1H), 2.41 – 2.33 (m, 1H *anti*), 2.22 – 2.14 (m, 1H), 2.15 – 2.07 (m, 1H *from minor isomer*), 2.06 – 1.98 (m, 1H), 1.63 (s, 2H), 1.34 (d, J = 7.0 Hz, 3H), 1.29 (d, J = 7.1 Hz, 1H *from minor isomer*).

$^{13}\text{C-NMR}$ (100 MHz, CDCl_3 , 25°C): δ = 144.4, 143.2, 135.04, 135.00, 128.48, 128.46 (2C), 128.1, 127.7 (2C), 126.6, 126.4, 118.1, 117.7, 74.99, 74.97, 45.4, 39.5, 38.9, 29.7, 17.7, 16.4; *major isomer*: δ = 144.4, 135.04, 128.46 (2C), 127.7 (2C), 126.4, 118.1, 74.97, 45.4, 39.5, 16.4.



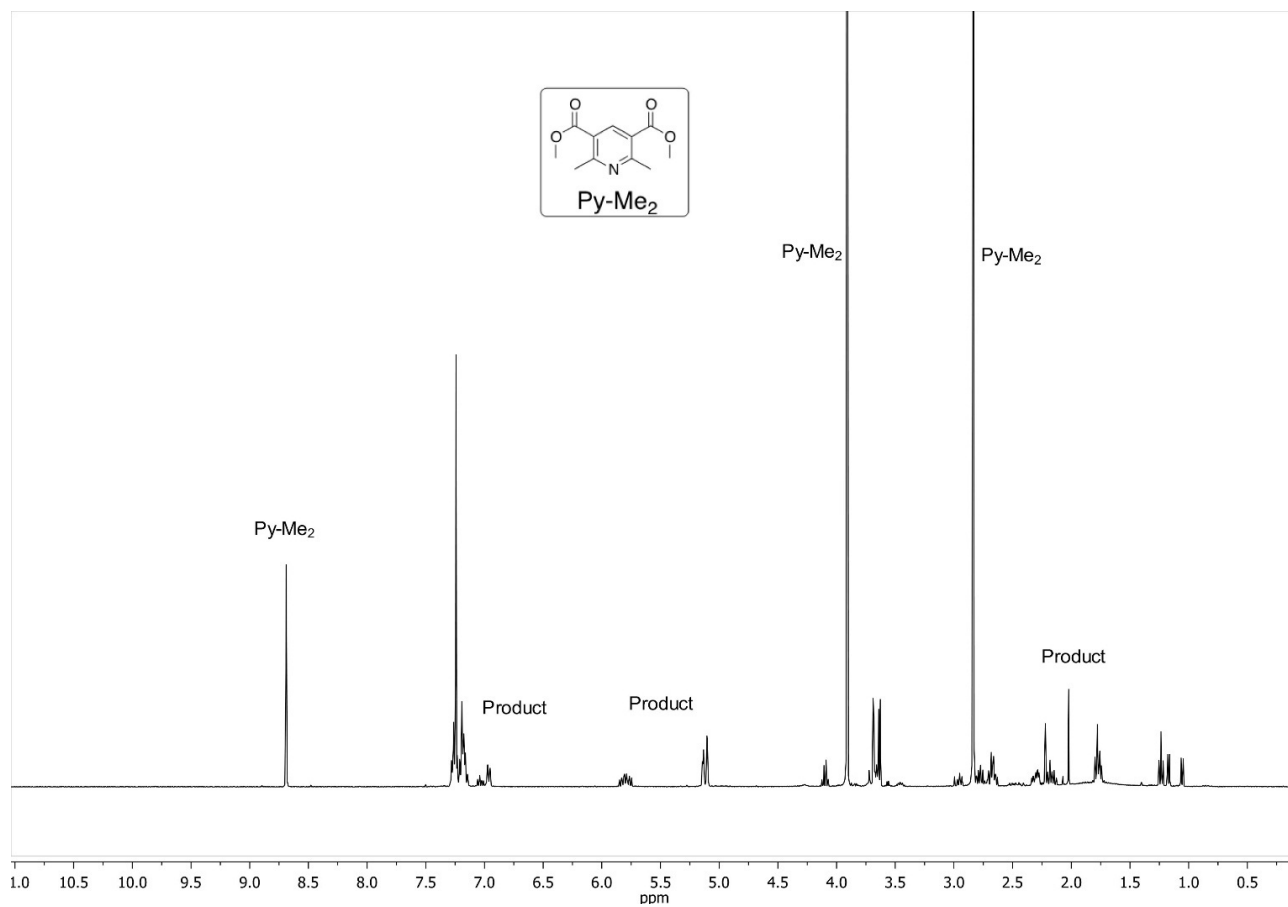
(3ab-3aa'): yellow oil, 50% as mixture regioisomer and diastereoisomer **3ab:3aa'** of >99:1, **3aa_{syn}:3aa_{anti}** dr of 91:9 (0.1 mmol, 19 mg). The general procedure was applied using **1a** (0.1 mmol 13 μ L) freshly distilled at 52°C/3 mbar and **2b** 85% technical grade (0.3 mmol, 37 μ L, 3 equiv.) and performed in duplicate. The title compound was isolated by flash column chromatography (100% DCM). Spectroscopic data are in agreement with those reported in the literature.¹⁸⁵



(3ea-3ea'): brown oil, 82% as mixture regioisomer and diastereoisomer **3ea:3ea'** of 84:16, **3ea_{anti}:3ea_{syn}** dr of 94:6 (0.18 mmol, 32 mg). The general procedure was applied using **1e** (0.1 mmol) and **2b** 85% technical grade (0.3 mmol, 37 μ L, 3 equiv.) and performed in duplicate. The title compound was isolated

¹⁸⁵ R. E. Taylor, F. C. Engelhardt, M. J. Schmitt, H. Yuan, *synthetic Methodology for the Construction of Structurally Diverse Cyclopropanes* *J. Am. Chem. Soc.* **2001**, *123*, 2964-2969. <https://doi.org/10.1021/ja0037163>

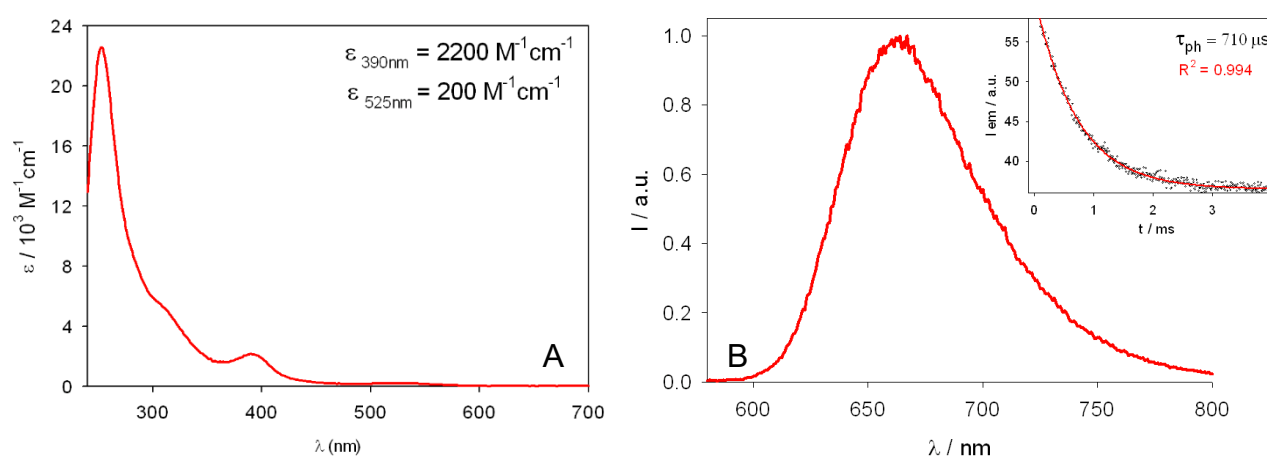
by flash column chromatography (100% DCM). Spectroscopic data are in agreement with those reported in the literature.¹⁸⁶



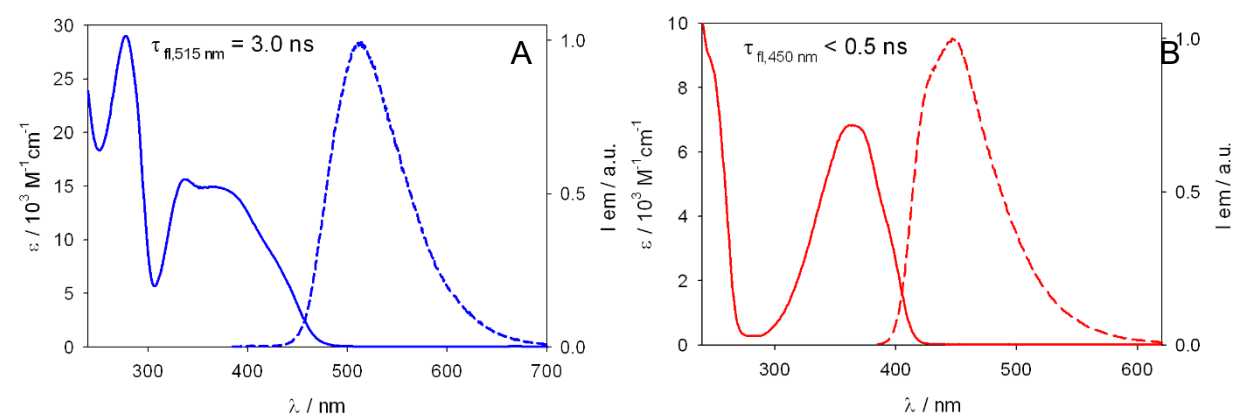
Chapter 3. Supplementary 5 ¹H-NMR (400 MHz, CDCl₃) spectrum of reaction crude. Reaction of aldehyde **1a** to give product **3a**

Photophysical and mechanistic studies

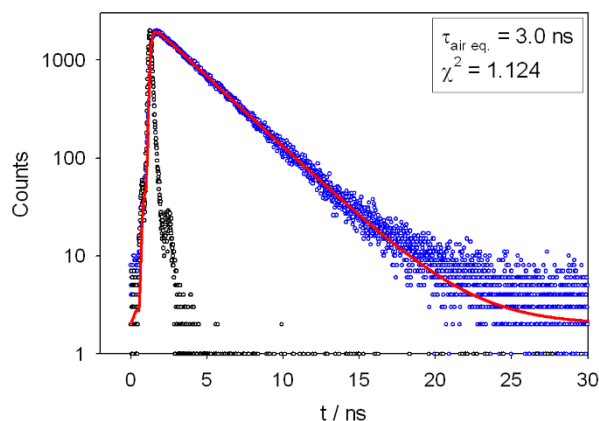
All the photophysical analyses were carried out in air-equilibrated tetrahydrofuran at 298 K unless otherwise specified. Luminescence measurements at 77 K were performed in dichloromethane/methanol (1:1 v/v) mixture. UV–vis absorption spectra were recorded with a PerkinElmer λ 40 spectrophotometer using quartz cells with path length of 1.0 cm. Luminescence spectra were performed with a PerkinElmer LS-50 or an Edinburgh FLS920 spectrofluorimeter equipped with a Hamamatsu R928 phototube. Lifetimes shorter than 10 μ s were measured by the above-mentioned Edinburgh FLS920 spectrofluorimeter equipped with a TCC900 card for data acquisition in time-correlated single-photon counting experiments (0.5 ns time resolution). The estimated experimental errors are 2 nm on the band maximum, 5% on the molar absorption coefficient and luminescence lifetime.



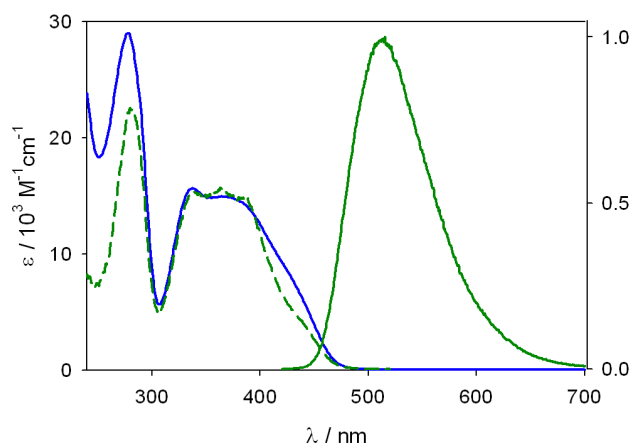
Chapter 3. Supplementary 6 A: molar absorptivity spectrum of $[\text{Cp}_2\text{TiCl}_2]$ recorded in air-equilibrated CH_3CN at r.t. B: phosphorescence spectrum of $[\text{Cp}_2\text{TiCl}_2]$ recorded in $\text{CH}_2\text{Cl}_2:\text{CH}_3\text{OH}$ (1:1 v/v) glassy matrix at 77 K; $\lambda_{\text{ex}} = 520$ nm. Inset: phosphorescence decay recorded on the same glassy matrix at $\lambda_{\text{em}} = 660$ nm.



Chapter 3. Supplementary 7. A: absorption (solid line) and emission spectrum (dashed line) recorded on a solution of 3DPAFIPN in air-equilibrated THF at r.t. $\lambda_{\text{ex}} = 365$ nm. For the fluorescence lifetime determination: $\lambda_{\text{ex}} = 405$ nm. B: absorption (solid line) and emission spectrum (dashed line) recorded on a solution of Hantzsch ester in air-equilibrated THF at r.t. $\lambda_{\text{ex}} = 365$ nm. For the fluorescence lifetime determination: $\lambda_{\text{ex}} = 405$ nm.



Chapter 3. Supplementary 8 Emission decay of 3DPAFIPN in air equilibrated THF (blue dots). The decay is fitted with a monoexponential function (red line); the instrument response function is also shown (black dots). $\lambda_{ex}=405$ nm, $\lambda_{em}=520$ nm.



Chapter 3. Supplementary 9 Comparison between normalized excitation (green dashed line) and emission (green solid line) spectra in degassed THF solutions of 3DPAFIPN at room temperature ($\lambda_{em}=530$ nm and $\lambda_{ex}=410$ nm) recorded in phosphorescence mode (delay=0.05 ms, gate 0.2 ms). The absorption spectrum is also shown (blue line).

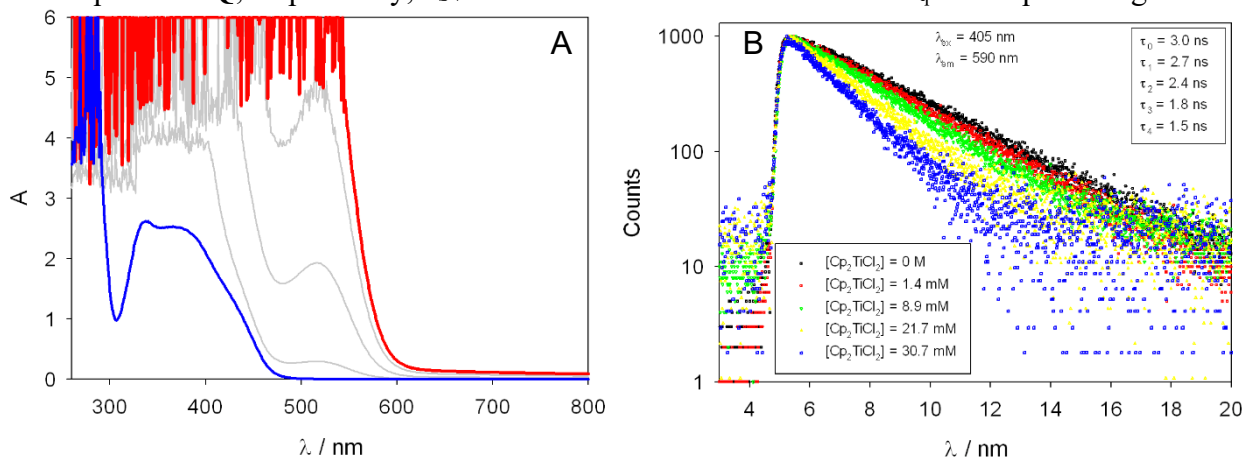
The Stern-Volmer relationship has been employed to evaluate in several experimental conditions the diffusional quenching occurring between 3DPAFIPN and the several species involved in the photoreactions taken into exam.

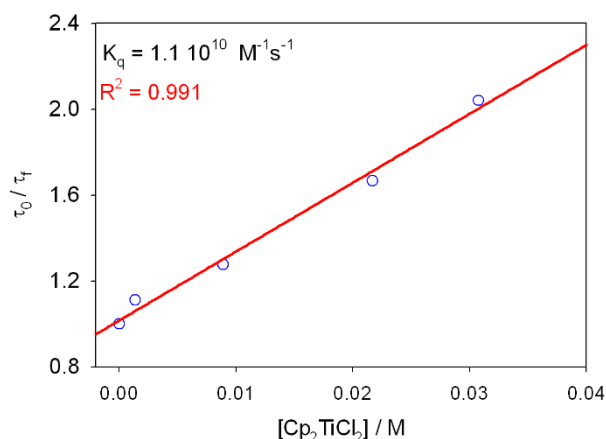
The Stern-Volmer kinetics show a linear correlation between the ratio τ_0/τ or I_0/I and the quencher concentration, as expected for a dynamic quenching process according to the Stern-Volmer equations:

$$\tau_0/\tau = 1 + k_{SV} [Q] = 1 + k_q \tau_0 [Q]$$

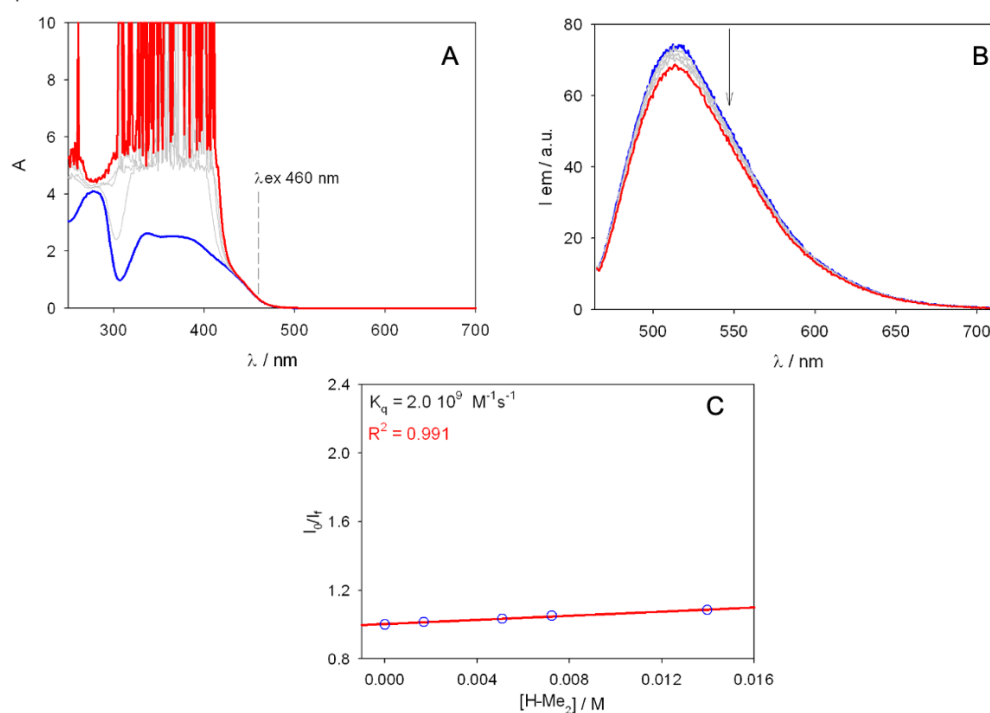
$$I_0/I = 1 + k_{SV} [Q] = 1 + k_q \tau_0 [Q]$$

where τ_0 and τ are the lifetimes, and I_0 and I are the emission intensities in the absence and in the presence of the quencher **Q**, respectively, k_{SV} is the Stern-Volmer constant and k_q is the quenching constant.

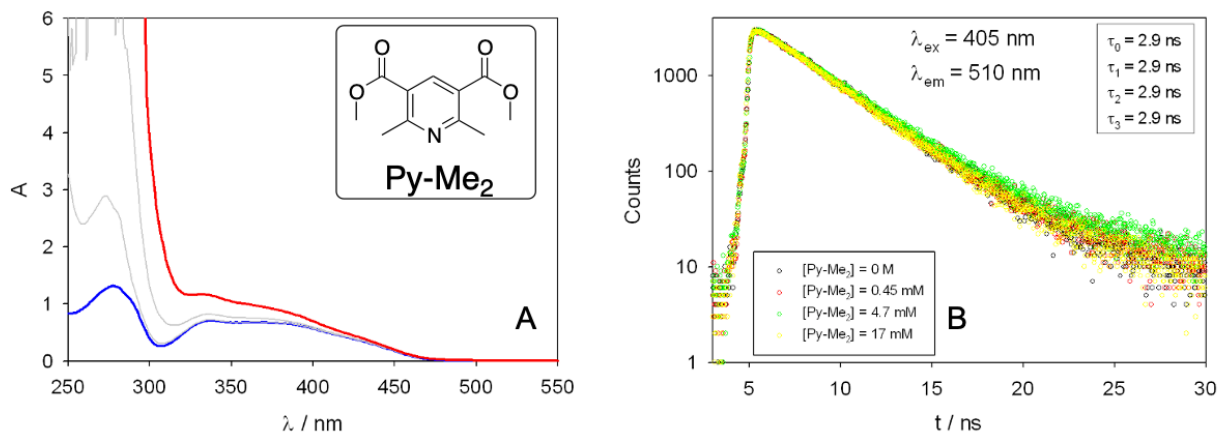




Chapter 3. Supplementary 10 a) absorption spectra of solutions of 3DPAFIPN in air-equilibrated THF (blue line) obtained upon addition of increasing amounts of $[\text{Cp}_2\text{TiCl}_2]$ (up to ca. 31 mM, red line). b) normalised fluorescence decays of 3DPAFIPN obtained from the same solutions at $\lambda_{em} = 590 \text{ nm}$ ($\lambda_{ex} = 405 \text{ nm}$). c) Stern-Volmer diagram relative to the fluorescence lifetimes shown in b.



Chapter 3. Supplementary 11: a) absorption spectra of solutions of 3DPAFIPN in air-equilibrated THF (blue line) obtained upon addition of increasing amounts of HE (up to ca. 14 mM, red line). b) fluorescence spectra of 3DPAFIPN obtained from the same solutions at $\lambda_{ex} = 460 \text{ nm}$. c) Stern-Volmer diagram relative to the fluorescence spectra shown in b.



Chapter 3. Supplementary 12 a) absorption spectra of solutions of 3DPAFIPN in THF (blue line) obtained upon addition of increasing amounts of Py-Me₂ (up to ca. 17 mM, red line). b) normalised fluorescence decays of 3DPAFIPN obtained from the same solutions at $\lambda_{em} = 510$ nm ($\lambda_{ex} = 405$ nm). Since the fluorescence lifetime of 3DPAFIPN is not significantly changing upon increasing additions of Py-Me₂, no Stern-Volmer plot is shown.

Determination of quantum yield

General procedure was applied on aldehyde **1a** (0.1 mmol scale) using allyl bromide **2a** under irradiation with Kessil® PR160L@456 nm. Three identical reactions were started, and one was stopped after 60 min., one after 90 and one after 120 min. Yield of the product **3a** was determined by ¹H NMR analysis on the reaction crude using benzyl alcohol as internal standard. A LP 10-BB sensor manufactured by Laserpoint connected to a Gentec TPM-300CE power meter was used to determine the total radiant power of the excitation light at the same distance from the source and with the same total irradiation area of the reaction vessel. The photon flux F_{ph} was calculated by taking into account the emission maximum of the lamp (456 nm, 2.72 eV; FWHM=0.12 eV) and approximated to monochromatic.¹⁵ The energy associated to a photon at a wavelength λ , E_{ph} , is calculated as

$$E_{ph} = \frac{h \cdot c}{\lambda}$$

where h is the Planck constant and c the speed of light. At 456 nm, E_{ph} corresponds to $4.36 \cdot 10^{-19}$ J.

The total photon flux F_{ph} was calculated as:

$$F_{ph} = \frac{P_i}{E_{ph}}$$

where P_i is the measured power (123 mW) and E_{ph} is the photon energy ($4.36 \cdot 10^{-19}$ J). From these data, a photon flux of $2.82 \cdot 10^{17}$ photons \cdot s⁻¹ was determined, corresponding to $1.02 \cdot 10^{21}$ photons \cdot h⁻¹ or $1.69 \cdot 10^3$ E \cdot h⁻¹. Considering that in our experimental condition the number of transmitted photons is negligible in the whole range of emission of the lamp, it can be assumed that all of the photons are absorbed by the 3DPAFIPN photocatalyst.

Quantum yield was determined as:

$$\Phi_{\%} = \frac{\text{mmol of } \mathbf{3a} \text{ formed}}{\text{mEinstein of light absorbed}} \cdot 100$$

Time (min)	3a (mmol)	Yield 3a (%)	Light absorbed (mEinstein)	Φ (%)
60	0.0189	18.9	1.7	1.1
90	0.0335	33.5	2.4	1.3
120	0.0530	53.0	3.6	1.6

Table 3.1.6 Determination of quantum yield.

Quantum yield could be considered, within the experimental error, constant during the time interval studied and the average quantum yield is 1.3%

¹⁸⁷ The results and the procedures described in this section are part of a published work:

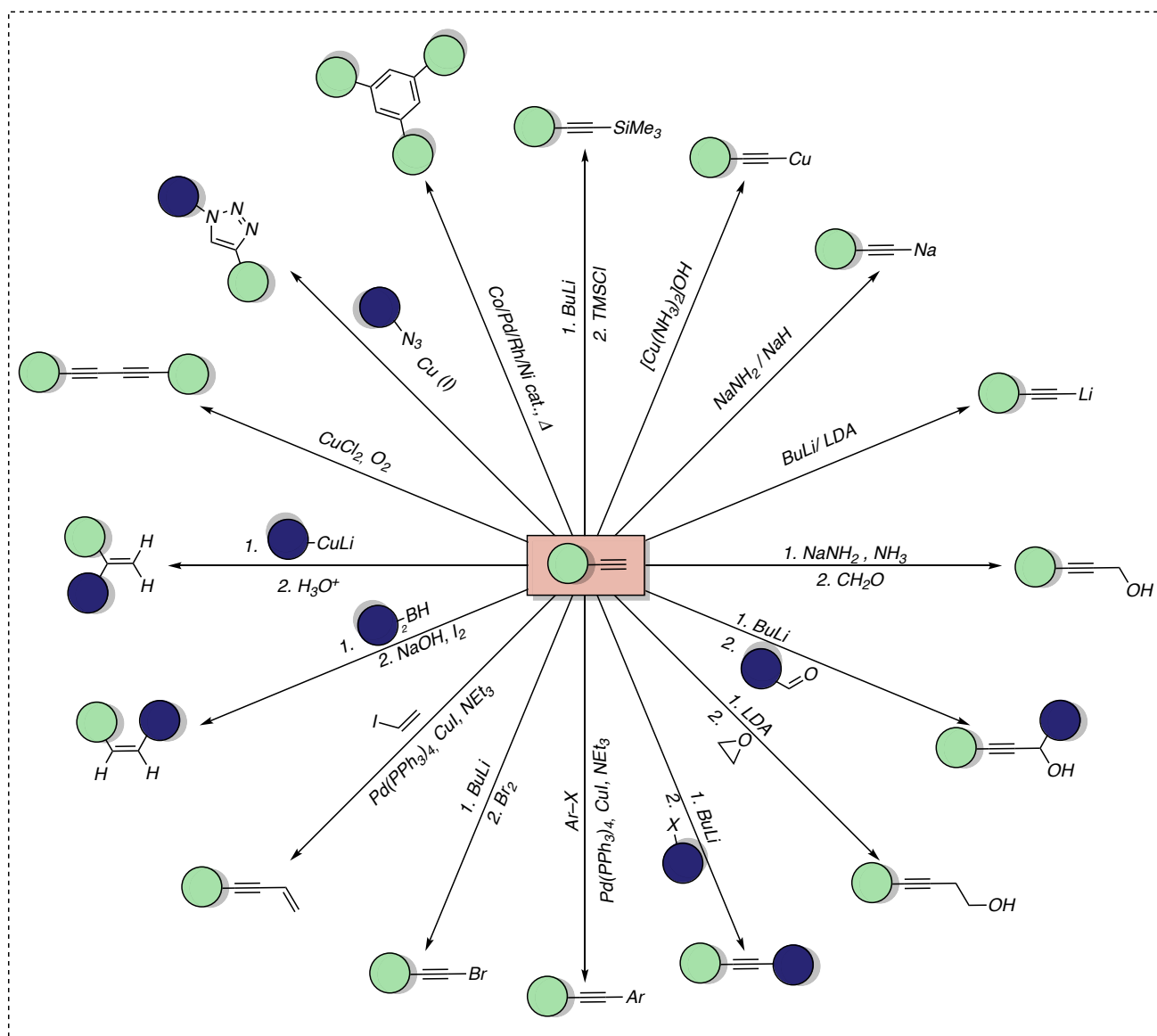
Calogero, F.; Gualandi, A.; Matteo, M. D.; Potenti, S.; Fermi, A.; Bergamini, G.; Cozzi, P. G. Photoredox Propargylation of Aldehydes Catalytic in Titanium. *J. Org. Chem.* **2021**, *86* (9), 7002–7009. <https://doi.org/10.1021/acs.joc.1c00521>.

A.F. carried out the photophysical investigations, supervised by G.B.

The complete characterization of the products introduced hereafter and discussed in the section “Supplementary Data” can be found in the Supporting Information of the above-mentioned work.

• Metal-catalyzed propargylation reaction

The addition of propargyl and allenyl nucleophiles to carbonyl compounds is a particularly convenient procedure for the synthesis of chemical motifs.¹⁸⁸ The obtained homoallenyl or homopropargyl alcohols are practical scaffolds allowing easy forthcoming functionalization. For this reason, these transformations find an intensive employment – especially if developed in stereocontrolled fashion– in total synthesis.¹⁸⁹



Chapter 3. Figure 8 Simplified scheme of the transformations of a terminal triple bond

¹⁸⁸ (a) Marshall, J. A. Synthesis and Reactions of Allylic, Allenic, Vinylic, and Arylmetal Reagents from Halides and Esters via Transient Organopalladium Intermediates. *Chem. Rev.* **2000**, *100* (8), 3163–3186. <https://doi.org/10.1021/cr000003u>. (b) Ding, C.-H.; Hou, X.-L. Catalytic Asymmetric Propargylation. *Chem. Rev.* **2011**, *111* (3), 1914–1937. <https://doi.org/10.1021/cr100284m>. (c) Yu, S.; Ma, S. Allenes in Catalytic Asymmetric Synthesis and Natural Product Syntheses. *Angew. Chem. Int. Ed.* **2012**, *51* (13), 3074–3112. <https://doi.org/10.1002/anie.201101460>.

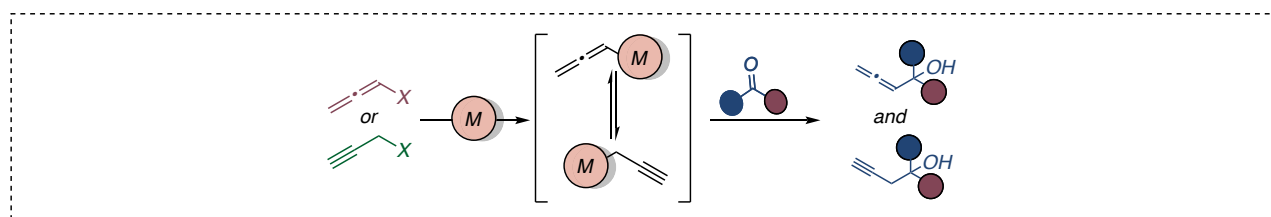
¹⁸⁹ (a) Pulkuri, K. K.; Chakraborty, T. K. Stereoselective Synthesis of the Monomeric Unit of Actin Binding Macrolide Rhizopodin. *Org. Lett.* **2012**, *14* (11), 2858–2861. <https://doi.org/10.1021/ol301103d>. (b) Francais, A.; Leyva, A.; Etxebarria-Jardi, G.; Ley, S. V. Total Synthesis of the Anti-Apoptotic Agents Isoand Bongkrekkic Acids. *Org. Lett.* **2010**, *12* (2), 340–343. <https://doi.org/10.1021/ol902676t>. (c) Trost, B. M.; Dong, G. Total Synthesis of Bryostatin 16 Using Atom-Economical and Chemoselective Approaches. *Nature* **2008**, *456* (7221), 485–488. <https://doi.org/10.1038/nature07543>. (d) Hirayama, L. C.; Dunham, K. K.; Singaram, B. Asymmetric Indium-Mediated Synthesis of Homopropargylic Alcohols *Tetrahedron Lett.* **2006**, *47*, 5173. [10.1055/s-2006-949314](https://doi.org/10.1055/s-2006-949314) (e) Ikeda, N.; Arai, I.; Yamamoto, H. Chiral allenylboronic esters as practical reagents for enantioselective carbon-carbon bond formation. Facile synthesis of (-)-ipenol. *J. Am. Chem. Soc.* **1986**, *108*, 483–486. <https://doi.org/10.1021/ja00263a020> (f) O'Sullivan, P. T.; Buhr, W.; Fuhr, M. A. M.; Harrison, J. R.; Davies, J. E.; Feeder, N.; Marshall, D. R.; Burton, J. W.; Holmes, A. B. A Concise Synthesis of the Octalactins. *J. Am. Chem. Soc.* **2004**, *126*, 2194–2207

As previously discussed in the case of allylation reactions, the use of transition metal catalysis is a convenient solution for the generation of reactive nucleophilic intermediates that are capable of promoting these types of processes. The mechanisms through which it is possible to obtain these transient species may include, oxidative addition, transmetalation, or generation of transient nucleophilic species from appropriate pronucleophiles under reductive Barbier type conditions.¹⁹⁰

Once the propargyl- or allenyl- metal nucleophile is formed, it is possible to describe its interaction with electrophile through an S_E2' -type mechanism. In other words, the generation of an allenyl-metal will determine the formation of the propargylation product, while the propargyl-metal species will determine the opposite regiochemical outcome.

However, although the use of a metal in presence of a pronucleophilic species is a convenient solution,¹⁹¹ in contrast to allylation reactions, an additional consideration is crucial. In fact, upon the generation of the organometallic species, an isomerization between the allenyl and the propargyl form of the organometallic species can arise.¹⁹²

Therefore, different regiochemical outcomes are allowed.



Chapter 3. Figure 9 Possible regiochemical outcome in Barbier-type allenylation/propargylation

The different product distribution depends on several factors including: (i) relative stability of the isomers, (ii) relative nucleophilicity of allenyl- and propargyl-metal complexes, (iii) identity and concentration of the metal, (iv) reaction conditions.

In this scenario, it is possible to depict two cases that allow an accurate description of this type of transformation.

If a rapid and reversible isomerization between its allenylic and propargylic form is allowed after the formation of transient organometallic species, the isomeric outcome of the nucleophilic addition will be ruled by the Curtin-Hammett principle.¹⁹³ In this case, starting with allenylic or propargylic pronucleophiles will provide the same regiochemical outcome.

On the contrary, if the new organometallic species does not isomerize rapidly, presenting an energetic barrier of isomerization higher than the activation barrier that determines the nucleophilic attack, the use

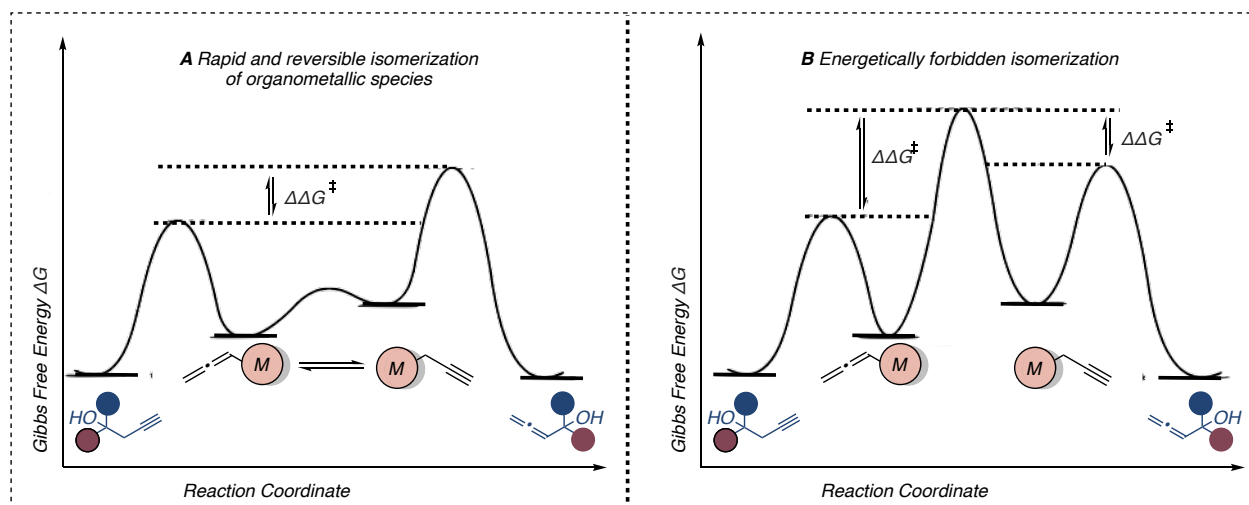
¹⁹⁰ C. Blomberg, *The Barbier Reaction and Related One- Step Processes*, Springer, Berlin, 1993.

¹⁹¹ H. P. Arcaya, K. Miyoshi, Y. Kobayashi, Mercury-Free Preparation and Selective Reactions of Propargyl (and Propargylic) Grignard Reagents *Org. Lett.* **2007**, *9*, 3535–3538. <https://doi.org/10.1021/ol071397f>

¹⁹² Wisniewska, H. M.; Jarvo, Enantioselective Propargylation and Allenylation Reactions of Ketones and Imines *E. R. J. Org. Chem.* **2013**, *78*, 11629–1163. <https://doi.org/10.1021/jo4019107>

¹⁹³ Carey, F. A.; Sundberg, R. J. *Structural Effects on Stability and Reactivity*. *Advanced Organic Chemistry Part A: Structure and Mechanisms*, 5th ed.; Springer: New York, 2007;

of allenylmetal reagent will provide the opposite product distribution with respect to the propargylmetal reagent.



Chapter 3. Figure 10 A Energetic profile for metal allenyl/propargyl species rapidly isomerizing. B Energetic profile for metal allenyl/propargyl witch isomerization is energetically forbidden.

Noteworthy, allenylation/propargylation reactions can be afforded with a complete regiochemical control and can also be developed in an enantioselective fashion if the reaction mechanism involves a transmetalation step of a nucleophile to an appropriate metal complex (i. e., copper complexes in presence of boronic esters).¹⁹⁴

On the contrary, although over the years many metals have been shown suitable for promoting propargylation/allenylation under Barbier-type reaction conditions, a complete regiochemical control is still difficult to achieve.¹⁹⁵

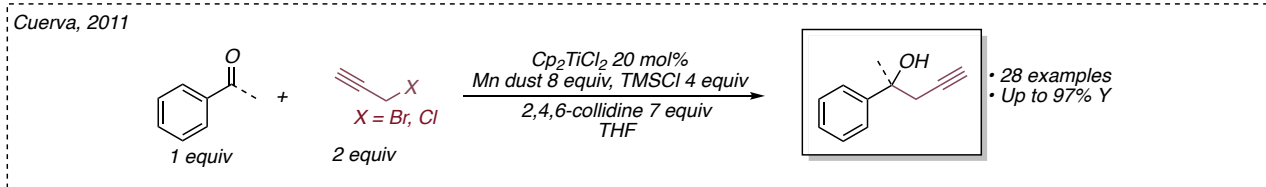
Remarkably, Justicia and Cuerva in 2009 disclosed the use of a catalytic amount of titanocene dichloride under reducing Barbier-type conditions for the propargylation of aldehydes and ketones.¹⁹⁶ A completely regioselective addition of propargylic moiety promoted by the formation of the transient Nugent-reagent was reported.

Under essentially analogous conditions to those reported by the authors in the case of allylations,¹⁷³ the reaction takes place under mild reaction conditions, it is compatible with different functional groups, producing only the homopropargylic isomer with good yields in the case of both aldehydes and ketones.

¹⁹⁴ (34) Shi, S.-L.; Xu, L.-W.; Oisaki, K.; Kanai, M.; Shibasaki, M. Identification of Modular Chiral Bisphosphines Effective for Cu(I)-Catalyzed Asymmetric Allylation and Propargylation of Ketones *J. Am. Chem. Soc.* **2010**, *132*, 6638. <https://doi.org/10.1021/ja101948s>
 (35) Fandrick, K. R.; Fandrick, D. R.; Reeves, J. T.; Gao, J.; Ma, S.; Li, W.; Lee, H.; Grinberg, N.; Lu, B.; Senanayake, C. H. A General Copper-BINAP-Catalyzed Asymmetric Propargylation of Ketones with Propargyl Boronates *J. Am. Chem. Soc.* **2011**, *133*, 10332-10335. <https://doi.org/10.1021/ja2028958>

¹⁹⁵ a) Place, P.; Delbecq, F.; Gore J. Utilisation d'un derive organique du chrome dans la synthese de composes alleniques *Tetrahedron Lett.* **1978**, 3801-3802;
 b) Hiyama, T.; Okude, Y.; Kimura, K.; Nozaki, H. Highly Selective Carbon-Carbon Bond Forming Reactions Mediated by Chromium(II) Reagents *Bull. Chem. Soc. Jpn.* **1982**, *55*, 561-568. <https://doi.org/10.1246/bcsj.55.561> c) Belyk, K.; Rozema, M. J.; Knochel, P. Preparation of Polyfunctional Allenic Alcohols by the Regioselective Addition of Functionalized Propargylic Chromium (III) Organometallics to Carbonyl Compounds *J. Org. Chem.* **1992**, *57*, 4070-4074; [10.1021/jo00041a006](https://doi.org/10.1021/jo00041a006) d) Wipf, P.; Lim, S. Addition of organochromium reagents to aldehydes, ketones and enones: a low-temperature version of the Nozaki-Hiyama reaction *J. Chem. Soc. Chem. Commun.* **1993**, 1654-1656. <https://doi.org/10.1039/C39930001654>

¹⁹⁶ Justicia, J.; Sancho-Sanz, I.; Álvarez-Manzaneda, E.; Oltra, J. E.; Cuerva, J. M. Efficient Propargylation of Aldehydes and Ketones Catalyzed by Titanocene(III). *Adv. Synth. Catal.* **2009**, *351* (14-15), 2295-2300. <https://doi.org/10.1002/adsc.200900479>.



Chapter 3. Scheme 9 Barbier-type propargylation of aldehydes and ketones catalytic in titanium

In light of the fact that from the analysis of the reaction crude there is no trace of the corresponding allenyl isomer, a reaction mechanism in which the interaction of the low oxidation state titanium complex with the propargyl halide leads the formation of a nucleophilic allenyl titanocene(IV) was proposed.

In an analogous way to what was disclosed for the allylation reaction, the proposed protocol is associated with some limitations that forbid a possible large-scale implementation and that reduce the range of substrates compatible with the reported protocol. Also in this context, satisfying yields are possible only if the reducing Mn(0) is at least forty times more than the catalyst. Similarly, seven equivalents of collidine (35 times more than the catalyst) and 4 four equivalents of TMSCl (20 times more than the catalyst) are compulsory.

• Presented work

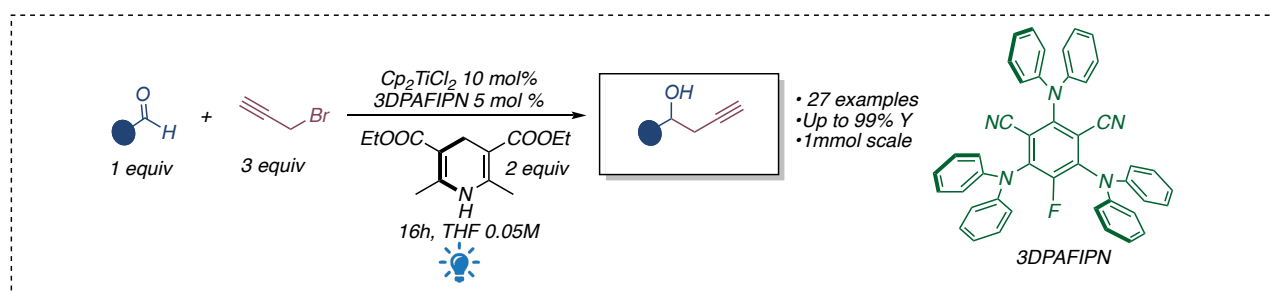
Thanks to the knowledge gained developing the allylation reaction, during my PhD the interest on the development of a propargylation reaction of aldehydes combining titanium complexes in low oxidation state with a photoredox system has arisen.

Quite recently, Glorius and co-workers had reported a carbonyl propargylation reaction via dual chromium/photoredox catalysis, taking advantage by a catalytic radical three components coupling of 1,3-enynes, aldehydes and a radical precursor in the presence of CrCl_3 under visible light.¹⁹⁷

However, the direct use of propargylic halides or alkynes for the generation of organometallic propargylic species represented an unexplored topic in the field of dual photoredox and transition metal catalysis.

We were pleased to realize that a practical and effective photoredox propargylation of aldehydes could be developed in the presence of a catalytic amount of titanocene dichloride.

Again, no scavengers were used for the process, but a catalytic amount of 3DPAFIPN, under visible light irradiation combined with a suitable organic reductant was shown able to replace the overstoichiometric $\text{Mn}(0)$ as the reductant for titanium. The reaction displayed a broad scope, and an enhanced selectivity only for the homopropargyl isomer.



Chapter 3. Scheme 10 Photoredox allylation of aldehydes catalytic in titanium

¹⁹⁷ Huang, H. M.; Bellotti, P.; Daniliuc, C. G.; Glorius, F. Radical Carbonyl Propargylation by Dual Catalysis. *Angew. Chem., Int. Ed.* **2021**, *60* (5), 2464–2471. <https://doi.org/10.1002/anie.202011996>

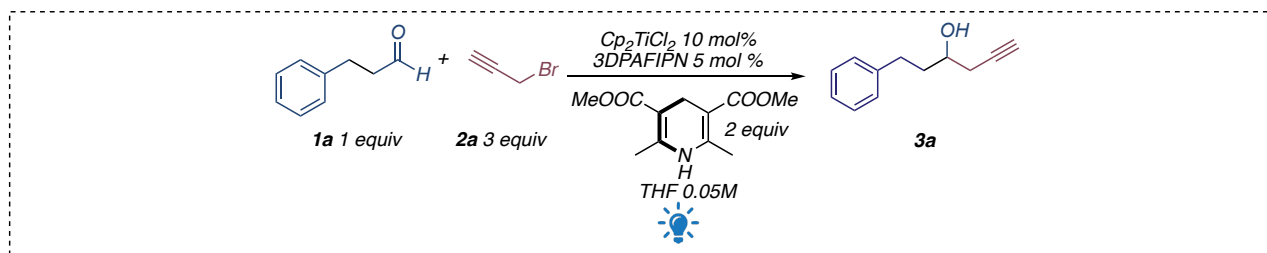
• Optimization of the reaction conditions

The salient results for the optimization of the reaction conditions are summarized in the **Table 3.2.1** and for our pleasure, the optimized parameters are consistent with the allylation protocol previously discussed. Starting by employing hydrocinnamic aldehyde (**1a**) as model substrate, we have optimized the model propargylation reaction using propargyl bromide as pronucleophile. 4CzIPN and 3CzCIIPN were tested in the model reaction leading to less satisfying results compared to the already employed 3DPAFIPN.

Reaching the electronically excited state, these two organic dyes show a less negative reduction potential, and for this reason the reaction outcome is less satisfactory when are employed. ($E(4\text{CzIPN}^{*+}/4\text{CzIPN}^*) = -1.18 \text{ V. vs SCE}$; $E(3\text{CzCIIPN}^{*+}/3\text{CzCIIPN}^*) = -0.93 \text{ V. vs. SCE}$; while $E(3\text{DPAFIPN}^{*+}/3\text{DPAFIPN}^*) = -1.38\text{V vs. SCE}$). For what concern the titanium source, all reactions were performed with the cheap and commercially available $[\text{Cp}_2\text{TiCl}_2]$. Analogously with the allylation protocol, the use of THF, with a titanium complex concentration of 0.005 M, was crucial to allow the desired transformation. Even for this reaction, Hantzsch's ester was found to be the most appropriate terminal reductant involved into the restoration of the photocatalyst. On the other hand, various sacrificial reductants (*e. g.*, TEA, DIPEA) were proved to be unsuited for the propargylation reaction. The protocol was quite sensitive to traces of water, and low yields were isolated performing the reaction in the presence of oxygen.

We were forced to observe even in this case that a positive outcome of the reaction is possible only under both extremely anhydrous conditions and strictly inert atmosphere (each successful reaction was performed in oven-dried Schlenk tubes and subjected to three 30-second freeze-pump-thaw cycles before irradiation).

It is worth noting that, even in this case, the photocatalyst do not decompose during the photoreaction but can be easily recovered (ca. 80%) at the end of the reaction by flash chromatography. The reaction could be scaled up to 1.0 mmol of starting material, increasing the reaction time to 48 h without observing an appreciable decrease of the yield.



Entry ^[a]	Deviations from standard conditions	Yield (%) ^[b]
1	none	>99(98)
2	1.0 mmol scale, 48 h, 3 mol% of 3DPAFIPN	>99(93)
3	4CzIPN instead of 3DPAFIPN	62
4	3CzClIPN instead of 3DPAFIPN	57
5	No Light	0
7	No Hantzsch's ester	0
8	No [Cp ₂ TiCl ₂]	0
9	No degassed solvent	75
10	No photocatalyst, with irradiation at 456 nm	0
11	In the presence of TEMPO (1 equiv.)	10
12	DMF instead of THF	traces

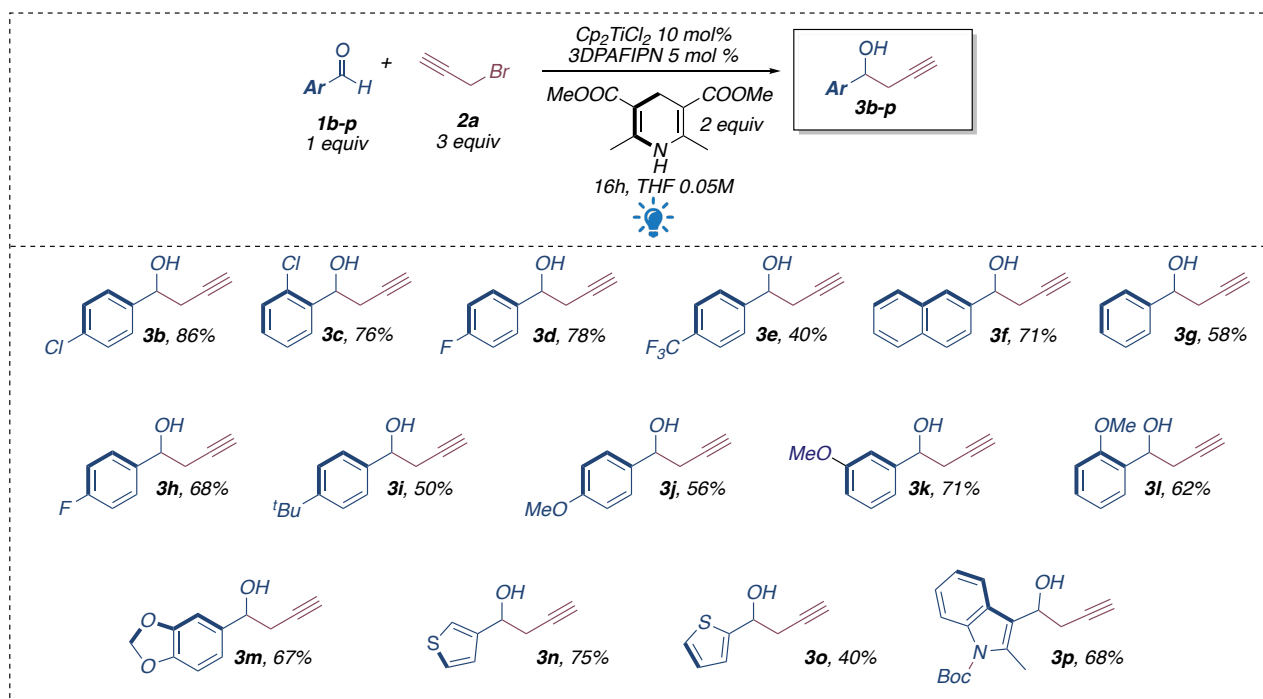
Table 3.2.1 Salient aspect of optimization of the reaction conditions

[a] Reactions performed on 0.1 mmol scale. [b] Determined by ¹H-NMR analysis. [c] Isolated yield after chromatographic purification, reaction performed on 0.2 mmol scale.

• Scope evaluation

The optimized reaction conditions were employed to test the scope of the reaction with aromatic and aliphatic aldehydes. In all reported examples with aromatic or aliphatic aldehydes, no traces of the possible allenylic product were detected by ^1H NMR analysis of the crude reaction mixture.

Aromatic and heteroaromatic aldehydes are suitable substrates for the reaction (**Scheme 11**). Yields are, in general, from good to moderate. The presence of electron-withdrawing groups on the aromatic ring reduced the outcome of the reaction. Either in presence of activating or deactivating functional groups, sterical hindrance in the *ortho*-position does not hamper the reactivity. Although the oxidized product of Hantzsch's ester (the corresponding protonated pyridinium) is strongly acidic and could favor undesired reaction pathways, indole substrates and variously substituted thiophene carboxaldehydes are reactive in the propargylation reaction. This different tolerance observed in the case of titanium-promoted propargylation reaction compared to the allylation, can be justified considering the different light sources employed in the two methodologies. In the case of allylation, indeed, most of the substrates were investigated employing a 22W blue LED stripe, while in the case of propargylations all the starting materials were functionalized employing a 456 nm-centered 40W Kessil lamp (*see the supplementary data of these section for the detailed reaction set-up description*). Probably, in this second case, the greater number of incident photons on the reaction mixture determines a decrease of the reaction time, thereby limiting the formation of parasite pathways for the starting material.



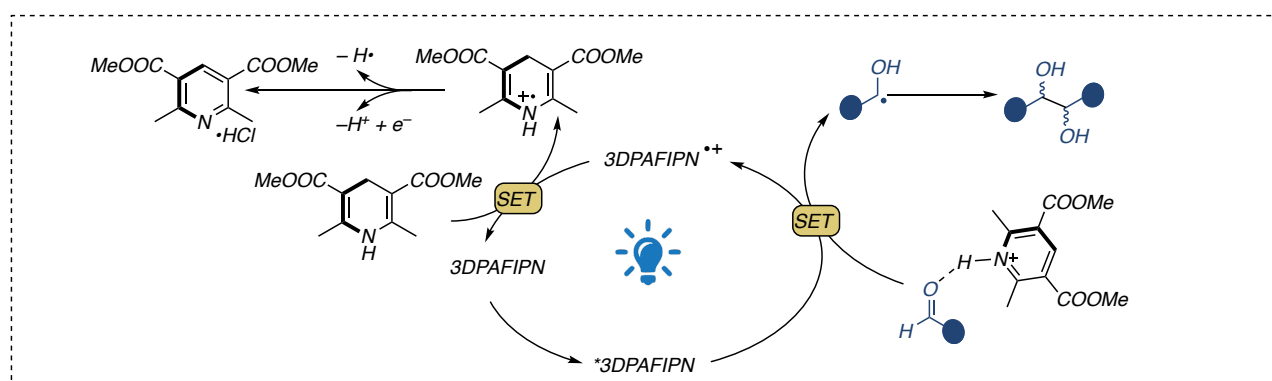
Chapter 3. Scheme 11 Propargylation of aromatic aldehydes

Comparing the presented protocol with the allylation reaction, it is noticeable that the yields of homopropargylic alcohols deriving from aromatic aldehydes are lower compared to the allylation

protocol. Although the reaction conditions are comparable for the two proposed methodologies it was observed that in the case of propargylations a non-negligible amount of starting material (5–15% depending on the substituents on the aromatic ring) was converted into an undesired and unavoidable byproduct. Analysis of the reaction crude showed in almost all the evaluated scope entries the formation of the pinacol coupling product. Because in every case the ratio between the *d/l* and *meso* isomer of the byproduct was close to 1:1, to the best of our knowledge, we believe that the formation does not derive from the titanium complex but results from the direct reduction of starting material by the photocatalyst in the excited state.

However, aromatic aldehydes possess a high reduction potential (e.g., $E(\text{benzaldehyde}/\text{benzaldehyde}^{\bullet-}) = -1.93 \text{ V vs. SCE}$) which would not allow the formation of the ketyl radical through SET with the photocatalyst. For this reason, it is likely that this unwanted pathway is favored by the presence in the reaction mixture of pyridinium salt derived from the oxidation of the Hantzsch's ester.¹⁹⁸

The acid proton of the deriving pyridinium can activate the carbonyl of the aldehyde, altering its electrochemical potential favoring the single electron reduction and consequent formation of the ketyl radical. The acid-promoted activation of redox active substrates, as presented in the introductory section, have represented a useful tool for the generation of otherwise inaccessible C-centered radicals in the early stage of the development of photoredox catalysis.⁸⁵



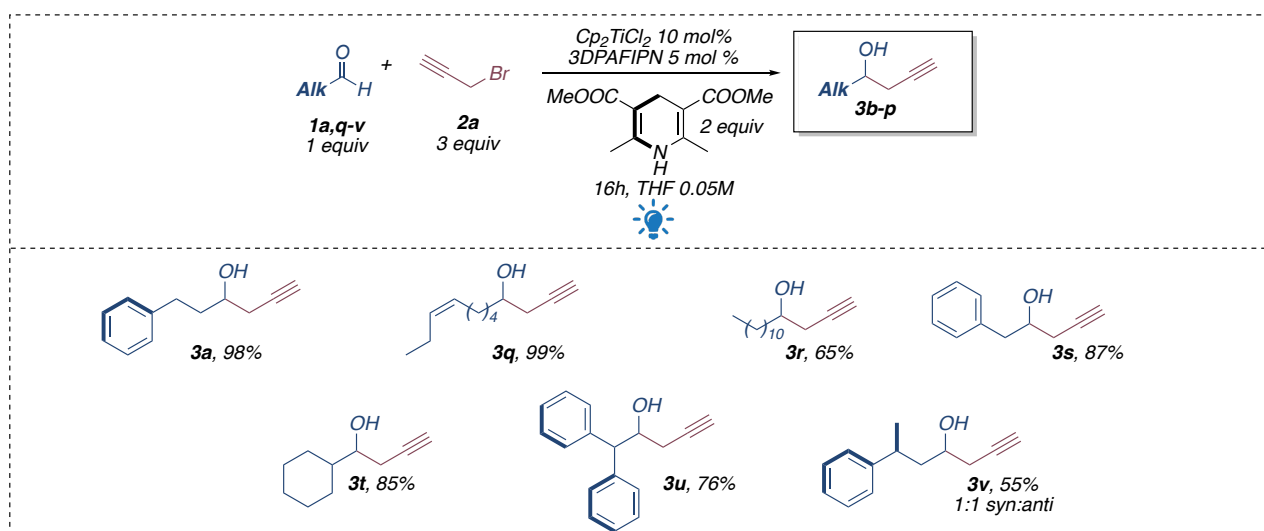
Chapter 3. Scheme 12 Plausible byprocess and consequent formation of pinacolization product.

Apparently, the protocol developed allows the formation of this by parasitic pathway because the transient allenyl/propargyl titanium complex is less reactive than the allyl titanium.

Due to the significant difference concerning their reduction potential, this byprocess is never observed when aliphatic substrates are considered. In this case, the methodology results effective and excellent results were obtained. Also branched aliphatic aldehydes were found reactive (**3t**), furnishing the corresponding homopropargylic alcohols in good yields. In addition, aliphatic aldehydes with acidic

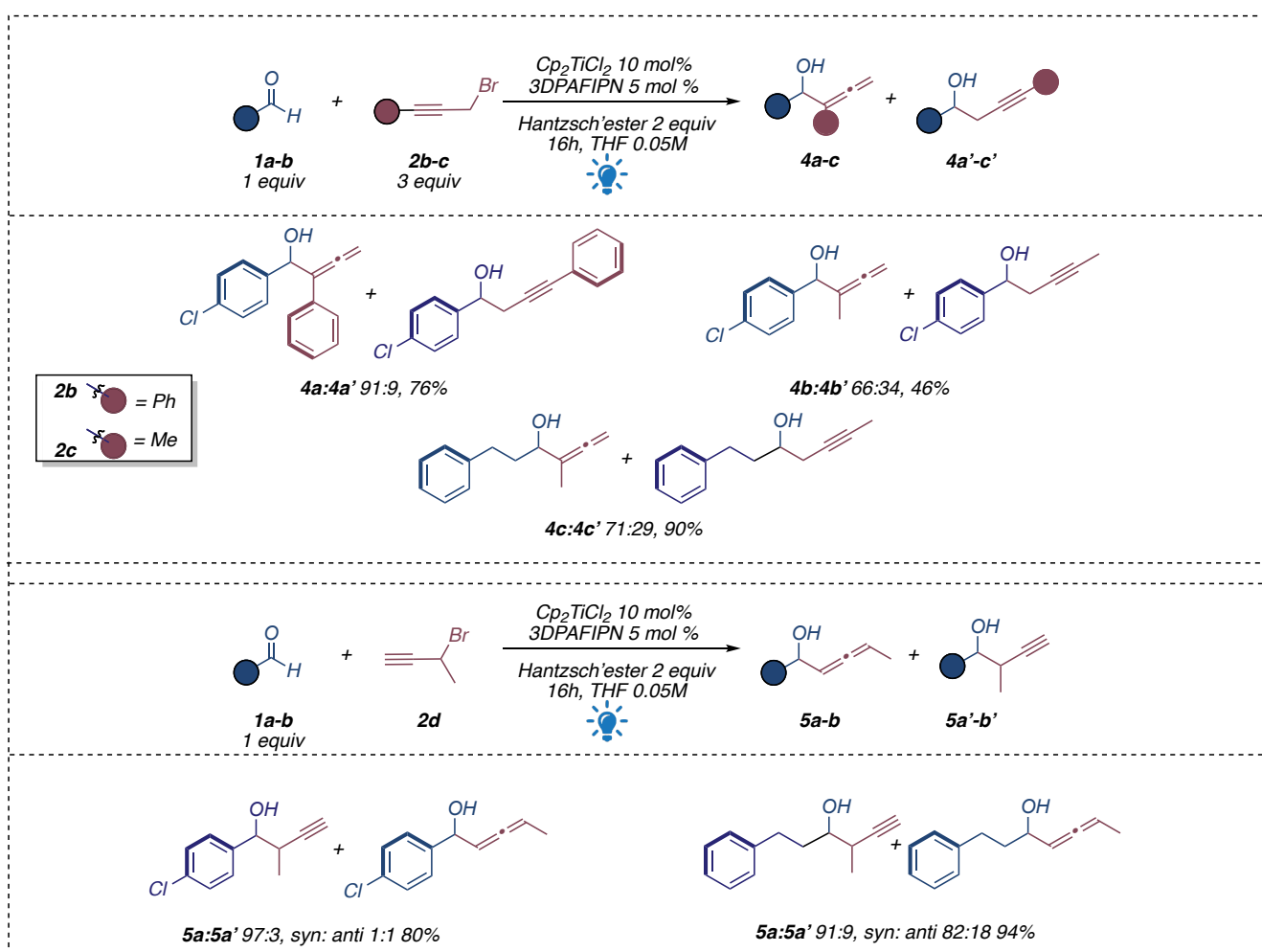
¹⁹⁸ Péter, Á.; Agasti, S.; Knowles, O.; Pye, E.; Procter, D. J. Recent Advances in the Chemistry of Ketyl Radicals. *Chem. Soc. Rev.* **2021**, *50* (9), 5349–5365. <https://doi.org/10.1039/D0CS00358A>.

protons, whose propargylation products can suffer from undesired water elimination pathways, are suitable in the reaction mixture (**3s**, **3u**).



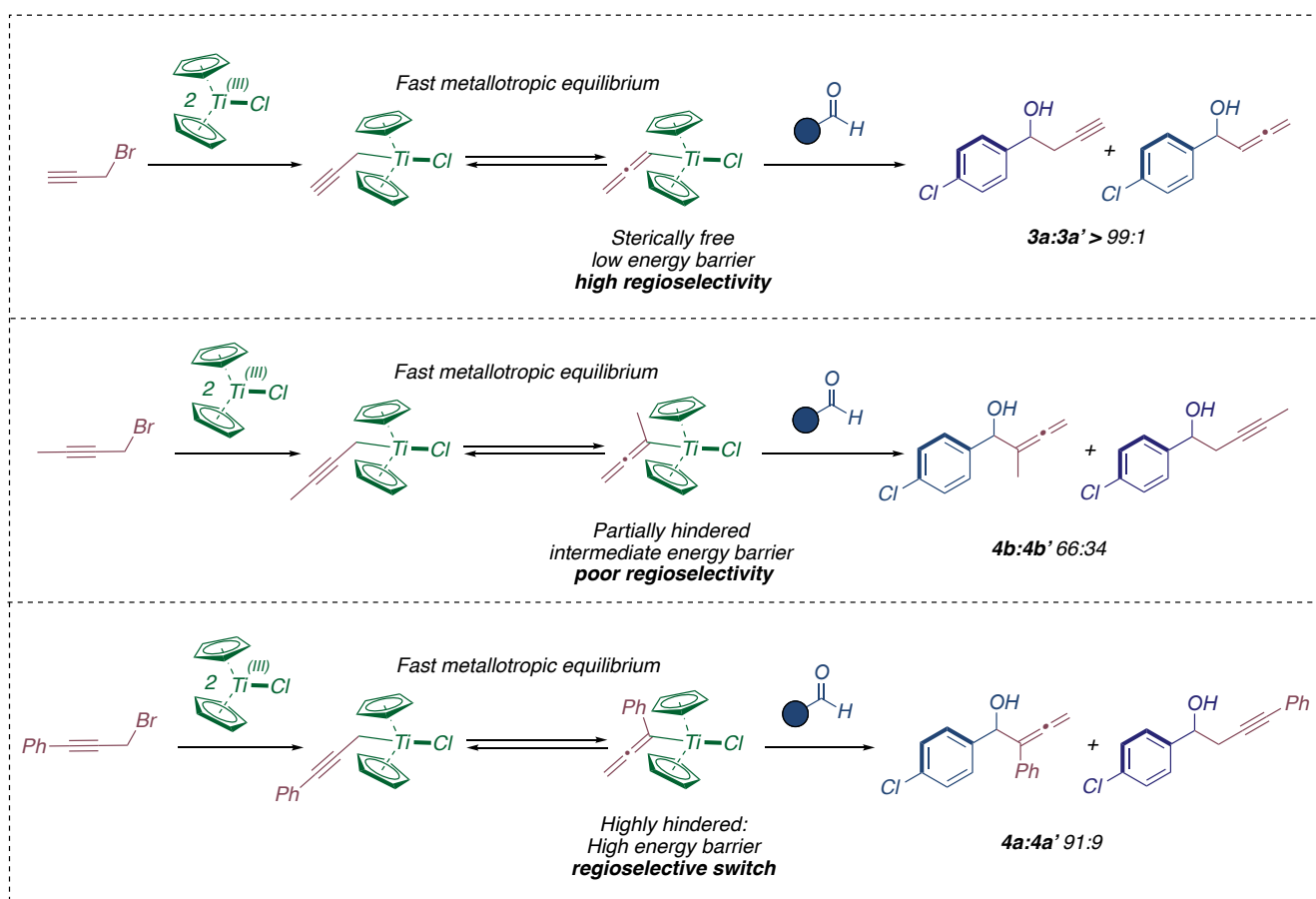
Chapter 3. Scheme 13 Propargylation of aliphatic aldehydes.

Furthermore, as in the case of the allylation protocol, we have briefly investigated the outcome of the reaction in the case of differently decorated propargyl bromides.



Chapter 3. Scheme 14 Effect of the substituents of the propargyl bromide on the regioselectivity outcome

Interestingly, the presence of aliphatic or aromatic substituents on the alkynyl moiety determines a switch of the regioselective outcome of the reaction favoring the formation of the allenylic product. This inversion derives probably due to the major sterical hindrance of the allenylic titanium intermediate, compared to the propargylic. To support our hypothesis, the synthesis and the characterizations of allenyl titanocene(IV) and propargyl titanocene(IV) were reported in literature. As confirmed by DFT calculations, these compounds in solution are involved in fast isomerization between the allenyl and propargyl before the electrophilic quenching.¹⁹⁰ Therefore, the reactivity of differently substituted propargylic halides are controlled by the different energy barriers that rule the reaction of the propargyl and allenyl titanium(IV) with carbonyls and not by their metallotropic equilibria.¹⁹⁹



Chapter 3. Scheme 15: Plausible justification for the different regiochemical outcomes

This motivation would also justify the fact that while the introduction of a phenyl group (**2b**) results in an almost total inversion of selectivity in favor of homoallenyl product, the presence of a less hindered methyl group, led the formation of a mixture of products.

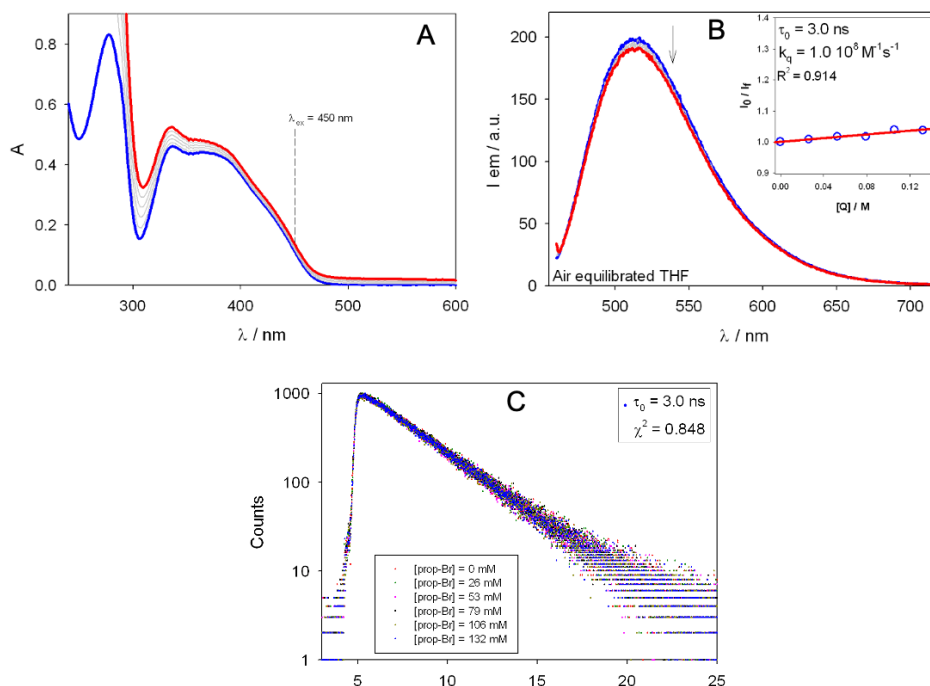
When secondary propargyl bromides were considered, the selectivity towards the formation of homopropargylic alcohol was re-established and good results were obtained in terms of yields. On the

¹⁹⁹ Ruiz-Muelle, A. B.; Oña-Burgos, P.; Ortuño, M. A.; Oltra, E. J.; Rodríguez-García, I.; Fernández, I. Unprecedented Spectroscopic and Computational Evidence for Allenyl and Propargyl Titanocene(IV) Complexes: Electrophilic Quenching of Their Metallotropic Equilibrium. *Chem. - Eur. J.* **2016**, *22*, 2427–2439. <https://doi.org/10.1002/chem.201504281>

other hand, poor diastereoselection was observed. In this case, the result could be imputable to the absence of control in the formation of the allenyl titanium intermediate.

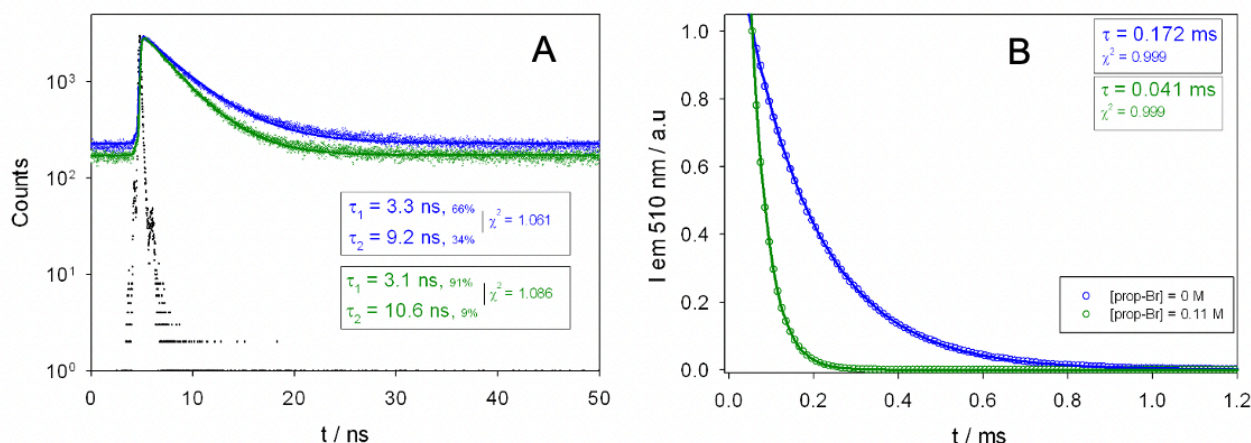
• Photophysical studies and reaction mechanism

The Stern–Volmer analysis of the reaction was conducted, similarly to the previously described study of allylation, by varying the concentration of propargyl bromide added (up to 0.13 M) to a solution of 3DPAFIPN. In air-equilibrated solution, the emission intensity of 3DPAFIPN is barely decreasing upon increasing the concentration of propargyl bromide, thus highlighting only a slow diffusional quenching ($k_q 1.0 \times 10^8 \text{ M}^{-1} \text{ s}^{-1}$).



Chapter 3. Figure 11 A: absorption spectra of solutions of 3DPAFIPN in air-equilibrated THF (blue line) obtained upon addition of increasing amounts of propargyl bromide (, up to ca. 0.13 M, red line). B: fluorescence spectra of 3DPAFIPN obtained from the same solutions at $\lambda_{ex} = 450 \text{ nm}$. Inset: Stern-Volmer diagram relative to the fluorescence spectra shown in B. C: fluorescence decays of 3DPAFIPN obtained from the same solutions as B, at $\lambda_{em} = 510 \text{ nm}$ ($\lambda_{ex} = 405 \text{ nm}$). Since the fluorescence lifetime of 3DPAFIPN is not significantly changing upon increasing additions of propargyl bromide, no Stern-Volmer constant has been calculated.

In degassed solutions, the long-excited state lifetime of 3DPAFIPN (172 μs) is decreasing to 41 μs upon the addition of propargyl bromide at high concentrations (ca. 0.11 M). The estimated quenching constant is three orders of magnitude lower than that determined for $[\text{Cp}_2\text{TiCl}_2]$ in the same experimental conditions ($k_q \approx 10^5$ and $5.2 \times 10^8 \text{ M}^{-1} \text{ s}^{-1}$, respectively), pointing out that a photoinduced electron transfer is more likely to occur to the latter.

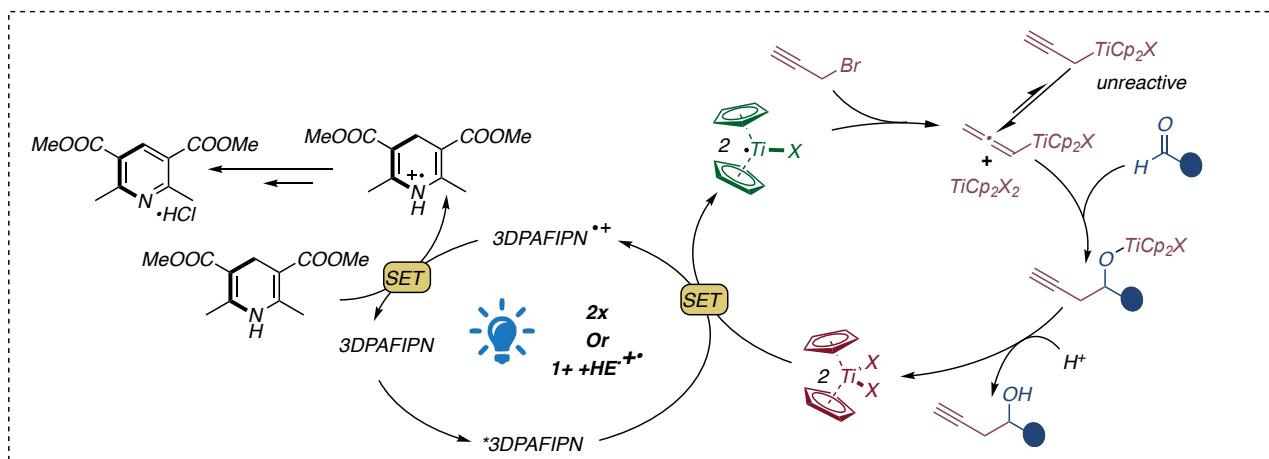


Chapter 3. Figure 12 A: prompt fluorescence decays of 3DPAFIPN obtained from degassed THF solutions at $\lambda_{em}=510$ nm (pump-freeze-thaw, 3 cycles; $\lambda_{ex}=405$ nm) in the absence and in the presence of 0.11 M (blue and green dots, respectively). The corresponding biexponential fitting curves are shown as the blue and green solid lines. The instrument response function is also shown (black dots). B: normalised emission decays of 3DPAFIPN in degassed THF solutions (pump-freeze-thaw, 3 cycles) in the absence (blue dots) and in the presence of 0.11 M (green dots). The decays are fitted with monoexponential functions (blue and green solid lines, respectively). $\lambda_{ex}=350$ nm, $\lambda_{em}=510$ nm; delay=0.05 ms; gate=0.01 ms. Based on these emission lifetimes, the quenching constant k_q is estimated as ca. $1.8 \cdot 10^5$ M⁻¹s⁻¹.

For this reason, we assume that the oxidative quenching of 3DPAFIPN* determines the formation of titanocene monochloride. The concomitantly formed 3DPAFIPN⁺ is a strong oxidant ($E(3DPAFIPN^+/3DPAFIPN) = +1.30$ vs SCE) and can be reduced by the Hantzsch's ester ($E(HE^+/HE) = +1.0$ vs SCE), restoring the 3DPAFIPN to its early oxidation state. This second event produces the strong reductant HE⁺ that can participate in further electron transfer events,¹⁸⁰ generating the rearomatized Hantzsch's ester.

The transient nucleophilic allenyl titanium species arises after a radical-mediated addition of 2[Cp₂TiCl] to the propargyl bromide. The active organometallic species is quenched by the aldehyde through an S_E2'-type mechanism leading the formation of the titanium-alkoxy derivative.

The desired product is released by acidic protons available from the oxidized Hantzsch's ester pyridinium salt that acts as scavenger for the reaction. Concurrently, this event allows the restoration of the pristine titanium complex that can be successively involved in a new catalytic cycle.



Chapter 3. Figure 13 Proposed catalytic cycle for dual propargylation of aldehydes

• Conclusions

In summary, we have described a new direct photoredox propargylation reactions mediated by a cheap and not toxic titanium complex. The large applicability of the protocol has been demonstrated with a broad scope in which various functional groups are tolerated in the case of both aromatic and aliphatic aldehydes. Compared to other proposed metal-catalyzed propargylation of carbonyl compounds, it was possible to realize a methodology under reducing conditions avoiding the use of stoichiometric metal reductants employing a visible light responsive photocatalyst.

Remarkably, the reaction in the presence of simple propargyl bromide turns out to be totally selective towards the formation of the corresponding homopropargyl product. The use of substituted propargyl bromides, instead, resulted in a switch in process selectivity. Although these latter results were only preliminarily investigated, important insights for possible future developments were provided. From these data, it would be possible to start an investigation that would allow to improve even more the allenyl-selectivity and extending the methodology to differently decorated propargyl bromides.

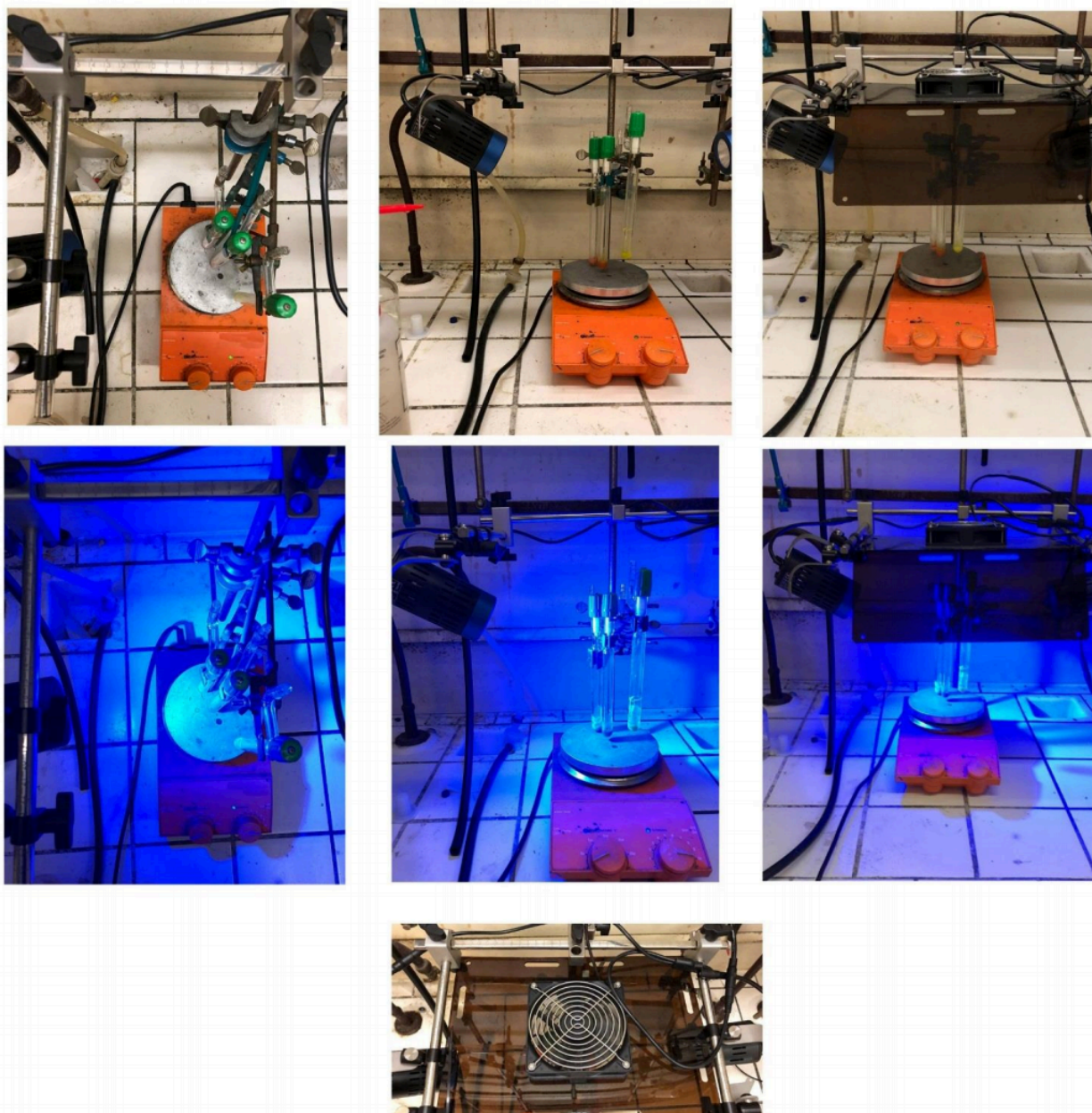
• Supplementary data**General methods and materials**

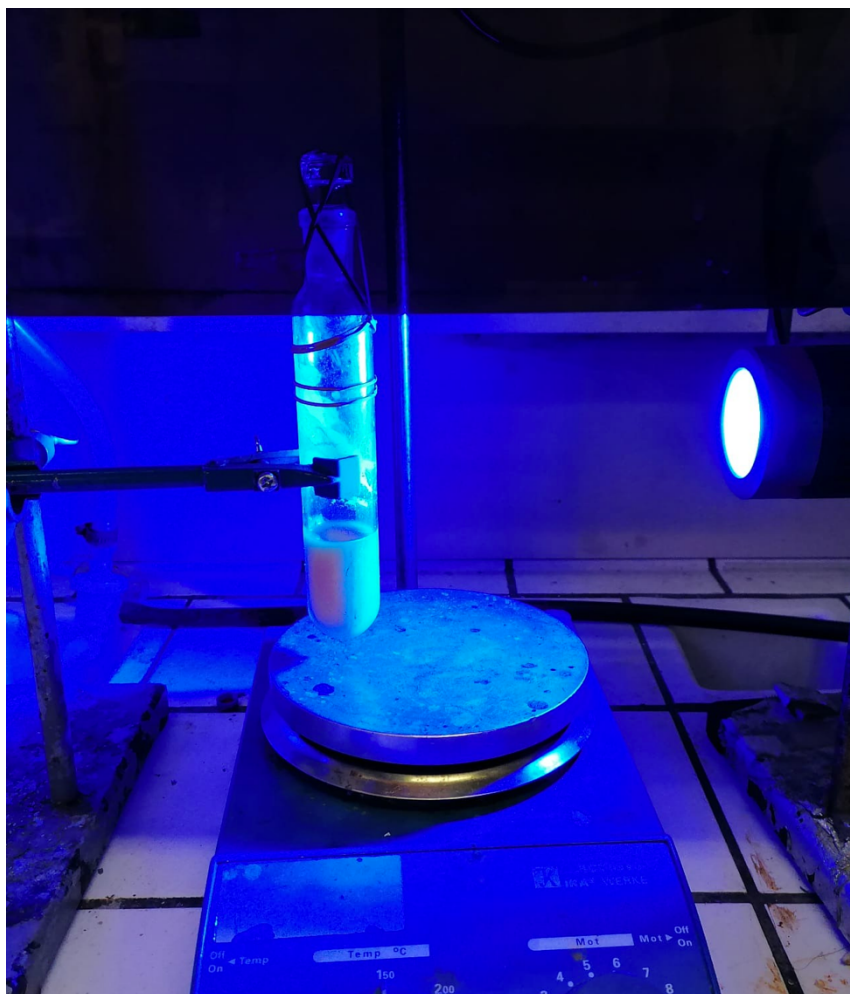
¹H-NMR spectra were recorded on Varian Mercury 400 spectrometer. Chemical shifts are reported in ppm from TMS with the solvent resonance as the internal standard (CHCl₃: δ = 7.26 ppm). Data are reported as follows: chemical shift, multiplicity (s = singlet, d = duplet, t = triplet, q = quartet, dd = double duplet, m = multiplet), coupling constants (Hz). ¹³C-NMR spectra were recorded on Varian Mercury 400 spectrometer. Chemical shifts are reported in ppm from TMS with the solvent as the internal standard (CDCl₃: δ = 77.0 ppm). Chromatographic purification was done with 240-400 mesh silica gel. All reactions were set up under an argon atmosphere in oven-dried glassware using standard Schlenk techniques.

Anhydrous solvents were supplied by Aldrich in Sureseal® bottles and were used, unless otherwise noted, without further purification. All the reagents were purchased from commercial sources (Sigma-Aldrich, Alfa Aesar, Fluorochem, Strem Chemicals, TCI) and used without further purification unless specified. Reaction mixture was irradiated with Kessil® PR160L@456 nm.

Photophysical and mechanistic studies

All the photophysical analyses were carried out in air-equilibrated tetrahydrofuran at 298 K unless otherwise specified. UV–vis absorption spectra were recorded with a PerkinElmer λ 40 spectrophotometer using quartz cells with optical path length of 1.0 cm. Degassed solutions are obtained by means of repeated pump-freeze-thaw cycles (ca. $4 \cdot 10^{-6}$ mbar) in sealed quartz cuvettes. Luminescence spectra were performed with a PerkinElmer LS-50, a Varian Cary Eclipse or an Edinburgh FLS920 spectrofluorimeter equipped with a Hamamatsu R928 phototube. Lifetimes shorter than 10 μ s were measured by the above-mentioned Edinburgh FLS920 spectrofluorimeter equipped with a TCC900 card for data acquisition in time-correlated single-photon counting experiments (0.5 ns time resolution). The estimated experimental errors are 2 nm on the band maximum, 5% on the molar absorption coefficient and luminescence lifetime.





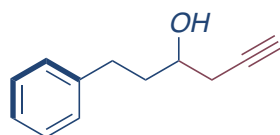
Chapter 3. Supplementary 14: Reaction set-up for 1 mmol scale

The reaction flasks were positioned approximately at 10 cm from the light source and Kessil® PR160 Rig with Fan Kit was used to control the temperature. The reaction temperature was close to room temperature during the irradiation as measured with a thermometer at 1 cm from reaction flask.

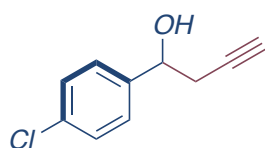
General procedure for photoredox titanium-catalyzed propargylation of aldehydes

Standard procedure: All the reactions were performed on 0.2 mmol scale of aldehyde. A dry 10 mL Schlenk tube, equipped with a Rotaflo stopcock, magnetic stirring bar, and argon supply tube, was first charged under argon with the organic photocatalyst 3DPAFIPN (5 mol%, 0.010 mmol, 6.4 mg), [Cp₂TiCl₂] catalyst (10 mol%, 0.02 mmol, 5.0 mg), diethyl 1,4-dihydro-2,6-dimethyl-3,5-pyridinedicarboxylate Hantzsch's ester (2 equivalents, 0.4 mmol, 100 mg). Inhibitor-free dry THF (4 mL, in order to obtain a 0.05 M solution of aldehyde) was then added and the reaction mixture was further subjected to a freeze-pump-thaw procedure (three cycles) and the vessel was refilled with argon. Then, propargyl bromide derivative **2a-d** (0.6 mmol, 3 equiv.) and the substrate **1a-v** (0.2 mmol) were added. The reaction was irradiated under vigorous stirring for 14 hours. After that the reaction mixture were quenched with H₂O (approx. 5 mL) and extracted with AcOEt (4 x 5 mL). The combined organic layers were dried over anhydrous Na₂SO₄ and the solvent was removed under reduced pressure. The crude was subject of flash column chromatography (SiO₂) to afford the products **3a-v**, **4a-c** and **5a-b** in the stated yields.

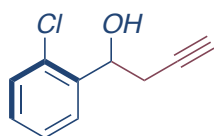
Procedure for 1 mmol scale: A dry 50 mL Schlenk tube, equipped with magnetic stirring bar and argon supply tube, was first charged under argon with the organic photocatalyst 3DPAFIPN (3 mol%, 0.03 mmol, 19 mg), [Cp₂TiCl₂] catalyst (8 mol%, 0.08 mmol, 0.020 g), diethyl 1,4-dihydro-2,6-dimethyl-3,5-pyridinedicarboxylate Hantzsch's ester (2 equivalents, 2 mmol, 0.500 g). Inhibitor-free dry THF (20 mL in order to obtain a 0.05 M solution of aldehyde) was then added and the reaction mixture was further subjected to a freeze-pump-thaw procedure (four cycles) and the vessel refilled with argon. Then, propargyl bromide **2a** (80% v/v in toluene, 3 mmol, 3 equiv. 0.280 mL) and the substrate **1a** (1 mmol, 0.134 g, 0.132 mL) were added. The reaction was irradiated under vigorous stirring for 48 hours. After that the solvent was removed under reduced pressure. The crude was subject of flash column chromatography (SiO₂) to afford the products **3a** in 93% yield (0.93 mmol, 0.162 g).



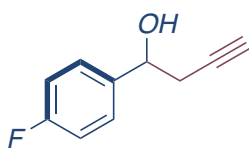
(3a): brown oil, 98% (0.195 mmol, 34 mg). The general procedure was applied using **1a** (0.2 mmol, 26 μ L) previously distilled and **2a** (solution 80% v/v in toluene, 0.6 mmol, 56 μ L, 3 equiv.). The title compound was isolated by flash column chromatography (100% DCM). Spectroscopic data are in agreement with those reported in the literature.²⁰⁰



(3b): brown oil, 86% (0.17 mmol, 31 mg). The general procedure was applied using **1b** (0.2 mmol, 28 mg) and **2a** (solution 80% v/v in toluene, 0.6 mmol, 56 μ L, 3 equiv.). The title compound was isolated by flash column chromatography (100% DCM). Spectroscopic data are in agreement with those reported in the literature.²⁰¹



(3c): brown oil, 76% (0.15 mmol, 27 mg). The general procedure was applied using **1c** (0.2 mmol, 22.4 μ L) previously distilled and **2a** (solution 80% v/v in toluene, 0.6 mmol, 56 μ L, 3 equiv.). The title compound was isolated by flash column chromatography (100% DCM). Spectroscopic data are in agreement with those reported in the literature.²⁰⁰

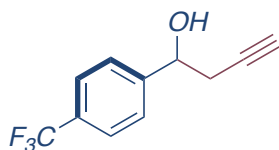


(3d): brown oil, 78% (0.16 mmol, 22.3 mg). The general procedure was applied using **1d** (0.2 mmol, 22 μ L) previously distilled and **2a** (solution 80% v/v in toluene, 0.6 mmol, 56 μ L, 3 equiv.). The title compound was isolated by flash column chromatography (100% DCM). Spectroscopic data are in agreement with those reported in the literature.²⁰²

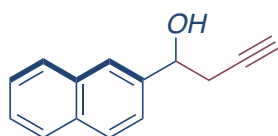
²⁰⁰ Liang, T.; Woo, S. K.; Krische, M. J. C-Propargylation Overrides O-Propargylation in Reactions of Propargyl Chloride with Primary Alcohols: Rhodium-Catalyzed Transfer Hydrogenation. *Angew. Chemie - Int. Ed.* **2016**, *55* (32), 9207–9211. <https://doi.org/10.1002/ange.201603575>

²⁰¹ Jain, P.; Wang, H.; Houk, K. N.; Antilla, J. C. Brønsted Acid Catalyzed Asymmetric Propargylation of Aldehydes. *Angew. Chemie - Int. Ed.* **2012**, *51* (6), 1391–1394. <https://doi.org/10.1002/anie.201107407>.

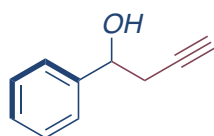
²⁰² Reddy, L. R. Chiral Brønsted Acid Catalyzed Enantioselective Propargylation of Aldehydes with Allenylboronate. *Org. Lett.* **2012**, *14* (4), 1142–1145. <https://doi.org/10.1021/ol300075n>



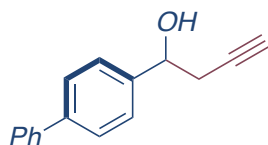
(3e): brown oil, 40% (0.08 mmol, 18 mg). The general procedure was applied using **1e** (0.2 mmol, 28 μ L) previously distilled and **2a** (solution 80% v/v in toluene, 0.6 mmol, 56 μ L, 3 equiv.). The title compound was isolated by flash column chromatography (100% DCM). Spectroscopic data are in agreement with those reported in the literature.²⁰³



(3f): brown oil, 71% (0.14 mmol, 28 mg). The general procedure was applied using **1f** (0.2 mmol, 32 mg) and **2a** (solution 80% v/v in toluene, 0.6 mmol, 56 μ L, 3 equiv.). The title compound was isolated by flash column chromatography (100% DCM). Spectroscopic data are in agreement with those reported in the literature.²⁰³



(3g): brown oil, 58% (0.12 mmol, 18 mg). The general procedure was applied using **1g** (0.2 mmol, 20.4 μ L) previously distilled and (solution 80% v/v in toluene, 0.6 mmol, 56 μ L, 3 equiv.). The title compound was isolated by flash column chromatography (100% DCM). Spectroscopic data are in agreement with those reported in the literature.²⁰⁴

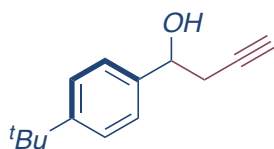


(3h): brown oil, 68% (0.14 mmol, 30.2 mg). The general procedure was applied using **1h** (0.2 mmol, 36 mg) and **2a** (solution 80% v/v in toluene, 0.6 mmol, 56 μ L, 3 equiv.). The title compound was isolated by

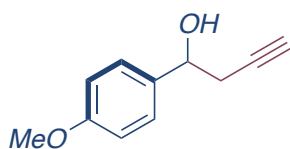
²⁰³ Chen, J.; Captain, B.; Takenaka, N. Helical Chiral 2,2'-Bipyridine N-Monoxides as Catalysts in the Enantioselective Propargylation of Aldehydes with Allenyltrichlorosilane. *Org. Lett.* **2011**, *13* (7), 1654–1657. <https://doi.org/10.1021/ol200102c>

²⁰⁴ Trost, B. M.; Ngai, M. Y.; Dong, G. Ligand-Accelerated Enantioselective Propargylation of Aldehydes via Allenylzinc Reagents. *Org. Lett.* **2011**, *13* (8), 1900–1903. <https://doi.org/10.1021/ol200043n>

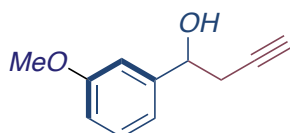
flash column chromatography (100% DCM). Spectroscopic data are in agreement with those reported in the literature.²⁰⁵



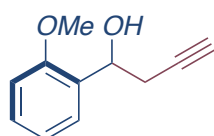
(3i): brown oil, 50% (0.1 mmol, 20.2 mg). The general procedure was applied using **1i** (0.2 mmol, 32 μ L) previously distilled and **2a** (solution 80% v/v in toluene, 0.6 mmol, 56 μ L, 3 equiv.). The title compound was isolated by flash column chromatography (100% DCM). Spectroscopic data are in agreement with those reported in the literature.²⁰⁶



(3j): brown oil, 56% (0.11 mmol, 19 mg). The general procedure was applied using **1j** (0.2 mmol, 26 μ L) and **2a** (solution 80% v/v in toluene, 0.6 mmol, 56 μ L, 3 equiv.). The title compound was isolated by flash column chromatography (100% DCM). Spectroscopic data are in agreement with those reported in the literature.²⁰⁷



(3k): brown oil, 71% (0.14 mmol, 25 mg). The general procedure was applied using **1k** (0.2 mmol, 26 μ L) and **2a** (solution 80% v/v in toluene, 0.6 mmol, 56 μ L, 3 equiv.). The title compound was isolated by flash column chromatography (100% DCM). Spectroscopic data are in agreement with those reported in the literature.²⁰¹

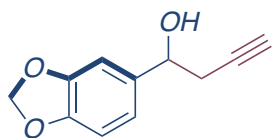


²⁰⁵ Li, Y.; Brand, J. P.; Waser, J. Gold-Catalyzed Regioselective Synthesis of 2- and 3-Alkynyl Furans. *Angew. Chemie - Int. Ed.* **2013**, *52* (26), 6743–6747. <https://doi.org/10.1002/anie.201302210>.

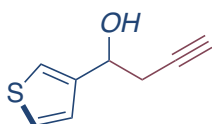
²⁰⁶ Borowiecki, P.; Dranka, M. A facile lipase-catalyzed KR approach toward enantiomerically enriched homopropargyl alcohols. *Bioorg. Chem.* **2019**, *93*, 102754–102769

²⁰⁷ Vaganov, V. Y.; Fukazawa, Y.; Kondratyev, N. S.; Shipilovskikh, S. A.; Wheeler, S. E.; Rubtsov, A. E.; Malkov, A. V. Optimization of Catalyst Structure for Asymmetric Propargylation of Aldehydes with Allenyltrichlorosilane. *Adv. Synth. Catal.* **2020**. <https://doi.org/10.1002/adsc.202000936>.

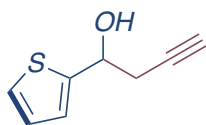
(3l): brown oil, 62% (0.12 mmol, 22 mg). The general procedure was applied using **1l** (0.2 mmol, 26 μ L) and **2a** (solution 80% v/v in toluene, 0.6 mmol, 56 μ L, 3 equiv.). The title compound was isolated by flash column chromatography (100% DCM). Spectroscopic data are in agreement with those reported in the literature.²⁰³



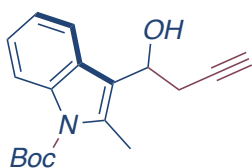
(3m): brown oil, 67% (0.13 mmol, 25 mg). The general procedure was applied using **1m** (0.2 mmol, 38 mg) and **2a** (solution 80% v/v in toluene, 0.6 mmol, 56 μ L, 3 equiv.). The title compound was isolated by flash column chromatography (100% DCM). Spectroscopic data are in agreement with those reported in the literature.²⁰³



(3n): brown oil, 75% (0.15 mmol, 23 mg). The general procedure was applied using **1n** (0.2 mmol, 18 μ l) and **2a** (solution 80% v/v in toluene, 0.6 mmol, 56 μ L, 3 equiv.). The title compound was isolated by flash column chromatography (100% DCM). Spectroscopic data are in agreement with those reported in the literature.²⁰⁸



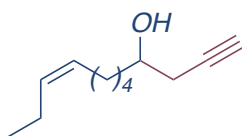
(3o): brown oil, 40% (0.08 mmol, 12 mg). The general procedure was applied using **1o** (0.2 mmol, 18 μ l) and **2a** (solution 80% v/v in toluene, 0.6 mmol, 56 μ L, 3 equiv.). The title compound was isolated by flash column chromatography (100% DCM). Spectroscopic data are in agreement with those reported in the literature.²⁰⁴



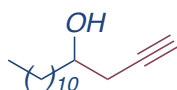
(3p): brown oil, 68% (0.14 mmol, 41 mg). The general procedure was applied using **1p** (0.2 mmol, 52 mg) and **2a** (solution 80% v/v in toluene, 0.6 mmol, 56 μ L, 3 equiv.). The title compound was isolated by flash column chromatography (100% DCM). ¹H NMR (401 MHz, CDCl₃) δ 8.10 (d, J = 8.0 Hz, 1H), 7.77 (d, J = 7.6 Hz, 1H), 7.30 – 7.16 (m, 2H overlapped with the residual peak of the solvent), 5.22 (dd, J = 7.9, 6.2 Hz, 1H), 2.96 (ddd, J = 16.7, 8.2, 2.4 Hz, 1H), 2.68 (ddd, J = 16.7, 5.8, 2.4 Hz, 1H), 2.60 (s,

²⁰⁸ Xu, M.; Ren, T. T.; Wang, K. B.; Li, C. Y. Synthesis of Cyclobutanones via Gold-Catalyzed Oxidative Rearrangement of Homopropargylic Ethers. *Adv. Synth. Catal.* **2013**, 355 (13), 2488–2494. <https://doi.org/10.1002/adsc.201300227>.

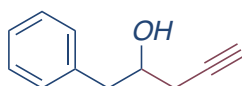
3H), 2.35 (s, 1H), 2.06 (t, $J = 2.3$ Hz, 1H), 1.68 (s, 9H). ^{13}C NMR (101 MHz, CDCl_3) δ 150.6, 136.0, 134.2, 127.3, 123.5, 122.4, 119.4, 118.4, 115.4, 83.9, 80.9, 70.5, 67.1, 28.2, 27.4, 14.2.



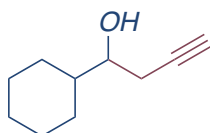
(3q): yellow oil, 99%. (0.2 mmol, 36 mg). The general procedure was applied using **1q** (0.2 mmol, 34 μL) and **2a** (solution 80% v/v in toluene, 0.6 mmol, 56 μL , 3 equiv). The title compound was isolated by flash column chromatography (100% DCM). ^1H NMR (400 MHz, CDCl_3) δ 5.50 – 5.19 (m, 2H), 3.80 – 3.71 (m, 1H), 2.43 (ddd, $J = 16.7, 4.7, 2.6$ Hz, 1H), 2.31 (ddd, $J = 16.7, 6.7, 2.6$ Hz, 1H), 2.11 – 1.98 (m, 5H), 1.97 – 1.85 (m, 1H), 1.57 – 1.51 (m, 2H), 1.44 – 1.35 (m, 3H), 1.25 (m, 1H), 0.95 (td, $J = 7.5, 2.2$ Hz, 3H). ^{13}C NMR (101 MHz, CDCl_3) δ 131.8, 128.8, 80.8, 70.7, 69.8, 36.1, 29.6, 27.3, 26.9, 25.2, 20.5, 14.3.



(3r): brown oil, 65% (0.13 mmol, 25 mg). The general procedure was applied using **1r** (0.2 mmol, 32 μL) and **2a** (solution 80% v/v in toluene, 0.6 mmol, 56 μL , 3 equiv.). The title compound was isolated by flash column chromatography (100% DCM). Spectroscopic data are in agreement with those reported in the literature.²⁰⁹



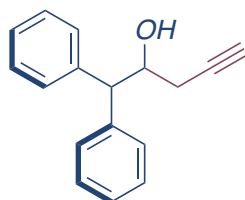
(3s): brown oil, 87% (0.17 mmol, 28 mg). The general procedure was applied using **1s** (0.2 mmol, 23 μL) and **2a** (solution 80% v/v in toluene, 0.6 mmol, 56 μL , 3 equiv.). The title compound was isolated by flash column chromatography (100% DCM). Spectroscopic data are in agreement with those reported in the literature.²¹⁰



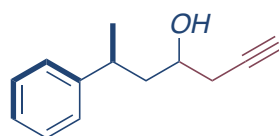
²⁰⁹ Motodate, S.; Kobayashi, T.; Fujii, M.; Mochida, T.; Kusakabe, T.; Katoh, S.; Akita, H.; Kato, K. Synthesis of β -Methoxyacrylate Natural Products Based on Box-Pd IIcatalyzed Intermolecular Methoxycarbonylation of Alkynes. *Chem. - An Asian J.* **2010**, *5* (10), 2221–2230. <https://doi.org/10.1002/asia.201000292>.

²¹⁰ Kim, J.; Jeong, W.; Rhee, Y. H. Flexible Tetrahydropyran Synthesis from Homopropargylic Alcohols Using Sequential Pd-Au Catalysis. *Org. Lett.* **2017**, *19* (1), 242–245. <https://doi.org/10.1021/acs.orglett.6b03532>

(3t): brown oil, 85% (0.17 mmol, 26 mg). The general procedure was applied using **1t** (0.2 mmol, 22 μ L) and **2a** (solution 80% v/v in toluene, 0.6 mmol, 56 μ L, 3 equiv.). The title compound was isolated by flash column chromatography (100% DCM). Spectroscopic data are in agreement with those reported in the literature.²⁰¹



(3u): brown oil, 76% (0.15 mmol, 36 mg). The general procedure was applied using **1u** (0.2 mmol, 39.2 mg) and **2a** (solution 80% v/v in toluene, 0.6 mmol, 56 μ L, 3 equiv.). The title compound was isolated by flash column chromatography (100% DCM). ¹H NMR (401 MHz, CDCl₃) δ 7.41 (dd, J = 8.2, 1.0 Hz, 2H), 7.37 – 7.18 (m, 8H), 4.54 (ddd, J = 8.7, 6.3, 4.5 Hz, 1H), 4.13 (d, J = 8.7 Hz, 1H), 2.46 (ddd, J = 16.9, 4.3, 2.7 Hz, 1H), 2.30 (ddd, J = 16.9, 6.4, 2.7 Hz, 1H), 2.17 – 2.08 (m, 1H), 2.04 (s, 1H). ¹³C NMR (101 MHz, CDCl₃) δ 141.7, 140.6, 128.8 (3C), 128.7 (2C), 128.6 (2C), 128.2, 126.8, 126.9, 80.6, 71.7, 71.1, 56.9, 25.3.



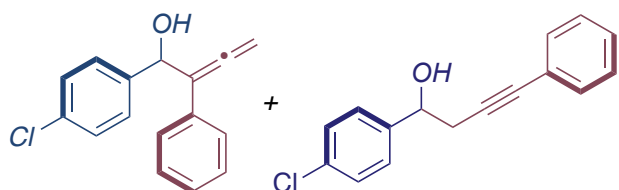
(3v): brown oil, 55% (0.11 mmol, 20 mg) as *syn:anti* mixture dr of 1:1. The general procedure was applied using **1v** (0.2 mmol, 29.6 mg) and **2a** (solution 80% v/v in toluene, 0.6 mmol, 56 μ L, 3 equiv.). The diastereoisomeric ratio was calculated considering the ¹H NMR spectrum of the reaction crude comparing the multiplet (1H) at 3.77 ppm and the multiplet (1H) at 3.49. The title compound was isolated by flash column chromatography (100% DCM). in analogy with the reported data in literature,²¹¹ it was possible to distinguish the *syn* and from the *anti* isomer as it follows.

3v_{syn} ¹H NMR (401 MHz, CDCl₃) δ 7.33 – 7.18 (m, 5H, overlapped with the residual peak of the solvent and peaks related to the other isomer aromatic protons), 3.77 (s, 1H), 3.09 – 2.97 (m, 1H), 2.52 – 2.39 (m, 1H), 2.05 (t, J = 12.0, 2.6 Hz, 2H), 1.93 – 1.83 (m, 3H), 1.33 – 1.29 (m, 3H). ¹³C NMR (101 MHz, CDCl₃) δ 146.9, 128.6 (2H), 127.1 (2H), 126.2, 80.8, 70.9, 68.0, 44.6, 36.5, 27.9, 23.1.

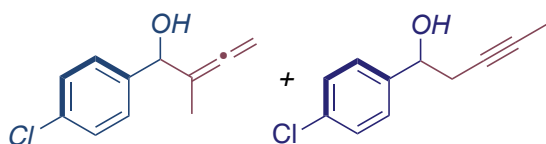
3v_{anti} ¹H NMR (401 MHz, CDCl₃) δ 7.33 – 7.18 (m, 5H, overlapped with the residual peak of the solvent and peaks related to the other isomer aromatic protons), 3.49 (s, 1H), 2.96 – 2.87 (m, 1H), 2.37 – 2.20 (m,

²¹¹ Arai, N.; Satoh, H.; Komatsu, R.; Ohkuma, T. Double Asymmetric Hydrogenation of Linear β,β -Disubstituted α,β -Unsaturated Ketones into γ -Substituted Secondary Alcohols Using a Dual Catalytic System. Chem. - Eur. J. 2017, 23 (37), 8806–8809. <https://doi.org/10.1002/chem.201701527>

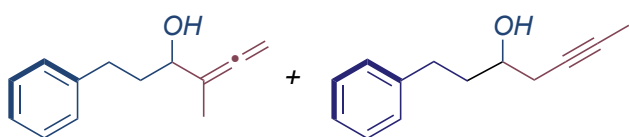
1H), 2.02 (t, $J = 12.0, 2.6$ Hz, 2H), 1.82 – 1.74 (m, 3H), 1.28 – 1.24 (m, 3H). ^{13}C NMR (101 MHz, CDCl_3) δ 146.3, 128.5 (2H), 126.8 (2H), 126.1, 80.6, 70.8, 67.7, 44.5, 36.4, 27.4, 22.0.



(**4a-4a'**): brown oil, 76% (0.14 mmol, 36 mg) as mixture regioisomer **4a:4a'** of 91:9. The general procedure was applied using **1b** (0.2 mmol, 28 mg) and **2b** (0.6 mmol, 117mg, 3 equiv). The regioisomeric ratio was calculated considering the ^1H NMR spectrum of the reaction crude comparing the multiplet (1H) at 5.71 ppm related to the product **4a** and the multiplet (1H) at 4.91 ppm related to the product **4a'**. The title compound was isolated by flash column chromatography (100% DCM). Spectroscopic data are in agreement with those reported in the literature.²¹²



(**4b-4b'**): brown oil, 46% (0.1 mmol, 18 mg) as mixture regioisomer **4b:4b'** of 66:34. The general procedure was applied using **1b** (0.2 mmol, 28 mg) and **2c** (0.6 mmol, 52 μL , 3 equiv.). The regioisomeric ratio was calculated considering the ^1H NMR spectrum of the reaction crude comparing the singlet (1H) at 5.10 ppm related to the product **4b** and the double doublet (1H) at 4.77 ppm related to the product **4b'**. The title compound was isolated by flash column chromatography (100% DCM). Spectroscopic data are in agreement with those reported in the literature.²¹³

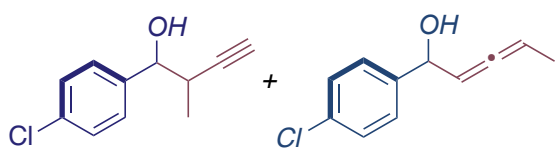


(**4c-4c'**): brown oil, 90% (0.18 mmol, 34 mg) as mixture regioisomer **4c:4c'** of 71:29. The general procedure was applied using **1v** (0.2 mmol, 26 μL) and **2c** (0.6 mmol, 52 μL , 3 equiv.). The regioisomeric ratio was calculated considering the ^1H NMR spectrum of the reaction crude comparing the triplet (1H) at 4.81 ppm related to the product **4c** and the multiplet (1H) at 4.72 ppm related to the product **4c'**. The title

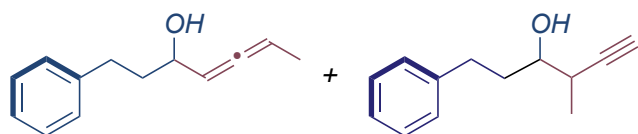
²¹² Banerjee, M.; Roy, S. Rhodium(I)-Catalyzed Carbonyl Allenylation versus Propargylation via Redox Transmetalation across Tetragonal Tin(II) Oxide. *Org. Lett.* **2004**, *6* (13), 2137–2140. <https://doi.org/10.1021/ol0493352>.

²¹³ Wang, M.; Khan, S.; Miliordos, E.; Chen, M. Enantioselective Allenylation of Aldehydes via Brønsted Acid Catalysis *Adv. Synth. Catal.* **2018**, *360* (23), 4634–4639. <https://doi.org/10.1002/adsc.201801080>.

compound was isolated by flash column chromatography (100% DCM). Spectroscopic data are in agreement with those reported in the literature.²¹⁴



(**5a-5a'**): brown oil, 80% (0.16 mmol, 31 mg) as mixture regioisomer and diastereoisomer **5a:5a'** of 97:3, **5a_{syn}:5a_{anti}** dr of 1:1. The regioisomeric ratio was calculated considering the ¹HNMR spectrum of the reaction crude comparing the doublet (1H) at 4.71 ppm related to the product **5a** and the multiplet (1H) at 5.29 ppm related to the product **5a'**. The diastereoisomeric ratio was calculated considering the ¹HNMR spectrum of the reaction crude comparing the doublet (1H) at 4.71 ppm related to the product **5a_{syn}** and the doublet (1H) at 4.51 ppm related to the product **5a_{anti}**. The general procedure was applied using **1b** (0.2 mmol, 28 mg) and **2d** (0.6 mmol, 79 mg, 3 equiv). The title compound was isolated by flash column chromatography (100% DCM). Spectroscopic data are in agreement with those reported in the literature.²¹⁵



(**5b-5b'**): brown oil, 94% (0.19 mmol, 35 mg) as mixture regioisomer and diastereoisomer of **5b:5b'** of 92:8, **5b_{syn}:5b_{anti}** dr of 18:82. The regioisomeric ratio was calculated considering the ¹HNMR spectrum of the reaction crude comparing the multiplet (1H) at 3.49 ppm related to the product **5b** and the multiplet (1H) at 4.80 ppm related to the product **5b'**. The diastereoisomeric ratio was calculated considering the ¹HNMR spectrum of the reaction crude comparing the multiplet (1H) at 3.54 ppm related to the product **5b_{syn}** and the multiplet (1H) at 3.49 ppm related to the product **5b_{anti}**. The general procedure was applied using **1a** (0.2 mmol, 26 μL) and **2d** (0.6 mmol, 79mg, 3 equiv). The title compound was isolated by flash column chromatography (100% DCM). Spectroscopic data are in agreement with those reported in the literature.²¹⁶

²¹⁴ Li, W.; Lin, Z.; Chen, L.; Tian, X.; Wang, Y.; Huang, S. H.; Hong, R. Highly Stereoselective Kinetic Resolution of α -Allenic Alcohols: An Enzymatic Approach. *Tetrahedron Lett.* **2016**, *57* (5), 603–606. <https://doi.org/10.1016/j.tetlet.2015.12.098>

²¹⁵ Miao, W.; Chung, L. W.; Wu, Y. D.; Chan, T. H. Experimental and Theoretical Studies of the Propargyl-Allenylindium System. *J. Am. Chem. Soc.* **2004**, *126* (41), 13326–13334. <https://doi.org/10.1021/ja049241n>

²¹⁶ Danheiser, L. D.; Carini, D. J.; Kwasigroch, A. C. Scope and stereochemical course of the addition of (trimethylsilyl)allenes to ketones and aldehydes. A regiocontrolled synthesis of homopropargylic alcohols. *J. Org. Chem.* **1986**, *51* (20), 3870–3878. <https://doi.org/10.1021/jo00370a023>

3.3 Diastereoselective and Enantioselective Pinacol Coupling of Aromatic Aldehydes Promoted by Titanium and a Red-Adsorbing Organic Dye²¹⁷

• Transition metal mediated pinacol coupling reactions.

The pinacol coupling reaction is a reductive coupling of carbonyl compounds that proceeds through the formation of ketyl radical in presence of a reductant, affording the corresponding 1,2-diols in one single step.²¹⁸ Owing to the usefulness of the pinacol coupling as valuable tool for the generation of umpolung intermediates in C-C bond-forming reactions, the development of diastereo- and enantioselective methodologies has been a hot topic in organic and organometallic chemistry since the second half of the last century. Several examples can be found in the literature for the ketyl radical coupling reaction in a non-light-driven manner. The common feature of most of the reported processes is the use of transition metals in low oxidation state promoting a single electron reduction in the presence of carbonyl compound (aldehydes, ketones and in some cases imines) generating the ketyl radical.

With the idea of following chronologically the developments of these techniques it is necessary to mention that the first developments involved the use of stoichiometric metal reagents capable of reducing a carbonyl system. The first *d/l*-selective pinacolization of aromatic aldehydes had been reported with modest results employing either a stannylene precursors²¹⁹ or a stoichiometric amount of TiCl₃ prepared from TiCl₄ and *n*BuLi.²²⁰

A key example was reported in 1987 by Inanaga and co-workers²²¹. Using an overstoichiometric amount of [Cp₂TiCl] – obtained after *in situ* reduction of [Cp₂TiCl₂] with ^sBuMgCl in THF, the reductive homocoupling of aromatic and α - β -unsaturated aldehydes was afforded with high *d/l*-selectivity.

²¹⁷ The results and the procedures described in this section are part of a published work:

Calogero, F.; Magagnano, G.; Potenti, S.; Pasca, F.; Fermi, A.; Gualandi, A.; Ceroni, P.; Bergamini, G.; Cozzi, P.G. Diastereoselective and Enantioselective Photoredox Pinacol Coupling Promoted by Titanium Complexes with a Red-Adsorbing Organic Dye, *Chem. Sci.*, **2022**, <https://doi.org/10.1039/D2SC00800A>. Photophysical analysis and interpretation of photophysical data were carried out by A.F. supervised by P.C. and G.B.

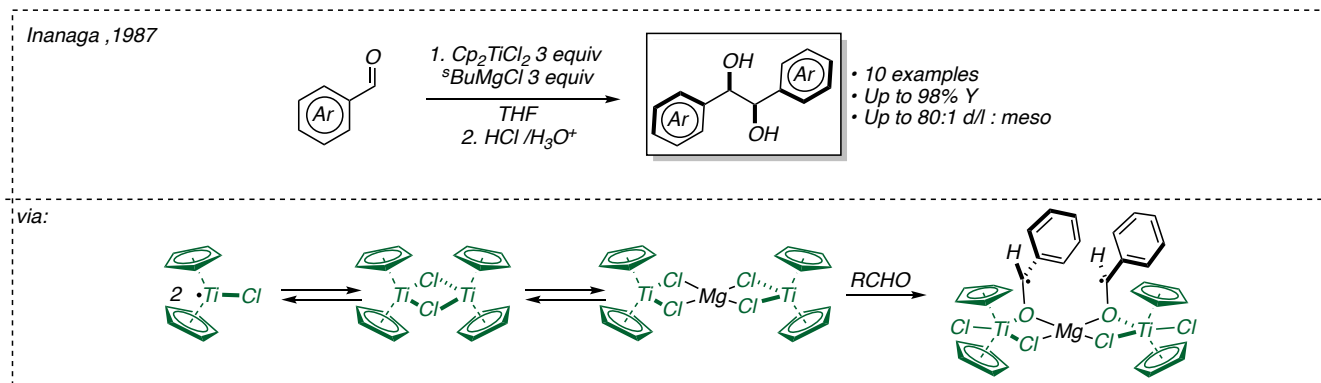
The complete characterization of the products introduced hereafter and discussed in the section “Supplementary Data” can be found in the Supporting Information of the above-mentioned work

²¹⁸ (a) Wirth, T. “New” Reagents for the “Old” Pinacol Coupling Reaction. *Angew. Chem. Int. Ed. Engl.* **1996**, *35* (1), 61–63. <https://doi.org/10.1002/anie.199600611>. (b) Fürstner, A. Chemistry of and with Highly Reactive Metals. *Angew. Chem. Int. Ed. Engl.* **1993**, *32* (2), 164–189. <https://doi.org/10.1002/anie.199301641>.

²¹⁹ Grugel, C.; Neumann, J.P.; Sauer J.; Seifert P.; A highly stereoselective C–C coupling of aldehydes forming glycols via a stannylene reaction, *Tetrahedron Lett.* **1978**, *19*, 2847–2850 [https://doi.org/10.1016/S0040-4039\(01\)94880-4](https://doi.org/10.1016/S0040-4039(01)94880-4)

²²⁰ Raubenheimer, H. G.; Seebach, D. *Chimia*, **1986**, *40*, 12–13.

²²¹ Handa, Y.; Inanaga, J. A highly stereoselective pinacolization of aromatic and α , β -unsaturated aldehydes.dta mediated by titanium(III)-magnesium(II) complex *Tetrahedron Lett.* **1987**, *28*, 5717–5718. [https://doi.org/10.1016/S0040-4039\(00\)96822-9](https://doi.org/10.1016/S0040-4039(00)96822-9)



Chapter 3. Scheme 16 Pinacol coupling of aromatic and α - β -unsaturated aldehydes in the presence of a stoichiometric quantity of titanocene dichloride

Remarkably, as reported by the authors, the stereoselectivity in the dimerization of benzaldehyde greatly depended by the other coexisting metal employed for the reduction of the titanocene complex and persistent during the reaction. In analogy with the literature reports,²²² it seemed possible that the metal ion determines the formation trimetal system (Ti(III)-Mg(II)-Ti(III)) and Ti(IV)-Mg(II)-Ti(IV)) contributing to the diastereoselective outcome of the reaction.

After these early reports, over the years the literature has been filled with examples in which other transition metals in a low oxidation state (e.g., magnesium,²²³ samarium,²²⁴ and ytterbium²²⁵ complexes) have been shown useful in promoting these diastereoselective transformations. A further powerful upgrade for the pinacol coupling reaction occurred with the development of catalytic methodologies. The first two reported works did not allow control of the diastereoselectivity of the process. Neither the utilization of a catalytic quantities of a binuclear ruthenium-based complex²²⁶ nor the employment of samarium iodide²²⁷ have been shown comparable to corresponding stoichiometric variants in the generation of a ketyl radical.

Based on the above-mentioned ability of cyclopentadienyl-titanium(III) complexes to promote stoichiometric pinacol couplings, in 1997 the first highly diastereoselective pinacol coupling of aromatic aldehydes catalyzed by a titanocene complex was reported by Gansäuer.¹⁶⁷

²²² Salzmann, J.-J.; Mosimann, P. Über die strukturellen Probleme des Di-cyclopentadienyl-titans *Helv. Chim. Acta*, **1958**, *50*, 526, 1831–1836 <https://doi.org/10.1002/hlca.19670500716>

²²³ Zhang, W.-C.; Li, C.-J. Magnesium in Water: Simple and Effective for Pinacol-Coupling. *J. Chem. Soc., Perkin Trans. 1* **1998**, No. 19, 3131–3132. <https://doi.org/10.1039/a806553e>.

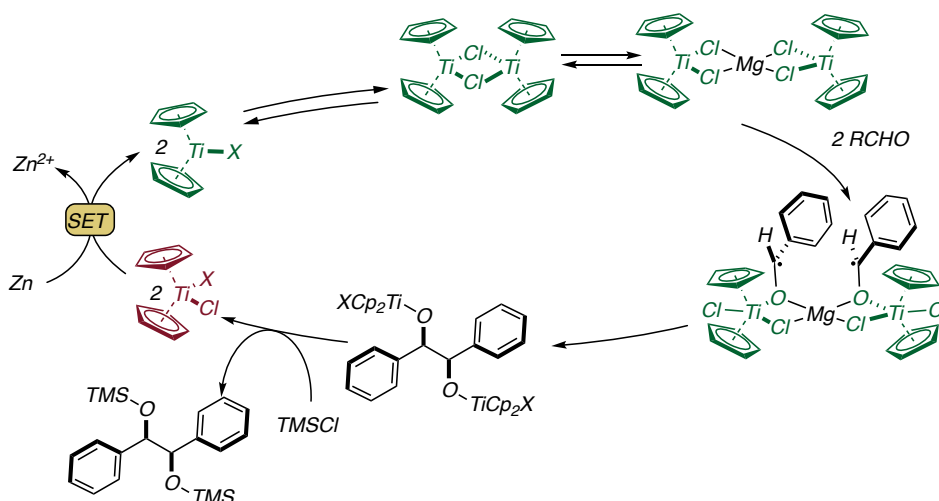
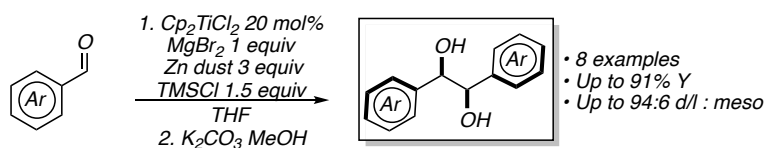
²²⁴ Namy, J. L.; Soupe J.; Kagan, H. B. Efficient formation of pinacols from aldehydes or ketones mediated by samarium diiodide *Tetrahedron Lett.*, **1983**, *24*, 765–766. [https://doi.org/10.1016/S0040-4039\(00\)81521-X](https://doi.org/10.1016/S0040-4039(00)81521-X)

²²⁵ Hou, Z.; Takamine, K.; Fujiwara Y.; Taniguchi, H. Ytterbium Metal Mediated Synthesis of Symmetrical and Unsymmetrical Pinacols from Carbonyl Compounds *Chem. Lett.*, **1987**, *16* 2061–2064.

²²⁶ Shinada, H.; Qu J.-P.; Matsuzaka, H.; Ishii Y.; Hidai, Y. Silylative Dimerization of Aromatic Aldehydes Catalyzed by a Thiolate-Bridged Diruthenium Complex *Chem. Lett.*, **1995**, *24*, 671–672. <https://doi.org/10.1246/cl.1995.671>

²²⁷ Nomura, R.; Matsuno, T.; Endo, T. Samarium Iodide-Catalyzed Pinacol Coupling of Carbonyl Compounds. *J. Am. Chem. Soc.* **1996**, *118* (46), 11666–11667. <https://doi.org/10.1021/ja962331a>.

Gansäuer, 1997



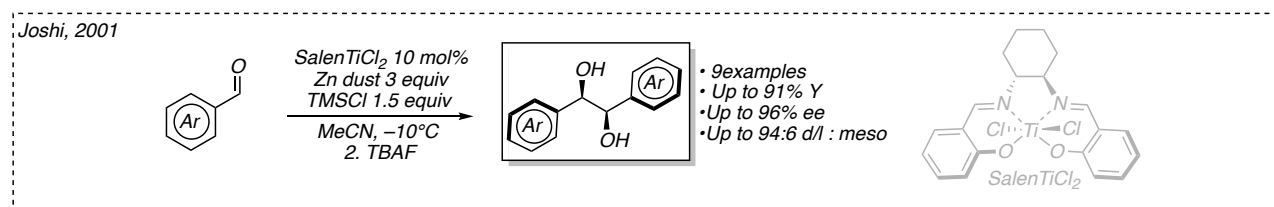
Chapter 3. Scheme 17 Pinacol coupling of aromatic aldehydes catalytic in titanium.

Under the optimized conditions a library of symmetrical 1,2-diols was synthesized in good yields and stereoselectivities. The success of the reaction is possible thanks to the presence of a significant excess of zinc dust that reduces the titanocene dichloride transiently generating the Nugent-reagent. This last can form the ketyl radical in the presence of an aromatic aldehyde after a single electron reduction. An important element that ensures this type of titanocene-mediated transformation, is the presence of an overstoichiometric amount of trimethylsilylchloride in the reaction mixture. The scavenger allows the breaking of the titanium-oxygen bond releasing the product and allowing the restoration of the catalyst. Worth mentioning, again, the formation of a transient trimetal species was found to be particularly beneficial to the diastereomeric outcome of the reaction. In fact, a marked increase in the ratio of diastereoisomers was observed in the presence of a stoichiometric amount of magnesium-based additives. Following Gansäuer's pioneering work, the use of chiral titanium-based complexes has also proven useful for the development of enantioselective variants for the pinacol coupling reaction. The first work reported by Dunlap and Nicholas,²²⁸ involving the use of chiral titanocene complexes, disclosed the possibility to obtain stereodefined symmetrical 1,2 diols with modest results. Only several years later, titanium Schiff bases²²⁹ complexes were found to be the best class of catalysts for these catalytic enantioselective

²²⁸ Dunlap M. S.; Nicholas K. M. Manganese-Promoted, Titanocene-Catalyzed Stereoselective Pinacol Coupling of Aldehydes. *Synt. Comm.* **1999**, *29*, 1097-1106. <https://doi.org/10.1080/00397919908086078>

²²⁹ (a) Shaw, S.; White, J. D. Asymmetric Catalysis Using Chiral Salen-Metal Complexes: *Recent Advances*. *Chem. Rev.* **2019**, *119*, 9381-9426; <https://doi.org/10.1021/acs.chemrev.9b00074> (b) Matsumoto, K.; Saito, B.; Katsuki, T. Asymmetric Catalysis of Metal Complexes with Non-planar ONNO Ligands: Salen, Salalen and Salan. *Chem. Commun.* **2007**, 3619-3627; DOI <https://doi.org/10.1039/B701431G> (d) Cozzi, P. G. Metal-Salen Schiff Base Complexes in Catalysis: Practical aspects. *Chem. Soc. Rev.* **2004**, *33*, 410-421; <https://doi.org/10.1039/B307853C> (e) Larrow, J. F.; Jacobsen, E. N. Asymmetric Processes Catalyzed by Chiral (Salen)Metal Complexes. *Top. Organomet. Chem.* **2004**, *6*, 123 - 152; [10.1007/b11772](https://doi.org/10.1007/b11772) (f) Canali, L.; Sherrington,

transformations. The two main contributions on this transformation were presented firstly by Riant and co-workers,²³⁰ then by Joshi and co-workers.²³¹ Both reported protocols involving the use two different chiral titanium Schiff base complexes led the formation of the desired symmetrical 1,2 diols with high yields and excellent enantioselectivity. Particularly noteworthy, the work published by Joshi reported the use of an unsubstituted chiral [(Salen)TiCl₂] complex (**Scheme 18**), simply prepared by Ti(OiPr)₄ followed by treatment with TMSCl.



Chapter 3. Scheme 18 Enantioselective pinacol coupling of aromatic aldehydes

For the reported protocol, again, the titanium complex was converted into the active Ti(III) species, through an in-situ reduction performed by a stoichiometric amount of Zn. As well as evidenced by Gansäuer, the presence of TMSCl was crucial to close the catalytic cycle, determining the pinacol silylation with concomitant restoration of Ti(IV) complex.

D. C. Utilisation of Homogeneous and Supported Chiral Metal(salen) Complexes in Asymmetric Catalysis. *Chem. Soc. Rev.* **1999**, 28, 85–93. <https://doi.org/10.1039/A806483K>

²³⁰ Bensari, A.; Renaud, J. L.; Riant, O. Enantioselective Pinacol Coupling of Aldehydes Mediated and Catalyzed by Chiral Titanium Complexes. *Org. Lett.* **2001**, 3, 3863. [10.1021/ol1016664a](https://doi.org/10.1021/ol1016664a)

²³¹ Chatterjee, A.; Bennur, T. H.; Joshi, N. N. Truly Catalytic and Enantioselective Pinacol Coupling of Aryl Aldehydes Mediated by Chiral Ti(III) Complexes. *J. Org. Chem.* **2003**, 68, 5668–5671; <https://doi.org/10.1021/jo0342875>

• Ketyl radical generation under photoredox conditions

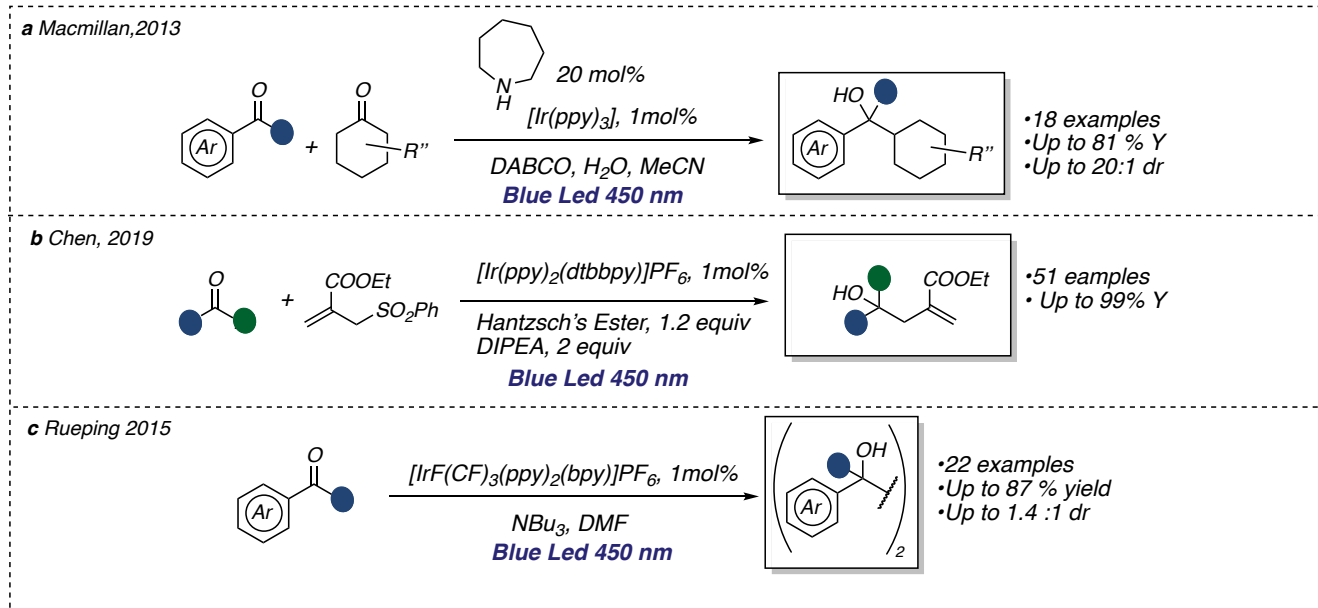
The visible light-promoted generation of ketyl radical intermediate have been accomplished using many photoactive metal complexes in presence of sacrificial donors. These approaches rely on the ability of the photocatalyst to convert visible light into chemical energy by engaging in single-electron transfer (SET) with organic substrates, thereby generating reactive ketyl radical intermediates. The first example of generation of a ketyl radical by visible light was described in 1978 by Kellogg and co-workers. The work reported the use of [Ru(bpy)₃]Cl₂ as a catalyst for the single electron reduction and fragmentation of aryl carbonyl compounds substituted by α -sulfonium groups.²³² After this report, photoredox methodologies have been applied for the generation of ketyl radicals from aldehydes or ketones, in different C-C bond forming reactions.²³³ A successful example of intramolecular ketyl radical-enabled coupling was reported by MacMillan through a dual photocatalytic and organocatalytic process for the direct β -functionalization of cyclic ketones with aryl ketones (**Scheme 19a**).²³⁴ In another example of C-C bond formation via ketyl radical, Chen and co-workers reported a visible light-mediated ‘polarity-reversed’ allylation reaction of aldehydes and ketones (**Scheme 19b**).¹⁸⁰ It is noteworthy that in this transformation, the Hantzsch’s ester acts both as an electron/proton donor and as the Lewis acid activating of the carbonyl group. Finally, the first photocatalytic pinacol coupling (**Scheme 19c**) was described by Rueping and co-workers.²³⁵ The reaction takes place through the formation of ketyl radical anions, after a direct reduction of the carbonyl moiety and concomitant oxidation of the photocatalyst.

²³² Hedstrand, D. M.; Kruizinga, W. H. Kellogg, R. M. Light Induced and Dye Accelerated Reductions of Phenacyl Onium Salts by 1,4-Dihydropyridines. *Tetrahedron Lett.*, **1978**, *19*, 1255 —1258. [https://doi.org/10.1016/S0040-4039\(01\)94515-0](https://doi.org/10.1016/S0040-4039(01)94515-0)

²³³ Xia, Q.; Dong, J.; Song, H.; Wang, Q. Visible-Light Photocatalysis of the Ketyl Radical Coupling Reaction. *Chem. Eur. J.* **2019**, *25*, 2949 – 2961. <https://doi.org/10.1002/chem.201804873>

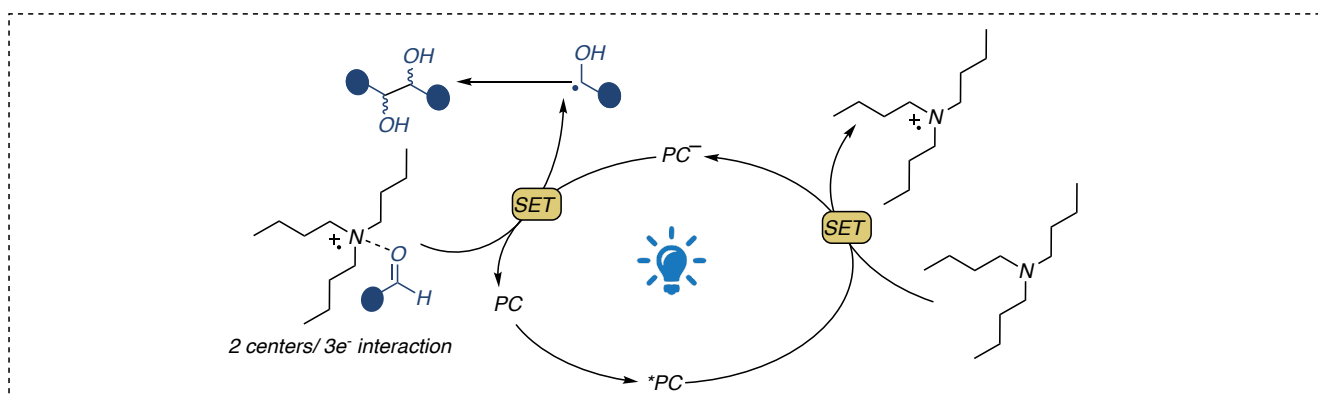
²³⁴ Petronijević, F. R.; Nappi, M.; MacMillan, D. W. C. J. Direct β -Functionalization of Cyclic Ketones with Aryl Ketones via the Merger of Photoredox and Organocatalysis. *J. Am. Chem. Soc.*, **2013**, *135*, 18323 —18326. <https://doi.org/10.1021/ja410478a>

²³⁵ Nakajima, M.; Fava, E.; Loescher, S.; Jiang, Z.; Rueping M. Photoredox-Catalyzed Reductive Coupling of Aldehydes, Ketones, and Imines with Visible Light. *Angew. Chem., Int. Ed.*, **2015**, *54*, 8828 —8832. <https://doi.org/10.1002/anie.201501556>



Chapter 3. Scheme 19 photoinduced ketyl radical generation and their application

Seminal studies reported by the same authors clarified that the tributylamine, (NBu_3), employed as terminal reductant plays a crucial role for the positive outcome of the reaction. The amine radical cation – formed upon reductive quenching of the photocatalyst – is able to interact with the carbonyl group of aromatic ketones and aldehydes, strongly influencing their reduction potentials and allowing the single electron reduction.



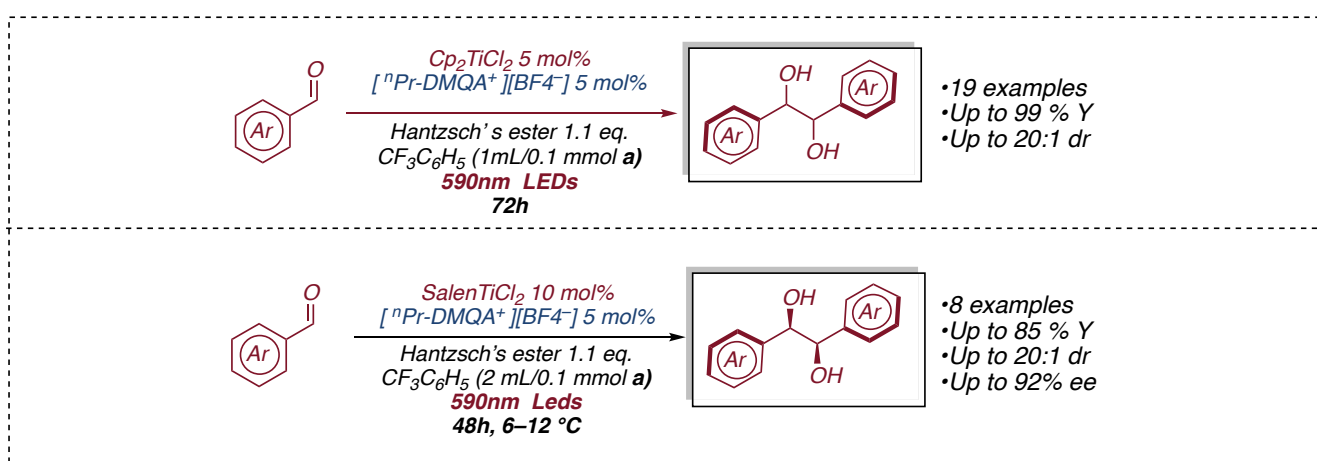
Chapter 3. Figure 14 Activation of carbonyl compounds proposed by Rueping

This interesting and mild methodology provides a simple and convenient catalytic access to symmetrical pinacols and diamines with good functional group tolerance, and good yields. However, as the radical-radical dimerization occurs fast, this step gives a mixture of diastereoisomeric diols, generally *d/l* : *meso* 1:1 in ratio in almost all catalytic processes described (dr up to 1.4 : 1).

• Presented work

The reasons why we decided to establish a protocol combining a photocatalytic system and titanium catalysis to achieve a pinacol coupling reaction stem from the desire to combine the strengths of both techniques in a way that would overcome their associated limitations. On one hand the use of titanium complexes in low oxidation state is extremely useful to realize reductive homocoupling of aromatic aldehydes, on the other hand both its catalytic and stoichiometric use is associated with a high production of wastes (that characterize -as already seen- many of the processes promoted by titanocene complexes). In the same way, the use of photocatalysis allows to promote single electron reduction and single electron oxidation processes in mild conditions and with minimum waste production. However, the use of a photocatalyst in the excited state, although capable of promoting single electron reduction of carbonyl compounds, cannot provide in the majority of cases the control to achieve a good diastereoselective outcome. For these reasons, we have hypothesized that the photo-induced generation of [Ti(III)] could be a straightforward method to perform the pinacol coupling with high diastereocontrol.

In the following paragraphs of the chapter, the detailed study of the reaction that provided a solution to the unexpected limitations originally encountered will be presented. After a long journey exploring the reactivity of the photoredox catalysis combined with titanium in low oxidation state, a highly diastereoselective ($dr > 20:1$ *d/l* : *meso* in most of the cases) pinacol coupling promoted by 5 mol% of the available [Cp₂TiCl₂] complex will be discussed. Moreover, the application of an easy to prepare chiral titanium Salen complex gave satisfactory yields in the presence of different aromatic aldehydes with a complete diastereoselection in favor of the *syn* diastereoisomers, and high enantiomeric excesses (up to 94%).



Chapter 3. Scheme 20 Red light-promoted diastereo- and enantioselective pinacol coupling of aromatic aldehydes catalytic in titanium

• Optimization of the reaction conditions

Firstly, we focused our investigation on the development of a diastereoselective version of the reaction employing $[\text{Cp}_2\text{TiCl}_2]$ as titanium complex. To evaluate all the parameters for the reaction, we chose *p*-chlorobenzaldehyde as the model substrate.

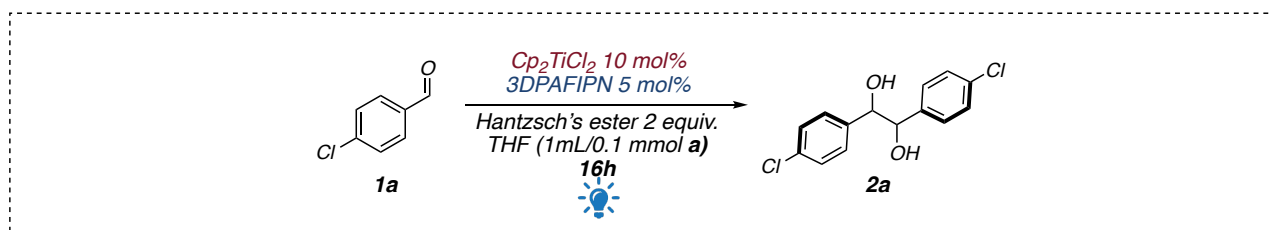
In view of the knowledge gained during the study of the previously presented methodologies, we began the development of this new reaction using as a starting point the optimized reaction conditions.

Since the previously carried out photophysical studies demonstrated the efficient formation of titanium in a low oxidation state promoted by the photoredox system, we believed that an effective diastereoselective pinacol coupling could be achieved simply removing the pronucleophilic species from the reaction environment.

In this way, once formed, the photoinduced titanium (III) species could selectively perform a single electron reduction in the presence of aromatic aldehydes leading the formation of the corresponding ketyl radical.

Already aware of the fact that the use of amine-based sacrificial agents has detrimental effects for photoredox reactions in the presence of titanium species, Hantzsch's ester was selected as an external reductant for the reaction.

Unexpectedly, performing the reaction in THF, all the attempts to use blue photon-absorbing organic dyes as well as $[\text{Ru}(\text{II})]$, $[\text{Ir}(\text{III})]$ photocatalyst, with the $[\text{Ti}(\text{IV})]$ complex, gave, always a 1:1 ratio.



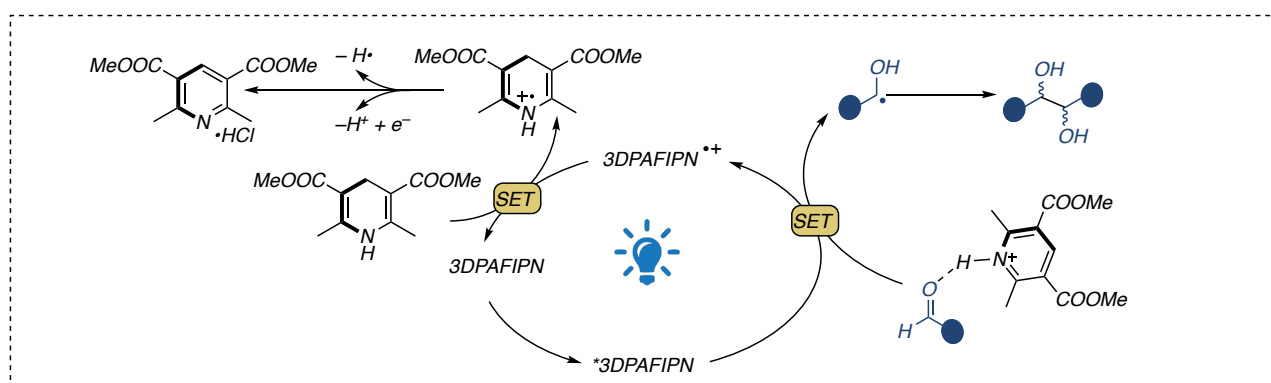
Entry ^[a]	Deviations from standard conditions	Conversion ^[b]	<i>d/l</i> : <i>meso</i> ^[c]
1	None	>99	1:1
2	5CzBn instead of 3DPAFIPN	>99	1:1
3	4CzIPN instead of 3DPAFIPN	>99	1:1
4	3CzCIPN instead of 3DPAFIPN	>99	1:1
5 ^[d]	(Ir[dF(CF ₃)ppy] ₂ (dtbbpy))PF ₆ instead of 3DPAFIPN	>99	1:1
6 ^[d]	[Ru(bpy) ₃]Cl ₂ •6H ₂ O	traces	–
7 ^[e]	No photocatalyst, no titanium	50	1:1

Table 3.3.1 Early optimization of the reaction conditions

[a] Reactions performed on 0.1 mmol scale. [b] Determined by ¹H-NMR analysis. [c] Determined by integration of benzylic CH ¹H NMR signal. [d] 1 mol% of photocatalyst were employed. [e] 60h irradiation time

In the light of these unsatisfactory results, we were forced to reanalyze all the components of the reaction questioning what was the reason that efficiently allowed us to obtain the desired product in terms of conversion of starting material but with a total absence of diastereocontrol.

We believe that this limitation is mainly related to the acidic activation of aldehydes in the presence of the pyridinium salt deriving from the oxidation of the sacrificial reductant. As already seen in the case of the propargylation reaction promoted by the same dual system, this species influences the redox potential of the carbonyl compound enabling its reduction in similar way to the one proposed by Rueping for his protocol.²³⁵



Chapter 3. Figure 15 Uncontrolled pinacol coupling reaction promoted by the Hantzsch's ester

Furthermore, performing the standard control experiments we realized that the reaction could be promoted also in absence of the photocatalyst and titanium complex leading to the conversion of the starting material but, again, without inducing diastereocontrol. The Hantzsch's ester used as sacrificial agent, is itself able to absorb light around 400 nm, and can behave as a strong reductant in its excited state. The so formed excited state is itself able to promote the reaction under blue light irradiation, preventing a possible metal-mediated mechanism.

Facing a situation more complex than expected, in order to avoid the direct formation of ketyl radical, we choose to evaluate a more tailored photoredox system. In order to prevent parasitic processes related to the photophysical properties of other species, we decided to move towards a photocatalyst able to absorb light in another region of the visible spectrum.

In order to obtain encouraging results from this choice, however, it is necessary that the newly chosen photoredox catalyst presents the appropriate photochemical properties.

The new selected molecule needs to have the ability to reduce titanium, either in its excited state (via a direct oxidative quenching with titanium), or in its reduced form (upon reductive quenching in the presence of the sacrificial reductant). In addition, due to the fact that titanium complexes used in

photoredox reactions are able to absorb light and behave as active photocatalysts,¹⁵⁹ molecules capable of exhibiting their photosensitizer activity under green light irradiation should be avoided.

Keeping these considerations in mind, we thought to use a red/orange-absorbing dye moving to a free region of the visible spectrum, non-interfering with the absorption neither of titanium complex nor of the Hantzsch's ester.

Red light-related advantages were recently illustrated by Rovis and co-workers reporting red-photon-absorbing osmium complexes to perform metallaphotoredox catalysis.²³⁶ Red light, indeed, brings the advantages of low energy, less health risks, and high penetration depth through various media.

However, considering the intrinsic toxicity of osmium, and the difficulties related to the preparation of the ligands, we wanted to use an organic dye to perform metallaphotoredox chemistry. Among all the red photons-absorbing organic dyes, we selected dimethoxyquinacridinium [DMQA]⁺ – a helical carbenium ion – for its interesting photophysical²³⁷ and electrochemical²³⁸ properties.

Moreover, the use of this molecule as photosensitizer for the conversion of red-light radiation into chemical energy to promote catalytic transformation has been recently reported in literature.

For instance, Lacour and co-workers employed [Pr-DMQA][BF₄], in aerobic photooxidation of benzylamine with modest results.²³⁹ More recently, Giannetti reported the use of the same photoactive species as a new organic photoredox catalyst for photoreductions and photooxidations under red light irradiation ($\lambda_{\text{max}} = 640 \text{ nm}$) with good results. The same authors introduced the use of the dye in metallaphotoredox catalysis, combining photoredox with palladium complexes.²⁴⁰

Further supporting our working plan, the photocatalyst exhibits suitable measured (photo)redox potentials for the reduction of Ti(IV) complexes and for the oxidation of Hantzsch's ester (**Scheme 21**).²⁴¹

²³⁶ Ravetz, B. D.; Tay, N. E. S.; Joe, C. L.; Sezen-Edmonds, M.; Schmidt, M. A.; Tan, Y.; Janey, J. M.; Eastgate, M. D.; Rovis, T. Development of a Platform for Near-Infrared Photoredox Catalysis. *ACS Cent. Sci.* **2020**, *6*, 2053–2059. <https://doi.org/10.1021/acscentsci.0c00948>

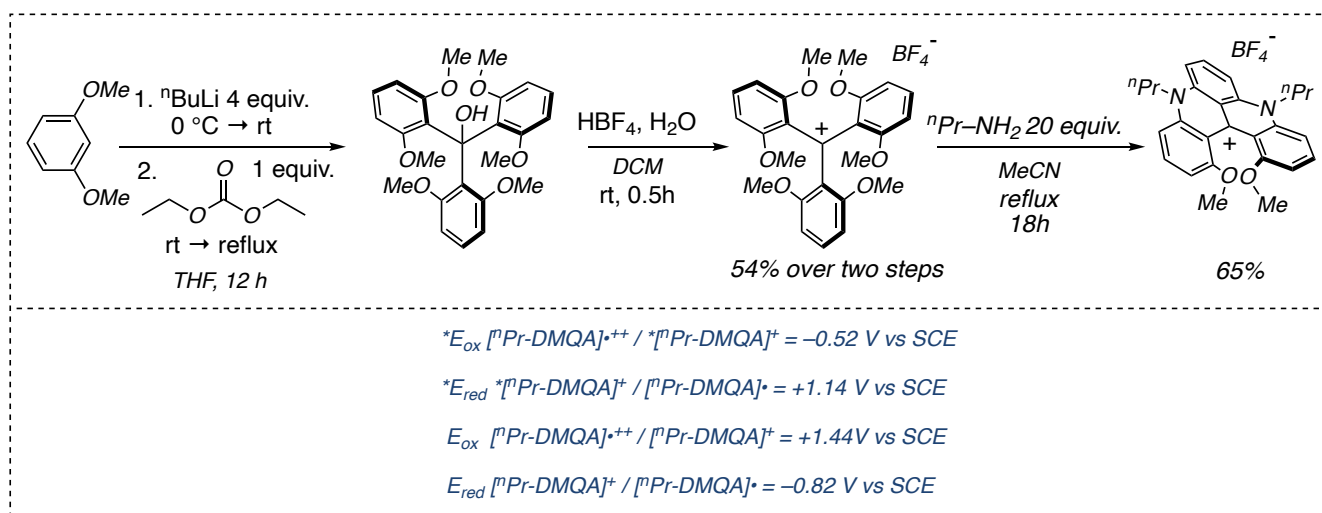
²³⁷ a) Laursen, B. W.; Krebs, F. C. Synthesis of a Triazatriangulenium Salt. *Angew. Chem. Int. Ed.* **2000**, *39*, 3432 – 3434; [https://doi.org/10.1002/1521-3773\(20001002\)39:19<3432::AID-ANIE3432>3.0.CO;2-S](https://doi.org/10.1002/1521-3773(20001002)39:19<3432::AID-ANIE3432>3.0.CO;2-S) b) Hernández Delgado, I.; Pascal, S.; Wallabregue, A.; Duwald, R.; Besnard, C.; Guénée, L.; Nançoz, C.; Vauthey, E.; Tovar, R. C.; Lunkley, J. L.; Muller, G.; Lacour, J. Functionalized Cationic [4]Helicenes With Unique Tuning of Absorption, Fluorescence and Chiroptical Properties up to the Far-Red Range. *Chem. Sci.* **2016**, *7*, 4685 – 4693. <https://doi.org/10.1039/C6SC00614K>

²³⁸ Sørensen, T. J.; Nielsen, M. F.; Laursen, B. W. Synthesis and Stability of *N,N'*-Dialkyl-1,13-dimethoxyquinacridinium (DMQA⁺): A [4]Helicene with Multiple Redox States. *ChemPlusChem* **2014**, *79*, 1030 – 1035. <https://doi.org/10.1002/cplu.201402058>

²³⁹ Duwald, R.; Pascal, S.; Bosson, J.; Grass, S.; Besnard, C.; Bürgi, T.; Lacour, J. Enantiospecific Elongation of Cationic Helicenes by Electrophilic Functionalization at Terminal Ends. *Chem. Eur. J.* **2017**, *23*, 13596. DOI: 10.1039/c9sc05407c

²⁴⁰ Mei, L.; Veleta, J. M.; Gianetti, T. L. Helical Carbenium Ion: A Versatile Organic Photoredox Catalyst for Red-Light-Mediated Reactions. *J. Am. Chem. Soc.* **2020**, *142*, 12056-12061. <https://doi.org/10.1021/jacs.0c05507>

²⁴¹ Liedtke, T.; Hilche, T.; Klare, S.; Gansäuer, A. Condition Screening for Sustainable Catalysis in Single-Electron Steps by Cyclic Voltammetry: Additives and Solvents. *ChemSusChem* **2019**, *12*, 3166-3171. <https://doi.org/10.1002/cssc.201900344>



Chapter 3. Scheme 21 Synthetic route and associated (photo)redox potential of $[{}^n\text{Pr-DMQA}][\text{BF}_4]$.

The synthesis of the photocatalyst is achieved in a few steps avoiding the use of chromatography columns to purify the synthetic intermediates. Although the overall yield is modest (35% over three steps), the use of inexpensive reagents as starting materials allows a possible scale up for its synthesis.

Practically, while the synthesis of the carbinol and its transformation in the corresponding air-stable carbocation proceeded smoothly with a high level of reproducibility, the final step of the synthesis resulted difficult to accomplish.

Although this reaction does not require a special set-up and can be carried out using the normal conventions of the Schlenk technique, the purification of the reaction crude for the synthesis of $[{}^n\text{Pr-DMQA}][\text{BF}_4]$ resulted particularly complex. During the early stages of the project, the synthesis of the red light-absorbing photocatalyst was carried out following the procedure recently reported by Giannetti.

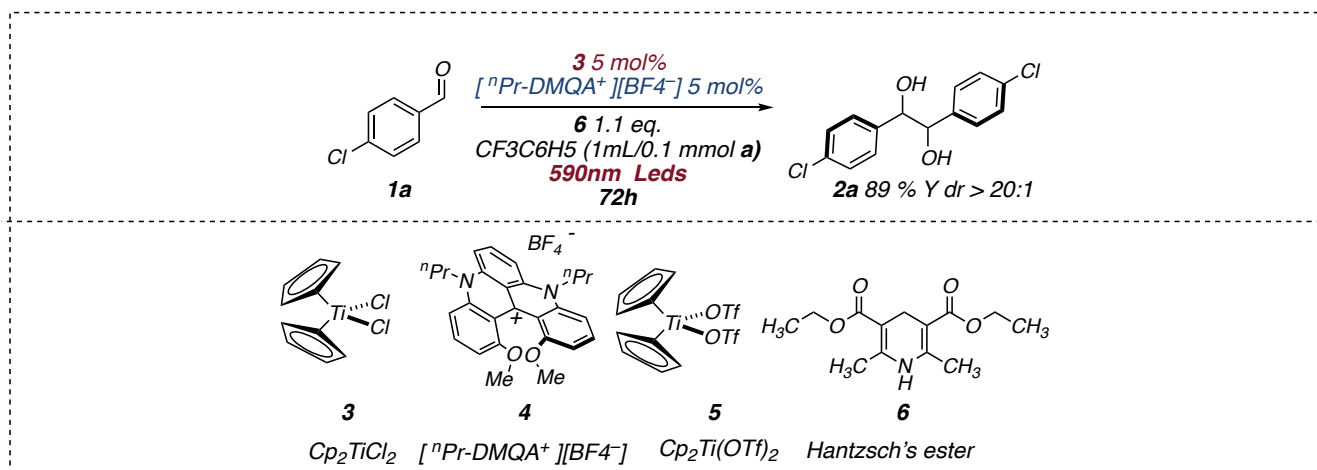
Following the procedure reported by the authors for the catalyst purification, it was not possible to faithfully reproduce the results reported. The observed drastic drop of the isolated yield initially limited, in its early stage, a possible development of this project.

While any efforts to use chromatographic methods led to unsatisfactory results, with almost total decomposition of the product of interest and poor isolated yields, after several attempts it was possible to develop an effective purification of the desired photocatalyst with good results. We were pleased to observe that, after the evaporation of the volatiles, by dissolving the reaction crude in the smallest possible amount of dichloromethane and slowly adding a large excess of ethyl acetate it was possible to precipitate and recover after simple filtration the product of interest with a high degree of purity (monitored by both NMR and HPLC/MS analyses) and in satisfying yields.

On those bases, we could focus on the development and new optimization of the reaction.

Since a different photocatalyst from those investigated so far was employed, all the components of the reaction have been evaluated in order to develop a new effective methodology that allows the formation of the desired product.

For sake of clarity the salient results obtained during the optimization of the reaction conditions are summarized in the **Table 3.3.2**



Entry ^[a]	Deviations from standard conditions	Yield (%) ^[b]	<i>d/l</i> : <i>meso</i> ^[c]
1	None	>99(89) ^[d]	>20:1
2	No photocatalyst	no reaction	–
3	No Titanium	traces	1:1
4 ^[e]	No Light	no reaction	–
5 ^[f]	10 mol % of [Cp ₂ TiCl ₂] and 2 ml/0.1 mmol a	>99	>20:1
6	Toluene instead of PhCF ₃	>99	7:1
7	Cp ₂ Ti(OTf) ₂ instead of [Cp ₂ TiCl ₂]	no reaction	–
8	Benzene instead of PhCF ₃	no reaction	–
9 ^[f]	DMF instead of PhCF ₃	53	1:2
10 ^[f]	MeCN instead of PhCF ₃	traces	–
11 ^[f]	THF instead of PhCF ₃	traces	–
12	2 equivalents of Hantzsch's Ester	>99	10:1
13	1.5 equivalents of Hantzsch's Ester	>99	>20:1
14	2,5 mol % of [Cp ₂ TiCl ₂] and 0.5 ml/0.1 mmol a	61	>20:1

Table 3.3.2 Salient aspect of optimization of the reaction conditions

[a] Reactions performed on 0.1 mmol scale. [b] Determined by ¹H-NMR analysis. [c] Determined by integration of benzylic CH ¹H NMR signal. [d] Reaction performed on 0.2 mmol scale and isolated after chromatographic purification. The value in parenthesis is the isolated yield [e] Reaction performed in presence of 10 mol % of [Cp₂TiCl₂], 2 equiv. of HE and 2 ml/0.1 mmol a of solvent. [f] 2 equivalents of HE were employed.

During the screening of the reaction conditions, we found that the protocol is extremely sensitive to the presence of oxygen and water. This latter, if present in the reaction mixture, is detrimental for the reaction outcome. For this reason, to perform the reactions, the solvents were freshly employed after distillation over 3 Å molecular sieves. In addition, each reaction was performed in oven-dried Schlenk tubes under strictly inert atmosphere and subjected to three 30-second freeze-pump-thaw cycles before irradiation centered at 590 nm. Screening the different parameters, we found that the reaction solvent plays a crucial role for the reaction outcome. While common solvents employed in photoredox and in titanium-catalyzed transformations gave only traces of the desired product (**Table 3.3.2** Entry 9–11), the first promising results were obtained performing the reaction in aromatic solvents (benzene excluded).

In these conditions, the pinacolization of the model substrate was successfully obtained both in terms of yields and of diastereoselectivity. Among all the aromatic solvent, yields and diastereoselection were found optimal in trifluorotoluene. Although further studies to clarify the precise role of the solvent for the reaction have not been performed yet, we assume that the employment of this aromatic solvent provides several important features for the reaction outcome. Firstly, trifluorotoluene, presenting an intermediate polarity between that of THF and ethyl acetate comparable to DCM,²⁴² should favor subsequent single electron transfer events maybe directly interacting with the photocatalyst. Moreover, it is plausible that the solvent molecules may also stabilize the transition state that leads to the formation of the product enhancing the diastereoselective outcome thanks to the engagement of non-covalent interactions with the ketyl radicals.

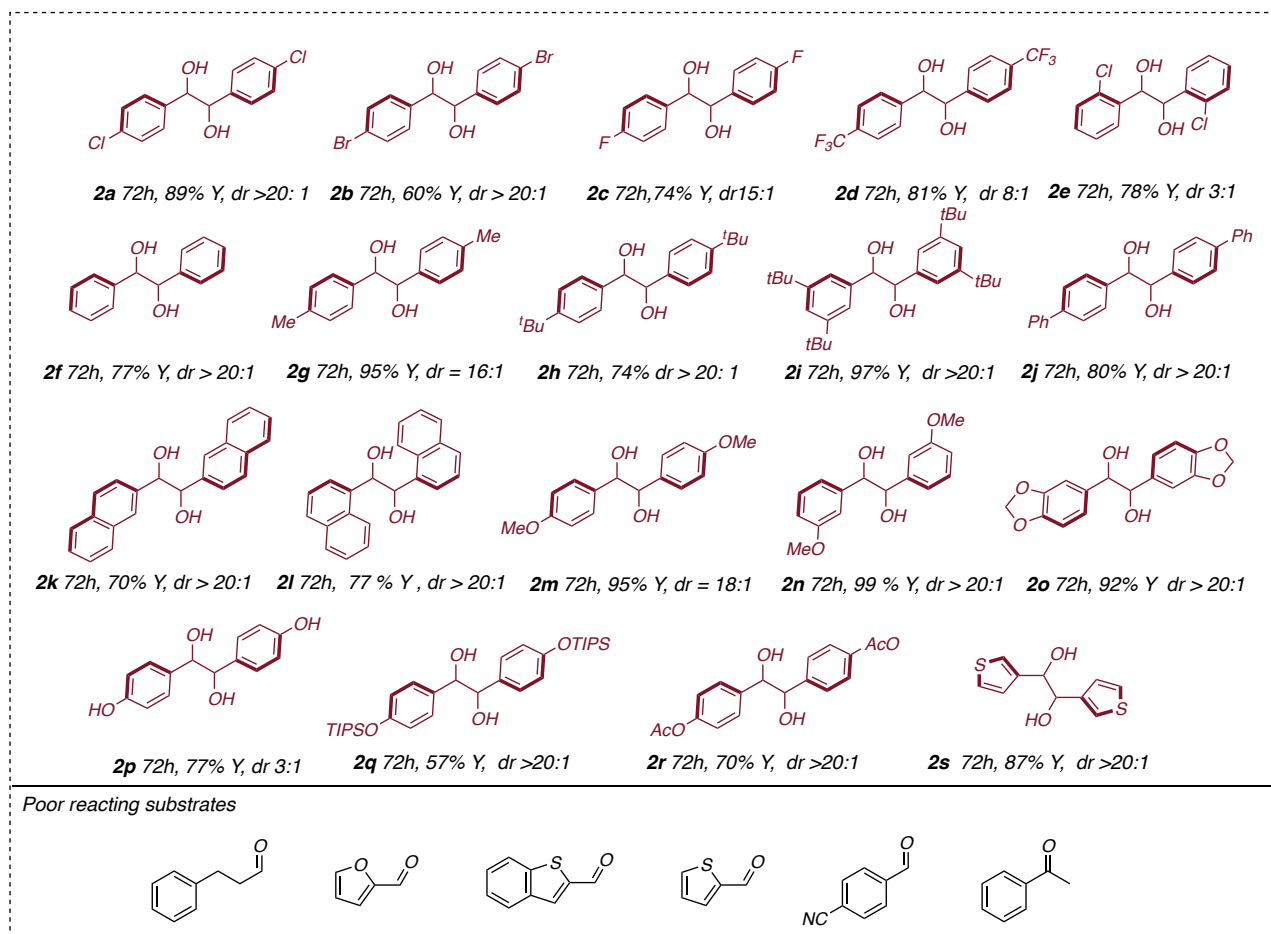
Once we obtained the first promising results, all the necessary control experiments were conducted to find a further confirmation to our initial assumptions. As expected, both titanium and light irradiation were necessary to allow the reaction. In contrast to what we have seen in the case of reactions performed under blue light irradiation, [Pr-DMQA][BF₄] was found mandatory since it is the only species present in the reaction mixture able to absorb light radiation at 590 nm. Continuing the optimization of the reaction conditions we were able to appreciate that both the solvent amount, the catalytic loading and the excess of sacrificial agent could be strongly reduced compared to previously developed allylation and propargylation protocols.

After the systematic evaluation of all reaction parameters, we were able to disclose the optimized conditions, obtaining **2a** in 89% isolated yield and dr >20:1 in favor of the *d/l* isomer after 72 h of irradiation.

²⁴² *Modern Solvents in Organic Synthesis*; Knochel, P., Augé, J., Augé, J., Eds.; Topics in current chemistry; Springer: Berlin Heidelberg, 1999.

•Scope evaluation

Once we obtained the best reaction conditions, we continued the study of this new reaction analyzing its generality in the presence of differently decorated aromatic aldehydes. We were pleased to observe that the conditions developed using the model aldehyde **1a** could be extended to a wide range of substrates. Both in the case of substrates bearing electron-donating or electron-withdrawing groups the pinacol coupling products were obtained with good to excellent yields and with enhanced diastereoselectivity.



Chapter 3. Scheme 22 Scope exploration for dual photoredox and titanium catalyzed diastereoselective pinacol coupling.

However, due to their greater ease of undergoing single electron reduction, a slight decrease in the diastereoselection has been observed in the presence of strongly electron withdrawing groups, as in the case of **2d**. Probably due to the fact that titanium complex in a low oxidation state is able to quickly generate the ketyl radical on these substrates, the formation of the pinacolization product occurs fast in an uncontrolled manner.

It is important to note that the steric hindrance around the carbonyl moiety was found detrimental for the diastereoselective outcome. While para- and meta- substituted substrates are well tolerated and led the

formation of the product with excellent results, ortho– substitution deeply affects the reaction, reducing dramatically the diastereoselectivity (**2e**) but not interfering substantially with the isolated yield.

Unfortunately, although most of the functional groups are tolerated and very satisfactory results can be obtained, during the survey of compatible substrates we encountered some limitations. The presence of an unprotected hydroxyl group (**2p**) on the aromatic ring, for example, has a detrimental effect on the diastereoselective outcome. Perhaps, since titanium complexes are highly oxyphilic, a possible coordination between the catalyst and the hydroxyl group can occur causing a drop on the efficiency.

In addition, while **1s** turned out to be perfectly compatible with the proposed protocol leading to pinacolization product with excellent yields and diastereoselection, some heteroaromatic substrates were found unreactive under the developed reaction conditions.

Substrates such as furfural, 2-thiophene carboxaldehyde, and thianaphthene-2-carboxaldehyde, indeed present a scaffold that can chelate the active titanium catalyst deactivating it and preventing a positive outcome of the reaction.

In conclusion, as expected, it was not possible to extend the protocol either to ketones or to aliphatic aldehydes. Both of these classes of carbonyl compounds exhibit a very different reduction potential than aromatic aldehydes and are way less prone to engage a single electron reduction.¹⁹⁸ In this context, only few non-light driven methodologies have been presented in literature reporting the dimerization of these ketyl radical in the presence of a titanium catalyst. In all the reported cases, however, the simple titanocene monochloride was not found able to promote the transformation. Either the presence of external Lewis acid²⁴³ or the preparation of hard to handle aryl titanium (III) complexes²⁴⁴ were found compulsory to achieve this transformation.

²⁴³ Paradas, M.; Campaña, A. G.; Estévez, R. E.; Álvarez de Cienfuegos, L.; Jiménez, T.; Robles, R.; Cuerva, J. M.; Oltra, J. E. Unexpected Ti^{III}/Mn-Promoted Pinacol Coupling of Ketones. *J. Org. Chem.* **2009**, *74* (9), 3616–3619. <https://doi.org/10.1021/jo9005238>.

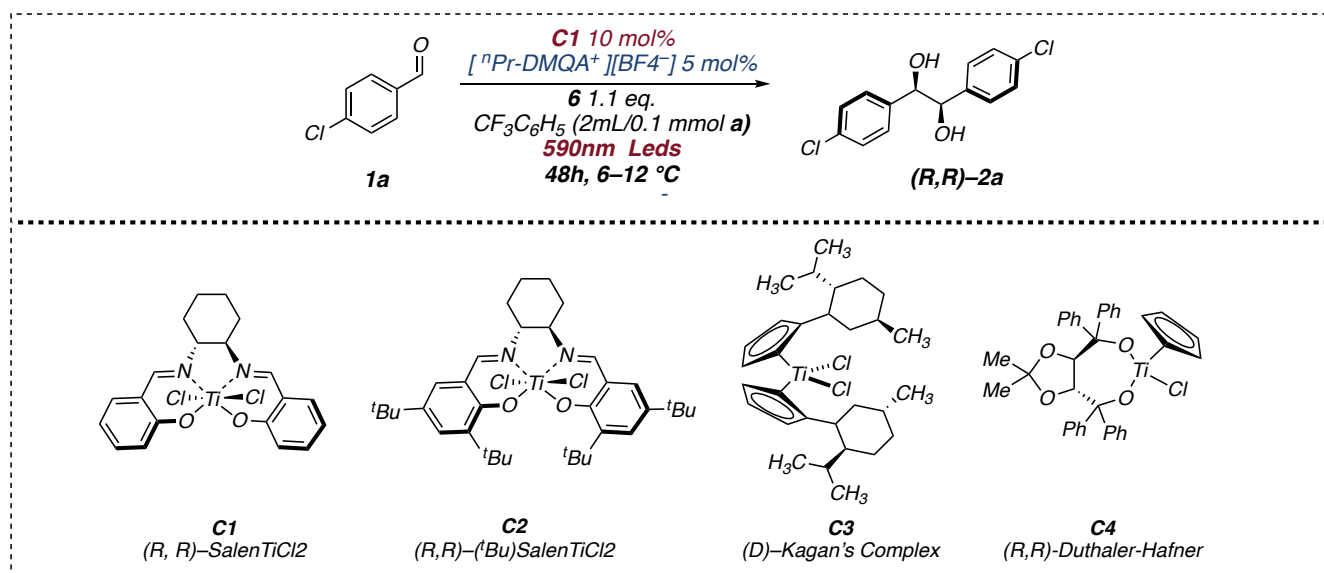
²⁴⁴ Yamamoto, Y.; Hattori, R.; Miwa, T.; Nakagai, Y.; Kubota, T.; Yamamoto, C.; Okamoto, Y.; Itoh, K. Diastereoselective Inter- and Intramolecular Pinacol Coupling of Aldehydes Promoted by Monomeric Titanocene(III) Complex Cp₂TiPh. *J. Org. Chem.* **2001**, *66* (11), 3865–3870. <https://doi.org/10.1021/jo001781p>.

- **Enantioselective variant**

Having completed the survey of tolerated substrates using the titanocene dichloride and having realized the high potential of this methodology in terms of applicability and tolerance, we decided to investigate the possibility to develop an enantioselective variant of the reaction.

In order to achieve this goal, we decided to select some of the most common chiral titanium complexes and evaluate their effect under the optimized reaction conditions replacing the previously employed $[\text{Cp}_2\text{TiCl}_2]$.

For clarity, the salient results regarding the optimization of the enantioselective variant of the reaction are summarized in the table below.



Entry ^[a]	Deviations from standard conditions	Yield (%) ^[b]	<i>d/l:meso</i> ^[c]	(<i>R,R:S,S</i>) ^[d]
1	None	74(67) ^[e]	>20:1	96:4
2	No photocatalyst	no reaction	–	–
3	No Titanium	traces	1:1	50:50
4	No Light	no reaction	–	–
5	24h	57	>20:1	96:4
6 ^[f]	10 mol % of (<i>S,S</i>)- C1	49	>20:1	3:97
7	5 mol % of C1 and 1 mL/0.1 mmol a	64	>20:1	96:4
8 ^[g]	5 mol % of C1 and 1 mL/0.1 mmol a	91	9:1 ^[h]	96:4
9	Toluene instead of PhCF ₃	traces	–	–
10	MeCN instead of PhCF ₃	no reaction	–	–
11	Benzene instead of PhCF ₃	no reaction	–	–
12	THF instead of PhCF ₃	traces	–	–
13	DME instead of PhCF ₃	traces	–	–
14 ^[i]	25 °C instead of 6–12 °C	92	9:1 ^h	64.5:35.5
15	C2 instead of C1	no reaction	–	–
16 ^[j]	5 mol% of C2 and 1 mL/0.1 mmol a	traces	–	–
17 ^[j]	5 mol% of C3 and 1 mL/0.1 mmol a	80	5:1 ^h	39.5:60.5
18	5 mol% of C4 and 1 mL/0.1 mmol a	no reaction	–	–

Table 3.3.3 Salient aspect of optimization of the enantioselective reaction conditions

[a] Reactions performed on 0.1 mmol scale. [b] Determined by ¹H NMR analysis. [c] Determined on the reaction crude by integration of benzylic CH ¹H NMR signals. [d] Determined by HPLC analysis on chiral column. [e] Reaction performed on 0.2 mmol scale. The value in parenthesis is the isolated yield after chromatographic purification. [f] For 16 h. [g] For 96 h. [h] Observed decomposition with reduction of aldehyde to alcohol. [i] 2 equivalents of **6** were employed. [j] At 25 °C.

As can be seen from the above reported data, the optimization of reaction conditions highlighted the similarity of reactivity between our dual photoredox/Ti mediated protocol and the one non-visible light mediated introduced by Joshi and co-workers described in the previous section. From the experimental evidence, we disclosed that the chiral Kagans's complex²⁴⁵ (**C3**) and the commercially available (*R,R*)-Duthaler-Hafner catalyst (**C4**) are unable to promote the reaction. (**Table 3.3.3** Entry 17-18)

On the other hand, we were pleased to observe that the unsubstituted [(Salen)TiCl₂] complex (**C1**) could promote the reaction at room temperature, allowing the formation of the desired product with a moderate diastereomeric ratio (d/l: meso 9:1) and a promising enantiomeric excess of 30%. Interestingly, during the screening of the different chiral complexes able to promote the transformation it was also possible to note that the presence of substituents on the scaffold of the Salen ligand has detrimental effects on the reaction. When **C2** was tested in the reaction, the presence of bulky ^tButyl moieties on the aromatic rings determined a total drop in the reactivity.

Having in hand promising, but still unsatisfactory results employing **C1** as chiral complex, we continued the optimization of the reaction conditions to evaluate how far we could improve the results in terms of yield, diastereoselection and enantioselectivity.

As already noted for the development of the diastereoselective reaction, deviations from aromatic solvents are not convenient and lead to a drop in the reactivity of the entire system. Remarkably, for the development of this enantioselective variant, even the use of toluene, which for the diastereoselective version of the process led to satisfactory results, turned out not to be helpful to the formation of the product of interest.

The big leap forward for process optimization was, again similarly to the protocol reported by Joshi, a careful temperature control. Thanks to the use of an inexpensive home-made refrigeration system, it was possible to maintain the reaction temperature between 6 and 12°C. (*See Supplementary Data section for detailed pictures of the reaction set-up*)

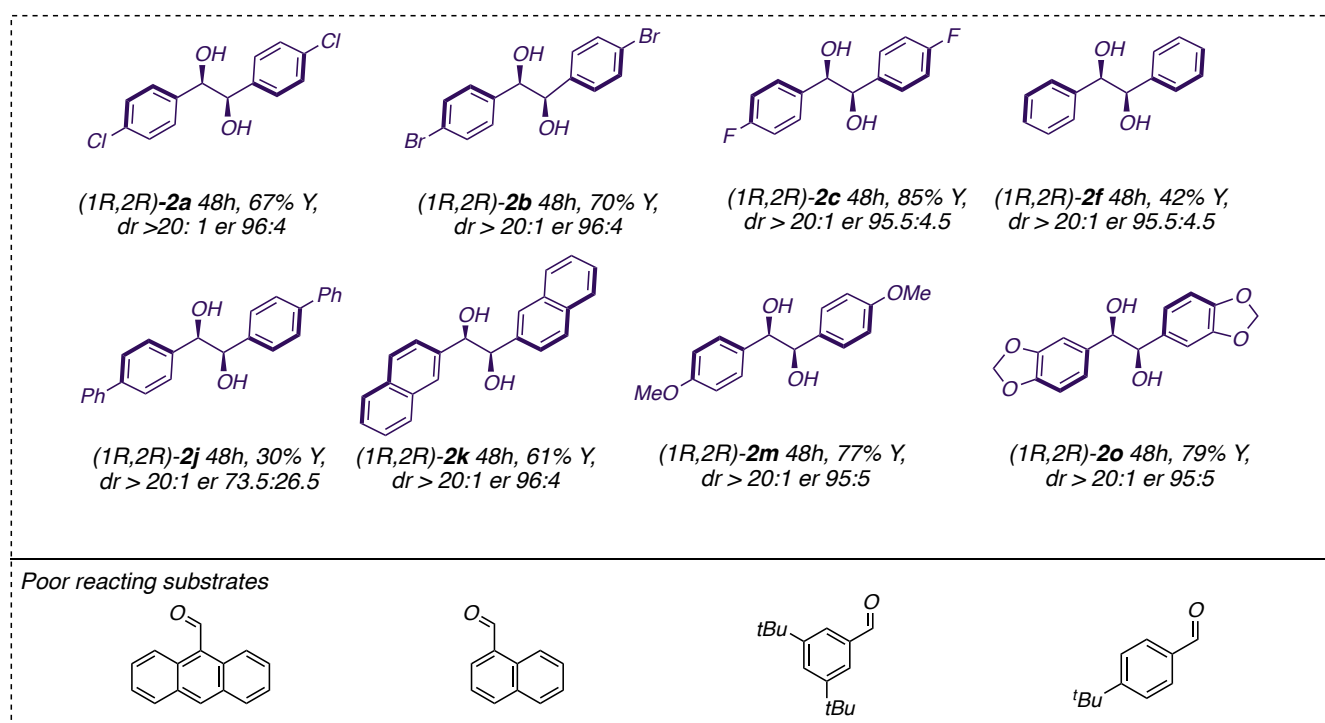
In this way, along with the increase of the catalytic loading from 5% to 10% it was possible to obtain the homocoupling product of the model *p*-chloro benzaldehyde with a yield of 57%, a total diastereoselection towards the *syn* isomer (*d/l:meso* > 20:1) and an enantiomeric excess of 92%.

²⁴⁵ Prof. Dr. A. Gansäuer and his research group are kindly acknowledged for the generous gift of the chiral complex.

To further improve the final yield of the product of interest, we tried to increase the reaction time from 24h to 48h. We were pleased to observe that extending the irradiation time a substantial increase in yield (67%) without affecting either the diastereoselectivity or the enantioselectivity was appreciated.

After completing the re-optimization of the reaction parameters for the development of an enantioselective protocol, we wanted to investigate if the novel dual photoredox and titanium promoted methodology had the same applicability as the previously presented diastereoselective protocol.

Reconsidering the substrates tested, unfortunately, we were forced to observe that the tolerance and applicability of the dual photoredox/Ti catalyzed enantioselective pinacol coupling reaction were slightly lower than what we disclosed employing the titanocene dichloride.



Chapter 3. Scheme 23: Scope exploration for dual photoredox and titanium catalyzed diastereoselective pinacol coupling.

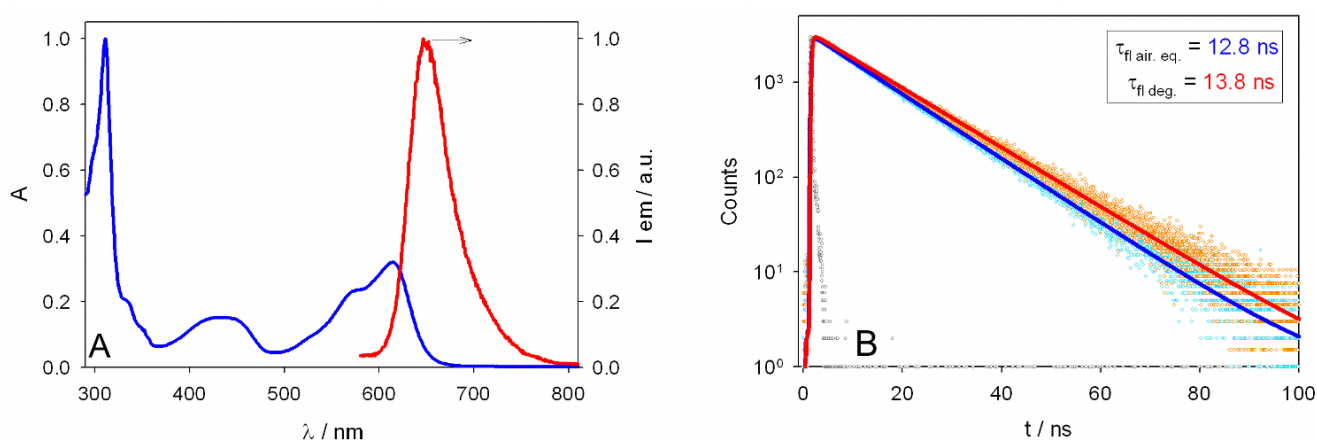
In general, the reaction was found effective with unhindered aldehydes. Electronic effects seem not to play a relevant role in the reactions. Both substrate (1*R*,2*R*)-**2c** and (1*R*,2*R*)-**2m** could be obtained with satisfactory yields and high enantiomeric excesses. Steric effects, on the contrary, are detrimental both for the enantioselectivity and the yield of the reaction limiting the presented protocol ((1*R*,2*R*)-**2c**). Probably due to the greater steric hindrance associated to the Salen ligand surrounding the metal center, it was not possible to extend this protocol to all the aldehydes that had been proven compatible with the diastereoselective method. Substrates that gave excellent results such as 4-tert-butylbenzaldehyde, 3,5-di-tert-butylbenzaldehyde and 1-naphthaldehyde, proved to be incompatible in the presence of the new chiral complex.

• Mechanistic details

To fully outline the mechanism of the reaction a careful photophysical analysis was performed.

Thanks to the collaboration with the research group supervised by Prof. P. Ceroni, the analysis of the photophysical behavior of [ⁿPr-DMQA][BF₄] in the presence of the various components of the reaction mixture, shed light on the key aspects that determined the positive outcome in the case of both diastereo- and enantioselective process.

As for the synthetic protocol, PhCF₃ was chosen as the main solvent for the photophysical characterization of **4**. In agreement with published results, **4** shows a low energy-lying absorption band with maximum at 614 nm ($\epsilon_{614\text{nm}} = 10300 \text{ M}^{-1}\text{cm}^{-1}$ in CH₂Cl₂, $\lambda_{\text{onset}} \sim 680 \text{ nm}$; **Figure 16a**) allowing its excitation with red light ($\lambda_{\text{max}} = 595 \text{ nm}$). The emission band of **4** is peaked at 648 nm – with a lifetime of 12.8 ns and a quantum yield of 0.26 in air-equilibrated PhCF₃ – corresponding to a spectroscopic energy $E_{0,0}$ of 1.96 eV. Considering the redox potentials reported by Giannetti and co-workers in DCM, in light of the fact that PhCF₃ exhibit a comparable polarity,²⁴⁶ the reported values can also be attributed to the present reaction conditions.

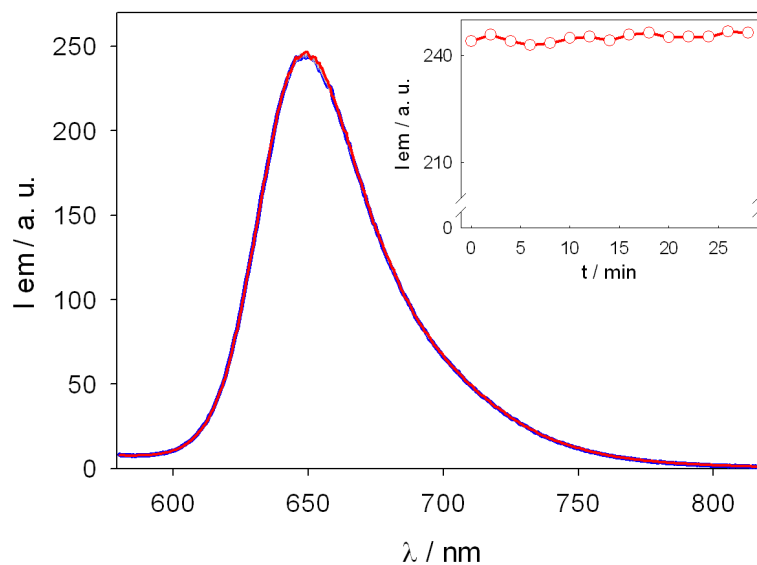


Chapter 3. Figure 16 A: Absorption (blue line) and fluorescence spectra (red line) of a PhCF₃ solution of **4** at r.t. ($\lambda_{\text{ex}} = 575 \text{ nm}$). B: comparison between fluorescence decays of air-equilibrated (blue dots) and N₂-saturated (red dots) PhCF₃ solutions of **4** at r.t. The corresponding monoexponential fitting functions are shown as solid lines. The instrument response function (IRF) is also reported (grey dots).

Remarkably, as expected for fluorescent dyes, the emission decay is not dramatically affected by the presence of molecular oxygen and a slightly increased lifetime was determined degassed solutions (13.8 ns vs. 12.8 ns **Figure 16b**). No phosphorescence has been detected in the visible and NIR spectral regions from deoxygenated PhCF₃ solutions at r.t. or in rigid matrix at 77 K in diethylether:ethanol:PhCF₃ mixtures (2:1:1 v/v/v). The compound shows excellent photostability in solution with no degradation upon prolonged irradiation at $\lambda_{\text{ex}} = 570 \text{ nm}$ (**Figure 17**), making it a good candidate as an active initiator

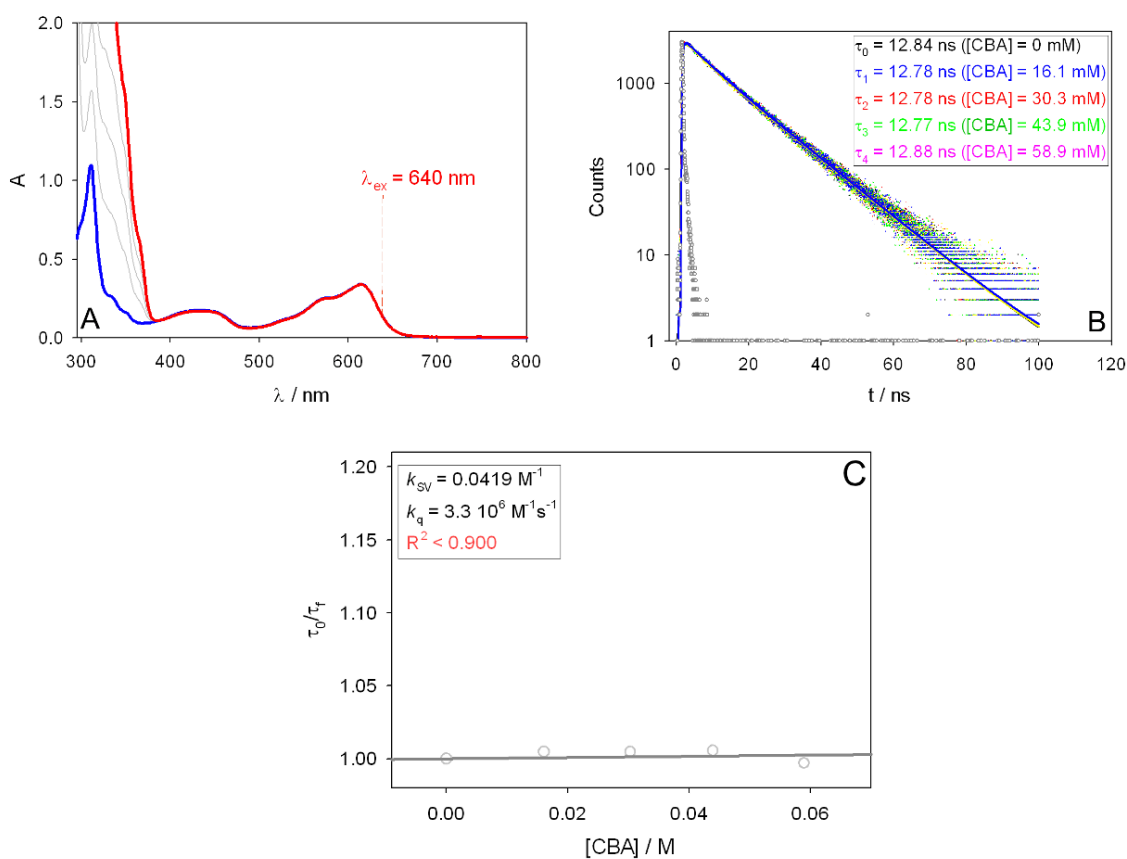
²⁴⁶ Freed, K. B.; Biesecker, J.; Middleton W.J. Spectral polarity index: a new method for determining the relative polarity of solvents J. Fluor. Chem., **1990**, *48*, 63–75 [https://doi.org/10.1016/S0022-1139\(00\)82602-0](https://doi.org/10.1016/S0022-1139(00)82602-0)

in photoredox processes. Since **4** is isolated and used as a racemic mixture, no investigations on electronic circular dichroism nor circular polarized luminescence have been carried out.



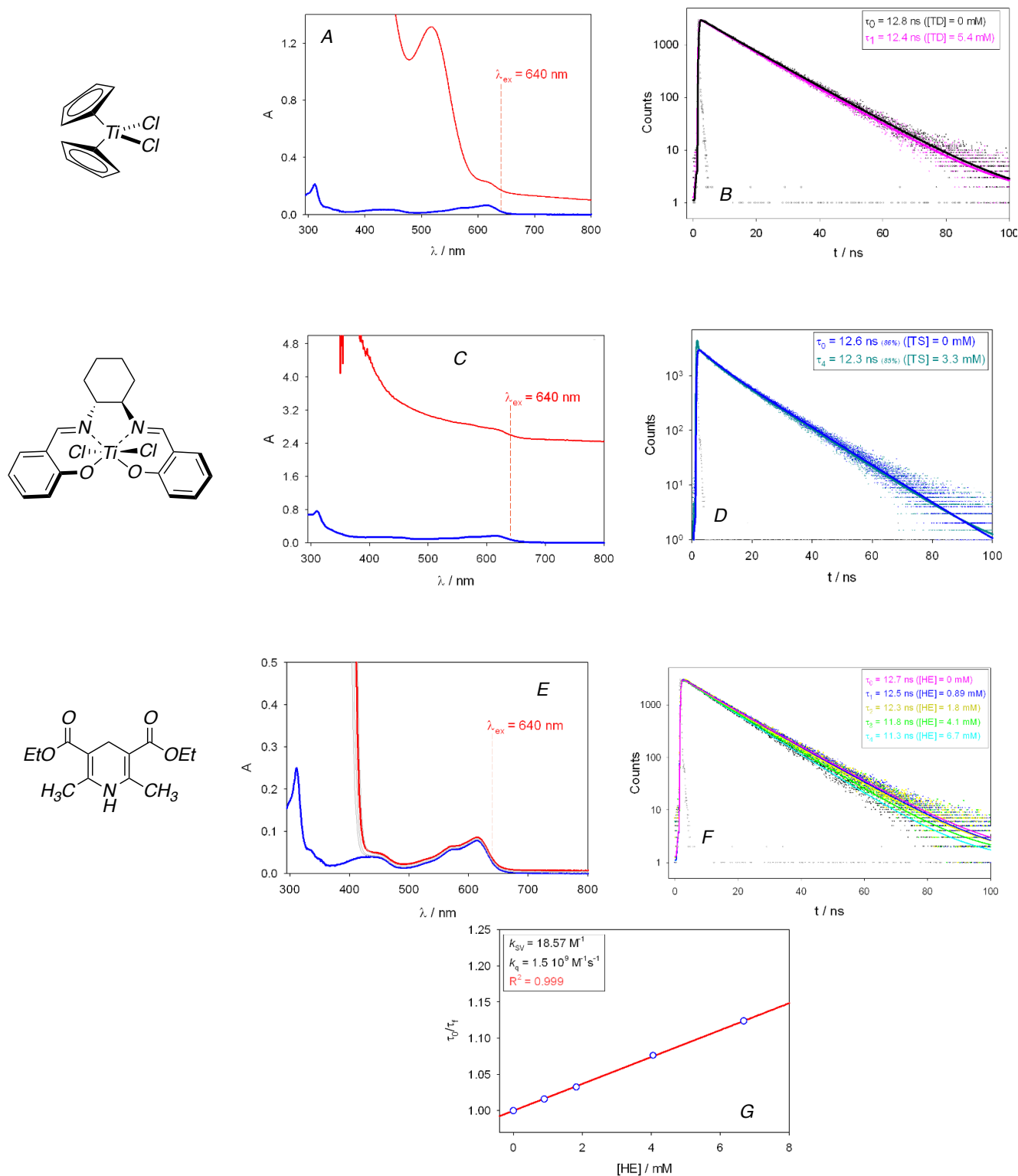
Chapter 3. Figure 17 Emission spectra collected on a diluted solution of **4** in air-equilibrated PhCF_3 at r.t. (ca. $10\ \mu\text{M}$) upon 30 minutes of continuous irradiation at $\lambda_{\text{exc}} = 570\ \text{nm}$. Inset: profile of the variations on emission maxima.

After having analyzed the main aspects regarding the photocatalyst, the analysis of the luminescence quenching in the presence of the reaction components has been undertaken. As expected by its low reduction potential, ($E(p\text{-chlorobenzaldehyde}/p\text{-chlorobenzaldehyde}^{\bullet-}) = -1.82\ \text{V vs. SCE}$) no relevant quenching mechanism has been observed upon additions of **1a**. (up to ca. $0.06\ \text{M}$, see)



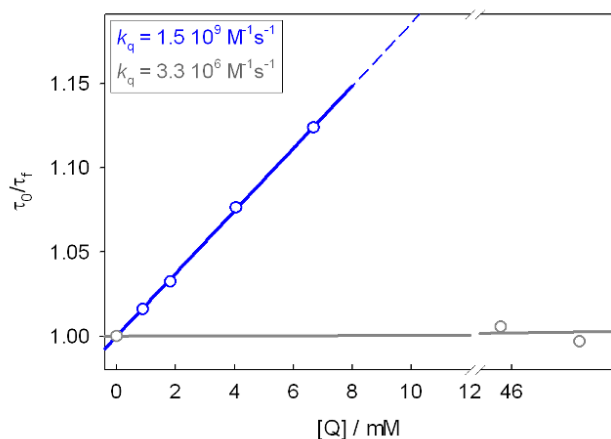
Chapter 3. Figure 18 A: absorption spectra of solutions of **4** in air-equilibrated PhCF_3 at r.t. (ca. 25 μM , blue line) obtained upon addition of increasing amounts of *p*-chlorobenzaldehyde (up to ca. 0.06 M, red line). B: fluorescence decays of **4** obtained from the same solutions at $\lambda_{\text{em}} = 690 \text{ nm}$ ($\lambda_{\text{ex}} = 640 \text{ nm}$). The instrument response function (IRF) is also shown (grey dots). C: Stern-Volmer diagram relative to the fluorescence lifetimes shown in B.

On the other hand, quenching processes have been observed for the two Ti(IV) complexes (**3** and **C1**) and the Hantzsch's ester **6** in air-equilibrated solutions, with compound **6** displaying the highest quenching constant ($k_{\text{q}} = 1.5 \cdot 10^9 \text{ M}^{-1} \text{ s}^{-1}$).



Chapter 3. Figure 19 A: absorption spectra of solutions of 4 in air-equilibrated PhCF_3 at r.t. (ca. 6.3 μM , blue line) obtained upon addition of 3 (TD, 5.4 mM, red line). The baseline is affected by the low solubility of 3. B: fluorescence decays of 4 obtained from the same solutions at $\lambda_{\text{em}} = 690 \text{ nm}$ ($\lambda_{\text{ex}} = 640 \text{ nm}$). The instrument response function (IRF) is also shown (grey dots). C: absorption spectra of solutions of 4 in air-equilibrated PhCF_3 at r.t. (ca. 16.2 μM , blue line) obtained upon addition of Cl (TS, up to 3.3 mM, red line). The baseline is affected by the low solubility of 4. D: fluorescence decays of 4 obtained from the same solutions at $\lambda_{\text{em}} = 690 \text{ nm}$ ($\lambda_{\text{ex}} = 640 \text{ nm}$). The instrument response function (IRF) is also shown (grey dots). Lifetimes are obtained from multiexponential fitting, taking into account the longest component (whose contribution to the fitting is expressed in percentage). E: absorption spectra of solutions of 4 in air-equilibrated PhCF_3 at r.t. (ca. 5.6 μM , blue line) obtained upon addition of increasing amounts of 6 (HE, up to 6.7 mM, red line). F: fluorescence decays of 4 obtained from the same solutions at $\lambda_{\text{em}} = 690 \text{ nm}$ ($\lambda_{\text{ex}} = 640 \text{ nm}$). The instrument response function (IRF) is also shown (grey dots). G: Stern-Volmer diagram relative to the fluorescence lifetimes shown in B.

Taking into account the concentrations used for the synthesis, the comparison between all substrates' contributions to the quenching efficiencies indicate that **6** is the most efficient quencher with an efficiency of ca. 67% compared to ca. 3% in the case of the Ti(IV) complexes.



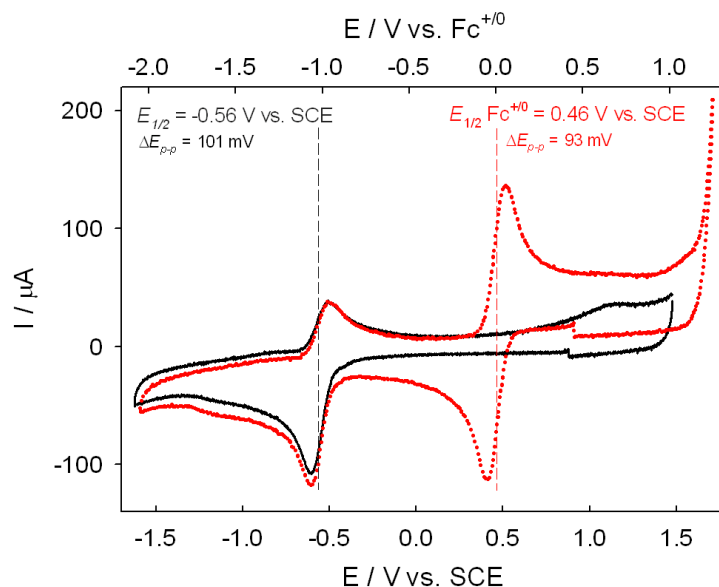
Quencher	[quencher] / mM	τ_0 / τ_q	$\eta_q / \%$
6	110	3.04	67
3	5.4	1.03	< 3
11	3.3	1.02	< 2
1a	59	~ 1.0	–

Chapter 3. Figure 20 Comparison between Stern-Volmer kinetics determined for the quenching of the luminescence of **4** in air-equilibrated PhCF₃ in the presence of the different quenchers (*Q*) in the reaction mixture (**6**: blue line; **1a**: grey line; the corresponding quenching constants are also explicated). The quenching efficiencies η are calculated taking into account, for each quencher, a concentration close to that used in the reaction medium (for **6**: data are extrapolated by using the relative quenching constant).

This experimental evidence demonstrates that the Hantzsch's ester can act as an efficient reductant of the dye's excited state¹⁸⁰ ($E(\mathbf{6}^+/\mathbf{6}) = 1.0$ V vs. SCE) leading to the formation of **4***. This latter, in a second stage, is able to reduce the Ti(IV) complexes triggering its redox activity towards aldehydes.

Indeed, Ti(IV) species are characterized by the following reduction potentials: ca. -0.8 V vs. SCE for **3** in CH₂Cl₂,²⁴¹ ca. -0.6 V vs. SCE for **C1** in CH₂Cl₂,²⁴⁷ (**Figure 21**), that are compatible with the reduction potential $E(\mathbf{4}^*/\mathbf{4}^+) = -0.82$ V vs. SCE. On the other hand, an oxidative quenching of the fluorescent excited state of **4**, is not thermodynamically feasible.

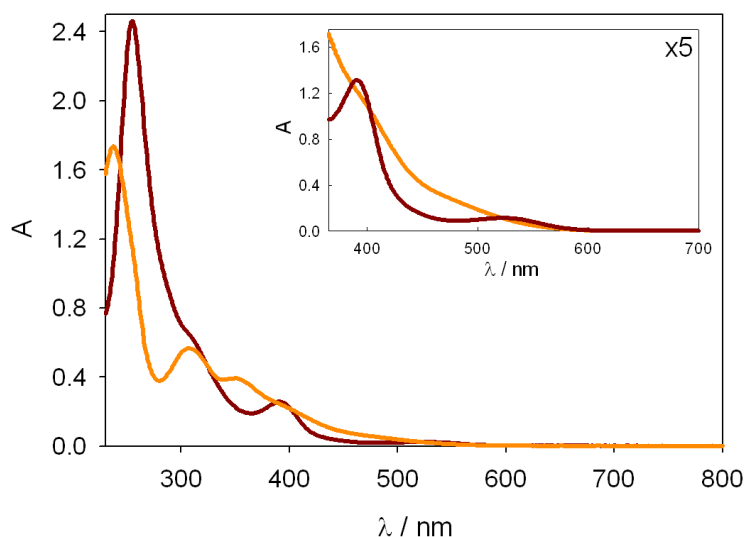
²⁴⁷Robinson, S. G.; Wu, X.; Jiang, B.; Sigman, M. S.; Lin, S. Mechanistic Studies Inform Design of Improved Ti(Salen) Catalysts for Enantioselective [3 + 2] Cycloaddition. *J. Am. Chem. Soc.* **2020**, *142* (43), 18471–18482. <https://doi.org/10.1021/jacs.0c07128>.



Chapter 3. Figure 21 Cyclic voltammogram (scan rate: 1 V/s) of a solution containing **C1** in CH_2Cl_2 (black line, 1.6 mM; tetrabutylammonium hexafluorophosphate 0.1 M is introduced as supporting electrolyte). For comparison purposes, the voltammogram of the same solution containing ferrocene as internal standard is also shown (red line; $\text{Fc}^{+/0} = 0.46 \text{ V vs. SCE}$).

To further demonstrate that the reaction proceeds through a photoredox net-reductive catalytic cycle which allows the formation of the transient Nugent–reagent, we wanted to show that other mechanisms for quenching the excited state of $[\text{}^n\text{Pr-DMQA}][\text{BF}_4]$ were excluded. The absorption spectra of **3** and **C1** are not compatible with a singlet-singlet Energy Transfer quenching from the excited singlet excited state of **4** (${}^1\mathbf{4}^*$, $\lambda_{\text{max}} = 648 \text{ nm}$, $\lambda_{\text{onset}} \sim 600 \text{ nm}$, **Figure 22**). Triplet-triplet EnT from **4** to **3** are also most unlikely due to the proximity in energy of ${}^1\mathbf{4}^*$ and ${}^3\mathbf{3}^*$ ($\lambda_{\text{max}} = 660 \text{ nm}$).²⁴⁸ In addition, no significant information on the excited states of **C1** is available, since the complex does not show any fluorescence or phosphorescence emission in deoxygenated solvents at r.t. or in rigid matrix ($\text{CH}_2\text{Cl}_2:\text{CH}_3\text{OH}$, 1:1 v/v) at 77 K.

²⁴⁸ Kenney, J. W.; Boone, D. R.; Striplin, D. R.; Chen, Y. H.; Hamar, K. B. Electronic Luminescence Spectra of Charge Transfer States of Titanium(IV) Metallocenes. *Organometallics* **1993**, 12 (9), 3671–3676. <https://doi.org/10.1021/om00033a045>.



Chapter 3. Figure 22 Comparison between qualitative absorption spectra of solutions of **3** (dark red line) and **C1** (orange line) in CH_2Cl_2 at r.t. Inset: the portions in the visible spectrum are enlarged 5 times.

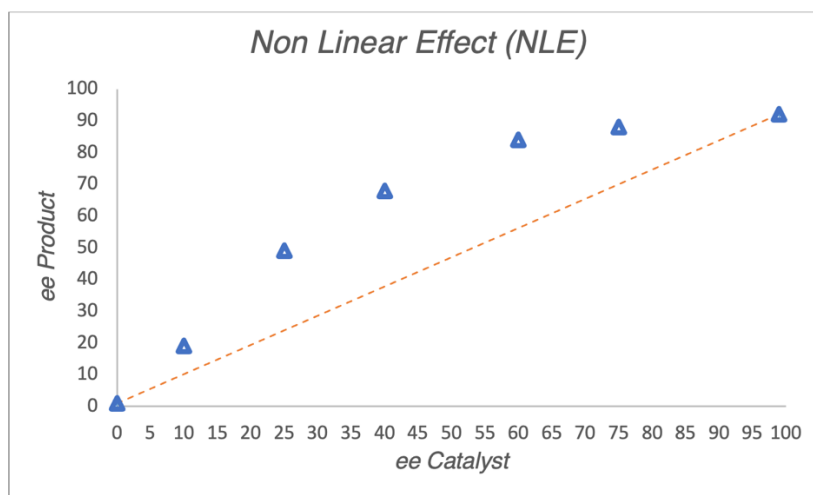
Once we obtained evidence that orange photon-absorbing organic dye could promote the reduction of the titanium complexes restoring the photocatalyst, we decided to focus on another mechanistic aspect of the reaction.

Indeed, many stereoselective protocols involving two $\text{M}(\text{Salen})$ complexes (where M is either Co , Cr or Ti), usually display non-linear effects,²⁴⁹ due to cooperative bimetallic mechanisms.²⁵⁰ According to what has been disclosed about titanocene–catalyzed pinacol coupling reactions, the stereoselective process would involve the coupling of two ketyl radicals mediated by two molecules of $[(\text{Salen})\text{TiCl}_2]$.

For this reason, we have conducted a non-linear effect study preparing the enantiomerically pure (*R,R*) and (*S,S*) $[(\text{Salen})\text{TiCl}_2]$ complexes, and using different ratio of the two complexes for promoting the reaction. The result of the study is depicted in **Figure 23**

²⁴⁹ Satyanarayana, T.; Abraham, S.; Kagan, H. B. Nonlinear effects in asymmetric catalysis. *Angew. Chem. Int. Ed.* **2009**, *48*, 456-494. <https://doi.org/10.1002/anie.200705241>

²⁵⁰ (a) Martinez, L. E.; Leighton, J. L.; Carsten, D. H.; Jacobsen, E. N. Highly Enantioselective Ring Opening of Epoxides Catalyzed by $(\text{salen})\text{Cr}(\text{III})$ Complexes. *J. Am. Chem. Soc.* **1995**, *117*, 5897-5898; <https://doi.org/10.1021/ja00126a048> (b) Larrow, J. F.; Schaus, S. E.; Jacobsen, E. N. Kinetic Resolution of Terminal Epoxides via Highly Regioselective and Enantioselective Ring Opening with TMSN_3 . An Efficient, Catalytic Route to 1,2-Amino Alcohols. *J. Am. Chem. Soc.* **1996**, *118*, 7420-7421 <https://doi.org/10.1021/ja961708+> (c) Hansen, K. B.; Leighton, J. L.; Jacobsen, E. N. On the Mechanism of Asymmetric Nucleophilic Ring-Opening of Epoxides Catalyzed by $(\text{Salen})\text{Cr}(\text{III})$ Complexes. *J. Am. Chem. Soc.* **1996**, *118*, 44, 10924-10925; <https://doi.org/10.1021/ja962600x> (d) Konsler, R. G.; Karl, J.; Jacobsen, E. N. Cooperative Asymmetric Catalysis with Dimeric Salen Complexes. *J. Am. Chem. Soc.* **1998**, *120*, 10780-10781 <https://doi.org/10.1021/ja982683c>



Chapter 3. Figure 23 Non-linear effect observed in the photoredox enantioselective reaction with [(Salen)TiCl₂]

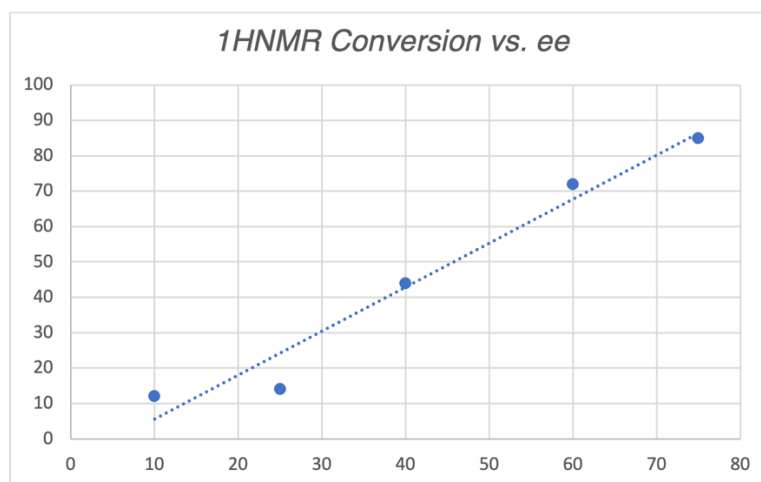
Clearly, a non-linear effect is registered, however the attribution of the proper model results nontrivial. Even if the best fitting model to describe the observed curve appears to be as a (ML)₂, suggesting a cooperative role played by two [(Salen)TiCl₂] complexes in the enantiodetermining step, a univocal establishment may result misleading. The main issue limiting our evaluation is related to the actual concentration of active chiral titanium complex in the reaction mixture. In analogy with the more studied [Cp₂TiCl₂], for instance, it is possible that the active chiral catalyst employed in the reaction is involved in dissociative equilibria during its reduction that can lead to the formation of different species.¹⁶⁶

In addition, considering the possible scenarios that can arise in the reaction mixture, a reservoir effect cannot be ruled out. As well as the Nugent–reagent is in equilibrium with its dimeric form, it is possible that the active chiral [(Salen)Ti(III)Cl] displays similar behavior.

Under these circumstances, it would not be possible to exclude that different kinetic constants are involved for the description of the equilibria between two Ti(III)-Salen complexes having the same or opposite configuration.

The formation of a stable, unreactive heterodimeric species ((*R,R*)-Ti(III)Salen—(*S,S*)-Ti(III)Salen) would lead to a formal increase in the overall enantiomeric excess, which would justify the asymmetric amplification observed.

In addition, performing the experiments to prove the presence of a non-linear effect in our reaction mechanism, it was possible to notice that the conversion of the starting material into the corresponding product, is directly proportional to the enantiomeric excess of the Ti(Salen) employed in the reaction.



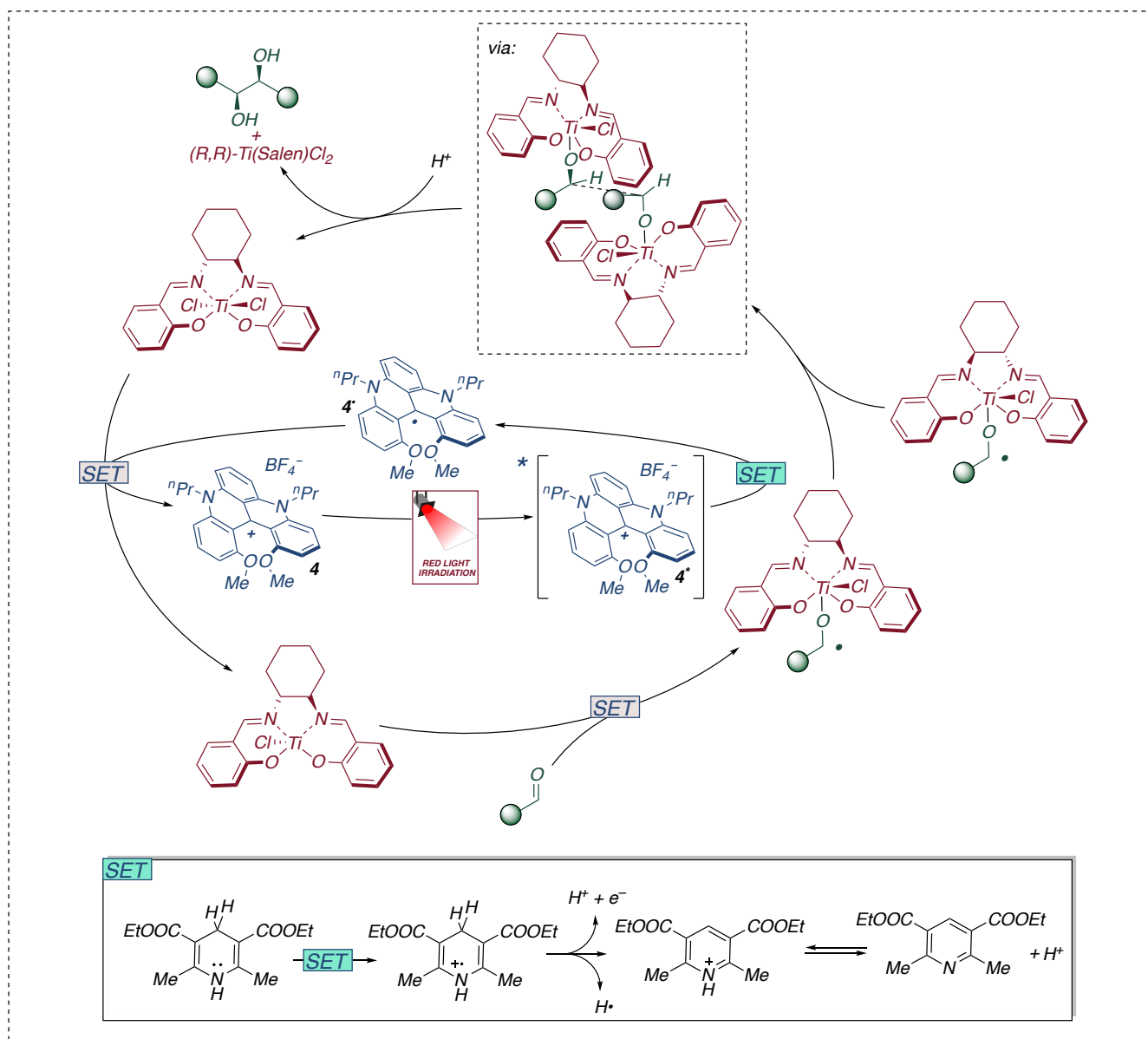
Chapter 3. Figure 24 Conversion of the reaction after 16 hours with the mixture of (R,R)- and (S,S)- [(Salen)TiCl₂] used in the studies of non-linear effect.

Although not conclusive, this experimental evidence could further support both a (ML)₂ type model and a reservoir effect.

In conclusion, combining the results deriving from photophysical study with the evidence obtained after the NLE experiments, we were able to propose a mechanistic cycle for the presented protocol. (**Figure 25**) For both the diastereo- and enantioselective reaction, the process is initiated by the absorption of visible radiation by the photocatalyst. The long-lasting excited state of the so formed **4*** is reductively quenched in the presence of Hantzsch's ester which is oxidized forming the corresponding radical cation. ($E(\mathbf{4}^*/\mathbf{4}^{\bullet}) = 1.32$ V vs. SCE while, $E(\mathbf{6}^+/\mathbf{6}) = 1.0$ V vs. SCE; $k_q = 1.5 \cdot 10^9$ M⁻¹ s⁻¹; $\eta_q = 67\%$)

The single electron transfer allows the generation of the reduced species **4*** which exhibits suitable redox potentials to trigger the reduction of both titanium (IV) complexes, restoring the photocatalyst in its early oxidation state. ($E(\mathbf{4}/\mathbf{4}^{\bullet}) = -0.82$ V vs. SCE, $E([\text{Cp}_2\text{TiCl}_2]/[\text{Cp}_2\text{TiCl}]) = -0.8$ V vs. SCE, $E([\text{(Salen)TiCl}_2]/[\text{(Salen)TiCl}]) = -0.6$ V vs. SCE)

Once formed, the titanium complex in a low oxidation state is involved in a single electron transfer in the presence of the aromatic aldehyde generating the active ketyl radical. The dimerization of this radical is the key step that determines the formation of the new carbon-carbon bond. In conclusion, oxygen-titanium bond breaking occurs due to the scavenging effect of the protons arising from the oxidative pathway of the Hantzsch's ester restoring the metal catalyst and releasing the desired product .



Chapter 3. Figure 25: Proposed dual catalytic cycle for enantio- and diastereoselective pinacol coupling of aromatic aldehydes

The scheme, following the reported literature,¹⁶⁵ depicts the diastereoselective /enantioselective step suggesting the encounter of two ketyl radicals, according to the Newman projections in the intermolecular dimerization. The most favorable projection, based on sterical reasons, does not determine the formation of the meso isomer, that is never detected in the reaction mixture. In the projection, an energetically favorable aryl-aryl interaction is shown. However, another projection, suggesting a Gauche effect between the two electronegative substituents (the two $\text{Ti}(\text{Salen})$ alkoxide) cannot be excluded.

• Conclusions

In conclusion, we have described an effective photoredox diastereo- and enantioselective pinacol coupling mediated by titanium complexes. The application of an orange/red absorbing organic dye, readily available and stable in the reaction conditions, is crucial in order to obtain good results. The direct and uncontrolled reduction of aldehydes either by a blue photon absorbing organic dyes or by the Hantzsch's ester, used as reductant is avoided. The enantioselective process is mediated by a simple prepared [(Salen)TiCl₂] metal complex, and good enantiomeric excesses are obtained. The above presented results open new directions and possibilities to many stereoselective photoredox reactions promoted by titanium or other metals with low reduction potentials. In addition, titanium complexed ketyl radicals generated in these conditions, could be used in different types of couplings.

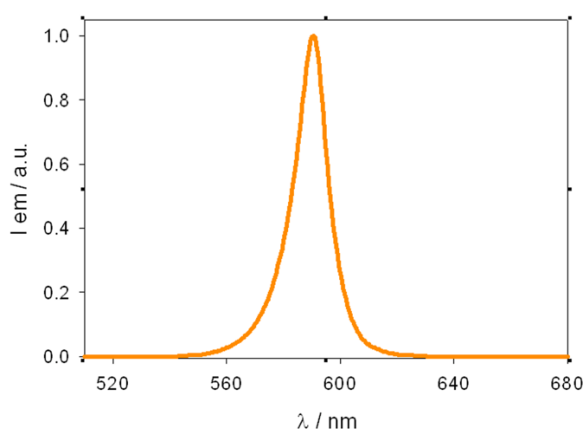
• Supplementary data

General methods and materials

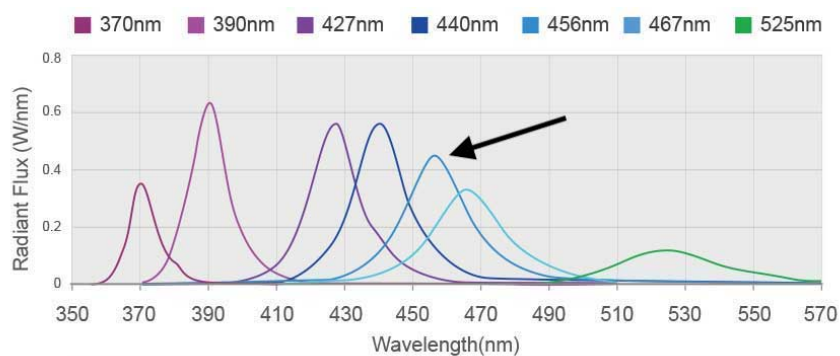
^1H -NMR spectra were recorded on Varian Mercury 400 MHz spectrometer. The chemical shift (δ) for ^1H are given in ppm relative to residual signals of the solvents and tetramethylsilane (TMS) @ 0 ppm (CDCl_3 : $\delta = 7.27$ ppm, DMSO-d_6 : $\delta = 2.50$ ppm, CD_3CN : $\delta = 1.94$ ppm, CD_3OD : $\delta = 3.31$ ppm). Data are reported as follows: chemical shift (δ), multiplicity (s = singlet, d = doublet, t = triplet, q = quartet, dd = doublet of doublets, m = multiplet), coupling constants (Hz). ^{13}C -NMR spectra were recorded on Varian Mercury 400 MHz spectrometer. The chemical shifts (δ) for ^{13}C are given in ppm relative to residual signals of the solvents and tetramethylsilane (TMS) @ 0 ppm (CDCl_3 : $\delta = 77.0$ ppm, DMSO-d_6 : $\delta = 39.5$ ppm, CD_3OD : $\delta = 49.0$ ppm). GC-MS spectra were taken by EI ionization at 70 eV on a Hewlett-Packard 5971 with GC injection. Analytical high-performance liquid chromatograph (HPLC) was performed on a HP 1090 liquid chromatograph equipped with a variable wavelength UV detector (deuterium lamp 190-600 nm), using either Daicel ChiralcelTM or PhenomenexTM columns (0.46 cm I.D. x 25 cm). HPLC grade isopropanol and hexane were used as the eluting solvents. Chromatographic purifications were done with 240-400 mesh silica gel. All reactions were set up under an argon atmosphere in oven-dried glassware using standard Schlenk techniques.

Anhydrous solvents were supplied by Aldrich in Sureseal[®] bottles. Anhydrous tetrahydrofuran was freshly distilled before the use in order to remove the radical inhibitor BHT present as stabilizer. Unless specified, other anhydrous solvents were used without further purifications. All the reagents were purchased from commercial sources (Sigma-Aldrich, Alfa Aesar, Fluorochem, Strem Chemicals, TCI) and used without further purification unless specified.

Reaction mixtures were irradiated with Kessil[®] PR160L@595 nm and Kessil[®] PR160L@456 nm.

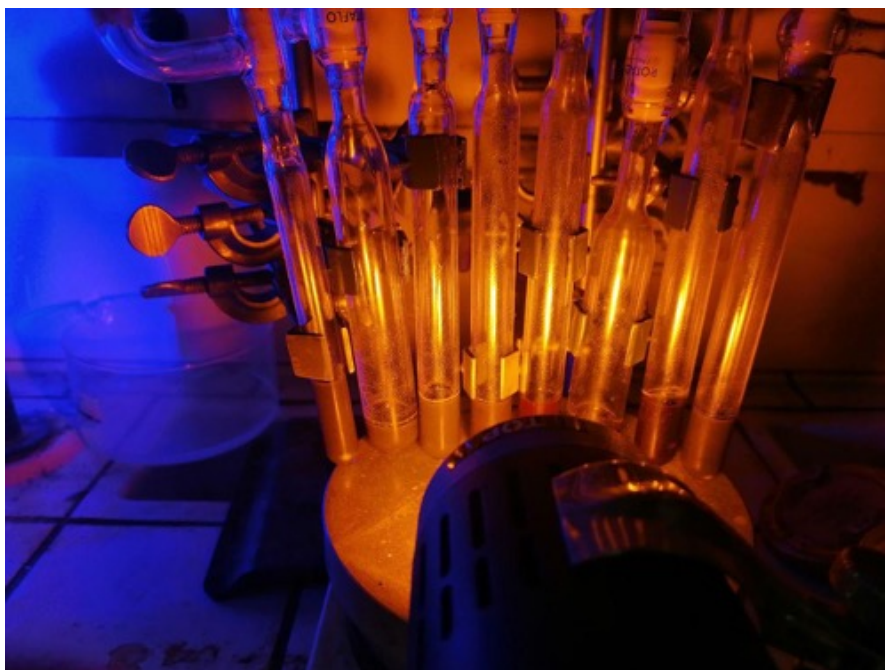


Chapter 3. Supplementary 15: Emission profile of the Kessil[®] PR160L@595 nm used to irradiate the reaction mixture.



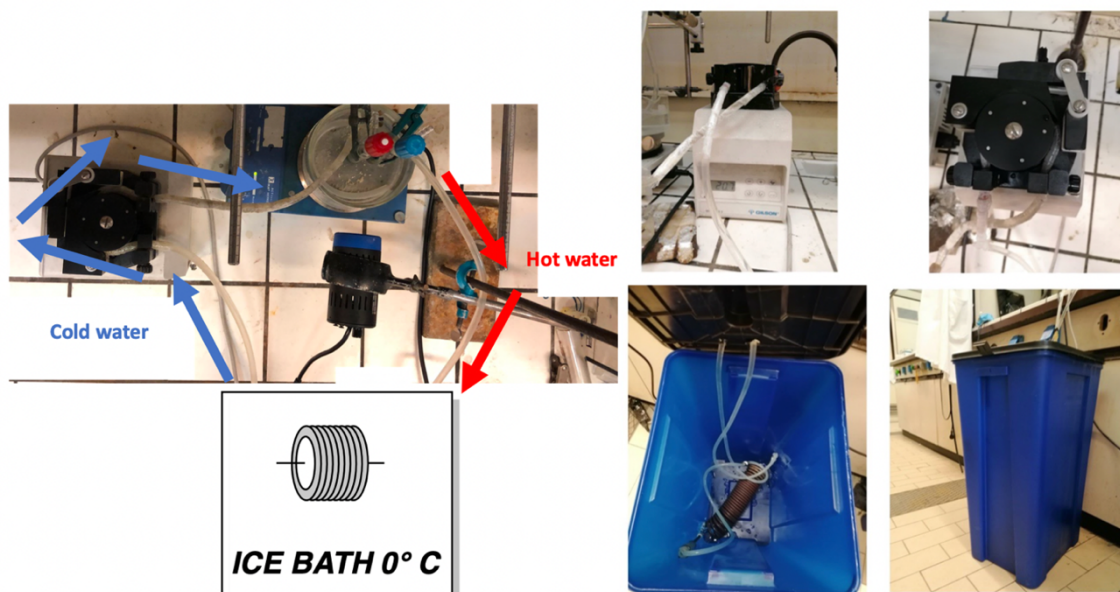
Chapter 3. Supplementary 16: Emission profile of the Kessil® PR160L@456 nm used to irradiate the reaction mixture (from Kessil® website)

The reaction flasks were positioned approximately at 10 cm from the light source and Kessil® PR160@595 nm. The reaction temperature was 25 °C during the irradiation as measured with a thermometer at 2 cm from reaction flask.



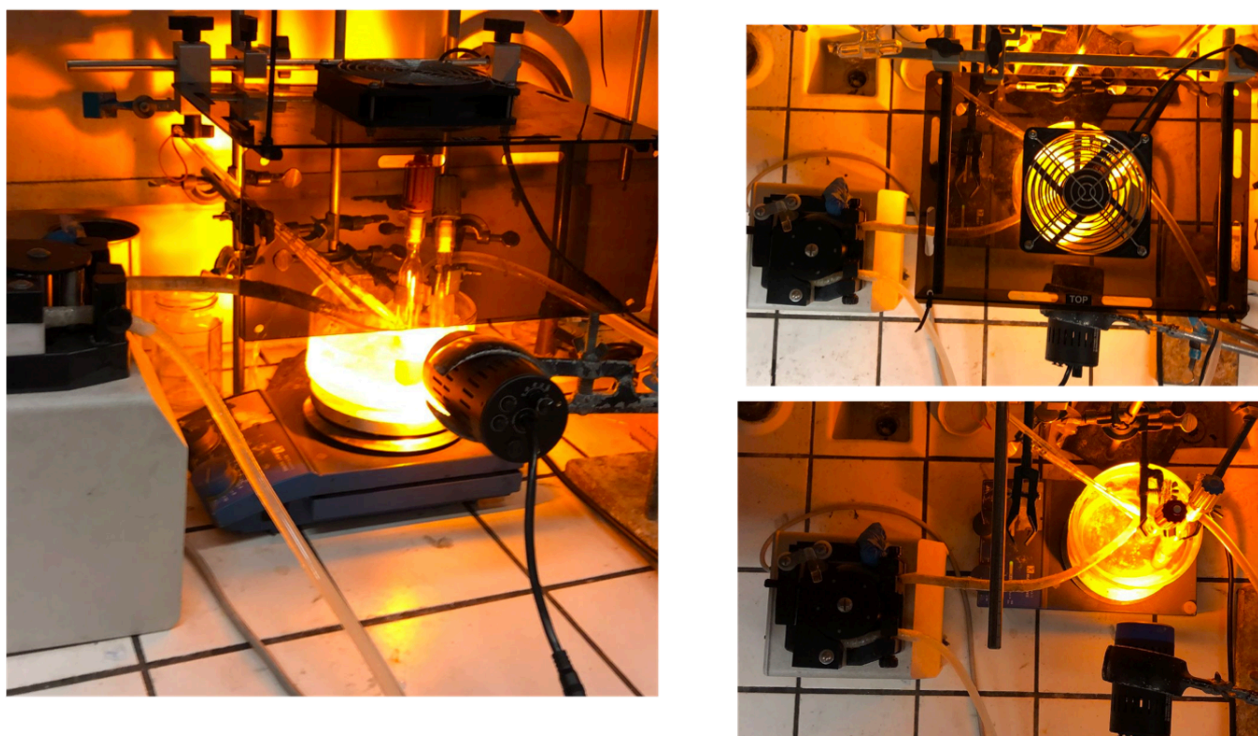
Chapter 3. Supplementary 17: Reaction set-up for diastereoselective pinacol coupling with Kessil® PR160L@595 nm lamp.

The home-made cryostat system was filled with ice allowing the control of the temperature. The reaction temperature was 10 °C during the irradiation as measured with a thermometer at 2 cm from reaction flask. The blue container was filled with ice in order to allow the refrigeration of the running water.



Chapter 3. Supplementary 18: : Home-made cryostat system.

The reaction flasks were positioned approximately at 10 cm from the light source and Kessil® PR160 Rig with Fan Kit.

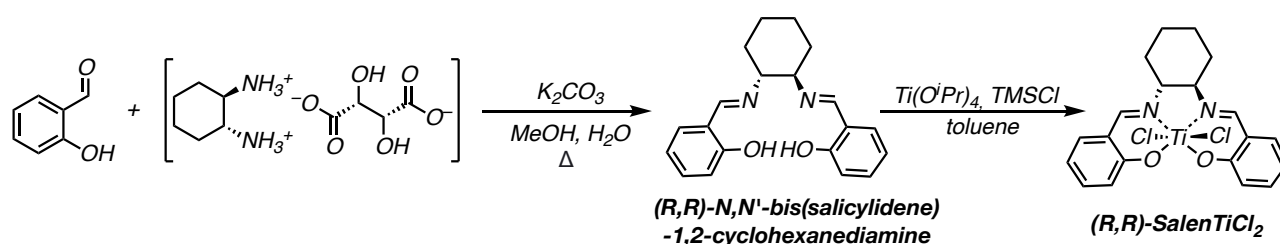


Chapter 3. Supplementary 19: Reaction set-up for enantioselective pinacol coupling with Kessil® PR160L@595 nm lamp.

Photophysical and Electrochemical Studies

All the photophysical analyses were carried out in α,α,α -trifluorotoluene at 298 K, unless otherwise specified. UV–vis absorption spectra were recorded with a PerkinElmer λ 40 spectrophotometer using quartz cells with path length of 1.0 cm. Luminescence spectra were performed with a PerkinElmer LS-50, an Edinburgh FS5 spectrofluorometer equipped with a Hamamatsu Photomultiplier R928P phototube or on an Edinburgh FLS920 equipped with a Ge detector for NIR emissions. Lifetimes shorter than 10 μ s were measured by the same Edinburgh FLS920 spectrofluorometer by time-correlated single-photon counting (TCSPC) technique. Quantum yields are determined with the method of Demas and Crosby (*J. Am. Chem. Soc.* 1971, 93:12, 2841-2847) using Cresyl Violet in air-equilibrated methanol as a standard ($\Phi = 0.54$). Experiments in absence of oxygen were carried out in sealed custom-made quartz cuvettes, upon degassing with repeated pump-freeze-thaw cycles in high vacuum. The estimated experimental errors are 2 nm on the band maximum, 5% on the molar absorption coefficient and luminescence lifetime. Cyclic voltammetry (CV) experiments were carried out in argon-purged dichloromethane solutions with tetrabutylammonium hexafluorophosphate as supporting electrolyte at room temperature with an Autolab 30 potentiostat interfaced to a personal computer. The working electrode was a glassy carbon electrode (0.08 cm², Amel); its surface was routinely polished with 0.3 mm alumina-water slurry on a felt surface, immediately prior to use. In all cases, the counter electrode was a Pt spiral and an Ag wire was used as a quasi-reference electrode. Ferrocene ($E_{1/2} = +0.46$ V vs. SCE) was introduced as an internal standard.

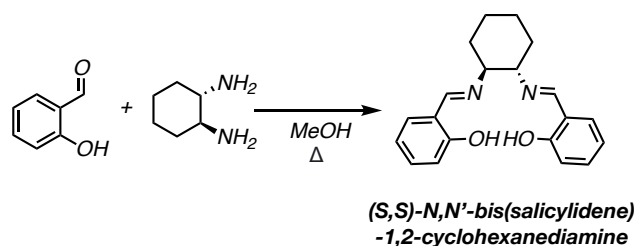
Synthesis of $(1R,2R)$ -[(Salen)TiCl₂]



• (R,R) - N,N' -bis(salicylidene)-1,2-cyclohexanediamine was obtained following the procedure reported by Chusov and co-workers.²⁵¹ Under argon atmosphere, a flame-dried 50 mL Schlenk tube, equipped with a magnetic stirring bar, was charged with mixture of $(1R,2R)$ -*trans*-cyclohexane-1,2-diammonium *L*-tartrate (2 mmol, 528 mg, 1.0 equiv.), K₂CO₃ (2 mmol, 276 mg, 1.0 equiv.) and H₂O (1.5 mL) and stirred for 30 min, then MeOH (5 mL) was added. After 15 min, a solution of 2-hydroxybenzaldehyde (488 mg, 4 mmol, 2 equiv.) in MeOH (2 mL) was added dropwise. The reaction mixture was refluxed until TLC analysis showed a full conversion of the starting material. The solvents were evaporated under *vacuum* and the residue was dissolved in EtOAc, washed with water (10 mL), dried (Na₂SO₄) and concentrated to afford the desired product in 75% yield (485 mg, 1.5 mmol). The crude product was employed in the next step without further purifications.

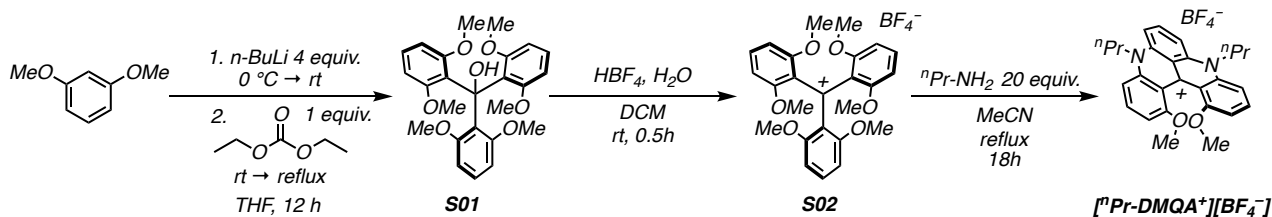
• (R,R) -[(Salen)TiCl₂] was obtained following the procedure reported by Joshi and co-workers.²³¹ Under argon atmosphere, in a flame-dried 5 mL Schlenk tube, equipped with a magnetic stirring bar, a solution of (R,R) - N,N' -bis(salicylidene)-1,2-cyclohexanediamine (322 mg, 1 mmol, 1 equiv.) in toluene (0.5 mL) was added to a solution of Ti(O^{*i*}Pr)₄ (1.0 M in toluene; 1 mL, 1 mmol, 1 equiv.). The solution was stirred at room temperature for 12h. The reaction mixture was diluted with 2 mL of toluene and treated dropwise with TMSCl (300 μL, 2.4 mmol, 2.4 equiv.). Immediately, the complex started precipitating as a red solid. After the mixture was stirred for 4 h, the solid was filtered through a sintered funnel and dried under reduced pressure to afford the desired (R,R) – [(Salen)TiCl₂] as a bright red solid (360 mg, 0.82 mmol, 82% yield).

²⁵¹ Tsygankov, A.; Chun, M.-S.; Samoylova, A.; Kwon, S.; Kreschenova, Y.; Kim, S.; Shin, E.; Oh, J.; Strelkova, T.; Kolesov, V.; Zubkov, F.; Semenov, S.; Fedyanin, I.; Chusov, D. Synthesis of *N,N'*-Dialkylated Cyclohexane-1,2-Diamines and Their Application as Asymmetric Ligands and Organocatalysts for the Synthesis of Alcohols. *Synlett* **2016**, 28 (05), 615–619. <https://doi.org/10.1055/s-0036-1588382>.

Synthesis of (S,S)-N,N'-bis(salicylidene)-1,2-cyclohexanediamine

Under argon atmosphere, a flame-dried 50 mL Schlenk tube, equipped with a magnetic stirring bar, was charged with mixture of (1*S*,2*S*)-*trans*-cyclohexane-1,2-diamine (2 mmol, 228 mg, 1.0 equiv.) in MeOH (5 mL) After 15 min a solution of 2-hydroxybenzaldehyde (488 mg, 4 mmol, 2 equiv.) in MeOH (2 mL) was added dropwise. The reaction mixture was refluxed until TLC analysis showed a full conversion of the starting material. The solvents were evaporated under vacuum and the residue was dissolved in EtOAc, washed with water (10 mL), dried (Na₂SO₄) and concentrated to afford the desired product in 65% yield (420 mg, 1.3 mmol). The crude product was employed in the next step without further purifications as reported above.

Synthesis of *N,N'*-di-*n*-propyl-1,13-dimethoxyquinacridinium [ⁿPr-DMQA]⁺ tetrafluoroborate



•**Synthesis of S01** Carbinol **S01** was synthesized modifying the procedure reported by Martin and Smith.²⁵² In a flame dried 250 mL three-necked round bottom flask equipped with a magnetic stirring bar, under argon atmosphere, 1,3-dimethoxybenzene (16 mmol, 2.2 g, 2.1 mL, 4 equiv.) was dissolved in dry THF (8 mL). The solution was cooled to 0 °C with an ice bath, and *n*-BuLi (2.5 M in hexane, 4 equiv.) was added dropwise. The solution was allowed to stir 4h at room temperature, then diethyl carbonate (4 mmol, 473 mg, 487 μL, 1 equiv.) was added to the reaction mixture. The solution was heated to reflux for 8h. The reaction was quenched at 0 °C upon slow addition of *ca.* 20 mL of water. Volatiles were removed under reduced pressure and the resulting mixture was extracted with DCM (3x10 mL). The combined organic phase was dried with Na₂SO₄ and concentrated under reduced pressure to yield a black solid which was employed in the next step without further purifications.

•**Synthesis of S02** Compound **S02** was synthesized adapting the procedure reported by Laursen and co-workers.²⁵³ In a one-necked round bottom flask equipped with a magnetic stir bar, the above-mentioned crude carbinol **S01** was dissolved in absolute EtOH (30 mL), and HBF₄ (48 wt. % in H₂O, 1.57 mL, 12 mmol, 3 equiv.) was added dropwise. After 0.5h a one-to-one solution of diethyl ether and hexane (60 mL) was added, and the formation of a violet precipitate was observed. **S02** was allowed to precipitate overnight in the reaction mixture. The crude was filtered and washed with hexane (*ca.* 20 mL). Compound **S02** was isolated as a dark violet solid (1.11 g, 2.2 mmol, 54% yield over two steps). Spectroscopic data matched those previously reported in the literature.

•**Synthesis of [ⁿPr-DMQA][BF₄]** Adapting the procedure reported by Giannetti and co-workers,²⁴⁰ in a flame dried 250 mL Schlenk tube equipped with a magnetic stirring bar, under argon atmosphere **S02** (1.1 g, 2.15 mmol, 1 equiv.) was dissolved in dry MeCN (25 mL, degassed). Propylamine (53.7 mmol, 3.18 g, 4.42 mL, 25 equiv.) was added to the solution, and the reaction mixture was heated to 80 °C and stirred for 18h, until HPLC/MS analysis showed a complete conversion of the starting material **S02**. Volatiles were removed under reduced pressure and the crude was washed with diethyl ether, then it was dissolved in the minimum volume of DCM (*ca.* 10 mL) and reprecipitated with EtOAc (*ca.* 100 mL). [ⁿPr-DMQA][BF₄] was isolated after filtration of the mixture as a dark green solid (700 mg, 1.4 mmol, 65%). Spectroscopic data matched those previously reported in the literature.

²⁵² Martin, J. C.; Smith, R. G. Factors Influencing the Basicities of Triarylcabinols. The Synthesis of Sesquixanthrol. *J. Am. Chem. Soc.* **1964**, *86* (11), 2252–2256. <https://doi.org/10.1021/ja01065a030>.

²⁵³ Laursen B. W.; Krebs, F. C. Synthesis, Structure, and Properties of Azatriangulenium Salts. *Chem. - A Eur. J.* **2001**, *7* (8), 1773–1783. [https://doi.org/10.1002/1521-3765\(20010417\)7:8<1773::AID-CHEM17730>3.0.CO;2-F](https://doi.org/10.1002/1521-3765(20010417)7:8<1773::AID-CHEM17730>3.0.CO;2-F).

General procedure A: diastereoselective photoredox pinacol coupling promoted by red-light-absorbing dye

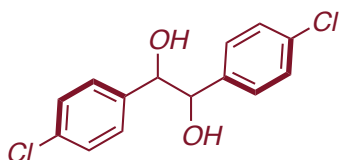
All the reactions were performed on 0.2 mmol scale of aldehyde in a flame dried 10 mL Schlenk tube, equipped with a Rotaflo stopcock, magnetic stirring bar and an argon supply tube.

Under vigorous argon flux, aldehydes **1a–s** (0.2 mmol), [Cp₂TiCl₂](5 mol%, 0.01 mmol, 2.5 mg), the organic photocatalyst [Pr-DMQA][BF₄] (5 mol%, 0.01 mmol, 5.0 mg) and diethyl 1,4-dihydro-2,6-dimethyl-3,5-pyridinedicarboxylate (Hantzsch's ester) (1.1 equiv., 0.22 mmol, 55 mg) were added. Dry trifluorotoluene (2 mL, in order to obtain a concentration of the titanium complex of 0.005 M) was then added and the reaction mixture was further subjected to a freeze-pump-thaw procedure (three cycles), and the vessel was then refilled with argon. The reaction was irradiated under vigorous stirring for 72h at room temperature. The solvent was then evaporated under reduced pressure and the reaction crude was monitored by NMR analysis to evaluate the diastereoselectivity of the reaction. The crude was subject of flash column chromatography (SiO₂) to afford products **2a–s** in the stated yields.

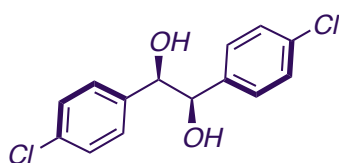
General procedure B: enantioselective photoredox pinacol coupling promoted by red-light-absorbing dye

All the reactions were performed on 0.2 mmol scale of aldehyde in a flame dried 10 mL Schlenk tube, equipped with a Rotaflo stopcock, magnetic stirring bar and an argon supply tube.

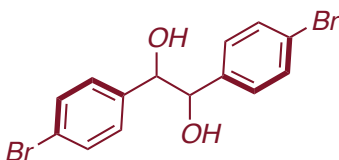
Under vigorous argon flux, selected aldehydes (0.2mmol), (*R,R*)-[(Salen)TiCl₂] (10 mol%, 0.02 mmol, 8.4 mg), the organic photocatalyst [ⁿPr-DMQA][BF₄] (5 mol%, 0.01 mmol, 5.0 mg) and diethyl 1,4-dihydro-2,6-dimethyl-3,5-pyridinedicarboxylate (Hantzsch's ester) (1.1 equiv., 0.22 mmol, 55 mg) were added. Dry trifluorotoluene (4 mL, in order to obtain a concentration of the titanium complex of 0.005 M) was then added and the reaction mixture was further subjected to a freeze-pump-thaw procedure (four cycles), and the vessel was then refilled with argon. The reaction was irradiated under vigorous stirring for 48h at 6–12°C. The solvent was then evaporated under reduced pressure and the reaction crude was monitored by NMR analysis to evaluate the diastereoselectivity of the reaction. The crude was subject of flash column chromatography (SiO₂) to afford the products in the stated yields.



(2a) white solid; 89% (0.089 mmol, 25 mg); d.r. > 20:1 (*d/l*-**2a**:*meso*-**2a**) was determined by integration of benzylic CH ¹H NMR signals. The general procedure A was applied using **1a** (0.2 mmol, 28 mg). The title compound was isolated by flash column chromatography (10–50% ethyl acetate in hexane). Spectroscopic data matched those previously reported in the literature.²⁵⁴



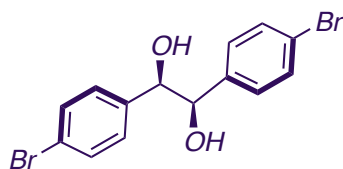
(R,R-2a) white solid; 67% (0.067 mmol, 19 mg); d.r. > 20:1 (*d/l*-**2a**:*meso*-**2a**) was determined by integration of benzylic CH ¹H NMR signals. The general procedure B was applied using **1a** (0.2 mmol, 28 mg). The title compound was isolated by flash column chromatography (10–50% ethyl acetate in hexane). Spectroscopic data matched those previously reported in the literature.²⁵⁴ HPLC analysis (LUX CELLULOSE 3, *n*-Hexane: *i*-PrOH = 95:5, 1 mL/min, 30 °C, 224 nm) indicated 96:4 e.r. (*t*-major = 31.83 min, *t*-minor = 35.19 min).



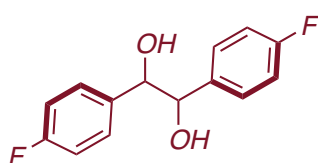
(2b) white solid; 60% (0.06 mmol, 22 mg); d.r. > 20:1 (*d/l*-**2b**:*meso*-**2b**) was determined by integration of benzylic CH ¹H NMR signals. The general procedure A was applied using **1b** (0.2 mmol, 37 mg). The title compound was isolated by flash column chromatography (10–50% ethyl acetate in hexane). Spectroscopic data matched those previously reported in the literature.²⁵⁵

²⁵⁴ Zhao, L.; Han, B.; Huang, Z.; Miller, M.; Huang, H.; Malashock, D. S.; Zhu, Z.; Milan, A.; Robertson, D. E.; Weiner, D. P.; Burk, M. J. Epoxide Hydrolase-Catalyzed Enantioselective Synthesis of Chiral 1,2-Diols via Desymmetrization of *meso*-Epoxides *J. Am. Chem. Soc.*, **2004**, *126* (36), 11156–11157. <https://doi.org/10.1021/ja0466210>

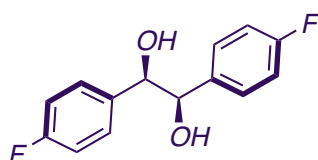
²⁵⁵ Jeong, K. S.; Kim, Y. S.; Kim, Y. J.; Lee, E.; Yoon, J. H.; Park, W. H.; Park, Y. W.; Kim, J.; Jeong, N. Lanthanitin: A Chiral Nanoball Encapsulating 18Lanthanum Ions by Ferritin-Like Assembly *Angew. Chem. Int. Ed.*, **2006**, *45*, 8134–8138. 10.1002/anie.200603622



(*R,R*-2b) white solid; 70% (0.07 mmol, 26 mg); d.r. > 20:1 (*d/l*-2b:*meso*-2b) was determined by integration of benzylic CH ¹H NMR signals. The general procedure B was applied using **1b** (0.2 mmol, 37 mg). The title compound was isolated by flash column chromatography (10–50% ethyl acetate in hexane). Spectroscopic data matched those previously reported in the literature. HPLC analysis (LUX CELLULOSE 3, *n*-Hexane: *i*-PrOH = 95:5, 1 mL/min, 30 °C, 220 nm) indicated 96:4 e.r. (*t*-minor = 25.98 min, *t*-major = 27.19 min).²⁵⁵

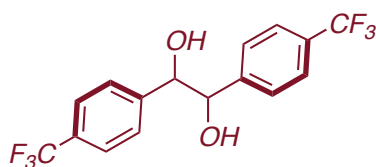


(2c) white solid; 74% (0.074 mmol, 18 mg); d.r. = 15:1 (*d/l*-2c:*meso*-2c) was determined by integration of benzylic CH ¹H NMR signals. The general procedure A was applied using previously distilled **1c** (0.2 mmol, 25 mg, 22 μL). The title compound was isolated by flash column chromatography (10–50% ethyl acetate in hexane). Spectroscopic data matched those previously reported in the literature.²⁵⁶

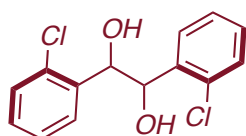


(*R,R*-2c) white solid; 85% (0.085 mmol, 21 mg); d.r. > 20:1 (*d/l*-2c:*meso*-2c) was determined by integration of benzylic CH ¹H NMR signals. The general procedure B was applied using previously distilled **1c** (0.2 mmol, 25 mg, 22 μL). The title compound was isolated by flash column chromatography (10–50% ethyl acetate in hexane). Spectroscopic data matched those previously reported in the literature.²⁵⁶ HPLC analysis (LUX CELLULOSE 3, *n*-Hexane: *i*-PrOH = 95:5, 1 mL/min, 30 °C, 224 nm) indicated 95.5:4.5 e.r. (*t*-major = 12.09 min, *t*-minor = 13.92 min).

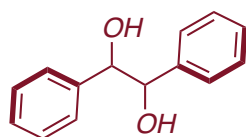
²⁵⁶ Tanner, D.; Johansson, F.; Harden, A.; Andersson, P. G. A comparative study of C₂-symmetric bis(aziridine) ligands in some transition metal-mediated asymmetric transformations *Tetrahedron*, **1998**, *54* (51), 15731–15738. [https://doi.org/10.1016/S0040-4020\(98\)00987-9](https://doi.org/10.1016/S0040-4020(98)00987-9)



(2d) white solid; 81% (0.081 mmol, 28 mg); d.r. = 8:1 (*d/l*-**2d**:*meso*-**2d**) was determined by integration of benzylic CH ¹H NMR signals. The general procedure A was applied using previously distilled **1d** (0.2 mmol, 35 mg, 27 μ L). The title compound was isolated by flash column chromatography (10–50% ethyl acetate in hexane). Spectroscopic data matched those previously reported in the literature.²⁵⁷



(2e) pale yellow oil; 78% (0.078 mmol, 22 mg); d.r. = 3:1 (*d/l*-**2e**:*meso*-**2e**) was determined by integration of benzylic CH ¹H NMR signals. The general procedure A was applied using previously distilled **1e** (0.2 mmol, 28 mg, 23 μ L). The title compound was isolated by flash column chromatography (10–50% ethyl acetate in hexane). Spectroscopic data matched those previously reported in the literature.²⁵⁸

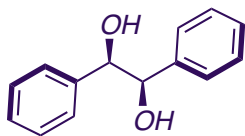


(2f) pale yellow solid; 77% (0.077 mmol, 16 mg); d.r. > 20:1 (*d/l*-**2f**:*meso*-**2f**) was determined by integration of benzylic CH ¹H NMR signals. The general procedure A was applied using previously distilled **1f** (0.2 mmol, 21 mg, 20 μ L). The title compound was isolated by flash column chromatography (10–50% ethyl acetate in hexane). Spectroscopic data matched those previously reported in the literature.²⁵⁹

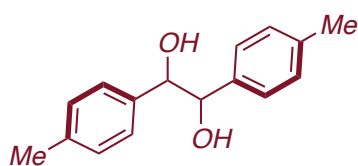
²⁵⁷ Brandolese, A.; Greenhalgh, M. D.; Desrues, T.; Liu, X.; Qu, S.; Bressy, C.; Smith, A. D. Horeau Amplification in the Sequential Acylative Kinetic Resolution of (\pm)-1,2-Diols and (\pm)-1,3-Diols in Flow. *Org. Biomol. Chem.* **2021**, *19* (16), 3620–3627. <https://doi.org/10.1039/d1ob00304f>.

²⁵⁸ Gualandi, A.; Rodeghiero, G.; Della Rocca, E.; Bertoni, F.; Marchini, M.; Perciaccante, R.; Jansen, T. P.; Ceroni, P.; Cozzi, P. G. Application of Coumarin Dyes for Organic Photoredox Catalysis. *Chem. Commun.* **2018**, *54* (72), 10044–10047. <https://doi.org/10.1039/C8CC04048F>.

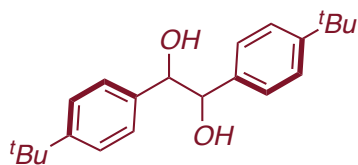
²⁵⁹ Fujii, K.; Mitsudo, K.; Mandai, H.; Suga, S. Hydrogen Bonding-Assisted Enhancement of the Reaction Rate and Selectivity in the Kinetic Resolution of *d,l*-1,2-Diols with Chiral Nucleophilic Catalysts. *Adv. Synth. Catal.* **2017**, *359* (16), 2778–2788. <https://doi.org/10.1002/adsc.201700057>.



(R,R-2f) pale yellow solid; 42% (0.042 mmol, 9 mg); d.r. > 20:1 (*d/l*-**2f**:*meso*-**2f**) was determined by integration of benzylic CH ¹H NMR signals. The general procedure B was applied using previously distilled **1f** (0.2 mmol, 21 mg, 20 μ L). The title compound was isolated by flash column chromatography (10–50% ethyl acetate in hexane). Spectroscopic data matched those previously reported in the literature. HPLC analysis (LUX CELLULOSE 3, *n*-Hexane: *i*-PrOH = 95:5, 1 mL/min, 30 $^{\circ}$ C, 214 nm) indicated 95.5:4.5 e.r. (*t*-minor = 12.43 min, *t*-major = 14.00 min).²⁵⁹



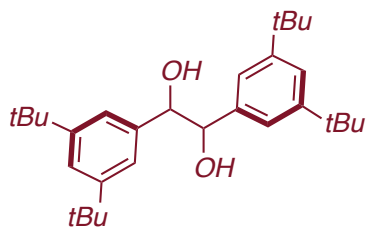
(2g) pale yellow solid; 95% (0.095 mmol, 23 mg); d.r. = 16:1 (*d/l*-**2g**:*meso*-**2g**) was determined by integration of benzylic CH ¹H NMR signals. The general procedure A was applied using previously distilled **1g** (0.2 mmol, 24 mg, 24 μ L). The title compound was isolated by flash column chromatography (10–50% ethyl acetate in hexane). Spectroscopic data matched those previously reported in the literature.²⁶⁰



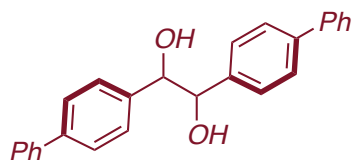
(2h) white solid; 74% (0.074 mmol, 24 mg); d.r. > 20:1 (*d/l*-**2h**:*meso*-**2h**) was determined by integration of benzylic CH ¹H NMR signals. The general procedure A was applied using previously distilled **1h** (0.2 mmol, 32 mg, 33 μ L). The title compound was isolated by flash column chromatography (10–50% ethyl acetate in hexane). Spectroscopic data matched those previously reported in the literature.²⁶¹

²⁶⁰ Mwangi, M. T.; Schulz, M. D.; Bowden, N. B. Sequential Reactions with Grubbs Catalyst and AD-mix- α/β Using PDMS Thimbles *Org. Lett.*, **2009**, *11*, (1), 33–36. <https://doi.org/10.1021/ol8022215>

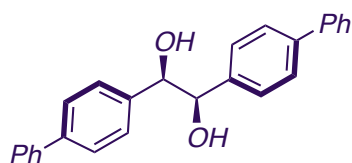
²⁶¹ Hong, S.; Tian, S.; Metz, M. V.; Marks, T. J. C₂-Symmetric Bis(Oxazolinato)Lanthanide Catalysts for Enantioselective Intramolecular Hydroamination/Cyclization. *J. Am. Chem. Soc.* **2003**, *125* (48), 14768–14783. <https://doi.org/10.1021/ja0364672>.



(2i) white solid; 97% (0.097 mmol, 42 mg); d.r. > 20:1 (*d/l*-**2i**:*meso*-**2i**) was determined by integration of benzylic CH ^1H NMR signals. The general procedure A was applied using **1i** (0.2 mmol, 44 mg). The title compound was isolated by flash column chromatography (10–50% ethyl acetate in hexane). ^1H NMR (400 MHz, CDCl_3) δ 7.19 (t, $J = 1.8$ Hz, 2H), 6.87 (d, $J = 1.9$ Hz, 4H), 4.67 (s, 2H), 2.83 (s, 2H), 1.18 (d, $J = 0.9$ Hz, 36H). ^{13}C NMR (101 MHz, CDCl_3) δ 150.3 (2C), 138.9 (4C), 121.5 (2C), 121.1 (4C), 80.6 (2C), 34.7 (4C), 31.4 (12C).

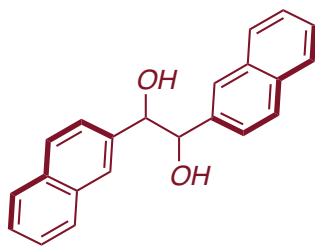


(2j) white solid; 80% (0.080 mmol, 29 mg); d.r. > 20:1 (*d/l*-**2j**:*meso*-**2j**) was determined by integration of benzylic CH ^1H NMR signals. The general procedure A was applied using **1j** (0.2 mmol, 36 mg). The title compound was isolated by flash column chromatography (10–50% ethyl acetate in hexane). Spectroscopic data matched those previously reported in the literature.²⁶²

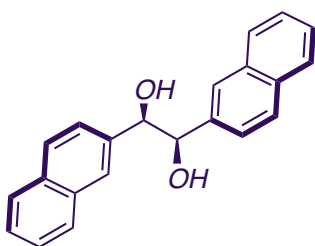


(R,R-2j) white solid; 30% (0.03 mmol, 11 mg); d.r. > 20:1 (*d/l*-**2j**:*meso*-**2j**) was determined by integration of benzylic CH ^1H NMR signals. The general procedure B was applied using **1j** (0.2 mmol, 36 mg). The title compound was isolated by flash column chromatography (10–50% ethyl acetate in hexane). Spectroscopic data matched those previously reported in the literature.²⁶² HPLC analysis (ID, *n*-Hexane: *i*-PrOH = 70:30, 1.5 mL/min, 40 °C, 254 nm) indicated 73.5:26.5 e.r. (*t*-major = 4.83 min, *t*-minor = 6.52 min).

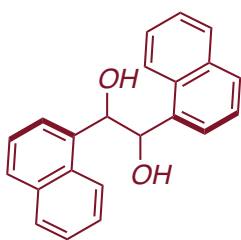
²⁶² Gök, Y.; Kiliçarslan, S.; Gök, H. Z.; Karayığit, İlker, Ü. *t* Synthesis, -Diaryl-BINOL Phosphoric Acids as Enantioselective Extractants of Benzylic Primary Amines. *Chirality*, **2011**, *43* (March 2010), 34–43. <https://doi.org/10.1002/chir>.



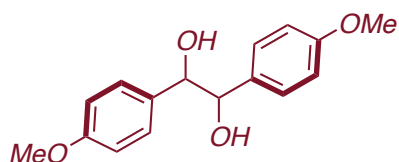
(2k) white solid; 70% (0.070 mmol, 22 mg); d.r. > 20:1 (*d/l*-**2k**:*meso*-**2k**) was determined by integration of benzylic CH ¹H NMR signals. The general procedure A was applied using **1k** (0.2 mmol, 31 mg). The title compound was isolated by flash column chromatography (10–50% ethyl acetate in *n*-Hexane). Spectroscopic data matched those previously reported in the literature.²⁵⁹



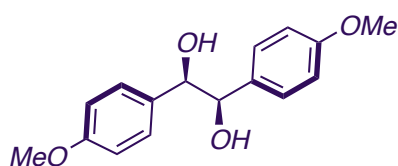
(*R,R*-2k) white solid; 61% (0.061 mmol, 19 mg); d.r. > 20:1 (*d/l*-**2k**:*meso*-**2k**) was determined by integration of benzylic CH ¹H NMR signals. The general procedure B was applied using **1k** (0.2 mmol, 31 mg). The title compound was isolated by flash column chromatography (10–50% ethyl acetate in *n*-Hexane). Spectroscopic data matched those previously reported in the literature.²⁵⁹ HPLC analysis (LUX CELLULOSE 3, *n*-Hexane: *i*-PrOH = 50:50, 1mL/min, 30 °C, 224 nm) indicated 96:4 e.r. (*t*-major = 11.33 min, *t*-minor = 19.25 min).



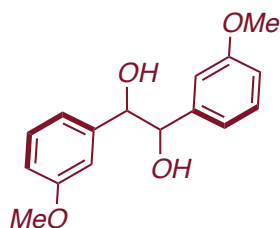
(2l) white solid; 77% (0.077 mmol, 24 mg); d.r. > 20:1 (*d/l*-**2l**:*meso*-**2l**) was determined by integration of benzylic CH ¹H NMR signals. The general procedure A was applied using **1l** (0.2 mmol, 31 mg, 27 μL). The title compound was isolated by flash column chromatography (10–50% ethyl acetate in *n*-Hexane). Spectroscopic data matched those previously reported in the literature.²⁵⁹



(2m) white solid; 95% (0.095 mmol, 26 mg); d.r. = 18:1 (*d/l*-**2m**:*meso*-**2m**) was determined by integration of benzylic CH ¹H NMR signals. The general procedure A was applied using previously distilled **1m** (0.2 mmol, 27 mg, 24 μL). The title compound was isolated by flash column chromatography (10–50% ethyl acetate in *n*-Hexane). Spectroscopic data matched those previously reported in the literature.²⁶⁰

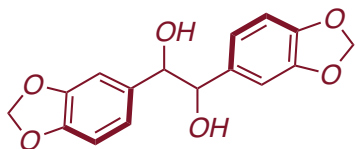


(R,R-2m) white solid; 77% (0.077 mmol, 21 mg); d.r. >² 20:1 (*d/l*-**2m**:*meso*-**2m**) was determined by integration of benzylic CH ¹H NMR signals. The general procedure B was applied using previously distilled **1m** (0.2 mmol, 27 mg, 24 μL). The title compound was isolated by flash column chromatography (10–50% ethyl acetate in *n*-Hexane). Spectroscopic data matched those previously reported in the literature. HPLC analysis (ID, *n*-Hexane: *i*-PrOH = 70:30, 1.5 mL/min, 40 °C, 214 nm) indicated 95:5 e.r. (*t*-major = 12.09 min, *t*-minor = 13.92 min).²⁶⁰

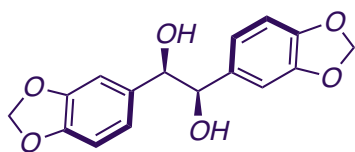


(2n) white solid; 99% (0.099 mmol, 27 mg); d.r. > 20:1 (*d/l*-**2n**:*meso*-**2n**) was determined by integration of benzylic CH ¹H NMR signals. The general procedure A was applied using previously distilled **1n** (0.2 mmol, 27 mg, 24 μL). The title compound was isolated by flash column chromatography (10–50% ethyl acetate in *n*-Hexane). Spectroscopic data matched those previously reported in the literature.²⁶³

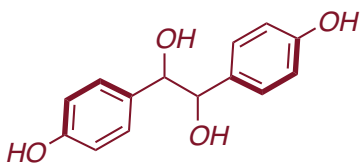
²⁶³ Sotto, N.; Billamboz, M.; Chevrin-Villette, C.; Len, C. Selective Pinacol Coupling on Regeneratable Supported Acids in Sole Water. *J. Org. Chem.* **2015**, *80* (12), 6375–6380. <https://doi.org/10.1021/acs.joc.5b00837>.



(2o) white solid; 92% (0.092 mmol, 27 mg); d.r. > 20:1 (*d/l*-**2o**:*meso*-**2o**) was determined by integration of benzylic CH ¹H NMR signals. The general procedure A was applied using **1o** (0.2 mmol, 30 mg). The title compound was isolated by flash column chromatography (10–50% ethyl acetate in *n*-Hexane). ¹H NMR (400 MHz, DMSO-*d*₆) δ 6.73 – 6.62 (m, 4H), 6.50 (dd, *J* = 8.0, 1.7 Hz, 2H), 5.90 (q, *J* = 1.1 Hz, 4H), 5.21 (s, 1.5 Hz, 2H), 4.41 (s, 2H). ¹³C NMR (101 MHz, DMSO-*d*₆) δ 146.9 (2C), 146.2 (2C), 136.9 (2C), 120.8 (2C), 107.9 (2C), 107.6 (2C), 101.0(2C), 77.7 (2C).

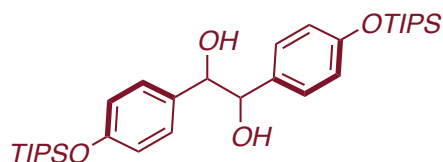


(*R,R*-2o) white solid; 79% (0.079 mmol, 24 mg); d.r. > 20:1 (*d/l*-**2o**:*meso*-**2o**) was determined by integration of benzylic CH ¹H NMR signals. The general procedure B was applied using **1o** (0.2 mmol, 30 mg). The title compound was isolated by flash column chromatography (10–50% ethyl acetate in *n*-Hexane). ¹H NMR (400 MHz, DMSO-*d*₆) δ 6.73 – 6.62 (m, 4H), 6.50 (dd, *J* = 8.0, 1.7 Hz, 2H), 5.90 (q, *J* = 1.1 Hz, 4H), 5.21 (s, 1.5 Hz, 2H), 4.41 (s, 2H). ¹³C NMR (101 MHz, DMSO-*d*₆) δ 146.9 (2C), 146.2 (2C), 136.9 (2C), 120.8 (2C), 107.9 (2C), 107.6 (2C), 101.0 (2C), 77.7 (2C). HPLC analysis (LUX CELLULOSE 3, *n*-Hexane: *i*-PrOH = 50:50, 1mL/min, 30 °C, 230 nm) indicated 95:5 e.r. (*t*-major = 7.26 min, *t*-minor = 8.34 min).

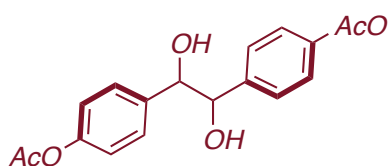


(2p) white solid; 77% (0.077 mmol, 19 mg); d.r. = 3:1 (*d/l*-**2p**:*meso*-**2p**) was determined by integration of benzylic CH ¹H NMR signals. The general procedure A was applied using **1p** (0.2 mmol, 24 mg). The title compound was isolated by flash column chromatography (10–50% ethyl acetate in *n*-Hexane). Spectroscopic data matched those previously reported in the literature.²⁶⁴

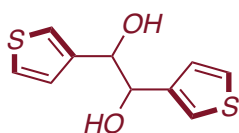
²⁶⁴ Nakatsuji, M.; Hata, Y.; Fujihara, T.; Yamamoto, K.; Sasaki, M.; Takekuma, H.; Yoshihara, M.; Minematsu, T.; Takekuma, S. I. Reactions of Azulenes with 1,2-Diaryl-1,2-Ethanediols in Methanol in the Presence of Hydrochloric Acid: Comparative Studies on Products, Crystal Structures, and Spectroscopic and Electrochemical Properties. *Tetrahedron* **2004**, *60* (28), 5983–6000. <https://doi.org/10.1016/j.tet.2004.05.022>.



(2q) white solid; 57% (0.057 mmol, 32 mg); d.r. > 20:1 (*d/l*-**2q**:*meso*-**2q**) was determined by integration of benzylic CH ^1H NMR signals. The general procedure A was applied using **1q** (0.2 mmol, 56 mg). The title compound was isolated by flash column chromatography (10–50% ethyl acetate in *n*-Hexane). ^1H NMR (400 MHz, DMSO- d_6) δ 6.76 (d, $J = 8.4$ Hz, 4H), 6.57 (d, $J = 8.4$ Hz, 4H), 5.30 (s, 2H), 4.39 (s, 2H), 1.22 – 1.13 (m, 6H), 1.03 (d, $J = 7.2$ Hz, 36H). ^{13}C NMR (101 MHz, DMSO- d_6) δ 154.5 (2C), 135.1 (2C), 128.7 (4C), 118.7 (4C), 78.3 (2C), 18.1 (6C), 12.4 (12C).

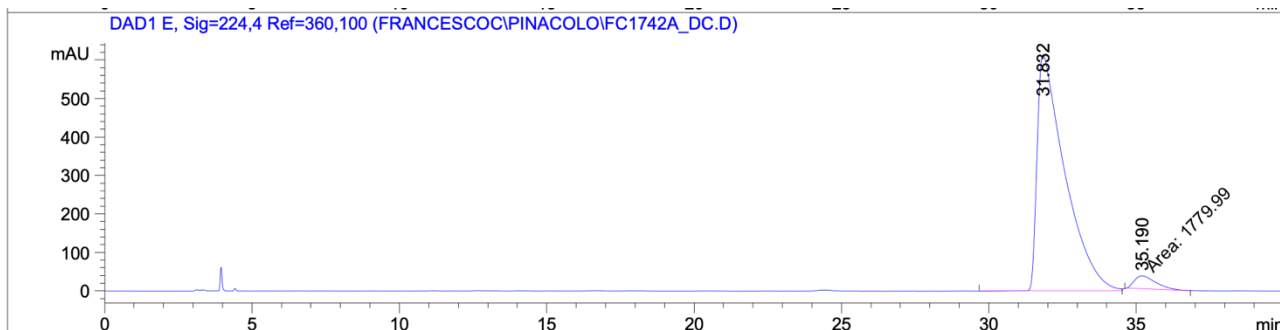
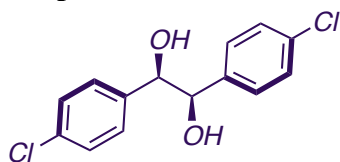


(2r) white solid; 70% (0.070 mmol, 23 mg); d.r. > 20:1 (*d/l*-**2r**:*meso*-**2r**) was determined by integration of benzylic CH ^1H NMR signals. The general procedure A was applied using **1r** (0.2 mmol, 33 mg, 28 μL). The title compound was isolated by flash column chromatography (10–50% ethyl acetate in *n*-Hexane). ^1H NMR (400 MHz, CDCl_3) δ 7.16 – 7.04 (m, 4H), 7.04 – 6.79 (m, 4H), 4.63 (s, 2H), 2.24 (s, 6H). ^{13}C NMR (101 MHz, CDCl_3) δ 169.5 (2C), 150.4 (2C), 137.6 (2C), 128.1 (4C), 121.4 (4C), 78.6 (2C), 21.3 (2C).

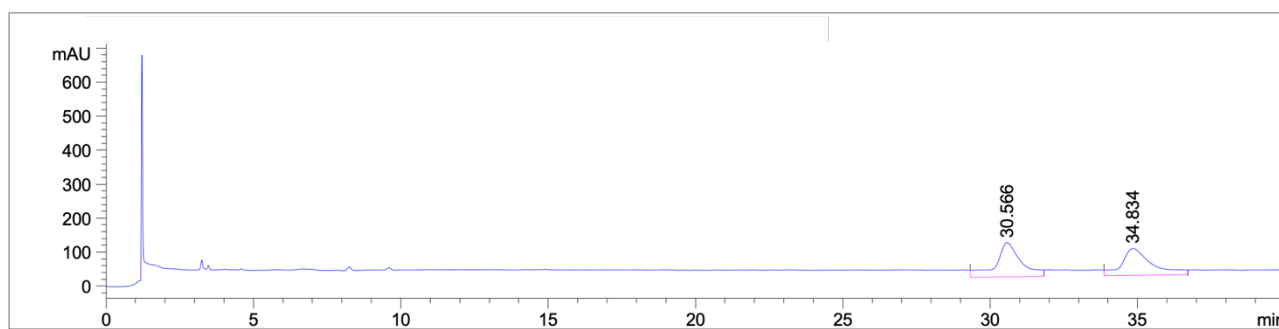


(2s) white solid; 87% (0.087 mmol, 20 mg); d.r. > 20:1 (*d/l*-**2s**:*meso*-**2s**) was determined by integration of benzylic CH ^1H NMR signals. The general procedure A was applied using previously distilled **1s** (0.2 mmol, 22 mg, 18 μL). The title compound was isolated by flash column chromatography (10–50% ethyl acetate in *n*-Hexane). ^1H NMR (400 MHz, DMSO- d_6) δ 7.29 (dd, $J = 5.0, 3.0$ Hz, 2H), 7.06 (dd, $J = 3.0, 1.2$ Hz, 2H), 6.83 (dd, $J = 5.0, 1.2$ Hz, 2H), 5.26 (s, 2H), 4.64 (s, 2H). ^{13}C NMR (101 MHz, DMSO- d_6) δ 144.4 (2C), 127.4 (2C), 125.1 (2C), 121.9 (2C), 74.0 (2C).

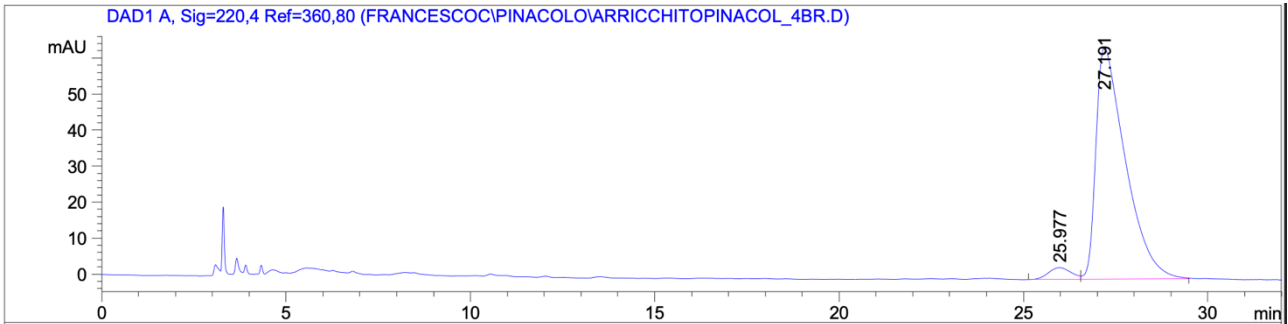
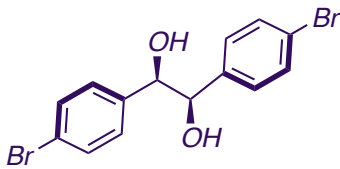
• Copies HPLC traces



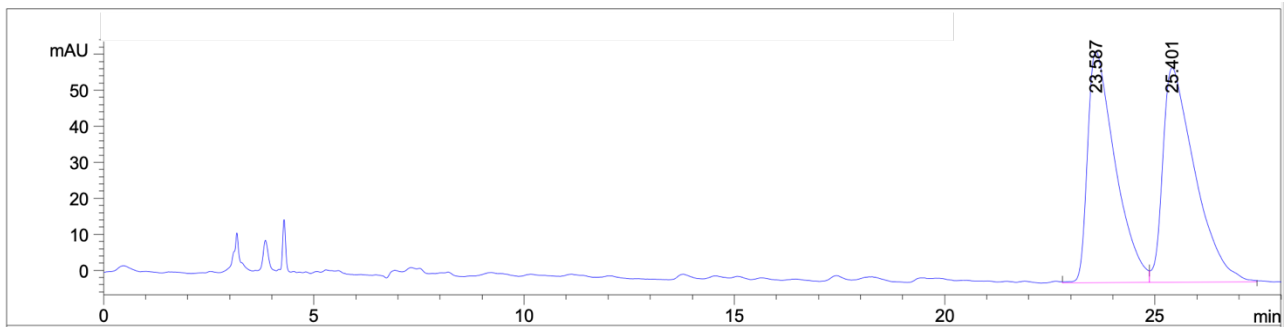
Peak #	RetTime [min]	Type	Width [min]	Area [mAU*s]	Height [mAU]	Area %
1	31.832	VV	0.8993	4.02516e4	613.60266	95.7651
2	35.190	MM	0.8792	1779.99146	33.74203	4.2349



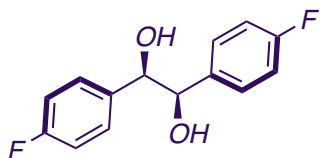
Peak #	RetTime [min]	Type	Width [min]	Area [mAU*s]	Height [mAU]	Area %
1	30.566	VV	0.8322	6113.87891	101.28490	51.2478
2	34.834	VV	1.0335	5816.15820	79.87313	48.7522



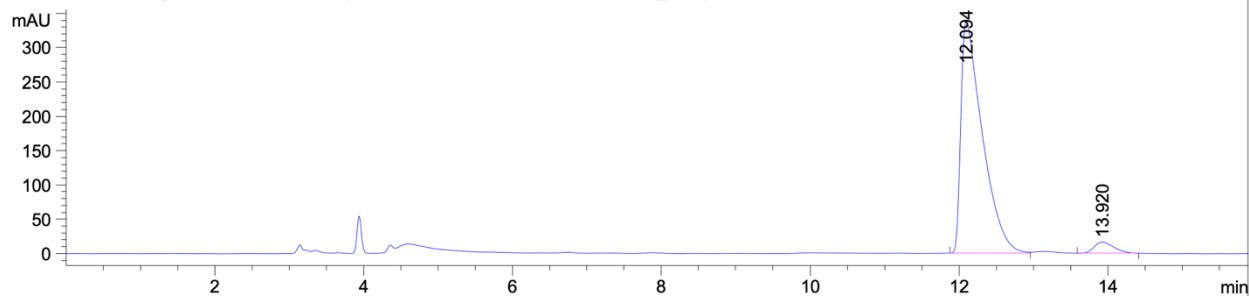
Peak #	RetTime [min]	Type	Width [min]	Area [mAU*s]	Height [mAU]	Area %
1	25.977	BV	0.5789	139.34477	3.25856	3.7586
2	27.191	VB	0.8117	3567.96436	64.26516	96.2414



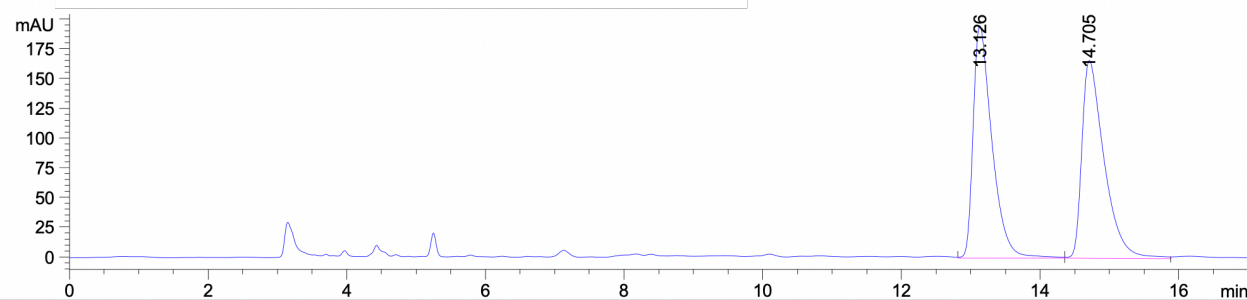
Peak #	RetTime [min]	Type	Width [min]	Area [mAU*s]	Height [mAU]	Area %
1	23.587	VV	0.6715	2929.68872	64.30592	48.0114
2	25.401	VB	0.7575	3172.37427	59.55227	51.9886



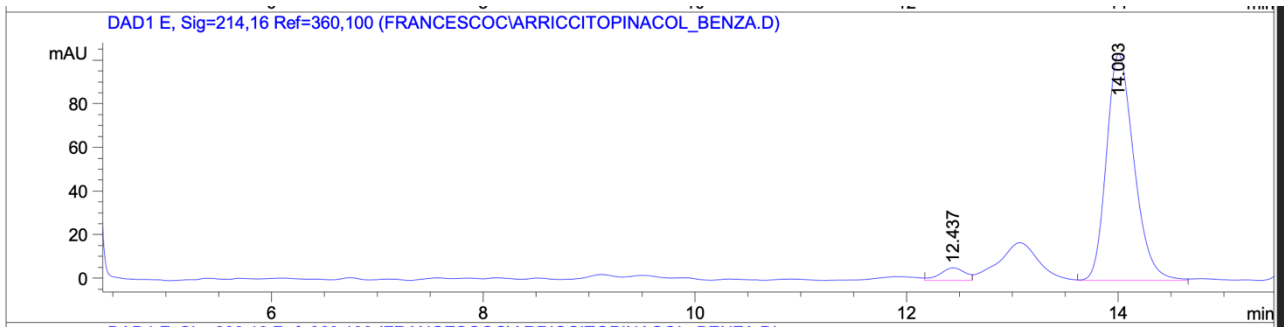
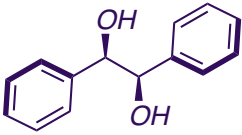
DAD1 B, Sig=224,16 Ref=360,100 (FRANCESCOCARRICITOPINACOL_4F.D)



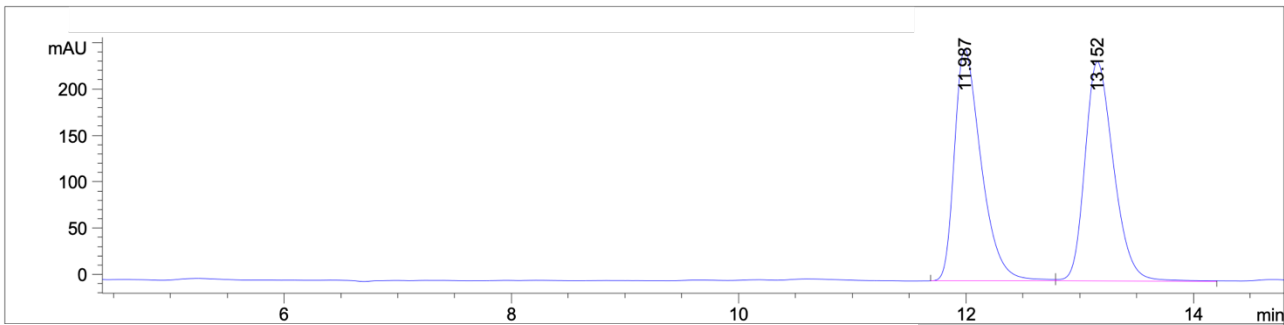
Peak #	RetTime [min]	Type	Width [min]	Area [mAU*s]	Height [mAU]	Area %
1	12.094	BB	0.2898	6773.72461	338.08020	95.6043
2	13.920	VB	0.2912	311.44299	16.42501	4.3957



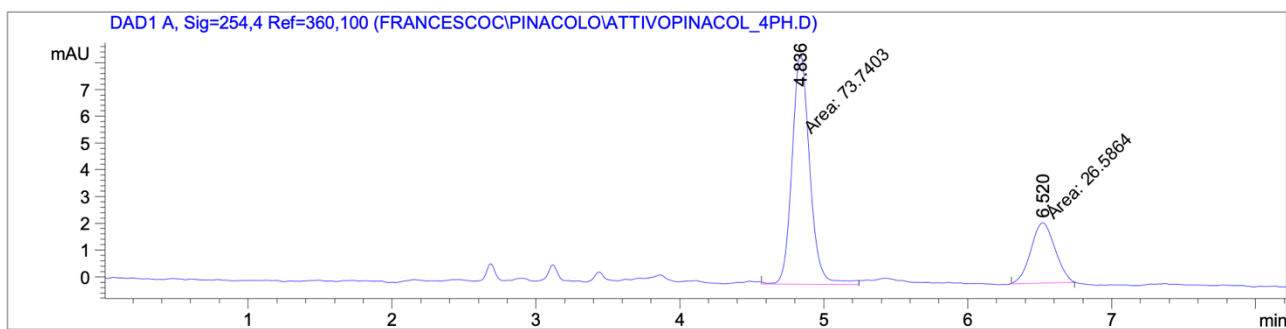
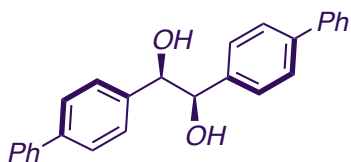
Peak #	RetTime [min]	Type	Width [min]	Area [mAU*s]	Height [mAU]	Area %
1	13.126	VV	0.2841	3725.70557	195.72293	49.9872
2	14.705	VV	0.3331	3727.61523	166.55109	50.0128



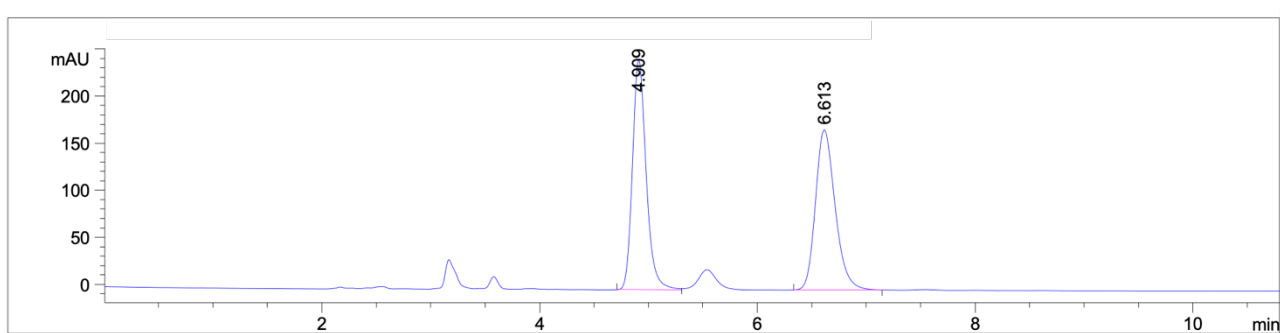
Peak #	RetTime [min]	Type	Width [min]	Area [mAU*s]	Height [mAU]	Area %
1	12.435	VV	0.2494	111.00645	6.69483	4.4730
2	14.004	VV	0.2794	2370.71362	130.81329	95.5270



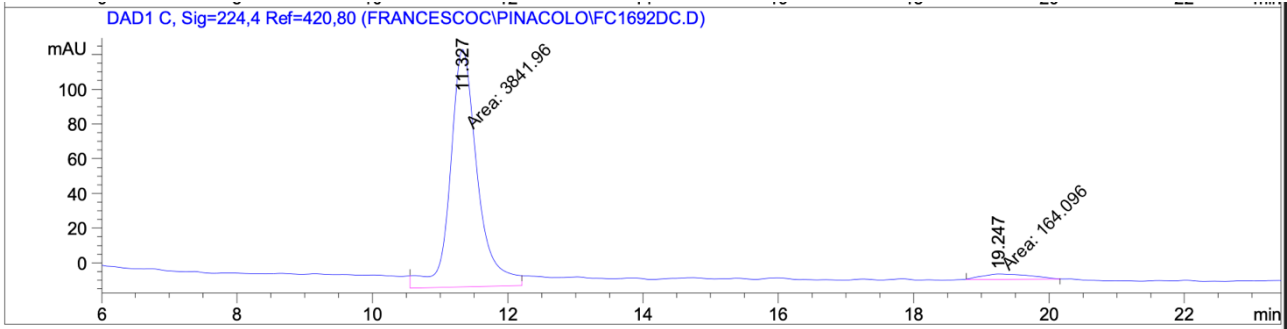
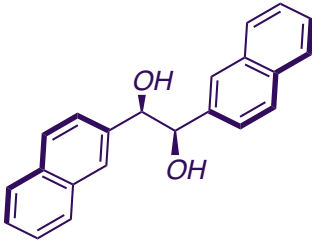
Peak #	RetTime [min]	Type	Width [min]	Area [mAU*s]	Height [mAU]	Area %
1	11.987	BV	0.2516	4110.92969	250.28018	49.6809
2	13.152	VB	0.2731	4163.74023	236.86893	50.3191



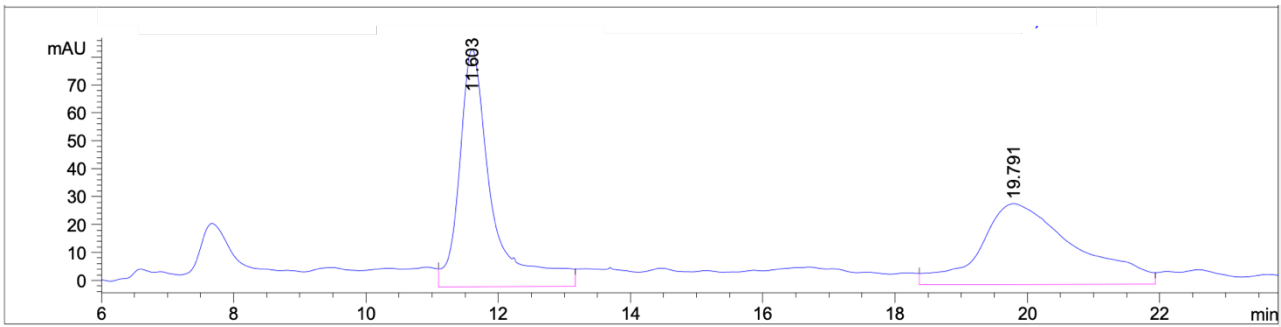
Peak #	RetTime [min]	Type	Width [min]	Area [mAU*s]	Height [mAU]	Area %
1	4.836	MM	0.1428	73.74026	8.60620	73.5002
2	6.520	MM	0.1951	26.58639	2.27089	26.4998



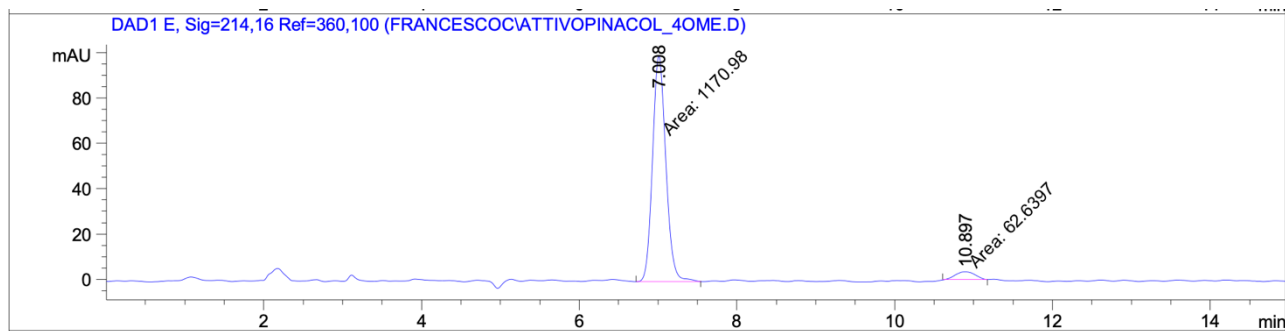
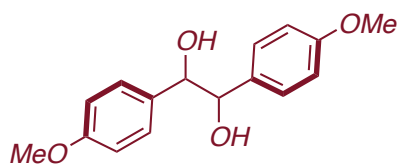
Peak #	RetTime [min]	Type	Width [min]	Area [mAU*s]	Height [mAU]	Area %
1	4.909	BV	0.1342	2141.13330	244.44960	50.0185
2	6.613	BB	0.1927	2139.55371	170.18555	49.9815



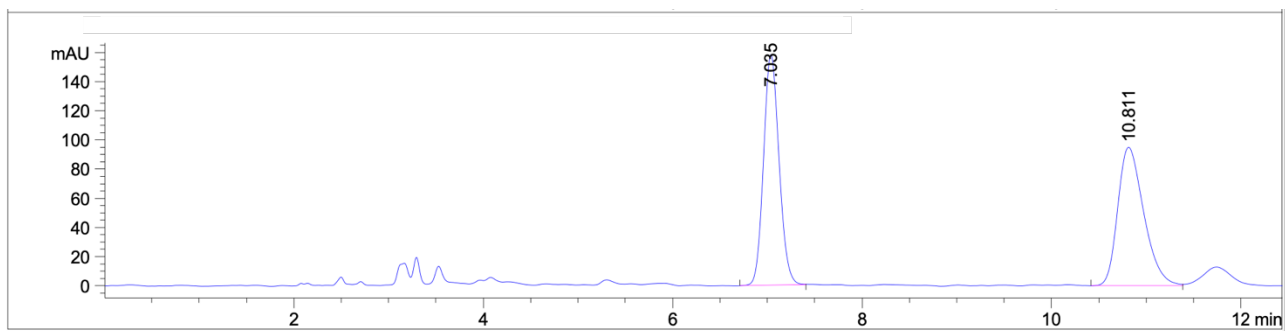
Peak #	RetTime [min]	Type	Width [min]	Area [mAU*s]	Height [mAU]	Area %
1	11.327	MM	0.4669	3841.96411	137.13683	95.9038
2	19.247	MM	0.8589	164.09592	3.18429	4.0962



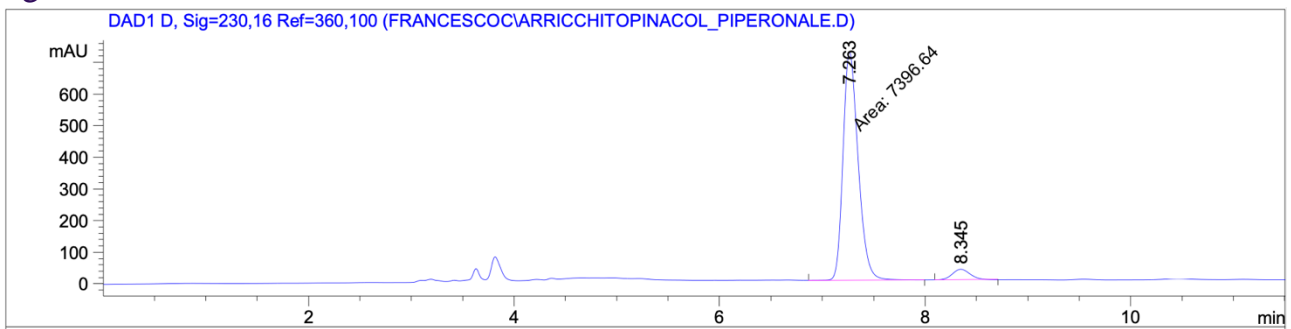
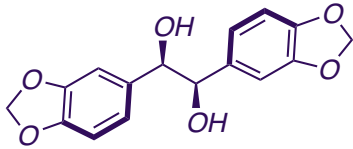
Peak #	RetTime [min]	Type	Width [min]	Area [mAU*s]	Height [mAU]	Area %
1	11.603	VV	0.4918	2883.87817	85.01467	49.8445
2	19.791	VV	1.3983	2901.86670	29.02757	50.1555



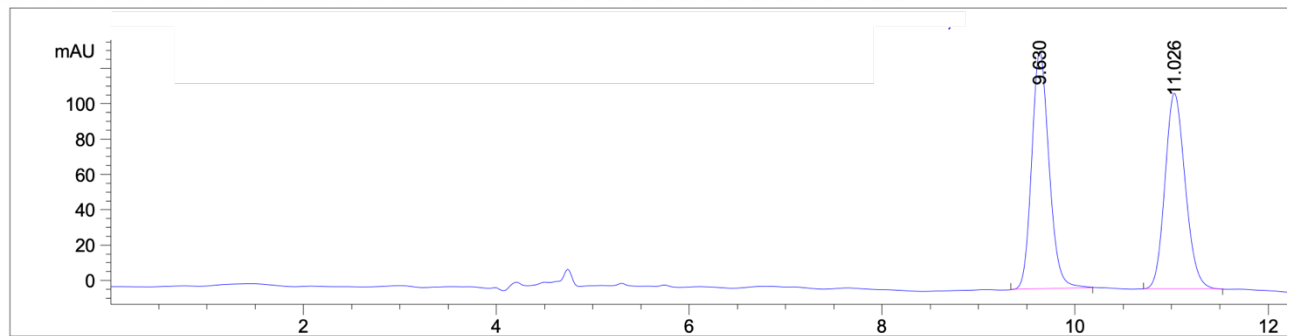
Peak #	RetTime [min]	Type	Width [min]	Area [mAU*s]	Height [mAU]	Area %
1	7.008	MM	0.1962	1170.98303	99.49201	94.9223
2	10.897	MM	0.2969	62.63968	3.51626	5.0777



Peak #	RetTime [min]	Type	Width [min]	Area [mAU*s]	Height [mAU]	Area %
1	7.035	BB	0.1770	1803.51257	158.25554	49.8518
2	10.811	VV	0.2929	1814.23694	94.96841	50.1482



Peak #	RetTime [min]	Type	Width [min]	Area [mAU*s]	Height [mAU]	Area %
1	7.263	MM	0.1705	7396.64014	723.12823	94.8271
2	8.345	BB	0.1873	403.49286	33.30582	5.1729



Peak #	RetTime [min]	Type	Width [min]	Area [mAU*s]	Height [mAU]	Area %
1	9.630	BB	0.1945	1685.87683	134.26591	50.9481
2	11.026	BB	0.2268	1623.13403	110.83760	49.0519

Chapter 4. Visible Light-Driven Formation of Transient Nucleophilic Organonickel Species for Functionalization of Carbonyl Compounds

Using the electrophilicity of carbonyl compounds as a chemical handle for the formation of new chemical bonds is certainly an efficient and functional way for the preparation of important molecular scaffolds of widespread interest. To do this, therefore, a fundamental goal for the synthetic chemical community is to design protocols that allow the formation of nucleophilic species – even transiently in the reaction mixture– that can be as selective as possible to expand the range of tolerable functional groups.²⁶⁵ Grignard-type reagents and organolithium compounds represent by far the class of organometallic compounds, markedly nucleophilic, able to promote this type of bond-forming.

However, the pronounced ionic character of the carbon-lithium and carbon-magnesium bonds determines that most of these compounds results extremely reactive, dramatically limiting the tolerated functional groups.

In addition, direct nucleophilic functionalization of a carbonyl moiety results in the formation of a stereocenter, tertiary in the case of aldehydes, quaternary in the case of asymmetric ketones. Development of enantioselective variant of these protocols provides additional interest in these transformations. As introduced in previous chapters, it is possible to find evidence in the literature that the most convenient response to this type of requirement is to operate in reductive conditions in the presence of an appropriate transition metal species and a (pseudo)halide that behaves as a pronucleophiles species.

In this scenario, the use of nickel as a transition metal both if present in stoichiometric or catalytic amount opens new routes to the direct functionalization of carbonyls, both in racemic and enantioselective fashion.

At the same time, the intrinsic property of nickel to have access to multiple oxidation states, the possibility of performing oxidative addition in the presence of an electrophile and its compatibility with reductive reaction conditions, makes it a valid alternative to other reported protocols.

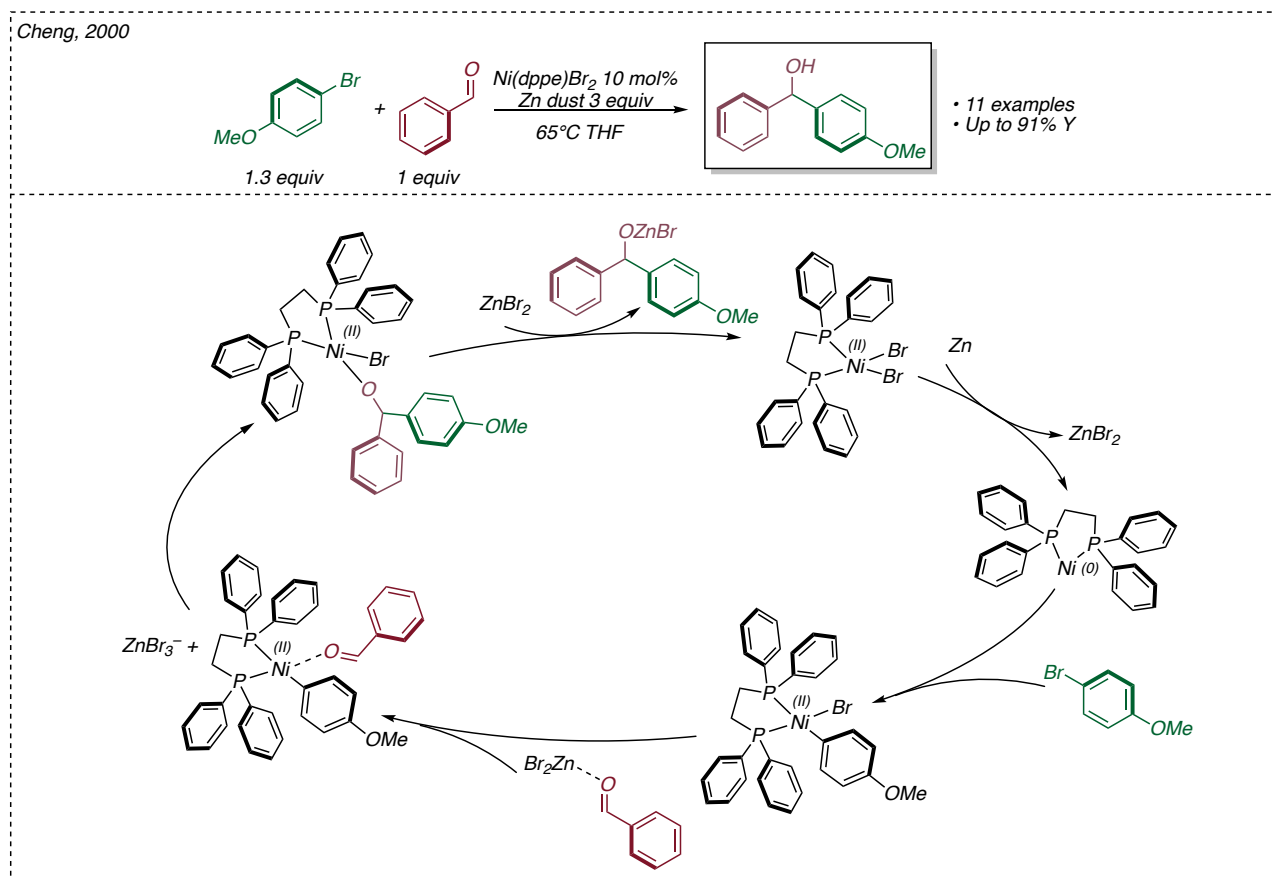
Although Corey and co-workers had already demonstrated in 1967 that starting from a stoichiometric amount of Ni(COD)₂, it was possible to generate a nucleophilic species capable of attacking an electrophile through a Grignard-type reaction in the presence of an alkyl-/aryl-halide,²⁶⁶ the recognition

²⁶⁵ Comprehensive Organic Synthesis, 2nd ed.; Knochel, P., Molander, G. A., Eds.; Elsevier: Oxford, 2014; Vols. 1 and 2

²⁶⁶ Corey, E. J.; Semmelhack, M. F. Organonickel Compounds as Reagents for Selective Carbon-Carbon Bond Formation between Unlike Groups. *J. Am. Chem. Soc.* **1967**, 89 (11), 2755–2757. <https://doi.org/10.1021/ja00987a056>.

of new methodologies remains a field decidedly underdeveloped compared to other metals such as rhodium²⁶⁷ and iridium.²⁶⁸

In this scenario, the use of nickel catalysis for the formation of transient organometallic nucleophilic species, for example, represents one of the few alternatives for the direct arylation of both aromatic and aliphatic aldehydes beyond the Co/Cr-catalyzed Nozaki-Hiyama-Kishi reaction.¹⁴⁹ The first example of this type of nickel-mediated transformation was reported by Cheng and co-workers.²⁶⁹



Chapter 4. Scheme 1 Nickel catalyzed arylation of aldehydes reported by Cheng

The authors reported an interesting proof of concept for the Grignard-type arylation of aromatic aldehydes in presence of different aryl bromides. The driving force of the reaction is the presence of a stoichiometric amount of elementary zinc, which plays several crucial roles in the reaction. Firstly, it enables the constant reduction of the nickel complex, allowing oxidative addition in the presence of aryl bromide and the formation of the organonickel nucleophilic species. In addition, the zinc(II) ions formed during the reaction are able to act as a Lewis acid towards the aldehyde, activating the carbonylic center and increasing its electrophilicity.

²⁶⁷ Swyka, R. A.; Zhang, W.; Richardson, J.; Ruble, J. C.; Krische, M. J. Rhodium-Catalyzed Aldehyde Arylation via Formate-Mediated Transfer Hydrogenation: Beyond Metallic Reductants in Grignard/Nozaki-Hiyama-Kishi-Type Addition. *J. Am. Chem. Soc.* **2019**, *141* (5), 1828–1832. <https://doi.org/10.1021/jacs.8b13652>.

²⁶⁸ Kim, I. S.; Ngai, M.-Y.; Krische, M. J. Enantioselective Iridium-Catalyzed Carbonyl Allylation from the Alcohol or Aldehyde Oxidation Level via Transfer Hydrogenative Coupling of Allyl Acetate: Departure from Chirally Modified Allyl Metal Reagents in Carbonyl Addition. *J. Am. Chem. Soc.* **2008**, *130* (44), 14891–14899. <https://doi.org/10.1021/ja805722e>.

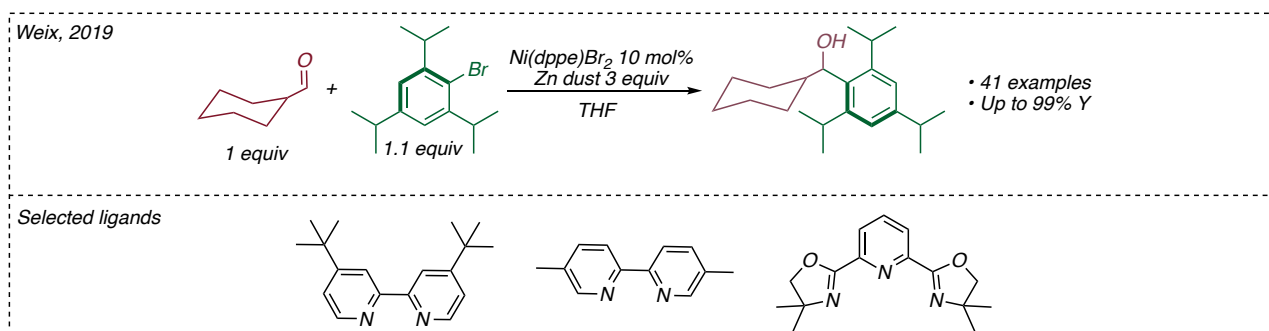
²⁶⁹ Majumdar, K. K.; Cheng, C.-H. Ni(II)/Zn-Mediated Chemoselective Arylation of Aromatic Aldehydes: Facile Synthesis of Diaryl Carbinols. *Org. Lett.* **2000**, *2* (15), 2295–2298. <https://doi.org/10.1021/ol006064w>.

The crucial role of the reducing agent was demonstrated by a series of control experiments. Remarkably, no arylation products were observed in the presence of a stoichiometric amount of $\text{Ni}(\text{COD})_2$ and dppe; but, upon addition of ZnBr_2 the arylation proceeds smoothly providing the desired carbinol. At the same time, however no arylation products were detected employing ArZnCl as preformed nucleophile neither in presence nor in absence of Ni-catalyst.

Even if the protocol exhibited a quite broad scope concerning the aryl halides explored, the reaction requires high temperature to be successful and is limited to the more reactive aromatic aldehydes.

These limitations have been overcome only in 2019 when Weix and co-workers reported a new nickel-catalyzed arylation of aldehydes.²⁷⁰

Replacing the bidentate phosphine ligands reported by Cheng with bipyridine ligands, and through a fine-tuning of the substituents on the heteroaromatic rings, the access to secondary alcohols deriving from polysubstituted aldehydes and hindered aryl bromides has been presented. Remarkably the reaction resulted suitable in the presence of hindered 2,6-disubstituted aromatic aldehydes, and 2,6-disubstituted aryl halides.



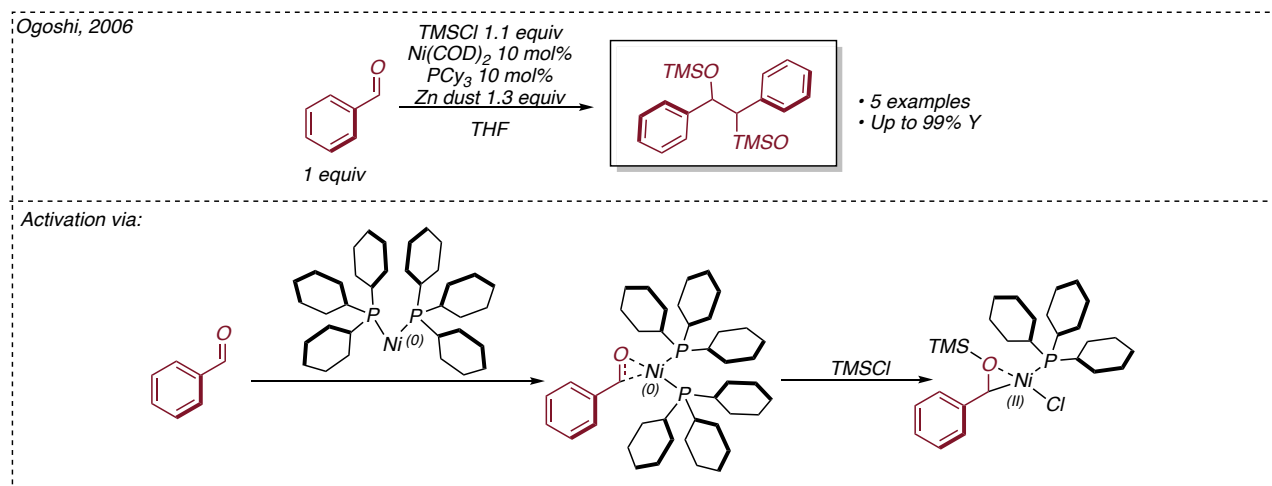
Chapter 4. Scheme 2 nickel catalyzed Arylation of hindered aldehydes reported by Weix

Representing a breakthrough for the nucleophilic organonickel chemistry, an extensive series of control experiments have been displaced, pointing out the active role of the reducing agent and its oxidized form. As in the protocol reported by Cheng, even in this case the formation of an organozinc derivative results unlikely. On the contrary, the reaction should proceed thanks to a 1,2-migratory insertion of an arylnickel in low oxidation state through the carbonyl of the aldehyde concomitantly activated by the previously generated Zn^{2+} . Although this type of activation and formation of transient organonickel nucleophiles compounds represents a reliable and tolerant protocol for the direct functionalization of carbonyls, a further improvement for the functionalization of unactivated sp^3 fragments remains unexplored. The alkylation of carbonyls by transition metal-catalyzed processes is a field of great interest, since only a few examples can be found in the literature.²⁷¹

²⁷⁰ Garcia, K. J.; Gilbert, M. M.; Weix, D. J. Nickel-Catalyzed Addition of Aryl Bromides to Aldehydes To Form Hindered Secondary Alcohols. *J. Am. Chem. Soc.* **2019**, *141* (5), 1823–1827. <https://doi.org/10.1021/jacs.8b13709>.

²⁷¹ a) Choi, H.; Nakajima, K.; Demeke, D.; Kang, F.-A.; Jun, H.-S.; Wan, Z.-K.; Kishi, Y. Asymmetric Ni(II)/Cr(II)-Mediated Coupling Reaction: Catalytic Process. *Org. Lett.* **2002**, *4* (25), 4435–4438. <https://doi.org/10.1021/ol026981x>.

A wise and clever alternative in this sense was proposed by Montgomery, reporting a formal reductive nickel-catalyzed alkylation of aliphatic aldehydes.²⁷² As originally reported by Ogoshi,²⁷³ a nickel (0) complex, in the presence of an aldehyde and tryalkylsilylhalide evolves into the corresponding α -silyloxy Ni(II) complex. This peculiar activation mode was exploited by the authors for the functionalization in umpolung fashion.

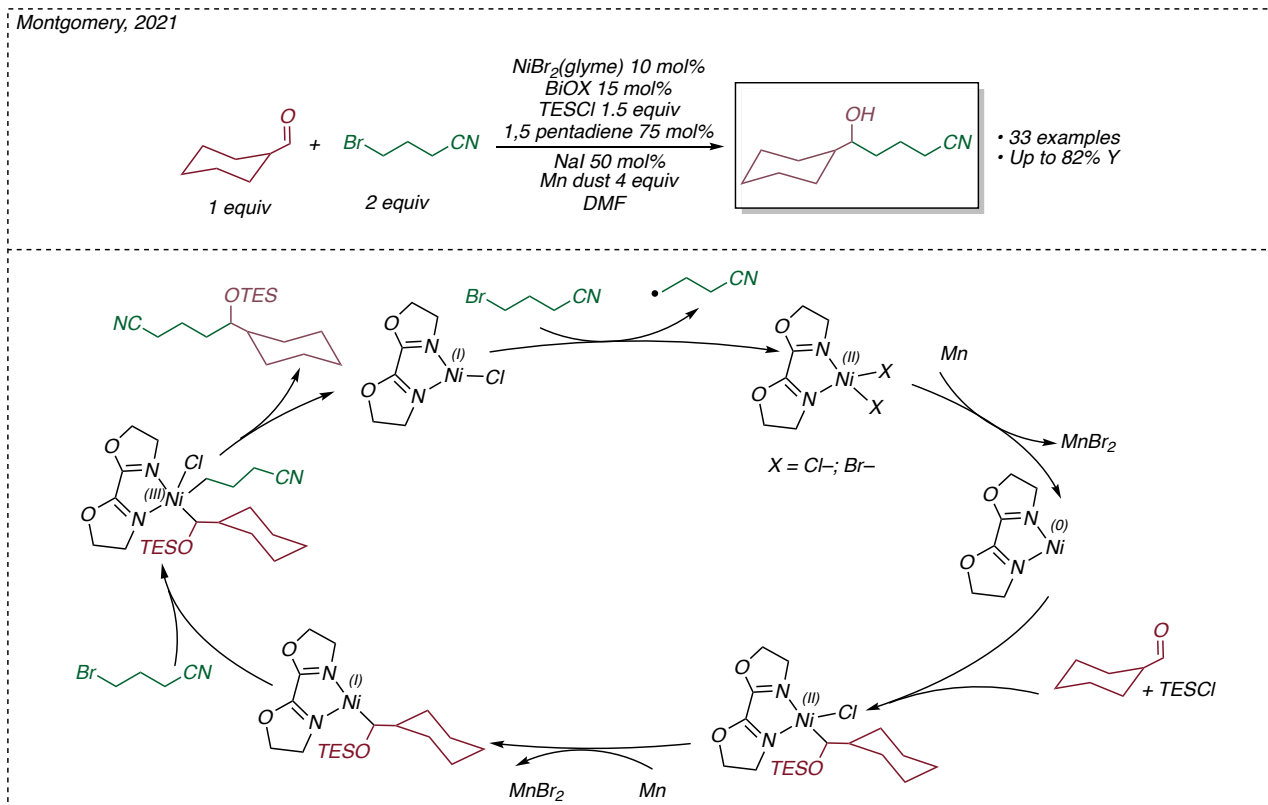


Chapter 4. Scheme 3 Activation of aromatic aldehydes in the presence of nickel in low oxidation state proposed by Ogoshi

The use of a large excess of manganese dust to ensure a reducing environment in the reaction mixture determines the reduction of the Nickel (II) complex to Nickel (0) allowing the generation of the α -silyloxy Ni(II) intermediate. The latter can in turn be reduced to form the corresponding Ni (I) complex, which undergoes through an oxidative addition in the presence of the appropriate alkyl halide. The formal alkylation product is formed after reductive elimination, restoring the nickel catalyst. The reaction shows generally high yields and a particularly wide scope both on the side of the aldehydes tested and on the side of the alkyl halides. The main limitation of the protocol is that it cannot be extended to aromatic aldehydes, since the α -silyloxy intermediate reacts rapidly, generating the pinacolization product.

²⁷² Cruz, C. L.; Montgomery, J. Nickel-Catalyzed Reductive Coupling of Unactivated Alkyl Bromides and Aliphatic Aldehydes. *Chem. Sci.* **2021**, *12* (36), 11995–12000. <https://doi.org/10.1039/D1SC03712A>.

²⁷³ Ogoshi, S.; Kamada, H.; Kurosawa, H. Reaction of (H₂-Arylaldehyde)Nickel(0) Complexes with Me₃SiX (X=OTf, Cl). Application to Catalytic Reductive Homocoupling Reaction of Arylaldehyde. *Tetrahedron* **2006**, *62* (32), 7583–7588. <https://doi.org/10.1016/j.tet.2006.03.124>.



Chapter 4. Scheme 4 Formal alkylation of aliphatic aldehydes reported by Montgomery

The utilization of aliphatic aldehydes, additionally, determines the possible formation of side reaction pathways which, to be minimized, require the presence in the reaction mixture of various (sub)stoichiometric additives which play no effective role in the formation of the product of interest.

A further alternative methodology that can be exploited for the functionalization of carbonyl compounds through the employment of nickel catalysis is the reductive cross coupling of π -systems. In fact, oligomerizations, hydrometallations and hydrocyanations of double and triple bonds represent one of the most studied fields of application of nickel catalysis.²⁷⁴ These types of transformations essentially concern the formation of a new σ -bond between two π -coupling partners in the presence of an opportune nickel complex and a stoichiometric amount of a reducing agent.

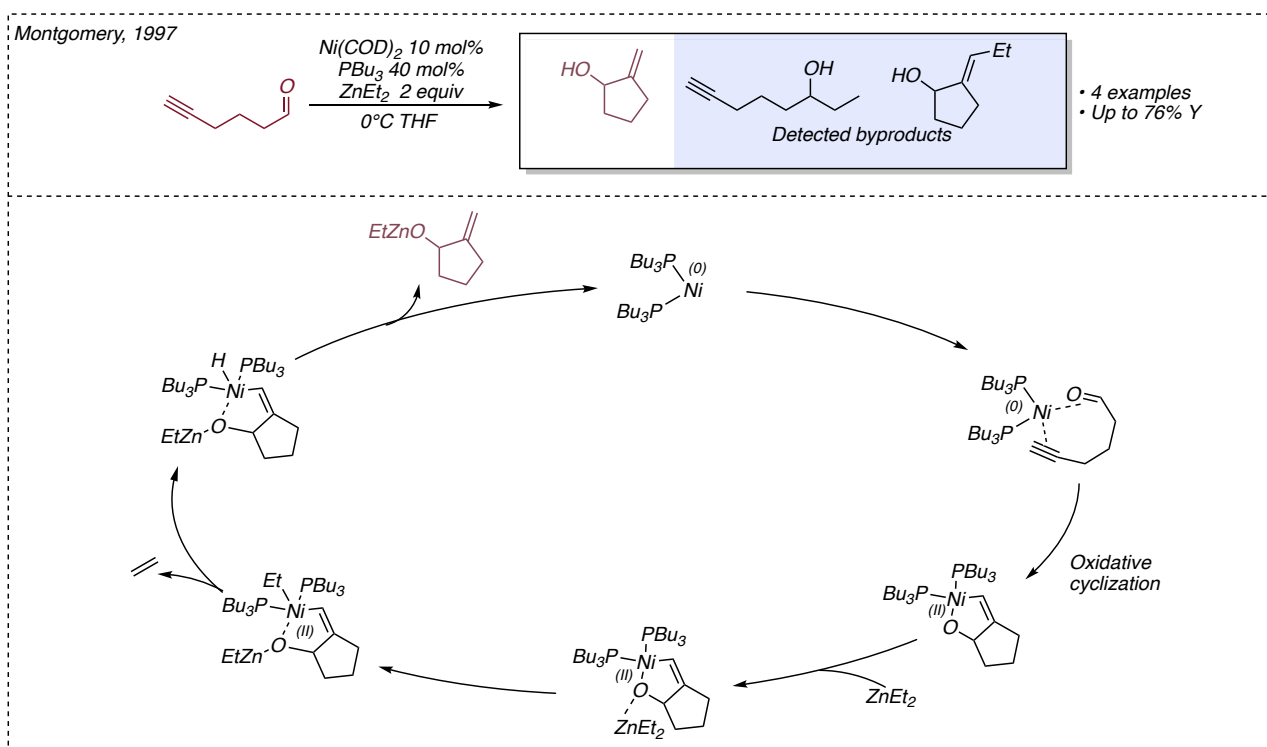
The reaction starts with a coordination of the nickel (0) complex with the two π -components of the reaction. Subsequently, the step that determines the formation of the new carbon-carbon bond involves an oxidative cyclization between these three components with the formation of a nickel(II) cycle. The so-formed intermediate evolves into the desired product after reductive elimination, by further action of the reducing agent. This type of methodology, initially implemented for the coupling of two C-C-based π -partners, has also found application for the functionalization of carbonyl compounds for the synthesis of secondary alcohols.

²⁷⁴ Montgomery, J. Nickel-Catalyzed Reductive Cyclizations and Couplings. *Angew. Chem. Int. Ed.* **2004**, 43 (30), 3890–3908. <https://doi.org/10.1002/anie.200300634>.

In this sense, the first reported protocols regarded the reductive coupling of aldehydes in presence of a suitable alkyne to allow the access to allylic alcohols.

The Montgomery group reported an intramolecular vinylation of aldehydes, employing a $\text{Ni}(\text{COD})_2/\text{PBu}_3$ catalytic system and using an overstoichiometric amount of organozinc (*e.g.*, Et_2Zn) as terminal reductant.²⁷⁵ Although the reaction is an excellent proof of concept and exhibits a good regioselectivity and a good tolerance to variously substituted alkynes and aldehydes, it is limited by the high amount of an alkylzinc reagent.

This latter, in fact, generates an unavoidable parasite reaction pathway determining the formation of undesired direct 1,2 carbonyl addition products which significantly hamper yields.



Chapter 4. Scheme 5 Intramolecular reductive coupling reported by Montgomery

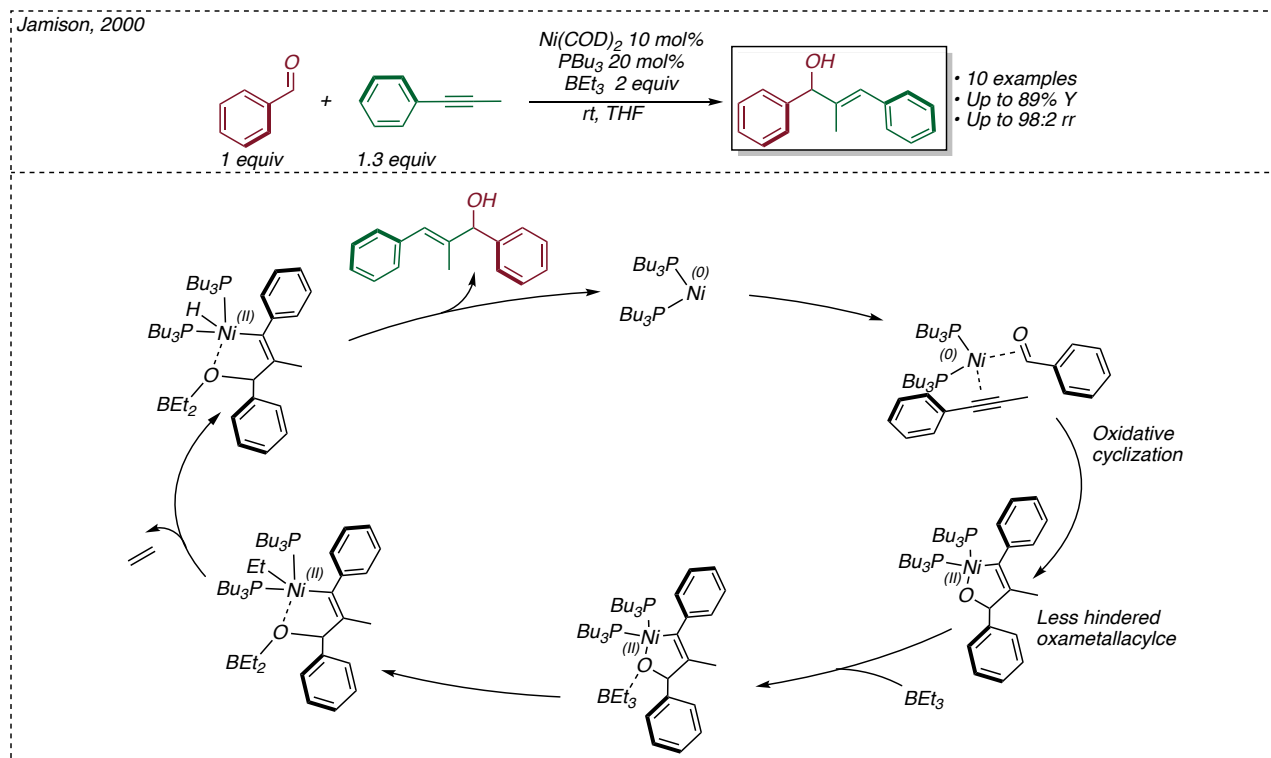
In addition, the incorporation of an ethyl-group into the desired final product was also observed with some investigated substrates. Only later the authors proposed a partial solution to these limitations by replacing organozinc with an overstoichiometric amount of the less nucleophilic triethylsilane.²⁷⁶

Although this modification dramatically decreased the formation of by-products, the access to intermolecular vinylation was prevented.

²⁷⁵ Oblinger, E.; Montgomery, J. A New Stereoselective Method for the Preparation of Allylic Alcohols. *J. Am. Chem. Soc.* **1997**, *119* (38), 9065–9066. <https://doi.org/10.1021/ja9719182>.

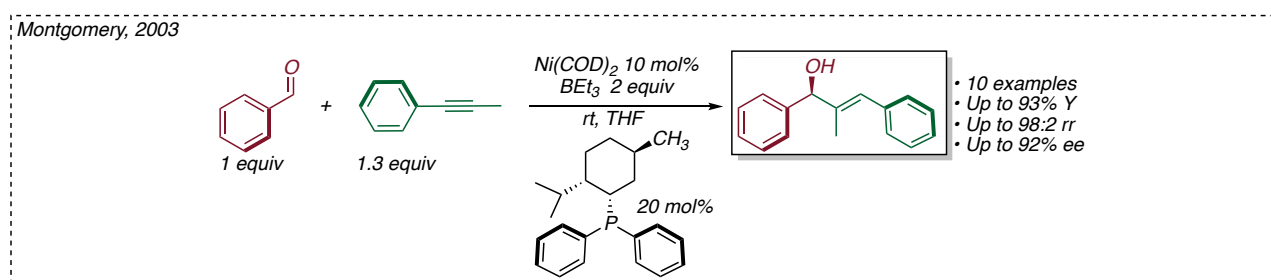
²⁷⁶ a) Tang, X.-Q.; Montgomery, J. Nickel Catalysis in the Stereoselective Preparation of Quinolizidine, Pyrrolizidine, and Indolizidine Alkaloids: Total Synthesis of (+)-Allopumiliotoxin 267A. *J. Am. Chem. Soc.* **1999**, *121* (25), 6098–6099. <https://doi.org/10.1021/ja990997+> b) Tang, X.-Q.; Montgomery, J. Nickel-Catalyzed Preparation of Bicyclic Heterocycles: Total Synthesis of (+)-Allopumiliotoxin 267A, (+)-Allopumiliotoxin 339A, and (+)-Allopumiliotoxin 339B. *J. Am. Chem. Soc.* **2000**, *122* (29), 6950–6954. <https://doi.org/10.1021/ja001440t>.

In this regard, the cornerstone work was published by Jamison and co-workers.²⁷⁷ Retaining basically the reaction conditions developed by Montgomery for the intramolecular process but using a different reducing agent (triethyl silane was replaced by BEt_3) a wide library of intermolecular reductive coupling products was developed with a particularly high regioselectivity.



Chapter 4. Scheme 6 Intermolecular reductive coupling of aldehydes and alkynes reported by Jamison

This presented protocol paved the way to the development of an enantioselective variants of the process maintaining very high regioselectivity and with enantiomeric excesses of up to 90%. The main aspect of the process is the use of a menthyl-based monodentate phosphine.²⁷⁸



Chapter 4. Scheme 7 Enantioselective reductive coupling of aldehydes and alkynes reported by Montgomery

²⁷⁷ Huang, W.-S.; Chan, J.; Jamison, T. F. Highly Selective Catalytic Intermolecular Reductive Coupling of Alkynes and Aldehydes. *Org. Lett.* **2000**, 2 (26), 4221–4223. <https://doi.org/10.1021/ol006781q>.

²⁷⁸ Miller, K. M.; Huang, W.-S.; Jamison, T. F. Catalytic Asymmetric Reductive Coupling of Alkynes and Aldehydes: Enantioselective Synthesis of Allylic Alcohols and α -Hydroxy Ketones. *J. Am. Chem. Soc.* **2003**, 125 (12), 3442–3443. <https://doi.org/10.1021/ja034366y>.

• Nickel-promoted allylation of aldehydes

The above-mentioned activation models allowing the access to transient nucleophilic organonickel species can also be found in literature for the design of allylation reactions.

The most known use of nickel catalysis in these transformations is related to the Nozaki-Hiyama reaction.²⁷⁹

In 1986 Kishi and co-workers reported that traces of nickel in the presence of an overstoichiometric amount of CrCl₂ were responsible for an increased ability of the salt to reduce vinyl and allyl halides better promoting the Nozaki-Hiyama reaction.²⁸⁰

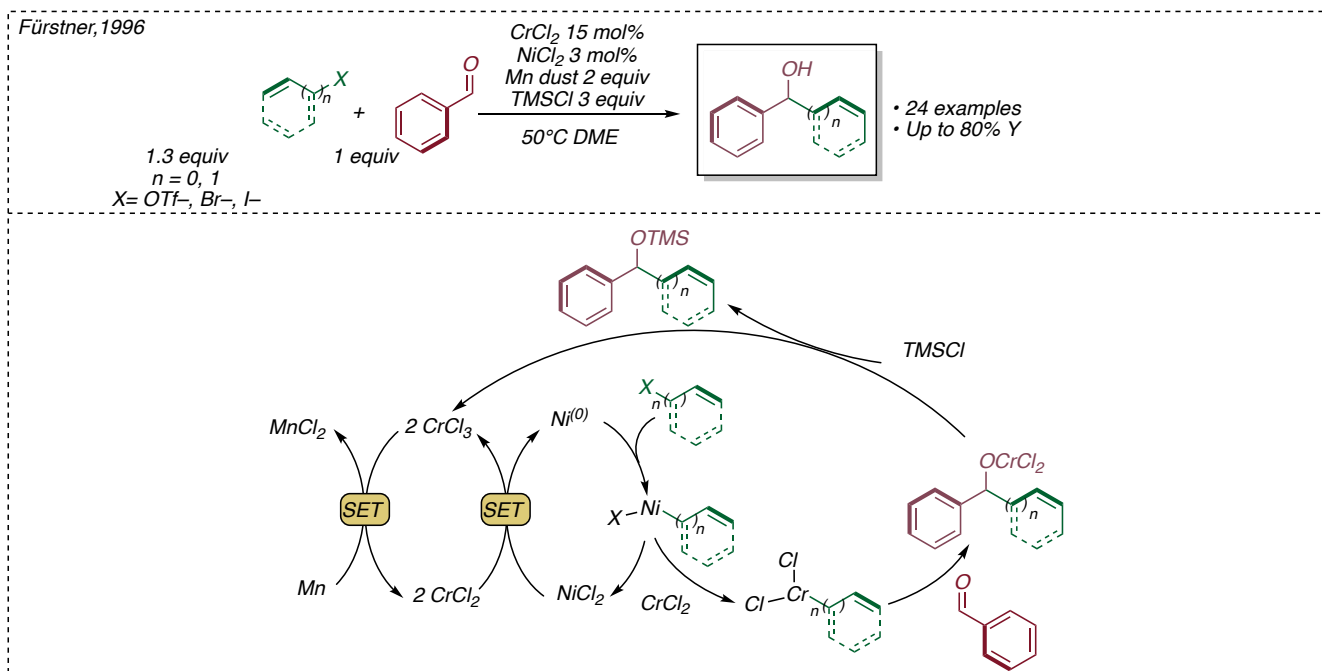
The reaction – later addressed as Nozaki-Hiyama-Kishi reaction– was developed, showing extraordinary tolerance for different functional groups and very high selectivity towards carbonyl groups of aldehydes. Another fundamental step forward in the development of this methodology was taken by Fürstner and co-workers in 1996. By using stoichiometric amounts of manganese dust, it was possible to decrease the amount of chromium to a catalytic fashion.²⁸¹ According to the mechanism proposed by the authors, the manganese dust is only able to reduce the chromium (III) salt leading to the formation of a catalytic amount of chromium (II). Two molecules of this intermediate are responsible for the reduction of Ni(II) to Ni(0). The low oxidation state nickel species is, then, involved into oxidative addition with the allyl or vinyl (pseudo)halide and then into transmetalation with the chromium (III) salt forming the nucleophilic organochromium reagent. The alkoxy-chromium species formed upon nucleophilic addition onto the carbonyl of the aldehyde evolves into the desired product, restoring the chromium (III) thanks to the presence of the stoichiometric TMSCl as additive. To shed even more light on the mechanism, a recent collaboration between Baran, Beckman and Doyle on an electrocatalytic version of the NHK reaction has further clarified the synergistic role of both metal species required to promote the reaction.²⁸²

²⁷⁹ Okude, Y.; Hirano, S.; Hiyama, T.; Nozaki, H. Grignard-Type Carbonyl Addition of Allyl Halides by Means of Chromous Salt. A Chemospecific Synthesis of Homoallyl Alcohols. *J. Am. Chem. Soc.* **1977**, *99* (9), 3179–3181. <https://doi.org/10.1021/ja00451a061>.

²⁸⁰ Takai, K.; Tagashira, M.; Kuroda, T.; Oshima, K.; Utimoto, K.; Nozaki, H. Reactions of Alkenylchromium Reagents Prepared from Alkenyl Trifluoromethanesulfonates (Triflates) with Chromium(II) Chloride under Nickel Catalysis. *J. Am. Chem. Soc.* **1986**, *108*, 19, 6048–6050 <https://doi.org/10.1021/ja00279a068>

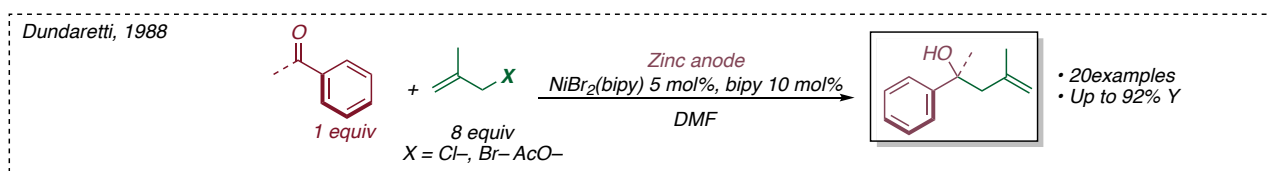
²⁸¹ Fürstner, A.; Shi, N. Nozaki-Hiyama-Kishi Reactions Catalytic in Chromium. *J. Am. Chem. Soc.* **1996**, *118* (49), 12349–12357. <https://doi.org/10.1021/ja9625236>.

²⁸² Gao, Y.; Hill, D. E.; Hao, W.; McNicholas, B. J.; Vantourout, J. C.; Hadt, R. G.; Reisman, S. E.; Blackmond, D. G.; Baran, P. S. Electrochemical Nozaki-Hiyama-Kishi Coupling: Scope, Applications, and Mechanism. *J. Am. Chem. Soc.* **2021**, *143* (25), 9478–9488. <https://doi.org/10.1021/jacs.1c03007>.



Chapter 4. Scheme 8 Nozaki-Hiyama-Kishi reaction catalytic in chromium developed by Fürstner.

Not only in combination with other metal species, but also independently, nickel catalysis has been shown to promote carbonyl allylation protocols. In 1989, Perichon and Dundaretti reported a new electrochemical-based strategy for nickel-catalyzed addition of the allyl moiety to both aromatic and aliphatic ketones and aldehydes.²⁸³ Zinc anode was found to be the best electron source promoting the formation of transient $Ni(0)$ species. According to the authors, this latter is able to generate π -allylnickel complexes in the presence of both an allyl halides and, surprisingly, allyl acetate with good tolerance and yields.



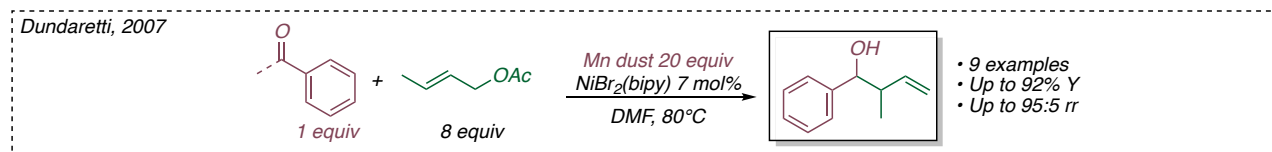
Chapter 4. Scheme 9 Nickel-mediated electrocatalytic allylation of aldehydes and ketones reported by Dundaretti

About 20 years after the first report, the same authors proposed a similar reaction using an excess of manganese dust instead of an electrocatalytic system to promote reduction.²⁸⁴ Remarkably, the method was suitable for addition of several substituted allyl acetates towards aldehydes. When crotyl acetates were employed as pronucleophilic allylic source, the major isomer observed was always the branched

²⁸³ Durandetti, S.; Sibille, S.; PBrichon, J. Electrochemical Allylation of Carbonyl Compounds Using Nickel Catalyst and Zinc(II) Species. *J. Org. Chem.* **1989**, *54*, 9, 2198–2204 <https://doi.org/10.1021/jo00270a033>

²⁸⁴ Durandetti, M.; Gosmini, C.; Périchon, J. Ni-Catalyzed Activation of α -Chloroesters: A Simple Method for the Synthesis of α -Arylesters and β -Hydroxyesters. *Tetrahedron* **2007**, *63* (5), 1146–1153. <https://doi.org/10.1016/j.tet.2006.11.055>.

product.



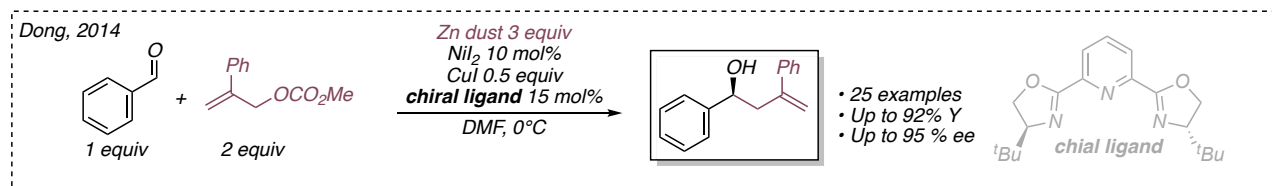
Chapter 4. Scheme 10 Nickel-catalyzed allylation of carbonyl compounds reported by Dundaretti.

The regioselective outcome is a result of the nucleophilic addition from the γ -position of η^3 -allylnickel complex. The regioselective outcome in this kind of transformation is strictly dependent on the nature of the organometallic reagent and with nickel the allylic transposition and the consequent formation of branched products is a common observed behavior.

The reductive generation of a Grignard-type organonickel species was also reported in an enantioselective fashion by Dong and co-workers in 2014.²⁸⁵

The work reported the enantioselective activation of allyl carbonates triggered by a PyBOX nickel complex formed in situ, leading to a wide variety of enantioenriched homoallylic alcohols with enantiomeric excesses up to 90% in the presence of both aromatic and aliphatic aldehydes

Thanks to the large access of zinc acting as reducing agent in the reaction mixture, a positive outcome was observed using both air-sensitive Ni(COD)₂ and bench-stable NiI₂.



Chapter 4. Scheme 11 Enantioselective nickel-catalyzed allylation of carbonyl compounds reported by Dundaretti.

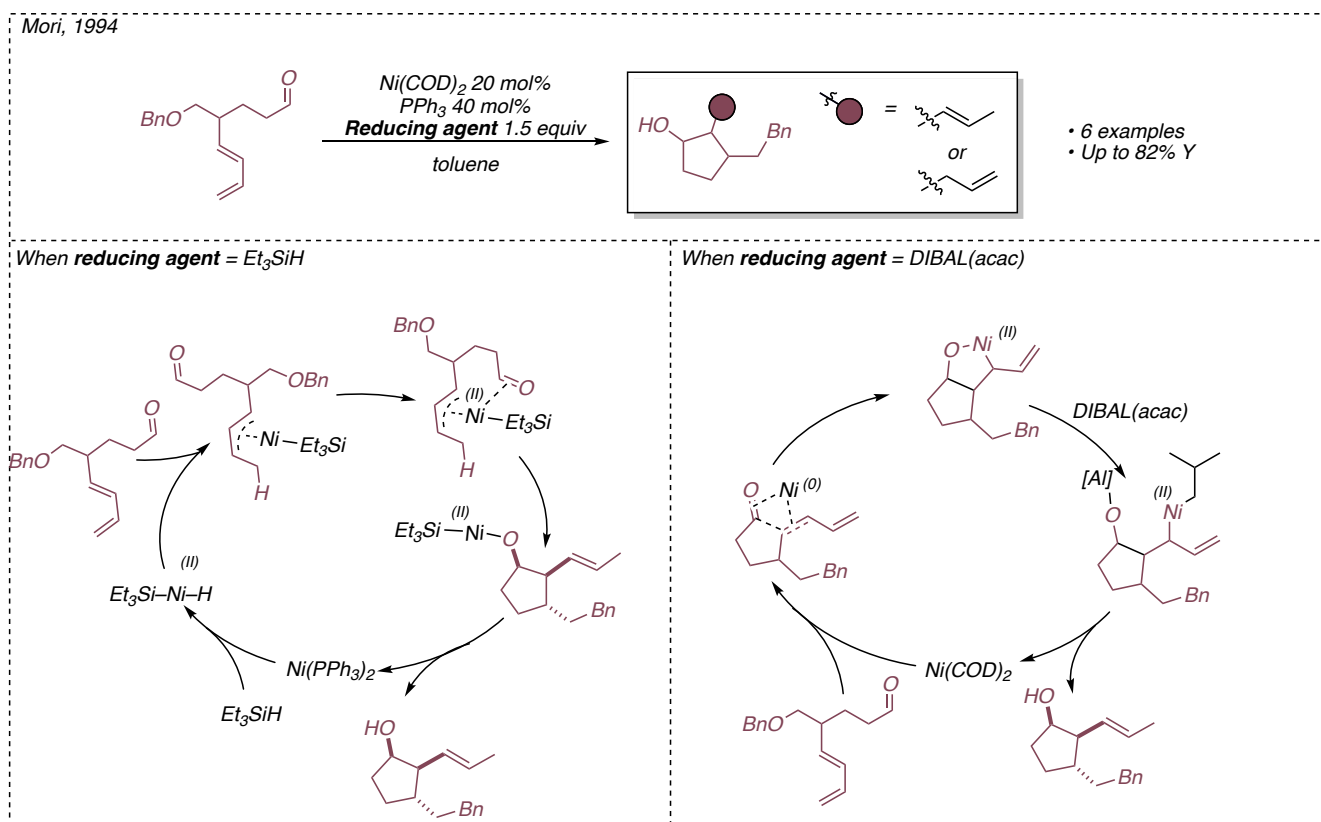
Effective allylation protocols has also been achieved through the exploitation of nickel-catalyzed reductive coupling of π -components. Indeed, in analogy to what was introduced for the case of vinylation reactions obtainable in the presence of alkynes, the reductive coupling of aldehydes with 1,3-dienes has been largely developed.

The first contribution in this respect was reported by Mori and co-workers in an intramolecular fashion.²⁸⁶ Notably, by fine-tuning the reaction conditions, it was possible to rationalize and predict the regiochemical outcome of the reaction discriminating selectively the synthesis of the corresponding homoallyl or bis-homoallyl alcohols.

²⁸⁵ Tan, Z.; Wan, X.; Zang, Z.; Qian, Q.; Deng, W.; Gong, H. Ni-Catalyzed Asymmetric Reductive Allylation of Aldehydes with Allylic Carbonates. *Chem. Commun.* **2014**, 50 (29), 3827–3830. <https://doi.org/10.1039/C3CC49859J>.

²⁸⁶ a) Sato, Y.; Takimoto, M.; Mori, M. Further Studies on Nickel-Promoted or -Catalyzed Cyclization of 1,3-Diene and a Tethered Carbonyl Group. *J. Am. Chem. Soc.* **2000**, 122 (8), 1624–1634. <https://doi.org/10.1021/ja991241d>. b) Sato, Y.; Takimoto, M.; Hayashi, K.; Katsuhara, T.; Takagi, K.; Mori, M. Novel Stereoselective Cyclization via π -Allylnickel Complex Generated from 1,3-Diene and Hydride Nickel Complex. *J. Am. Chem. Soc.* **1994**, 116 (21), 9771–9772. <https://doi.org/10.1021/ja00100a061>.

As proposed by the authors, the nature of the stoichiometric reductant used to promote the reaction and restore the nickel catalyst can also determine whether the evolution of the reaction will lead to either the terminal or the internal alkene. Indeed, the use of DIBAL(acac) as a reducing agent gave bis-homoallyl alcohol as the only reaction outcome, whereas if a stoichiometric amount of trialkylsilane was used it was possible to reverse the regioselectivity and obtain the formal allylation product. To justify the experimental results, the authors proposed two different mechanisms depending on the reducing agent used. In the case of DIBAL(acac), the reaction proceeds analogously to the protocol employed in the presence of alkynes.



Chapter 4. Scheme 12 Reductive cross-coupling nickel-catalyzed regiodivergent allylation and homoallylation of aldehydes reported by Mori

The first step after the coordination by nickel in the low oxidation state is the oxidative cyclization, then DIBAL acts as an indirect reductant through transmetalation and subsequent β -hydride elimination.

The scenario changes when the reductant does not have any β -hydrogen to allow the conventional reaction pathway to take place. In this case, indeed, trialkyl silane is thought to be responsible for the initial formation of a nickel hydride species which can perform an hydrometallation onto a double bond, generating an η^3 -allylnickel intermediate that can act as a nucleophile.

Likewise, the intermolecular variant of this protocol was developed by Kimura and co-workers.²⁸⁷ Even in this case, the presence of stoichiometric organometallic reducing agents with or without β -hydrogens proved decisive in predicting the selectivity of the process.

²⁸⁷ a) Kimura, M.; Ezo, A.; Shibata, K.; Tamaru, Y. Novel and Highly Regio- and Stereoselective Nickel-Catalyzed Homoallylation of Benzaldehyde with 1,3-Dienes. *J. Am. Chem. Soc.* **1998**, *120* (16), 4033–4034. <https://doi.org/10.1021/ja973847c>. b) Kimura, M.; Fujimatsu, H.; Ezo, A.; Shibata, K.; Shimizu, M.; Matsumoto, S.; Tamaru, Y. Nickel-Catalyzed Homoallylation of Aldehydes and Ketones with 1,3-Dienes and Complementary Promotion by Diethylzinc or Triethylborane. *Angew. Chem. Int. Ed.* **1999**, *38* (3), 397–400. [https://doi.org/10.1002/\(SICI\)1521-3773\(19990201\)38:3<397::AID-ANIE397>3.0.CO;2-Y](https://doi.org/10.1002/(SICI)1521-3773(19990201)38:3<397::AID-ANIE397>3.0.CO;2-Y).

4.1 Photoredox Allylation of Aldehydes Catalytic in Nickel²⁸⁸

• Presented work

As described in the previous chapters, the combination of photoredox conditions and nickel catalysis has been shown to be a perfect match for the realization of exciting transformations. We decided to extend the range of allowed possibilities to the functionalization of carbonyl compounds.

Again, the decision to develop a protocol that would allow the use of nickel catalysis under photoredox and/or radical polar cross over conditions is meant to propose a partial solution to the limits characterizing nonvisible light-driven analogous methodologies.

Since photoredox catalysis allows both net-reductive and net-oxidative transformations under extremely mild reaction conditions, a dual photoredox nickel-catalyzed allylation of aldehydes would allow access to homoallylic alcohols without the need for either metal additives, harsh conditions, or air-sensitive catalysts.

Consequently, this protocol would extend the range of compatible substrates and would increase the survey of functional groups that can be tolerated during the process.

Furthermore, the photocatalytic generation of a transient allylnickel nucleophiles would also represent a further improvement on the dual photoredox and chromium catalyzed allylation protocols (*presented in the Introduction*).

The combination of photoredox reduction of a nickel species with the ability of the metal to perform oxidative addition in the presence of the appropriate allyl pronucleophile opens the possibility to transient nucleophilic organonickel species from unsubstituted allyl sources.

On the contrary, in dual chromium photocatalytic methods, the transient nucleophilic Cr(III)allyl reagent derives from the formation of an allyl radical by oxidation of the corresponding alkene and subsequent interception by the catalytic Cr(II)Cl₂. Both because of the difficulties associated with its use and the high electrochemical potentials related, these processes cannot be extended to the simple propene. The approach for the realization of this project was firstly to develop a methodology to obtain allylation products with satisfactory results using a racemic ligand for the nickel complex. Once we obtained the best conditions and investigated the level of applicability

²⁸⁸ The results and the procedures described in this section are part of a published work:

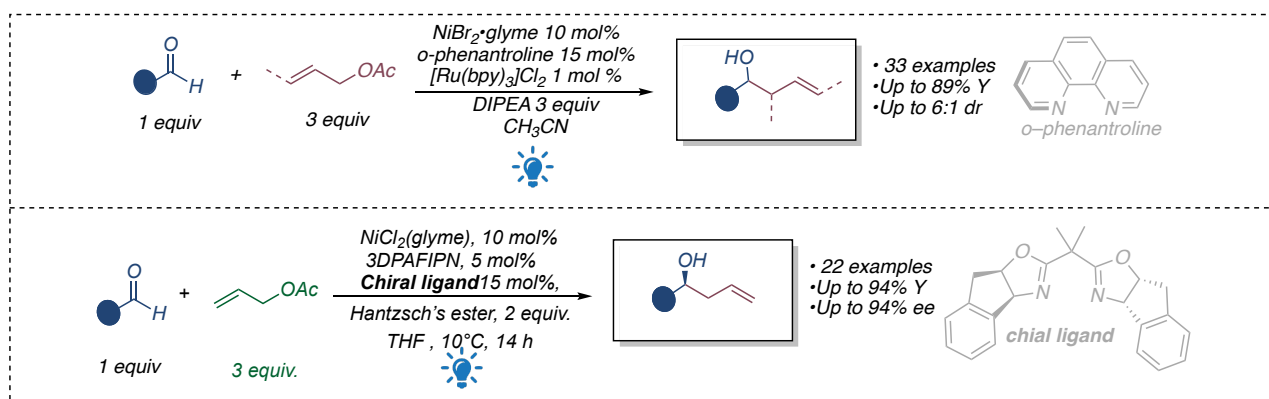
Gualandi, A.; Rodeghiero, G.; Faraone, A.; Patuzzo, F.; Marchini, M.; Calogero, F.; Perciaccante, R.; Jansen, T. P.; Ceroni, P.; Cozzi, P. G. Allylation of Aldehydes by Dual Photoredox and Nickel Catalysis. *Chem. Commun.* **2019**, 55 (48), 6838–6841. <https://doi.org/10.1039/C9CC03344K>.

M. M. carried out the photophysical investigations, supervised by P.C.

The complete characterization of the products introduced hereafter and discussed in the section “Supplementary Data” can be found in the Supporting Information of the above-mentioned work

of the methodology by probing differently functionalized aldehydes both aromatic and aliphatic, we decided to investigate a possible enantioselective variant– *which is described in detail in the chapter 4.2* –.

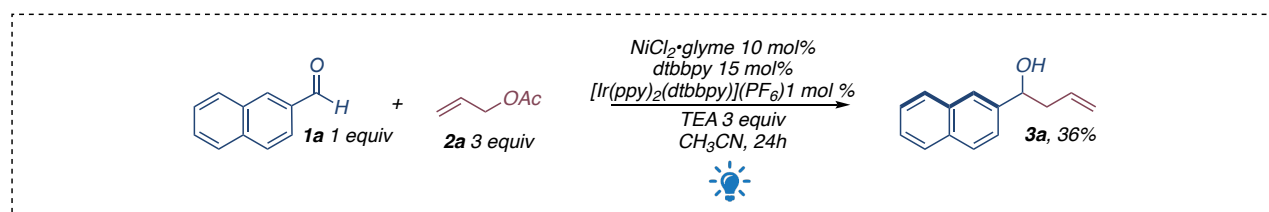
The following sections will be devoted, first to the description of the non-stereoselective process: the optimization of the reaction conditions, the survey of compatible substrates and both photophysical and electrochemical studies will be exploited. Then, the route that led to the achievement of a dual photoredox/Ni catalyzed allylation protocol of both aromatic and aliphatic aldehydes with high yields, high tolerability to different functional groups and enantiomeric excess up to 94% will be discussed.



• Optimization of the reaction conditions

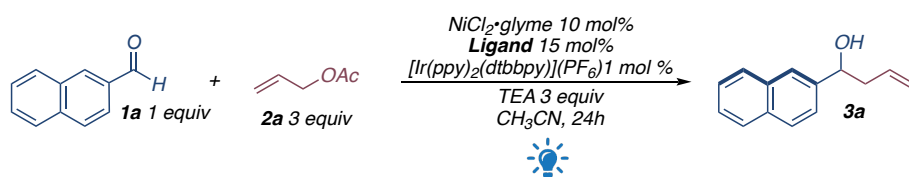
The investigation for the best reaction conditions began by employing 2-naphthaldehyde (**1a**) as model substrate. Using as reference point the nucleophilic properties of organonickel compounds disclosed in analogous non-visible light-driven processes, the evaluation of the reaction parameters involved: (i) the best nickel precatalyst and ligand combination to promote the process; (ii) the photocatalyst that was most efficient in allowing a continuous reduction of the nickel complex; (iii) the best sacrificial agent that would also bypass the use of an external scavenger; (iv) the allyl source that could be involved in oxidative addition processes generating the desired organometallic species.

As a starting point for the optimization, we began introducing a photoredox system by replacing the metal reductant under the best reaction conditions reported for the non-visible light-driven protocols.²⁸⁴ The firstly chosen reaction conditions were: $[\text{NiCl}_2(\text{glyme})]$ (10 mol%), allylacetate **2a** (3 equiv.), triethylamine (TEA, 3 equiv.), $[\text{Ir}(\text{ppy})_2(\text{dtbbpy})]\text{PF}_6$, (1 mol%), 4,4'-di-tert-butyl-2,2'-dipyridyl (dtbbpy, 15 mol%) as ligand for nickel(II), under blue LEDs irradiation at 450 nm in acetonitrile.



Chapter 4. Scheme 13 Preliminary results

We were pleased to observe that this initial reaction set-up enabled the formation of the desired product with encouraging preliminary results. To improve the reaction outcome, we started by comparing different ligands that are commonly known for nickel-mediated transformation. The main results of this screening are shown in **Table 4.1.1**.

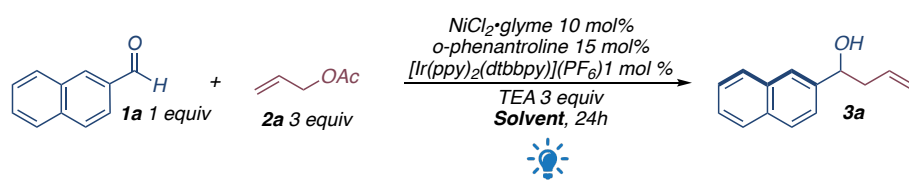


Entry ^[a]	Ligand	Yield ^[b]
1	terpyridine	17
2	dppe	22
3	<i>o</i> -phenanthroline	48
4	dtbbpy	36
5	neocuproine	20
6	pyridine ^[c]	0
7	4,7-diphenyl-1,10-phenanthroline	37
8	5,6-dimethyl-1,10-phenanthroline	36
9	4,4'-dimethoxy-2,2'-bipyridine	35
10	No ligand	21

Table 4.1.1 Screening of photocatalysts.

[a] Reaction conditions reported in the above figure on 0.1 mmol scale. [b] Determined by ¹H-NMR analysis. [c] 30 mol%

Interestingly, it was noted that the reaction can partially work even in the absence of ligand, while the best results were obtained using nitrogen-bidentate ligands (with *o*-phenanthroline giving the best results). On the other hand, poor results were obtained using phosphorus-based ligands. Probably in this case the photocatalyst used can oxidize the ligand by a single electron transfer, leading to its consequent deactivation. Therefore, while continuing to use *o*-phenanthroline as ligand, we tested different solvents to see which would give the best results.



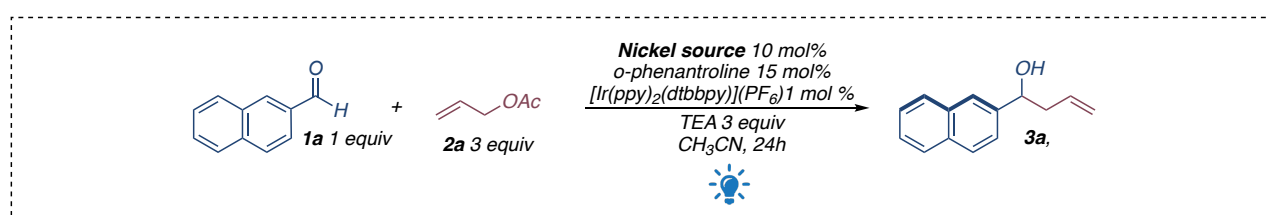
Entry ^[a]	Solvent	Yield ^[b]
1	DMF	46
2	CH_3CN	48
3	DCE	29
4	THF	39
5	DMSO	35
6	DME	27
7	MeOH	14
8	Dioxane	25
9	DMF/ H_2O 9/1	46

Table 4.1.2 Screening of the reaction solvent.

[a] Reaction conditions reported in the above figure on 0.1 mmol scale. [b] Determined by ¹H-NMR analysis.

We were pleased to note that the protocol was compatible with several of the most common organic solvents. In analogy to Perichón, Dundaretti and Dong, good results were obtained using DFM; however, a slight improvement in yield was observed in the presence of acetonitrile. This screening also made it possible to appreciate that the dual Ni/photoredox protocol was compatible in an aqueous environment.

At this point we evaluated which was the best nickel precatalyst for the reaction. While simple Nickel(II) halides gave unsatisfactory results due to their reduced solubility in organic solvents, Nickel(II) halides complexes surrounded by glyme ligand gave the highest conversions towards the desired product. Due to its increased reactivity [NiBr₂(glyme)] led to the highest conversion of the starting material into the desired product

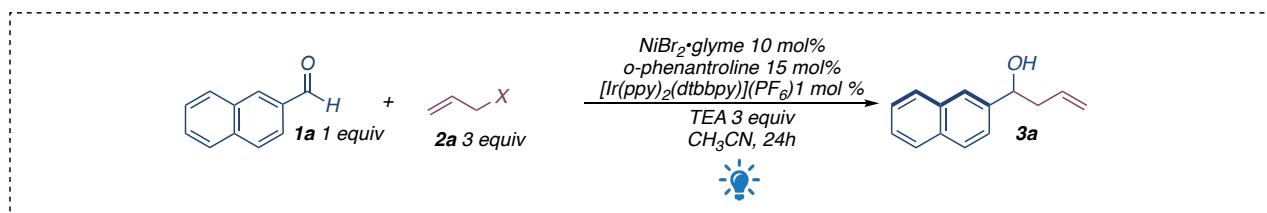


Entry ^[a]	Nickel source	Yield ^[b]
1	[NiCl ₂ (glyme)]	48
2	Ni(ClO ₄) ₂	32
3	NiBr ₂	36
4	NiI ₂	47
5	Ni(COD) ₂	35
6	[Ni(<i>o</i> -phenanthroline) ₃](BF ₄) ₂ ^[c]	45
7	Ni(acac) ₂	35
8	[NiBr ₂ (glyme)]	56

Table 4.1.3 Screening of nickel source.

[a] Reaction conditions reported in the above figure on 0.1 mmol scale. [b] Determined by ¹H-NMR analysis. [c] reaction performed in absence of external *o*-phenanthroline.

At this point we evaluated which was the best allyl source. As shown in the table, the protocol is consistent with previous non-light driven reports. Allyl halides are not compatible substrates with the formation of transient nucleophilic organonickel species, while allyl ethers, acetates and carbonates determine a positive outcome of the reaction.



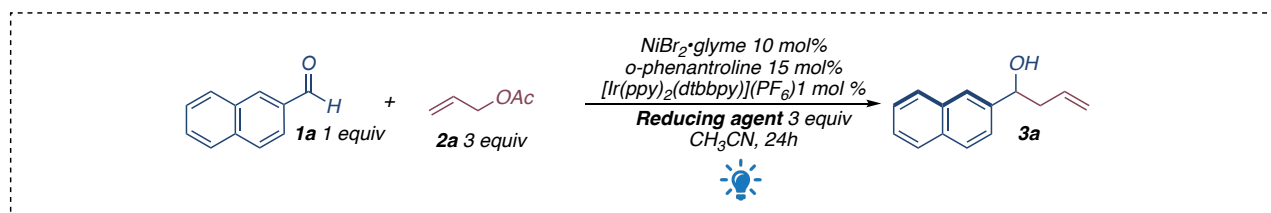
Entry ^[a]	X	Yield ^[b]
1	OAc	48
2	Cl	0
3	Br	5
4	I	0
5	OC(O) <i>O</i> <i>t</i> Bu	40
6	OC(O) <i>t</i> Bu	42
7	OH	8
8	OPh	11

Table 4.1.4 Screening of allyl source.

[a] Reaction conditions reported in the above figure on 0.1 mmol scale. [b] Determined by $^1\text{H-NMR}$ analysis.

Although the results of these initial evaluations started to be satisfactory, we wanted to investigate whether other amines were able to act as sacrificial reductants improving the reaction outcome.

Despite its higher reduction potential, an effective increase in yield has been found employing DIPEA in the reaction mixture, (0.86 V for DIPEA vs. 0.69 V for TEA vs SCE). On the other hand, product formation was not observed when triphenylamine was evaluated as reducing agent. This outcome can be interpreted in two respects. First of all, the potential associated to this molecule is higher (0.98 V vs SCE), so even if possible, its oxidation is energetically more disadvantageous. In addition, unlike the other amines used to promote this kind of reactions, the oxidative pathway of TPA do not lead to a proton release. In this case, thus, the double role played by the sacrificial agent in all the above reported protocols lacks. The desired transformation can occur, but the scavenger action is lost determining a deactivation of the catalytic system.

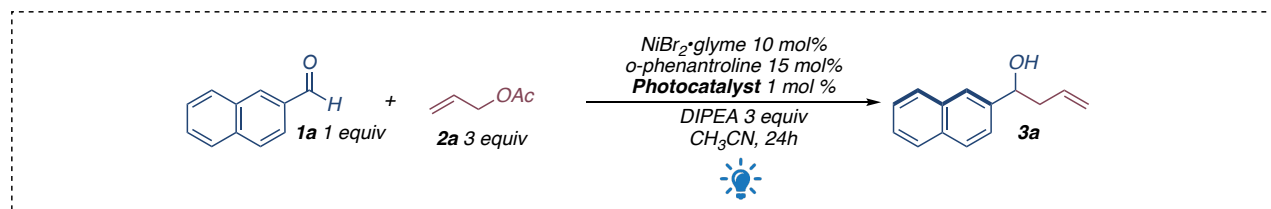


Entry ^[a]	Reducing agent	Yield ^[b]
1	-	0
2	TEA	56
3	Ph ₃ N	0
4	DIPEA	65
5	DIPEA ^[c]	60
6	DIPEA ^[d]	35

Table 4.1.5 Screening of reducing agent.

[a] Reaction conditions reported in the above figure on 0.1 mmol scale. [b] Determined by ¹H-NMR analysis. [c] 4 equiv. of DIPEA were used. [d] 2 equiv of DIPEA were used.

Making appropriate modifications, we considered different photosensitizers to promote transformation. Although the [Ru(bpy)₃]Cl₂ complex in its excited state is a worse reductant than the previously employed [Ir(ppy)₂(dtbbpy)]PF₆, its employment brought the best results. This allowed us to optimize the process by using a cheaper and whose synthesis was more easily feasible photocatalyst.

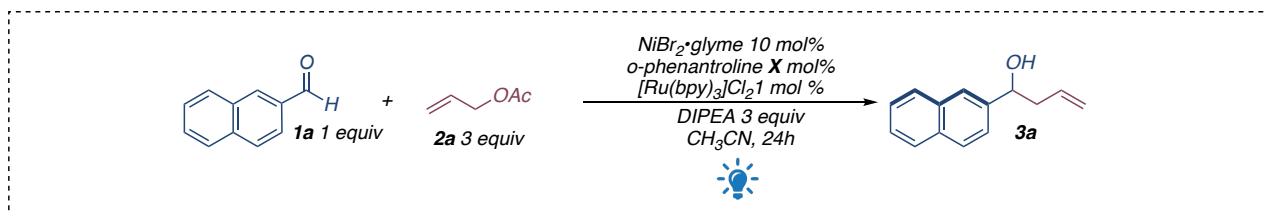


Entry ^[a]	Photocatalyst	Yield ^[b]
1	-	0
2	[Ir(ppy) ₂ (dtbbpy)]PF ₆	65
3	(Ir[dF(CF ₃)ppy] ₂ (dtbbpy))PF ₆	31
4	Cu(dap) ₂ Cl	0
5	[Ru(bpy) ₃]Cl ₂	68

Table 4.1.6 Screening of reducing agent.

[a] Reaction conditions reported in the above figure on 0.1 mmol scale. [b] Determined by ¹H-NMR analysis.

In conclusion, the evaluations about the most appropriate ligand:nickel ratio and about the minimum catalytic loading for the reaction were carried out.

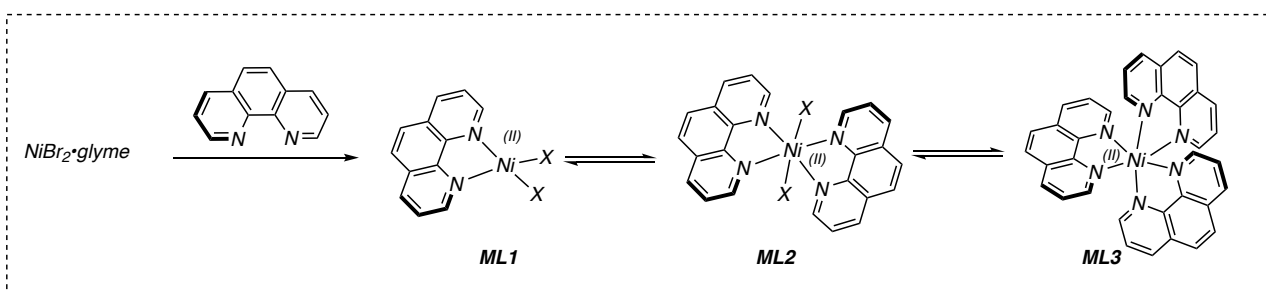


Entry ^[a]	mol% <i>o</i> -phenanthroline	Yield ^[b]
1	15	68
2	30	51
3	60	42
4	1.5 ^[c]	47

Table 4.1.7 Screening of nickel to ligand ratio.

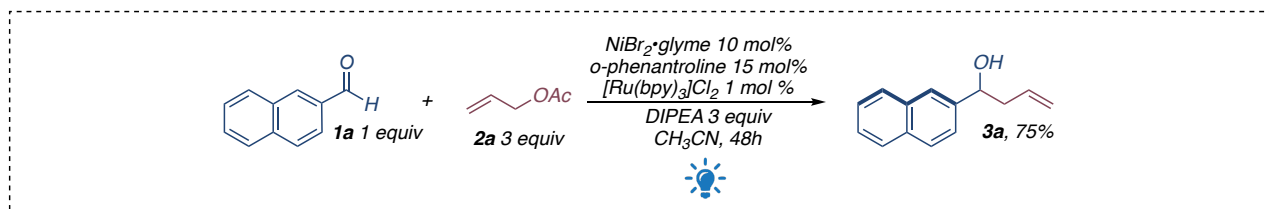
[a] Reaction conditions reported in the above figure on 0.1 mmol scale. [b] Determined by $^1\text{H-NMR}$ analysis. [c] 1 mol% of $[\text{NiBr}_2(\text{glyme})]$ employed.

It was possible to notice that the yield of the reaction decreased increasing the amount of ligand surrounding the metal center. This trend can be explained because more than one ligand can coordinate the nickel center. An unbalanced ratio between the two reaction partners probably results in the prevalent formation of an ML_3 species (**Scheme 14**). This species, lacking free coordination sites to promote oxidative addition, is unable for the desired process. Keeping the optimal ratio unchanged, we have noticed that the reaction is able to operate even with a drastic reduction in catalytic loading, but the system's turnover is not efficient enough to provide satisfactory yields.



Chapter 4. **Scheme 14** Possible Nickel complexes formed during the reaction

After the systematic evaluation of all reaction parameters, we were able to disclose the optimized conditions, obtaining **3a** in 75% isolated yield after 48 h of irradiation: [NiBr₂(glyme)] (10 mol%), allylacetate **2a** (3 equiv.), diisopropylethylamine (DIPEA, 3 equiv.), [Ru(bpy)₃]Cl₂ photocatalyst (1 mol%), *o*-phenanthroline (15 mol%) as ligand for nickel(II), under blue LEDs irradiation at 450 nm.



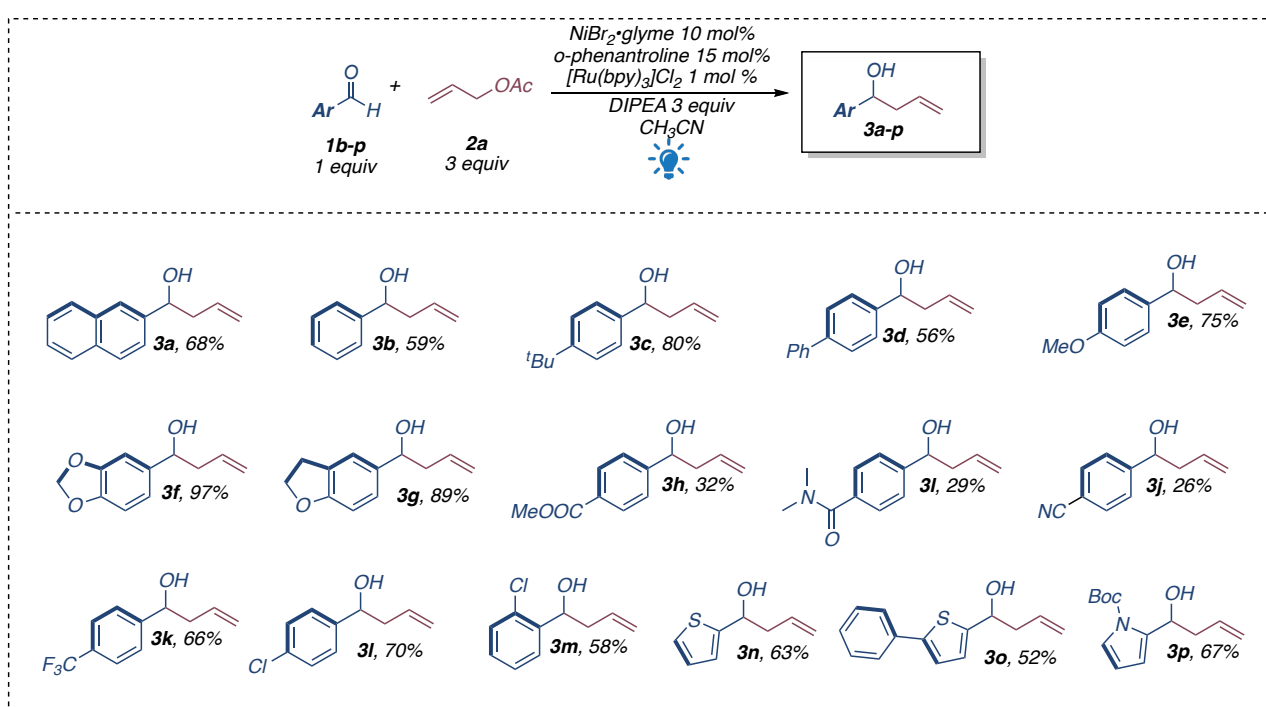
Chapter 4. Scheme 15 Optimized reaction conditions for dual Ni/photoredox allylation of aldehydes

• Scope evaluation

The generality of our initial finding was studied with a variety of aromatic and aliphatic aldehydes.

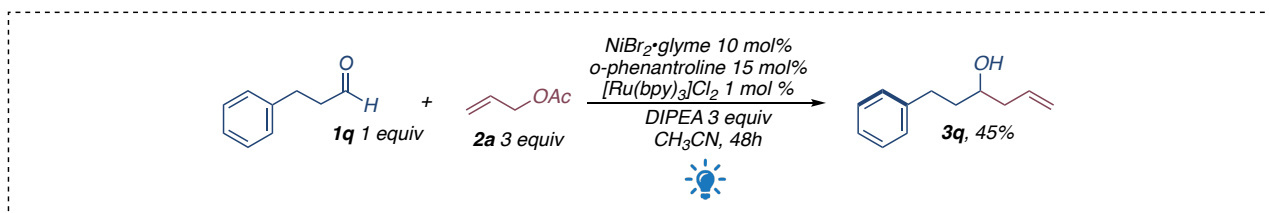
We started our investigation evaluating a range of suitable aromatic substrates. Yields are from good to moderate as a function of the presence of electron-withdrawing groups, that have an impact on the isolated yields. In general, functional groups were well tolerated, including halides, CF₃, esters, nitriles, ethers. Interestingly, acidic NH groups were also tolerated. In addition, sensitive pyrrole or electron rich substrates are quite compelling reactants.

In the case of aromatic aldehydes, the reaction is clean, and no reduction or pinacol coupling byproducts were observed. In the ¹H-NMR spectra of the crude reaction mixtures just signals of the unconsumed aldehydes are present.

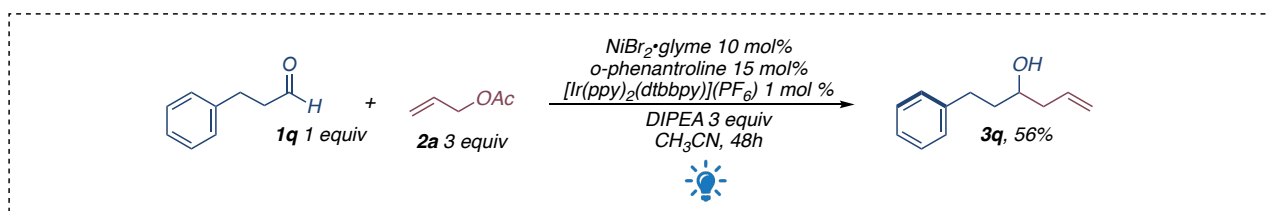


Chapter 4. Figure 1 Survey of aromatic aldehydes suitable for the reported protocol.

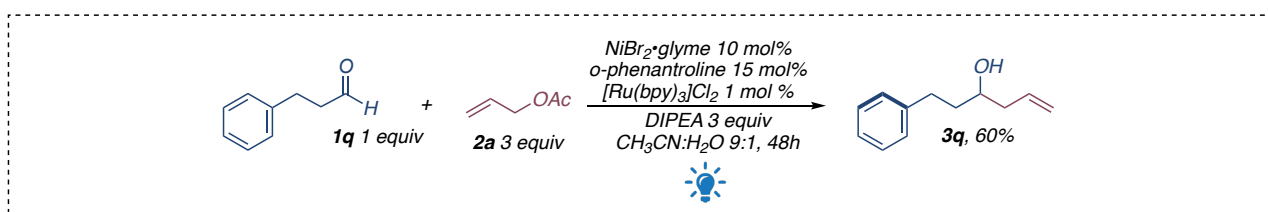
Due to the proximity of the aromatic ring to the carbonyl group, aromatic aldehydes resulted more reactive compared with aliphatic substrates and a slight modification of the reaction condition resulted compulsory to increase the reactivity and extend the generality of the protocol. In this case, dihydrocinnamaldehyde was selected as a model substrate for the re-optimization of the reaction parameters. Thanks to the presence of a phenyl ring relatively close to the reactive center, under the best conditions used for aromatic aldehydes, the formation of the desired allylation product could be observed, albeit with modest results.



The first consideration was about the nature of the photocatalyst. As a first hypothesis, it was thought that moving back to a photocatalyst with an enhanced reducing character, both in its excited state and in its reduced form, might be the solution to the lack of reactivity observed. However, the use of $[\text{Ir}(\text{ppy})_2(\text{dtbbpy})]\text{PF}_6$ as a photosensitizer in our optimized reaction conditions led only to a slight increase of the yield.



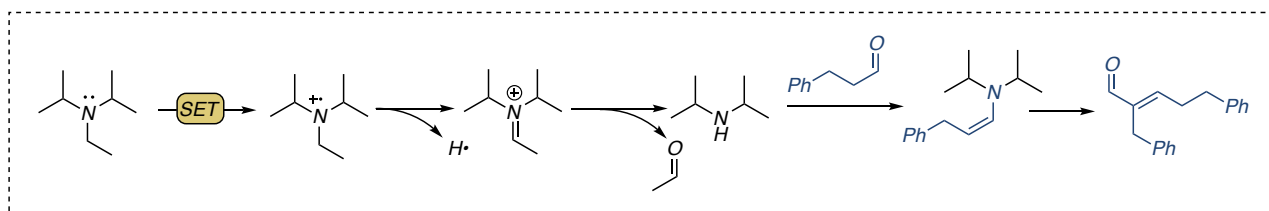
Satisfactory results were achieved by the employment of water as co-solvent to the reaction mixture, with a final yield in product of 60%. Under this reaction environment it was possible to promote the transformation in the presence of the same ruthenium photocatalyst used in the case of aromatic substrates.



Chapter 4. Scheme 16 Optimized reaction conditions for dual Ni/photoredox allylation of aliphatic substrates

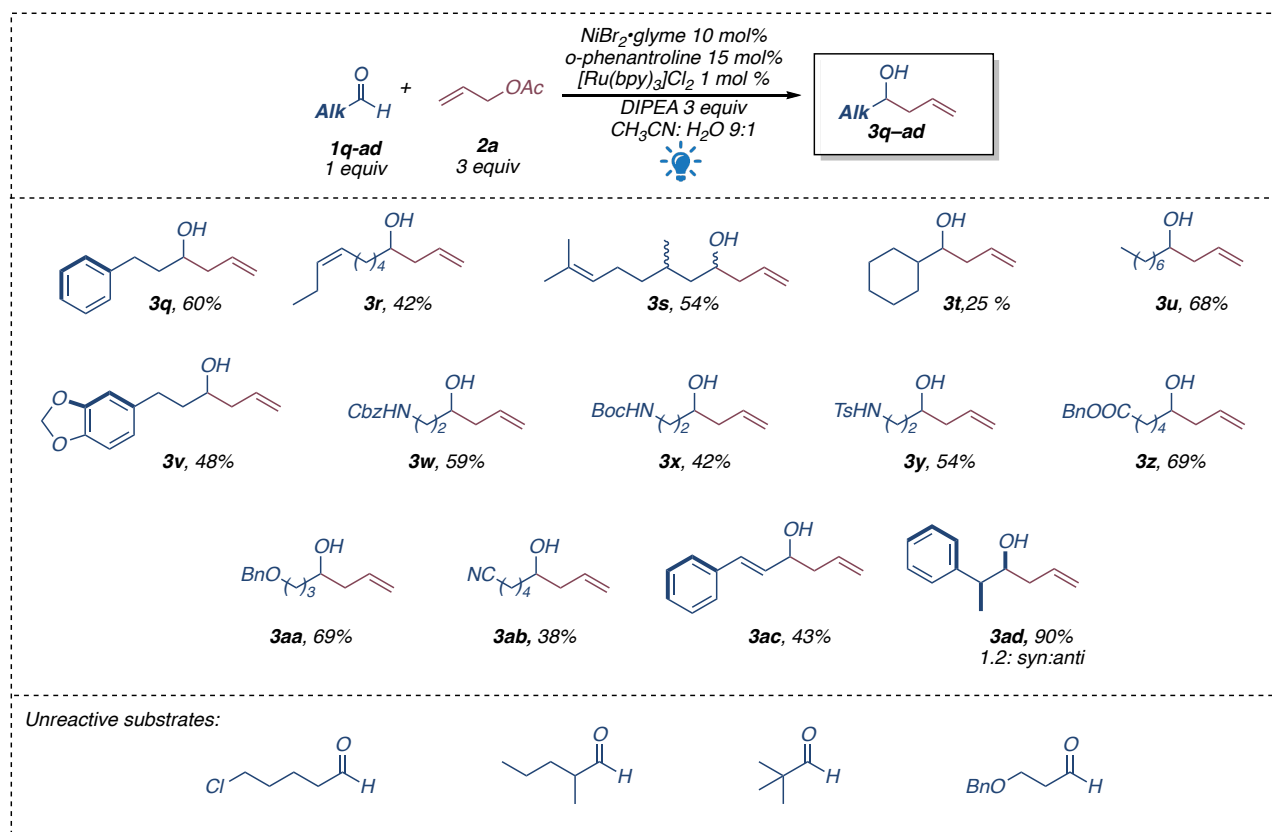
Probably, there are several roles played by the water in the reaction mixture. First of all, it promotes hydrolysis of the final nickel alcoholate into the desired homoallylic alcohol restoring faster the transition metal catalyst. In addition, the low reactivity observed screening aliphatic aldehydes is not solely related to the lower electrophilicity of the carbonyl center. The analysis of the crude of these reactions, compared with the case of aromatic aldehydes, is more complex and various parasitic pathways were identified. The main encountered by-product in these reactions corresponds to the aldol condensation of the starting material. To the best of our knowledge, we believe that these undesirable reaction pathways arise from the oxidation of the sacrificial agent present in the reaction mixture. The oxidation of the tertiary amine

first leads to the formation of the corresponding radical cation. This highly reactive species then evolves to the corresponding di-isopropyl amine releasing acetaldehyde. We, therefore, believe that the so formed diisopropylamine can interact with aliphatic substrates, generating a transient enamine capable of promoting aldol condensation. The addition of water to the reaction mixture inhibits the formation of the enamine intermediate preventing the byprocess.



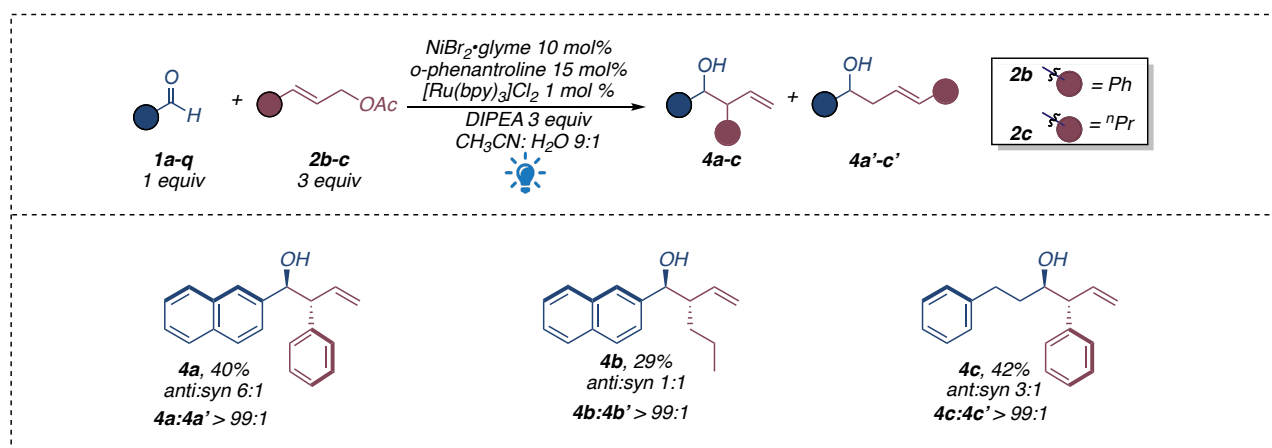
Chapter 4. Figure 2 Plausible parasitic reaction pathway of aliphatic aldehydes in the presence of DIPEA

Although the introduction of water allows access to the functionalization of aliphatic aldehydes, analyzing the survey of substrates compatible with the new presented protocol, however fairly low reactivity was found. Linear aliphatic and unsaturated aldehydes were found suitable substrates leading to the formation of the desired product with yields from poor to moderate. More hindered alkyl aldehydes showed a reduced reactivity while α -disubstituted aliphatic aldehydes were unreactive. Reaction with chiral aldehydes **1ad** gave poor diastereoisomeric ratio. The major diastereoisomer obtained can be explained by the Felkin-Ahn model.



Chapter 4. Figure 3 Survey of aliphatic aldehydes suitable for the reported protocol.

Once the scope was evaluated in the presence of an unsubstituted allyl source, we investigated the possibility of promoting the same reaction in the presence of a more decorated allyl pronucleophile. For this purpose, the model aromatic and aliphatic aldehydes were evaluated in the presence of the commercially available cinnamyl acetate and 2-hexenyl acetate.

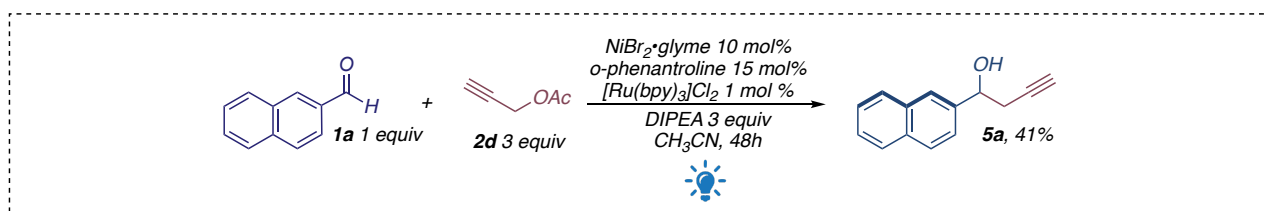


Chapter 4. Figure 4 Survey of substituted allylating agents.

It was pleasing to note that the protocol allows the desired transformation in the presence of these allylating agents. As reported for other protocols involving the formation of transient nucleophilic

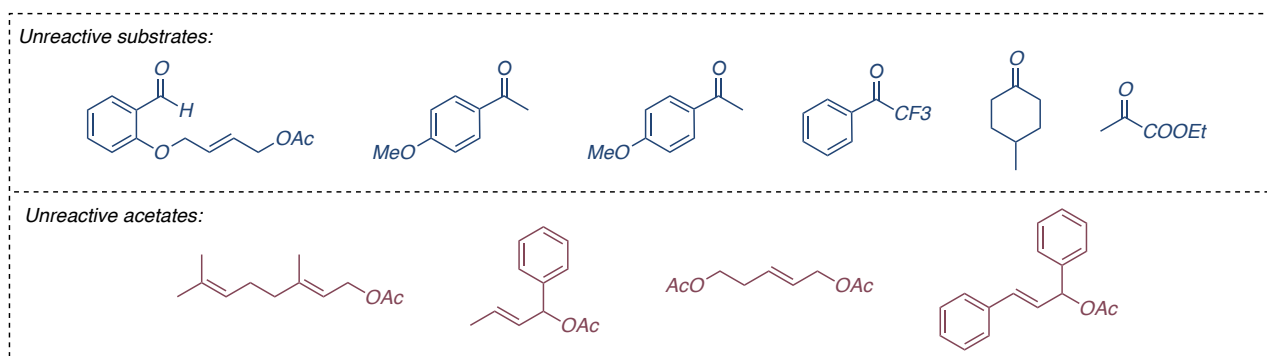
organonickel species, it was possible to observe that in all the considered cases, the regiochemical outcome always leads to the exclusive formation of the branched product. The isolated yields of the final homoallylic alcohols, however, are lower compared to the less steric hindered allyl acetate. In addition, it was also not possible to obtain satisfactory results in terms of diastereoselectivity in the presence of neither aromatic nor aliphatic aldehydes.

In conclusion, it was also possible to preliminarily examine the access to a propargylation protocol in these reaction conditions. To our delight, using 2-naphthaldehyde as model substrate the reaction has a positive outcome in the presence of propargyl acetate.



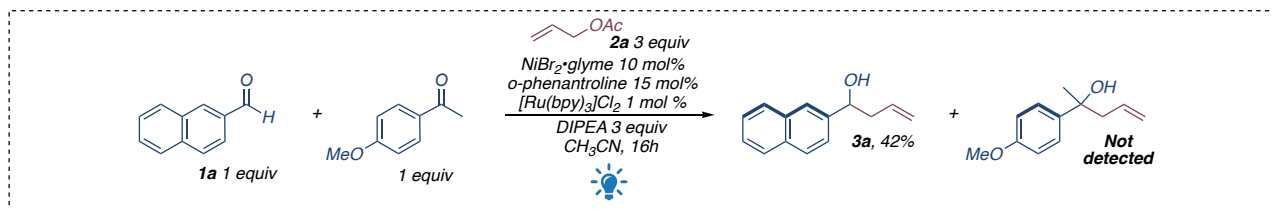
Chapter 4. Scheme 17 Dual photoredox and nickel catalyzed propargylation of 2-naphthaldehyde

Despite careful and in-depth analysis of the best reaction conditions, due to the intrinsic reduced nucleophilicity of the organonickel transient compounds, some severe limitations were encountered evaluating the possibilities of the proposed new dual protocol. The use of (E)-4-(2-formylphenoxy)but-2-en-1-yl acetate for an intramolecular variant of the reaction is forbidden under the presented reaction conditions. Similarly, due to the steric hindrance and the reduced electrophilicity, it is not possible to promote the functionalization of either aliphatic or aromatic ketones.



Chapter 4. Figure 5 Poor reactive substrates.

In addition, several acetates precursors have proved ineffective in the dual photoredox/Ni protocol. As the steric hindrance increases, the oxidative addition process becomes more unfavorable, determining deactivation of the process. Interestingly, the methodology is completely selective towards aldehydes, and when the model reaction was performed in the presence of an aromatic ketone, only the selective reaction with aldehyde occurred.

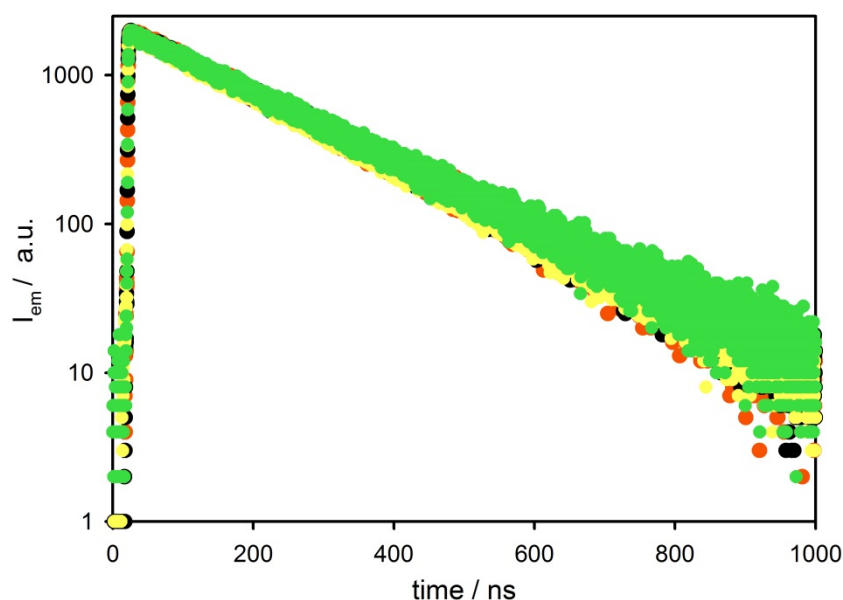


• Mechanistic investigation

Thanks to the collaboration with Professor P. Ceroni's research group, a detailed photophysical and electrochemical investigation was conducted to clarify the mechanism of the new dual nickel and photoredox protocol.

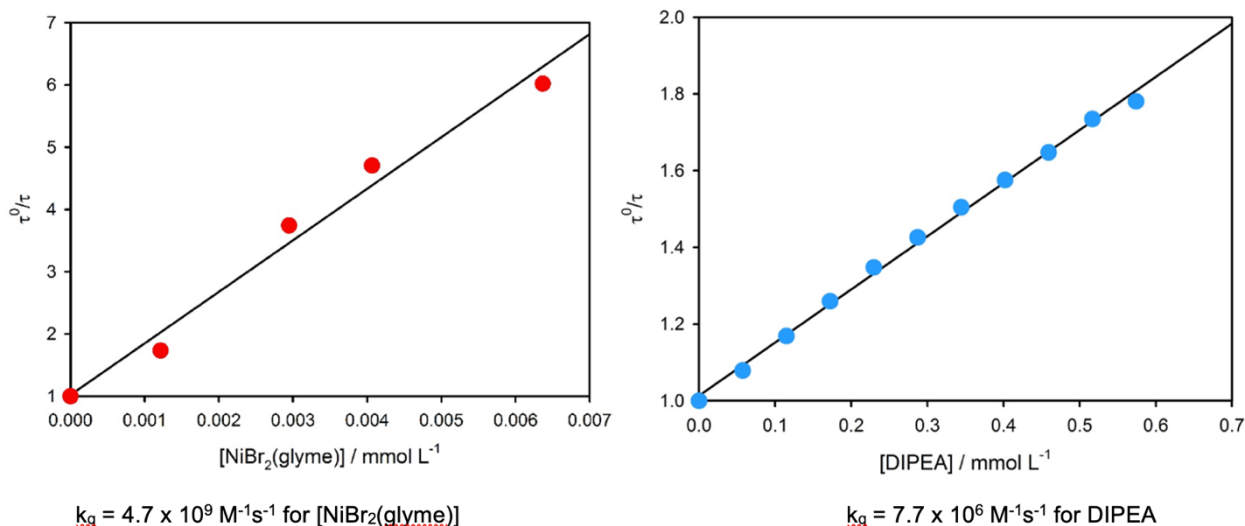
As already introduced for the previous dual transformations, each component of the reaction mixture was evaluated as quenchers of the excited state of the photocatalyst.

In particular, no change of the decay of the emission intensity of the excited state of $[\text{Ru}(\text{bpy})_3]\text{Cl}_2$ was observed upon addition of allyl acetate 0.6 M, o-phenanthroline 0.03 M or hydrocinnamaldehyde 0.2 M (same concentrations used to perform the reaction).



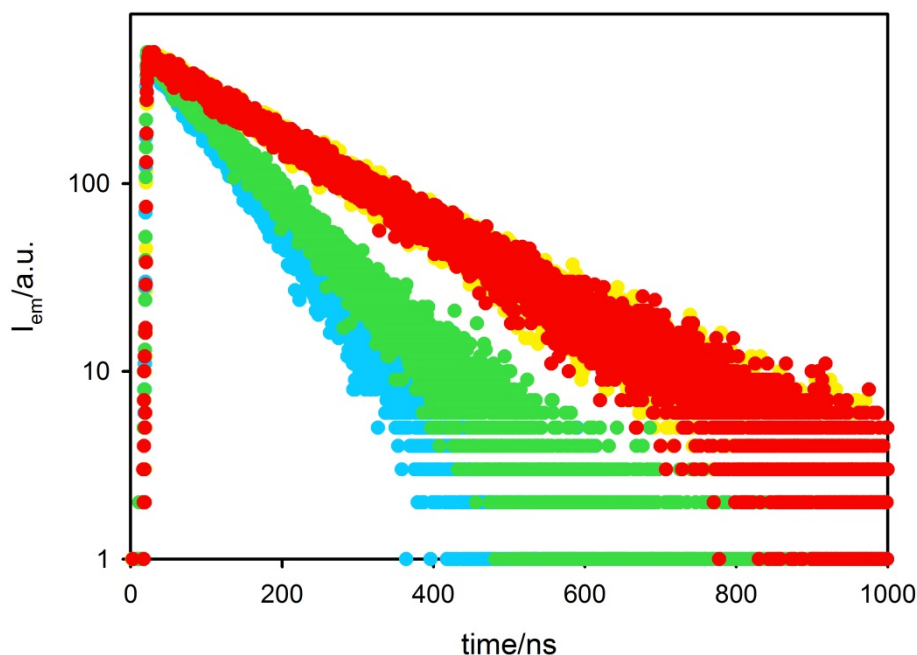
Chapter 4. Figure 6 Emission intensity decays of $[\text{Ru}(\text{bpy})_3]\text{Cl}_2$ (4×10^{-5} M) in acetonitrile solution in absence (orange dots) and in presence of allyl acetate 0.6 M (black dots), o-phenanthroline 0.03 M (yellow dots) and hydrocinnamaldehyde 0.2 M (green dots), upon excitation at 405 nm.

On the other hand, as determined by Stern-Volmer plots, DIPEA and $[\text{NiBr}_2(\text{glyme})]$ are able to quench the emission of the photocatalyst with quenching constants of $7.7 \times 10^6 \text{ M}^{-1}\text{s}^{-1}$ and $4.7 \times 10^9 \text{ M}^{-1}\text{s}^{-1}$, respectively,



Chapter 4. Figure 7 Emission intensity decays of $[\text{Ru}(\text{bpy})_3]\text{Cl}_2$ in acetonitrile solution in the absence (τ^0) and in the presence (τ) of increasing amount of DIPEA (blue dots) and $[\text{NiBr}_2(\text{glyme})]$ (red dots). The slopes represent the Stern-Volmer constant (K_{SV}), i.e., the product of the quenching constant (k_q) and τ^0

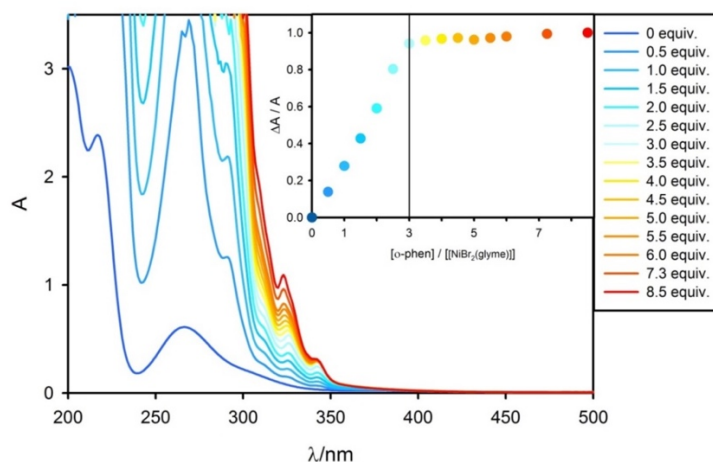
Interestingly, quenching of the photocatalyst is no longer observed upon concomitant addition of $[\text{NiBr}_2(\text{glyme})]$ precatalyst and o-phenanthroline ligand (ca. 3 equiv. per Ni(II) ion).



Chapter 4. Figure 8 Emission intensity decays of $[\text{Ru}(\text{bpy})_3]\text{Cl}_2$ ($4 \times 10^{-5} \text{ M}$) in air-equilibrated acetonitrile solution (yellow dots) and upon addition of (i) $[\text{NiBr}_2(\text{glyme})]$ 0.02 M (light-blue dots), (ii) $[\text{NiBr}_2(\text{glyme})]$ 0.02 M and o-phenanthroline 0.03 M (green dots), (iii) $[\text{NiBr}_2(\text{glyme})]$ 0.02 M and o-phenanthroline 0.1 M (red dots). Excitation at 405 nm.

This experimental evidence stems from the fact that $[\text{NiBr}_2(\text{glyme})]$ is simply the reaction precatalyst. In fact, as confirmed by the titration experiment (**Figure 9**), under reaction conditions the interaction between $[\text{NiBr}_2(\text{glyme})]$ and o-phenanthroline results in the formation of several species in equilibrium with each other. Specifically, it is believed that

these species correspond to the formation of nickel complexes with one, two or three ligand molecules, capable of replacing both the bromide and the glyme.²⁸⁹



Chapter 4. Figure 9 Titration experiment: Absorption spectrum (blue solid line) of $[\text{NiBr}_2(\text{glyme})] 2 \times 10^{-4} \text{ M}$ in MeCN upon addition of *o*-phenanthroline up to 8.5 equivalents (red solid line). Inset shows normalized absorption changes at 344 nm as function of *o*-phenanthroline equivalents added. The stoichiometry of the system results in 1:3 $[\text{NiBr}_2(\text{glyme})]$: *o*-phenanthroline.

This result demonstrates that the actual Ni(II) catalyst containing the *o*-phenanthroline ligand(s) is not able to quench the photocatalyst, so, under the reaction conditions, the only active quencher is DIPEA.²⁹⁰

In addition, considering the reported photoredox potentials associated to the excited state of the photocatalyst ($E(\text{Ru}^{\text{II}*}/\text{Ru}^{\text{III}}) = -0.86 \text{ V vs SCE}$)²⁹¹ and the reduction potential calculated for the nickel precatalyst ($E(\text{NiBr}_2/\text{NiBr}) = -2.63 \text{ V vs SCE}$) it is thermodynamically forbidden that the reaction proceeds through oxidative quenching. It is more likely that the interaction between the two species occurs through an energy transfer process.

	$E_{1/2}$ (V vs SCE)
$[\text{NiBr}_2(\text{glyme})]$	-2.63 ^a
$[\text{NiBr}_2(\text{glyme})] + 1.5 \text{ equiv. } o\text{-phenanthroline}$	-1.31 ^a
$[\text{Ni}(\text{phen})_3](\text{BF}_4)_2$	-1.30 ^b

Table 4.1.8 First reduction potential estimated from cyclic voltammetry

[a] Chemical irreversible one-electron transfer process, E_{pc} at 0.2 V/s. [b] Similar value of $E_{1/2}$ was estimated for $[\text{NiBr}_2(\text{glyme})]$ upon addition of 3 equivalents of *o*-phenanthroline.

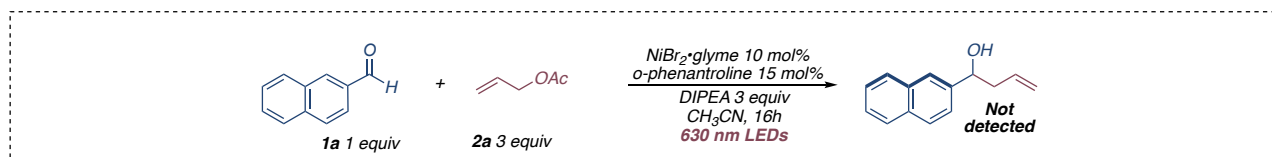
The presumably formed excited state of $\text{NiBr}_2(\text{glyme})$, however does not determine any outcome on the reaction. This hypothesis was confirmed by the control experiment

²⁸⁹ Broomhead, J. A.; Dwyer, F. O. The preparation and resolution of the bis-(2,2'-bipyridine)-1,10-phenanthroline-nickel(II) and the bis-(1,10-phenanthroline)-2,2'-bipyridine-nickel(II) ions. *Aust. J. Chem.* **1962**, *16*, 51-65. <https://doi.org/10.1071/CH9620453>

²⁹⁰ Wrighton, M.; Markham, J. Quenching of the Luminescent State of Tris(2,2'-Bipyridine)Ruthenium(II) by Electronic Energy Transfer. *J. Phys. Chem.* **1973**, *77* (26), 3042-3044. <https://doi.org/10.1021/j100644a002>; b) Pitre, S. P.; McTiernan, C. D.; Ismaili, H.; Scaiano, J. C. Mechanistic insights and kinetic analysis for the oxidative hydroxylation of arylboronic acids by visible light photoredox catalysis: a metal-free alternative. *J. Am. Chem. Soc.* **2013**, *135*, 13286-13289. [10.1021/ja406311g](https://doi.org/10.1021/ja406311g)

²⁹¹ Tokel-Takvoryan, N. E.; Hemingway, R. E.; Bard, A. J. Electrogenerated chemiluminescence. XIII. Electrochemical and electrogenerated chemiluminescence studies of ruthenium chelates. *J. Am. Chem. Soc.* **1973**, *95*, 6582-6589. <https://doi.org/10.1021/ja00801a011>

performed under red light irradiation (Single red LED 630 nm 2.7W) that would trigger the direct excitation of $[\text{NiBr}_2(\text{glyme})]$.



In light of these photophysical evidence, we believe that the dual catalytic cycle is initiated by the reductive quenching of the $[\text{Ru}(\text{bpy})_3]^{2+}$ photocatalyst by DIPEA, ($E(\text{DIPEA}^+/\text{DIPEA}) = 0.86 \text{ V vs SCE}$, while $E(\text{Ru}^{\text{II}}/\text{Ru}^{\text{I}}) = 0.84 \text{ V vs SCE}$) producing the reduced $[\text{Ru}(\text{bpy})_3]^+$ complex ($E(\text{Ru}^{\text{II}}/\text{Ru}^{\text{I}}) = -1.28 \text{ V vs SCE}$).²⁸ The ruthenium complex is able to reduce the *in situ* formed Ni(II)phenanthroline complexes, leading to the formation of the corresponding Ni(I) complex.

The formation of this intermediate would result, however, in contrast with what has been reported in other nonvisible-light driven nickel-catalyzed processes involving the formation of transient nucleophilic organonickel species.²⁹² In fact, from these works it is reported that the involved species include mostly Ni (II) and Ni (0) intermediates.

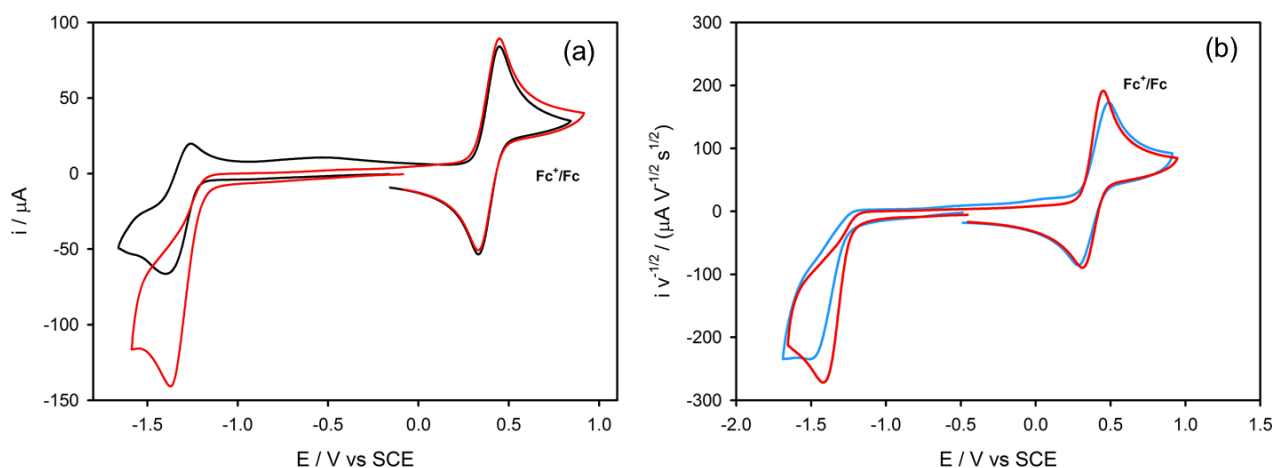
However, a careful electrochemical investigation suggested a different scenario.

Performing the cyclic voltammogram of $[\text{Ni}^{\text{II}}(\text{phen})_3]^{2+}$ in CH_3CN ²⁹³ a reversible reduction process at -1.31 V vs SCE is observed.

Upon addition of allyl acetate, the cyclic voltammogram displays a chemically irreversible reduction process with a cathodic peak at almost the same potential value and higher cathodic current, compared to $[\text{Ni}^{\text{II}}(\text{phen})_3]^{2+}$. These experimental results can be accounted for a chemical reaction of $[\text{Ni}^{\text{I}}(\text{phen})_3]^+$ with allyl acetate, immediately followed by its one-electron reduction at less negative potential compared to the pristine $[\text{Ni}^{\text{II}}(\text{phen})_3]^{2+}$ complex.

²⁹² Anka-Lufford, L. L.; Prinsell, M. R.; Weix, D. J. Selective cross-coupling of organic halides with allylic acetates. *J. Org. Chem.* **2012**, *77*, 9989-10000. <https://doi.org/10.1021/jo302086g>

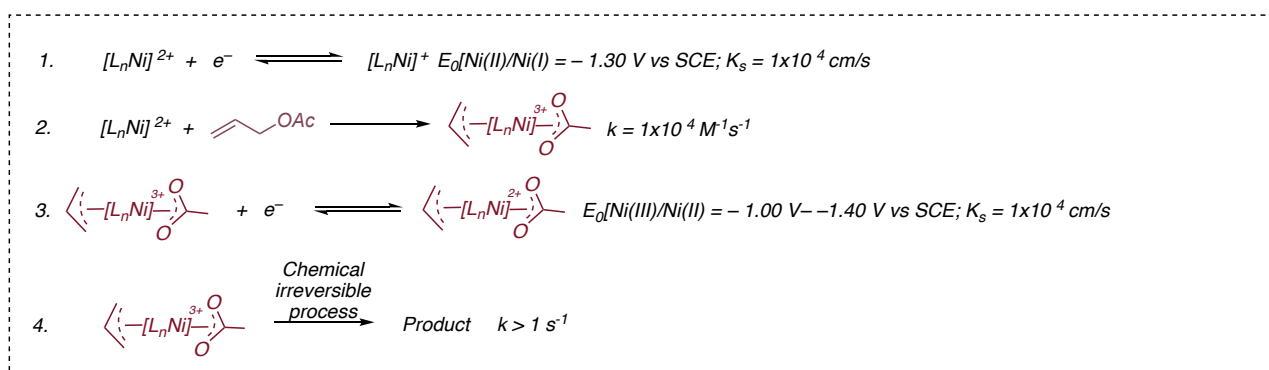
²⁹³ Smith, W. H.; Kuo, Y.-M. Electrochemical studies of nickel tris(phenanthroline) in nonaqueous solvents part ii. electrocatalytic polymerization of activated olefins. *J. Electroanal. Chem.* **1985**, *188*, 203-218. [https://doi.org/10.1016/S0022-0728\(85\)80062-0](https://doi.org/10.1016/S0022-0728(85)80062-0)



Chapter 4. Figure 10 a). Cyclic voltammetry of an argon-purged solution of $[\text{Ni}(\text{phen})_3](\text{BF}_4)_2$ (3mM) in CH_3CN in the presence of 0.3M tetraethylammonium tetrafluoroborate (TEABF_4) (black solid line) and upon addition of allyl acetate (0.6M) (red solid line). Scan rate = 0.2Vs^{-1} ; working electrode: glassy carbon. Ferrocene (Fc) was used as internal standard (plot (b)). Cyclic voltammetry of an argon-purged solution of $[\text{Ni}(\text{phen})_3](\text{BF}_4)_2$ (3mM) in CH_3CN in the presence of 0.3M tetraethylammonium tetrafluoroborate (TEABF_4) upon addition of allyl acetate (0.6M) at 0.2 V/s (red solid line) and 2 V/s (blue solid line). Working electrode: glassy carbon. Ferrocene (Fc) was used as internal standard (plot (b)).

The photogenerated $[\text{Ru}(\text{bpy})_3]^+$ complex is able to reduce not only $[\text{L}_n\text{Ni}^{\text{II}}]^{2+}$ to $[\text{L}_n\text{Ni}^{\text{I}}]^+$, but also the nickel complex intermediate obtained after the oxidative addition onto the allyl acetate generating the transient nucleophilic organometallic species $[\text{L}_n\text{Ni}^{\text{II}}(\eta^3\text{-allyl})(\text{OAc})]$.²⁹⁴

This mechanism is confirmed by digital simulation obtained by using the software package DigiSim 3.05. of cyclic voltammograms.²⁹⁵

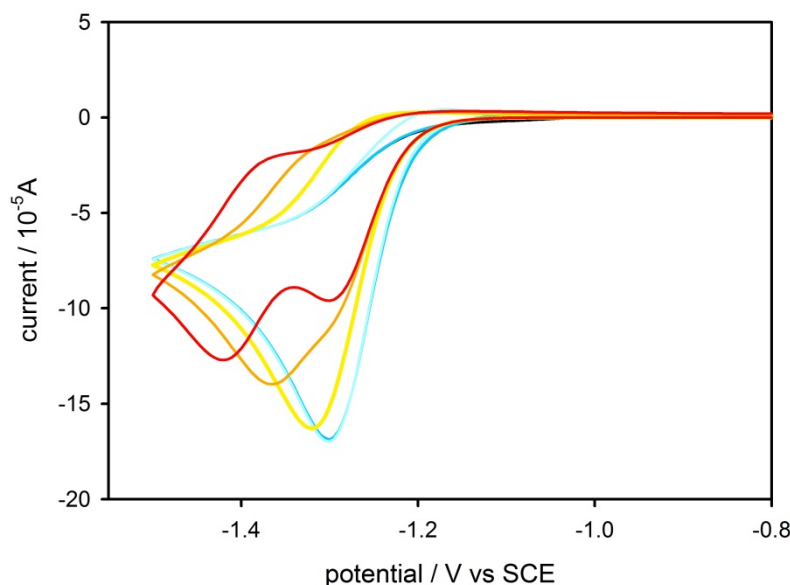


Chapter 4. Figure 11 mechanism proposed for the simulation. k_s is defined as the heterogeneous electron transfer rate constant with the electrode, k is the reaction rate constant, $E_0[\text{Ni}(\text{II})/\text{Ni}(\text{I})]$ is the reduction potential estimated with experimental CV and $E_0[\text{Ni}(\text{III})/\text{Ni}(\text{II})]$ is the variable parameter, i.e., the reduction potential for process.

From simulated voltammograms, it is possible to conclude that the reduction potential $E(\text{Ni}^{\text{III}}/\text{Ni}^{\text{II}})$ must be lower or at least equal to the potential for the electron transfer 1 estimated experimentally; indeed, if it is higher, two electron transfer processes should be visible in the cyclic voltammetry (orange and red solid lines in **Figure 12**).

²⁹⁴ Kraikivskii, P. B.; Klein, H.-F.; Saraev, V. V.; Meusinger, R.; Svoboda, I.; Pashchanka, M. Conversion of Imine Ligands in Allyl-Nickel(II) Complexes. *Journal of Organometallic Chemistry* **2009**, 694 (24), 3912–3917. <https://doi.org/10.1016/j.jorganchem.2009.08.010>.

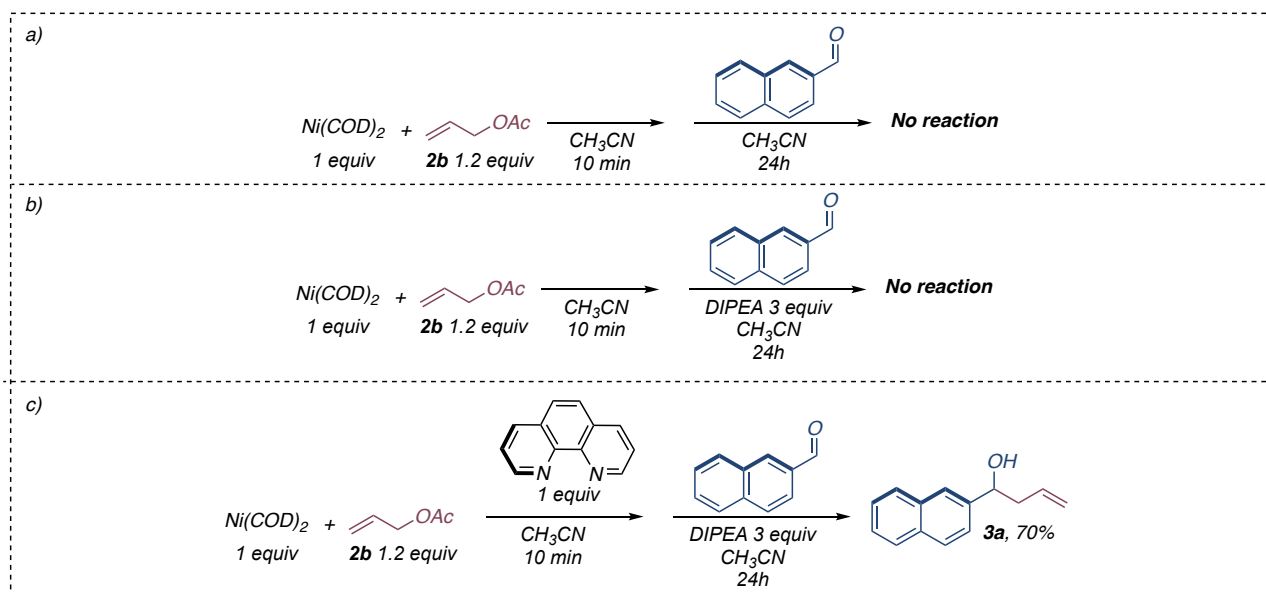
²⁹⁵ Digit simulation: DigiSim 3.05, BioAnalytical Systems, West Lafa.



Chapter 4. Figure 12 Simulated cyclic voltammograms using DigiSim considering the reaction mechanism. Simulation parameters: 25 °C, 0.2V/s, concentration of $[\text{LnNi}^{\text{II}}]^{2+}$ 3mM and allyl acetate 0.6M, $E_0(\text{Ni(II)/Ni(I)}) = -1.30$ V vs SCE, $k_s(4) = 1 \times 10^4$ cm/s, $k(5) = 1 \times 10^4$ M⁻¹s⁻¹, $k_s(6) = 1 \times 10^4$ cm/s and $k(7) > 1$ s⁻¹. The variable parameter is the reduction potential $E_0(\text{Ni(III)/Ni(II)})$: -1.00 V (black solid line), -1.10 V (blue solid line), -1.20 V (light blue solid line); -1.30 V (yellow solid line), -1.35V (orange solid line) and -1.40 V (red solid line).

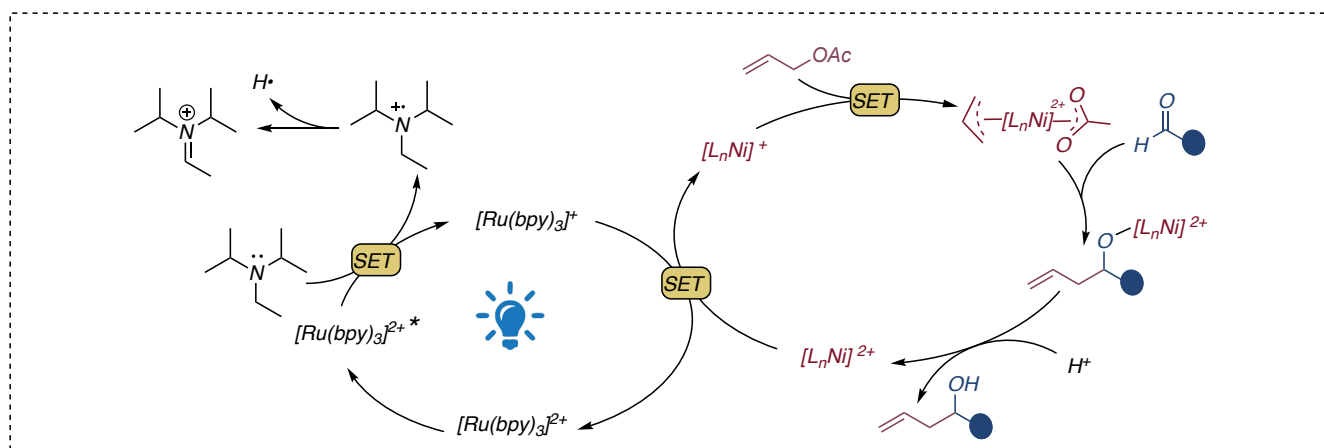
In order to find the accordance between the electrochemical investigations and the experimental evidence, several control experiments were conducted. We have performed the allylation reaction of 2-naphthaldehyde in the dark with allyl acetate using a stoichiometric amount of $\text{Ni}(\text{COD})_2$ both with or without o-phenanthroline ligand and DIPEA. We were pleased to observe the presence of homoallylic **3a** alcohol only when the reaction was performed in the presence of o-phenanthroline demonstrating the importance of the ligand in the reaction. The intermediate $[\text{LnNi}^{\text{II}}((\eta^3\text{-allyl})(\text{OAc}))]$, formed by oxidative addition of $\text{Ni}(0)$ to allyl acetate, was confirmed to be the allylating species.^{266,296}

²⁹⁶ a) Hegedus, L. S.; Wagner, S. D.; Waterman, E. L.; Siirala-Hansen, K. Reaction of π -Allylnickel Bromide Complexes with Ketones and Aldehydes. Synthesis of α -Methylene- γ -Butyrolactones. *J. Org. Chem.* **1975**, *40* (5), 593–598. <https://doi.org/10.1021/jo00893a012>. b) Hegedus, L. S.; Varaprath, S. Unsaturated (π -allyl)nickel halide complexes. Reactions to produce dienes. *Organometallics* **1982**, *1*, 259–263. <https://doi.org/10.1021/om00062a006>. d) Hegedus, L. S.; Thompson, D. P. The reactions of organic halides with (π -allyl)nickel halide complexes: a mechanistic study. *J. Am. Chem. Soc.* **1985**, *107*, 5663–5669. <https://doi.org/10.1021/ja00306a012>



Chapter 4. Scheme 18 control experiments with stoichiometric Ni(COD)_2

In conclusion, by combining the experimental results with the detailed photo-electrochemical analysis, it is possible to depict a general picture of the reaction as shown **Scheme 19**.

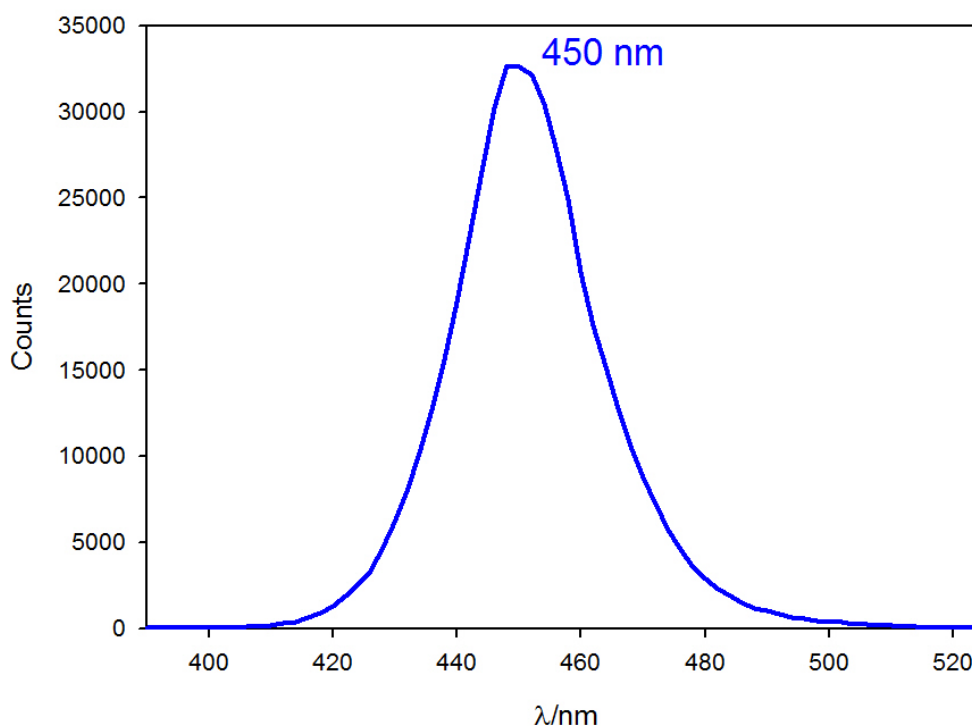


Chapter 4. Scheme 19 Proposed dual catalytic cycle

• Supplementary data**General methods and materials**

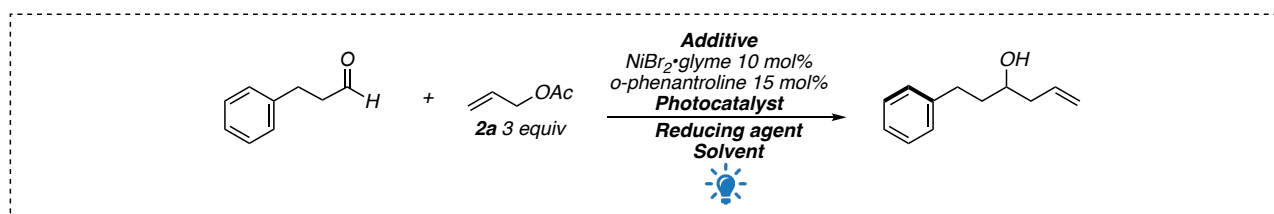
^1H -NMR spectra were recorded on Varian Mercury 400 spectrometer. Chemical shifts are reported in ppm from TMS with the solvent resonance as the internal standard (CDCl_3 ; $\delta = 7.27$ ppm). Data are reported as follows: chemical shift, multiplicity (s = singlet, d = duplet, t = triplet, q = quartet, dd = double duplet, dt = double triplet, bs = broad signal, m = multiplet), coupling constants (Hz). ^{13}C -NMR spectra were recorded on Varian MR400 spectrometer. Chemical shifts are reported in ppm from TMS with the solvent as the internal standard (CDCl_3 ; $\delta = 77.0$ ppm). GC-MS spectra were taken by EI ionization at 70 eV on a Hewlett-Packard 5971 with GC injection. LC-electrospray ionization mass spectra (ESI-MS) were obtained with Agilent Technologies MSD1100 single-quadrupole mass spectrometer. Chromatographic purification was done with 240-400 mesh silica gel. All reactions were set up under an argon atmosphere in oven-dried glassware using standard Schlenk techniques.

Anhydrous solvents were supplied by Aldrich in Sureseal® bottles and were used without further purification. All the reagents were purchased from Aldrich and used without further purification unless specified. Triethylamine and DIPEA were stirred one day over KOH and distilled before their use.



Chapter 4. Supplementary 1 Emission profile of the 16W Blue LED strip used to irradiate the solutions.

Screening of the conditions for aliphatic aldehydes.

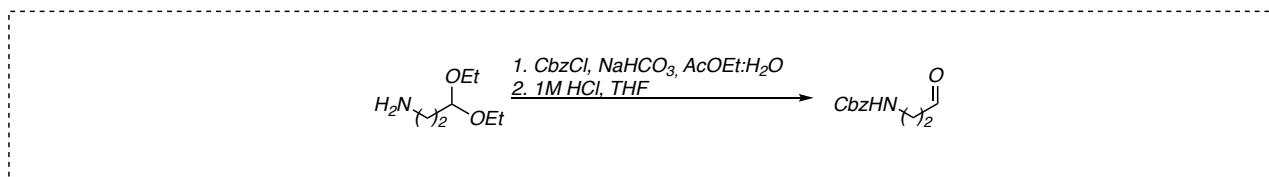


Entry ^[a]	Photocatalyst	R. A.	Solvent	Additive	Yield ^[b]
1	[Ru(bpy) ₃]Cl ₂	DIPEA	CH ₃ CN	-	45
2	[Ir(ppy) ₂ (dtbbpy)]PF ₆	DIPEA	CH ₃ CN	-	56
3	[Ru(bpy) ₃]Cl ₂	DIPEA	CH ₃ CN/H ₂ O 10/1	-	60
4	[Ir(ppy) ₂ (dtbbpy)]PF ₆	DIPEA	CH ₃ CN/H ₂ O 10/1	-	60
5	[Ru(bpy) ₃]Cl ₂	DIPEA	CH ₃ CN	H ₃ BO ₃ (30 mol%)	43
6	[Ru(bpy) ₃]Cl ₂	TEOA ^[c]	CH ₃ CN	-	25

Table 4.1.9 Further optimization of the reaction conditions in the presence of aliphatic aldehydes

[a] Reaction conditions reported in the above figure on 0.2 mmol scale. [b] Determined by ¹H-NMR analysis after chromatographic purification. [c] Triethanol amine.

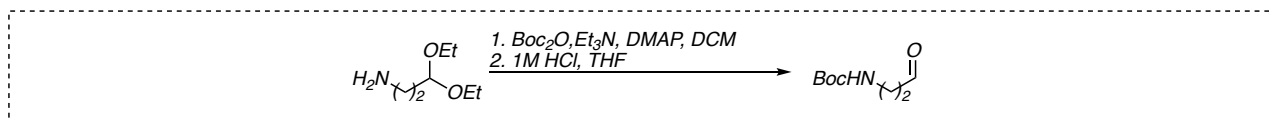
Synthesis of aldehyde 1w



To a solution of 3,3-diethoxy-1-aminopropane (250 μ L, 1.54 mmol) in AcOEt (3 mL) were added NaHCO_3 (650 mg, 7.7 mmol, 5 equiv.), water (3 mL) and benzyl chloroformate (331 μ L, 2.3 mmol, 1.5 equiv.). The resulting mixture was allowed to stir overnight at room temperature and checked by GC-MS and TLC (cHex/AcOEt 6/4) to complete conversion. After that, the layers were separated, and the aqueous phase was extracted with AcOEt (3 x 5 mL), dried over Na_2SO_4 and concentrated. The crude was dissolved in THF (0.5 mL), treated with 1M HCl (250 μ L, 12 mol%) at 0°C and stirred overnight at room temperature. After the reaction mixture was diluted with Et_2O (10 mL) and washed with a saturated solution of NaHCO_3 (5 mL), the combined organic phase was dried over Na_2SO_4 and concentrated to obtain a yellowish oil. The crude was further purified by flash column chromatography (cHex/AcOEt 7/3) to obtain 1w as yellow solid, 51% yield (0.79 mmol, 164 mg). Spectroscopic data are in agreement with those reported in the literature.²⁹⁷

²⁹⁷ B.-L. Zhao, Y. Lin, H.-H. Yan and D.-M. Du, *Org. Biomol. Chem.*, **2015**, *13*, 11351-11361. 10.1039/C5OB01749A.

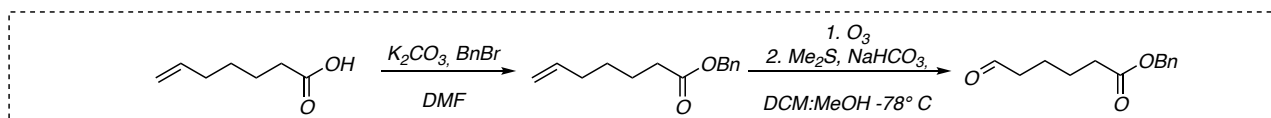
Synthesis of aldehyde **1x**



To a solution of 3,3-diethoxy-1-aminopropane (250 μL , 1.54 mmol) in DCM (3 mL) were added Et_3N (428 μL , 3.1 mmol, 2 equiv.), 4-(dimethylamino)pyridine (2 mg, 0.016 mmol, 1.0 mol%) and a solution of di-tert-butyl dicarbonate (371 mg, 1.7 mmol, 1.1 equiv.) in DCM (1.5 mL) drop-wise at 0°C . The resulting mixture was allowed to stir overnight at room temperature and checked by GC-MS and TLC (cHex/AcOEt 6/4). After the mixture was quenched with H_2O (10 mL), the layers separated, and the aqueous phase was extracted with Et_2O (3 x 10 mL), the combined organic phase washed with Brine (10 mL), dried over Na_2SO_4 and concentrated. The crude was dissolved in THF (1 mL), treated with 1M HCl (550 μL , 40 mol%) at 0°C and left stirring at room temperature and it was monitored by TLC (cHex/AcOEt 7/3). A saturated solution of NaHCO_3 was added, extracted with Et_2O (3 x 10 mL), the combined organic phase was dried over Na_2SO_4 and concentrated to obtain a yellowish oil. The crude was further purified by flash column chromatography (cHex/AcOEt 8/2) to obtain **1x** as yellowish oil, 31% yield (0.47 mmol, 82 mg). Spectroscopic data are in agreement with those reported in the literature.²⁹⁸

²⁹⁸ Kitajima, M.; Murakami, Y.; Takahashi, N.; Wu, Y.; Kogure, N.; Zhang, R.-P.; Takayama, H. Asymmetric Total Synthesis of Novel Pentacyclic Indole Alkaloid, Kopsiyunnanine E, Isolated from *Kopsia Arborea*. *Org. Lett.* **2014**, *16* (19), 5000–5003. <https://doi.org/10.1021/ol502265q>.

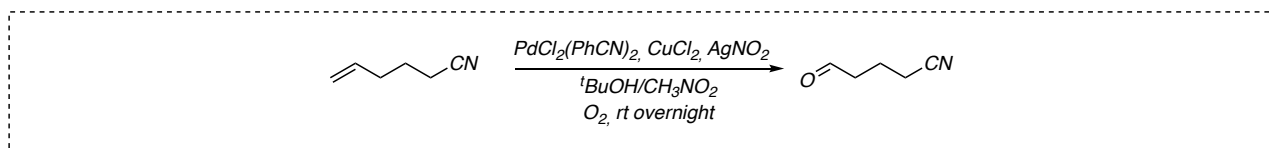
Synthesis of aldehyde **1z**



To a solution of 6-heptenoic acid (400 μL , 2.95 mmol) in dry DMF (9 mL), potassium carbonate (1.22 g, 8.8 mmol, 3 equiv.) and benzyl bromide (421 μL , 3.54 mmol, 1.2 equiv.) were added sequentially. The mixture was left stirring at room temperature overnight and after the consumption of the starting material (monitored by TLC cHex/AcOEt 6/4), water was added (5 mL) and the aqueous phase extracted with AcOEt (1 x 5 mL) and DCM (2 x 10 mL), the combined organic phases were dried over Na_2SO_4 and concentrated to a yellow oil. The residue was dissolved in a mixture of DCM/MeOH 3/1 (15 mL), cooled to -78°C and ozone was bubbled until the mixture turned blue. Oxygen was then bubbled for few minutes, dimethyl sulfide (685 μL , 9.3 mmol, 3.2 equiv.) and sodium bicarbonate (780 mg, 9.27 mmol, 3 equiv.) were added in sequence. The suspension was warmed to room temperature, left stirring overnight, then filtered on Celite® and the solvents removed under reduced pressure. The crude was purified by flash column chromatography (cHex/AcOEt 9/1) to obtain **1z** as colorless oil, 70% yield (2.1 mmol, 455 mg). Spectroscopic data are in agreement with those reported in the literature.²⁹⁹

²⁹⁹ a Kusuma, B. R.; Peterson, L. B.; Zhao, H.; Vielhauer, G.; Holzbeierlein, J.; Blagg, B. S. J. Targeting the Heat Shock Protein 90 Dimer with Dimeric Inhibitors. *J. Med. Chem.* **2011**, *54* (18), 6234–6253. <https://doi.org/10.1021/jm200553w>. b) Aguilar, A. L.; Escibano, J.; Wentworth, P.; Butters, T. D. Synthetic 1-Deoxynojirimycin N-Substituted Peptides Offer Prolonged Disruption to N-Linked Glycan Processing. *ChemMedChem* **2014**, *9* (12), 2809–2813. <https://doi.org/10.1002/cmdc.201402186>.

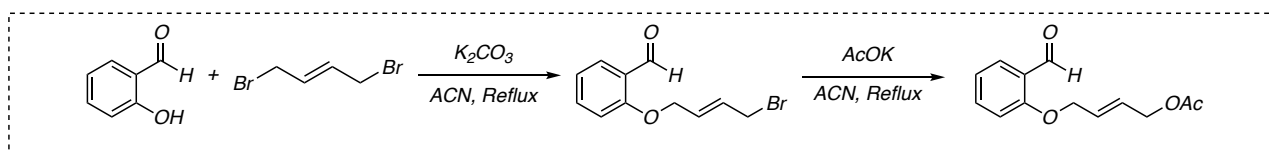
Synthesis of aldehyde 1ab



A solution of bis(benzonitrile)palladium(II) chloride (25 mg, 0.06 mmol, 12 mol%), copper(II) chloride (4 mg, 0.03 mmol, 6 mol%) and silver nitrite (5 mg, 0.03 mmol, 6 mol%) in tert-butanol (9 mL) and nitromethane (1 mL) mixture was sparged with oxygen gas for few minutes and after that, 5-hexenenitrile (60 μL , 0.5 mmol) was added. The reaction mixture was left stirring overnight at room temperature under oxygen atmosphere. After complete consumption of the alkene, the mixture was diluted with H_2O (5 mL) and extracted with DCM (3 x 10 mL). The dark organic phase was filtered through Celite®, dried over Na_2SO_4 and concentrated to obtain a yellow oil. Purification by flash column chromatography (cHex/AcOEt 9/1) gave a mixture of the aldehyde and the ketone, as colorless oil, 44% yield (0.24 mmol, 35 mg pur. 74%). The purity of the aldehyde was calculated by integrating in the $^1\text{H-NMR}$ spectrum the signals of the CHO proton (9.77 ppm, s, 1H) and the methyl group of the ketone (2.16 ppm, s, 3H).³⁰⁰

³⁰⁰ Kim, K. E.; Li, J.; Grubbs, R. H.; Stoltz, B. M. Catalytic Anti-Markovnikov Transformations of Hindered Terminal Alkenes Enabled by Aldehyde-Selective Wacker-Type Oxidation. *J. Am. Chem. Soc.* **2016**, *138* (40), 13179–13182. <https://doi.org/10.1021/jacs.6b08788>.

Synthesis of aldehyde for intramolecular reaction



To a solution of salicylaldehyde (250 μ L, 2.35 mmol) in dry ACN (6 mL), K_2CO_3 (357 mg, 2.58 mmol, 1.1 equiv.) and (E)-1,4-dibromo-2-butene (554 mg, 2.58 mmol, 1.1 equiv.) were added. The mixture was stirred under reflux for 4 hours and was cooled to room temperature and filtered on Celite®. The filtrate was then concentrated under reduced pressure and the crude purified by flash column chromatography (cHex/AcOEt 9/1) to give the intermediate **ii** as a yellowish oil (49% yield, 1.16 mmol, 295 mg).³⁰¹ To a suspension of potassium acetate (183 mg, 1.86 mmol, 1.6 equiv.), previously flamed under vacuum with a heating gun in dry ACN (5 mL), intermediate **ii** was added and the mixture was refluxed overnight. After the consumption of **ii** (monitored by TLC, cHex/AcOEt 8/2), the mixture was cooled to room temperature and filtered on Celite®. The filtrate was then concentrated under reduced pressure to give the desired product as yellowish oil in 44% yield (1.04 mmol, 245 mg).

¹H-NMR (400 MHz, $CDCl_3$, 25°C): δ = 10.51 (d, J = 0.7 Hz, 1H), 7.83 (dd, J = 7.7, 1.8 Hz, 1H), 7.52 (ddd, J = 8.4, 7.4, 1.8 Hz, 1H), 7.05 – 7.00 (m, 1H), 6.95 (d, J = 8.4 Hz, 1H), 6.00 – 5.97 (m, 2H), 4.66 – 4.61 (m, 4H), 2.07 (s, 3H); ¹³C-NMR (100 MHz, $CDCl_3$, 25°C): δ = 189.6, 170.6, 160.7, 135.8, 128.6, 128.2, 127.7, 121.0 (2C), 112.7, 68.0, 63.8, 20.8; GC-MS: rt 18.64; m/z = 234 (M^+ , 0.5), 174 ($[M - AcOH]^+$, 6), 121 ($C_7H_5O_2^+$, 46), 113 ($[M - PhCHOO\cdot]^+$, 100).

³⁰¹ Zhao, M.; Yang, H.; Li, M.-M.; Chen, J.; Zhou, L. *N*-Heterocyclic Carbene Catalyzed Intramolecular Acylation of Allylic Electrophiles. *Org. Lett.* **2014**, *16* (11), 2904–2907. <https://doi.org/10.1021/ol501046p>.

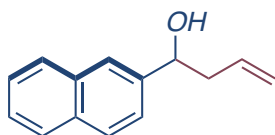
Synthesis of [Ni(phen)₃](BF₄)₂ complex

The complex was prepared following the reported procedure³⁰² using NaBF₄ instead of NaClO₄. NiCl₂•6H₂O (0.2 mmol, 48 mg), o-phenanthroline (0.6 mmol, 108 mg) and NaBF₄ (0.4 mmol, 44 mg) were added to distilled water (10 mL). The solution was heated at 80 °C for 2 hours, the pink precipitate was filtered off and washed with distilled water (2 x 3 mL). The title compound was obtained as pink solid in 63% yield (0.13 mmol, 100 mg).

³⁰² W. H. Smith and Y.-M. Kuo, *J. Electroanal. Chem. Interfacial Electrochem.*, 1985, **188**, 189-202.

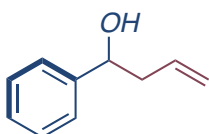
General procedure for photoredox nickel-catalyzed allylation of aldehydes

A dry 10 mL Schlenk tube, equipped with a Rotaflo stopcock, magnetic stirring bar and an argon supply tube, was first charged under argon with the ruthenium photocatalyst (1 mol%, 0.002 mmol, 1.0 mg), [NiBr₂(glyme)] catalyst (10 mol%, 0.02 mmol, 6 mg) and phenanthroline ligand (15 mol%, 0.03 mmol, 6 mg). Dry ACN (1 mL in order to obtain a 0.2 M substrate solution) was then added (the protocol was changed in the case of the aliphatic substrates, where 100 μ L of H₂O were added to the solvent ACN) and the reaction mixture was further subjected to a freeze-pump-thaw procedure (three cycles) and the vessel refilled with argon. Then DIPEA (0.6 mmol, 3 equiv., 104 μ L), allyl acetate 2a (0.6 mmol, 3 equiv.) and the substrate 1 (0.2 mmol) were added. The reaction was irradiated with 16W blue LEDs and stirred from 48 h to 64h. After that the reaction mixture was quenched with aqueous HCl 1M (approx. 1 mL) and extracted with AcOEt (4 x 3 mL). The combined organic layers were dried over anhydrous Na₂SO₄ and the solvent was removed under reduced pressure. The crude was studied by ¹H-NMR spectroscopy and purified by flash column chromatography (SiO₂) to afford the products **3** in the stated yields.



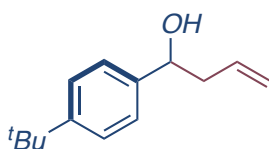
(3a): brown oil, 75% (0.15 mmol, 30 mg). The general procedure was applied using 1a (0.2 mmol, 32 mg) and 2a (0.6 mmol, 64 μ L, 3 equiv.). The title compound was isolated by flash column chromatography (cyclohexane/ethyl acetate).

^1H NMR (400 MHz, CDCl_3 , 25 $^\circ\text{C}$): δ = 7.85 – 7.78 (m, 4H), 7.51 – 7.42 (m, 3H), 5.88 – 5.77 (m, 1H), 5.21 – 5.12 (m, 2H), 4.89 (dd, J = 7.2, 5.9 Hz, 1H), 2.66 – 2.52 (m, 2H); ^{13}C NMR (100 MHz, CDCl_3 , 25 $^\circ\text{C}$): δ = 141.2, 134.3, 133.2, 132.9, 128.2, 127.9, 127.6, 126.1, 125.8, 124.4, 124.0, 118.5, 73.3, 43.7;



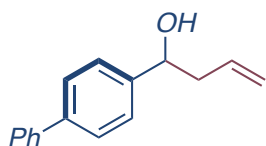
(3b): brown oil, 59% (0.12 mmol, 17 mg). The general procedure was applied using 1b (0.2 mmol, 20.4 μ L) and 2a (0.6 mmol, 64 μ L, 3 equiv.). The title compound was isolated by flash column chromatography (cyclohexane/ethyl acetate).

^1H -NMR (400 MHz, CDCl_3 , 25 $^\circ\text{C}$): δ = 7.36 – 7.12 (m, 5H), 5.86 – 5.74 (m, 1H), 5.18 – 5.11 (m, 2H), 4.72 (dd, J = 7.6, 5.4 Hz, 1H), 2.56 – 2.44 (m, 2H), 2.06 (br s, 1H); ^{13}C -NMR (100 MHz, CDCl_3 , 25 $^\circ\text{C}$): δ = 143.8, 134.4, 128.4 (2C), 127.5, 125.8 (2C), 118.4, 73.3, 43.8.



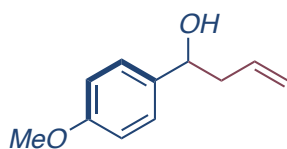
(3c): brown oil, 80% (0.16 mmol, 33 mg). The general procedure was applied using 1c (0.2 mmol, 33 μ L) and 2a (0.6 mmol, 64 μ L, 3 equiv.). The title compound was isolated by flash column chromatography (cyclohexane/ethyl acetate).

^1H -NMR (400 MHz, CDCl_3 , 25 $^\circ\text{C}$): δ = 7.37 (d, J = 8.3 Hz, 2H), 7.28 (d, J = 8.4 Hz, 2H), 5.82 (ddt, J = 17.1, 10.1, 7.1 Hz, 1H), 5.20 – 5.10 (m, 2H), 4.70 (t, J = 6.5 Hz, 1H), 2.57 – 2.44 (m, 2H), 1.32 (s, 9H); ^{13}C -NMR (100 MHz, CDCl_3 , 25 $^\circ\text{C}$): δ = 150.4, 140.9, 134.7, 125.5 (2C), 125.3 (2C), 118.1, 73.1, 43.6, 34.5, 31.3 (3C).



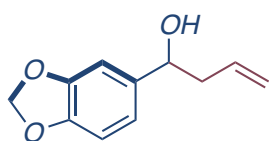
(3d): brown oil, 56% (0.11 mmol, 25 mg). The general procedure was applied using 1d (0.2 mmol, 36 mg) and 2a (0.6 mmol, 64 μ L, 3 equiv.). The title compound was isolated by flash column chromatography (cyclohexane/ethyl acetate).

$^1\text{H-NMR}$ (400 MHz, CDCl_3 , 25 $^\circ\text{C}$): δ = 7.60 – 7.56 (m, 4H), 7.45 – 7.41 (m, 4H), 7.36 – 7.30 (m, 1H), 5.89 – 5.79 (m, 1H), 5.22 – 5.15 (m, 2H), 4.78 (t, J = 5.4 Hz, 1H), 2.62 – 2.48 (m, 2H); $^{13}\text{C-NMR}$ (100 MHz, CDCl_3 , 25 $^\circ\text{C}$): δ = 142.9, 140.8, 140.5, 134.4, 128.7 (2C), 127.2, 127.1 (2C), 127.0 (2C), 126.2 (2C), 118.5, 73.02, 43.8.



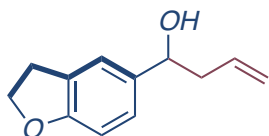
(3e): brown oil, 73% (0.15 mmol, 26 mg). The general procedure was applied using 1e (0.2 mmol, 24 μ L) and 2a (0.6 mmol, 64 μ L, 3 equiv.). The title compound was isolated by flash column chromatography (cyclohexane/ethyl acetate).

$^1\text{H-NMR}$ (400 MHz, CDCl_3 , 25 $^\circ\text{C}$): δ = 7.30 – 7.23 (m, 2H), 6.90 – 6.84 (m, 2H), 5.78 (ddt, J = 17.2, 10.2, 7.1 Hz, 1H), 5.17 – 5.08 (m, 2H), 4.67 (t, J = 6.5 Hz, 1H), 3.79 (s, 3H), 2.51 – 2.46 (m, 2H); $^{13}\text{C-NMR}$ (100 MHz, CDCl_3 , 25 $^\circ\text{C}$): δ = 159.0, 136.0, 134.6, 127.0 (2C), 118.2, 113.8 (2C), 73.0, 55.2, 43.7.



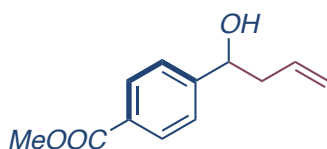
(3f): brown oil, 97% (0.19 mmol, 37 mg). The general procedure was applied using 1f (0.2 mmol, 38 mg) and 2a (0.6 mmol, 64 μ L, 3 equiv.). The title compound was isolated by flash column chromatography (cyclohexane/ethyl acetate).

$^1\text{H-NMR}$ (400 MHz, CDCl_3 , 25 $^\circ\text{C}$): δ = 6.85 (d, J = 1.5 Hz, 1H), 6.80 – 6.72 (m, 2H), 5.92 (s, 2H), 5.82 – 5.70 (m, 1H), 5.16 – 5.09 (m, 2H), 4.62 (t, J = 6.5 Hz, 1H), 2.48 – 2.42 (m, 2H); $^{13}\text{C-NMR}$ (100 MHz, CDCl_3 , 25 $^\circ\text{C}$): δ = 147.7, 146.8, 138.0, 134.4, 119.2, 118.3, 108.0, 106.4, 100.9, 73.2, 43.8.



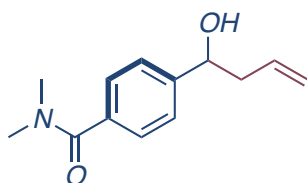
(3g): brown oil, 89% (0.18 mmol, 34 mg). The general procedure was applied using 1g (0.2 mmol, 24 μ L) and 2a (0.6 mmol, 64 μ L, 3 equiv.). The title compound was isolated by flash column chromatography (cyclohexane/ethyl acetate).

$^1\text{H-NMR}$ (400 MHz, CDCl_3 , 25 $^\circ\text{C}$): δ = 7.21 – 7.19 (m, 1H), 7.08 – 7.04 (m, 1H), 6.73 (d, J = 8.2 Hz, 1H), 5.79 (ddt, J = 17.2, 10.2, 7.1 Hz, 1H), 5.17 – 5.09 (m, 2H), 4.64 (t, J = 6.6 Hz, 1H), 4.55 (t, J = 8.7 Hz, 2H), 3.18 (t, J = 8.7 Hz, 2H), 2.50 – 2.44 (m, 2H); $^{13}\text{C-NMR}$ (100 MHz, CDCl_3 , 25 $^\circ\text{C}$): δ = 159.6, 136.1, 134.7, 127.2, 125.8, 122.5, 118.1, 108.9, 73.3, 71.3, 43.8, 29.7.



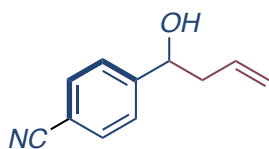
(3h): brown oil, 32% (0.06 mmol, 13 mg). The general procedure was applied using 1h (0.2 mmol, 33 mg) and 2a (0.6 mmol, 64 μ L, 3 equiv.). The title compound was isolated by flash column chromatography (cyclohexane/ethyl acetate).

$^1\text{H-NMR}$ (400 MHz, CDCl_3 , 25 $^\circ\text{C}$): δ = 8.00 (dt, J = 8.4, 1.9 Hz, 1H), 7.44 – 7.40 (m, 2H), 5.83 – 5.71 (m, 1H), 5.19 – 5.15 (m, 1H), 5.15 – 5.12 (m, 1H), 4.80 (ddd, J = 8.0, 4.8, 3.6 Hz, 1H), 3.90 (s, 3H), 2.58 – 2.40 (m, 2H); $^{13}\text{C-NMR}$ (100 MHz, CDCl_3 , 25 $^\circ\text{C}$): δ = 166.8, 148.9, 133.8, 129.7 (2C), 129.3, 125.7 (2C), 119.0, 72.7, 52.0, 43.8.



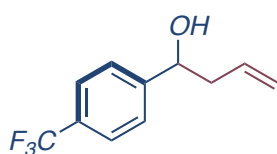
(3i): brown oil, 28% (0.06 mmol, 12 mg). The general procedure was applied using 1i (0.2 mmol, 35 mg) and 2a (0.6 mmol, 64 μ L, 3 equiv.). The title compound was isolated by flash column chromatography (cyclohexane/ethyl acetate).

$^1\text{H-NMR}$ (400 MHz, CDCl_3 , 25 $^\circ\text{C}$): δ = 7.39 – 7.34 (m, 4H), 5.77 (dddd, J = 17.0, 10.3, 7.6, 6.6 Hz, 1H), 5.17 – 5.11 (m, 2H), 4.74 (dd, J = 7.7, 5.0 Hz, 1H), 3.08 (s, 3H), 2.95 (s, 3H), 2.55 – 2.40 (m, 2H); $^{13}\text{C-NMR}$ (100 MHz, CDCl_3 , 25 $^\circ\text{C}$): δ = 171.4, 145.3, 135.4, 134.0, 127.2 (2C), 125.7 (2C), 118.7, 72.8, 43.8, 39.6, 39.5.



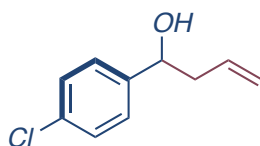
(3j): brown oil, 26% (0.05 mmol, 9 mg). The general procedure was applied using 1j (0.2 mmol, 39 mg) and 2a (0.6 mmol, 64 μ L, 3 equiv.). The title compound was isolated by flash column chromatography (cyclohexane/ethyl acetate).

$^1\text{H-NMR}$ (400 MHz, CDCl_3 , 25°C): δ = 7.58 (d, J = 8.4 Hz, 2H), 7.43 (d, J = 8.5 Hz, 2H), 5.79 – 5.67 (m, 1H), 5.14 – 5.08 (m, 2H), 4.76 (dd, J = 7.7, 4.9 Hz, 1H), 2.54 – 2.36 (m, 2H); $^{13}\text{C-NMR}$ (100 MHz, CDCl_3 , 25°C): δ = 149.2, 133.3, 132.1 (2C), 126.4 (2C), 119.2, 118.7, 110.9, 72.3, 43.6.



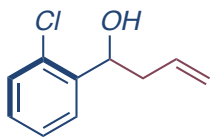
(3k): brown oil, 66% (0.13 mmol, 28 mg). The general procedure was applied using 1k (0.2 mmol, 27 μ L) and 2a (0.6 mmol, 64 μ L, 3 equiv.). The title compound was isolated by flash column chromatography (cyclohexane/ethyl acetate).

$^1\text{H-NMR}$ (400 MHz, CDCl_3 , 25°C): δ = 7.59 (d, J = 8.2 Hz, 2H), 7.46 (d, J = 8.1 Hz, 2H), 5.83 – 5.71 (m, 1H), 5.18 (m, 1H), 5.16 – 5.13 (m, 1H), 4.78 (dd, J = 7.9, 4.8 Hz, 1H), 2.57 – 2.40 (m, 2H), 2.19 (br s, 1H); $^{13}\text{C-NMR}$ (100 MHz, CDCl_3 , 25°C): δ = 147.7, 133.7, 129.7 (q, J = 32.4 Hz), 126.1 (2C), 125.3 (q, J = 3.6 Hz), 124.3 (q, J = 272.1 Hz), 119.2 (2C), 72.5, 43.9; $^{19}\text{F-NMR}$ (377 MHz, CDCl_3 , 25°C): δ = -61.28.



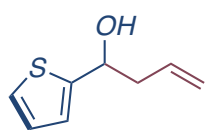
(3l): brown oil, 70% (0.14 mmol, 15 mg). The general procedure was applied using 1l (0.2 mmol, 28 mg) and 2a (0.6 mmol, 64 μ L, 3 equiv.). The title compound was isolated by flash column chromatography (cyclohexane/ethyl acetate).

$^1\text{H-NMR}$ (400 MHz, CDCl_3 , 25°C): δ = 7.32 – 7.25 (m, 4H), 5.82 – 5.71 (m, 1H), 5.17 – 5.14 (m, 1H), 5.12 (m, 1H), 4.70 (dd, J = 7.8, 5.1 Hz, 1H), 2.53 – 2.39 (m, 2H); $^{13}\text{C-NMR}$ (100 MHz, CDCl_3 , 25°C): δ = 142.2, 133.9, 133.1, 128.5 (2C), 127.2 (2C), 118.8, 72.5, 43.8.



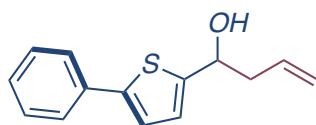
(3m): brown oil, 58% (0.12 mmol, 21 mg). The general procedure was applied using 1m (0.2 mmol, 22.4 μ L) and 2a (0.6 mmol, 64 μ L, 3 equiv.). The title compound was isolated by flash column chromatography (cyclohexane/ethyl acetate).

$^1\text{H-NMR}$ (400 MHz, CDCl_3 , 25 $^\circ\text{C}$): δ = 7.55 (dd, J = 7.7, 1.3 Hz, 1H), 7.34 – 7.16 (m, 3H), 5.91 – 5.80 (m, 1H), 5.20 – 5.13 (m, 3H), 2.66 – 2.59 (m, 1H), 2.42 – 2.32 (m, 1H); $^{13}\text{C-NMR}$ (100 MHz, CDCl_3 , 25 $^\circ\text{C}$): δ = 141.1, 134.2, 131.7, 129.4, 128.4, 127.04, 126.99, 118.7, 69.6, 42.0.



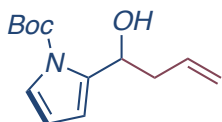
(3n): brown oil, 63% (0.13 mmol, 19 mg). The general procedure was applied using 1n (0.2 mmol, 39 mg) and 2a (0.6 mmol, 64 μ L, 3 equiv.). The title compound was isolated by flash column chromatography (cyclohexane/ethyl acetate).

$^1\text{H-NMR}$ (400 MHz, CDCl_3 , 25 $^\circ\text{C}$): δ = 7.29 (dd, J = 5.0, 3.0 Hz, 1H), 7.19 (d, J = 2.9 Hz, 1H), 7.07 (dd, J = 5.0, 1.2 Hz, 1H), 5.86 – 5.73 (m, 1H), 5.22 – 5.10 (m, 2H), 4.83 (dt, J = 8.0, 4.2 Hz, 1H), 2.61 – 2.46 (m, 2H); $^{13}\text{C-NMR}$ (100 MHz, CDCl_3 , 25 $^\circ\text{C}$): δ = 145.3, 134.2, 126.0, 125.6, 120.7, 118.5, 69.5, 43.0.



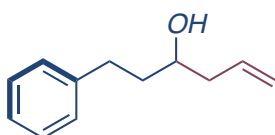
(3o): brown oil, 52% (0.10 mmol, 24 mg). The general procedure was applied using 1o (0.2 mmol, 38 mg) and 2a (0.6 mmol, 64 μ L, 3 equiv.). The title compound was isolated by flash column chromatography (cyclohexane/ethyl acetate).

$^1\text{H-NMR}$ (400 MHz, CDCl_3 , 25 $^\circ\text{C}$): δ = 7.57 (d, J = 8.1, 2H), 7.38 – 7.33 (m, 2H), 7.27 (d, J = 7.2 Hz, 1H), 7.15 (d, J = 3.6 Hz, 1H), 6.93 (d, J = 3.6 Hz, 1H), 5.85 (ddt, J = 17.2, 10.2, 7.1 Hz, 1H), 5.25 – 5.15 (m, 2H), 4.96 (t, J = 6.3 Hz, 1H), 2.70 – 2.58 (m, 2H), 2.20 (br s, 1H); $^{13}\text{C-NMR}$ (100 MHz, CDCl_3 , 25 $^\circ\text{C}$): δ = 147.2, 143.5, 134.4, 133.7, 128.8 (2C), 127.4, 125.7 (2C), 124.6, 122.5, 118.9, 69.5, 43.6.



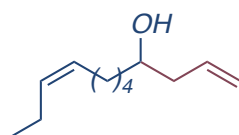
(3p): brown oil, 67% (0.14 mmol, 33 mg). The general procedure was applied using 1p (0.2 mmol, 39 mg) and 2a (0.6 mmol, 64 μ L, 3 equiv.). The title compound was isolated by flash column chromatography (cyclohexane/ethyl acetate).

$^1\text{H-NMR}$ (400 MHz, CDCl_3 , 25°C): δ = 7.14 (dd, J = 3.4, 1.7 Hz, 1H), 6.20 – 6.18 (m, 1H), 6.08 (t, J = 3.4 Hz, 1H), 5.90 (ddt, J = 17.1, 10.2, 6.9 Hz, 1H), 5.17 – 5.04 (m, 2H), 4.93 (t, J = 6.4 Hz, 1H), 3.94 (br s, 1H), 2.68 – 2.62 (m, 2H), 1.59 (s, 9H); $^{13}\text{C-NMR}$ (100 MHz, CDCl_3 , 25°C): δ = 150.2, 137.5, 135.3, 121.9, 116.9, 111.7, 110.2, 84.5, 66.2, 39.2, 28.0 (3C).



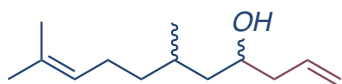
(3q): brown oil, 60% (0.12 mmol, 21 mg). The general procedure was applied using 4e (0.2 mmol, 26 μ L) previously distilled and 2a (0.6 mmol, 64 μ L, 3 equiv.). The title compound was isolated by flash column chromatography (cyclohexane/ethyl acetate).

$^1\text{H-NMR}$ (400 MHz, CDCl_3 , 25°C): δ = 7.29 – 7.14 (m, 5H), 5.86 – 5.76 (m, 1H), 5.16 – 5.10 (m, 2H), 3.67 (ddd, J = 12.2, 7.6, 4.7 Hz, 1H), 2.84 – 2.75 (m, 1H), 2.72 – 2.64 (m, 1H), 2.35 – 2.28 (m, J = 12.2, 6.9, 4.3, 1.3 Hz, 1H), 2.24 – 2.12 (m, 1H), 1.81 – 1.75 (m, 2H), 1.61 (br s, 1H); $^{13}\text{C-NMR}$ (100 MHz, CDCl_3 , 25°C): δ = 142.0, 134.6, 128.4 (2C), 128.4 (2C), 125.8, 118.3, 69.9, 42.0, 38.4, 32.0.



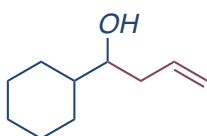
(3r): yellow oil, 42%. (0.08 mmol, 14 mg). The general procedure was applied using 4b (0.2 mmol, 34 μ L) freshly distilled at 68°C/13 mbar and 2a (0.6 mmol, 64 μ L, 3 equiv.). The title compound was isolated by flash column chromatography (cyclohexane/ethyl acetate).

$^1\text{H-NMR}$ (400 MHz, CDCl_3 , 25°C): δ = 5.81 (dddd, J = 12.5, 9.6, 7.6, 6.4 Hz, 1H), 5.38-5.26 (m, 2H), 5.14-5.08 (m, 2H), 3.66-3.60 (m, 1H), 2.32-2.24 (m, 1H), 2.16-2.10 (m, 1H), 1.98 (m, 5H), 1.56 (br s, 1H), 1.49-1.29 (m, 7H), 0.94 (t, J = 7.5 Hz, 3H); $^{13}\text{C-NMR}$ (100 MHz, CDCl_3 , 25°C): δ = 134.8, 131.7, 128.9, 118.0, 70.6, 41.9, 36.7, 29.7, 27.0, 25.2, 20.5, 14.3.



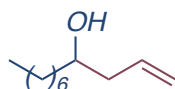
(3s): colorless oil, 54% (0.11 mmol, 21 mg) as a mixture of syn and anti diastereomers. The general procedure was applied using 1c (0.2 mmol, 38 μ L) and 2a (0.6 mmol, 64 μ L, 3 equiv.). The title compound was isolated by flash column chromatography (cyclohexane/ethyl acetate).

$^1\text{H-NMR}$ (400 MHz, CDCl_3 , 25 $^\circ\text{C}$) mixture of diastereoisomers: δ = 5.86 – 5.76 (m, 1H), 5.13 – 5.03 (m, 3H), 3.76 – 3.70 (m, 1H), 2.31 – 2.22 (m, 1H), 2.16 – 2.04 (m, 1H), 2.04 – 1.87 (m, 2H), 1.66 (s, 3H), 1.69 – 1.55 (m, 2H), 1.58 (s, 3H), 1.51 – 1.05 (m, 4H), 0.90 (dd, J = 6.4, 6.4 Hz, 3H); $^{13}\text{C-NMR}$ (100 MHz, CDCl_3 , 25 $^\circ\text{C}$) mixture of diastereoisomers: δ = 134.9, 134.8, 131.2, 124.7, 118.1, 118.0, 68.7, 68.3, 44.3, 44.2, 42.8, 42.1, 37.8, 36.7, 29.3, 28.9, 25.7, 25.4, 25.3, 20.2, 19.1, 17.6.



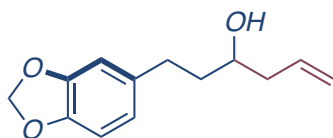
(3t): brown oil, 25% (0.05 mmol, 8 mg). The general procedure was applied using 1d (0.2 mmol, 24 μ L) freshly distilled at 44 $^\circ\text{C}$ /27 mbar and 2a (0.6 mmol, 64 μ L, 3 equiv.). The title compound was isolated by flash column chromatography (cyclohexane/ethyl acetate).

$^1\text{H-NMR}$ (400 MHz, CDCl_3 , 25 $^\circ\text{C}$): δ = 5.82 (dddd, J = 12.5, 9.2, 8.0, 6.4 Hz, 1H), 5.15 – 5.09 (m, 2H), 3.39-3.35 (m, 1H), 2.35-2.28 (m, 1H), 2.11 (dt, J = 14, 8.4 Hz, 1H), 1.84 (d, J = 12.6 Hz, 1H), 1.77-1.63 (m, 4H), 1.54 (d, J = 16 Hz, 1H), 1.38-0.95 (m, 6H); $^{13}\text{C-NMR}$ (100 MHz, CDCl_3 , 25 $^\circ\text{C}$): δ = 135.4, 117.9, 74.7, 43.0, 38.8, 29.1, 28.1, 26.5, 26.2, 26.1.



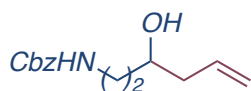
(3u): brown oil, 68% (0.14 mmol, 24 mg). The general procedure was applied using 4a (0.2 mmol, 31 μ L) freshly distilled at 59 $^\circ\text{C}$ /21 mbar and 2a (0.6 mmol, 64 μ L, 3 equiv.). The title compound was isolated by flash column chromatography (cyclohexane/ethyl acetate).

$^1\text{H-NMR}$ (400 MHz, CDCl_3 , 25 $^\circ\text{C}$): δ = 5.86 – 5.75 (m, 1H), 5.13 – 5.08 (m, 2H), 3.63 (ddt, J = 9.7, 7.8, 4.9 Hz, 1H), 2.36 – 2.24 (m, 2H), 2.16 – 2.08 (m, 2H), 2.03 (br s, 1H), 1.63 – 1.20 (m, 10H), 0.85 (dd, J = 6.8, 5.9 Hz, 3H); $^{13}\text{C-NMR}$ (100 MHz, CDCl_3 , 25 $^\circ\text{C}$): δ = 134.9, 118.0, 70.7, 41.9, 36.8, 31.8, 29.6, 29.3, 25.7, 22.6, 14.1.



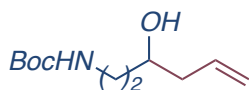
(3v): brown oil, 48% (0.10 mmol, 21 mg). The general procedure was applied using 4f (0.2 mmol, 36 mg) previously synthesized and 2a (0.6 mmol, 64 μ L, 3 equiv.). The title compound was isolated by flash column chromatography (cyclohexane/ethyl acetate).

$^1\text{H-NMR}$ (400 MHz, CDCl_3 , 25°C): δ = 6.72 (s, 1H), 6.69 (d, J = 7.8 Hz, 1H), 6.63 (d, J = 7.9 Hz, 1H), 5.90 (s, 2H), 5.85 – 5.74 (m, 1H), 5.15 – 5.10 (m, 2H), 3.67 – 3.61 (m, 1H), 2.65 (ddt, J = 30.1, 13.9, 7.9 Hz, 2H), 2.33 – 2.26 (m, 1H), 2.15 (dt, J = 7.9, 4.3 Hz, 1H), 1.75 – 1.69 (m, 2H), 1.59 (br s, 1H); $^{13}\text{C-NMR}$ (100 MHz, CDCl_3 , 25°C): δ = 147.5, 145.6, 135.8, 134.5, 121.1, 118.3, 108.9, 108.1, 100.7, 69.7, 42.1, 38.6, 31.7.



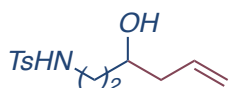
(3w): yellow oil, 59% (0.12 mmol, 29 mg). The general procedure was applied using 4g (0.2 mmol, 41 mg) previously synthesized and 2a (0.6 mmol, 64 μ L, 3 equiv.). The title compound was isolated by flash column chromatography (cyclohexane/ethyl acetate).

$^1\text{H-NMR}$ (400 MHz, CDCl_3 , 25°C): δ = 7.36 – 7.27 (m, 5H), 5.79 (dt, J = 16.8, 7.3 Hz, 1H), 5.21 – 5.04 (m, 5H), 3.72 – 3.66 (m, 1H), 3.52 – 3.44 (m, 1H), 3.21 (dt, J = 19.3, 5.3 Hz, 1H), 2.60 (br s, OH), 2.28 – 2.15 (m, 2H), 1.67 (dddd, J = 14.2, 8.7, 5.6, 3.1 Hz, 1H), 1.52 (ddd, J = 14.6, 10.6, 5.4 Hz, 1H); $^{13}\text{C-NMR}$ (100 MHz, CDCl_3 , 25°C): δ = 157.0, 136.5, 134.5, 128.5 (2C), 128.1 (3C), 118.1, 68.5, 66.7, 41.9, 38.1, 36.6.



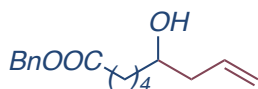
(3x): yellow oil, 42% (0.09 mmol, 20 mg). The general procedure was applied using 4h (0.22 mmol, 39 mg) previously synthesized and 2a (0.6 mmol, 64 μ L, 3 equiv.). The title compound was isolated by flash column chromatography (cyclohexane/ethyl acetate).

$^1\text{H-NMR}$ (400 MHz, CDCl_3 , 25°C): δ = 5.86 – 5.75 (m, 1H), 5.12 – 5.07 (m, 2H), 4.87 (br s, 1H), 3.71 – 3.64 (m, 1H), 3.46 – 3.36 (m, 1H), 3.15 – 3.07 (m, 1H), 2.93 (br s, 1H), 2.28 – 2.16 (m, 2H), 1.67 – 1.36 (m, 2H), 1.41 (s, 9H); $^{13}\text{C-NMR}$ (100 MHz, CDCl_3 , 25°C): δ = 156.9, 134.8, 117.8, 79.4, 68.3, 41.8, 37.4, 37.0, 28.4 (3C).



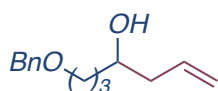
(3y): brown oil, 54% (0.09 mmol, 25 mg). The general procedure was applied using 4i (pur. 70%, 0.2 mmol, 56 mg) previously synthesized and 2a (0.6 mmol, 64 μ L, 3 equiv.). The title compound was isolated by flash column chromatography (cyclohexane/ethyl acetate).

$^1\text{H-NMR}$ (400 MHz, CDCl_3 , 25 $^\circ\text{C}$): δ = 7.72 (d, J = 8.3 Hz, 2H), 7.32 – 7.25 (m, 2H), 5.71 (dddd, J = 16.9, 10.3, 7.9, 6.5 Hz, 1H), 5.22 (br s, 1H), 5.13 – 5.05 (m, 2H), 3.72 (ddd, J = 12.3, 7.8, 4.4 Hz, 1H), 3.16 (dtd, J = 12.5, 7.5, 4.9 Hz, 1H), 3.00 (ddt, J = 12.2, 7.1, 4.9 Hz, 1H), 2.40 (s, 3H), 2.25 – 2.16 (m, 1H), 2.13 – 2.05 (m, 1H), 2.01 (br s, 1H), 1.66 (dddd, J = 14.4, 7.8, 5.0, 3.0 Hz, 1H), 1.52 (dddd, J = 14.3, 9.3, 7.1, 4.9 Hz, 1H); $^{13}\text{C-NMR}$ (100 MHz, CDCl_3 , 25 $^\circ\text{C}$): δ = 143.3, 136.9, 133.9, 129.6 (2C), 127.1 (2C), 118.8, 69.5, 42.0, 41.0, 35.2, 21.5.



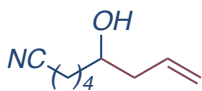
(3z): yellow oil, 46% (0.10 mmol, 25 mg). The general procedure was applied using 4j (0.2 mmol, 46 mg) previously synthesized and 2a (0.6 mmol, 64 μ L, 3 equiv.). The title compound was isolated by flash column chromatography (cyclohexane/ethyl acetate).

$^1\text{H-NMR}$ (400 MHz, CDCl_3 , 25 $^\circ\text{C}$): δ = 7.37 – 7.28 (m, 5H), 5.79 (dddd, J = 21.1, 9.4, 7.9, 6.5 Hz, 1H), 5.13 – 5.07 (m, 4H), 3.64 – 3.58 (m, 1H), 2.36 (t, J = 7.5 Hz, 2H), 2.26 (dddt, J = 12.1, 6.8, 4.2, 1.3 Hz, 1H), 2.14 – 2.06 (m, 1H), 1.74 – 1.30 (m, 7H); $^{13}\text{C-NMR}$ (100 MHz, CDCl_3 , 25 $^\circ\text{C}$): δ = 173.4, 136.0, 134.7, 128.5 (2C), 128.16 (2C), 128.15, 118.1, 70.3, 66.1, 41.9, 36.3, 34.2, 25.1, 24.8.



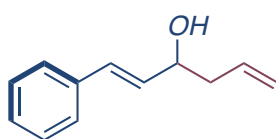
(3aa): yellow oil, 69% (0.14 mmol, 30 mg). The general procedure was applied using 4k (0.2 mmol, 36 mg) previously synthesized and 2a (0.6 mmol, 64 μ L, 3 equiv.). The title compound was isolated by flash column chromatography (cyclohexane/ethyl acetate).

$^1\text{H-NMR}$ (400 MHz, CDCl_3 , 25 $^\circ\text{C}$): δ = 7.35 – 7.25 (m, 5H), 5.87 – 5.76 (m, 1H), 5.13 – 5.08 (m, 2H), 4.50 (s, 2H), 3.68 – 3.62 (m, 1H), 3.50 (t, J = 6.0 Hz, 2H), 2.35 (br s, 1H), 2.30 – 2.11 (m, 2H), 1.81 – 1.59 (m, 3H), 1.48 (ddd, J = 14.3, 11.1, 7.2 Hz, 1H); $^{13}\text{C-NMR}$ (100 MHz, CDCl_3 , 25 $^\circ\text{C}$): δ = 138.2, 135.0, 128.4 (2C), 127.7 (2C), 127.6, 117.7, 73.0, 70.5, 70.4, 42.0, 34.0, 26.2.



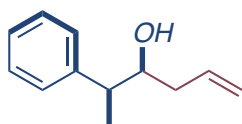
(3ab): yellow oil, 38% (0.08 mmol, 13 mg). The general procedure was applied using 4l (pur. 74%, 0.2 mmol, 33 mg) previously synthesized and 2a (0.6 mmol, 64 μ L, 3 equiv.). The title compound was isolated by flash column chromatography (cyclohexane/ethyl acetate).

$^1\text{H-NMR}$ (400 MHz, CDCl_3 , 25°C): δ = 5.84 – 5.74 (m, 1H), 5.15 – 5.10 (m, 2H), 3.64 (tt, J = 8.5, 4.3 Hz, 1H), 2.34 (t, J = 7.0 Hz, 2H), 2.32 – 2.25 (m, 1H), 2.16 – 2.09 (m, 1H), 1.75 – 1.40 (m, 7H); $^{13}\text{C-NMR}$ (100 MHz, CDCl_3 , 25°C): δ = 134.4, 119.6, 118.4, 70.1, 42.0, 35.7, 25.4, 24.8, 17.1.



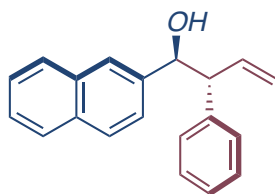
(3ac): yellow oil, 43%. (0.09 mmol, 15 mg). The general procedure was applied using 1m (0.2 mmol, 26 μ L) and 2a (0.6 mmol, 64 μ L, 3 equiv.). The title compound was isolated by flash column chromatography (cyclohexane/ethyl acetate).

$^1\text{H-NMR}$ (400 MHz, CDCl_3 , 25°C): δ = 7.39 – 7.35 (m, 2H), 7.33 – 7.27 (m, 2H), 7.25 – 7.20 (m, 1H), 6.60 (d, J = 16.0 Hz, 1H), 6.23 (dd, J = 15.9, 6.3 Hz, 1H), 5.90 – 5.79 (m, 1H), 5.21 – 5.13 (m, 2H), 4.39 – 4.31 (m, 1H), 2.48 – 2.32 (m, 2H); $^{13}\text{C-NMR}$ (100 MHz, CDCl_3 , 25°C): δ = 136.6, 134.0, 131.5, 130.3, 128.5 (2C), 127.6, 126.4 (2C), 118.5, 71.7, 42.0.



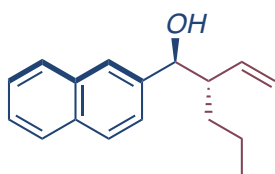
(3ad): yellow oil, 30% with syn:anti dr of 3:1 (0.06 mmol, 11 mg). The general procedure was applied using 1n (0.2 mmol, 26 μ L) freshly distilled at 52°C/3 mbar and 2a (0.6 mmol, 64 μ L, 3 equiv.). The title compound was isolated by flash column chromatography (cyclohexane/ethyl acetate).

$^1\text{H-NMR}$ (400 MHz, CDCl_3 , 25°C): δ = 7.38 – 7.18 (m, 5H), 5.93 – 5.83 (m, 1H anti), 5.84 – 5.73 (m, 1H), 5.14 – 5.06 (m, 2H), 3.76 – 3.68 (m, 1H), 2.83 – 2.73 (m, 1H), 2.41 – 2.33 (m, 1H anti), 2.22 – 2.14 (m, 1H), 2.15 – 2.07 (m, 1H from minor isomer), 2.06 – 1.98 (m, 1H), 1.63 (s, 2H), 1.34 (d, J = 7.0 Hz, 3H), 1.29 (d, J = 7.1 Hz, 1H from minor isomer); $^{13}\text{C-NMR}$ (100 MHz, CDCl_3 , 25°C): δ = 144.4, 143.2, 135.04, 135.00, 128.48, 128.46 (2C), 128.1, 127.7 (2C), 126.6, 126.4, 118.1, 117.7, 74.99, 74.97, 45.4, 39.5, 38.9, 29.7, 17.7, 16.4; major isomer: δ = 144.4, 135.04, 128.46 (2C), 127.7 (2C), 126.4, 118.1, 74.97, 45.4, 39.5, 16.4.



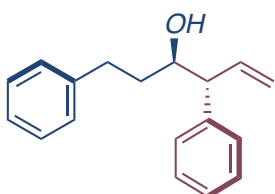
(4a): brown oil, 40% (0.08 mmol, 22 mg) with 6a as the major isomer (6a:6a' > 99:1, d.r. 6:1) The general procedure was applied using 1a (0.2 mmol, 36 mg) and 2b (0.6 mmol, 106 mg, 3 equiv.). The title compound was isolated by flash column chromatography (cyclohexane/ethyl acetate).

¹H-NMR (400 MHz, CDCl₃, 25°C) major diastereoisomer: δ = 7.79 – 7.66 (m, 3H), 7.61 (s, 1H), 7.44 – 7.40 (m, 2H), 7.30 – 7.23 (m, 2H), 7.21 – 7.05 (m, 4H), 6.36 – 6.22 (m, 1H), 5.33 – 5.17 (m, 2H), 5.02 (dd, J = 7.5, 1.6 Hz, 1H), 3.67 (t, J = 8.2 Hz, 1H), 2.46 (bs, 1H); ¹³C-NMR (100 MHz, CDCl₃, 25°C) δ = 140.6, 139.4, 137.7, 133.0, 132.9, 128.4, 128.3, 127.9, 127.5 (2C), 126.6, 125.8, 125.7 (2C), 124.7, 118.5, 77.3, 59.0.



(4b): brown oil, 56% (0.11 mmol, 25 mg) with 6b as the major isomer (6b:6b' > 99:1, d.r. 1:1). The general procedure was applied using 1a (0.2 mmol, 36 mg) and 2c (0.6 mmol, 85 mg, 3 equiv.). The title compound was isolated by flash column chromatography (cyclohexane/ethyl acetate).

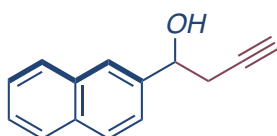
¹H-NMR (400 MHz, CDCl₃, 25°C) mixture of diastereoisomer: δ = 7.79 (m, 8H), 7.51 – 7.36 (m, 6H), 5.69 (ddd, J = 17.1, 10.2, 9.2 Hz, 1H), 5.55 (ddd, J = 17.1, 10.3, 9.1 Hz, 1H), 5.31 – 5.16 (m, 2H), 5.11 – 4.97 (m, 2H), 4.82 – 4.74 (m, 1H), 4.54 (dd, J = 8.0, 1.5 Hz, 1H), 2.51 (m, 1H), 2.41 (m, 1H), 1.45 – 1.03 (m, 8H), 0.85 (t, J = 7.2 Hz, 3H), 0.75 (t, J = 7.1 Hz, 3H); ¹³C-NMR (100 MHz, CDCl₃, 25°C) δ = 140.1, 140.0, 139.3, 138.6, 133.2, 133.1, 133.0, 132.9, 128.0, 127.95, 127.93, 127.7, 127.6, 126.1, 126.0, 125.8, 125.7, 125.5, 124.8, 124.7, 118.8, 117.3, 77.1, 76.8, 52.4, 51.1, 32.6, 31.7, 20.4, 20.3, 14.0, 13.9.



(4c): brownish oil, 42% (0.08 mmol, 21 mg) with 6c as the major isomer (6c:6c' > 99:1, d.r. 3:1). The general procedure was applied using 4e (0.2 mmol, 26 μ L) previously distilled and 2b (0.6 mmol, 106 mg, 3 equiv.) previously synthesized. The title compound was isolated by flash column chromatography (cyclohexane/ethyl acetate).

272

$^1\text{H-NMR}$ (400 MHz, CDCl_3 , 25°C): $\delta = 7.35 - 7.04$ (m, 10H), 6.25 (ddd, $J = 17.1, 10.2, 8.9$ Hz, 1H from minor isomer), 6.10 (ddd, $J = 16.7, 10.4, 9.2$ Hz, 1H), 6.00 (dd, $J = 18.5, 8.8$ Hz, 1H from minor isomer), 5.24 – 5.17 (m, 2H), 5.14 – 5.08 (m, 1H from minor isomer), 3.88 (t, $J = 8.8$ Hz, 1H from minor isomer), 3.82 – 3.77 (m, 1H), 3.55 (dd, $J = 12.4, 4.4$ Hz, 1H from minor isomer), 3.33 (dd, $J = 12.4, 4.4$ Hz, 1H from minor isomer), 3.29 – 3.23 (m, 1H), 2.86 – 2.78 (m, 1H + 1H from minor isomer), 2.61 (ddd, $J = 13.8, 9.6, 7.1$ Hz, 1H + m, 1H from minor isomer), 1.87 (br s, 1H), 1.73 – 1.58 (m, 2H); $^{13}\text{C-NMR}$ (100 MHz, CDCl_3 , 25°C) major diastereoisomer: $\delta = 142.0, 141.3, 138.3, 128.7, 128.4, 128.3, 127.9, 126.7, 118.0, 77.3, 76.7, 73.2, 57.5, 36.0, 32.0$.



(5a): yellowish oil, 41% (0.08 mmol, 14 mg). The general procedure was applied using 1a (0.2 mmol, 28 mg) and 2d (80 wt. % in toluene 0.6 mmol, 67 μL , 3 equiv.). The title compound was isolated by flash column chromatography (cyclohexane/ethyl acetate).

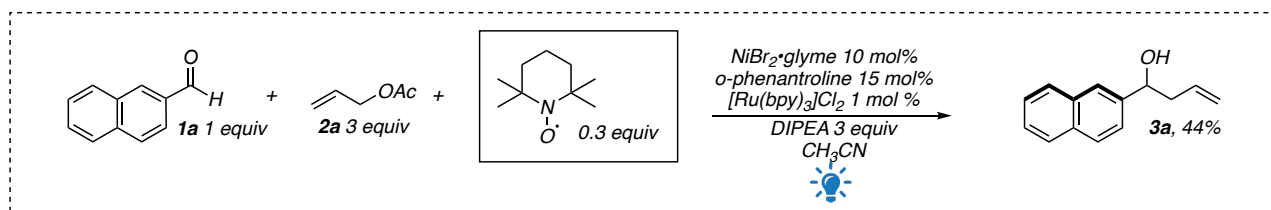
$^1\text{H-NMR}$ (400 MHz, CDCl_3 , 25°C): $\delta = 7.94 - 7.71$ (m, 4H), 7.54 – 7.40 (m, 3H), 5.04 (t, $J = 6.3$ Hz, 1H), 2.79 – 2.65 (m, 2H), 2.49 (bs, 1H), 2.08 (t, $J = 2.6$ Hz, 1H); $^{13}\text{C-NMR}$ (100 MHz, CDCl_3 , 25°C): $\delta = 139.9, 133.3, 133.2, 128.5, 128.2, 127.8, 126.4, 126.2, 124.8, 123.8, 80.7, 72.6, 71.3, 29.6$.

Procedure for the allylation reaction with Ni(COD)₂

A dry 10 mL Schlenk tube, equipped with a Rotaflo stopcock, magnetic stirring bar and an argon supply tube, was first charged in glove box with the Ni(COD)₂ (0.1 mmol, 28 mg) and phenanthroline (0.1 mmol, 20 mg). Dry ACN (1 mL) and allyl acetate 2a (0.12 mmol, 12 mg, 13 μ L) were then added. After 10 min aldehyde 1a (0.1 mmol, 16 mg) was added and the reaction was stirred for 24h. After that the reaction mixture was quenched with HCl 1M (approx. 1 mL) and extracted with AcOEt (4 x 3 mL). The combined organic layers were dried over anhydrous Na₂SO₄ and the solvent was removed under reduced pressure. The crude was purified by flash column chromatography (SiO₂) to afford the product 3a in 70% yield (0.07 mmol, 14 mg). The test without ligand and DIPEA was performed using the same procedure reported above and no product was observed.

Further mechanistic studies

Reaction in the presence of radical scavenger TEMPO. Reaction was conducted using typical procedure on 0.1 mmol scale.



4.2 Enantioselective Photoredox Allylation of Aldehydes Catalytic in Nickel³⁰³

• Optimization of the reaction conditions

After having optimized the racemic version of the process with satisfactory results and having obtained a complete and detailed picture of the mechanism of the reaction, we focused our attention on the development of an enantioselective variant of the process.

We started our optimization moving from the replacement of o-phenanthroline with a chiral ligand whose characteristics were known to be suitable for an enantioselective nickel catalyzed transformation, unchanging the other reaction parameters.³⁰⁴

Following the experimental evidence disclosed for the non-asymmetrical protocol, our attention was mainly focused on bidentate nitrogen-based chiral ligands. In this regard many ligands were tested under the optimized reaction conditions.³⁰⁵ As can be seen in the table, ligands belonging to different commonly used classes were considered evaluating the effect of different decorations on the molecular scaffolds.

³⁰³ The results and the procedures described in this section are part of a published work:

Calogero, F.; Potenti, S.; Bassan, E.; Fermi, A.; Gualandi, A.; Monaldi, J.; Dereli, B.; Maity, B.; Cavallo, L.; Ceroni, P.; Giorgio Cozzi, P. Nickel-Mediated Enantioselective Photoredox Allylation of Aldehydes with Visible Light. *Angew. Chem. Int. Ed.* **2022**. <https://doi.org/10.1002/anie.202114981>

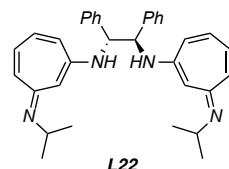
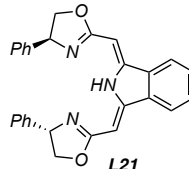
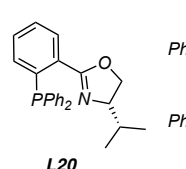
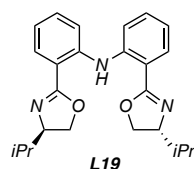
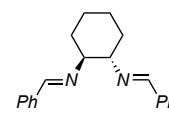
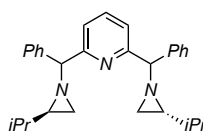
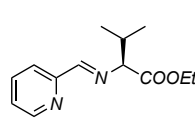
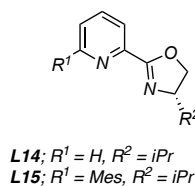
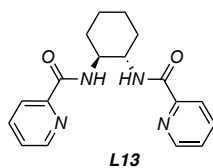
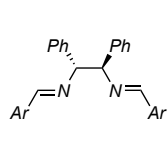
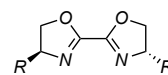
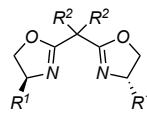
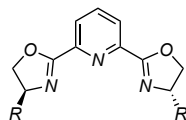
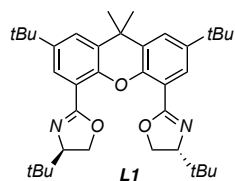
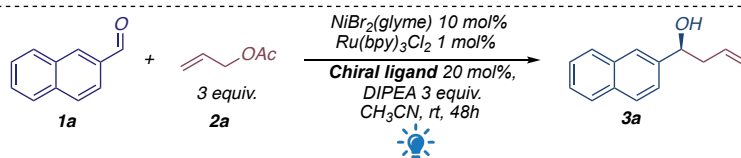
E.B. and A.F. carried out the photophysical investigations, supervised by C.P.

B.M. and B.D. carried out the computational investigations, supervised by L.C.

The complete characterization of the products introduced hereafter and discussed in the section “Supplementary Data” can be found in the Supporting Information of the above-mentioned work

³⁰⁴ Poremba, K. E.; Dibrell, S. E.; Reisman, S. E. Nickel-Catalyzed Enantioselective Reductive Cross-Coupling Reactions. *ACS Catal.* **2020**, *10* (15), 8237–8246. <https://doi.org/10.1021/acscatal.0c01842>.

³⁰⁵ Dr. Andrea Gualandi and by Jacopo Monaldi of our research group are kindly acknowledged for their contribution on the preliminary investigation.



Entry ^[a]	Ligand	Yield (%) ^[b]	ee (%) ^[c]
1	L1	47	4
2	L2	37	27
3	L3	16	27
4	L4	12	36
5	L5	0	-
6	L6	40	25
7	L7	55	3
8	L8	36	5
9	L9	50	44
10	L10	44	3
11	L11	56	2
12 ^[d]	L12	70	0
13 ^[d]	L13	0	-
14 ^[d]	L14	14	10
15 ^[d]	L15	8	0
16	L16	0	-
17	L17	29	0
18	L18	7	0
19	L19	0	-
20	L20	16	0
21	L21	0	-
22	L22	0	-

Table 4.2.1 Preliminary enantioselective studies.

[a] Reaction conditions reported in the above figure on 0.1 mmol scale. [b] Determined by ¹H-NMR analysis. [c] Determined by HPLC analysis using chiral stationary phase. [d] DMF was used instead of CH₃CN.

Interestingly, although it was the class that gave the best results in the analogous non-light-driven transformation PyBOx ligands deriving from different amino alcohols led to modest results in terms of both yield and stereoselection.²⁸⁵

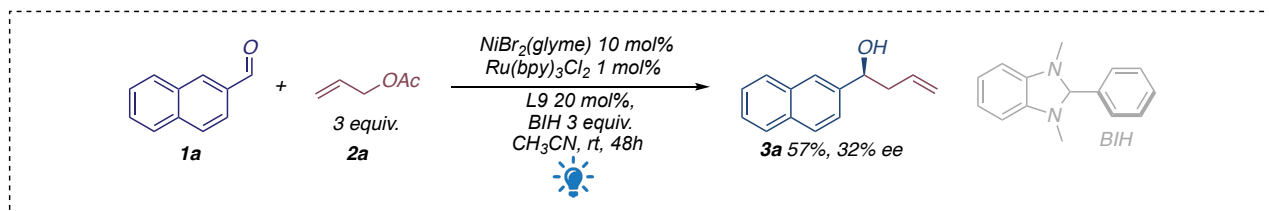
Various chiral Schiff bases also proved incompatible with the reaction conditions, deactivating the process in many cases and not being able to promote the enantioselective reaction.

Similar considerations derived from the use of phOx and pyOx ligands which not only proved unsuitable to promote an asymmetric version of the reaction but also led to a drop of the reactivity of the process.

The only encouraging results were appreciated using BOx ligands deriving from different amino alcohols.

The best enantioselective result was obtained using the chiral bisoxazoline derived from D-Phenylalaninol

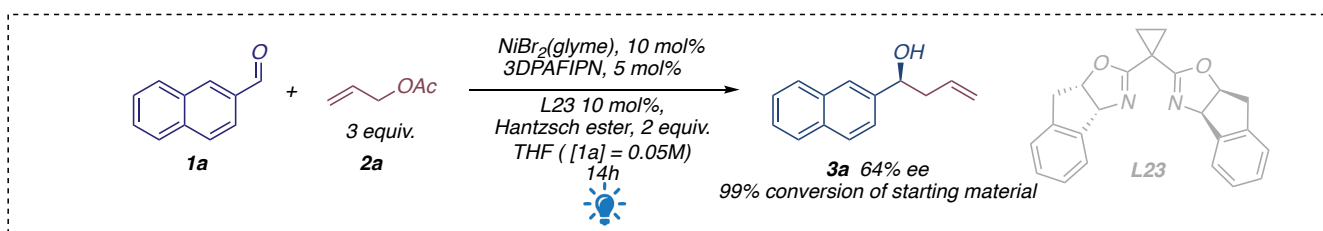
L9. Benzyl moieties proved to be the best compromise between conversion of the starting material into the desired product and enantioselective induction. However, the employment of this ligand determined a ¹H-NMR conversion of 50% and an unsatisfactory enantiomeric excess of 44%. In the light of all the insufficient results obtained, we asked ourselves what the problem preventing a satisfying enantioselective outcome could be. Reanalyzing all the parameters of our reaction, we realized that many of species present in the reaction mixture could be detrimental for the enantioselective outcome. Both the solvent used for the reaction (MeCN) and the tertiary amine used as a sacrificial reductant are known to be coordinating species for the metal centers. To the best of our knowledge, we believe that the poor results obtained in the above-described trials depend on the effect of these species on the nickel coordination sphere. We assumed that the Lewis basicity of the diisopropylethylamine deriving from the lone pair centered on the nitrogen atom determine an interaction with the metal center of the nickel precatalyst. This interaction can drastically disfavor the formation of the chiral complex, determining the rise of an equilibrium between the desired chiral complex and an achiral nickel species still able to promote the allylation reaction. Having identified this as the main problem for the optimization, we first tried to evaluate our protocol with the best chiral ligand tested so far in the presence of a less coordinating stoichiometric reductant. Among the various sacrificial agents commonly used in photoredox transformations, we identified 1,3-dimethyl-2-phenyl-2,3-dihydro-1H-benzo[d]imidazole (BIH) as the best candidate. This substrate was chosen due to its electrochemical potential (0.31 V vs SCE) that can trigger a reductive quenching of the excited state of the ruthenium photocatalyst. In addition, compared with aliphatic tertiary amines, BIH should be less prone to coordinating the nickel center, not interfering with the formation of the transient chiral complex. However, when BIH was tested under optimized reaction conditions the result continued to be inadequate. Only a slight increase in yield and a further decrease of enantiomeric excess were observed.



Chapter 4. Scheme 20 Enantioselective dual Ni/photoredox catalyzed allylation of aldehydes in presence of BIH as reducing agent and **L9** as chiral ligand

This last test further demonstrated the impossibility of directly translating the optimized protocol for the non-stereocontrolled reaction into an enantioselective version. A long and unsuccessful journey was necessary to obtain results that showed a significant improvement in the implementation of the desired protocol. There were two determining factors in achieving the desired quality leap for our protocol. Firstly, the development of our dual photoredox and titanium-catalyzed propargylation and allylation reactions demonstrated a suitable and highly efficient dual photoredox system to overcome the reactivity-related limitations found in the nickel-mediated protocols. Secondly, the publication in the literature of the dual photoredox and chromium mediated enantioselective allylation from Kanai's group elucidated the nature of the scaffold of the chiral ligand able to promote this type of process.¹⁵⁴

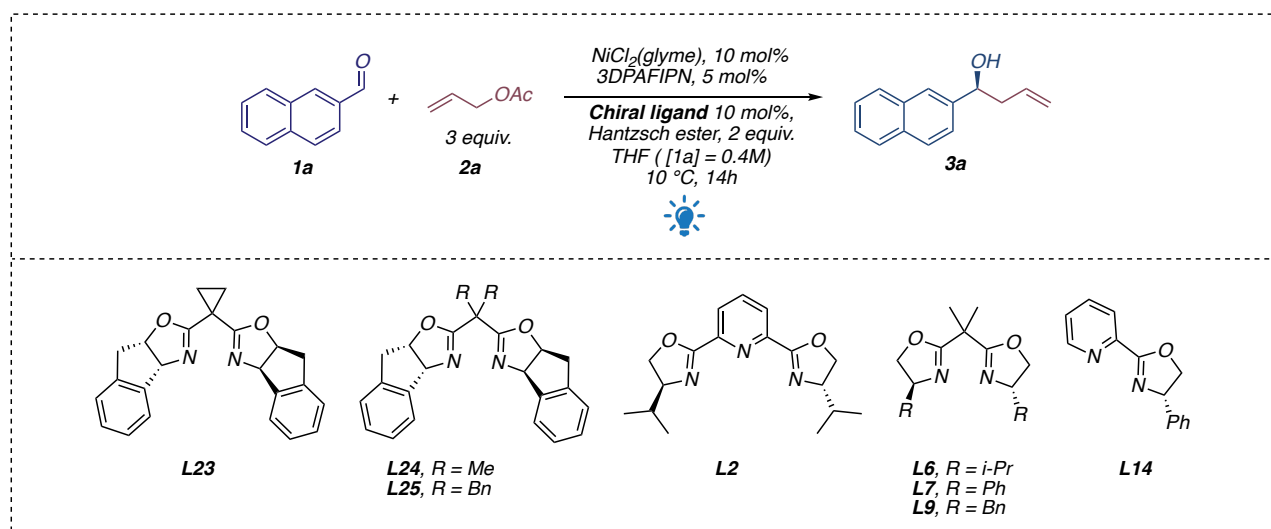
In the light of this, as a first attempt we decided to combine these two elements trying to improve the results so far obtained. We were pleased to observe that carrying out the reaction in THF (in a volume to ensure a 0.05M concentration of starting material), using 3DPAFIPN as a photocatalyst, Hantzsch's ester as an organic reductant in the presence of catalytic amounts of $[\text{NiBr}_2(\text{glyme})]$ and the chiral ligand **L23** (10 mol% each), it was possible to promote the coupling between the model substrate **1a** and allyl acetate with results never achieved before. Indeed, as depicted in **Scheme 21**, it was possible to obtain the desired homoallylic alcohol with an enantiomeric excess of 64% and a total conversion of the model starting material **1a**.



Chapter 4. Scheme 21 Preliminary enantioselective results with the new reaction conditions

Having a solid starting point, we decided to evaluate if it was possible to further optimize the reaction conditions up to a general method, leading to even higher enantiomeric excesses. In the first instance, we considered that, unlike titanium-mediated processes, the nickel-catalyzed enantioselective allylation of aldehydes did not require such a low concentration. On the contrary, drastically decreasing the dilution of the entire reaction environment would have brought a further benefit additionally promoting the in-situ

formation of the active chiral complex. Secondly, we wanted to investigate if it was possible to further improve the enantioselectivity tuning the ligand surrounding the metal center.



Entry ^[a]	Ligand	Yield ^[b] (%) ^[c]	ee (%) ^[d]
1 ^[e]	L24	91	25
2 ^[f]	L24	45	76
3 ^[g]	L24	>99	79
4	L24	90	90
5 ^[h]	L24	90 (87)	92
6 ^[h,i]	L25	90	89
7 ^[f]	L2	70	71
8	L23	>99	67
9	L2	93	0
10 ^[f]	L6	33	0
11 ^[f]	L7	25	3
12 ^[f]	L9	98	67
13 ^[f]	L14	Traces	n.d.

Table 4.2.2 Optimization of the reaction conditions

[a] Reaction conditions reported in the above scheme. [b] Determined by ¹H-NMR analysis. [c] Isolated yield after chromatographic purification. [d] Determined by chiral HPLC analysis. [e] [1a] = 0.05. [f] [1a] = 0.1M. [g] [1a] = 0.2 M. [h] Reaction was carried out using 15 mol% of chiral ligand and 10 mol% of [NiCl₂(glyme)]. [i] Reaction performed in absence of 3Å MS.

As can be seen from the optimization table, increasing the concentration of reaction mixture has beneficial effects on the enantioselective outcome in the presence of different ligands. Even under the new reaction conditions bisoxazoline ligands proved to be the class able to give the best results. While the **L9** ligand determined an enantiomeric excess of 67%; in analogy with others dual photoredox and transition metal mediated functionalization of aldehydes, employing aminoindanol-based Box ligands (**L23**, **L24** and **L25**) the best enantioselective outcomes were achieved.

It was possible to further improve both the enantiomeric excess and the yield of the transformation tuning the bite angle of the ligand scaffold modifying the substituents on the methylene group between the two oxazoline moieties. As described in the table, the best results were obtained by replacing the originally employed cyclopropane ring (**L23**) with two methyl groups (**L24**). On the contrary, the introduction of a

benzyl group on the methylene portion determined a slight drop in yield and enantiomeric excess, probably due to the generated steric hindrance.

On the other hand, pyOx **L14** and pyBOX **L2** ligands were again found unable to induce stereochemical control in formation of the product. Remarkably, by testing various reaction conditions it was possible to note that the presence of small amounts of water plays a crucial role in the stereoselective outcome. Water molecules in the reaction mixture hamper the ability of the metal center to coordinate the chiral ligand, generating parasitic coordination pathways, so the optimization process required the introduction of freshly activated 3 Å molecular sieves to overcome this limitation. A similar consideration can be made for the reaction temperature. The optimal reaction temperature for the process was found to be around 10 °C. This experimental evidence can be attributed to the relative instability of the nickel complexes in a low oxidation state coordinated to bisoxazoline ligands.³⁰⁶

Having in hand a powerful methodology, a further improvement of the reaction outcome came from the screening of other common organic solvents.

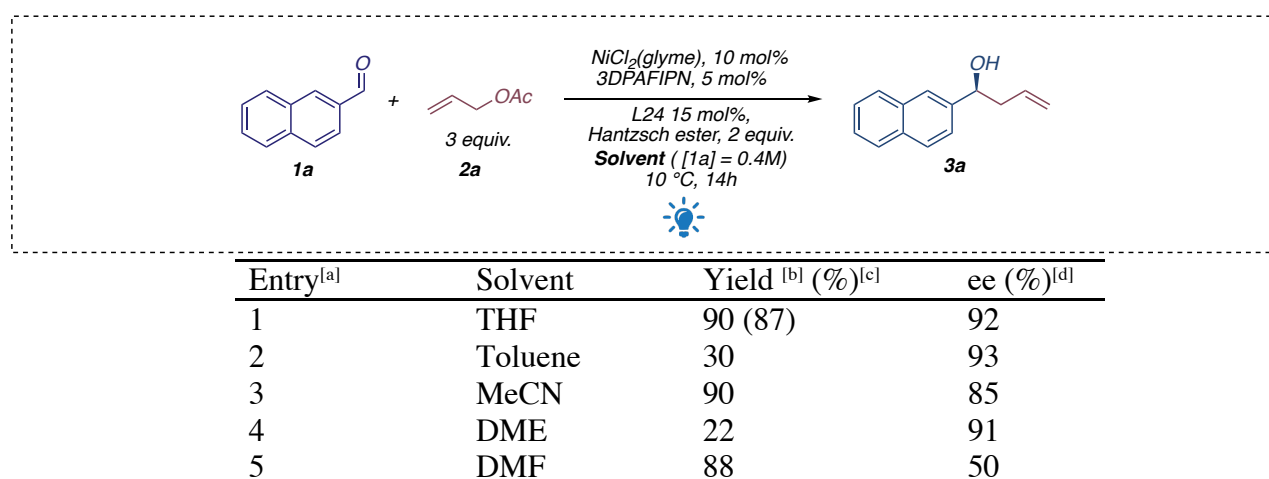


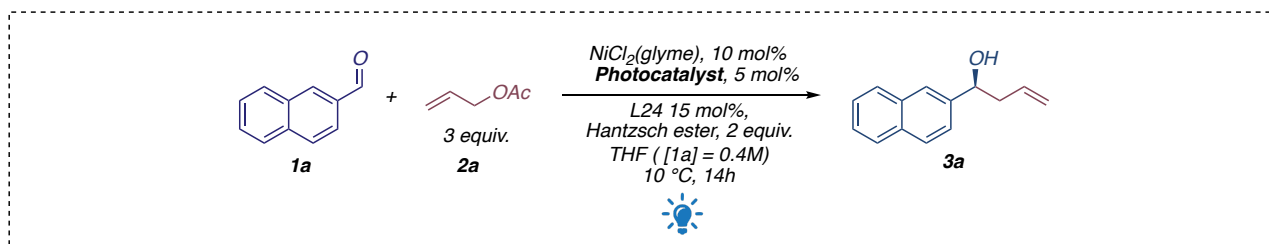
Table 4.2.3 Screening of reaction solvent.

[a] Reaction conditions reported in the above scheme on 0.1 mmol scale. [b] Determined by ¹H-NMR analysis. [c] Isolated yield after chromatographic purification. [d] Determined by chiral HPLC analysis.

Poor enantioselectivity was observed in the presence of highly polar and coordinating solvents such as DMF. Although results from moderate to good could be obtained in the presence of various organic solvents, it was not possible to replace the originally employed THF. Remarkably, toluene allowed a slightly higher enantiomeric outcome than THF, however, the employment of this solvent reduces the reactivity of the system leading to an inadequate conversion of the starting material into the desired product. The initial choice of using a photocatalyst with a marked reducing character in its excited state proved to be correct, since several of the most common less reducing photocatalysts were screened with worse results. In addition, to further demonstrate that all the components of the reaction cooperate to achieve a good enantioselective outcome, we decided to re-test the conditions initially used for the non-

³⁰⁶ Yin, H.; Fu, G. C. Mechanistic Investigation of Enantioconvergent Kumada Reactions of Racemic α -Bromoketones Catalyzed by a Nickel/Bis(Oxazoline) Complex. *J. Am. Chem. Soc.* **2019**, *141* (38), 15433–15440. <https://doi.org/10.1021/jacs.9b08185>.

asymmetrical version of the protocol in the presence of the new chiral ligand. As can be seen in the table, the presence of DIPEA and acetonitrile plays a detrimental role in the reaction.

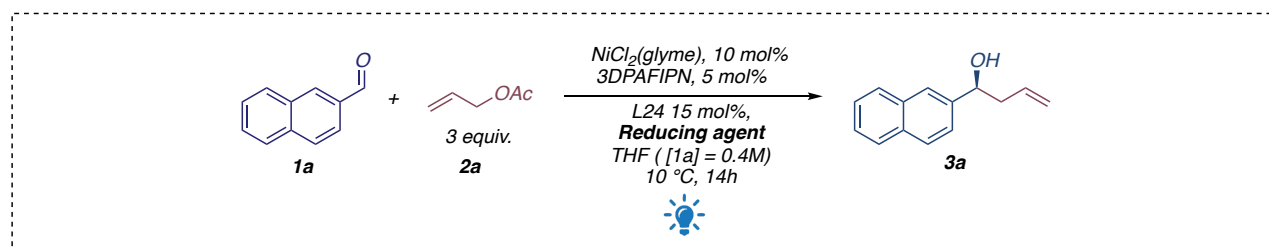


Entry ^[a]	Photocatalyst	Yield ^[b] (%) ^[c]	ee (%) ^[d]
1	-	0	-
2	3DPAFIPN	90 (87)	93
3 ^[e]	(Ir[dF(CF ₃)ppy] ₂ (dtbbpy))PF ₆	25	92
4	4CzIPN	51	89
5	[Ru(bpy) ₃]Cl ₂ •6H ₂ O	-	-
6 ^[e,f]	[Ru(bpy) ₃]Cl ₂ •6H ₂ O	50	25

Table 4.3.4 Screening of photocatalyst.

[a] Reaction conditions reported in the above scheme on 0.1 mmol scale. [b] Determined by ¹H-NMR analysis. [c] Isolated yield after chromatographic purification. [d] Determined by chiral HPLC analysis. [e]. 1 mol % of the photocatalyst was used. [f]. Reaction was carried out using 3 equiv. of DIPEA as reducing agent and 0.5 mL of MeCN as solvent.

The choice of the right stoichiometric organic reductant also proved to be crucial to the process. Due to its low-coordinating nature and suitable oxidation potential, the employment of Hantzsch's ester provided incomparable results than other common tertiary amines used. DIPEA and BIH, for example, were found to be unsuitable with the new reaction environment. Similarly, triethylamine can promote the process, but –probably due to the Lewis basicity of the nitrogen atom present - a drop in stereoinduction is observed.

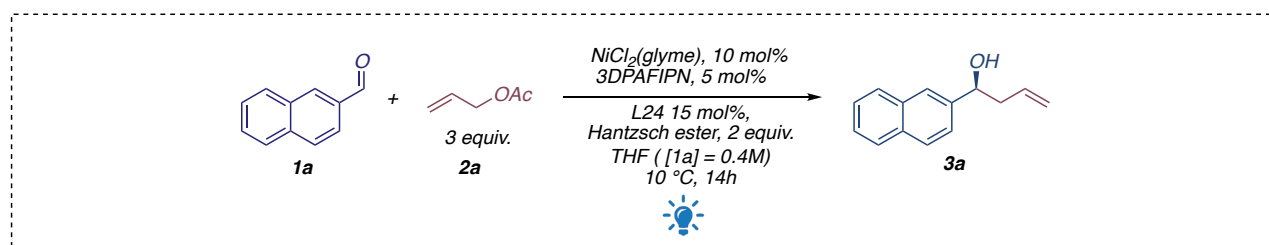


Entry ^[a]	Reducing agent	Yield ^[b]	ee (%) ^[c]
1	DIPEA, 3 equivalents	No reaction	–
2	BIH, 2 equivalents	No reaction	–
3	TEA, 3 equivalents	61	53

Table 4.2.5 Screening of reducing agent.

[a] Reaction conditions reported in the above scheme on 0.1 mmol scale. [b] Determined by ¹H-NMR analysis. [c] Determined by chiral HPLC analysis.

To conclude, all the necessary control experiment were conducted. We were pleased to observe that each component in the reaction mixture were necessary to promote enantioselective transformation.



Entry ^[a]	Deviation from standard conditions	Yield ^[b] (%) ^[c]	ee (%) ^[d]
1	none	>99(87) ^d	92
2	No photocatalyst, with irradiation at 456 nm	0	–
3	Allyl bromide instead of allyl acetate	traces	–
4	No Nickel	0	–
5	No Light	0	–

Table 4.2.6 Control experiments

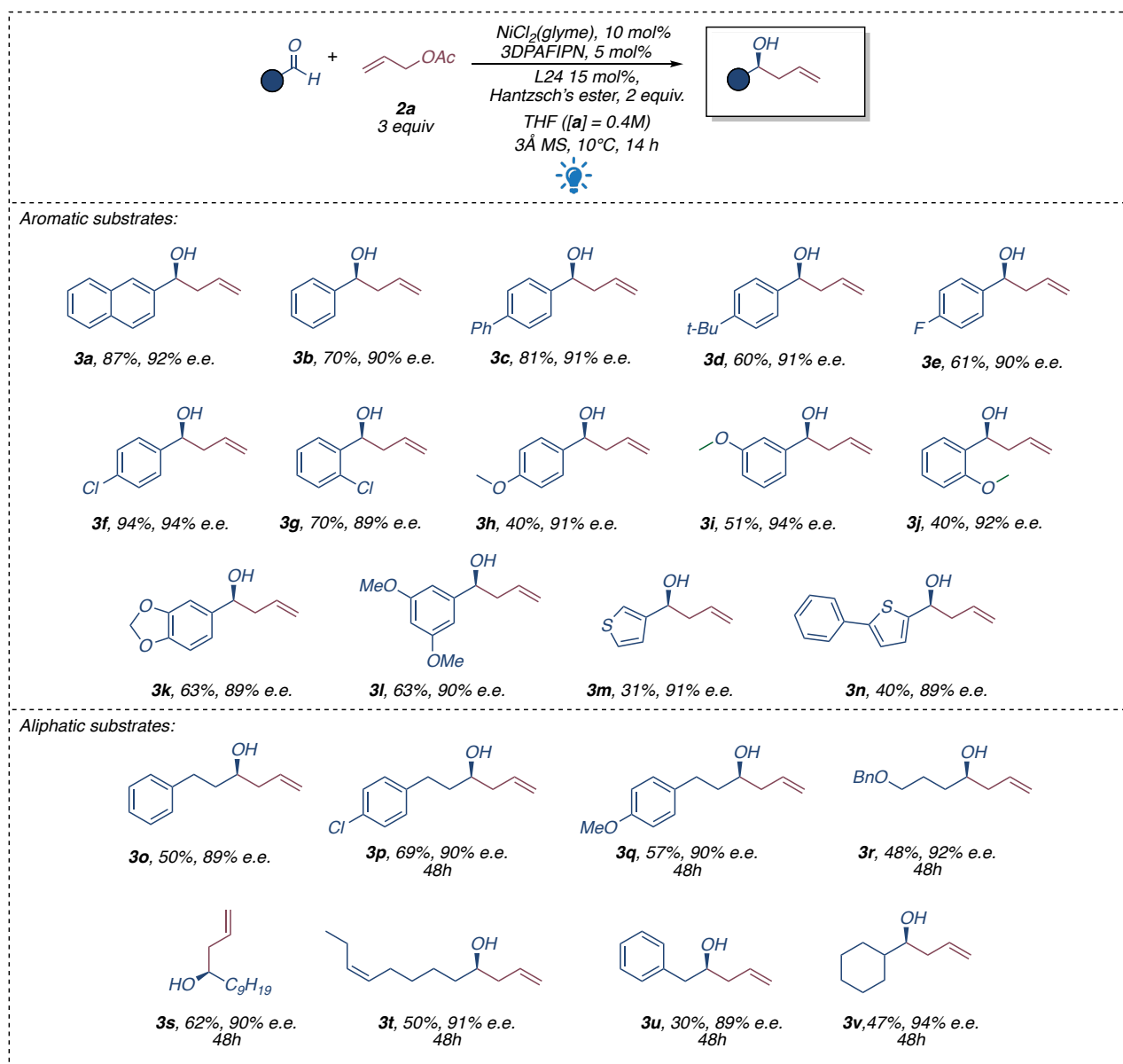
[a] Reaction conditions reported in the above scheme on 0.1 mmol scale. [b] Determined by ¹H-NMR analysis. [c] Determined by chiral HPLC analysis.

After the systematic evaluation of all reaction parameters, we were able to disclose the optimized conditions, obtaining **3a** in 87% isolated yield and 93% of enantiomeric excess after 16 h of irradiation at 8-12° C: [$\text{NiCl}_2(\text{glyme})$] (10 mol%), L24 (15 mol%) as chiral ligand, allylacetate **2a** (3 equiv.), Hantzsch's (HE, 2 equiv.), 3DPAFIPN (5 mol%) under blue LEDs irradiation at 456 nm.

• Scope Evaluation

The selected reaction conditions were employed with a variety of aromatic and aliphatic aldehydes.

The collected results revealed that the applicability of this methodology is quite broad, with both aromatic and aliphatic substrates reacting nicely, leading to the desired products with high enantioselectivities.



Chapter 4. Figure 13 Scope evaluation of aromatic and aliphatic substrate in enantioselective dual Ni/photoredox enantioselective allylation reaction.

Electron rich (**3h–l**) or electron poor (**3e–g**) aromatic aldehydes are suitable substrates for our enantioselective allylation protocol. *Ortho*, *meta* or *para* substituents seem to influence neither reactivity nor stereoselectivity of this nickel mediated allylation. Heterocyclic substrates are tolerated in certain cases (**3m,n**).

For all the substrates studied the allylating agent was found to attack the prochiral *Si*-face of carbonyl group. The absolute configurations of the homoallylic alcohol isolated after purification was established in the case of **S-3a** and **S-3q** comparing the data reported in literature.³⁰⁷

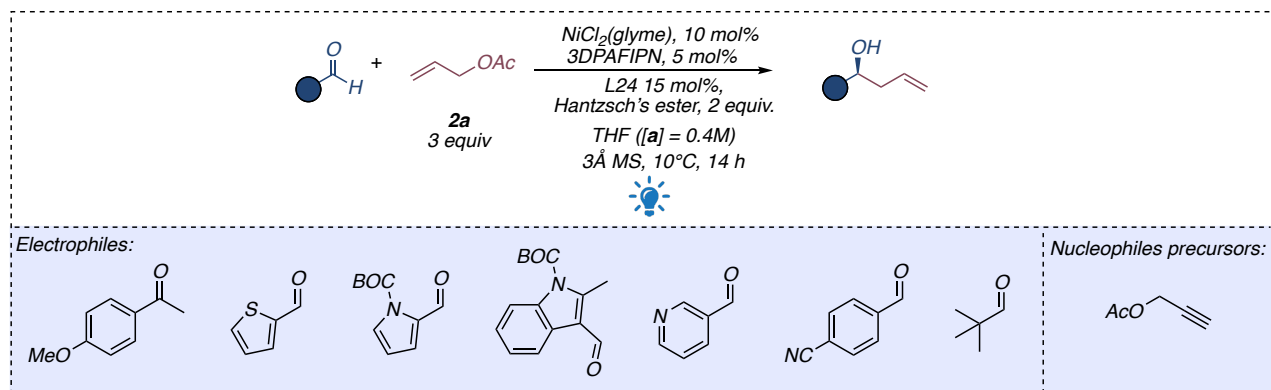
Remarkably, as already seen with the non-asymmetric version of the process, aliphatic substrates proved to be less reactive than aromatic aldehydes. Fortunately, it was possible to achieve satisfactory results in terms of yield simply increasing the reaction time to 48h. The investigation of the tolerated aliphatic aldehydes disclosed that hindered cyclohexyl aldehyde is compatible with the developed reaction conditions. The best results were obtained with linear aliphatic aldehydes (**3o-v**). Especially hydrocinnamic derivatives with different electron-withdrawing and electron donating decorations on the aromatic ring displayed the best reactivity and the desired products were isolated with e.e.s ranging from 89% to 94% and moderate yields.

Unsuccessful results were observed for some aromatic aldehydes, due either to the chelation ability of the heteroatom, or to the limited stability of the products.

As far as the latter drawback is concerned, the low isolated yields are determined by the presence of a strong Brønsted acid in the reaction mixture, *i.e.*, the pyridinium ion derived by oxidation of Hantzsch's ester. As in the case of titanium mediated processes, acid sensitive substrates containing pyrrole or indole rings gave unsatisfactory results due to decomposition pathways promoted by the presence of Brønsted acids.

We were forced to note that the process cannot be extended to neither aromatic ketones nor to highly hindered aliphatic aldehydes such as pivalaldehyde. Similarly, the use of propargyl acetate as a pronucleophile did not lead to the formation of neither the propargylation nor the allenylation product. Both limitations can be attributed to the low nucleophilicity of nucleophilic transient organonickel species.

³⁰⁷ Prévost, S.; Thai, K.; Schützenmeister, N.; Coulthard, G.; Erb, W.; Aggarwal, V. K. Synthesis of Prostaglandin Analogues, Latanoprost and Bimatoprost, Using Organocatalysis via a Key Bicyclic Enal Intermediate. *Org. Lett.* **2015**, *17* (3), 504–507. <https://doi.org/10.1021/ol503520f>.



Chapter 4. Scheme 22 Unreactive substrates.

In conclusion, the employed photocatalyst had been shown quite stable in the reaction conditions (we have determined, by means of internal standard experiments involving ^{19}F -NMR, the amount of the catalyst present in the reaction mixture at the end of the reaction).

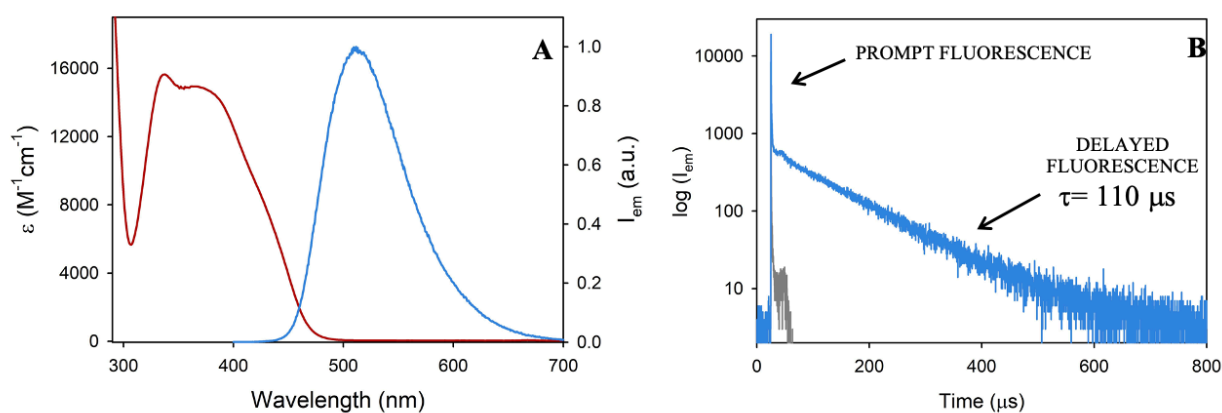
• Photophysical and computational studies

To provide a complete picture of the mechanism involved in the enantioselective process, we have carried out both a photophysical investigation and a computational modelling of the overall reaction mechanism. The photophysical investigation was carried out in collaboration with the research group supervised by Professor P. Ceroni of our department. The theoretical and computational treatment was carried out in collaboration with the research group led by Professor L. Cavallo of the King Abdullah University of Science and Technology in Thuwal, Saudi Arabia.

The study of the reaction mechanism began with the photophysical investigation of the process.

The photocatalyst used for the reported transformation is 3DPAFIPN. As described in the previous chapters, this molecule has some particularly interesting characteristics that make it an excellent candidate for photoredox processes. Among all, the Thermally Activated Delayed Fluorescence (TADF), shared by the majority of cyanoarene-based photosensitizers, makes these molecules a convenient and cheaper substitute for the common rare metal-based photosensitizers.

3DPAFIPN in deaerated, stabilizer-free THF solution has shown an absorption band in the visible region ($\epsilon = 14900 \text{ M}^{-1}\text{cm}^{-1}$ at $\lambda = 370 \text{ nm}$; abs onset at 470 nm in THF) and an emission band peaked at 520 nm due to prompt fluorescence ($\tau = 3.6 \text{ ns}$) and delayed fluorescence ($\tau = 110 \text{ }\mu\text{s}$).



Chapter 4. Figure 14 A) Absorption spectrum (red line) and emission spectrum ($\lambda_{exc} = 380 \text{ nm}$; blue line) of 3DPAFIPN in THF at r.t. B) Emission intensity decay of 3DPAFIPN in degassed THF at r.t. ($\lambda_{exc} = 440 \text{ nm}$; $\lambda_{em} = 520 \text{ nm}$; blue line) and the instrument response function (IRF, gray line).

Like the previously described protocols, the ability of each species to quench or modify the excited state of the photocatalyst was evaluated.

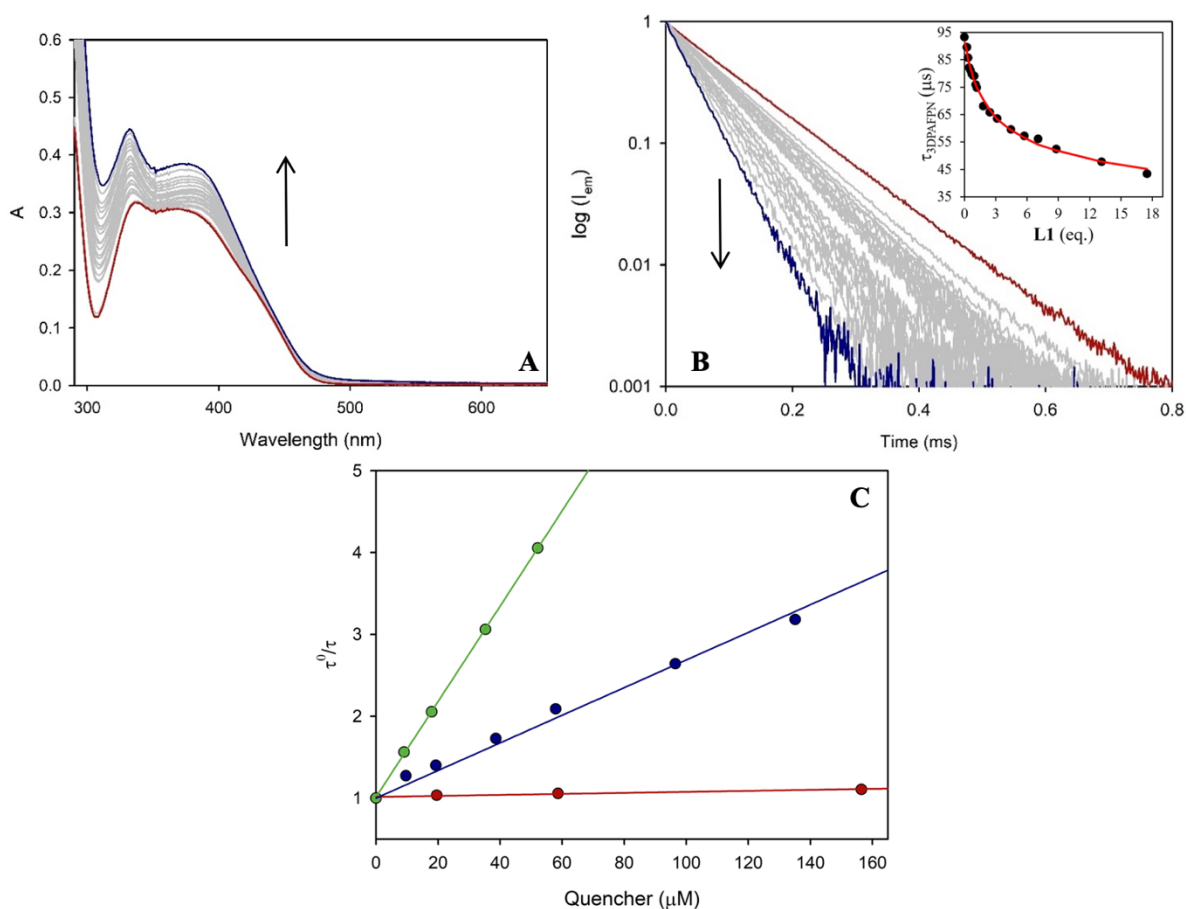
In order to have a clear picture of the reaction mixture, the determination of the association constant between the nickel precatalyst and the chiral bisoxazoline ligand was considered.

A titration experiment was carried out to determine the equilibrium constant (K_{eq}) for the complexation of **L24** by $[\text{NiCl}_2(\text{glyme})]$. Given the low value of $[\text{NiCl}_2\text{L24}]$'s molar absorption coefficient and the low solubility of $[\text{NiCl}_2(\text{glyme})]$ in THF, a UV-Vis titration was not possible, and an indirect method was

used. Firstly, the quenching ability of $[\text{NiCl}_2(\text{glyme})]$ and its correlated Stern-Volmer plot were evaluated in absence of ligand.

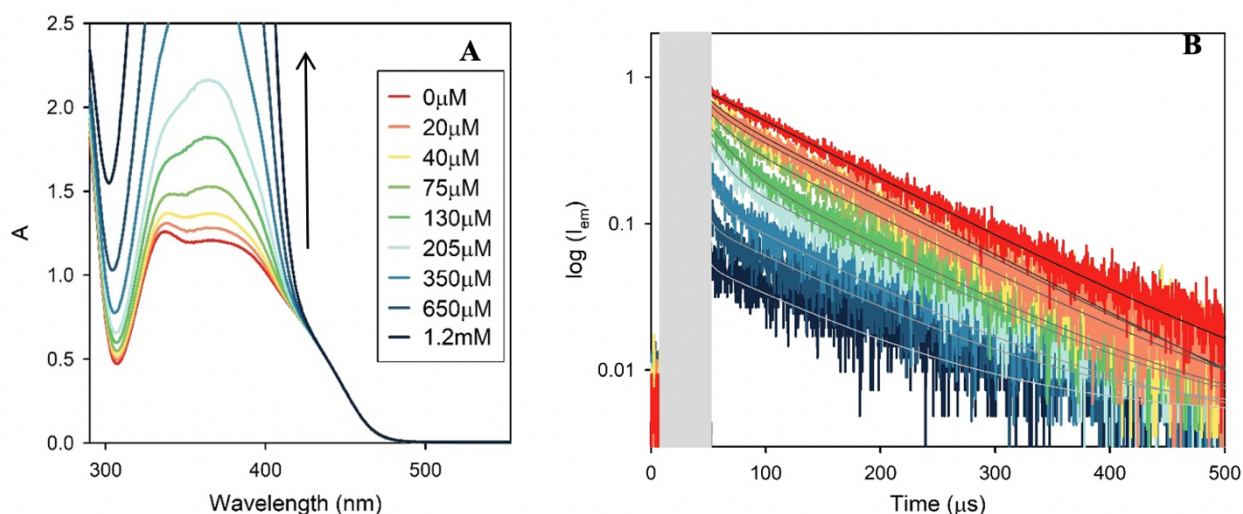
Then, the same procedure was applied for **L24**. As expected, the chiral ligand employed for the transformation was found unable to quench the excited state of the photocatalyst.

At this point, after preparing a solution containing $[\text{NiCl}_2(\text{glyme})]$ ($20 \mu\text{M}$) and 3DPAFIPN, it was possible to monitor 3DPAFIPN's lifetime upon addition of increasing amounts of **L24** (up to 18 eq, 0.36 mM). $[\text{NiCl}_2(\text{glyme})]$ and $[\text{NiCl}_2\text{L24}]$ presented different quenching constants for 3DPAFIPN. After fitting the data to a 1:1 binding model using Specfit[®], K_{eq} was determined to be 44700 M^{-1} .



Chapter 4. Figure 15 A) Absorption spectra for a solution containing 3DPAFIPN and $[\text{NiCl}_2(\text{glyme})]$ ($20 \mu\text{M}$, red line) upon addition of increasing amounts of L24 (up to 18 eq, 0.36 mM). B) Corresponding normalized emission intensity decays ($\lambda_{\text{exc}} = 405 \text{ nm}$, emission cutoff filter = 435 nm); inset: 3DPAFIPN's lifetime as a function of added L24 equivalents (black dots). C) Stern-Volmer plots between 3DPAFIPN and L24 (red), $[\text{NiCl}_2(\text{glyme})]$ (blue) or $[\text{NiCl}_2\text{L24}]$ (green).

Once it has been established that the reaction conditions allow quantitative formation of the desired chiral nickel complex and having evaluated its quenching properties, a Stern-Volmer experiment was carried out to determine the dynamic quenching constant between 3DPAFIPN and Hantzsch's ester. Unexpectedly, the emission intensity showed a biexponential emission decay of 18 and 110 μs : upon increasing the concentration of Hantzsch's ester up to 130 μM (Figure 16).



Chapter 4. Figure 16 A) Dilution-corrected absorption spectra for solutions of 3DPAFIPN upon addition of increasing amounts of HE (up to 1.2 mM). B) Corresponding normalized emission intensity decays of 3DPAFIPN with fitting ($\lambda_{exc} = 440$ nm, $\lambda_{em} = 520$ nm) (the IRF has been grayed out).

The longer lifetime shows a constant value and corresponds to the typical one of 3DPAFIPN, while its relative weight decreases upon increasing Hantzsch's ester concentration. The shorter component decreases upon further addition of the quencher (**Table 4.2.7**).

HE (μM)	0	20	40	75	130	205	350	650	1200
τ_{SHORT} (μs)	/	18	16	18	22	14	9	6	5
τ_{LONG} (μs)					110				

Table 4.2.7 Lifetimes resulting from the fitting of the emission intensity decays reported in Figure 16B the longer lifetime's value was held constant during iterations.

This behavior has been attributed to the formation of a complex between 3DPAFIPN and Hantzsch's ester (3DPAFIPN•HE), whose lifetime is 18 μs .

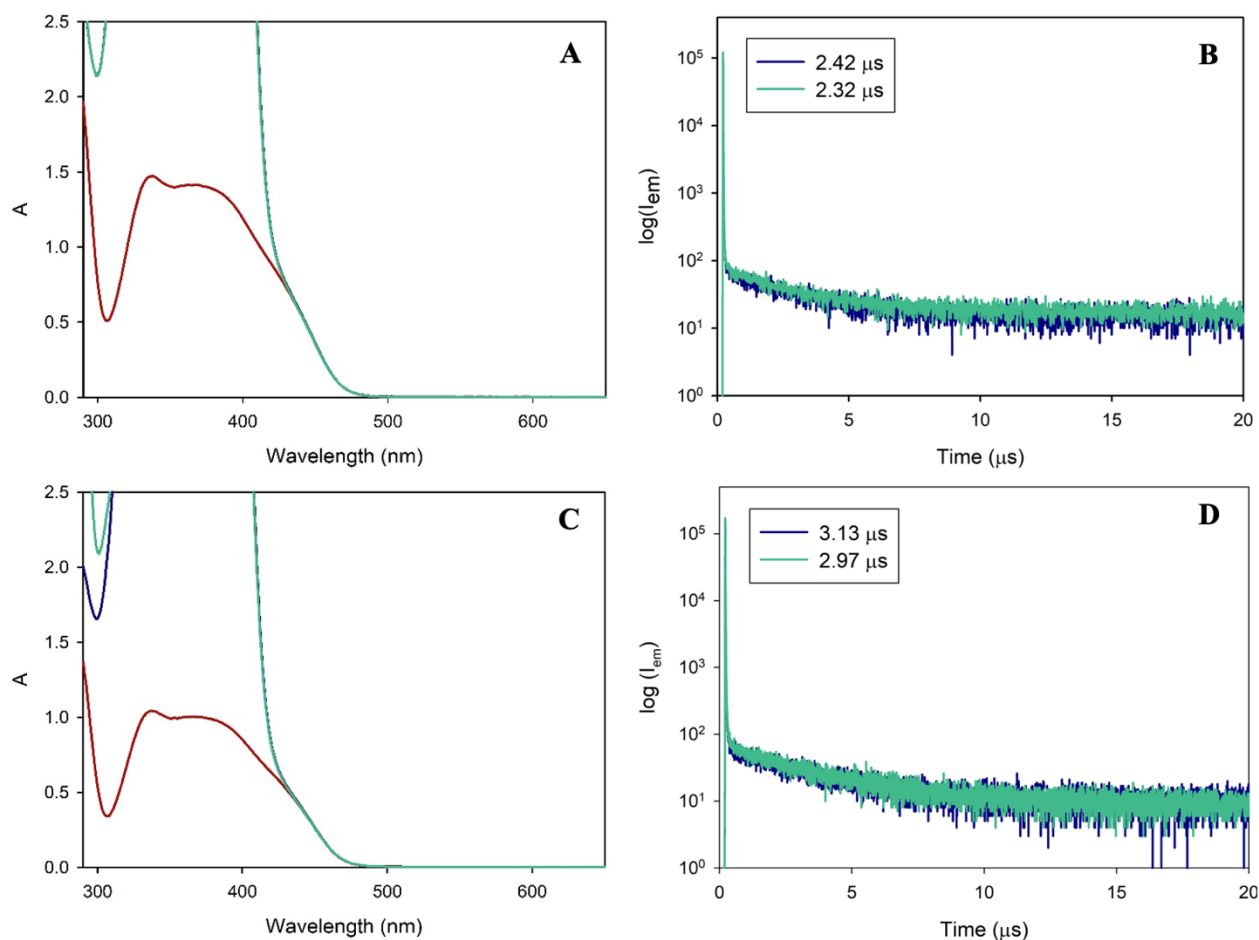
Under the experimental conditions used to perform the reaction, the formation of this complex is considered quantitative in view of the large excess of Hantzsch's ester presents in the reaction mixture. Therefore, we considered the complex 3DPAFIPN•HE as the photoredox active species.

The extent of the complex's quenching caused by the other redox active species involved in the reaction was evaluated by single point measurements according to the Stern-Volmer equation:

$$\tau^0/\tau = 1 + k_q\tau^0[\text{Q}]$$

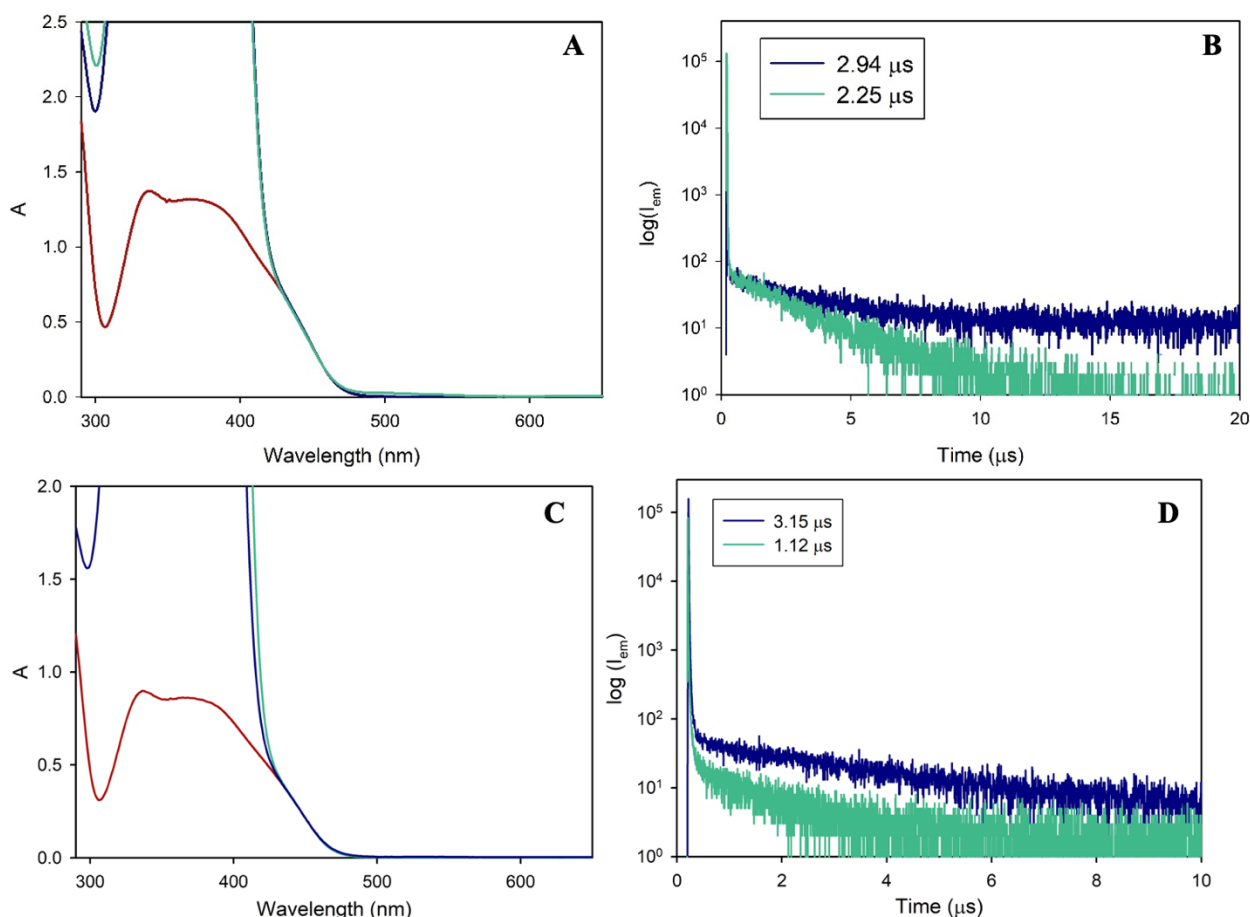
where τ^0 and τ are the lifetimes of 3DPAFIPN in the presence of an excess amount of Hantzsch's ester and in the additional presence of the quencher, respectively, k_q is the dynamic quenching constant and $[\text{Q}]$ is the concentration of the quencher.

Taking into account each component of the reaction, no significant lifetime change was observed upon addition of allyl acetate or naphthaldehyde, indicating that no bimolecular quenching processes occur between the complex and these two species.



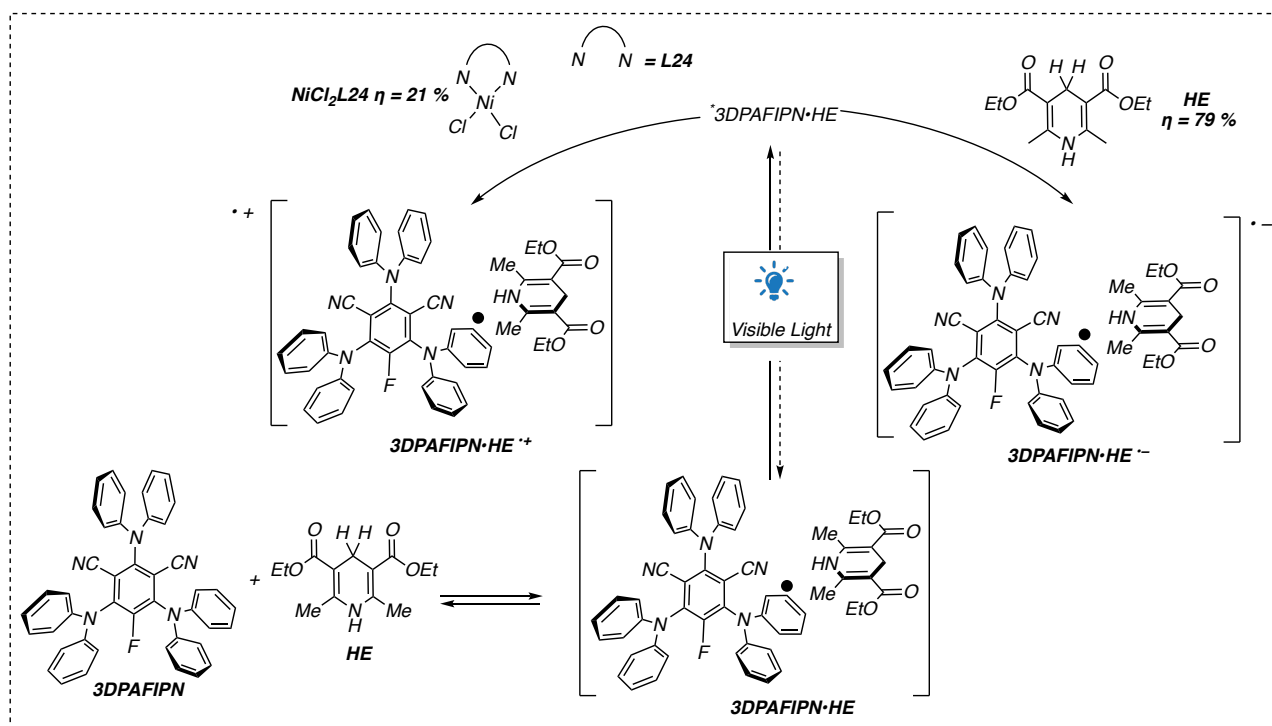
Chapter 4. Figure 17 A) Absorption spectra for a solution of 3DPAFIPN (red line), following addition of HE 2.20 mM (blue line), and the further addition of allylacetate 400 μ M (green line). B) Corresponding emission intensity decays of 3DPAFIPN ($\lambda_{exc}= 405$ nm, pulsed laser; $\lambda_{em}= 520$ nm) following the addition of HE (blue line) and the further addition of allylacetate (green line). C) Absorption spectra for a solution of 3DPAFIPN (red line), following addition of HE 2.15 mM (blue line), and the further addition of naphthaldehyde 335 μ M (green line). D) Corresponding emission intensity decays of 3DPAFIPN ($\lambda_{exc}= 405$ nm, pulsed laser; $\lambda_{em}= 520$ nm) following the addition of HE (blue line) and the further addition of naphthaldehyde (green line).

On the contrary, upon further addition both of Hantzsch's ester (concentration higher than 130 μ M) and **[NiCl₂L24]**, a dynamic quenching of the emission of the 3DPAFIPN·HE complex was observed in both cases ($k_q = 2.11 \times 10^8 \text{ M}^{-1}\text{s}^{-1}$ and $k_q = 5.49 \times 10^8 \text{ M}^{-1}\text{s}^{-1}$ respectively).



Chapter 4. Figure 18 A) Absorption spectra for a solution of 3DPAFIPN (red line) following addition of HE 2.20 mM (blue line), and the further addition of [NiCl₂(glyme)] 190 μM + 1.5 eq. L24 (green line). B) Corresponding emission intensity decays of 3DPAFIPN (λ_{exc} = 405 nm, pulsed laser; λ_{em} = 520 nm) following the addition of HE (blue line) and the further addition of [NiCl₂(glyme)] + 1.5 eq. L24 (green line). C) Absorption spectra for a solution of 3DPAFIPN (red line) following addition of HE 1.88 mM (blue line), and a further addition of HE 2.73 mM (green line). D) Corresponding emission intensity decays of 3DPAFIPN (λ_{exc} = 405 nm, pulsed laser; λ_{em} = 520 nm) following the addition of HE (blue line) and a further addition of HE (green line).

Given the higher concentration of Hantzsch's ester in the reaction conditions compared to that of [NiCl₂L24], the quenching efficiency is higher for the former (79%) compared to the latter (21%) and the first single electron transfer (SET) that takes place leads to the reductive quenching of the lowest excited state of the 3DPAFIPN·HE complex.



Chapter 4. Figure 19 Schematic picture of the photocatalytic mechanism.

For clarity, quenching efficiency of species i was calculated according to the following formula:

$$\eta^i = \frac{k_q^i \cdot [Q]^i}{k_{nr} + k_r + \sum_0^n k_q^n \cdot [Q]^n} \cdot 100$$

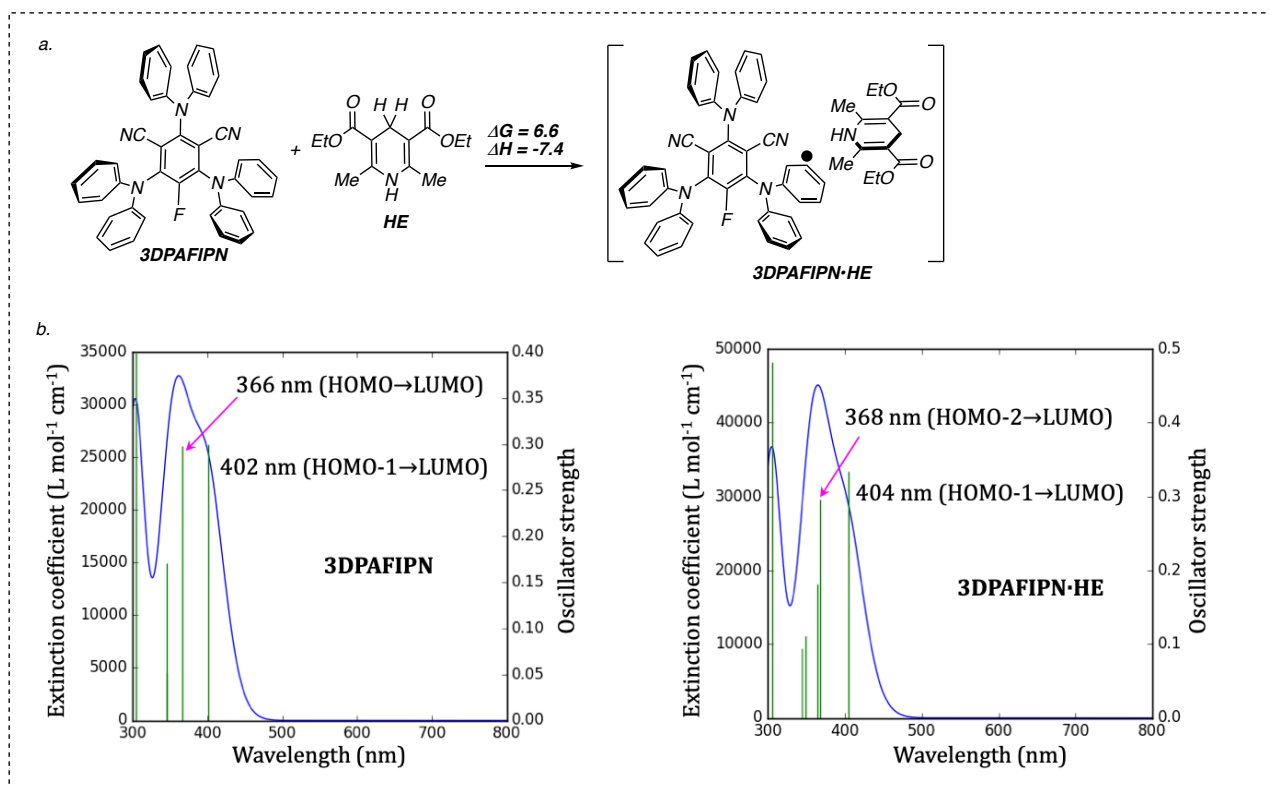
Entry ^[a]	Quencher	k_q ($M^{-1}s^{-1}$)	[Q] (M)
1	Allylacetate	not significant	1.2
2	2-Naphthaldehyde	not significant	0.4
3	[NiCl ₂ L24]	5.49×10^8	0.01
4	HE	2.11×10^8	0.1

Table 4.2.8 Quenching efficiency of species of the component of the reaction mixture

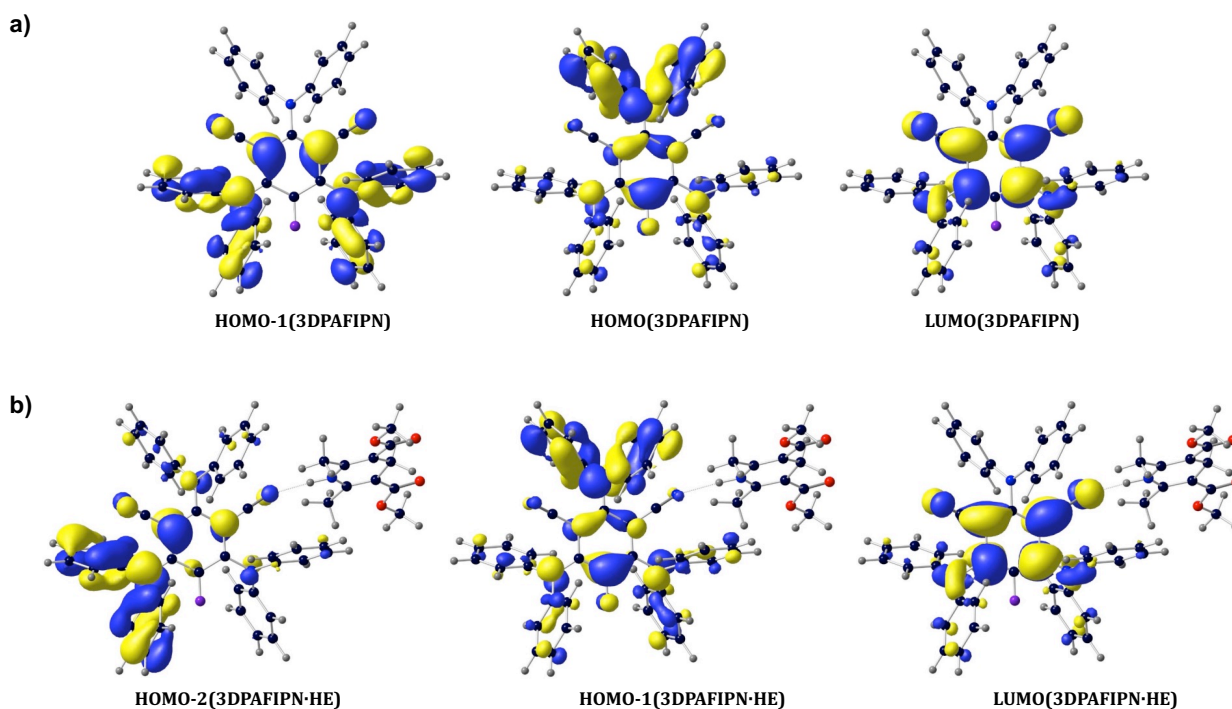
To shed further light on the reaction mechanism and explore the origin of enantioselectivity, density functional theory (DFT) calculations have been performed. In the DFT study, **1a** and **2a** were selected as the reactants, and **L24** as the Ni(II) ligand. The complete mechanism evaluation was divided into two main sections corresponding to the photoredox catalytic cycle and to the nickel catalytic cycle.

To provide further support to the photophysical evidence on the formation of a **3DPAFIPN·HE** complex, the DFT calculations were performed considering this complex reacting along the reductive or oxidative cycles. The first step involved the modelling of the formation of complex between **3DPAFIPN** and Hantzsch's ester. As can be seen from the figures below, the formation of the **3DPAFIPN·HE** complex

can take place under the reaction conditions with a moderate energy effort (6.6 kcal/mol). Similarly, the calculated absorption spectra of 3DPAFIPN and 3DPAFIPN•HE shows no significant differences.



Then two possible reductive or oxidative photoredox catalytic cycles were evaluated. In both cases, the process starts with the photoinduced excitation of 3DPAFIPN•HE to the singlet excited state, eventually transformed into triplet $^T3DPAFIPN\cdot HE$ by ISC (intersystem crossing).



Chapter 4. Figure 21 Most relevant frontier molecular orbitals (isosurface = 0.03 a.u.) involved in the photoexcitation of 3DPAFIPN and 3DPAFIPN·HE.

Along the reductive cycle ${}^1\text{3DPAFIPN}\cdot\text{HE}$ (or the singlet excited state ${}^*\text{3DPAFIPN}\cdot\text{HE}$ in equilibrium with it) is reduced to ${}^1\text{3DPAFIPN}\cdot\text{HE}^-$ by oxidation of HE to HE^{2+} (**SET1**), and the so-formed ${}^1\text{3DPAFIPN}\cdot\text{HE}^-$ is then oxidized to ${}^1\text{3DPAFIPN}\cdot\text{HE}$ by the reduction of ${}^{\text{I}}\text{1-Ni}^{\text{II}}$ to ${}^{\text{I}}\text{2-Ni}^{\text{I}}$ (**SET2**). The calculated $1e^-$ reduction potential of the ${}^1\text{3DPAFIPN}\cdot\text{HE}/{}^1\text{3DPAFIPN}\cdot\text{HE}^-$ pair is lower than that of the HE^{2+}/HE , pointing out that the **SET1** is thermodynamically less favored.

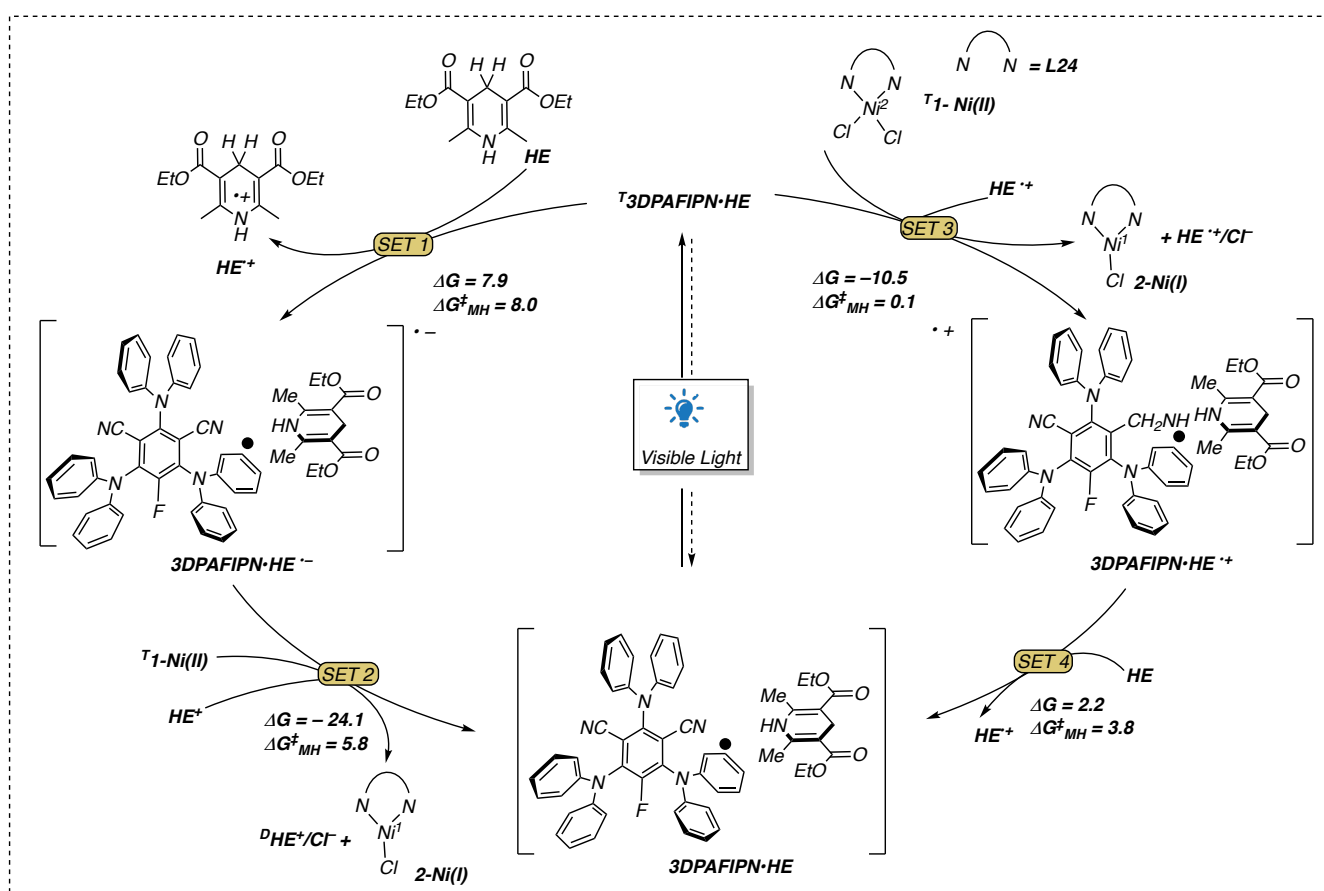
Differently, **SET2** is highly favored because of the lower $1e^-$ reduction potential of the ${}^1\text{3DPAFIPN}\cdot\text{HE}/{}^1\text{3DPAFIPN}\cdot\text{HE}^-$ pair than that of the ${}^{\text{I}}\text{1-Ni}^{\text{II}}/{}^{\text{I}}\text{2-Ni}^{\text{I}}$ pair. (**Table 9**)

Half Reaction	$E_{1/2}^{\text{red}}$ (V)
${}^1\text{3DPAFIPN}\cdot\text{HE} + 1e^- \rightarrow {}^1\text{3DPAFIPN}\cdot\text{HE}^-$	0.58
${}^1\text{3DPAFIPN}\cdot\text{HE} + 1e^- \rightarrow {}^1\text{3DPAFIPN}\cdot\text{HE}^-$	-1.63
${}^1\text{3DPAFIPN}\cdot\text{HE}^{2+} + 1e^- \rightarrow {}^1\text{3DPAFIPN}\cdot\text{HE}$	-1.38
${}^1\text{3DPAFIPN}\cdot\text{HE}^{2+} + 1e^- \rightarrow {}^1\text{3DPAFIPN}\cdot\text{HE}$	0.83
$\text{HE}^{2+} + 1e^- \rightarrow \text{HE}$	0.93
${}^{\text{I}}\text{1-Ni}^{\text{II}} + \text{HE}^{2+} + 1e^- \rightarrow {}^{\text{I}}\text{2-Ni}^{\text{I}} + \text{HE}^{2+}/\text{Cl}^-$	-0.58
${}^{\text{I}}\text{2-Ni}^{\text{I}} + \text{HE}^{2+} + 2a + 1e^- \rightarrow {}^{\text{I}}\text{3-Ni}^{\text{0}} + \text{HE}^{2+}/\text{Cl}^-$	-1.46

Table 4.2.9. Calculated reduction potentials, $E_{1/2}^{\text{red}}$ in V, of the most relevant species involved in the catalytic cycles. The potentials are reported against the saturated calomel electrode (SCE) at 298.15 K in acetonitrile solvent.

Along the oxidative cycle ${}^1\text{3DPAFIPN}\cdot\text{HE}$ is oxidized to ${}^1\text{3DPAFIPN}\cdot\text{HE}^{2+}$ by the reduction of ${}^{\text{I}}\text{1-Ni}^{\text{II}}$ to ${}^{\text{I}}\text{2-Ni}^{\text{I}}$ (**SET3**), and the so formed ${}^1\text{3DPAFIPN}\cdot\text{HE}^{2+}$ is then reduced to ${}^1\text{3DPAFIPN}\cdot\text{HE}$ by the oxidation of

HE to HE^{•+} (**SET4**). **SET3** is thermodynamically favored as the calculated 1e⁻ reduction potential of the ^T1-Ni^{II}/2-Ni^I pair is higher than that of 3DPAFIPN·HE^{•+}/^T3DPAFIPN·HE, while **SET4** is unfavored as the 1e⁻ reduction potential of the 3DPAFIPN·HE^{•+}/3DPAFIPN·HE pair is lower than that of HE^{•+}/HE pair. In accordance with the calculated 1e⁻ reduction potentials, both the oxidative cycle and reductive cycle are characterized by one exergonic SET step and one endergonic SET with lower activation barriers. Therefore, consistently with the above photophysical experimental study, the DFT analysis suggests that both cycles are possible, with the experimental preference for the reductive quenching explained by the higher concentration of the Hantzsch's ester.

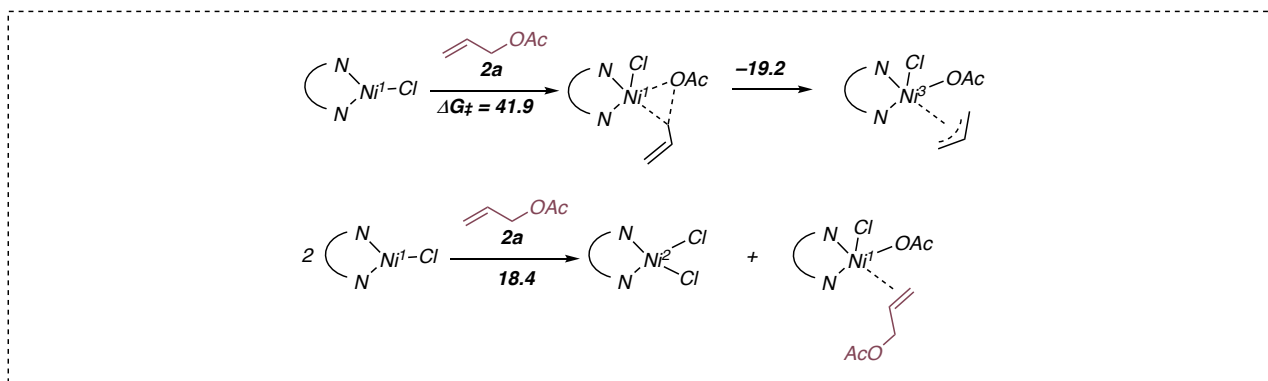


Chapter 4. Figure 22 Two alternative mechanisms for the photoredox catalytic cycle. Free energy values at M06(SMD-THF)/Def2-TZVPP/SDD//PBE(SMD-THF)/Def2-SVP/SDD level of theory are presented. ΔG_{MH}^\ddagger have been approximated using Marcus-Hush theory.

Once the formation of the complex between the photocatalyst and Hantzsch's ester had been confirmed by computational modelling, it was possible to evaluate by means of DFT calculations the formation pathway of the transient nucleophilic organonickel species. In the same way, it was possible to establish how the latter interacts with the model substrate, giving rise to enantioenriched product.

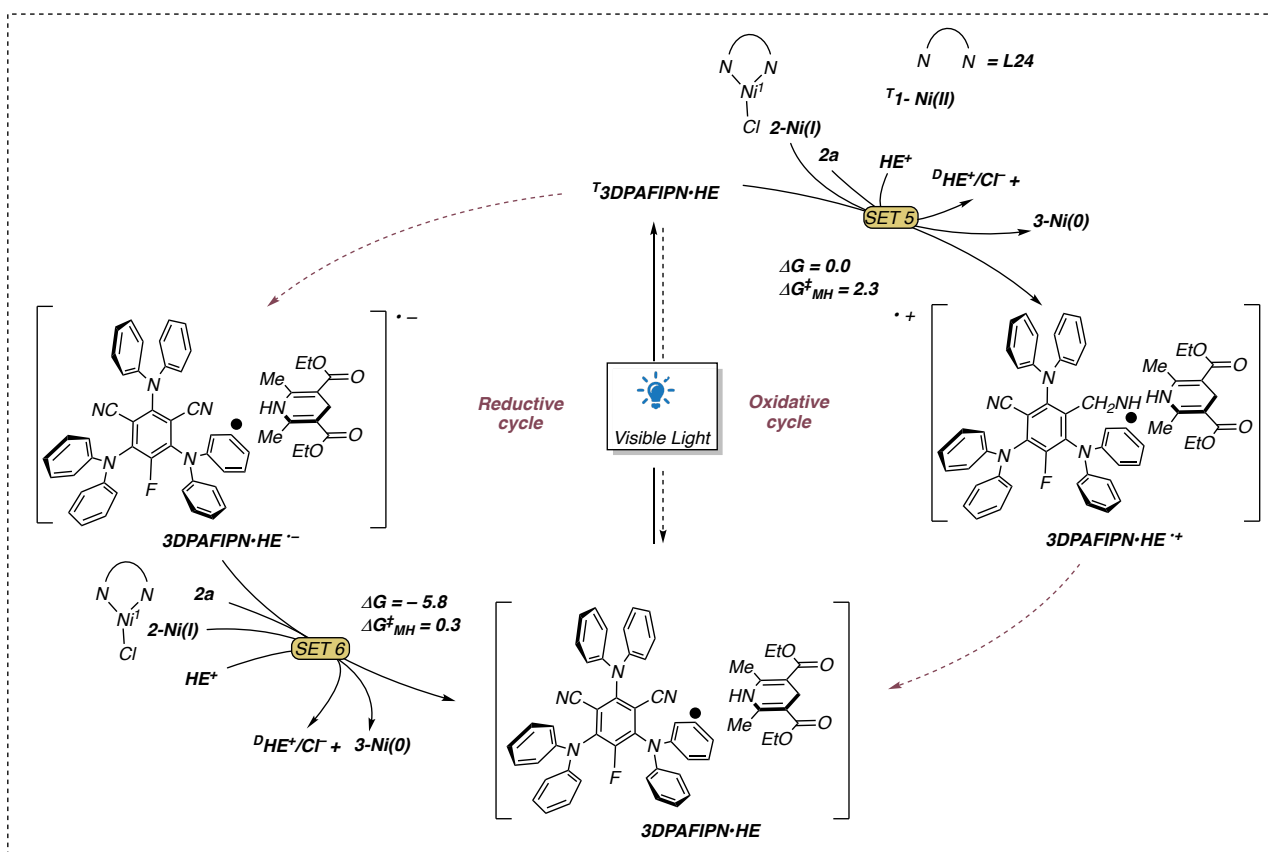
As discussed before, the nickel precatalyst ^T1-Ni^{II} is reduced to 2-Ni^I, however, the step corresponding to oxidative addition of **2a** to 2-Ni^I, requires a very high activation barrier of 41.9 kcal/mol.³⁰⁸ These results indicates that 2-Ni^I is catalytically inactive for the studied reaction.

³⁰⁸ a) Maity, B.; Zhu, C.; Yue, H.; Huang, L.; Harb, M.; Minenkov, Y.; Rueping, M.; Cavallo, L. Mechanistic Insight into the Photoredox-Nickel-HAT Triple Catalyzed Arylation and Alkylation of α -Amino Csp³-H Bonds. *J. Am. Chem. Soc.* **2020**, *142*, 16942–16952. <https://dx.doi.org/10.1021/jacs.0c05010>. b)



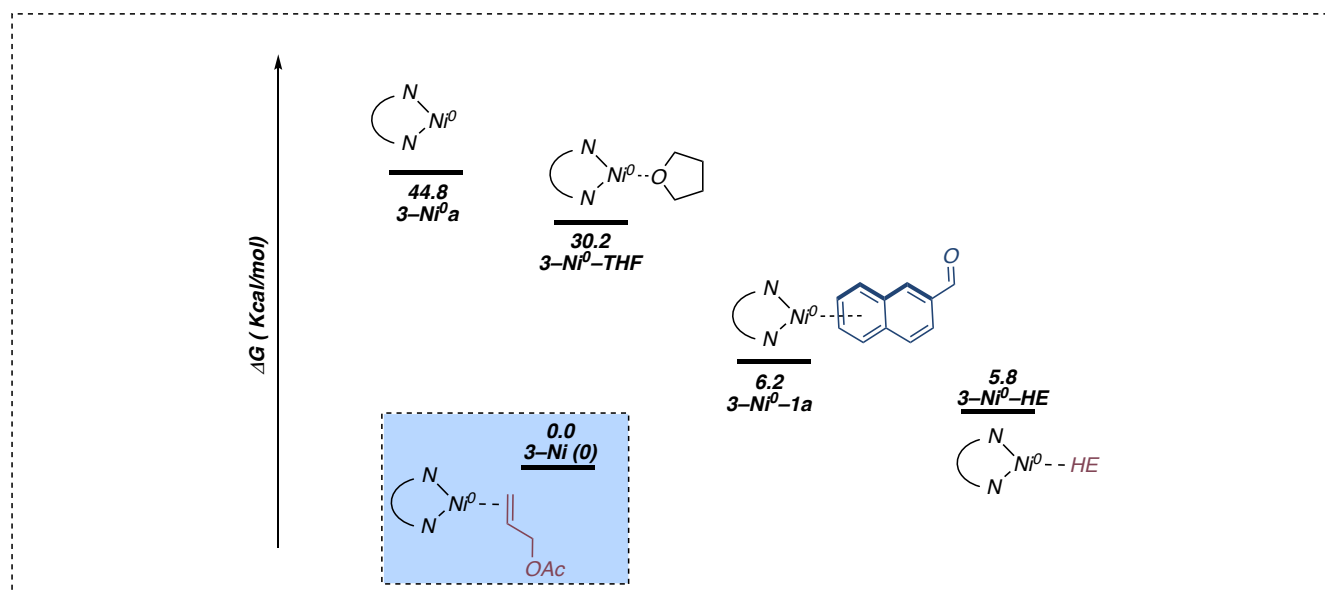
Chapter 4. Figure 23 Free energy values (in kcal/mol) for a) oxidative addition of **2a** to **2-Ni^I** complex and b) disproportionation step of **2-Ni^I**.

Nevertheless, as depicted in **Figure 24**, similarly to **^T1-Ni^{II}** to **2-Ni^I**, **2-Ni^I** can be reduced to **3-Ni⁰** by either **^T3DPAFIPN** or **3DPAFIPN·HE⁻** along the reductive and the oxidative quenching cycles.



Chapter 4. Figure 24 Two alternative photoredox catalytic cycles for the Ni^I/Ni⁰ reduction.

In light of that, as described in **Figure 25** the associated energies of possible Ni⁰-complexes involved in the allylation reaction were evaluated.



Chapter 4. Figure 25 Energetics of possible Ni⁰-complexes involved in the allylation of aldehydes.

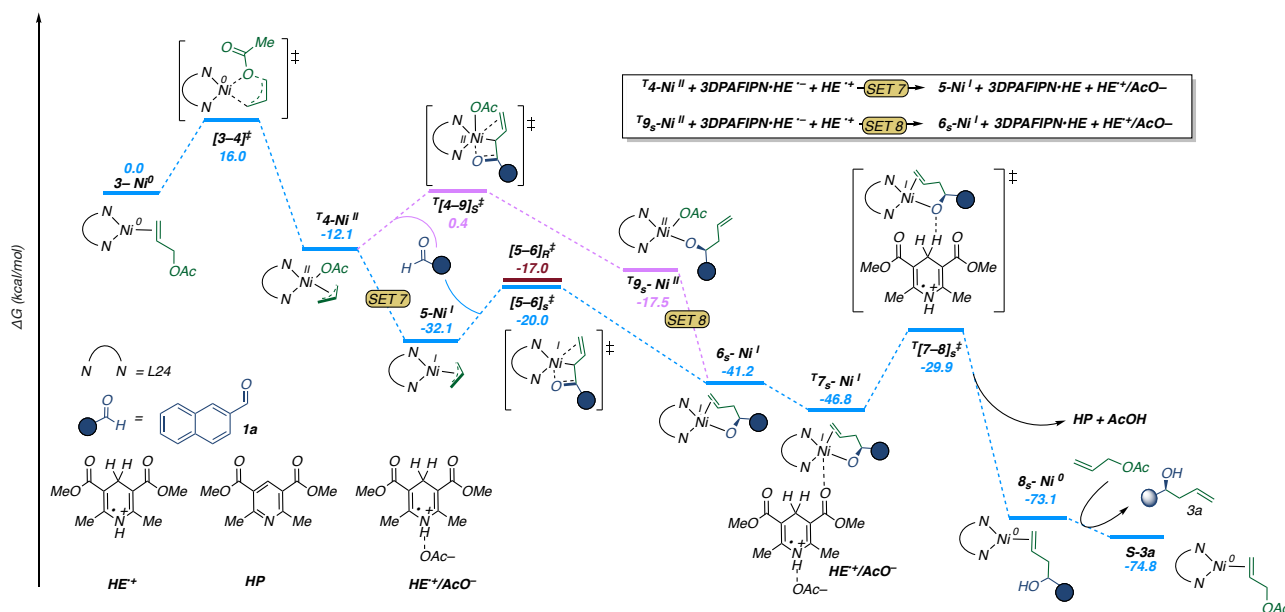
Once the most stable involved species in the process had been identified, it was possible to evaluate through DFT modelling the most favorable pathway for the reaction. The nickel catalytic cycle starts with the oxidative addition of coordinated allyl acetate **2a** to the nickel atom of **3-Ni⁰** via transition state [**3-4**][‡] and an energy barrier of 16.0 kcal/mol, leading to ^T**4-Ni^{II}**. The moderate barrier along with high the exergonicity (−12.1 kcal/mol) indicates that this oxidative addition step is facile. The resulting Ni^{II}-intermediate ^T**4-Ni^{II}** undergoes exergonic 1e[−] reduction coupled with 3DPAFIPN·HE⁺/3DPAFIPN·HE oxidation generating the Ni^I-intermediate **5-Ni^I**, through **SET7**. **SET7** is a highly exergonic process, with a Δ*G* of −19.9 kcal/mol. The reaction continues with the insertion of the carbonyl group of 2-naphthaldehyde into the Ni-allyl bond in **5-Ni^I** via transition state [**5-6**]_s[‡] and an energy barrier of 11.9 kcal/mol, leading to **6_s-Ni^I**. This corresponds to the enantioselective step, with formation of the stereocenter.

As an alternative, we tried to interchange the sequence of SET and C=O insertion steps (pink line). Along this pathway insertion of the carbonyl group of **1a** into the Ni-allyl bond in ^T**4-Ni^{II}**, via transition state ^T[**4-9**]_s[‡] and an energy barrier of 12.5 kcal/mol, leads to ^T**9_s-Ni^{II}**, from which 1e[−] reduction, *i.e.*, **SET8**, leads to the common intermediate **6_s-Ni^I**. However, this alternative pathway is energetically disfavored, and was not considered further.

However, at this point in the process, computational modelling has also made it possible to elucidate the mechanism by which the radical cation resulting from the oxidation of HE performs its scavenger function.

The breaking of the nickel-oxygen bond is believed to occur through an initial coordination of one carbonyl moiety of the Hantzsch's ester derivative **HE⁺/AcO[−]** onto the metal center of **6_s-Ni^I** and the

consequent formation of the stable complex of ${}^T7_S\text{-Ni}^I$, an exergonic step by 5.6 kcal/mol. Then a proton-coupled electron transfer occurs via transition state ${}^T[7-8]_S^\ddagger$ and a free energy barrier of 16.9 kcal/mol, leading to 8_S-Ni^0 with the liberation of **HP** (Hantzsch's ester pyridine) and acetic acid. The desired product, already formed in the 8_S-Ni^0 intermediate, is replaced by another molecule of allyl acetate allowing a further catalytic cycle to begin.

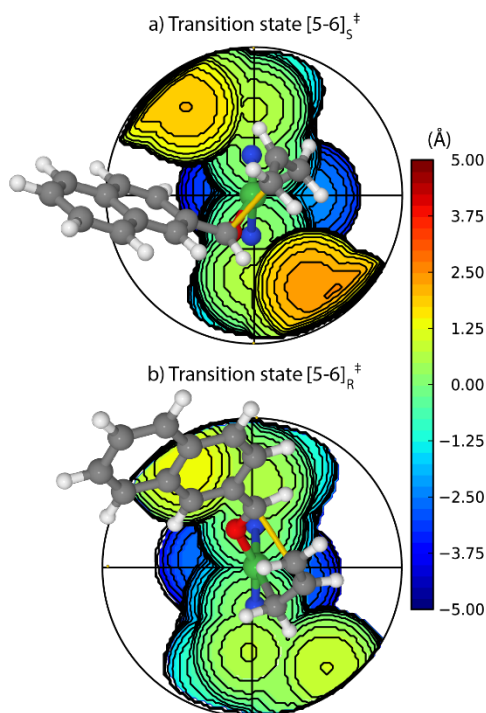


Chapter 4. Figure 26 Proposed mechanism for the nickel catalytic cycle of allylation of aldehydes.

Having clarified the overall mechanism leading to formation of the experimentally favored *S*-product, the enantioselective steps from 5-Ni^I to 6_S-Ni^I , leading to the formation of the *S*-product was in-depth investigated. Calculations indicate that transition state $[5-6]_S^\ddagger$, leading to the *S*-product, is favored by 3.0 kcal/mol over transition state $[5-6]_R^\ddagger$, leading to the *R*-product, which is in agreement with the experimentally observed high enantioselectivity. The comparison of the competing transition state geometries indicates that the **L24** ligand shapes a chiral catalytic pocket³⁰⁹ with hindered north-west (NW) and south-east (SE) quadrants, and unhindered north-east (NE) and south-west quadrants (SW) quadrants. In the favored $[5-6]_S^\ddagger$ transition state, the reacting substrates are placed in the unhindered SW and NE quadrants, minimizing steric interaction with the **L24** ligand. In contrast, the substrate is placed in the more hindered NW and SE quadrants in transition state $[5-6]_R^\ddagger$, with the **L24** ligand bending away from the substrate, as evidenced by a flattening of the bumps in NW and SE quadrants (note the greenish color

³⁰⁹ a) Falivene, L.; Credendino, R.; Poater, A.; Petta, A.; Serra, L.; Oliva, R.; Scarano, V.; Cavallo, L. SambVca 2. A Web Tool for Analyzing Catalytic Pockets with Topographic Steric Maps. *Organometallics* **2016**, *35* (13), 2286–2293. <https://doi.org/10.1021/acs.organomet.6b00371>. b) Falivene, L.; Cao, Z.; Petta, A.; Serra, L.; Poater, A.; Oliva, R.; Scarano, V.; Cavallo, L. Towards the Online Computer-Aided Design of Catalytic Pockets. *Nat. Chem.* **2019**, *11* (10), 872–879. <https://doi.org/10.1038/s41557-019-0319-5>.

of the bumps in $[5-6]_{\text{R}}^{\ddagger}$, compared to the orange bumps in $[5-6]_{\text{S}}^{\ddagger}$. This steric clash between the substrate and the **L24** ligand explains the higher energy of in $[5-6]_{\text{R}}^{\ddagger}$.



Chapter 4. Figure 27 Optimized geometries of transition states pro-S, i.e. $[5-6]_{\text{S}}^{\ddagger}$ (a), and pro-R, i.e. $[5-6]_{\text{R}}^{\ddagger}$ (b), with the Ni atom, the N atom of the **L24** ligand and the substrates represented as ball and stick, overlapped to the steric map of the **L24** ligand. The emerging C-C bond is colored in gold.

• Conclusions

In summary, we have reported a novel allylation photoredox methodology based on the use of the nickel catalysis. Disclosing this new protocol has shown that the combination of photoredox and nickel catalysis is excellent not only for cross-coupling protocols, but also for new, more sustainable and less waste-producing Grignard-type reactions. In fact, compared to other allylation reactions allowed by the formation of catalytic transient nucleophilic organonickel species, the presented reaction does not require external overstoichiometric metal reductants or additives. In-depth optimization of the reaction conditions and fine-tuning of all the parameters enabled the development of a methodology that was compatible in the presence of both aromatic and aliphatic aldehydes with yields from moderate to good. Moreover, it was possible to extend the protocol not only to the use of simple allyl acetate, but more decorated allyl species have been found suitable for the process, exhibiting an excellent regiochemical outcome. In the same way, it was also possible to preliminarily establish that the process can be extended to the propargylation reaction.

A careful photophysical and electrochemical analysis of the reaction provided a detailed picture of the mechanism, also highlighting some differences with non-light-driven analogues protocol already present in the literature. After a long and unsuccessful journey and through a drastic modification of the previously optimized reaction conditions, it was also possible to establish a dual photoredox and nickel catalyzed protocol for an enantioselective version of the process. The introduction of a photocatalyst with a marked reducing character in the excited state, together with the introduction of Hantzsch's ester as a new organic sacrificial reductant, made it possible to re-design the reaction conditions to obtain an excellent stereoselective protocol. We were pleased to note that the use of a chiral bisoxazoline-based ligand surrounding the nickel center allowed the realization of a large library of highly enantioenriched homoallylic alcohols deriving from both aromatic and aliphatic aldehydes. The role of 3DPAFIPN was thoroughly analyzed and carefully interpreted from the photophysical point of view, allowing to draw a mechanistic picture of the reaction which is additionally supported by theoretical calculations. A distinctive mechanism for the turnover of the nickel catalyst is suggested, adding a new feature to the multifaceted reactivity of the Hantzsch's ester. An inexpensive cooling apparatus guarantees the control of temperature necessary for obtaining e.e.s from 89% to 94%. Further studies will aim to extend this protocol to ketones and to exploit other redox-active metals for enantioselective photoredox reactions.

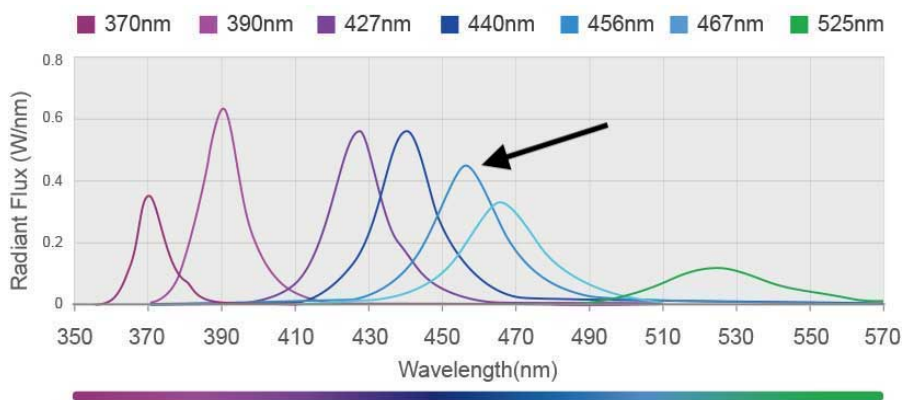
• Supplementary data

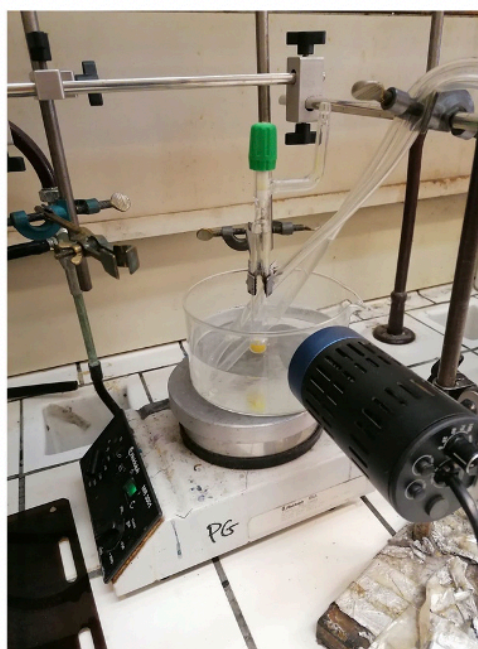
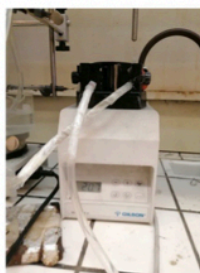
General methods and materials

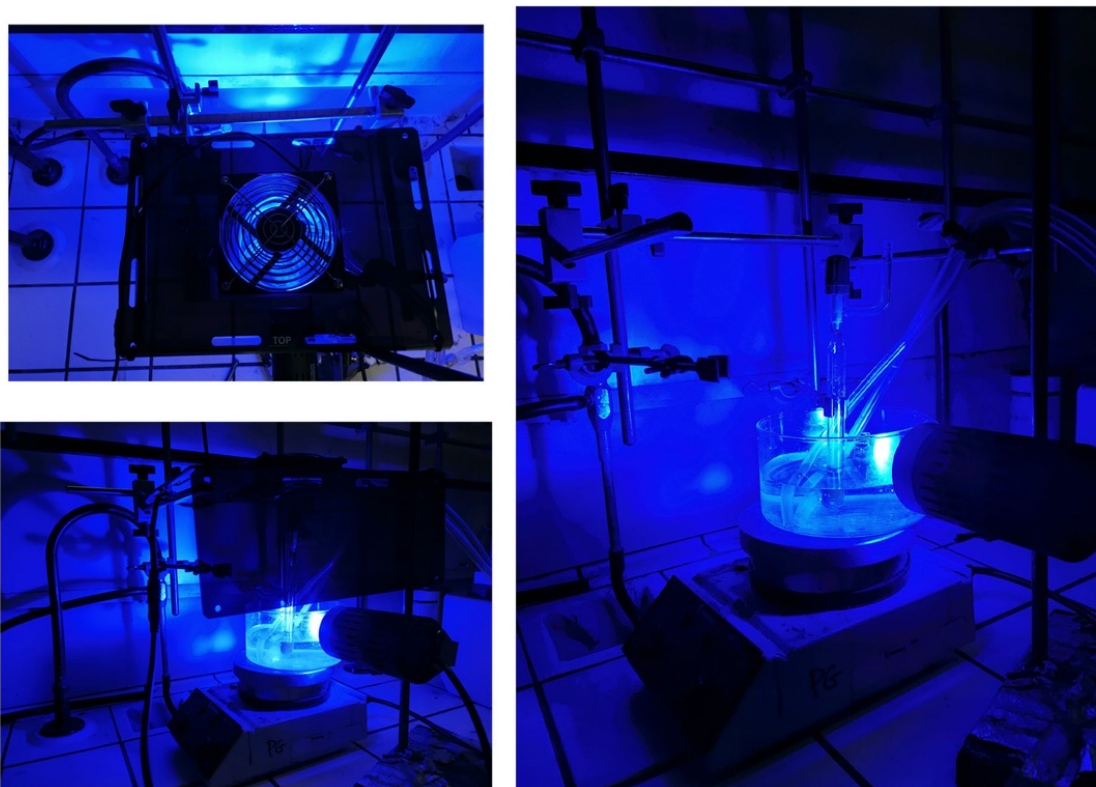
^1H -NMR spectra were recorded on Varian Mercury 400 spectrometer. Chemical shifts are reported in ppm from TMS with the solvent resonance as the internal standard (CHCl_3 : $\delta = 7.27$ ppm). Data are reported as follows: chemical shift, multiplicity (s = singlet, d = doublet, t = triplet, q = quartet, dd = doublet of doublets, m = multiplet), coupling constants (Hz). ^{13}C -NMR spectra were recorded on Varian Mercury 400 spectrometer. Chemical shifts are reported in ppm from TMS with the solvent as the internal standard (CDCl_3 : $\delta = 77.0$ ppm). GC-MS spectra were taken by EI ionization at 70 eV on a Hewlett-Packard 5971 with GC injection. Analytical high-performance liquid chromatograph (HPLC) was performed on a HP 1090 liquid chromatograph equipped with a variable wavelength UV detector (deuterium lamp 190-600 nm), using Daicel ChiralcelTM or PhenomenexTM columns (0.46 cm I.D. x 25 cm). HPLC grade isopropanol and hexane were used as the eluting solvents. Chromatographic purifications were done with 240-400 mesh silica gel. All reactions were set up under an argon atmosphere in oven-dried glassware using standard Schlenk techniques.

Anhydrous solvents were supplied by Aldrich in Sureseal[®] bottles. Anhydrous tetrahydrofuran was freshly distilled before the use in order to remove the radical inhibitor BHT present as stabilizer. Unless specified, other anhydrous solvents were used without further purifications. All the reagents were purchased from commercial sources (Sigma-Aldrich, Alfa Aesar, Fluorochem, Strem Chemicals, TCI) and used without further purification unless specified. 3Å molecular sieves were supplied by Sigma-Aldrich and activated before the use. Activation of the MS was performed through five 6-minute cycles in microwave (750W). Once the cycles are completed the MS are rapidly inserted in Schlenk tube, equipped with a Rotaflo[®] stopcock and then flame-dried for 5 minutes under vacuum.

Reaction mixture was irradiated with Kessil[®] PR160L@456 nm.







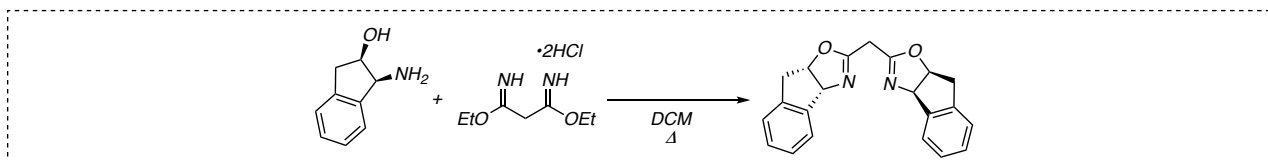
Chapter 4. Supplementary 3 Reaction set-up with Kessil® PR160L@456 nm lamp.

The reaction flasks were positioned approximately at 10 cm from the light source and Kessil® PR160 Rig with Fan. with a home-made cryostat system filled with ice that allows the control of the temperature. The reaction temperature was close to 10 °C during the irradiation as measured with a thermometer at 2 cm from the reaction flask.

The blue flask was filled with ice in order to allow the refrigeration of the running water.

Representative procedure for the synthesis of (1R,2S) amino-indanol substituted bis(oxazolines)

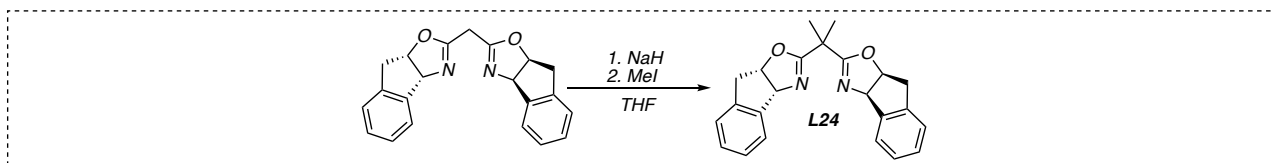
Synthesis of bis((3aR,8aS)-3a,8a-dihydro-8H-indeno[1,2-d]oxazol-2-yl)methane



Following the procedure reported by Reisman *et al.*³¹⁰, a flame-dried 250 mL Schlenk tube, equipped with a magnetic stirring bar, was charged with (1R,2S)-(+)-*cis*-1-amino-2-indanol (500 mg, 3.35 mmol, 2.1 equiv.) and diethyl malonimidate dihydrochloride (360 mg, 1.56 mmol, 1 equiv.) under argon atmosphere. Then dry DCM (40 mL) was added, and the solution was heated at 40 °C for two days. The reaction was monitored by direct NMR analysis of the reaction mixture until disappearance of the starting material was observed. Then, the reaction was quenched with water (ca. 20 mL). The layers were separated, the aqueous layer was extracted three times with DCM (ca. 3 x 10 mL), The organic layers were combined, dried with Na₂SO₄, filtered, and concentrated. Crude bis((3aR,8aS)-3a,8a-dihydro-8H-indeno[1,2-d]oxazol-2-yl)methane was isolated as white crystals after recrystallization from hot ethanol (220 mg, 0.67 mmol, 43% yield). Spectroscopic data agree with those reported in literature.

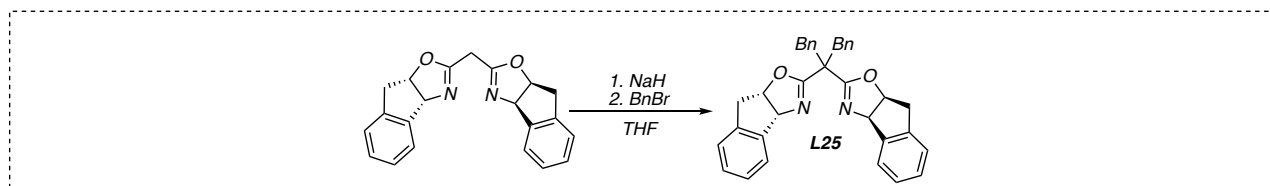
³¹⁰ Hofstra, J. L.; DeLano, T. J.; Reisman, S. E. Synthesis of Chiral Bisoxazoline Ligands: (3aR,3a'R,8aS,8a'S)-2,2'-(cyclopropane-1,1-diyl)bis(3a,8adihydro-8H-indeno[1,2-d]oxazole) *Org. Synth.* **2020**, *97*, 172-188. 10.15227/orgsyn.097.0172

Synthesis of (3a*R*,3a'*R*,8a*S*,8a'*S*)-2,2'-(propane-2,2-diyl)bis(3a,8a-dihydro-8*H*-indeno[1,2-*d*]oxazole
(**L24**)



Chiral bis(oxazoline) ligand **L24** was obtained adapting the procedure reported by Reisman et al.³¹⁰ A flame-dried 20 mL Schlenk tube, equipped with a magnetic stirring bar, was charged with NaH (60 wt% in mineral oil, 72 mg, 1.8 mmol, 3 equiv.) under argon atmosphere. In order to remove the mineral oil, sodium hydride was washed once with 3 mL of hexane and then twice with 3 mL of dry THF. The compound was then suspended in 3 mL of dry THF and cooled to 0 °C with an ice bath. Subsequently, bis((3a*R*,8a*S*)-3a,8a-dihydro-8*H*-indeno[1,2-*d*]oxazol-2-yl)methane (200 mg, 0.6 mmol, 1 equiv.) was added and the reaction mixture was stirred at room temperature for 90 minutes. Then, iodomethane (341 mg, 149 μ L, 2.4 mmol, 4 equiv.) was added dropwise under argon flux. The reaction mixture was refluxed until GC/MS analysis showed a full conversion of the starting material. The reaction mixture was cooled to room temperature, quenched with *ca.* 5 mL of saturated aqueous NH₄Cl, extracted with ethyl acetate (*ca.* 4 x 5 mL), dried with Na₂SO₄, filtered, and concentrated. Chiral ligand **L24** was isolated as white crystals after recrystallization from hot ethanol (145 mg, 0.4 mmol, 67% yield). Spectroscopic data agree with those reported in literature.

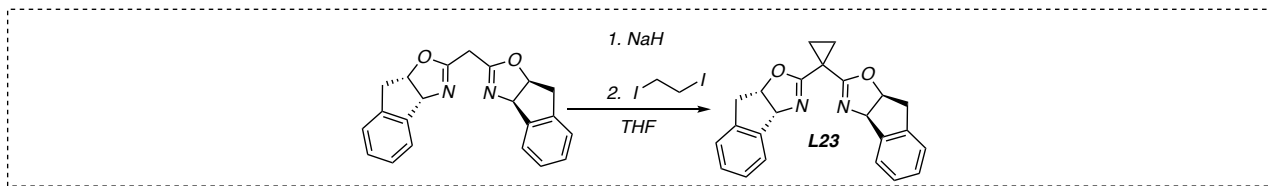
Synthesis of (3aR,3a'R,8aS,8a'S)-2,2'-(1,3-diphenylpropane-2,2-diyl)bis(3a,8a-dihydro-8H-indeno[1,2-d]oxazole (L25)



Chiral bis(oxazoline) ligand **L25** was obtained adapting the procedure reported by Reisman *et al.*³¹⁰ A flame-dried 20 mL Schlenk tube, equipped with a magnetic stirring bar, was charged with NaH (60 wt% in mineral oil, 36 mg, 0.9 mmol, 3 equiv.) under argon atmosphere. In order to remove the mineral oil, sodium hydride was washed once with 2 mL of hexane and then twice with 2 mL of dry THF. The compound was, then, suspended in 2 mL of dry THF and cooled to 0 °C with an ice bath. Subsequently, bis((3aR,8aS)-3a,8a-dihydro-8H-indeno[1,2-d]oxazol-2-yl)methane (100 mg, 0.3 mmol, 1 equiv.) was added and the reaction mixture was stirred at room temperature for 90 minutes. Then, benzyl bromide (205 mg, 143 μ L, 1.2 mmol, 4 equiv.) was added dropwise under argon flux. The reaction mixture was refluxed until GC/MS analysis showed a full conversion of the starting material. The reaction mixture was cooled to room temperature, quenched with *ca.* 5 mL of saturated aqueous NH₄Cl, extracted with ethyl acetate (*ca.* 4 x 5 mL), dried with Na₂SO₄, filtered, and concentrated. Chiral ligand **L25** was isolated as white crystals after recrystallization from hot ethanol (59 mg, 0.12 mmol, 38% yield). Spectroscopic data agree with those reported in literature.³¹¹

³¹¹ Burguete, M. I.; Fraile, J. M.; García, J. I.; García-Verdugo, E.; Herrerías, C. I.; Luis, S. V.; Mayoral, J. A. Bis(Oxazoline)Copper Complexes Covalently Bonded to Insoluble Support as Catalysts in Cyclopropanation Reactions. *J. Org. Chem.* **2001**, *66* (26), 8893–8901. <https://doi.org/10.1021/jo0159338>.

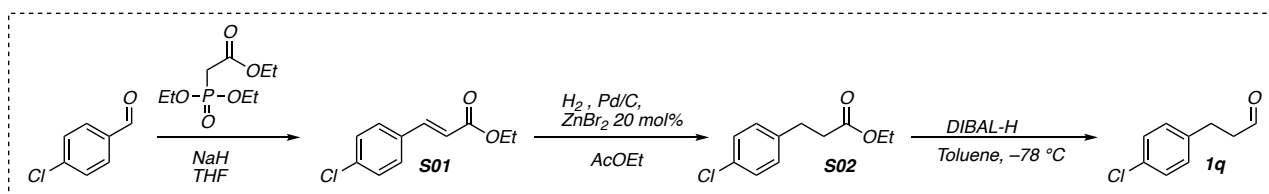
Synthesis of (3aR,3a'R,8aS,8a'S)-2,2'-(cyclopropane-1,1-diyl)bis(3a,8a-dihydro-8H-indeno[1,2-d]oxazole) (**L23**)



Chiral bis(oxazoline) ligand **L23** was obtained adapting the procedure reported by Reisman *et al.* 310 A flame-dried 20 mL Schlenk tube, equipped with a magnetic stirring bar, was charged with NaH (60 wt% in mineral oil, 36 mg, 0.9 mmol, 3 equiv.) under argon atmosphere. In order to remove the mineral oil, sodium hydride was washed once with 2 mL of hexane and then twice with 2 mL of dry THF. The compound was, then, suspended in 2 mL of dry THF and cooled to 0 °C with an ice bath. Subsequently, bis((3aR,8aS)-3a,8a-dihydro-8H-indeno[1,2-d]oxazol-2-yl)methane (100 mg, 0.3 mmol, 1 equiv.) was added and the reaction mixture was stirred at room temperature for 90 minutes. Then, 1,2-diiodoethane (101 mg, 47 μ L, 0.36 mmol, 1.2 equiv.) was added dropwise under argon flux. The reaction mixture was refluxed until GC/MS analysis showed a full conversion of the starting material. The reaction mixture was cooled to room temperature, quenched with *ca.* 5 mL of saturated aqueous NH₄Cl, extracted with ethyl acetate (*ca.* 4 x 5 mL), dried with Na₂SO₄, filtered, and concentrated. Chiral ligand **L23** was isolated as white crystals after recrystallization from hot ethanol (89 mg, 0.25 mmol, 83% yield). Spectroscopic data agree with those reported in literature.

Synthesis and characterization of the substrates

Synthesis of aldehyde **1q**



•**Synthesis of S01:** **S01** was prepared following a standard Horner–Wadsworth–Emmons (HWE) procedure: a flame-dried two-necked round bottom flask, equipped with a magnetic stirring bar, was charged with triethyl phosphonoacetate (1.09 mL, 5.5 mmol, 1.1 equiv.) and dry THF (7.5 mL) under argon atmosphere. The solution was cooled to 0 °C and NaH (60 wt% in mineral oil, 260 mg, 6.5 mmol, 1.3 equiv.) was added. The solution was stirred for 15 minutes, then, a solution of 4-chlorobenzaldehyde (700 mg, 5 mmol, 1 equiv.) in dry THF (13 mL) was added dropwise to the reaction mixture. The reaction mixture was stirred at room temperature until the TLC showed a complete conversion of the starting material. The reaction mixture was cooled to 0 °C and was quenched with water (ca. 10 mL). The organic solvent was evaporated under reduced pressure and 10 mL ethyl acetate were added. The layers were separated, the aqueous layer was extracted three times with ethyl acetate (ca. 3x10 mL), The organic layers were combined, dried with Na₂SO₄, filtered, and concentrated. **S01** was isolated after flash chromatography (silica, cyHex:Et₂O 9:1) in 75% yield (790 mg, 3.75 mmol). Spectroscopic data are in agreement with those reported in literature.³¹²

•**Synthesis of S02:** **S02** was prepared according to the procedure reported by Wu *et al.*³¹³ A flame-dried two-necked round bottom flask, equipped with a magnetic stirring bar, was charged with **S01** (790 mg, 3.75 mmol, 1. equiv.) and EtOAc (30 mL) under argon atmosphere. Then, ZnBr₂ (166 mg, 0.74 mmol, 0.2 equiv.) and palladium on activated carbon (Pd/C 10 wt. % loading, 80 mg, 10% w/w) were added. The apparatus was partially evacuated and then refilled with hydrogen (balloon), and the reaction mixture was stirred for 20 hours at room temperature. When GC/MS analysis showed a full conversion of the starting material, the reaction mixture was filtered over a Celite® pad and concentrated in vacuum. Spectroscopically pure compound **S02** was obtained in quantitative yield (797 mg, 3.75 mmol) and used as such in the next step. Spectroscopic data are in agreement with those reported in literature.³¹⁴

³¹² Song, C.; Yang, C.; Zeng, H.; Zhang, W.; Guo, S.; Zhu, J. Rh(III)-Catalyzed Enaminone-Directed C–H Coupling with α -Diazo- α -phosphonoacetate for Reactivity Discovery: Fluoride-Mediated Dephosphonation for C–C Coupling Reactions. *Org. Lett.* **2018**, *20*, 3819–3823. <https://doi.org/10.1021/acs.orglett.8b01406>

³¹³ Wu, G.; Huang, M.; Richards, M.; Poirier, M.; Wen, X.; Draper, R. W. Novel ZnX₂-modulated Pd/C and Pt/C catalysts for chemoselective hydrogenation and hydrogenolysis of halogen-substituted nitroarenes, alkenes, benzyl ethers, and aromatic ketones. *Synthesis*, **2003**, 2003(11), 1657–1660. 10.1055/s-2003-40878

³¹⁴ Nestl, B. M.; Glueck, S. M.; Hall, M.; Kroutil, W.; Stuermer, R.; Hauer, B.; Faber, K. Biocatalytic Racemization of (Hetero)Aryl-aliphatic α -Hydroxycarboxylic Acids by *Lactobacillus* spp. Proceeds via an Oxidation–Reduction Sequence *Eur. J. Org. Chem.* **2006**, 4573–4577. <https://doi.org/10.1002/ejoc.200600454>

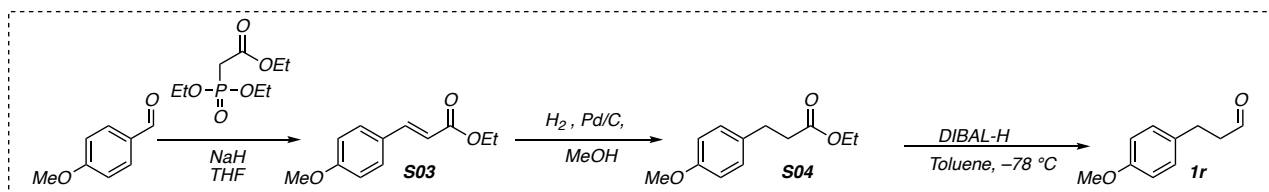
•*Synthesis of 1q*:

1q was obtained adapting the procedure reported by Papai *et al.*³¹⁵ a flame-dried A flame-dried two-necked round bottom flask, equipped with a magnetic stirring bar, was charged with **S02** (425 mg, 2 mmol, 1 equiv.) and anhydrous toluene (8 mL) under argon atmosphere. The solution was cooled to -78 °C and DIBAL-H (1.5 M in toluene, 1.47 mL, 2.2 mmol, 1.1 equiv.) was added dropwise. The solution was stirred 1h at -78 °C and monitored by TLC (cyHex:Et₂O 9:1) until a full conversion of the starting material was observed. The reaction was quenched at -78 °C adding 1.1 mL of ethanol (dropwise) and allowed to warm to room temperature. The mixture was washed with 1 M HCl (*ca.* 3x5 mL), followed by NaHCO₃ (*ca.* 10 mL) and brine (*ca.* 10 mL). Upon separation, the organic layer was dried with Na₂SO₄, filtered, and concentrated. Compound **1q** was isolated as a colorless oil after flash chromatography (silica, cyHex:Et₂O 95:5) in 68% yield (229 mg, 1.36 mmol). Spectroscopic data are in agreement with those reported in literature.³¹⁶

³¹⁵ Földes, T., Madarász, Á., Révész, Á., Dobi, Z., Varga, S., Hamza, A., Nagy, P.R., Pihko, P.M. Pápai, I. Stereocontrol in diphenylprolinol silyl ether catalyzed Michael additions: steric shielding or Curtin–Hammett scenario? *J. Am. Chem. Soc.* **2017**, *139*, 17052–17063. <https://doi.org/10.1021/jacs.7b07097>

³¹⁶ Santi, N.; Morrill, L. C.; Świderek, K.; Moliner, V.; Luk, L. Y. P. Transfer hydrogenations catalyzed by streptavidin-hosted secondary amine organocatalysts *Chem. Commun.*, **2021**, *57*, 1919–1922. <https://doi.org/10.1039/D0CC08142F>

Synthesis of aldehyde **1r**



•**Synthesis of **S03****: **S03** was prepared following a standard Horner–Wadsworth–Emmons (HWE) procedure: a flame-dried two-necked round bottom flask, equipped with a magnetic stirring bar, was charged with triethyl phosphonoacetate (1.09 mL, 5.5 mmol, 1.1 equiv.) and dry THF (7.5 mL), under argon atmosphere. The solution was cooled to 0 °C and NaH (60 wt% in mineral oil, 260 mg, 6.5 mmol, 1.3 equiv.) was added. The solution was stirred for 15 minutes, then, a solution of 4-methoxybenzaldehyde (680 mg, 5 mmol, 1 equiv.) in dry THF (13 mL) was added dropwise to the reaction mixture. The reaction stirred at room temperature until the TLC showed a complete conversion of the starting material. The reaction mixture was cooled to 0 °C and was quenched with water (*ca.* 10 mL). The layers were separated, and the aqueous layer was extracted three times with ethyl acetate (*ca.* 3x10 mL). The organic layers were combined, dried with Na₂SO₄, filtered, and concentrated. **S03** was isolated as a colorless oil after flash chromatography (silica, cyHex:Et₂O 9:1) in 80% yield (825 mg, 4 mmol). Spectroscopic data are in agreement with those reported in literature.³¹⁷

•**Synthesis of **S04****: A flame-dried two-necked round bottom flask, equipped with a magnetic stirring bar, was charged with **S03** (825 mg, 4 mmol, 1 equiv.) and EtOH (30 mL), under argon atmosphere. Then, palladium on activated carbon (Pd/C 10 wt. % loading, 83 mg, 10% w/w) was added. The apparatus was partially evacuated and then refilled with hydrogen (balloon), and the reaction mixture was stirred for 20 hours at room temperature. When GC/MS analysis showed a full conversion of the starting material, the reaction mixture was filtered over a Celite® pad and concentrated in vacuum. Spectroscopically pure compound **S04** was obtained as a pale-yellow oil without further purification (89%, 741 mg, 3.56 mmol) and used as such for the next step. Spectroscopic data are in agreement with those reported in literature.³¹⁸

•**Synthesis of **1r****: **1r** was obtained adapting the procedure reported by Papai *et al.*³¹⁷ A flame-dried two-necked round bottom flask, equipped with a magnetic stirring bar, was charged with was prepared a solution of **S04** (741 mg, 3.56 mmol, 1 equiv.) and anhydrous toluene (14 mL) under argon atmosphere. The solution was cooled to -78 °C and a solution of DIBAL-H (1.5 M in toluene, 2.6 mL, 3.9 mmol, 1.1 equiv.) was added dropwise. The solution was stirred 1h at -78 °C, and monitored by TLC

³¹⁷ Sarvi, I.; Gholizadeh, M.; Izadyar, M.; Threonine stabilizer-controlled well-dispersed small palladium nanoparticles on modified magnetic nanocatalyst for Heck cross-coupling process in water *Appl Organometal Chem.* 2019; 33:e4645. <https://doi.org/10.1002/aoc.4645> © 2018 John Wiley & Sons,

³¹⁸ Zhang, X.-W.; Jiang, G.-Q.; Lei, S.-H.; Shan, X.-H.; Qu, J.-P.; Kang, Y.-B. Iron-Catalyzed α,β-Dehydrogenation of Carbonyl Compounds *Org. Lett.* **2021**, 23, 5, 1611–1615. <https://doi.org/10.1021/acs.orglett.1c00043>

(cyHex:Et₂O 9:1) until a full conversion of the starting material was observed. The reaction was quenched at -78 °C adding 1.9 mL of ethanol (dropwise) and allowed to warm to room temperature. The mixture was washed with 1 M HCl (*ca.* 3x5 mL), followed by NaHCO₃ (*ca.* 10 mL) and brine (*ca.* 10 mL). Upon separation, the organic layer was dried with Na₂SO₄, filtered, and concentrated. Compound **1r** was isolated as a colorless oil after flash chromatography (silica, cyHex:Et₂O 95:5) in 69% yield (405 mg, 2.47 mmol). Spectroscopic data are in agreement with those reported in literature.³¹⁹

³¹⁹Schaubach, S.; Gebauer, K.; Ungeheuer, F.; Hoffmeister, L.; Ilg, M. K.; Wirtz, C.; Fürstner, A. A Two-Component Alkyne Metathesis Catalyst System with an Improved Substrate Scope and Functional Group Tolerance: Development and Applications to Natural Product Synthesis *Chem. Eur. J.*, **2016**, *22*, 8494–8507. <https://doi.org/10.1002/chem.201601163>

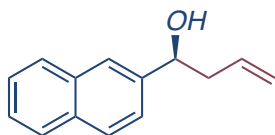
General procedure for enantioselective photoredox nickel-catalyzed allylation of aldehydes

Standard procedure:

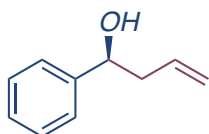
All the reactions were performed on 0.2 mmol scale of aldehyde. A dry 10 mL Schlenk tube, equipped with a Rotaflo® stopcock, magnetic stirring bar and an argon supply tube, was first charged under argon with activated 3Å molecular sieves and [NiCl₂(glyme)] (10 mol%, 0.02 mmol, 4.4 mg) that was flame-dried under vacuum to eliminate the presence of water. Then, all the solids, the substrate if solid **1** (0.2 mmol the organic photocatalyst 3DPAFIPN (5 mol%, 0.01 mmol, 6.5 mg), diethyl 1,4-dihydro-2,6-dimethyl-3,5-pyridinedicarboxylate Hantzsch's ester (2 equivalents, 0.4 mmol, 101 mg) and the chiral ligand **L24** (15 mol %, 0.03 mmol, 10.8 mg) were added. Inhibitor-free dry THF (0.5 mL in order to obtain a 0.4 M substrate solution) was then added and the reaction mixture was further subjected to a freeze-pump-thaw procedure (three cycles) and the vessel refilled with argon. Then, allyl acetate **2** (0.6 mmol, 3 equiv., 60 mg, 65 µL) and the substrate if liquid **1** (0.2 mmol) were added. The reaction mixture was irradiated under vigorous stirring for 14h. After that, the reaction mixture was quenched with water (approx. 4 mL) and extracted with EtOAc (4x3 mL). The combined organic layers were dried over anhydrous Na₂SO₄ and the solvent was removed under reduced pressure. The crude was purified by flash column chromatography (SiO₂) to afford products **3** in the stated yields.

Standard procedure for functionalization for UV/VIS inactive substrates:

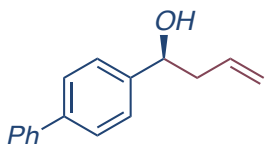
A flame-dried two-necked round bottom flask, equipped with a magnetic stirring bar, was charged with UV/Vis inactive substrate (**3t**, **3u** and **3w**, 1 equiv., appropriately purified by flash chromatography and fully characterized) and dry DCM (6 mL/mmol) under argon atmosphere. The solution was cooled to 0 °C and pyridine (2 equiv.) and 3,5-dinitrobenzoyl chloride (2 equiv.) were subsequently added. The reaction mixture was stirred for 3h at room temperature and monitored by TLC (cyHex:Et₂O 9:1) until a full conversion of the starting material was observed. The reaction was quenched with water and the mixture was extracted three times with EtOAc. The combined organic layer was washed with brine, dried over anhydrous Na₂SO₄, filtered, and concentrated under reduced pressure. The enantiomeric excess of the derivatives was evaluated without further purifications.



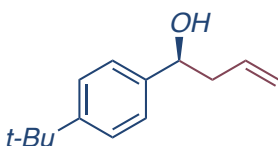
(3a) pale yellow oil, 87% (0.17 mmol, 34 mg). The general procedure was applied using **1a** (0.2 mmol, 32 mg) and **2** (0.6 mmol, 3 equiv., 60 mg, 65 μ L). The title compound was isolated by flash column chromatography (100% DCM) Spectroscopic data are in agreement with those reported in the previous chapters. HPLC analysis (Chiralcel OD-H, *n*-Hexane: *i*-PrOH = 90:10, 0.70 mL/min, 40 $^{\circ}$ C, 224 nm) indicated 93% ee (*t*-major = 17.87 min, *t*-minor = 19.76 min).



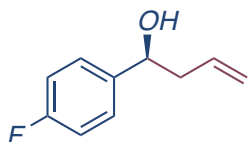
(3b) pale yellow oil, 64% (0.13 mmol, 19 mg). The general procedure was applied using previously distilled **1b** (0.2 mmol, 20 μ L), and **2** (0.6 mmol, 3 equiv., 60 mg, 65 μ L). The title compound was isolated by flash column chromatography (100% DCM). Spectroscopic data are in agreement with those reported in the previous chapters. HPLC analysis (Phenomenex LUX CELLULOSE 3, *n*-Hexane: *i*-PrOH = 85:15, 0.70 mL/min, 40 $^{\circ}$ C, 214 nm) indicated 90% ee (*t*-major = 11.53 min, *t*-minor = 12.13 min).



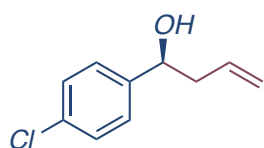
(3c) brown oil, 81% (0.16 mmol, 36 mg). The general procedure was applied using **1c** (0.2 mmol, 36 mg) and **2** (0.6 mmol, 3 equiv., 60 mg, 65 μ L). The title compound was isolated by flash column chromatography (100% DCM). Spectroscopic data are in agreement with those reported in the previous chapters. HPLC analysis (Chiralcel AD, *n*-Hexane: *i*-PrOH = 95:5, 1 mL/min, 40 $^{\circ}$ C, 214 nm) indicated 91% ee (*t*-major = 10.94 min, *t*-minor = 12.12 min).



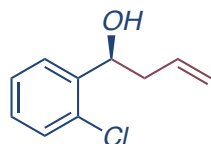
(3d) pale yellow oil, 60% (0.12 mmol, 24 mg). The general procedure was applied using previously distilled **1d** (0.2 mmol, 32 mg, 34 μ L) and **2** (0.6 mmol, 3 equiv., 60 mg, 65 μ L). The title compound was isolated by flash column chromatography (100% DCM). Spectroscopic data are in agreement with those reported in the previous chapters. HPLC analysis (Chiralcel IA, *n*-Hexane: *i*-PrOH = 9:1, 0.5 mL/min, 40 $^{\circ}$ C, 210 nm) indicated 91% ee (*t*-minor = 9.33 min, *t*-major = 9.79 min).



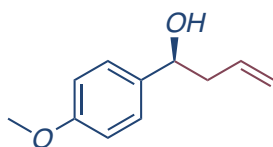
(3e) pale yellow oil, 61% (0.12 mmol, 21 mg). The general procedure was applied using previously distilled **1e** (0.2 mmol, 25 mg, 22 μ L), and **2** (0.6 mmol, 3 equiv., 60 mg, 65 μ L). The title compound was isolated by flash column chromatography (100% DCM). Spectroscopic data are in agreement with those reported in the previous chapters. HPLC analysis (Phenomenex LUX CELLULOSE 3, *n*-Hexane: *i*-PrOH = 95:5, 1 mL/min, 40 $^{\circ}$ C, 220 nm) indicated 90% ee (*t*-major = 6.67 min, *t*-minor = 7.00 min).



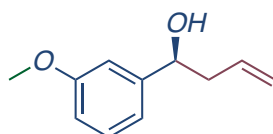
(3f) pale yellow oil, 94% (0.18 mmol, 34 mg). The general procedure was applied using **1f** (0.2 mmol, 28 mg) and **2** (0.6 mmol, 3 equiv., 60 mg, 65 μ L). The title compound was isolated by flash column chromatography (100% DCM). Spectroscopic data are in agreement with those reported in the previous chapters. HPLC analysis (Chiralcel AD, *n*-Hexane: *i*-PrOH = 95:5, 0.7 mL/min, 40 $^{\circ}$ C, 220 nm) indicated 89% ee (*t*-minor = 7.35 min, *t*-major = 7.63 min).



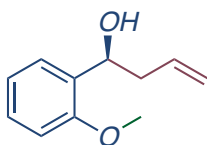
(3g) pale yellow oil, 70 % (0.14 mmol, 25 mg). The general procedure was applied using previously distilled **1g** (0.2 mmol, 28 mg, 23 μ L), and **2** (0.6 mmol, 3 equiv., 60 mg, 65 μ L). The title compound was isolated by flash column chromatography (100% DCM). Spectroscopic data are in agreement with those reported in the previous chapters. HPLC analysis (Chiralcel AD, *n*-Hexane: *i*-PrOH = 97:3, 0.7 mL/min, 40 $^{\circ}$ C, 210 nm) indicated 89% ee (*t*-minor = 11.46 min, *t*-major = 12.09 min).



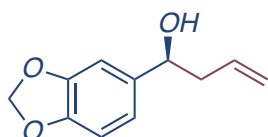
(3h) pale yellow oil, 40 % (0.08 mmol, 14 mg). The general procedure was applied using previously distilled **1h** (0.2 mmol, 27 mg, 24 μ L), and **2** (0.6 mmol, 3 equiv., 60 mg, 65 μ L). The title compound was isolated by flash column chromatography (100% DCM). Spectroscopic data are in agreement with those reported in the previous chapters. HPLC analysis (Chiralcel IC, *n*-Hexane: *i*-PrOH = 98:2, 0.7 mL/min, 40 °C, 210 nm) indicated 91% ee (*t*-minor = 24.60 min, *t*-major = 26.45 min).



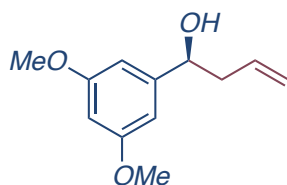
(3i) pale yellow oil, 51 % (0.1 mmol, 15 mg). The general procedure was applied using previously distilled **1i** (0.2 mmol, 27 mg, 24 μ L), and **2** (0.6 mmol, 3 equiv., 60 mg, 65 μ L). The title compound was isolated by flash column chromatography (100% DCM). Spectroscopic data are in agreement with those reported in literature.¹²⁰ HPLC analysis (Phenomenex LUX CELLULOSE 3, *n*-Hexane: *i*-PrOH = 95:5, 1 mL/min, 40 °C, 280 nm) indicated 94% ee (*t*-major = 9.25 min, *t*-minor = 9.77 min).



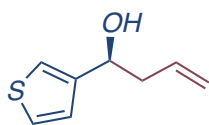
(3j) pale yellow oil, 40 % (0.08 mmol, 14 mg). The general procedure was applied using previously distilled **1j** (0.2 mmol, 27 mg, 24 μ L), and **2** (0.6 mmol, 3 equiv., 60 mg, 65 μ L). The title compound was isolated by flash column chromatography (100% DCM). Spectroscopic data are in agreement with those reported in literature.¹²⁰ HPLC analysis (Chiralcel OD-H, *n*-Hexane: *i*-PrOH = 95:5, 0.7 mL/min, 40 °C, 254 nm) indicated 92% ee (*t*-major = 10.94 min, *t*-minor = 11.92 min).



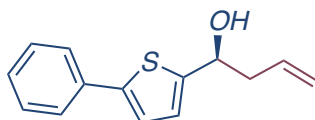
(3k) pale yellow oil, 63 % (0.13 mmol, 24 mg). The general procedure was applied using **1k** (0.2 mmol, 30 mg) and **2** (0.6 mmol, 3 equiv., 60 mg, 65 μ L). The title compound was isolated by flash column chromatography (100% DCM). Spectroscopic data are in agreement with those reported in the previous chapters. HPLC analysis (Chiralcel IA, *n*-Hexane: *i*-PrOH = 9:1, 1 mL/min, 40 °C, 260 nm) indicated 89% ee (*t*-minor = 16.27 min, *t*-major = 18.09 min).



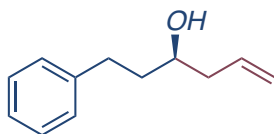
(3l) pale yellow oil, 63 % (0.13 mmol, 26 mg). The general procedure was applied using **1l** (0.2 mmol, 33 mg) and **2** (0.6 mmol, 3 equiv., 60 mg, 65 μ L). The title compound was isolated by flash column chromatography (100% DCM). Spectroscopic data are in agreement with those reported in the previous chapters. HPLC analysis (Chiralcel IC, *n*-Hexane: *i*-PrOH = 9:1, 1 mL/min, 30 $^{\circ}$ C, 220 nm) indicated 90% ee (*t*-major = 15.36 min, *t*-minor = 18.47 min).



(3m) pale yellow oil, 31 % (0.06 mmol, 9 mg). The general procedure was applied using previously distilled **1m** (0.2 mmol, 23 mg, 19 μ L), and **2** (0.6 mmol, 3 equiv., 60 mg, 65 μ L). The title compound was isolated by flash column chromatography (100% DCM). Spectroscopic data are in agreement with those reported in literature.¹²⁰ HPLC analysis (Phenomenex LUX CELLULOSE 3, *n*-Hexane: *i*-PrOH = 97:3, 0.7 mL/min, 40 $^{\circ}$ C, 220 nm) indicated 91% ee (*t*-major = 5.90 min, *t*-minor = 6.24 min).

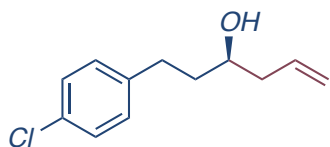


(3n) pale yellow oil, 40 % (0.08 mmol, 18 mg). The general procedure was applied using **1n** (0.2 mmol, 38 mg) and **2** (0.6 mmol, 3 equiv., 60 mg, 65 μ L). The title compound was isolated by flash column chromatography (100% DCM). Spectroscopic data are in agreement with those reported in the previous chapters. HPLC analysis (Chiralcel IA, *n*-Hexane: *i*-PrOH = 95:5, 0.5 mL/min, 40 $^{\circ}$ C, 220 nm) indicated 89% ee (*t*-major = 23.92 min, *t*-minor = 25.19 min).

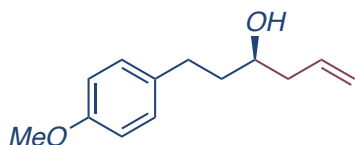


(3o) pale yellow oil, 50 % (0.1 mmol, 18 mg). The general procedure was applied using previously distilled **1o** (0.2 mmol, 26 mg, 24 μ L), and **2** (0.6 mmol, 3 equiv., 60 mg, 65 μ L). The title compound was isolated by flash column chromatography (100% DCM). Spectroscopic data are in agreement with

those reported in the previous chapters. HPLC analysis (Chiralcel OD–H, *n*-Hexane: *i*-PrOH = 9:1, 0.7 mL/min, 40 °C, 214 nm) indicated 89% ee (*t*-minor = 8.35 min, *t*-major = 10.83 min).



(3p) pale yellow oil, 69 % (0.14 mmol, 29 mg). The general procedure was applied using **1p** (0.2 mmol, 34 mg) and **2** (0.6 mmol, 3 equiv., 60 mg, 65 μ L). The reaction time was extended to 48h. The title compound was isolated by flash column chromatography (100% DCM). Spectroscopic data are in agreement with those reported in literature.³²⁰ HPLC analysis (Chiralcel OZ–H, *n*-Hexane: *i*-PrOH = 98:2, 0.7 mL/min, 30 °C, 230 nm) indicated 90% ee (*t*-major = 19.77 min, *t*-minor = 21.15 min).

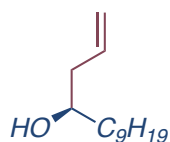


(3q) pale yellow oil, 57 % (0.11 mmol, 23 mg). The general procedure was applied using **1q** (0.2 mmol, 33 mg) and **2** (0.6 mmol, 3 equiv., 60 mg, 65 μ L). The reaction time was extended to 48h. The title compound was isolated by flash column chromatography (100% DCM). Spectroscopic data are in agreement with those reported in literature.¹²⁰ HPLC analysis (Chiralcel OD–H, *n*-Hexane: *i*-PrOH = 9:1, 0.7 mL/min, 30 °C, 230 nm) indicated 90% ee (*t*-minor = 10.02 min, *t*-major = 11.65 min).



(3r) pale yellow oil, 48 % (0.09 mmol, 23 mg). The general procedure was applied using **1r** (0.2 mmol, 36 mg) and **2** (0.6 mmol, 3 equiv., 60 mg, 65 μ L). The reaction time was extended to 48h. The title compound was isolated by flash column chromatography (100% DCM). Spectroscopic data are in agreement with those reported in the previous chapters. HPLC analysis (Phenomenex LUX CELLULOSE 3, *n*-Hexane: *i*-PrOH = 95:5, 0.7 mL/min, 30 °C, 210 nm) indicated 91% ee (*t*-major = 13.33 min, *t*-minor = 14.08 min).

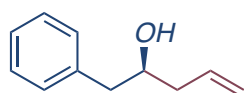
³²⁰ Voigt, T.; Geiding-Reimers, C.; Tran, T. T. N.; Bergmann, S.; Lachance, H.; Schölermann, B.; Brockmeyer, A.; Janning, P.; Ziegler, Sl.; Waldmann, H. A Natural Product Inspired Tetrahydropyran Collection Yields Mitosis Modulators that Synergistically Target CSE1L and Tubulin *Angew. Chem. Int. Ed.* **2013**, *52*, 410–414. <https://doi.org/10.1002/anie.201205728>



(3s) pale yellow oil, 62 % (0.12 mmol, 24 mg). The general procedure was applied using previously distilled **1s** (0.2 mmol, 31 mg, 37 μ L), and **2** (0.6 mmol, 3 equiv., 60 mg, 65 μ L). The reaction time was extended to 48h. The title compound was isolated by flash column chromatography (100% DCM). Spectroscopic data are in agreement with those reported in literature.³²¹ HPLC analysis was performed on the corresponding 3,5-dinitrobenzoyl derivative (Chiralcel AD, *n*-Hexane: *i*-PrOH = 97:3, 0.6 mL/min, 30 °C, 210 nm) indicated 92% ee (*t*-minor = 8.65 min, *t*-major = 9.28 min) of the corresponding ester obtained after functionalization of the product with 3,5-dinitrobenzoyl derivative.

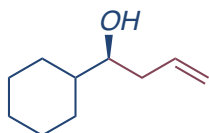


(3t) pale yellow oil, 50 % (0.1 mmol, 18 mg). The general procedure was applied using **1t** (0.2 mmol, 28 mg, 33 μ L), and **2** (0.6 mmol, 3 equiv., 60 mg, 65 μ L). The reaction time was extended to 48h. The title compound was isolated by flash column chromatography (100% DCM). Spectroscopic data are in agreement with those reported in the previous chapters. HPLC analysis was performed on the corresponding 3,5-dinitrobenzoyl derivative (Chiralcel AD *n*-Hexane: *i*-PrOH = 97:3, 0.6 mL/min, 30 °C, 210 nm) indicated 91% ee (*t*-minor = 9.61 min, *t*-major = 10.44 min) of the corresponding ester obtained after functionalization of the product with 3,5-dinitrobenzoyl derivative.



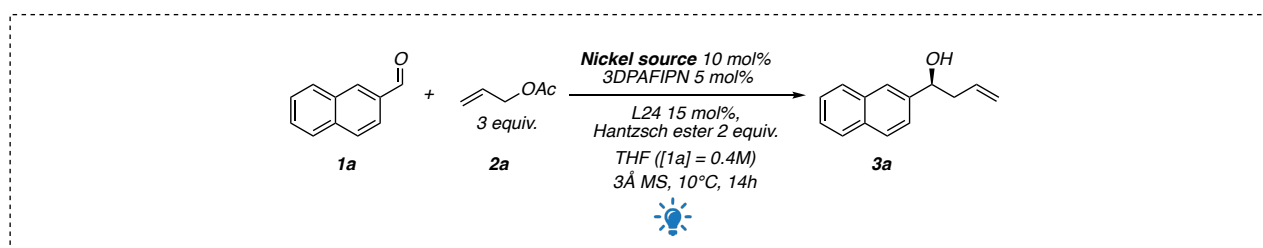
(3u) pale yellow oil, 30 % (0.06 mmol, 10 mg). The general procedure was applied using previously distilled **1u** (0.2 mmol, 24 mg, 22 μ L), and **2** (0.6 mmol, 3 equiv., 60 mg, 65 μ L). The reaction time was extended to 48h. The title compound was isolated by flash column chromatography (100% DCM). Spectroscopic data are in agreement with those reported in the previous chapters. HPLC analysis (Chiralcel OD–H, *n*-Hexane: *i*-PrOH = 9:1, 0.7 mL/min, 40 °C, 214 nm) indicated 88% ee (*t*-major = 6.80 min, *t*-minor = 7.63 min).

³²¹ Goswami, D.; Chattopadhyay, A.; Sharma, A.; Chattopadhyay, S. [Bmim][Br] as a Solvent and Activator for the Ga-Mediated Barbier Allylation: Direct Formation of an *N*-Heterocyclic Carbene from Ga Metal. *J. Org. Chem.* **2012**, *77* (24), 11064–11070. <https://doi.org/10.1021/jo3020775>.



(**3v**) pale yellow oil, 47 % (0.09 mmol, 14 mg). The general procedure was applied using **1v** (0.2 mmol, 22 mg, 24 μ L) previously distilled and **2** (0.6 mmol, 3 equiv., 60 mg, 65 μ L). The reaction time was extended to 48h. The title compound was isolated by flash column chromatography (100% DCM). Spectroscopic data are in agreement with those reported in the previous chapters. HPLC analysis was performed on the corresponding 3,5-dinitrobenzoyl derivative (Chiralcel OD-H *n*-Hexane: *i*-PrOH = 95:5, 0.6 mL/min, 30 °C, 210 nm) indicated 93% ee (*t*-minor = 18.79 min, *t*-major = 19.60 min) of the corresponding ester obtained after functionalization of the product with 3,5-dinitrobenzoyl derivative.

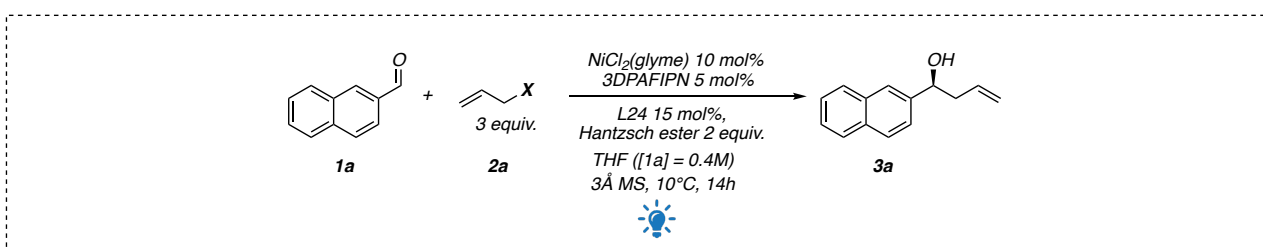
Further optimization studies



Entry ^[a]	Deviation from standard conditions	Yield ^[b] (%) ^[c]	ee (%) ^[d]
1	[NiCl ₂ (glyme)]	90 (87)	93
2	[NiBr ₂ (glyme)]	90	91
3	NiCl ₂	84	92

Table 4.2.10 Screening of nickel source

[a] Reaction conditions reported in the above scheme on 0.1 mmol scale. [b] Determined by ¹H-NMR analysis. [c] Isolated yield after chromatographic purification. [d] Determined by chiral HPLC analysis.

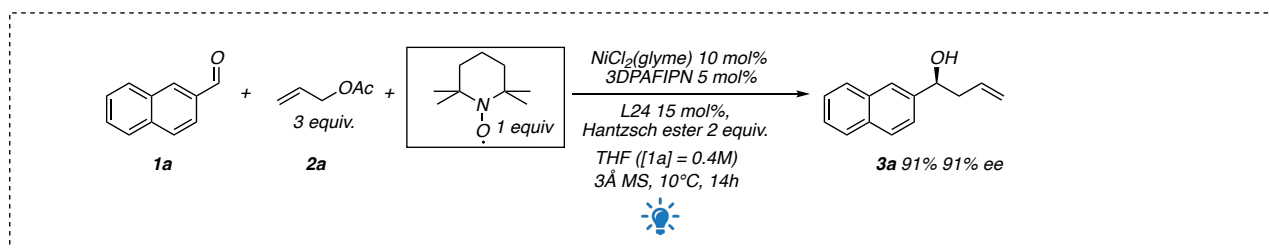


Entry ^[a]	Deviation from standard conditions	Yield ^[b] (%) ^[c]	ee (%) ^[d]
1	-OAc	90 (87) ^d	93
2	-Br	Traces	–

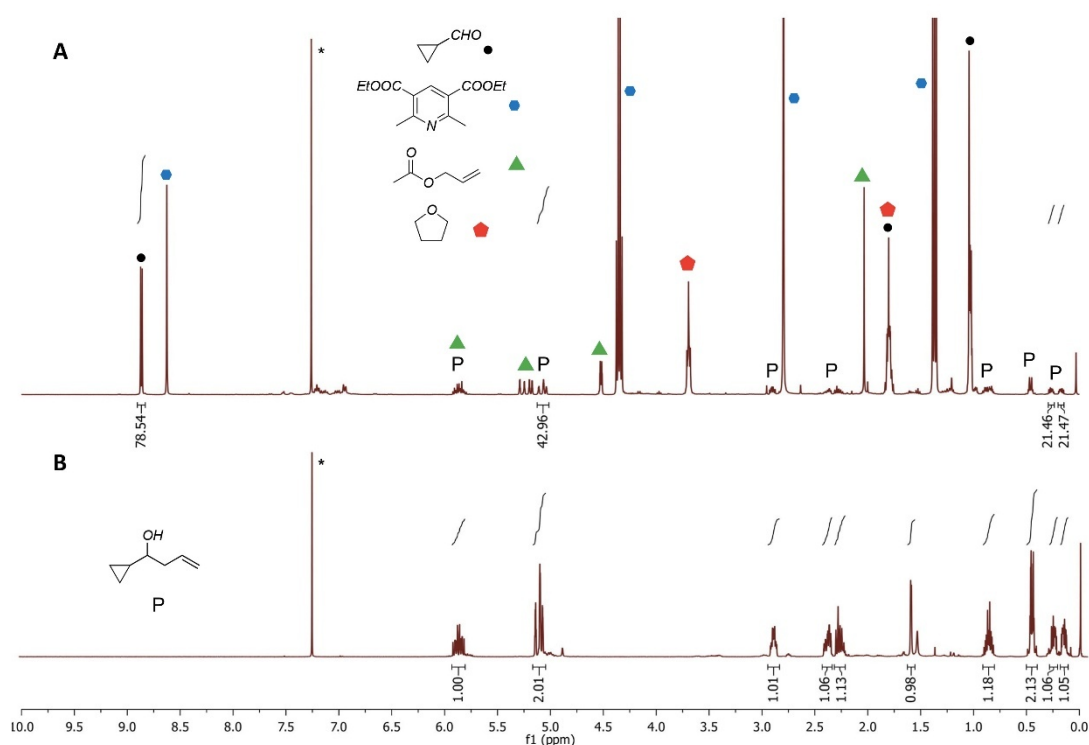
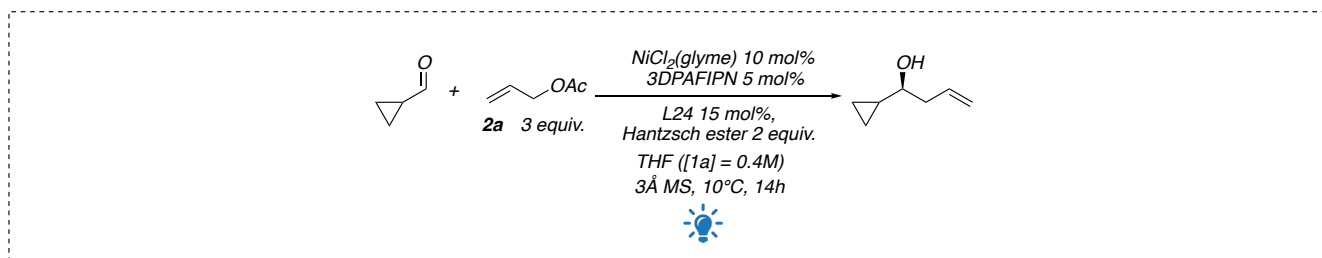
Table 4.2.11 Screening of allyl source

[a] Reaction conditions reported in the above scheme on 0.1 mmol scale. [b] Determined by ¹H-NMR analysis. [c] Isolated yield after chromatographic purification. [d] Determined by chiral HPLC analysis.

Radical trap experiments

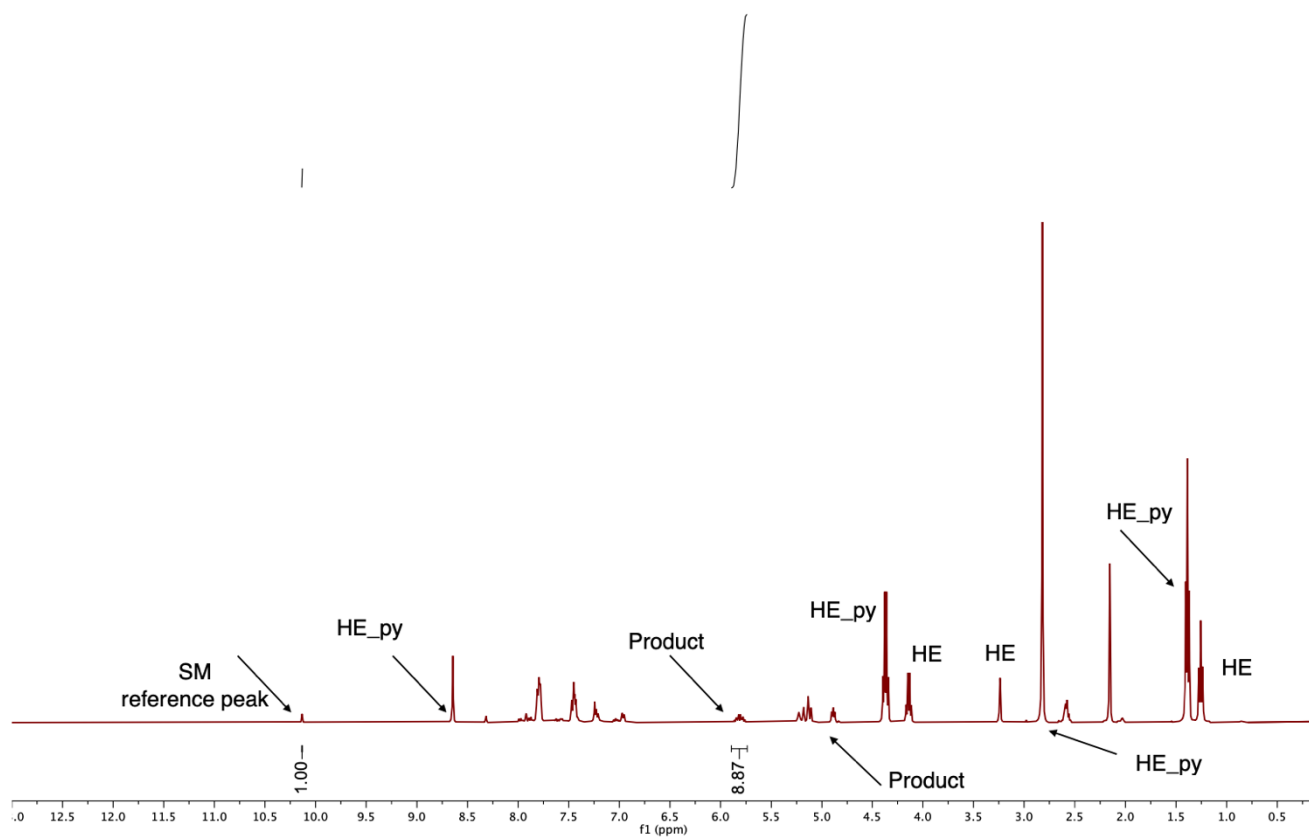


The reaction was performed using the general procedure but adding 1 equiv. of TEMPO. ^1H NMR and GC-MS analysis of the reaction mixture gave no evidence of trapped ketyl radical the standard reaction in the presence of TEMPO gave 91% yields and 91% ee, as TEMPO was not stopping the reaction.



Chapter 4. Supplementary 4 a) $^1\text{H-NMR}$ (400 MHz, CDCl_3) spectrum of reaction crude performed on cyclopropyl carbaldehyde under photoredox standard conditions; b) $^1\text{H-NMR}$ (400 MHz, CDCl_3) spectrum of allylated product of cyclopropyl carbaldehyde obtained under Grignard conditions.

The reaction was performed using the general procedure on 0.2 mmol of cyclopropyl carbaldehyde. Unfortunately, as cyclohexyl carbaldehyde, cyclopropyl carbaldehyde was found not reactive, and only traces of the desired product were found in the reaction mixture. By GCMS, HPLC-MS and $^1\text{H-NMR}$ were not found evidence of open products due to radical formation and rearrangements.

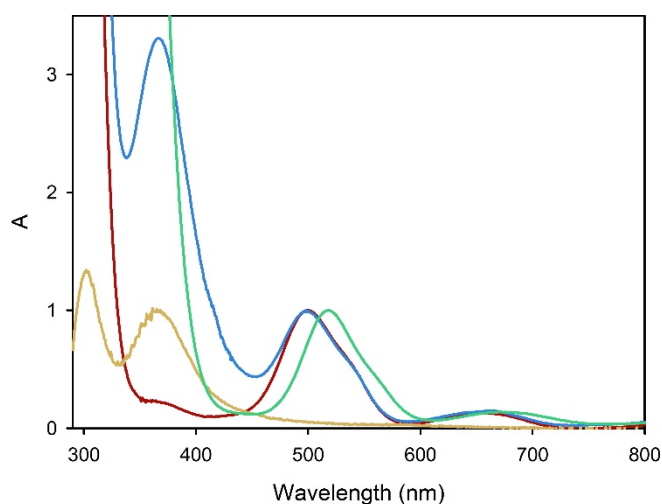


Chapter 4. Supplementary 5 $^1\text{H-NMR}$ (400 MHz, CDCl_3) spectrum of reaction crude. Reaction of aldehyde 1a to give product 3a

Photophysical Investigation

General methods

All the photophysical analyses were carried out in deoxygenated, stabilizer-free tetrahydrofuran (THF) at 298 K, unless otherwise specified. Experiments in absence of oxygen were carried out in a nitrogen-filled glovebox in a custom-made quartz cuvette. UV–vis absorption spectra were recorded with a PerkinElmer λ 40 spectrophotometer using quartz cells with path length of 1.0 cm or cuvettes with two compartments (1.0 cm optical path). Luminescence spectra were performed with a PerkinElmer LS-50 or an Edinburgh FS5 spectrofluorometer equipped with a Hamamatsu Photomultiplier R928P phototube. Lifetimes shorter than 10 μ s were measured by an Edinburgh FLS920 spectrofluorometer by time-correlated single-photon counting (TCSPC) technique. Lifetimes longer than 10 μ s were measured by the above-mentioned Edinburgh FS5 spectrofluorometer equipped with a TCC900 card for data acquisition in TCSPC experiments or by a homemade time-resolved phosphorimeter equipped with an Avalanche PhotoDiode C12703 with a 405 nm pulsed LED as the excitation source. The estimated experimental errors are 2 nm on the band maximum, 5% on the molar absorption coefficient and luminescence lifetime.

Photophysical characterization of compounds

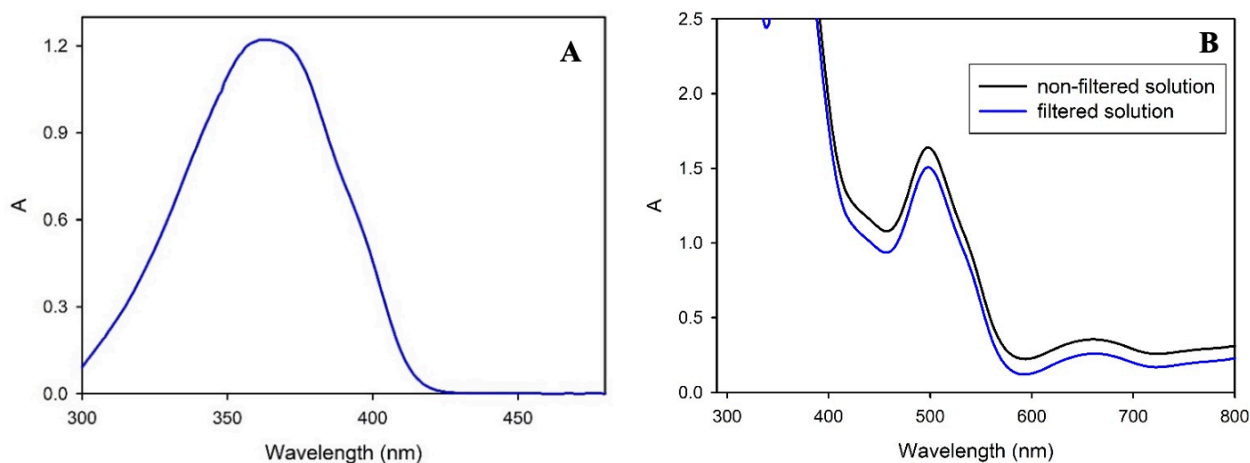
Chapter 4. Supplementary 6 Normalized absorption spectra for air-equilibrated THF solutions of synthesized [NiCl₂L24] (red line), L24 (yellow line), [NiCl₂(glyme)] + 1.5 eq. L24 (blue line) and NiCl₂(glyme) + 1.5 eq. L24 (green line).

Given the good match of the absorption spectrum of synthesized [NiCl₂L24] and the one obtained upon mixing [NiCl₂(glyme)] and L24, we can deduce that the species formed in situ is [NiCl₂L24]. In fact, the two chlorides must be part of nickel's first coordination sphere since the absorption spectrum obtained by mixing [NiBr₂(glyme)] and L24 is red shifted, as expected from the spectrochemical series.

Determination of solubilities

The maximum solubility of HE in THF was determined to be 0.1 M from the absorption spectrum of a saturated solution following dilution and its molar absorption coefficient ($\epsilon = 5150 \text{ M}^{-1}\text{cm}^{-1}$ at 363 nm in THF).

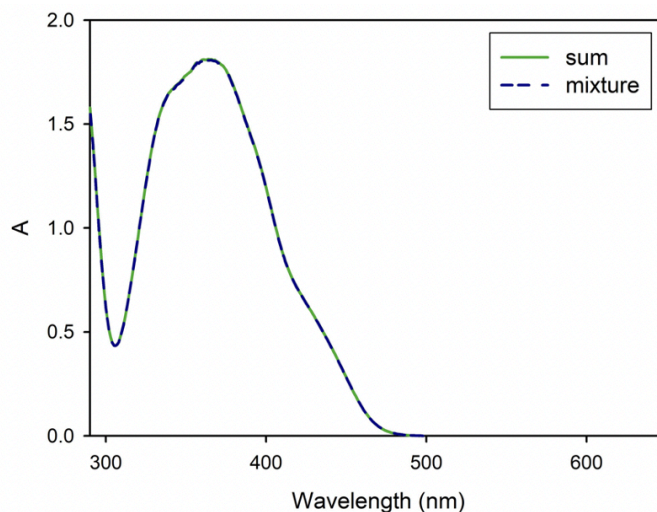
In order to measure $[\text{NiCl}_2\text{L24}]$'s solubility, a solution was prepared by adding 5.6 mg of $[\text{NiCl}_2(\text{glyme})]$ + 1.5 eq. L24 to 2 ml THF and sonicated for 30 minutes at r.t. Given the slight difference in the absorption spectra recorded before and after filtration (PTFE filter, $0.20 \mu\text{m}$), the non-filtered solution was considered to be only marginally above the solubility limit and thus the maximum concentration of $[\text{NiCl}_2\text{L24}]$ in THF was determined to be 0.01 M.



Chapter 4. Supplementary 7 a) Absorption spectrum of a saturated HE solution after dilution 1:440. b) Absorption spectrum of a solution containing $[\text{NiCl}_2(\text{glyme})]$ (5.6 mg in 2 ml) + 1.5 eq. L24 before (black line) and after filtration (blue line).

Sum-mixture experiment

In order to prove the formation of the complex between the two species, absorption spectra of the sum and the mixture of two solutions, containing 3DPAFIPN $73 \mu\text{M}$ and HE $140 \mu\text{M}$ respectively were collected using two-compartment cuvettes.



Chapter 4. Supplementary 8 Absorption spectra of the sum (green line) of a 3DPAFIPN solution ($73 \mu\text{M}$ in THF) and a HE solution ($140 \mu\text{M}$ in THF), and their mixture (blue line).

However, by superimposing two spectra, no substantial differences could be appreciated, suggesting that the interaction between the two species is weak.

Computational Details

Full geometry optimizations were performed at the generalized-gradient approximation (GGA) PBE functional³²² in Gaussian 09.³²³ Numerical integrations were performed with an ultrafine grid. For geometry optimizations, the Def2-SVP³²⁴ basis set was used for light elements, and the SDD³²⁵ pseudopotential and its associated double- ζ basis set was employed for Ni. Optimizations were performed in solution using the SMD³²⁶ continuum solvation model with the solvent parameters for THF ($\epsilon = 7.6$). The natures of all stationary points were determined by calculation of the analytical vibrational frequencies. These were also used to compute the molecular partition functions (298 K, 1 atm) with the conventional particle-in-a-box, rigid-rotator, quantum-mechanical harmonic oscillator approximation, except that all vibrational frequencies below 50 cm^{-1} were replaced with values of 50 cm^{-1} (the quasi-harmonic-oscillator approximation). Single point energy calculations were carried out at M06³²⁷ level of theory using def2-TZVPP and SDD basis sets for nonmetal atoms and Ni, respectively. For Ni species, the most stable spin states are reported as the ground-states. Unless specified otherwise, the ΔG was used throughout the text. The ΔG value was obtained by augmenting the ΔE_e^S energy terms at M06(SMD-THF)/Def2-TZVPP/SDD with the respective free energy corrections at the PBE(SMD-THF)/Def2-SVP/SDD level. TD-DFT calculations were performed at the CAM-B3LYP (SMD-THF)/Def2-TZVPP level of theory.

³²² Perdew, J. P.; Burke, K.; Ernzerhof, M., Generalized gradient approximation made simple. *Phys. Rev. Lett.* **1996**, *77*, 3865-3868. <https://doi.org/10.1103/PhysRevLett.77.3865>

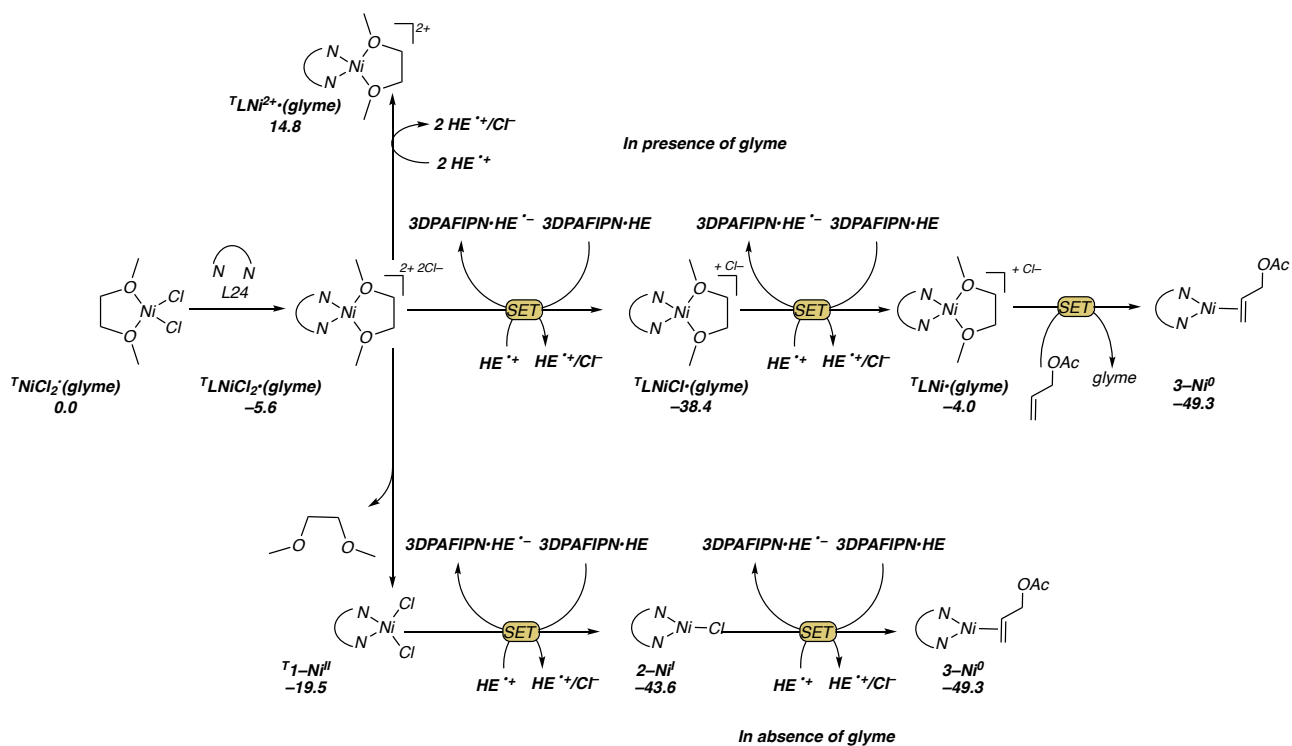
³²³ Frisch, M. J.; Trucks, G. W.; Schlegel, H. B.; Scuseria, G. E.; Robb, M. A.; Cheeseman, J. R.; Scalmani, G.; Barone, V.; Mennucci, B.; Petersson, G. A.; Nakatsuji, H.; Caricato, M.; Li, X.; Hratchian, H. P.; Izmaylov, A. F.; Bloino, J.; Zheng, G.; Sonnenberg, J. L.; Hada, M.; Ehara, M.; Toyota, K.; Fukuda, R.; Hasegawa, J.; Ishida, M.; Nakajima, T.; Honda, Y.; Kitao, O.; Nakai, H.; Vreven, T.; Peralta, J. E., Jr.; Ogliaro, F.; Bearpark, M.; Heyd, J. J.; Brothers, E.; Kudin, K. N.; Staroverov, V. N.; Kobayashi, R.; Normand, J.; Raghavachari, K.; Rendell, A.; Burant, J. C.; Iyengar, S. S.; Tomasi, J.; Cossi, M.; Rega, N.; Millam, J. M.; Klene, M.; Knox, J. E.; Cross, J. B.; Bakken, V.; Adamo, C.; Jaramillo, J.; Gomperts, R.; Stratmann, R. E.; Yazyev, O.; Austin, A. J.; Cammi, R.; Pomelli, C.; Ochterski, J. W.; Martin, R. L.; Morokuma, K.; Zakrzewski, V. G.; Voth, G. A.; Salvador, P.; Dannenberg, J. J.; Dapprich, S.; Daniels, A. D.; Farkas, Foresman, J. B.; Ortiz, J. V.; Cioslowski, J.; Fox, D. J., Gaussian 09, revision D.01 2013, Gaussian Inc., Wallingford, CT.

³²⁴ Dunning Jr., T. H., and Hay, P. J. *Modern Theoretical Chemistry*, Ed. H. F. Schaefer III, Vol. 3 (Plenum, New York, 1977) 1-28.

³²⁵ Marenich, A. V.; Cramer, C. J.; Truhlar, D. G., Universal Solvation Model Based on Solute Electron Density and on a Continuum Model of the Solvent Defined by the Bulk Dielectric Constant and Atomic Surface Tensions. *J. Phys. Chem. B* **2009**, *113*, 6378-6396. <https://doi.org/10.1021/jp810292n>

³²⁶ Zhao, Y.; Truhlar, D. G., The M06 suite of density functionals for main group thermochemistry, thermochemical kinetics, noncovalent interactions, excited states, and transition elements: two new functionals and systematic testing of four M06-class functionals and 12 other functionals. *Theor. Chem. Acc.* **2008**, *120*, 215-241. <http://dx.doi.org/10.1007/s00214-007-0401-8>.

³²⁷ Hush, N. S., Adiabatic Rate Processes at Electrodes .1. Energy-Charge Relationships. *J. Chem. Phys.* **1958**, *28*, 962-972. <https://doi.org/10.1063/1.1744305>



Chapter 4. Supplementary 9 Energetic of precatalyst activation by SET step associated to the photoredox cycle. Free energy values (in kcal/mol) at M06(SMD-THF)/Def2-TZVPP/SDD//PBE(SMD-THF)/Def2-SVP/SDD level of theory are presented.

Energy barriers of single electron transfer steps, involved in this whole study, by using Marcus-Hush theory^{23,328}

Applying the Marcus-Hush theory of electron transfer, the free energy barrier of a single electron transfer process can be estimated according to the following equation:

$$\Delta G_{\text{MH}}^{\ddagger} = \frac{(\Delta G_{\text{r}} + \lambda)^2}{4\lambda}$$

ΔG_{r} is the free energy change of the step, λ is the reorganization energy, which has two components, inner sphere and outer sphere. However, the first one is considered to be negligible and, hence, the total λ will be equal to the outer sphere reorganization energy, which can be calculated by the equation:

$$\lambda = \lambda_{\text{outer}} = 332 \left(\frac{1}{2a_1} + \frac{1}{2a_2} - \frac{1}{R} \right) \left(\frac{1}{\epsilon_{\text{opt}}} - \frac{1}{\epsilon} \right)$$

a_1 and a_2 are the radii of donor and acceptor, R is the sum of a_1 and a_2 , ϵ_{opt} and ϵ is the optical dielectric constant and static dielectric constant of solvent respectively (for THF $\epsilon_{\text{opt}} = 1.98$ $\epsilon = 7.43$) [$\epsilon_{\text{opt}} = (\text{refractive index})^2$].

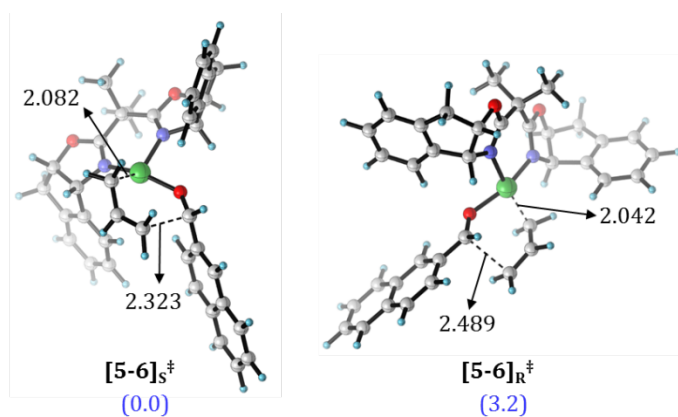
	a_1 (Å)	a_2 (Å)	R (Å)	λ	ΔG_{r}	$\Delta G_{\text{MH}}^{\ddagger}$
SET1	7.55	5.29	12.84	10.19	7.9	8.0
SET2	7.66	5.95	13.61	9.33	-24.1	5.8
SET3	7.55	5.95	13.50	9.37	-18.4	2.2
SET4	7.14	5.29	12.43	10.34	2.2	3.8
SET5	7.55	5.98	13.53	9.34	0.0	2.3
SET6	7.66	5.98	13.64	9.29	-5.8	0.3

Table 4.2.12 Calculated free energy barriers ($\Delta G_{\text{MH}}^{\ddagger}$) of single electron transfer steps and their relevant parameters.

³²⁸ a) Marcus, R. A., On the Theory of Oxidation-Reduction Reactions Involving Electron Transfer. *J. Chem. Phys.* **1956**, *24*, 966-978. <https://doi.org/10.1063/1.1742723>; b) Marcus, R. A., Electrostatic Free Energy and Other Properties of States Having Nonequilibrium Polarization. *J. Chem. Phys.* **1956**, *24*, 979-989. <https://doi.org/10.1063/1.1742724>; c) Marcus, R. A., Theory of Oxidation-Reduction Reactions Involving Electron Transfer .3. Applications to Data on the Rates of Organic Redox Reactions. *J. Chem. Phys.* **1957**, *26*, 872-877 <https://doi.org/10.1063/1.1743424>; d) Marcus, R. A., On the Theory of Electrochemical and Chemical Electron Transfer Processes. *Can. J. Chem.* **1959**, *37*, 155-163. <https://doi.org/10.1139/v59-022>; e) Marcus, R. A., The 2nd Robinson, R. A. Memorial Lecture - Electron, Proton and Related Transfers. *Faraday Discuss.* **1982**, *74*, 7-15. DOI <https://doi.org/10.1039/DC9827400007>; f) Marcus, R. A.; Sutin, N., Electron Transfers in Chemistry and Biology. *Biochim Biophys Acta* **1985**, *811*, 265-322. [https://doi.org/10.1016/0304-4173\(85\)90014-X](https://doi.org/10.1016/0304-4173(85)90014-X); g) Weigend, F.; Ahlrichs, R., Balanced basis sets of split valence, triple zeta valence and quadruple zeta valence quality for H to Rn: Design and assessment of accuracy. *Phys. Chem. Chem. Phys.* **2005**, *7*, 3297-3305. <https://doi.org/10.1039/B508541A>

Entry	Complex	$\Delta G_{T \rightarrow S}$ (kcal/mol)
1	[NiCl ₂ (Glyme)]	15.2
2	[LNi ²⁺ (Glyme)]	12.9
3	[LNiCl ₂ (Glyme)]	18.9
4	1-Ni ^{II}	14.5
5	4-Ni ^{II}	4.0
6	[4-9] _R [‡]	19.5
7	9 _S -Ni ^{II}	11.4
8	[4-9] _R [‡]	8.8

Table 4.2.13 The relative stability of the triplet state (*T*) compared to the singlet state (*S*) of Ni^{II}-intermediates and transition states. For all the structures the triplet states are more stable than singlet states.



Chapter 4. Supplementary 10 Optimized geometries of transition states pro-*R* and pro-*S* for L24 ligand.

Entry	Half reaction	$E_{1/2}^{\text{red}}$
1	^T 3DPAFIPN + 1e ⁻ → 3DPAFIPN ^{•-}	0.50
2	3DPAFIPN + 1e ⁻ → 3DPAFIPN ^{•-}	-1.72
3	3DPAFIPN ^{•+} + 1e ⁻ → ^T 3DPAFIPN	-1.03
4	3DPAFIPN ^{•+} + 1e ⁻ → 3DPAFIPN	1.22

Table 4.2.14 Calculated reduction potentials, $E_{1/2}^{\text{red}}$ in V, of 3DPAFIPN. The potentials are reported against the saturated calomel electrode (SCE) at 298.15 K in acetonitrile solvent.

Cartesian coordinates (Å) of the optimized structures of all intermediates and transition states at PBE/SDD(Ni)/Def2-SVP(other atoms) level of theory. E_e^S represents the absolute electronic energy in Hartree at M06(SMD)/SDD(Ni)/Def2-TZVPP(other atoms) level of theory in THF solvent.

1a

20

 E_e^S : -499.040989

0 1

C -4.505209 -7.530273 0.567115
 H -4.794731 -6.672904 1.245402
 O -3.330240 -7.824056 0.388962
 C -5.654940 -8.227249 -0.052865
 H -7.109637 -6.951083 0.917596
 C -6.952083 -7.801673 0.233140
 C -6.516696 -9.975857 -1.516321
 C -8.080709 -8.447636 -0.345685
 C -5.440812 -9.328718 -0.939215
 C -7.859528 -9.561356 -1.242034
 C -9.418834 -8.033036 -0.069893
 H -4.404817 -9.638970 -1.144240
 H -8.821896 -11.055920 -2.506356
 H -6.356455 -10.824588 -2.200228
 C -10.496048 -8.686561 -0.651832
 H -9.581086 -7.185060 0.614212
 H -11.524224 -8.360297 -0.431764
 C -10.278521 -9.780358 -1.533801
 H -11.141331 -10.290619 -1.989518
 C -8.988639 -10.208173 -1.823145

2a

15

 E_e^S : -345.704360

0 1

C 0.293933 0.273429 0.978613
 H 0.651210 1.261792 1.310328
 H -0.270799 -0.329052 1.711287
 C 0.547059 -0.183384 -0.260007
 H 1.113493 0.440581 -0.975465
 C 0.150163 -1.536865 -0.757552
 H 1.040297 -2.171577 -0.961194
 H -0.480015 -2.077235 -0.018552
 O -0.589694 -1.377032 -1.993508
 C -0.615007 -2.447009 -2.830008
 O -0.057826 -3.503711 -2.587758
 C -1.418244 -2.138399 -4.068105
 H -2.470732 -1.920559 -3.794201
 H -1.386857 -2.996999 -4.761562
 H -1.021362 -1.232569 -4.569014

3DPAFINP·HE

80

 E_e^S : -2067.562417

0 1

C -1.046225 -0.036709 0.948213
 C -1.136882 -0.326323 3.759666
 C -1.357891 -1.296230 1.534768
 C -0.781023 1.074750 1.797608
 C -0.887888 0.954028 3.222043
 C -1.344954 -1.469663 2.957983
 F -1.177139 -0.463290 5.094928
 N -0.999483 0.107588 -0.453444
 N -0.687535 2.058963 4.064598
 N -1.591202 -2.719875 3.544547
 C -1.816477 -2.360694 0.704226
 N -2.240073 -3.217983 0.019907
 C -0.270433 2.281460 1.235621
 N 0.198041 3.255785 0.773036
 C -1.787937 1.117603 -1.082776
 C -3.358836 3.122396 -2.304665
 C -3.086840 1.397787 -0.604320
 C -1.281069 1.851137 -2.178205
 C -2.069202 2.837189 -2.786262
 C -3.858737 2.401062 -1.208256
 H -3.495443 0.820077 0.238183
 H -0.263697 1.652431 -2.544967
 H -1.660265 3.402771 -3.638005
 H -4.869823 2.608054 -0.824280
 H -3.969730 3.903820 -2.781598
 C -0.169578 -0.763585 -1.221081
 C 1.483291 -2.497885 -2.717678
 C -0.603267 -1.259290 -2.470517
 C 1.097211 -1.145702 -0.727087
 C 1.909557 -2.015146 -1.469573
 C 0.225612 -2.111038 -3.212549
 H -1.596174 -0.982739 -2.853447
 H 1.448488 -0.751402 0.238295
 H 2.894844 -2.304523 -1.071922
 H -0.126343 -2.491197 -4.184241
 H 2.126433 -3.173582 -3.301748
 C -1.414311 3.264036 3.814131
 C -2.862109 5.630719 3.300147
 C -2.766619 3.198743 3.414434
 C -0.790929 4.522793 3.955464

C -1.518180 5.694523 3.708107
 C -3.478565 4.377880 3.149662
 H -3.260457 2.220010 3.318278
 H 0.267635 4.578565 4.247992
 H -1.020018 6.670300 3.818139
 H -4.532292 4.313427 2.836748
 H -3.425280 6.554533 3.098369
 C 0.212979 1.964957 5.166351
 C 2.011102 1.769676 7.336162
 C -0.081259 2.597821 6.394498
 C 1.413057 1.232449 5.035494
 C 2.298186 1.131542 6.118240
 C 0.818901 2.503579 7.464254
 H -1.020261 3.158013 6.511151
 H 1.657504 0.749892 4.076981
 H 3.231264 0.558980 5.999884
 H 0.576718 3.001774 8.415995
 H 2.712556 1.696339 8.181091
 C -0.863885 -3.863490 3.091593
 C 0.583305 -6.111319 2.188551
 C -1.503040 -5.115993 2.965124
 C 0.504080 -3.744789 2.763356
 C 1.215809 -4.862794 2.304598
 C -0.776293 -6.230382 2.525876
 H -2.572596 -5.210153 3.202197
 H 1.010796 -2.774517 2.876200
 H 2.281726 -4.756559 2.049643
 H -1.286583 -7.201169 2.428136
 H 1.146337 -6.988375 1.834898
 C -2.538971 -2.835858 4.605609
 C -4.423585 -3.046889 6.696449
 C -3.748084 -2.109663 4.551012
 C -2.278600 -3.668576 5.715945
 C -3.221966 -3.775077 6.746607
 C -4.677676 -2.211837 5.595937
 H -3.963890 -1.474162 3.678633
 H -1.332224 -4.225616 5.772940
 H -3.006334 -4.425826 7.608300
 H -5.618226 -1.642084 5.539432
 H -5.158652 -3.130795 7.511305

¹³DPAFINP-HE

80

 E_c^s : -2067.477587

0 3

C -1.039841 -0.038632 0.972013
 C -1.120308 -0.335180 3.784216
 C -1.467275 -1.273978 1.536945
 C -0.650937 1.048689 1.804820
 C -0.779473 0.926420 3.255447
 C -1.424041 -1.456642 2.986134

F -1.159825 -0.475115 5.117212
 N -1.002551 0.110640 -0.434640
 N -0.628538 2.050134 4.100067
 N -1.628994 -2.727957 3.570484
 C -2.019295 -2.295825 0.728224
 N -2.483923 -3.171527 0.084337
 C -0.053182 2.210485 1.260667
 N 0.451031 3.196093 0.846329
 C -1.689258 1.198218 -1.039114
 C -3.060415 3.366458 -2.207654
 C -2.928734 1.625968 -0.508501
 C -1.139496 1.867427 -2.157258
 C -1.829799 2.938446 -2.736902
 C -3.601817 2.707613 -1.090074
 H -3.366486 1.092963 0.348268
 H -0.161594 1.558311 -2.552864
 H -1.389552 3.457968 -3.601909
 H -4.567423 3.031265 -0.671936
 H -3.594364 4.213796 -2.663936
 C -0.282303 -0.830800 -1.218605
 C 1.151731 -2.720218 -2.742217
 C -0.772021 -1.247032 -2.478729
 C 0.928276 -1.371752 -0.726085
 C 1.632623 -2.314362 -1.485297
 C -0.050411 -2.179877 -3.232869
 H -1.729236 -0.854542 -2.850600
 H 1.319347 -1.035214 0.245127
 H 2.575303 -2.726895 -1.093989
 H -0.443787 -2.504519 -4.208481
 H 1.710110 -3.459040 -3.336889
 C -1.487292 3.167482 3.907210
 C -3.196342 5.366957 3.446389
 C -2.837562 2.958540 3.541418
 C -0.995627 4.489868 4.022818
 C -1.851499 5.575445 3.802084
 C -3.680434 4.053709 3.313618
 H -3.220834 1.930813 3.456006
 H 0.063170 4.659555 4.265951
 H -1.456175 6.599280 3.889956
 H -4.732333 3.877820 3.039605
 H -3.861863 6.224813 3.266513
 C 0.363008 2.035928 5.107630
 C 2.332943 1.933343 7.134670
 C 0.162706 2.712243 6.338106
 C 1.559212 1.301605 4.911238
 C 2.529654 1.254483 5.918190
 C 1.144361 2.658904 7.334035
 H -0.774560 3.258330 6.516743
 H 1.724571 0.783073 3.955308
 H 3.458475 0.689024 5.745235
 H 0.970478 3.180869 8.287913

H 3.099255 1.894117 7.923562
 C -0.761575 -3.794522 3.205408
 C 0.972724 -5.874214 2.403421
 C -1.257244 -5.108515 3.025745
 C 0.606941 -3.530978 2.963109
 C 1.462111 -4.566255 2.564954
 C -0.389423 -6.135860 2.636808
 H -2.327207 -5.314865 3.171990
 H 0.993926 -2.511154 3.106257
 H 2.527102 -4.348923 2.388763
 H -0.788285 -7.152338 2.495387
 H 1.647707 -6.685170 2.090385
 C -2.690252 -2.905728 4.487747
 C -4.798312 -3.185753 6.353314
 C -3.865776 -2.123189 4.367602
 C -2.581088 -3.825353 5.561966
 C -3.630554 -3.960137 6.477838
 C -4.904936 -2.266418 5.293768
 H -3.960383 -1.414954 3.531192
 H -1.661214 -4.413959 5.687830
 H -3.526876 -4.671254 7.312167
 H -5.816246 -1.659155 5.179363
 H -5.617596 -3.294622 7.079960

3DPAFINP·HE²⁺

80

E_c^s : -2067.356343

+1 2

C -1.088199 -0.037000 0.952513
 C -1.139628 -0.320646 3.764231
 C -1.392832 -1.298724 1.541778
 C -0.820346 1.083595 1.791713
 C -0.900357 0.963117 3.214138
 C -1.361125 -1.468807 2.961152
 F -1.154481 -0.453777 5.087040
 N -1.044205 0.095956 -0.446340
 N -0.723121 2.064321 4.061427
 N -1.554088 -2.716536 3.562954
 C -1.853879 -2.376038 0.728367
 N -2.283278 -3.254398 0.076558
 C -0.343760 2.305749 1.231493
 N 0.093110 3.303714 0.791125
 C -1.763902 1.145799 -1.083335
 C -3.185430 3.231144 -2.325238
 C -3.035906 1.525277 -0.594527
 C -1.206963 1.815979 -2.197599
 C -1.922535 2.848276 -2.812624
 C -3.735021 2.567580 -1.214297
 H -3.480988 0.988305 0.256024
 H -0.206651 1.539229 -2.559535
 H -1.480084 3.372690 -3.673122

H -4.727629 2.854343 -0.835068
 H -3.740365 4.047468 -2.811523
 C -0.264631 -0.819852 -1.210122
 C 1.272210 -2.647961 -2.693307
 C -0.742855 -1.300958 -2.451031
 C 0.986297 -1.256794 -0.716022
 C 1.743665 -2.171259 -1.457652
 C 0.030254 -2.206523 -3.184949
 H -1.728554 -0.982796 -2.819578
 H 1.370288 -0.859363 0.235213
 H 2.720538 -2.502627 -1.073924
 H -0.350459 -2.587061 -4.144852
 H 1.872183 -3.364972 -3.273682
 C -1.466247 3.260228 3.819206
 C -2.941461 5.603722 3.334172
 C -2.824483 3.173659 3.441969
 C -0.847100 4.522976 3.950241
 C -1.590709 5.685677 3.714123
 C -3.552035 4.344714 3.196095
 H -3.308983 2.189151 3.359110
 H 0.217561 4.587017 4.217103
 H -1.102131 6.667042 3.811551
 H -4.612530 4.273066 2.910159
 H -3.518324 6.521229 3.143541
 C 0.209866 1.989209 5.132576
 C 2.060462 1.818724 7.245828
 C -0.060212 2.633071 6.362804
 C 1.411069 1.261738 4.966868
 C 2.324392 1.175407 6.024523
 C 0.867231 2.546897 7.406442
 H -1.002016 3.182802 6.501110
 H 1.637204 0.787229 4.000199
 H 3.261573 0.615331 5.885443
 H 0.649268 3.044991 8.363487
 H 2.785082 1.755791 8.071619
 C -0.820310 -3.848961 3.091600
 C 0.636391 -6.069253 2.169420
 C -1.456125 -5.102724 2.957559
 C 0.545270 -3.708798 2.760374
 C 1.264086 -4.817598 2.296465
 C -0.721799 -6.205576 2.504512
 H -2.525710 -5.202913 3.191455
 H 1.043311 -2.735965 2.887882
 H 2.330530 -4.706064 2.047700
 H -1.223183 -7.179221 2.395477
 H 1.206268 -6.938695 1.808502
 C -2.484714 -2.849665 4.631664
 C -4.322597 -3.074350 6.748715
 C -3.688257 -2.109206 4.606112
 C -2.205154 -3.707041 5.720960
 C -3.127042 -3.816125 6.767596

334

C -4.596478 -2.221045 5.666035
H -3.919400 -1.470031 3.740601
H -1.259836 -4.267390 5.751068
H -2.901595 -4.477723 7.617799
H -5.536216 -1.648907 5.637097
H -5.041791 -3.164197 7.576749

3DPAFINP·HE⁻

80

E_c^s : -2067.658213

-1 2

C -1.055454 -0.030737 0.955078
C -1.146841 -0.331238 3.763334
C -1.451927 -1.273263 1.516444
C -0.701084 1.061367 1.791390
C -0.829516 0.935526 3.245987
C -1.417712 -1.457738 2.969381
F -1.190441 -0.476761 5.107401
N -1.012576 0.125006 -0.461187
N -0.587843 2.043662 4.096850
N -1.685331 -2.724791 3.549348
C -1.947012 -2.309813 0.689604
N -2.366339 -3.190833 0.020288
C -0.154974 2.241107 1.232654
N 0.302192 3.237041 0.786145
C -1.834589 1.113011 -1.067824
C -3.484292 3.098269 -2.235553
C -3.117046 1.385918 -0.538219
C -1.383924 1.856404 -2.183790
C -2.209809 2.829053 -2.764179
C -3.926799 2.374580 -1.115272
H -3.478468 0.810552 0.327030
H -0.377201 1.676938 -2.588065
H -1.839937 3.399504 -3.630871
H -4.922138 2.572232 -0.686968
H -4.124657 3.869794 -2.689874
C -0.165970 -0.721189 -1.224717
C 1.530612 -2.436600 -2.713383
C -0.542763 -1.164157 -2.514565
C 1.067720 -1.158556 -0.687859
C 1.899497 -2.012862 -1.425297
C 0.306055 -2.003024 -3.250027
H -1.510823 -0.857728 -2.935862
H 1.373777 -0.819125 0.312734
H 2.854676 -2.342944 -0.987162
H -0.007681 -2.338218 -4.251341
H 2.188709 -3.103062 -3.291680
C -1.392088 3.203801 3.946951
C -3.004068 5.506801 3.560027
C -2.739750 3.081596 3.532416
C -0.857956 4.500702 4.146055

C -1.662400 5.632766 3.965492
C -3.530531 4.223314 3.338735
H -3.161992 2.078784 3.368667
H 0.197503 4.617164 4.431892
H -1.225960 6.631729 4.124545
H -4.577389 4.103475 3.017207
H -3.627650 6.401089 3.408470
C 0.423646 1.953326 5.085220
C 2.434578 1.697376 7.075704
C 0.273878 2.574458 6.350402
C 1.592505 1.192082 4.840957
C 2.580208 1.066575 5.826933
C 1.273325 2.449776 7.324961
H -0.639028 3.146086 6.572037
H 1.720854 0.700005 3.865213
H 3.482736 0.473256 5.610089
H 1.131936 2.938199 8.302425
H 3.213359 1.598476 7.847230
C -0.810165 -3.802074 3.246743
C 0.952235 -5.915490 2.554816
C -1.293345 -5.124982 3.096673
C 0.565564 -3.553767 3.027306
C 1.431821 -4.601173 2.682446
C -0.416237 -6.165530 2.765341
H -2.365447 -5.331881 3.227684
H 0.948836 -2.528033 3.135299
H 2.499322 -4.383761 2.518773
H -0.814095 -7.186444 2.650764
H 1.634368 -6.736081 2.284667
C -2.784458 -2.868908 4.430245
C -4.978867 -3.082400 6.224660
C -3.947070 -2.079469 4.252645
C -2.736677 -3.759714 5.532035
C -3.825002 -3.864169 6.408943
C -5.025152 -2.186910 5.141065
H -3.998846 -1.379899 3.405033
H -1.833694 -4.362049 5.707641
H -3.760558 -4.560225 7.260674
H -5.919781 -1.565557 4.975906
H -5.828160 -3.164974 6.919951

HE

31

E_c^s : -783.687719

0 1

H 0.752106 -0.014288 0.347663
C 0.682150 -0.106526 1.452977
C 0.532600 1.768887 3.133257
C -1.376375 0.230045 2.872827
N -0.702138 1.261847 3.506460
C -0.746528 -0.443754 1.848578

C 1.219578 1.155987 2.107913
 H 1.355229 -0.969199 1.676201
 H -1.190457 1.739894 4.266641
 C 0.952050 2.977237 3.926657
 H 1.995059 2.889006 4.280097
 H 0.288524 3.113211 4.804129
 H 0.905339 3.898440 3.311331
 C -2.762740 -0.009508 3.408998
 H -2.981329 0.675898 4.251523
 H -2.886260 -1.051630 3.759778
 H -3.528248 0.145845 2.624407
 C 2.511542 1.597171 1.562891
 O 3.121133 0.972979 0.696435
 O 2.991732 2.769829 2.076661
 C 4.246527 3.204610 1.543986
 H 4.181402 3.389410 0.451661
 H 5.045917 2.455772 1.721854
 H 4.494951 4.146718 2.067356
 C -1.328848 -1.546669 1.070974
 O -0.720815 -2.133162 0.177402
 O -2.607821 -1.887387 1.413687
 C -3.175070 -2.971513 0.672070
 H -2.571681 -3.896434 0.780187
 H -3.247907 -2.730227 -0.408733
 H -4.187087 -3.132762 1.087892

HE⁺

31

 E_c^S : -783.490082

+1 2

H 0.540816 0.254324 0.243629
 C 0.562234 0.055757 1.346873
 C 0.498172 1.822827 3.108745
 C -1.414449 0.268390 2.856977
 N -0.739449 1.318790 3.433496
 C -0.781266 -0.387448 1.800727
 C 1.174791 1.209328 2.054829
 H 1.274523 -0.810434 1.349208
 H -1.222044 1.788362 4.213109
 C 0.956742 2.974342 3.945097
 H 1.969324 2.789715 4.350076
 H 0.258814 3.150949 4.786035
 H 1.022413 3.898301 3.336526
 C -2.754647 -0.035742 3.446730
 H -2.982870 0.642736 4.290616
 H -2.795977 -1.081884 3.805955
 H -3.549436 0.063747 2.682113
 C 2.526606 1.592182 1.545066
 O 3.115189 0.919835 0.711496
 O 3.005229 2.732872 2.073777
 C 4.302806 3.147411 1.602586

H 4.282528 3.323473 0.508542
 H 5.066092 2.376841 1.829848
 H 4.534669 4.085505 2.137015
 C -1.334716 -1.546054 1.035645
 O -0.713380 -2.073504 0.124960
 O -2.557245 -1.934076 1.442001
 C -3.130087 -3.051939 0.735426
 H -2.489040 -3.949934 0.839313
 H -3.246998 -2.815669 -0.340998
 H -4.116809 -3.229278 1.198345

HP

29

 E_c^S : -782.494418

0 1

C 0.497521 0.135460 1.399681
 C 0.426596 1.827271 3.122400
 C -1.402302 0.350019 2.876454
 N -0.788851 1.378916 3.495079
 C -0.767069 -0.326210 1.792724
 C 1.121690 1.218021 2.035951
 C 0.955749 2.974845 3.938157
 H 1.953421 2.749825 4.363788
 H 0.241285 3.186705 4.754680
 H 1.084354 3.885507 3.319119
 C -2.761454 0.004394 3.420227
 H -2.994840 0.694777 4.251405
 H -2.800874 -1.041163 3.785491
 H -3.544142 0.085641 2.639836
 C 2.466980 1.597063 1.490842
 O 3.052740 0.951290 0.633852
 O 2.967702 2.731513 2.026699
 C 4.251254 3.143686 1.529372
 H 4.210506 3.338529 0.438670
 H 5.019871 2.368719 1.723783
 H 4.505372 4.072698 2.070989
 C -1.299883 -1.489662 1.009637
 O -0.690960 -2.020027 0.091635
 O -2.522133 -1.899171 1.413334
 C -3.076119 -3.014869 0.696924
 H -2.430548 -3.910582 0.797344
 H -3.189913 -2.778012 -0.380095
 H -4.065315 -3.207404 1.149969
 H 1.013517 -0.364264 0.567078

HE⁺/CI

32

 E_c^S : -1243.871597

0 2

C 0.532992 0.113323 1.266670
 C 0.494094 1.810462 3.103609

336

C -1.384789 0.245497 2.866707
N -0.720837 1.285256 3.470904
C -0.789367 -0.363748 1.761699
C 1.149439 1.250822 2.006333
H -1.212903 1.743805 4.342050
C 0.972756 2.950508 3.952453
H 1.951821 2.710516 4.410586
H 0.234642 3.169140 4.748682
H 1.132231 3.855981 3.335376
C -2.701478 -0.110603 3.490615
H -2.901482 0.546434 4.359505
H -2.706177 -1.169045 3.815537
H -3.521791 -0.009429 2.753675
C 2.463300 1.682085 1.456021
O 2.967177 1.145652 0.477004
O 3.041823 2.703238 2.123917
C 4.309081 3.145491 1.609029
H 4.207494 3.503302 0.564537
H 5.054126 2.324743 1.632351
H 4.632141 3.973363 2.265234
C -1.349267 -1.499951 0.980206
O -0.757540 -1.989609 0.026158
O -2.552171 -1.935789 1.412267
C -3.115104 -3.038830 0.682217
H -2.453991 -3.927274 0.736706
H -3.266208 -2.772315 -0.383213
H -4.086099 -3.257534 1.161445
H 1.252019 -0.743852 1.219892
H 0.466617 0.360786 0.177037
Cl -2.043712 2.516421 5.826461

HE⁺/OAc⁻

38

E_c^s : -1012.120053

0 2

C 0.528262 0.078958 1.373874
C 0.344850 1.680688 3.278688
C -1.508955 0.216700 2.816121
N -0.915935 1.210286 3.536058
C -0.825588 -0.406627 1.757164
C 1.077854 1.198282 2.188583
H -1.795446 1.971696 4.728268
C 0.821727 2.707649 4.268021
H 1.918953 2.805403 4.281956
H 0.450454 2.430944 5.275936
H 0.399968 3.705956 4.021137
C -2.904514 -0.141946 3.255043
H -3.251348 0.560873 4.033027
H -2.936857 -1.171689 3.663879
H -3.612880 -0.127836 2.405100
C 2.422244 1.653784 1.740244

O 3.133846 0.980024 1.004214
O 2.768437 2.889763 2.169016
C 4.056013 3.359602 1.737609
H 4.115386 3.390982 0.630974
H 4.866653 2.705728 2.118217
H 4.164062 4.377681 2.153417
C -1.313121 -1.530053 0.916535
O -0.675630 -1.966358 -0.036220
O -2.510438 -2.038676 1.292713
C -2.997880 -3.128274 0.495133
H -2.304169 -3.992391 0.537428
H -3.118796 -2.823244 -0.564025
H -3.976932 -3.407001 0.924836
H 1.257644 -0.770606 1.367024
C -2.081284 2.375695 6.632708
O -1.013502 1.892323 6.997959
O -2.475323 2.443642 5.357307
C -3.100130 2.971335 7.579814
H -3.337471 4.012964 7.282537
H -2.716569 2.955337 8.615382
H -4.049400 2.399597 7.527218
H 0.537887 0.345887 0.286567

¹Ni^{II}

52

E_c^s : -2240.791373

0 3

C 0.460789 -5.830441 0.423686
C -0.867398 -5.157539 0.130057
Ni -2.579709 -7.177286 1.411833
N -0.733702 -7.884563 1.309589
N -2.068796 -5.613316 0.299332
C 0.305199 -7.289246 0.813476
C -0.344126 -9.266854 1.671524
C 1.090462 -9.406586 1.080537
O 1.416880 -8.027928 0.687063
C -3.016264 -4.588111 -0.196207
C -2.114869 -3.339504 -0.422415
O -0.760176 -3.908668 -0.348141
C 1.120813 -5.099217 1.629617
H 2.098820 -5.564411 1.859427
H 1.288903 -4.035413 1.374117
H 0.478934 -5.155755 2.530597
C 1.360633 -5.712071 -0.831459
H 1.503371 -4.646688 -1.089291
H 2.350279 -6.160842 -0.629359
H 0.909270 -6.229558 -1.701192
Cl -3.737470 -8.829164 0.389874
Cl -3.084825 -6.085943 3.323120
H -1.086198 -9.967288 1.238226
H 1.149293 -10.010302 0.154905

H -3.809869 -4.433467 0.562136
 H -2.173241 -2.576387 0.377541
 C -0.153298 -9.464658 3.165823
 C 0.629274 -9.903745 5.811890
 C -1.108337 -9.350192 4.187734
 C 1.185501 -9.798963 3.457114
 C 1.582351 -10.021527 4.785447
 C -0.706439 -9.571470 5.516023
 H -2.150648 -9.081904 3.957463
 H 2.625471 -10.285042 5.021601
 H -1.442435 -9.482942 6.330114
 H 0.930133 -10.074173 6.857527
 C 2.016870 -9.906152 2.198373
 H 2.315186 -10.957900 2.002088
 H 2.954997 -9.314790 2.235678
 H -3.331961 -3.189632 -4.556971
 C -3.612941 -3.973581 -3.836061
 C -4.340388 -5.998116 -1.984798
 C -3.207433 -3.887067 -2.494655
 C -4.382269 -5.075683 -4.247159
 C -4.742727 -6.080380 -3.329149
 C -3.572481 -4.895585 -1.578382
 H -4.704067 -5.154494 -5.297490
 H -5.342316 -6.940222 -3.666461
 H -4.601506 -6.795388 -1.270624
 C -2.412230 -2.790474 -1.822627
 H -3.006042 -1.855116 -1.740703
 H -1.478328 -2.525371 -2.359254

2-Ni^I

51

 E_c^s : -1780.547281

0 2

C 0.591418 -5.844833 0.297715
 C -0.764423 -5.191900 0.121784
 Ni -2.411593 -7.476254 0.907109
 N -0.559328 -7.994657 1.011395
 N -1.945437 -5.706127 0.292518
 C 0.497860 -7.296724 0.720256
 C -0.093375 -9.326792 1.474388
 C 1.434586 -9.320515 1.169753
 O 1.690329 -7.921725 0.820337
 C -2.937752 -4.669173 -0.088964
 C -2.079876 -3.386740 -0.309401
 O -0.708941 -3.898945 -0.262668
 C 1.371841 -5.071796 1.398524
 H 2.380128 -5.509777 1.524400
 H 1.481546 -4.010219 1.106659
 H 0.840365 -5.120137 2.369811
 C 1.354608 -5.764121 -1.052645
 H 1.466591 -4.707694 -1.361101

H 2.361209 -6.209465 -0.942283
 H 0.811713 -6.309485 -1.850270
 Cl -4.339805 -8.440556 1.299106
 H -0.655383 -10.114444 0.933398
 H 1.727803 -9.923521 0.288631
 H -3.687209 -4.572639 0.722273
 H -2.162659 -2.636881 0.500933
 C -0.171568 -9.487545 2.983052
 C 0.130998 -9.780794 5.745145
 C -1.311844 -9.453874 3.801406
 C 1.113455 -9.672939 3.533380
 C 1.269499 -9.820433 4.921319
 C -1.150586 -9.601017 5.190091
 H -2.311588 -9.309096 3.360652
 H 2.269458 -9.965459 5.360170
 H -2.033283 -9.575560 5.847943
 H 0.242541 -9.893698 6.835032
 C 2.173775 -9.721546 2.455901
 H 2.591154 -10.745889 2.351692
 H 3.034189 -9.048468 2.650353
 H -3.480002 -3.160406 -4.391899
 C -3.726050 -3.959242 -3.674469
 C -4.370455 -6.019519 -1.832469
 C -3.253996 -3.901803 -2.352984
 C -4.517593 -5.051341 -4.070647
 C -4.839100 -6.073247 -3.156770
 C -3.575882 -4.929444 -1.442700
 H -4.890864 -5.107014 -5.105361
 H -5.462419 -6.921211 -3.480982
 H -4.614011 -6.818081 -1.112531
 C -2.422886 -2.821543 -1.697261
 H -3.000333 -1.878202 -1.593310
 H -1.503519 -2.568049 -2.264340

TS-Ni^I-ox

66

 E_c^s : -2123.462393

0 2

C -0.533278 -1.587431 -0.097343
 C -1.759975 -0.700792 0.010039
 Ni -0.373947 1.946063 -0.208447
 N 0.944200 0.456690 -0.385901
 N -1.851682 0.592093 0.040618
 C 0.763524 -0.814089 -0.205793
 C 2.390630 0.650983 -0.645053
 C 3.032701 -0.698309 -0.226131
 O 1.866119 -1.589482 -0.170504
 C -3.297314 0.936817 0.142402
 C -4.012898 -0.449456 0.147595
 O -2.909170 -1.401983 0.059835
 C -0.663396 -2.435651 -1.396842

H 0.206686 -3.112599 -1.490340
H -1.585351 -3.045528 -1.357789
H -0.704602 -1.784869 -2.292971
C -0.484952 -2.519661 1.141791
H -1.410598 -3.122307 1.196152
H 0.378258 -3.206370 1.063081
H -0.388153 -1.937366 2.080022
Cl -1.691973 3.540132 -1.253772
C 0.702788 1.464919 2.577970
H -0.067562 0.679609 2.480674
C 0.345539 2.785134 2.148130
C 1.925162 1.138178 3.102416
H 0.926509 3.644045 2.511644
H -0.720177 3.009331 1.978313
H 2.144218 0.117595 3.454748
H 2.728784 1.889202 3.187423
O 1.128344 3.274118 0.305096
C 1.217368 4.594220 0.161865
C 1.675724 5.017049 -1.225682
H 2.540782 4.417968 -1.570819
H 0.834205 4.836398 -1.926193
H 1.932050 6.092812 -1.229726
O 0.976449 5.408712 1.051123
H -4.652064 -0.629953 -0.737175
H -3.541556 1.589132 -0.719705
H 2.743956 1.527803 -0.068982
H 3.482095 -0.702992 0.786499
H -2.818403 3.551932 1.289633
C -3.396961 2.863152 1.925904
C -4.962947 1.089056 3.487531
C -3.697463 1.573127 1.459850
C -3.869194 3.254550 3.190947
C -4.638134 2.369138 3.969977
C -4.492814 0.694308 2.224188
H -3.641313 4.262875 3.570484
H -5.001735 2.687378 4.959713
H -5.586715 0.409750 4.090030
C -4.777384 -0.590505 1.479669
H -4.440391 -1.494421 2.029377
H -5.865014 -0.720118 1.300431
H 4.703504 -1.176301 -4.167426
C 4.007836 -0.380279 -3.857847
C 2.204083 1.662129 -3.072677
C 3.597634 -0.272081 -2.519636
C 3.512431 0.536871 -4.801372
C 2.615607 1.549703 -4.412485
C 2.704975 0.749471 -2.131375
H 3.824517 0.458853 -5.854661
H 2.229690 2.257347 -5.162654
H 1.494302 2.446736 -2.770629
C 3.999872 -1.123796 -1.336136

H 5.044552 -0.910697 -1.022340
H 3.944806 -2.214304 -1.530712

2-Ni^{III}-ox

66

 E_c^s : -2126.236596

O 2

C 0.101246 -7.088671 -0.730360
C -0.745003 -5.906823 -0.285888
Ni -2.821363 -7.561548 1.073259
N -1.016142 -8.524971 1.056300
N -1.853515 -5.898774 0.383943
C -0.126731 -8.315445 0.135074
C -0.672470 -9.808715 1.707624
C 0.367034 -10.447244 0.747780
O 0.763549 -9.300175 -0.078972
C -2.193704 -4.480512 0.683345
C -1.196376 -3.696249 -0.216328
O -0.235413 -4.707970 -0.632460
C 1.600399 -6.699147 -0.595437
H 2.233273 -7.545596 -0.917697
H 1.820170 -5.828569 -1.239410
H 1.862430 -6.441063 0.449960
C -0.209592 -7.424451 -2.215901
H -0.035439 -6.525267 -2.839330
H 0.480009 -8.219226 -2.561621
H -1.251970 -7.772111 -2.352621
Cl -3.092135 -6.602491 3.125090
C -5.265924 -8.807190 1.802391
H -5.572234 -8.201792 2.674170
C -3.848419 -9.150929 1.714806
C -6.212048 -9.172041 0.897978
H -3.607455 -9.914158 0.952871
H -3.368483 -9.329846 2.693593
H -7.269279 -8.890069 1.030212
H -5.957238 -9.769620 0.005814
O -3.055854 -8.230553 -0.748479
C -3.859089 -7.851480 -1.713503
C -5.005489 -6.901080 -1.401275
H -5.909162 -7.213821 -1.960604
H -5.245702 -6.839015 -0.324133
H -4.735900 -5.886501 -1.761857
O -3.673490 -8.240556 -2.875866
H -0.625451 -2.919670 0.325029
H -2.049829 -4.338833 1.773960
H -0.044260 -11.206638 0.054316
H -1.581079 -10.427061 1.836523
H 3.210290 -10.732396 3.975564
C 2.228854 -10.235029 4.028004
C -0.291919 -8.938532 4.166428
C 1.840434 -9.548791 5.191890

C 1.351614 -10.271283 2.932549
 C 0.096020 -9.632366 3.009690
 C 0.591175 -8.903250 5.259883
 H 2.522554 -9.511270 6.055756
 H 0.305089 -8.360951 6.174602
 H -1.259169 -8.412280 4.206288
 C 1.538736 -10.954242 1.596133
 H 2.514269 -10.735871 1.115540
 H 1.475409 -12.059128 1.696119
 H -4.512499 -2.065436 -2.450221
 C -4.589135 -2.668155 -1.531466
 C -4.797602 -4.192038 0.852558
 C -3.442984 -3.231630 -0.948373
 C -5.838563 -2.872241 -0.918039
 C -5.942347 -3.622061 0.268622
 C -3.554901 -3.999352 0.230516
 H -6.742781 -2.430055 -1.365111
 H -6.925608 -3.760002 0.744774
 H -4.863841 -4.779416 1.781550
 C -2.003972 -3.119380 -1.401630
 H -1.816710 -3.721147 -2.317569
 H -1.711447 -2.077262 -1.640718

3-Ni⁰_a

50

 E_c^S : -1320.201680

0 1

Ni -1.196749 -7.612869 0.904228
 C 0.318215 -5.109314 1.635655
 C -0.937446 -5.032780 0.759995
 N 0.301432 -7.682755 1.934230
 N -1.733580 -5.977892 0.311930
 C 0.818180 -6.484223 2.091889
 C 1.178372 -8.641598 2.681537
 C 2.394894 -7.778512 3.125794
 O 1.981149 -6.417199 2.795476
 C -2.768582 -5.313333 -0.546295
 C -2.499358 -3.791275 -0.358859
 O -1.262341 -3.756990 0.416501
 C 0.019360 -4.294153 2.928484
 H 0.922263 -4.250796 3.566687
 H -0.280881 -3.262283 2.664704
 H -0.800082 -4.764223 3.508386
 C 1.471164 -4.436710 0.836791
 H 1.185278 -3.407143 0.551245
 H 2.386829 -4.393534 1.455713
 H 1.696767 -5.008263 -0.085927
 H 1.441304 -9.476725 2.003196
 C 0.554049 -9.107581 3.979000
 C -0.301161 -9.704056 6.573524
 C 1.319790 -8.686703 5.086359

C -0.639949 -9.825557 4.157654
 C -1.063420 -10.120961 5.465729
 C 0.895159 -8.986015 6.390891
 H -1.234279 -10.145998 3.286981
 H -1.997324 -10.682468 5.624995
 H 1.488422 -8.663437 7.261274
 H -0.643346 -9.943145 7.592771
 C 2.569258 -7.957466 4.643938
 H 3.479839 -8.557301 4.857442
 H 2.709479 -6.979432 5.149521
 H 3.324491 -7.974569 2.555933
 H -3.265154 -3.264907 0.243681
 H -3.768982 -5.641197 -0.201504
 C -2.540717 -5.559807 -2.020976
 C -1.971480 -5.599067 -4.757904
 C -2.560602 -6.785929 -2.706333
 C -2.237866 -4.357590 -2.693160
 C -1.953705 -4.372460 -4.068322
 C -2.272970 -6.797110 -4.082803
 H -2.792876 -7.720313 -2.170690
 H -1.719082 -3.437992 -4.602470
 H -2.283832 -7.749029 -4.636491
 H -1.748770 -5.621527 -5.836342
 C -2.304101 -3.172197 -1.755334
 H -3.159367 -2.508860 -2.005848
 H -1.393409 -2.538611 -1.787075

3-Ni⁰

65

 E_c^S : -1666.001741

0 1

C -0.094050 -0.968460 -0.963938
 C -1.155774 -0.844415 0.117538
 Ni 0.251731 1.319915 1.403464
 N 1.571274 0.177333 0.527842
 N -1.119312 -0.016220 1.117639
 C 1.265392 -0.770706 -0.309669
 C 3.032580 0.060623 0.777511
 C 3.402796 -1.331584 0.185341
 O 2.241366 -1.636276 -0.654960
 C -2.321127 -0.284450 1.941696
 C -3.176501 -1.249744 1.065252
 O -2.248138 -1.629706 -0.003169
 C -0.314346 0.177697 -1.993611
 H 0.461597 0.131953 -2.783922
 H -1.309200 0.072455 -2.470903
 H -0.257923 1.165551 -1.493649
 C -0.180997 -2.334671 -1.668077
 H -1.175168 -2.453323 -2.137114
 H 0.588069 -2.400257 -2.460129
 H -0.025389 -3.174752 -0.964078

C -0.466348 2.837649 2.368460
H -0.741560 2.597517 3.417556
C -1.459219 3.753950 1.694524
C 0.940371 2.989291 2.055227
H -1.102946 4.042433 0.684420
H -1.640025 4.675817 2.288136
H 1.692057 2.887567 2.864283
H 1.231302 3.738056 1.289058
O -2.764303 3.132071 1.473555
C -3.795419 3.523265 2.261484
C -5.083930 2.861714 1.831324
H -5.498218 3.415301 0.962211
H -4.926480 1.815279 1.506667
H -5.820621 2.903606 2.653912
O -3.701763 4.328037 3.174275
H 3.227167 0.148157 1.865038
C 3.878774 1.028341 -0.039801
C 5.611910 2.431611 -1.734976
C 4.776661 0.327067 -0.873491
C 3.850039 2.431550 -0.042989
C 4.721693 3.129339 -0.897180
C 5.646509 1.026462 -1.725308
H 3.151619 2.973902 0.609907
H 4.706689 4.230419 -0.910775
H 6.347029 0.482056 -2.378499
H 6.287625 2.990370 -2.401477
C 4.665020 -1.166267 -0.666929
H 5.546571 -1.561588 -0.117666
H 4.594750 -1.743700 -1.611443
H 3.474270 -2.145650 0.934056
H -4.046690 -0.773492 0.571611
H -2.816974 0.678517 2.169536
C -2.014003 -1.096377 3.189013
C -1.673474 -2.918386 5.283323
C -1.176015 -0.756110 4.262672
C -2.683611 -2.337175 3.158913
C -2.514670 -3.255235 4.208369
C -1.009942 -1.676786 5.312099
H -0.652199 0.212590 4.274938
H -3.033738 -4.226741 4.191007
H -0.355803 -1.425745 6.161665
H -1.532860 -3.632030 6.110323
C -3.556779 -2.461461 1.929747
H -4.634146 -2.415592 2.198075
H -3.409645 -3.411704 1.376232

3-Ni⁰-1a

70

 E_c^s : -1819.325965

0 1

Ni -2.238345 -7.263845 1.015449

C 0.515393 -5.292999 1.620781
C -0.759981 -4.773128 0.995193
N -0.499080 -7.616615 1.787179
N -1.765534 -5.447809 0.514968
C 0.514077 -6.796940 1.796762
C 0.021468 -8.915695 2.289747
C 1.560031 -8.778348 2.156119
O 1.724010 -7.321768 2.086065
C -2.605437 -4.459696 -0.209942
C -2.134402 -3.088900 0.342154
O -0.812415 -3.427033 0.880660
C 0.691380 -4.663895 3.032048
H 1.635943 -5.017268 3.488093
H 0.729211 -3.560913 2.949972
H -0.148950 -4.941531 3.698956
C 1.692890 -4.873412 0.700136
H 1.715279 -3.772426 0.596272
H 2.651734 -5.209060 1.137177
H 1.589334 -5.320315 -0.308689
H -0.409960 -9.746985 1.697476
C -0.178369 -9.106034 3.789838
C -0.076964 -9.501227 6.562261
C 1.060130 -9.331003 4.429944
C -1.368673 -9.073260 4.533802
C -1.310373 -9.272813 5.924542
C 1.115489 -9.529856 5.818322
H -2.333189 -8.884579 4.040663
H -2.237618 -9.247734 6.517968
H 2.080696 -9.702568 6.320427
H -0.044991 -9.654825 7.652331
C 2.195212 -9.335573 3.431741
H 2.562220 -10.367925 3.244441
H 3.074049 -8.737809 3.748519
H 1.986304 -9.194651 1.221499
H -2.735117 -2.692364 1.185204
H -3.677575 -4.670597 -0.030394
C -2.263127 -4.367085 -1.693709
C -1.524883 -3.749540 -4.322807
C -2.227224 -5.390123 -2.654101
C -1.914826 -3.043019 -2.039091
C -1.548341 -2.728194 -3.357021
C -1.858019 -5.071483 -3.972939
H -2.473258 -6.426695 -2.378295
H -1.274480 -1.696838 -3.630422
H -1.824705 -5.864470 -4.736306
H -1.235741 -3.514507 -5.359191
C -2.011248 -2.126184 -0.840716
H -2.918530 -1.485819 -0.892881
H -1.145356 -1.442511 -0.727551
C -1.906484 -13.514161 1.424175
H -1.875908 -13.343770 2.543949

O -1.571609 -14.597288 0.948802
 C -2.369363 -12.346853 0.658592
 H -2.639097 -11.132207 2.436447
 C -2.714852 -11.158015 1.335456
 C -2.944488 -11.295748 -1.457167
 C -3.154042 -10.005918 0.647119
 C -2.479670 -12.402676 -0.757582
 C -3.300913 -10.086790 -0.789714
 C -3.474974 -8.755915 1.342161
 H -2.204366 -13.336557 -1.271556
 H -3.952897 -9.029510 -2.594170
 H -3.054698 -11.340308 -2.553332
 C -4.104241 -7.670477 0.599169
 H -3.684818 -8.853264 2.423155
 H -4.756304 -6.940178 1.113485
 C -4.246282 -7.817941 -0.827302
 H -4.715419 -6.998397 -1.397495
 C -3.839278 -8.958794 -1.500515

3-Ni⁰-THF

63

 E_c^s : -1552.625924

0 1

Ni -3.013325 -7.231651 0.627851
 C -1.244740 -5.043714 2.407557
 C -1.634887 -4.810546 0.961738
 N -1.152260 -7.284146 3.539938
 N -2.315524 -5.641044 0.205707
 C -0.803717 -6.490322 2.582244
 C -0.287111 -8.469449 3.416951
 C 0.508867 -8.265426 2.086149
 O 0.203147 -6.883273 1.749261
 C -2.446151 -4.990946 -1.132435
 C -1.966487 -3.529367 -0.888526
 O -1.334156 -3.600180 0.423525
 C -2.459336 -4.741830 3.313081
 H -2.198241 -4.907240 4.376675
 H -2.772246 -3.686579 3.183306
 H -3.311860 -5.401434 3.052314
 C -0.052308 -4.137951 2.805563
 H -0.332568 -3.071194 2.714676
 H 0.228787 -4.339154 3.858069
 H 0.831658 -4.323671 2.165791
 H -0.905710 -9.393514 3.417701
 C 0.793451 -8.517591 4.485186
 C 3.062653 -8.534208 6.122112
 C 2.079683 -8.480647 3.906540
 C 0.633462 -8.557359 5.879042
 C 1.777257 -8.567261 6.696233
 C 3.220764 -8.490422 4.725591
 H -0.373334 -8.572744 6.325450

H 1.668371 -8.598129 7.791750
 H 4.228531 -8.461299 4.281306
 H 3.951659 -8.540153 6.772365
 C 2.003207 -8.458077 2.395123
 H 2.365795 -9.415382 1.962426
 H 2.615688 -7.653973 1.937340
 H 0.150368 -8.890155 1.243001
 H -2.789202 -2.790642 -0.809964
 H -3.500242 -5.062481 -1.465927
 C -1.477008 -5.528610 -2.169591
 C 0.483297 -6.111410 -4.077716
 C -1.364354 -6.840128 -2.656929
 C -0.616490 -4.509842 -2.628824
 C 0.368837 -4.798439 -3.587488
 C -0.378206 -7.125903 -3.617091
 H -2.035191 -7.628078 -2.275757
 H 1.046160 -4.008567 -3.949648
 H -0.275671 -8.150021 -4.009208
 H 1.254826 -6.348747 -4.827222
 C -0.944494 -3.181782 -1.983007
 H -1.392901 -2.478233 -2.717121
 H -0.058130 -2.670458 -1.553856
 H -3.552586 -8.711460 3.176582
 C -4.299738 -9.128319 2.474998
 O -3.809118 -8.887681 1.129824
 C -4.589522 -9.739054 0.246039
 C -4.890888 -11.008586 1.070629
 C -4.471818 -10.644792 2.518584
 H -5.265950 -8.590869 2.612613
 H -5.517569 -9.200003 -0.044781
 H -3.977861 -9.909899 -0.659845
 H -4.320930 -11.880428 0.695800
 H -5.967007 -11.261529 1.006253
 H -3.509037 -11.126385 2.782734
 H -5.222417 -10.949828 3.273125

3-Ni⁰-HE

81

 E_c^s : -2103.977530

0 1

C 0.518565 -5.651194 1.567385
 C -0.797325 -5.150891 0.989042
 Ni -2.148588 -7.343989 2.181615
 N -0.376885 -8.005467 1.539252
 N -1.932474 -5.781247 1.064654
 C 0.569372 -7.148838 1.285815
 C 0.055691 -9.309982 0.946923
 C 1.547741 -9.044102 0.581115
 O 1.681892 -7.600444 0.667962
 C -2.910628 -4.996610 0.278567
 C -2.178125 -3.649762 -0.003404

O -0.792124 -3.952992 0.368728
 C 0.517788 -5.418426 3.102506
 H 1.458899 -5.805457 3.542401
 H 0.448860 -4.333645 3.320256
 H -0.341455 -5.936510 3.574325
 C 1.712314 -4.920525 0.925879
 H 1.643367 -3.836910 1.135937
 H 2.659500 -5.298724 1.353645
 H 1.747681 -5.061316 -0.171024
 H -2.993502 -10.364342 3.569268
 C -3.775172 -9.586050 3.555941
 C -3.823943 -7.055672 3.113958
 C -5.296819 -8.617593 1.817835
 N -4.969646 -7.384624 2.300417
 C -4.672955 -9.746524 2.345285
 C -3.124963 -8.204718 3.680983
 H -4.365491 -9.774695 4.490383
 H -5.439282 -6.586495 1.866667
 C -4.047943 -5.712867 3.789047
 H -4.409496 -4.962706 3.052522
 H -3.128610 -5.327338 4.257447
 H -4.829194 -5.785464 4.581244
 C -6.335681 -8.625402 0.726938
 H -6.701153 -7.598698 0.520678
 H -7.197000 -9.267864 0.994188
 H -5.928765 -9.054707 -0.209293
 C -2.173503 -8.140243 4.807276
 O -1.678890 -9.127585 5.351286
 O -1.837831 -6.871324 5.241729
 C -0.865837 -6.820046 6.287082
 H 0.097568 -7.276532 5.976990
 H -1.217784 -7.344831 7.199553
 H -0.711783 -5.747520 6.512386
 C -4.975117 -11.067978 1.816243
 O -5.695282 -11.359684 0.855763
 O -4.330898 -12.062809 2.533182
 C -4.532787 -13.388850 2.051193
 H -5.611167 -13.646984 2.000240
 H -4.023929 -14.063551 2.765651
 H -4.099187 -13.527819 1.037459
 H -2.500252 -2.806931 0.639095
 H -3.849619 -4.879708 0.855638
 H -0.598162 -9.502986 0.070328
 H 1.810318 -9.331627 -0.454004
 C 0.124176 -10.510016 1.866027
 C 0.707184 -12.700359 3.506860
 C -0.913522 -11.364648 2.262602
 C 1.457027 -10.766807 2.255484
 C 1.753279 -11.861190 3.082325
 C -0.615603 -12.458960 3.093433
 H -1.946267 -11.191884 1.927765

H 2.791808 -12.069940 3.384755
 H -1.424725 -13.132060 3.416399
 H 0.928964 -13.563130 4.154599
 C 2.412363 -9.773294 1.635109
 H 3.304698 -10.256828 1.189080
 H 2.784890 -9.041565 2.384986
 H -2.602598 -4.297171 -4.251650
 C -2.894442 -5.007705 -3.462062
 C -3.639993 -6.849137 -1.438660
 C -3.387229 -6.280590 -3.799622
 C -2.774951 -4.658352 -2.107092
 C -3.151081 -5.576843 -1.105447
 C -3.757837 -7.195929 -2.795914
 H -3.481536 -6.565165 -4.859355
 H -4.138550 -8.190792 -3.075123
 H -3.916550 -7.564860 -0.649024
 C -2.299142 -3.354385 -1.505296
 H -3.038669 -2.541866 -1.672495
 H -1.336789 -2.996862 -1.925640

[3-4]‡

65

 E_c^S : -1663.568839

0 1

C 0.348318 -1.601879 -0.404265
 C -0.903758 -0.793011 -0.140682
 Ni 0.446054 1.732476 0.413471
 N 1.783938 0.410372 0.202533
 N -1.000782 0.435384 0.265096
 C 1.611771 -0.864706 -0.011313
 C 3.252891 0.627990 0.272440
 C 3.826413 -0.795159 0.490436
 O 2.715966 -1.637766 0.030909
 C -2.442489 0.682642 0.529252
 C -3.153647 -0.503405 -0.173856
 O -2.055547 -1.463001 -0.352697
 C 0.440032 -1.890539 -1.931399
 H 1.330398 -2.511927 -2.147535
 H -0.462807 -2.439202 -2.262166
 H 0.516918 -0.947093 -2.507261
 C 0.251415 -2.931602 0.386804
 H -0.648091 -3.492617 0.072982
 H 1.144117 -3.553147 0.188879
 H 0.187245 -2.744229 1.477312
 C -0.053151 3.588700 0.936174
 H -0.690759 3.482791 1.833299
 C -0.656092 4.014921 -0.265829
 C 1.369604 3.318231 1.002687
 H -0.039572 4.524409 -1.020356
 H -1.742016 4.181536 -0.324228
 H 1.837131 3.214035 2.000614

H 2.024720 3.810792 0.257892
 O -0.861835 2.691634 -1.969359
 C -2.089913 2.530199 -2.329477
 C -2.254529 1.859579 -3.704000
 H -1.550553 2.287825 -4.445284
 H -2.013525 0.778395 -3.618136
 H -3.294717 1.959433 -4.069215
 O -3.110081 2.835555 -1.671205
 H 3.487965 1.337041 1.088985
 H 4.014724 -1.064860 1.548784
 H -3.542878 -0.267195 -1.183973
 H -2.735400 1.666504 0.104285
 H 5.777564 1.572783 -4.420479
 C 5.240721 1.419450 -3.471162
 C 3.861606 1.045873 -1.062626
 C 5.563778 0.320165 -2.656867
 C 4.230875 2.320945 -3.086278
 C 3.533500 2.139533 -1.879178
 C 4.868091 0.135287 -1.451910
 H 6.348465 -0.389125 -2.964329
 H 3.980283 3.173266 -3.736815
 H 2.733213 2.835658 -1.588531
 C 5.045763 -0.954918 -0.419338
 H 5.973502 -0.802455 0.173758
 H 5.107268 -1.975473 -0.849081
 C -2.815863 0.499333 1.993987
 C -3.773981 -0.188224 4.536587
 C -3.802179 -0.501745 2.134101
 C -2.302076 1.154583 3.124135
 C -2.787451 0.805674 4.396809
 C -4.286862 -0.847040 3.405419
 H -1.523334 1.924939 3.018855
 H -2.390034 1.312337 5.290152
 H -5.055778 -1.628035 3.516852
 H -4.144308 -0.454336 5.539086
 C -4.211102 -1.054390 0.787062
 H -4.260594 -2.161940 0.753338
 H -5.214735 -0.681251 0.488979

^{T4}-Ni^{II}

65

E_g^S : -1666.014939

0 3

C 0.148825 -4.887564 0.220322
 C -0.997882 -4.066900 0.788397
 Ni -2.383138 -6.344051 2.161885
 N -0.440994 -6.770066 1.817113
 N -2.053177 -4.483161 1.415817
 C 0.349291 -6.193772 0.967368
 C 0.253214 -7.982735 2.308574
 C 1.478272 -8.127062 1.357084

O 1.496348 -6.833953 0.664640
 C -2.930985 -3.307399 1.644579
 C -2.094797 -2.103123 1.107051
 O -0.912684 -2.746819 0.534994
 C 1.464186 -4.072261 0.280333
 H 2.288286 -4.660856 -0.162172
 H 1.353977 -3.133350 -0.291843
 H 1.735646 -3.817421 1.323981
 C -0.196220 -5.218506 -1.261869
 H -0.333390 -4.279998 -1.833774
 H 0.634541 -5.789417 -1.720184
 H -1.124648 -5.817952 -1.333702
 C -4.515385 -7.899602 0.802923
 H -5.290183 -7.141187 0.576462
 C -4.957183 -9.095434 1.295517
 C -3.141509 -7.479407 0.580467
 H -4.255924 -9.910603 1.547670
 H -6.029562 -9.288172 1.463169
 H -3.019902 -6.776858 -0.268637
 H -2.418184 -8.319855 0.520115
 O -2.817294 -7.712981 3.761041
 C -3.869121 -7.033876 4.010935
 C -4.874473 -7.530938 5.023765
 H -5.663800 -8.092738 4.480251
 H -4.407185 -8.216304 5.755598
 H -5.364675 -6.687735 5.547466
 O -4.095137 -5.948863 3.373368
 H -3.166497 -3.245781 2.725737
 H -1.725649 -1.418582 1.894200
 C -4.156444 -2.247349 -0.144049
 C -6.334880 -4.013267 -0.056219
 C -4.184043 -3.305400 0.787262
 C -5.218485 -2.078004 -1.047663
 C -6.303833 -2.970140 -1.001640
 C -5.274090 -4.187527 0.849698
 H -5.205275 -1.254693 -1.779561
 H -7.140712 -2.846899 -1.707031
 H -5.285810 -4.990767 1.602332
 H -7.197924 -4.696801 -0.024709
 C -2.923953 -1.387757 0.025176
 H -3.190507 -0.360704 0.352374
 H -2.336288 -1.277060 -0.909928
 H 1.367597 -8.901864 0.573626
 H -0.446119 -8.841680 2.275986
 C 2.279909 -7.931988 3.618402
 C 1.019013 -7.315766 6.047401
 C 3.057699 -7.764472 4.775589
 C 0.878244 -7.787346 3.681718
 C 0.235554 -7.483336 4.892193
 C 2.419238 -7.452671 5.988770
 H 4.152985 -7.875856 4.735450

344

H -0.861752 -7.389609 4.920463
H 3.019824 -7.316560 6.901963
H 0.533265 -7.077160 7.006651
C 2.731767 -8.306220 2.224304
H 3.070122 -9.363828 2.184406
H 3.574375 -7.690735 1.847810

T[4-9]_s‡

85

E_c^s : -2161.861267

0 3

C -2.488971 -4.497331 -0.437530
C -1.766508 -3.122437 -0.532973
N -1.460026 -5.395545 0.134004
C -0.327630 -4.765462 0.102346
O -0.359789 -3.489814 -0.321468
Ni -1.854180 -7.182355 0.915667
N 0.057888 -7.386188 1.431095
C 1.058782 -6.631494 1.109385
O 2.285987 -7.091653 1.410188
C 2.137475 -8.440148 1.967390
C 0.593695 -8.575492 2.128371
C 1.062317 -5.278369 0.424923
C 1.824959 -5.420650 -0.924839
C -3.584049 -10.677223 2.741208
C -4.749466 -10.084037 2.382512
C -5.006764 -9.418565 1.102264
C -4.792678 -7.512687 1.281970
O -3.555845 -7.217610 1.708810
O -2.048104 -8.540703 -0.500320
C -1.168319 -8.715596 -1.448995
O -0.118014 -8.073267 -1.603204
C -1.515796 -9.846927 -2.421440
C 1.783348 -4.263775 1.350573
H 2.809914 -4.615465 1.563536
H 1.845012 -3.278029 0.853590
H 1.244886 -4.142781 2.311856
H 1.836356 -4.447813 -1.452339
H 2.870311 -5.725659 -0.727660
H 1.335904 -6.185407 -1.558475
H -5.563792 -10.047745 3.131783
H -2.741227 -10.761360 2.033562
H -3.442341 -11.113821 3.743595
H -6.045196 -9.515075 0.731853
H -4.255096 -9.626104 0.318201
H -2.546920 -10.226175 -2.290996
H -1.377439 -9.494662 -3.463478
H -0.806121 -10.687113 -2.267445
C -5.910483 -7.053645 2.180375
H -7.375000 -6.906376 0.591563
C -7.184993 -6.800357 1.673289

C -6.708811 -6.504230 4.432410
C -8.262545 -6.402756 2.517159
C -5.683917 -6.890349 3.582481
C -8.023484 -6.251648 3.935404
C -9.573937 -6.142404 2.011979
H -4.670670 -7.073142 3.970446
H -8.913896 -5.740678 5.860633
H -6.519666 -6.383619 5.511644
C -10.601529 -5.755910 2.861488
H -9.757046 -6.256576 0.931265
H -11.607072 -5.561240 2.456413
C -10.365179 -5.610112 4.257208
H -11.188906 -5.303825 4.920843
C -9.102001 -5.852738 4.780549
H -5.003038 -7.241865 0.218718
H -3.378002 -4.491131 0.224324
H -2.025394 -2.408769 0.273042
H 2.583280 -9.132269 1.227831
H 0.173523 -9.488718 1.659850
H -2.557217 -2.981722 -4.770806
C -2.788152 -3.828506 -4.105321
C -3.376986 -6.016825 -2.398864
C -2.542983 -3.738246 -2.725742
C -3.329269 -5.016060 -4.626983
C -3.619936 -6.103003 -3.780689
C -2.841067 -4.827469 -1.880726
H -3.523524 -5.098235 -5.707914
H -4.034959 -7.030748 -4.204500
H -3.571503 -6.878064 -1.741176
C -1.995415 -2.565351 -1.943749
H -1.060757 -2.146252 -2.369645
H -2.727711 -1.730772 -1.904492
C 0.367746 -8.529654 3.629731
C 0.393301 -8.388455 6.419379
C -0.852741 -8.510125 4.322630
C 1.597058 -8.481155 4.318796
C 1.613475 -8.411083 5.721370
C -0.831328 -8.438241 5.726353
H -1.810086 -8.553441 3.778094
H 2.568381 -8.374103 6.269267
H -1.779290 -8.422916 6.286398
H 0.395802 -8.332703 7.519309
C 2.769016 -8.547548 3.364264
H 3.313310 -9.510852 3.462433
H 3.517563 -7.745459 3.528232

5-Ni^I

58

E_c^s : -1437.514763

0 2

C -3.398905 -5.538951 -1.491219

C -2.954652 -4.088132 -1.147272
 N -2.851838 -6.357042 -0.385674
 C -1.975003 -5.612182 0.217287
 O -1.882171 -4.319999 -0.173192
 Ni -3.556774 -8.083759 0.403316
 N -1.774267 -8.425364 1.163107
 C -0.856058 -7.520361 1.343377
 O 0.398211 -7.954622 1.594240
 C 0.389868 -9.411530 1.425931
 C -1.131668 -9.733980 1.442637
 C -1.077530 -6.016766 1.376132
 C 0.262254 -5.257507 1.301499
 C -5.207192 -8.933950 1.331570
 C -5.439275 -8.419508 0.012894
 C -4.801374 -8.983995 -1.132922
 C -1.813504 -5.666598 2.702607
 H -1.180543 -5.942598 3.569644
 H -2.015179 -4.578108 2.748533
 H -2.774236 -6.214707 2.775740
 H 0.078546 -4.168416 1.347866
 H 0.905505 -5.541237 2.155067
 H 0.810004 -5.479522 0.364860
 H -6.041236 -7.496217 -0.108890
 H -5.037397 -10.020004 1.461124
 H -5.708259 -8.447626 2.186899
 H -4.987653 -8.539301 -2.124829
 H -4.511617 -10.050980 -1.141285
 H -4.498423 -5.669407 -1.547485
 H -3.723346 -3.474909 -0.635809
 H 0.896823 -9.624128 0.463632
 H -1.439512 -10.472129 0.675490
 H -1.791969 -7.990937 -5.290224
 C -1.898991 -7.043854 -4.738554
 C -2.144719 -4.624191 -3.341674
 C -2.591546 -7.023807 -3.515255
 C -1.337311 -5.863275 -5.260552
 C -1.455167 -4.647441 -4.564411
 C -2.715278 -5.807538 -2.826124
 H -3.021157 -7.945039 -3.092552
 H -0.796001 -5.893095 -6.219240
 H -1.006956 -3.727239 -4.971796
 C -2.409016 -3.448054 -2.428221
 H -1.510567 -2.829992 -2.225580
 H -3.173050 -2.766362 -2.860721
 C -1.365245 -10.239610 2.861621
 C -1.334488 -11.152235 5.508831
 C -2.581391 -10.497577 3.512873
 C -0.136762 -10.433157 3.529650
 C -0.116909 -10.891426 4.856515
 C -2.558254 -10.955324 4.841882
 H -3.535867 -10.329662 2.993141

H 0.839540 -11.041521 5.382139
 H -3.505501 -11.158306 5.365602
 H -1.330640 -11.509141 6.550741
 C 1.033185 -10.105380 2.629923
 H 1.556518 -11.027524 2.296637
 H 1.798808 -9.462308 3.110168

¹⁹S-Ni^{II}

85

E_c^S : -2165.090007

0 3

C 0.690038 -6.838651 0.715600
 C 0.100502 -5.583377 0.093407
 Ni -2.634734 -6.029159 1.197767
 N -1.583671 -7.763361 1.297198
 N -1.148701 -5.261239 -0.008177
 C -0.373689 -7.917266 0.855274
 C -2.173886 -9.117304 1.439897
 C -1.160731 -10.039706 0.699873
 O 0.013006 -9.167873 0.553886
 C -1.206092 -3.983282 -0.749479
 C 0.270767 -3.490947 -0.770118
 O 1.004985 -4.699369 -0.368312
 C 1.190931 -6.480720 2.146055
 H 1.614049 -7.383344 2.630000
 H 1.987614 -5.713857 2.079866
 H 0.361663 -6.089204 2.766865
 C 1.867321 -7.335181 -0.151275
 H 2.640239 -6.547508 -0.212619
 H 2.319853 -8.235385 0.303789
 H 1.542907 -7.589023 -1.179416
 O -3.775525 -6.157982 3.011319
 C -2.868826 -5.484963 3.612850
 C -2.981266 -5.218730 5.095616
 H -4.037881 -5.207810 5.423012
 H -2.463376 -6.036322 5.641361
 H -2.485450 -4.267874 5.369028
 O -1.848831 -5.077648 2.963468
 C -5.303833 -6.469715 0.209993
 O -4.058299 -5.911767 -0.056887
 C -5.527853 -7.792108 -0.532255
 H -3.785477 -7.592567 -1.774192
 C -4.654314 -8.221416 -1.525641
 C -6.868760 -9.824510 -0.847991
 C -4.849198 -9.456616 -2.215225
 C -6.644419 -8.620728 -0.198009
 C -5.985535 -10.280760 -1.874006
 C -3.955938 -9.908886 -3.234061
 H -7.333361 -8.297816 0.599983
 H -7.047541 -12.139103 -2.298909
 H -7.733078 -10.451737 -0.575518

C -4.170794 -11.116080 -3.886876
H -3.091765 -9.277263 -3.496842
H -3.474057 -11.450117 -4.671802
C -5.290573 -11.925875 -3.549548
H -5.451628 -12.880275 -4.074970
C -6.178284 -11.515258 -2.563164
H -3.188849 -9.126068 0.994444
H -1.464171 -10.328307 -0.325578
H 0.512725 -2.713180 -0.019582
H -1.901768 -3.287511 -0.238530
C -2.162529 -9.644009 2.869120
C -1.862436 -10.933399 5.334279
C -2.802634 -9.113945 4.000517
C -1.385634 -10.818224 2.962037
C -1.231704 -11.467726 4.197471
C -2.645199 -9.767381 5.235489
H -3.407858 -8.197853 3.913619
H -0.626513 -12.384892 4.275455
H -3.138971 -9.362936 6.133129
H -1.746110 -11.433768 6.308519
C -0.849337 -11.232342 1.610709
H -1.371258 -12.138516 1.235269
H 0.234359 -11.469447 1.612318
H -3.669034 -5.342618 -4.622723
C -2.782014 -4.872057 -4.169650
C -0.502784 -3.685711 -3.038716
C -2.682867 -4.776089 -2.770302
C -1.753297 -4.377471 -4.995111
C -0.607355 -3.784138 -4.435902
C -1.541692 -4.173650 -2.220179
H -3.456576 -5.179674 -2.093852
H -1.843305 -4.461157 -6.089736
H 0.197708 -3.406888 -5.086460
C 0.610777 -3.084156 -2.209835
H 0.621782 -1.976022 -2.292476
H 1.622733 -3.432291 -2.502017
C -6.448963 -5.448058 -0.105741
H -6.259812 -4.572077 0.553755
H -7.423475 -5.883893 0.201044
C -6.509651 -4.997362 -1.534679
H -5.624102 -4.450188 -1.906006
C -7.535997 -5.215708 -2.378909
H -7.511274 -4.859830 -3.422485
H -8.442887 -5.758806 -2.058421
H -5.422407 -6.704521 1.299345

[5-6]_R[‡]

78

E_c^s : -1933.757308

0 2

C -3.620107 -3.881634 0.141125

C -2.599545 -2.717391 0.009642
N -2.778552 -5.060146 0.476661
C -1.560884 -4.724046 0.178848
O -1.337565 -3.441175 -0.177132
Ni -3.383312 -6.624483 1.608648
N -1.528645 -7.318673 1.571393
C -0.591006 -6.965696 0.733505
O 0.370249 -7.875762 0.468553
C -0.028958 -9.127252 1.123012
C -1.065950 -8.612063 2.146573
C -0.350481 -5.621029 0.084653
C -0.023580 -5.804362 -1.422473
C -3.983274 -7.795641 3.170807
C -4.869754 -6.983827 3.965368
C -6.243728 -6.930188 3.848532
C -6.204146 -5.783600 1.639934
O -5.232945 -6.390293 1.065500
C -7.597125 -6.034485 1.282814
C -8.618157 -5.152492 1.774646
C -9.947170 -5.342295 1.449360
C -10.356126 -6.429146 0.608953
C -9.337836 -7.328435 0.105171
C -7.978180 -7.106042 0.454473
C -9.746017 -8.414504 -0.732767
C -11.083286 -8.604761 -1.057828
C -12.078726 -7.719333 -0.562516
C -11.716149 -6.652249 0.255296
C 0.853722 -4.965091 0.815173
H 1.747402 -5.611479 0.726806
H 1.080149 -3.983498 0.357583
H 0.633323 -4.812185 1.890299
H 0.161769 -4.818158 -1.888941
H 0.883143 -6.427240 -1.539177
H -0.862380 -6.293952 -1.955978
H -4.390045 -6.261230 4.655763
H -4.455736 -8.677576 2.688146
H -3.041890 -8.061160 3.679167
H -6.844919 -6.257261 4.481121
H -6.793182 -7.710129 3.298451
H -6.010320 -4.859434 2.231534
H -7.203718 -7.788112 0.070051
H -8.323313 -4.310428 2.422658
H -12.483275 -5.962466 0.643370
H -10.717186 -4.654722 1.835245
H -8.975895 -9.102267 -1.117875
H -11.376580 -9.447461 -1.703809
H -13.135555 -7.879852 -0.826871
H -4.379275 -3.721847 0.930749
H -2.481288 -2.096019 0.919768
H -0.437787 -9.790267 0.334118
H -1.921250 -9.298699 2.290086

H -3.974312 -1.872028 -3.976436
 C -4.283584 -2.731833 -3.360923
 C -5.079590 -4.950746 -1.783342
 C -5.127920 -3.721021 -3.894681
 C -3.838752 -2.856609 -2.035225
 C -4.237325 -3.961277 -1.251651
 C -5.522660 -4.821906 -3.111327
 H -5.481399 -3.634461 -4.934245
 H -6.184621 -5.589907 -3.541248
 H -5.379846 -5.807235 -1.161628
 C -2.956990 -1.916606 -1.245110
 H -2.049961 -1.585011 -1.790621
 H -3.508475 -0.995843 -0.956120
 C -0.228778 -8.441373 3.414206
 C 1.642932 -8.390351 5.501041
 C -0.535470 -7.751685 4.598475
 C 1.021054 -9.083184 3.265073
 C 1.958506 -9.065257 4.308913
 C 0.406875 -7.733502 5.642266
 H -1.491609 -7.219043 4.711697
 H 2.933122 -9.565177 4.192682
 H 0.176088 -7.194617 6.574349
 H 2.372874 -8.366656 6.325369
 C 1.139833 -9.728147 1.903201
 H 1.015258 -10.831181 1.963300
 H 2.111413 -9.542649 1.401651

[5-6]_s[‡]

78

E_c^s : -1933.761429

0 2

C -3.345389 -4.634837 -0.660974
 C -2.747558 -3.207649 -0.847712
 N -2.214690 -5.432672 -0.122745
 C -1.156829 -4.686987 -0.183239
 O -1.316085 -3.422348 -0.627388
 Ni -2.422507 -7.287394 0.600965
 N -0.510366 -7.260964 1.137405
 C 0.405930 -6.388776 0.837821
 O 1.676801 -6.686454 1.185252
 C 1.680757 -8.029715 1.761005
 C 0.162216 -8.341948 1.905257
 C 0.277490 -5.052049 0.134856
 C 1.058642 -5.120456 -1.209064
 C -2.454498 -9.197336 -0.226177
 C -3.268019 -9.871072 0.723423
 C -4.664584 -9.997575 0.656985
 C -5.376449 -7.830536 1.095347
 O -4.349284 -7.095914 0.834976
 C 0.891495 -3.957487 1.048305
 H 1.951526 -4.191534 1.258517

H 0.838797 -2.974756 0.544382
 H 0.346524 -3.889541 2.011059
 H 0.997713 -4.144825 -1.728177
 H 2.123139 -5.351909 -1.014672
 H 0.639675 -5.901719 -1.874024
 H -2.771596 -10.226052 1.648021
 H -2.887880 -9.033938 -1.232704
 H -1.377374 -9.441748 -0.249509
 H -5.196846 -10.583629 1.422085
 H -5.158498 -9.937594 -0.327136
 C -5.885423 -8.001961 2.470197
 H -7.796016 -8.822544 1.851248
 C -7.165389 -8.524948 2.706389
 C -5.570017 -7.740824 4.890831
 C -7.678077 -8.690142 4.021354
 C -5.097768 -7.596391 3.597570
 C -6.862549 -8.294238 5.151118
 C -8.978122 -9.231346 4.276948
 H -4.109214 -7.150739 3.408186
 H -6.748722 -8.156090 7.323374
 H -4.953330 -7.418054 5.745979
 C -9.447826 -9.380141 5.574664
 H -9.602592 -9.532008 3.420104
 H -10.450442 -9.800901 5.751204
 C -8.642847 -8.992646 6.682456
 H -9.026757 -9.115503 7.707189
 C -7.376524 -8.459749 6.469802
 H -6.162856 -7.932145 0.307818
 H -0.130746 -9.324041 1.483341
 H 2.217421 -8.681134 1.043752
 H -3.074727 -2.471329 -0.088159
 H -4.187826 -4.694422 0.054971
 H -4.589013 -5.577950 -5.833160
 C -4.353961 -5.422757 -4.768368
 C -3.756352 -5.049682 -2.063073
 C -4.575481 -6.463212 -3.845707
 C -3.840816 -4.185192 -4.341912
 C -3.541892 -4.001505 -2.981908
 C -4.279467 -6.282423 -2.483447
 H -4.984209 -7.424730 -4.193875
 H -3.677264 -3.371340 -5.066156
 H -4.449162 -7.081857 -1.746572
 C -3.030196 -2.757647 -2.290090
 H -2.121331 -2.330128 -2.761904
 H -3.796659 -1.953427 -2.296178
 C -0.089738 -8.260480 3.401431
 C -0.121800 -8.009082 6.186068
 C -1.310949 -8.365851 4.083651
 C 1.114445 -8.042475 4.102433
 C 1.102043 -7.913882 5.500868
 C -1.320026 -8.238715 5.483573

348

H -2.246495 -8.546200 3.531928
H 2.038307 -7.742651 6.055405
H -2.271074 -8.321691 6.032422
H -0.142313 -7.908690 7.282606
C 2.301446 -8.029892 3.166037
H 2.927802 -8.936799 3.305547
H 2.971651 -7.157480 3.308880

6s-Ni^I

78

E_c^S : -1936.592820

0 2

C -6.706575 -8.381797 6.266815
C -8.202478 -8.139841 6.232547
Ni -8.656160 -8.952905 3.450078
N -6.886693 -9.527503 4.009442
N -9.028027 -8.319543 5.244472
C -6.231220 -9.199546 5.083137
C -5.990233 -10.392085 3.202506
C -4.606991 -10.274338 3.908245
O -4.943780 -9.603672 5.165098
C -10.363879 -7.847831 5.695092
C -10.155091 -7.485509 7.197802
O -8.712422 -7.637077 7.378660
C -6.340138 -9.131033 7.573976
H -5.248110 -9.298094 7.619704
H -6.643236 -8.528928 8.450547
H -6.849244 -10.113963 7.629229
C -5.987852 -7.001602 6.229903
H -6.291328 -6.393269 7.103899
H -4.890999 -7.148204 6.267390
H -6.241822 -6.446080 5.305356
C -9.463860 -8.163181 0.757376
O -9.552154 -9.028898 1.835874
C -10.693686 -8.256647 -0.152754
H -11.463091 -10.012051 0.806566
C -11.626590 -9.274937 0.005369
C -12.013915 -7.343574 -2.009465
C -12.780222 -9.371396 -0.830374
C -10.907281 -7.282400 -1.176852
C -12.982881 -8.383701 -1.865724
C -13.749379 -10.409233 -0.676261
H -10.179951 -6.462499 -1.298460
H -14.286026 -7.722941 -3.486737
H -12.164845 -6.582689 -2.792481
C -14.863200 -10.475138 -1.503564
H -13.596384 -11.161760 0.114132
H -15.600483 -11.282752 -1.372108
C -15.059753 -9.502848 -2.522962
H -15.946552 -9.565195 -3.173030
C -14.137718 -8.478812 -2.698490

H -11.102252 -8.658187 5.528953
H -10.635262 -8.189450 7.904309
H -3.879306 -9.622772 3.386236
H -5.987979 -10.036985 2.152595
H -11.634591 -4.789096 2.239731
C -11.420266 -4.998895 3.299364
C -10.890187 -5.515124 6.008126
C -11.517802 -3.966876 4.252631
C -11.054483 -6.298295 3.692229
C -10.787881 -6.542564 5.048533
C -11.257189 -4.218428 5.611177
H -11.806117 -2.953353 3.932054
H -10.972134 -7.114663 2.956723
H -11.342109 -3.408620 6.353137
C -10.604209 -6.027405 7.402321
H -11.512949 -5.988072 8.039490
H -9.822725 -5.443220 7.931497
H -8.369515 -11.926869 2.524624
C -7.537747 -12.504271 2.959280
C -5.396253 -13.972871 4.100698
C -7.658897 -13.887602 3.178361
C -6.339345 -11.866298 3.315672
C -5.271757 -12.590839 3.884532
C -6.595303 -14.615379 3.745794
H -8.592113 -14.404838 2.906258
H -6.703623 -15.698450 3.913794
H -4.567544 -14.546976 4.544673
C -4.082053 -11.696913 4.155644
H -3.246206 -11.919907 3.458407
H -3.673916 -11.802155 5.181907
C -8.148710 -8.386684 -0.065342
H -7.320161 -8.196094 0.655784
H -8.062395 -7.624188 -0.868809
C -8.008297 -9.765844 -0.636299
H -8.121616 -10.593058 0.088363
C -7.767450 -10.061219 -1.927991
H -7.678219 -11.104398 -2.274731
H -7.652736 -9.270817 -2.691107
H -9.413181 -7.086422 1.08050

17s-Ni^I

116

E_c^S : -2948.747486

0 3

C 7.663202 -15.006026 -6.843101
C 6.500777 -14.179666 -6.331288
Ni 6.180206 -12.387862 -8.701914
N 7.683498 -13.683791 -9.015552
N 5.966414 -13.108440 -6.833487
C 8.200953 -14.528184 -8.177187
C 8.541900 -13.683102 -10.229012

C 9.781113 -14.528376 -9.810896
O 9.353296 -15.114448 -8.535390
C 4.956323 -12.621963 -5.856708
C 4.819117 -13.799860 -4.847577
O 5.982517 -14.633778 -5.180178
C 7.194712 -16.477215 -7.027598
H 8.041011 -17.097451 -7.378481
H 6.838827 -16.881063 -6.061266
H 6.374159 -16.545544 -7.769087
C 8.793805 -14.932260 -5.780756
H 8.420691 -15.306531 -4.809457
H 9.647249 -15.560129 -6.096716
H 9.149223 -13.891102 -5.646727
C 6.411147 -9.537226 -9.221333
O 5.715297 -10.733352 -9.391524
H 3.764711 -12.445216 -12.239211
C 3.431922 -11.686332 -11.486265
C 1.312746 -10.429135 -12.000816
C 1.240286 -12.120878 -10.298659
N 0.621243 -11.217244 -11.097325
C 2.626159 -12.371813 -10.396934
C 2.678448 -10.578764 -12.193707
C 0.443415 -9.405404 -12.693342
H 0.732816 -8.375229 -12.403229
H -0.616768 -9.562749 -12.423470
H 0.550892 -9.453297 -13.793533
C 0.322041 -12.779284 -9.296915
H 0.175983 -13.852267 -9.532780
H -0.662209 -12.277283 -9.305972
H 0.741675 -12.741091 -8.274081
C 3.522475 -9.778278 -13.090335
O 4.723352 -9.996776 -13.268224
O 2.888279 -8.750679 -13.733763
C 3.706377 -7.975889 -14.612568
H 4.519556 -7.458508 -14.061587
H 3.037176 -7.226574 -15.075643
H 4.169010 -8.605606 -15.400538
C 3.362294 -13.299950 -9.582840
O 4.618901 -13.440809 -9.631161
O 2.630657 -14.120671 -8.772246
C 3.302290 -15.235339 -8.183928
H 3.588781 -15.979382 -8.957871
H 2.577590 -15.697669 -7.487828
H 4.213196 -14.932272 -7.636112
C 5.508188 -8.434564 -8.659095
H 3.684667 -9.425615 -9.217446
C 4.124633 -8.525508 -8.762106
C 5.283240 -6.244970 -7.578791
C 3.270586 -7.484408 -8.289270
C 6.082083 -7.274456 -8.053616
C 3.860181 -6.312063 -7.684382
C 1.848238 -7.559651 -8.399418
H 7.178430 -7.202623 -7.958668
H 3.458602 -4.378027 -6.755022
H 5.739401 -5.357452 -7.110968
C 1.043547 -6.527187 -7.935906
H 1.399209 -8.452675 -8.863448
H -0.051450 -6.598016 -8.030064
C 1.625313 -5.374102 -7.339348
H 0.976033 -4.562120 -6.975974
C 3.004663 -5.270282 -7.215837
H 4.376611 -11.284591 -11.063660
H -0.817059 -11.216152 -11.131755
C -2.470243 -12.218115 -11.754866
O -1.834406 -13.182181 -12.179351
O -1.936610 -11.158841 -11.161819
C -3.986345 -12.123272 -11.860335
H -4.434959 -12.004374 -10.852514
H -4.399727 -13.025841 -12.346421
H -4.274041 -11.223869 -12.443067
H 10.688271 -13.934257 -9.588227
H 8.789215 -12.635610 -10.492155
H 3.925353 -14.436465 -4.995299
H 4.017712 -12.376091 -6.393085
C 5.460923 -11.470392 -5.000026
C 6.368041 -9.647542 -3.083817
C 5.489820 -11.835723 -3.637799
C 5.869564 -10.193147 -5.411017
C 6.325580 -9.282387 -4.442627
C 5.946057 -10.923729 -2.672721
H 5.822560 -9.902328 -6.470716
H 6.645687 -8.275063 -4.750926
H 5.970930 -11.202346 -1.607397
H 6.728998 -8.924891 -2.335322
C 4.943238 -13.229319 -3.430531
H 5.581866 -13.871667 -2.790420
H 3.942426 -13.198030 -2.949429
H 5.485913 -14.819166 -13.739343
C 6.409530 -15.019128 -13.174070
C 8.765719 -15.544268 -11.745427
C 7.219293 -16.117936 -13.518983
C 6.769167 -14.173662 -12.110582
C 7.948483 -14.447483 -11.400470
C 8.402298 -16.386243 -12.808769
H 6.924521 -16.772041 -14.354559
H 6.127075 -13.325837 -11.830335
H 9.035730 -17.243973 -13.085121
C 10.003923 -15.607851 -10.879447
H 10.918294 -15.377843 -11.466549
H 10.170001 -16.602173 -10.415905
C 7.015109 -9.045519 -10.579354
H 7.493577 -8.056861 -10.416555

350

H 6.160291 -8.905234 -11.276038
C 7.996085 -9.996891 -11.194870
H 7.572508 -10.943456 -11.575743
C 9.319927 -9.777945 -11.322189
H 9.786404 -8.840054 -10.971212
H 9.986432 -10.516577 -11.798238
H 7.278001 -9.642819 -8.513034

T[7-8]_s[‡]

116

E_c^s: -2944.236462

0 3

C -7.289046 -9.024809 6.417016
C -8.414608 -9.782341 5.741124
Ni -7.967634 -8.782458 3.034423
N -6.852085 -7.729520 4.272277
N -8.836082 -9.695912 4.515809
C -6.726333 -7.911837 5.551888
C -6.016937 -6.553895 3.908663
C -5.511742 -6.009433 5.281038
O -5.963507 -7.028631 6.226679
C -10.035204 -10.565714 4.406595
C -10.017286 -11.395602 5.722940
O -9.046176 -10.664373 6.542381
C -6.133925 -10.020849 6.726450
H -5.310590 -9.491955 7.244129
H -6.502425 -10.828539 7.387890
H -5.735841 -10.472119 5.796341
C -7.833326 -8.420633 7.738487
H -8.215368 -9.227044 8.391127
H -7.023794 -7.888902 8.271083
H -8.657369 -7.705412 7.543899
C -8.747531 -6.870719 0.785380
O -8.193449 -8.106303 1.232580
H -6.059581 -9.686819 0.153857
C -7.049045 -9.871881 -0.304209
C -7.997893 -10.352891 -2.536959
C -8.654874 -11.720556 -0.673190
N -8.811161 -11.307055 -1.961582
C -7.731294 -11.083807 0.180077
C -7.085714 -9.636092 -1.754672
H -9.978017 -11.780314 -2.713994
C -8.198263 -10.213637 -4.023607
H -7.267235 -9.929416 -4.542112
H -8.942251 -9.417683 -4.247943
H -8.586346 -11.165725 -4.437864
C -9.531863 -12.880062 -0.270750
H -8.944088 -13.820929 -0.234015
H -10.346457 -13.011424 -1.006314
H -9.965004 -12.744309 0.737377
C -6.123825 -8.617330 -2.233986

O -5.197338 -8.183152 -1.548662
O -6.354636 -8.149463 -3.493584
C -5.441742 -7.150000 -3.961016
H -5.516240 -6.224958 -3.352122
H -5.732700 -6.933012 -5.005532
H -4.393169 -7.509993 -3.927105
C -7.442715 -11.458091 1.562149
O -6.841070 -10.708419 2.360217
O -7.837096 -12.710192 1.934994
C -7.434039 -13.148120 3.235794
H -6.343556 -13.359140 3.259929
H -7.990909 -14.082943 3.434206
H -7.659301 -12.394920 4.015444
C -10.227489 -6.994367 0.434745
H -10.015801 -8.858811 -0.647899
C -10.703157 -8.060383 -0.325496
C -12.483630 -6.035276 0.493707
C -12.074332 -8.151483 -0.709174
C -11.141913 -5.978127 0.844060
C -12.989955 -7.114043 -0.290915
C -12.573186 -9.231087 -1.502347
H -10.770122 -5.137045 1.451655
H -15.055445 -6.410848 -0.351937
H -13.177507 -5.243354 0.818969
C -13.912933 -9.284980 -1.861658
H -11.882366 -10.021634 -1.836984
H -14.280861 -10.121588 -2.476565
C -14.815343 -8.266760 -1.444425
H -15.875604 -8.323970 -1.736683
C -14.362141 -7.203931 -0.675456
H -7.677776 -8.846162 0.381198
O -10.982177 -12.041108 -3.112233
C -10.963396 -12.701441 -4.260171
O -9.943947 -12.978162 -4.894472
C -12.343548 -13.105301 -4.755820
H -12.386841 -14.209568 -4.851926
H -13.154146 -12.763884 -4.085790
H -12.502695 -12.691105 -5.772078
H -6.646717 -5.832620 3.348807
H -5.985980 -5.059970 5.595739
H -9.627999 -12.426618 5.613245
H -9.960307 -11.183217 3.488918
H -3.241396 -8.144344 0.353723
C -3.337235 -7.716684 1.363117
C -3.603583 -6.585766 3.918823
C -4.621434 -7.469130 1.876971
C -2.195047 -7.408998 2.126205
C -2.320972 -6.838796 3.405441
C -4.745770 -6.909210 3.157337
H -5.511253 -7.711555 1.278282
H -1.192826 -7.608423 1.715087

H -1.423982 -6.588561 3.993967
 C -3.976536 -5.928424 5.228379
 H -3.524311 -6.422457 6.113281
 H -3.643923 -4.869264 5.255062
 C -11.339924 -9.788107 4.485382
 C -13.795807 -8.568865 5.030751
 C -11.800301 -8.770193 3.636578
 C -12.099749 -10.201256 5.599995
 C -13.334124 -9.592180 5.876695
 C -13.035742 -8.161255 3.918272
 H -11.205658 -8.449258 2.767096
 H -13.932614 -9.909195 6.745505
 H -13.409047 -7.359940 3.262217
 H -14.761258 -8.081766 5.239547
 C -11.419988 -11.331032 6.340005
 H -11.949024 -12.294043 6.173912
 H -11.373318 -11.180802 7.438034
 C -7.935209 -6.304554 -0.411632
 H -6.861205 -6.369317 -0.130792
 H -8.085289 -6.954545 -1.298247
 C -8.267164 -4.881640 -0.758062
 H -8.123470 -4.141141 0.052402
 C -8.704114 -4.452849 -1.956750
 H -8.866378 -5.153452 -2.794539
 H -8.914285 -3.387329 -2.146353
 H -8.659683 -6.140179 1.622344

8_R-Ni⁰

79

 E_c^S : -1937.195508

0 1

C 1.429486 -0.137838 3.841345
 C 0.487779 -1.095975 3.135005
 Ni 0.211815 0.526222 0.741138
 N 1.900768 0.931533 1.598036
 N -0.171339 -0.870880 2.034835
 C 2.219396 0.676489 2.833495
 C 3.033505 1.699645 1.022677
 C 3.894648 2.097299 2.256574
 O 3.354385 1.237008 3.310310
 C -1.132884 -1.996609 1.890686
 C -0.621426 -3.059783 2.903296
 O 0.251069 -2.265032 3.771084
 C 2.394956 -0.903652 4.771562
 H 3.051851 -0.189921 5.301602
 H 1.821182 -1.477021 5.522721
 H 3.032511 -1.611260 4.205737
 C 0.557890 0.846131 4.678980
 H -0.022922 0.285090 5.438003
 H 1.208877 1.573739 5.202893
 H -0.147505 1.399296 4.028018

C -0.445660 3.951328 -1.924957
 O -0.133563 5.307941 -1.607156
 C -0.098754 3.127915 -0.657473
 H -0.829481 3.394578 0.137002
 C -0.029796 1.622483 -0.839971
 H 0.667135 1.318368 -1.651884
 H -1.324970 -0.133279 -1.225518
 C -1.160759 0.758131 -0.585269
 H -2.109120 1.217632 -0.238732
 H 0.885316 3.532593 -0.328024
 H -0.376105 5.846699 -2.386182
 H 3.757763 3.142972 2.596396
 H 2.638358 2.566672 0.458201
 H -1.138928 -2.345467 0.839225
 H 0.008790 -3.855945 2.458789
 H 2.654185 0.090908 -1.377084
 C 3.675024 0.095785 -0.964721
 C 6.294031 0.099958 0.121301
 C 3.970732 0.842399 0.186573
 C 4.699742 -0.651270 -1.571629
 C 5.999927 -0.649256 -1.031413
 C 5.272445 0.846380 0.730602
 H 4.483166 -1.243488 -2.474466
 H 6.793420 -1.240172 -1.515392
 H 7.312545 0.098220 0.541007
 C 5.355549 1.743027 1.946137
 H 5.850448 1.266955 2.817371
 H 5.929441 2.668042 1.722709
 H -3.106772 0.040799 1.186750
 C -3.402833 -0.651653 1.987791
 C -4.154796 -2.432433 4.060660
 C -4.653569 -0.526637 2.617507
 C -2.531106 -1.670615 2.402536
 C -2.904808 -2.559211 3.434152
 C -5.026763 -1.409982 3.647799
 H -5.344724 0.270665 2.302316
 H -6.008298 -1.298927 4.134984
 H -4.448685 -3.122940 4.867154
 C -1.827650 -3.590360 3.683540
 H -2.124873 -4.584791 3.285591
 H -1.586669 -3.737044 4.756310
 C -1.889462 3.790991 -2.380817
 H -2.587215 5.526415 -1.307153
 C -2.870982 4.683344 -1.956643
 C -3.581859 2.537032 -3.635244
 C -4.234551 4.539211 -2.349203
 C -2.265425 2.709577 -3.235803
 C -4.604586 3.436181 -3.205939
 C -5.250486 5.447460 -1.921131
 H -1.489675 2.010838 -3.586022
 H -6.246161 2.449323 -4.251730

H -3.856180 1.699694 -4.296956
 C -6.570077 5.278016 -2.317868
 H -4.966938 6.287650 -1.266950
 H -7.342606 5.985660 -1.978333
 C -6.933036 4.192012 -3.162409
 H -7.983208 4.068280 -3.470071
 C -5.969520 3.291670 -3.597389
 H 0.214564 3.582132 -2.749702

NiCl₂(Glyme)

19

 E_c^s : -1400.276841

0 1

Ni -1.951491 -6.714035 1.136567
 C -4.061735 -8.254423 2.353924
 H -3.695252 -9.265961 2.067760
 H -4.797681 -8.358095 3.180271
 C -4.700136 -7.549713 1.181134
 H -5.123669 -6.565139 1.481222
 H -5.513313 -8.178760 0.758792
 O -3.672534 -7.357658 0.189496
 C -4.121347 -6.679024 -0.994965
 H -4.493677 -5.660955 -0.756496
 H -4.924220 -7.275515 -1.477032
 H -3.254540 -6.610515 -1.678084
 O -2.955930 -7.441238 2.791128
 C -2.215037 -8.000095 3.887974
 H -1.401773 -7.290166 4.126149
 H -1.787232 -8.988974 3.620730
 H -2.884059 -8.103432 4.768166
 Cl -2.205086 -4.500346 1.186213
 Cl -0.373252 -8.225959 0.726764

¹⁵LNiCl₂(Glyme)

68

 E_c^s : -2549.579274

0 3

C -0.016999 -5.394704 -0.593815
 C -0.978970 -4.560151 0.230384
 Ni -2.491578 -6.825828 1.430861
 N -0.816737 -7.508426 0.589046
 N -1.946809 -4.944682 1.000509
 C -0.082535 -6.877095 -0.278749
 C -0.344413 -8.913763 0.599665
 C 0.480180 -9.030399 -0.704677
 O 0.782915 -7.612115 -0.981245
 C -2.550198 -3.743937 1.630660
 C -1.774286 -2.564800 0.967552
 O -0.770567 -3.235907 0.141007
 C 1.426622 -4.911230 -0.272764
 H 2.155416 -5.512118 -0.847293

H 1.538451 -3.849278 -0.559467
 H 1.653395 -5.014785 0.807121
 C -0.320674 -5.193674 -2.104369
 H -0.392453 -4.114405 -2.338627
 H 0.502030 -5.628958 -2.702253
 H -1.255670 -5.707433 -2.398801
 C -4.093459 -9.164248 0.506968
 H -3.255980 -9.554458 -0.116166
 H -4.820649 -9.979816 0.710399
 C -4.772427 -8.039755 -0.237218
 H -5.770254 -7.791089 0.191349
 H -4.875850 -8.355834 -1.296424
 O -3.935653 -6.874874 -0.159820
 C -4.049628 -6.034858 -1.315094
 H -5.102702 -5.699040 -1.440249
 H -3.700228 -6.605232 -2.204517
 H -3.414263 -5.148031 -1.149275
 O -3.596121 -8.634661 1.750770
 C -3.304505 -9.632382 2.734080
 H -2.909721 -9.099524 3.617806
 H -2.556912 -10.366288 2.361221
 H -4.236577 -10.172774 3.007603
 Cl -2.172615 -6.553757 3.699296
 Cl -2.345190 -8.775638 -2.630938
 H -0.120571 -9.376204 -1.572804
 H -1.210960 -9.601829 0.619585
 H -1.213653 -1.938624 1.685748
 H -2.402026 -3.837131 2.725904
 H 3.865121 -10.488442 1.519594
 C 2.934642 -10.090774 1.955123
 C 0.549229 -9.047513 3.083464
 C 2.811887 -9.932909 3.346867
 C 1.859893 -9.726392 1.128871
 C 0.670550 -9.217025 1.695350
 C 1.630617 -9.410453 3.906122
 H 3.650892 -10.211689 4.003746
 H 1.553956 -9.278099 4.996769
 H -0.362105 -8.606595 3.517741
 C 1.755953 -9.806150 -0.379013
 H 2.638343 -9.392102 -0.908520
 H 1.646565 -10.857563 -0.722761
 C -4.119435 -2.402524 0.391234
 C -6.391981 -3.841409 1.198377
 C -3.999345 -3.504837 1.261917
 C -5.383992 -2.019048 -0.084585
 C -6.516204 -2.748343 0.319140
 C -5.128396 -4.226636 1.678325
 H -5.490297 -1.156667 -0.761445
 H -7.512198 -2.454607 -0.047652
 H -5.026045 -5.072632 2.376044
 H -7.290197 -4.393432 1.515884

C -2.779336 -1.753118 0.122251
 H -2.775532 -0.682359 0.412494
 H -2.499634 -1.788003 -0.952127

LNi²⁺(Glyme)

66

E_c^s : -1628.779906

+2 1

C 0.257084 -5.021526 0.129837
 C -1.005398 -4.381518 0.666899
 Ni -2.601486 -6.826690 0.798009
 N -0.890296 -7.300894 -0.017641
 N -2.105369 -4.966241 1.046257
 C 0.046591 -6.446944 -0.346235
 C -0.481983 -8.634863 -0.540613
 C 0.652163 -8.286658 -1.544013
 O 1.000837 -6.907020 -1.143371
 C -3.061748 -3.923987 1.502706
 C -2.228529 -2.609113 1.409120
 O -0.955476 -3.063379 0.817302
 C 1.274993 -5.098080 1.312907
 H 2.225592 -5.536209 0.953196
 H 1.478569 -4.077245 1.688889
 H 0.884194 -5.719318 2.142193
 C 0.831775 -4.155075 -1.015322
 H 1.032470 -3.133745 -0.644938
 H 1.782582 -4.588701 -1.372953
 H 0.126566 -4.091219 -1.867242
 C -3.977102 -8.613958 2.656338
 H -3.290570 -9.481545 2.757508
 H -4.667083 -8.599596 3.525674
 C -4.759538 -8.661622 1.365857
 H -5.572465 -7.901689 1.341353
 H -5.205138 -9.669089 1.228310
 O -3.820768 -8.390902 0.297474
 C -4.381233 -8.503677 -1.027789
 H -5.237011 -7.808187 -1.155488
 H -4.714351 -9.547618 -1.198401
 H -3.578749 -8.248938 -1.744654
 O -3.203404 -7.387385 2.639634
 C -2.408040 -7.163641 3.823255
 H -1.885623 -6.199176 3.688550
 H -1.669682 -7.981177 3.955064
 H -3.077324 -7.109676 4.705780
 H 0.340591 -8.223159 -2.604082
 H -1.349935 -9.138058 -1.010160
 H -1.964469 -2.162103 2.384752
 H -3.400534 -4.166707 2.530748
 H 3.381238 -10.854273 0.562573
 C 2.358204 -10.606966 0.885913
 C -0.276087 -9.981272 1.720346

C 1.866665 -11.080984 2.113793
 C 1.527920 -9.814998 0.077504
 C 0.217341 -9.502704 0.497246
 C 0.557801 -10.771940 2.528978
 H 2.510551 -11.701520 2.755970
 H 0.184438 -11.152892 3.491960
 H -1.297452 -9.742816 2.048341
 C 1.822213 -9.235056 -1.285912
 H 2.795744 -8.708470 -1.352411
 H 1.836842 -10.026583 -2.065293
 C -4.118870 -2.460246 -0.088139
 C -6.164389 -4.259778 -0.779672
 C -4.203809 -3.724624 0.527997
 C -5.062893 -2.092963 -1.060679
 C -6.079399 -3.000914 -1.404596
 C -5.223745 -4.629898 0.197419
 H -5.011188 -1.106490 -1.546830
 H -6.823148 -2.720768 -2.166410
 H -5.305606 -5.604524 0.706545
 H -6.976861 -4.951334 -1.051008
 C -2.972791 -1.645525 0.469830
 H -3.343668 -0.768116 1.039523
 H -2.294602 -1.245932 -0.311813

LNiCl(Glyme)

67

E_c^s : -2089.343961

0 2

C 1.135106 -5.755949 0.229169
 C -0.374119 -5.700637 0.108997
 Ni -0.878836 -8.561793 -0.096782
 N 1.028811 -8.293410 0.155505
 N -1.215915 -6.675660 -0.062712
 C 1.678348 -7.169930 0.215135
 C 2.027803 -9.385362 0.282980
 C 3.401040 -8.654484 0.191821
 O 3.024654 -7.242958 0.289669
 C -2.561742 -6.069308 -0.235458
 C -2.347701 -4.570117 0.119422
 O -0.887903 -4.452661 0.173203
 C 1.558500 -5.089167 1.567225
 H 2.661422 -5.081164 1.653709
 H 1.192792 -4.045587 1.598812
 H 1.139521 -5.638092 2.434153
 C 1.744170 -4.975031 -0.968624
 H 1.387681 -3.927673 -0.954933
 H 2.848273 -4.974915 -0.896532
 H 1.451857 -5.435284 -1.933491
 C -3.724673 -8.231413 3.060538
 H -3.157810 -8.977810 2.450138
 H -3.798468 -8.642306 4.099068

C -5.127640 -8.084319 2.513049
 H -5.664909 -7.279897 3.075988
 H -5.679701 -9.039309 2.698703
 O -5.092366 -7.788612 1.129091
 C -6.378819 -7.649123 0.566550
 H -6.958464 -6.818166 1.038521
 H -6.982203 -8.584248 0.666896
 H -6.255970 -7.426656 -0.511981
 O -3.065772 -6.977576 3.065171
 C -1.763695 -7.057511 3.604182
 H -1.327250 -6.038612 3.588624
 H -1.102398 -7.739693 3.015891
 H -1.771236 -7.418006 4.662864
 Cl -1.786151 -10.554050 -0.299763
 H 1.859732 -10.125659 -0.524456
 H 3.920843 -8.776013 -0.778442
 H -2.724027 -4.282215 1.120297
 H -3.286363 -6.585342 0.427798
 C 2.036501 -10.019857 1.664430
 C 2.450095 -10.980844 4.256399
 C 0.999023 -10.713124 2.308671
 C 3.277337 -9.812513 2.301978
 C 3.488886 -10.293672 3.604376
 C 1.215813 -11.192207 3.612523
 H 0.036371 -10.873246 1.795841
 H 4.455146 -10.136157 4.109603
 H 0.413247 -11.737283 4.133683
 H 2.604720 -11.360211 5.278846
 C 4.249320 -9.089663 1.396451
 H 5.064153 -9.767632 1.063380
 H 4.740251 -8.218539 1.877035
 C -3.184783 -4.719362 -2.135418
 C -3.607998 -6.879362 -3.876426
 C -3.004608 -6.044804 -1.687839
 C -3.579768 -4.470638 -3.459987
 C -3.787952 -5.557573 -4.327360
 C -3.214543 -7.132492 -2.550428
 H -3.722894 -3.438348 -3.817200
 H -4.094969 -5.373209 -5.368941
 H -3.066491 -8.164507 -2.193133
 H -3.775550 -7.720886 -4.566674
 C -2.935904 -3.725941 -1.021668
 H -3.884142 -3.250314 -0.691050
 H -2.251766 -2.900383 -1.307452

LNi(Glyme)

66

 E_c^s : -1629.006235

0 1

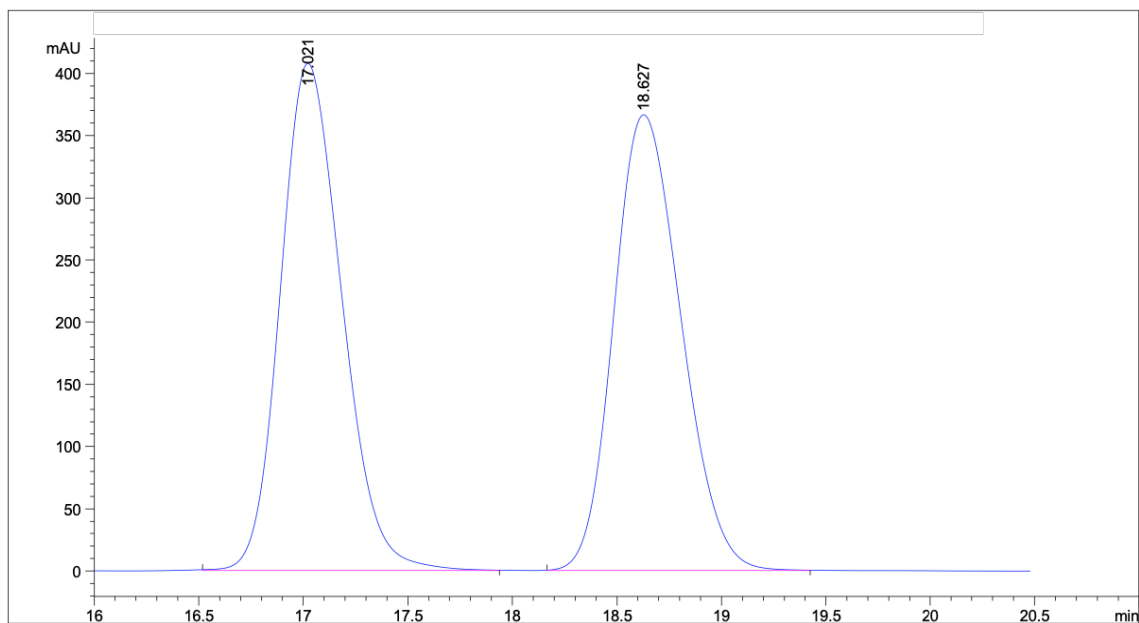
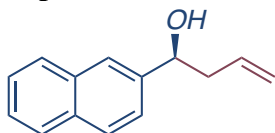
C 0.088691 -5.095361 -0.174789
 C -1.178705 -4.685229 0.553070

Ni -1.971064 -7.280008 1.270974
 N -0.551715 -7.534488 0.143057
 N -2.306095 -5.341966 0.664193
 C 0.121615 -6.584728 -0.457383
 C -0.046038 -8.833270 -0.404106
 C 0.996822 -8.416474 -1.489096
 O 1.040588 -6.965669 -1.386191
 C -3.262807 -4.392509 1.279808
 C -2.390900 -3.198239 1.778562
 O -1.117691 -3.436317 1.113290
 C 1.332176 -4.753069 0.694797
 H 2.256081 -5.056855 0.164982
 H 1.380187 -3.665182 0.892055
 H 1.291627 -5.286638 1.665792
 C 0.157981 -4.301085 -1.508967
 H 0.127522 -3.214443 -1.297803
 H 1.096915 -4.527705 -2.050276
 H -0.697246 -4.552647 -2.167494
 C -4.390905 -8.387655 2.719525
 H -3.917038 -9.380556 2.901115
 H -5.087861 -8.173773 3.562576
 C -5.196247 -8.409860 1.440643
 H -5.559890 -7.377872 1.207480
 H -6.104430 -9.035432 1.635451
 O -4.445728 -8.941188 0.370397
 C -5.166228 -8.955879 -0.843130
 H -5.467068 -7.930381 -1.168847
 H -6.092374 -9.577843 -0.774424
 H -4.507404 -9.389072 -1.621561
 O -3.380501 -7.364412 2.710656
 C -2.835835 -7.154834 4.019939
 H -2.107034 -6.326428 3.952511
 H -2.312325 -8.065972 4.385971
 H -3.651630 -6.882939 4.729666
 H 0.685646 -8.654664 -2.524993
 H -0.909441 -9.397591 -0.808958
 H -2.195314 -3.197312 2.870140
 H -3.817184 -4.911276 2.089273
 H 4.097518 -10.436669 0.766669
 C 3.035052 -10.374282 1.051270
 C 0.298240 -10.228868 1.788927
 C 2.584147 -10.959147 2.248702
 C 2.109940 -9.711475 0.224603
 C 0.754341 -9.634046 0.600805
 C 1.225620 -10.894493 2.612832
 H 3.300271 -11.480472 2.903885
 H 0.886897 -11.368802 3.547545
 H -0.767158 -10.160390 2.063100
 C 2.351225 -9.051804 -1.114809
 H 3.150727 -8.281752 -1.082130
 H 2.661088 -9.794683 -1.880297

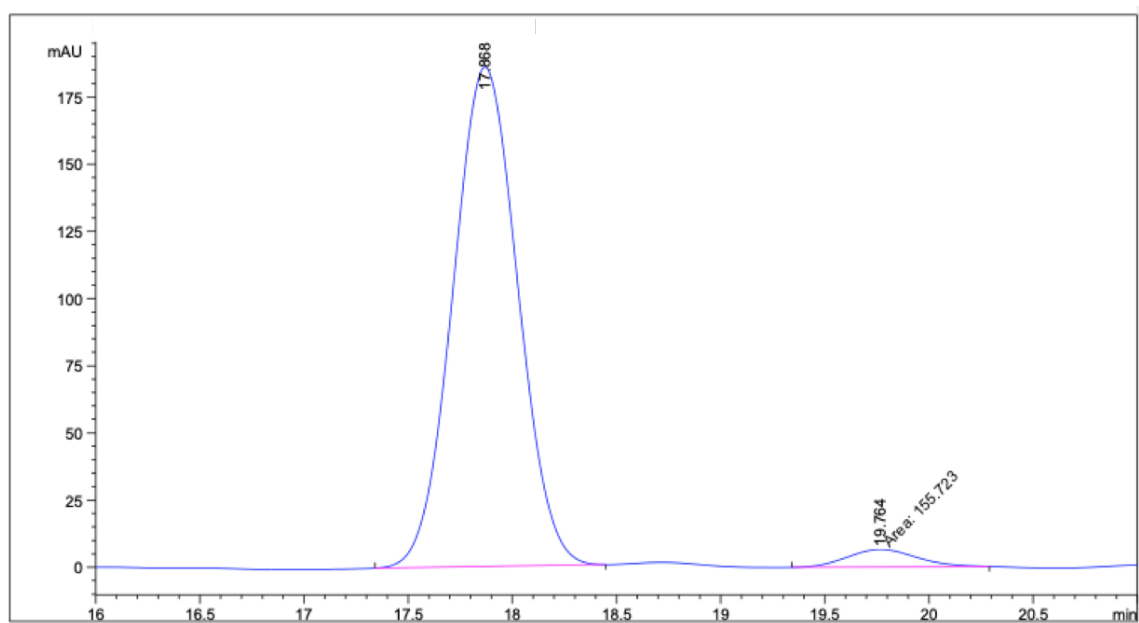
C -4.045922 -2.355539 0.242479
C -5.837586 -3.619011 -1.510238
C -4.190908 -3.758720 0.259714
C -4.800631 -1.578671 -0.651324
C -5.697571 -2.218319 -1.527192
C -5.082830 -4.399239 -0.616066
H -4.690861 -0.482549 -0.671499
H -6.292439 -1.618262 -2.233803
H -5.178235 -5.496678 -0.608631

H -6.539991 -4.106568 -2.204599
C -3.046943 -1.898884 1.283442
H -3.556578 -1.383259 2.126112
H -2.291416 -1.188514 0.888481

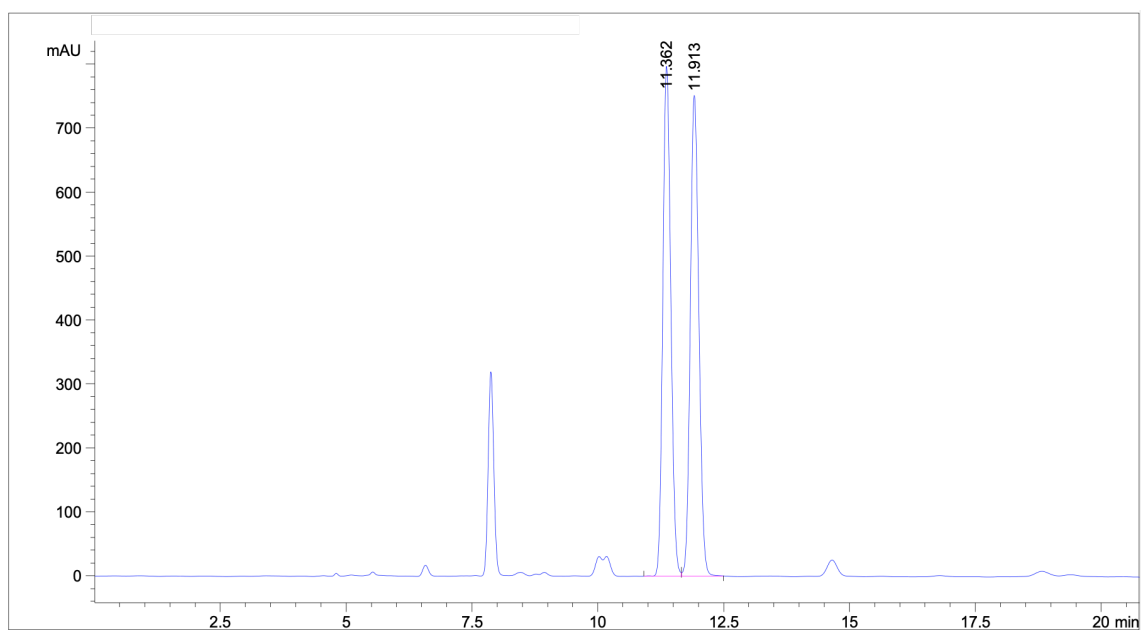
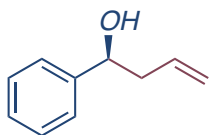
Copies of HPLC traces



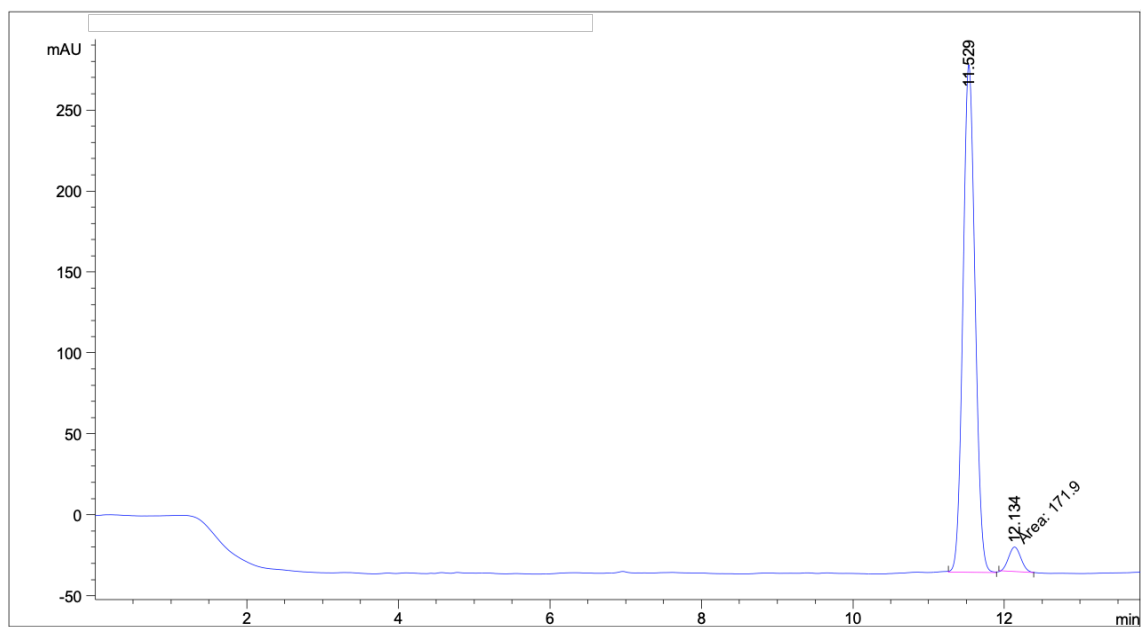
Peak #	RetTime [min]	Type	Width [min]	Area [mAU*s]	Height [mAU]	Area %
1	17.021	BB	0.3182	8327.83203	407.83405	50.4227
2	18.627	BB	0.3507	8188.20752	366.48590	49.5773



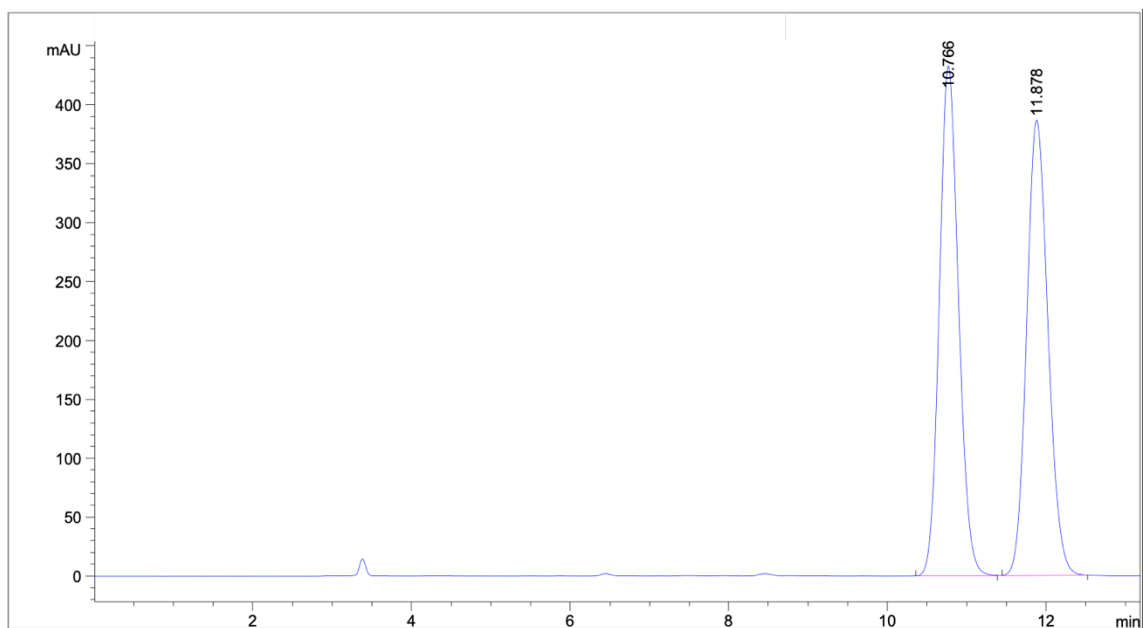
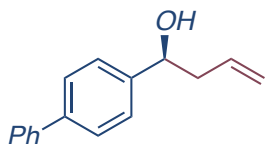
Peak #	RetTime [min]	Type	Width [min]	Area [mAU*s]	Height [mAU]	Area %
1	17.868	BB	0.3388	4029.04150	185.94078	96.2788
2	19.764	MM	0.3933	155.72350	6.59941	3.7212



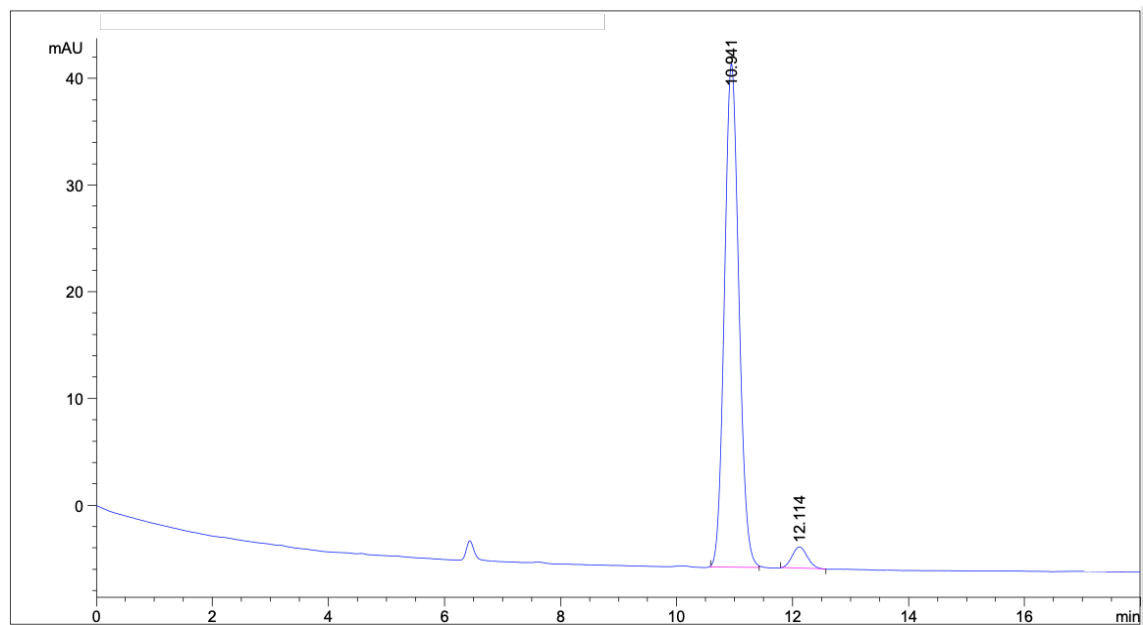
Peak #	RetTime [min]	Type	Width [min]	Area [mAU*s]	Height [mAU]	Area %
1	11.362	BV	0.1728	8804.08008	797.44043	49.8186
2	11.913	VB	0.1835	8868.18750	752.23218	50.1814



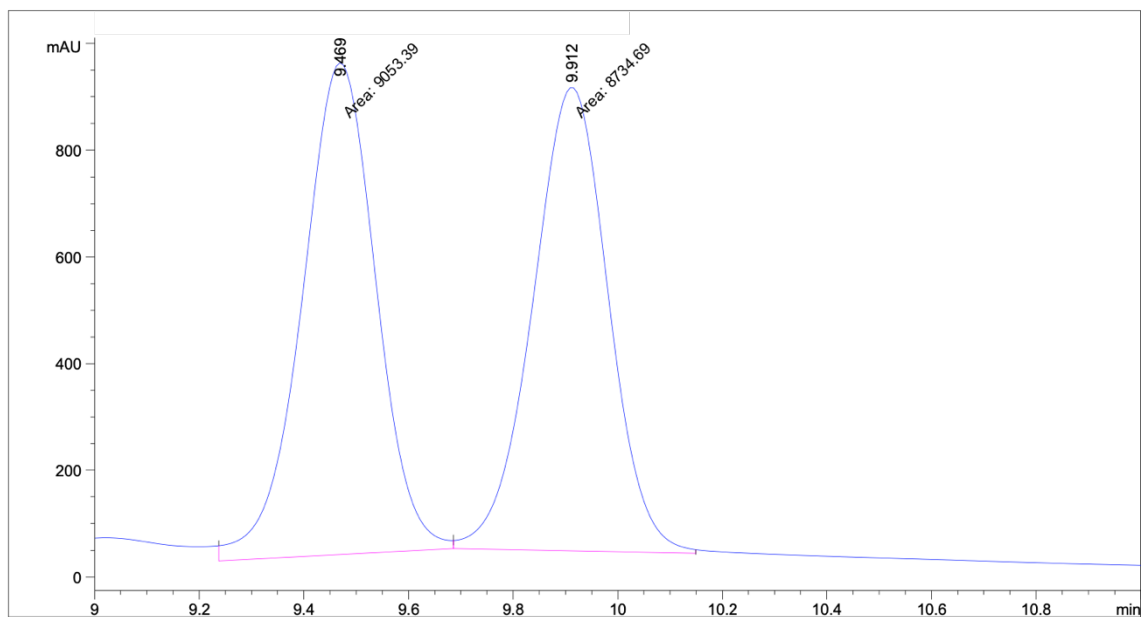
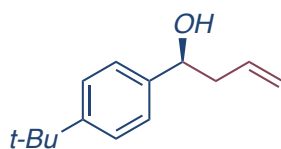
Peak #	RetTime [min]	Type	Width [min]	Area [mAU*s]	Height [mAU]	Area %
1	11.529	BB	0.1734	3479.35474	313.66684	95.2920
2	12.134	MM	0.1884	171.90015	15.20836	4.7080



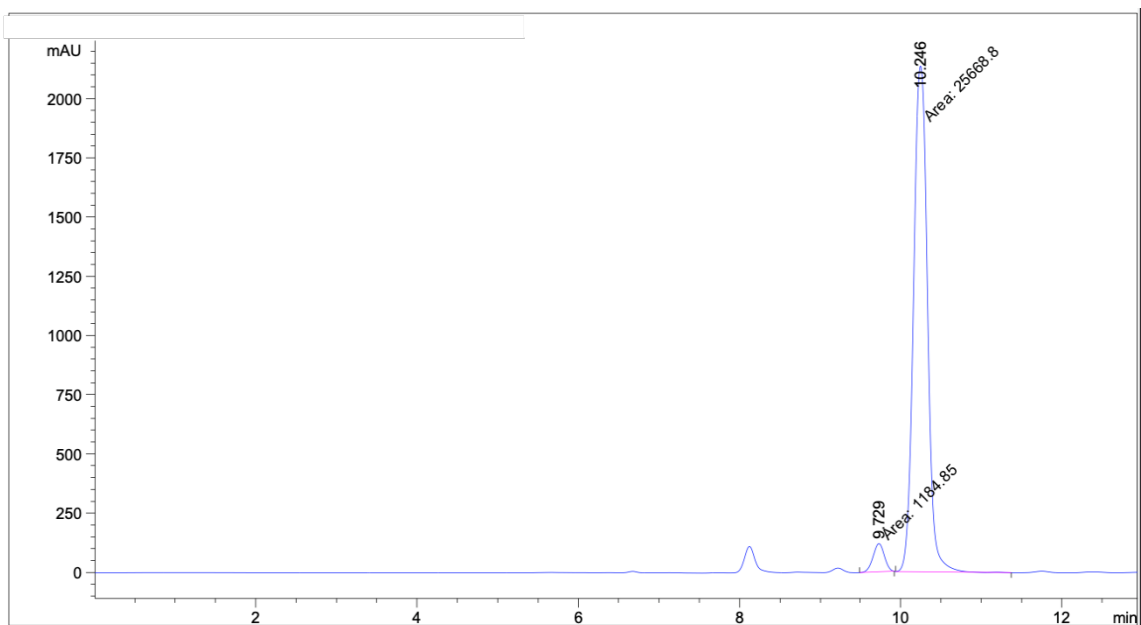
Peak #	RetTime [min]	Type	Width [min]	Area [mAU*s]	Height [mAU]	Area %
1	10.766	BB	0.2603	7286.15527	433.00293	50.1851
2	11.878	BB	0.2902	7232.41162	386.72256	49.8149



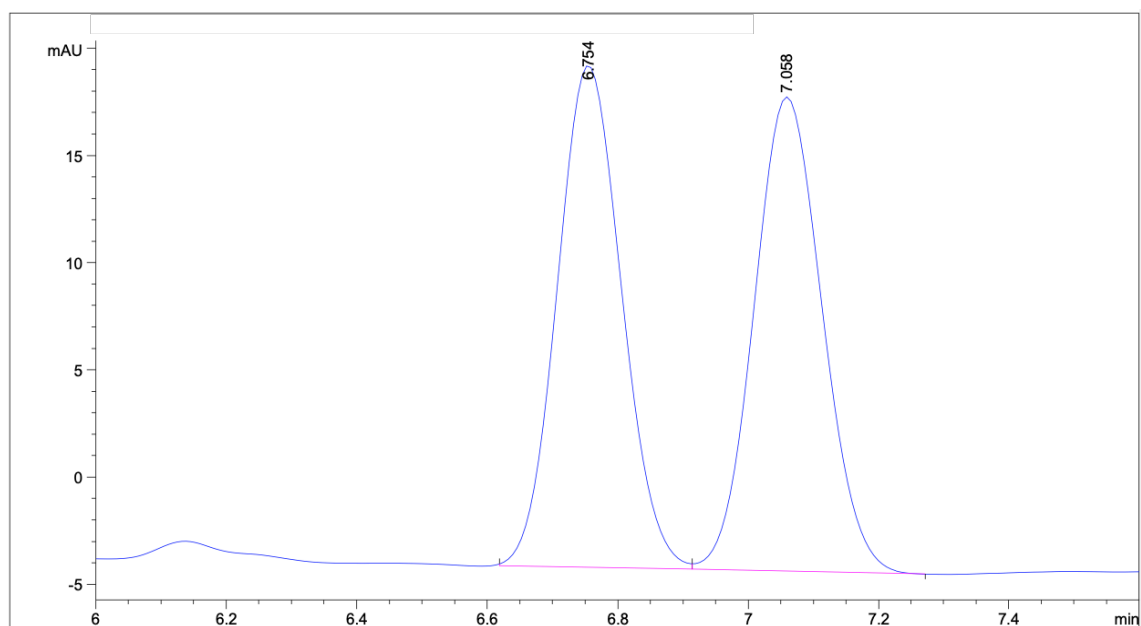
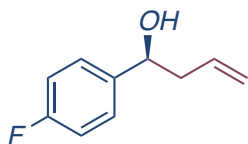
Peak #	RetTime [min]	Type	Width [min]	Area [mAU*s]	Height [mAU]	Area %
1	10.941	BB	0.2695	815.21820	47.19833	95.6955
2	12.114	BB	0.2818	36.66916	2.00113	4.3045



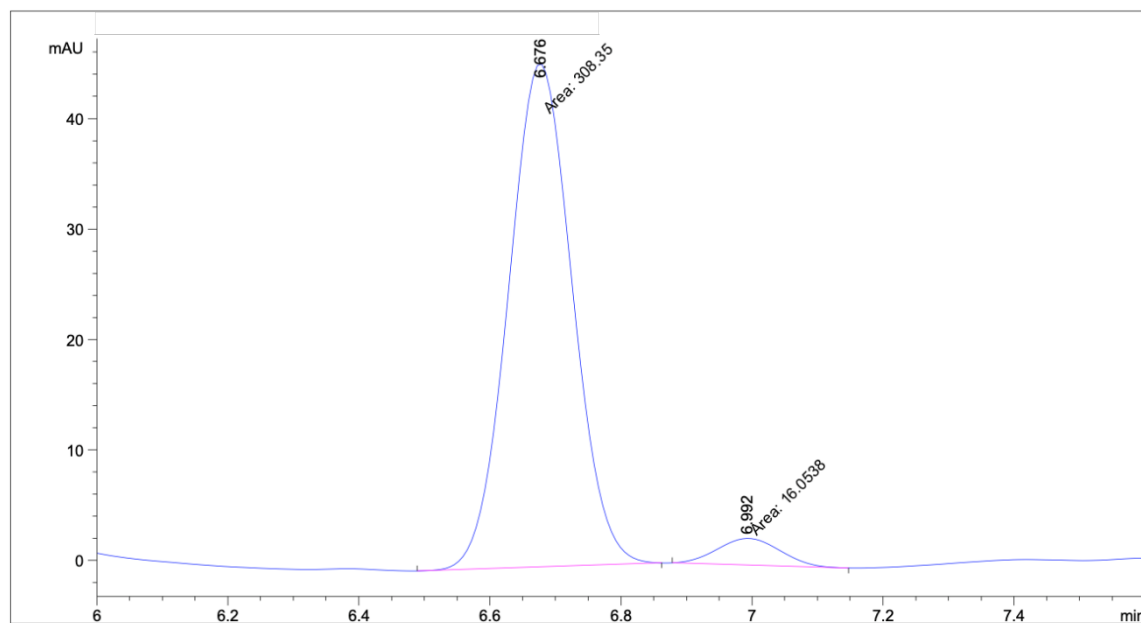
Peak #	RetTime [min]	Type	Width [min]	Area [mAU*s]	Height [mAU]	Area %
1	9.469	MM	0.1635	9053.38770	922.79181	50.8958
2	9.912	MM	0.1673	8734.69238	870.20752	49.1042



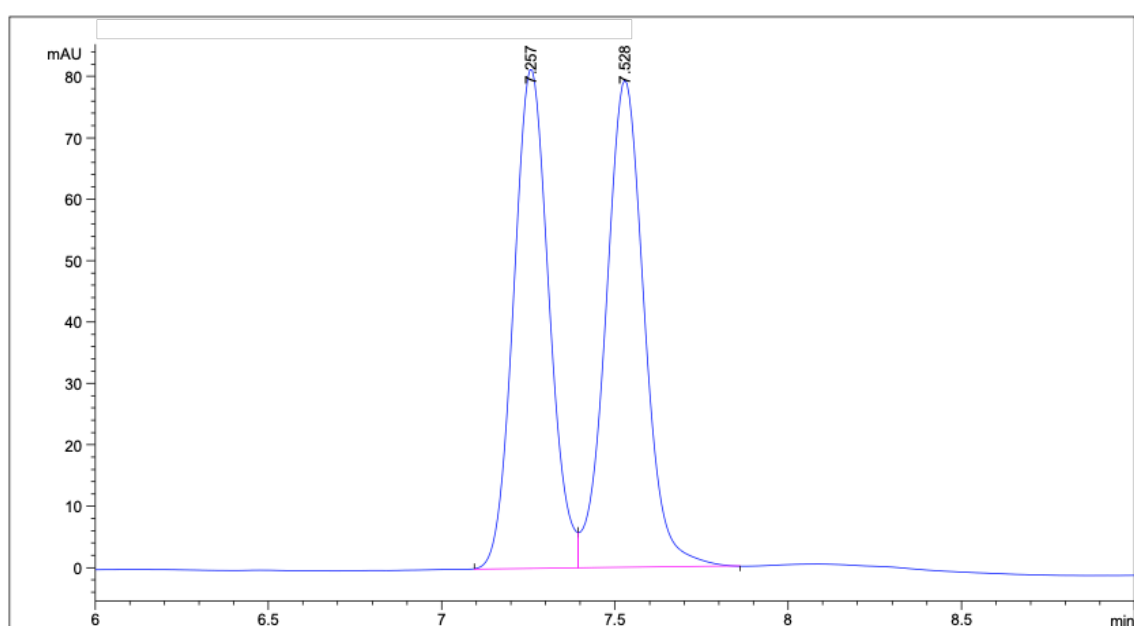
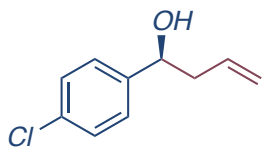
Peak #	RetTime [min]	Type	Width [min]	Area [mAU*s]	Height [mAU]	Area %
1	9.729	MM	0.1640	1184.84741	120.42715	4.4122
2	10.246	MM	0.2002	2.56688e4	2136.43018	95.5878



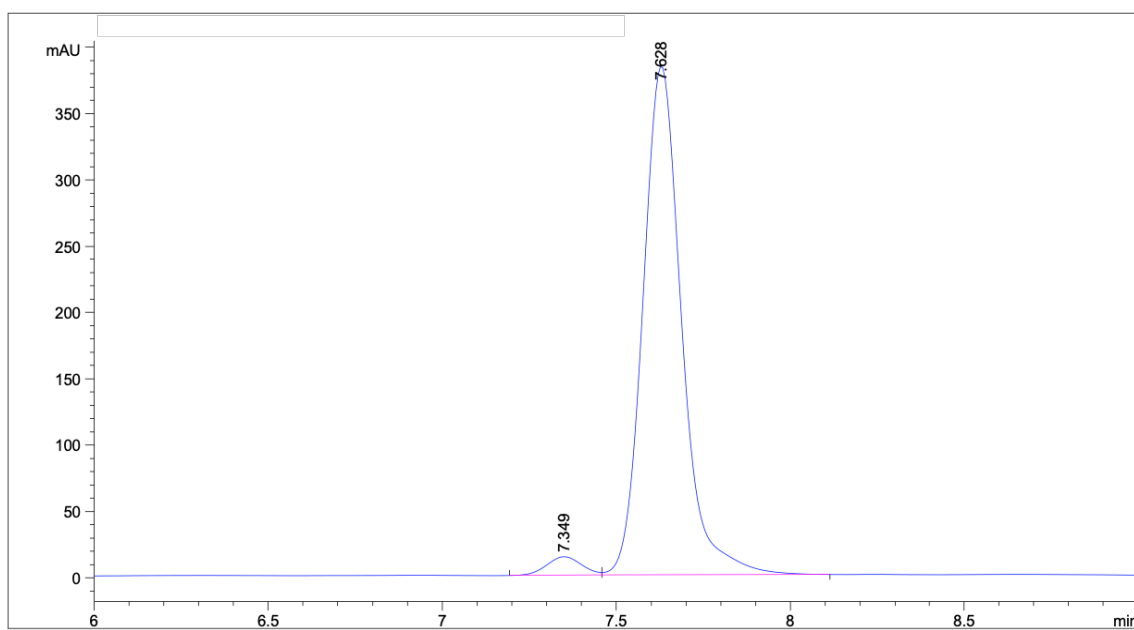
Peak #	RetTime [min]	Type	Width [min]	Area [mAU*s]	Height [mAU]	Area %
1	6.754	BV	0.1079	160.39395	23.41419	49.9659
2	7.058	VB	0.1147	160.61284	22.12551	50.0341



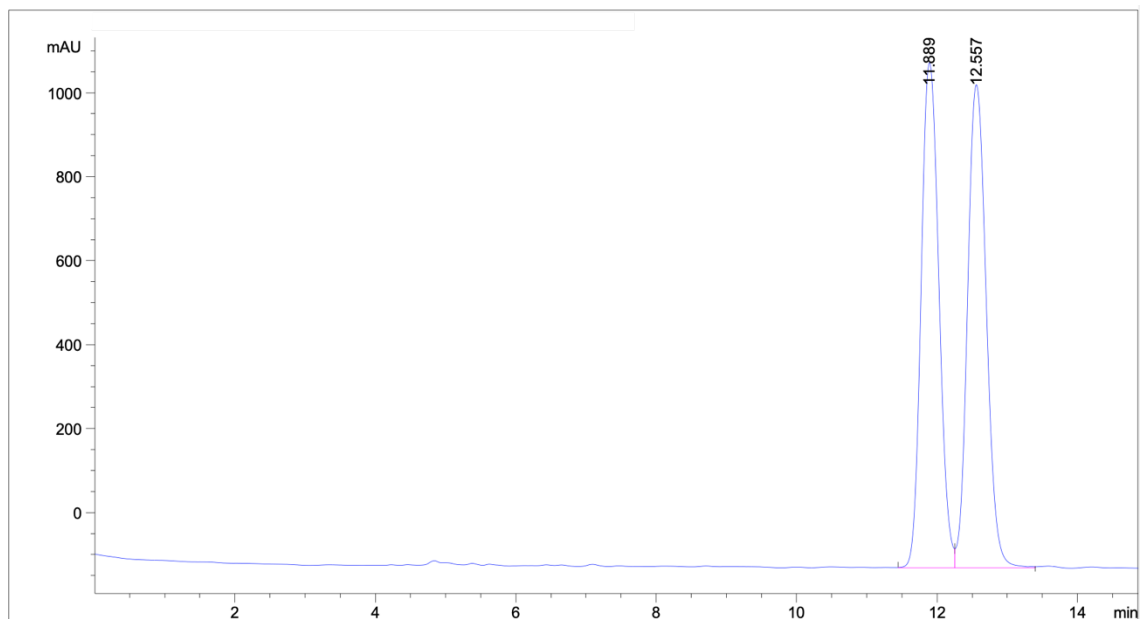
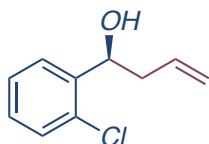
Peak #	RetTime [min]	Type	Width [min]	Area [mAU*s]	Height [mAU]	Area %
1	6.676	MM	0.1125	308.35019	45.67260	95.0513
2	6.992	MM	0.1108	16.05376	2.41399	4.9487



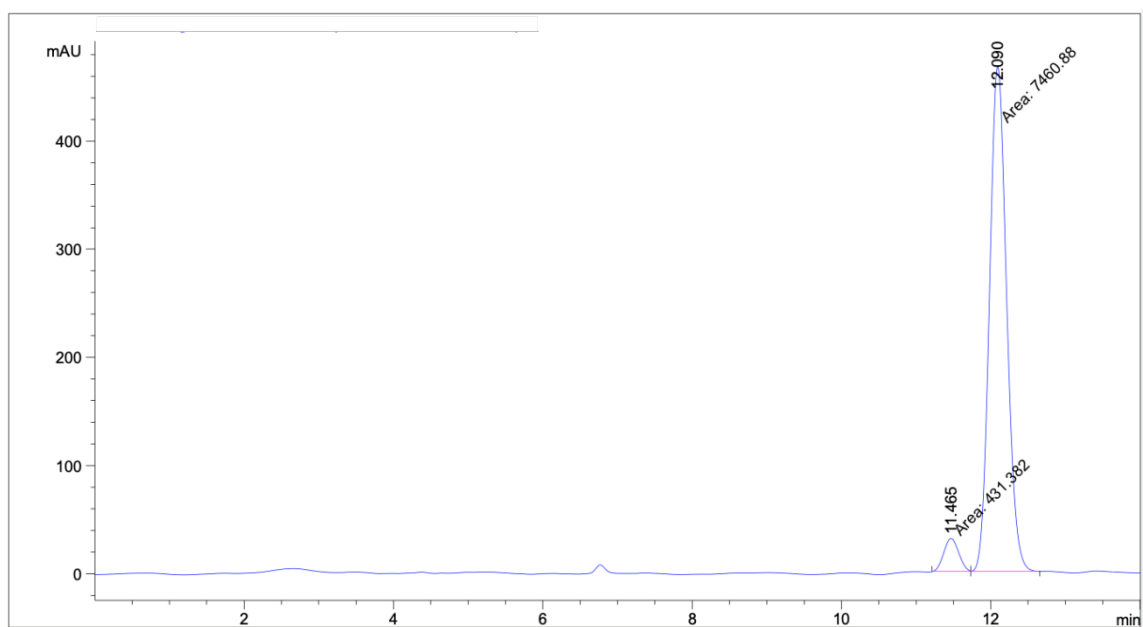
Peak #	RetTime [min]	Type	Width [min]	Area [mAU*s]	Height [mAU]	Area %
1	7.257	BV	0.1107	577.49689	81.44855	48.6495
2	7.528	VB	0.1195	609.55933	79.43860	51.3505



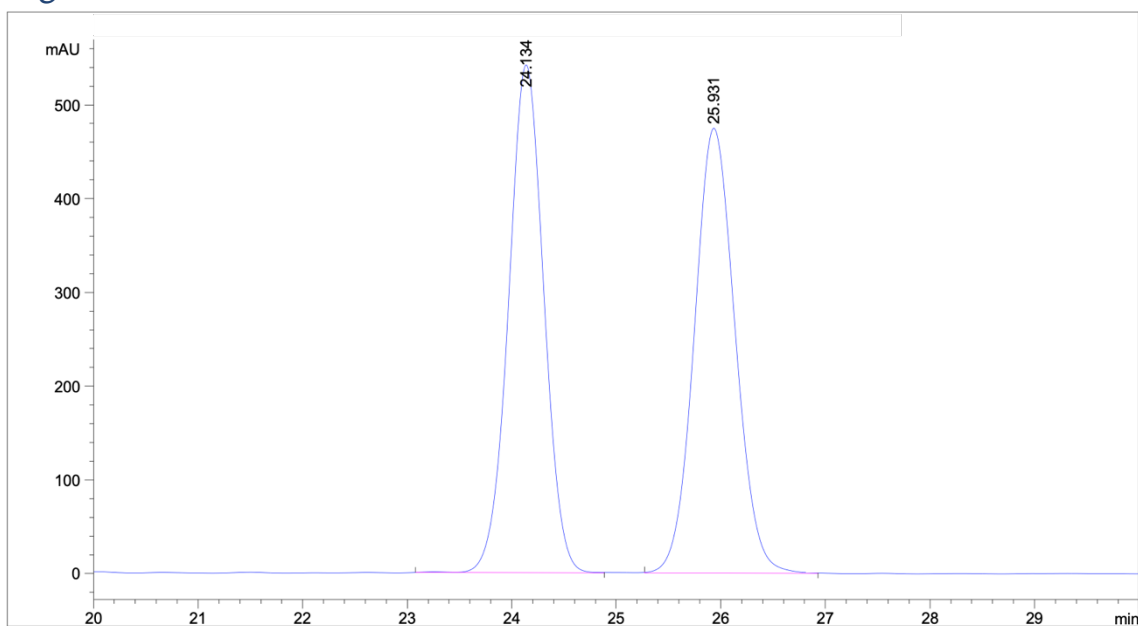
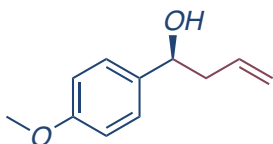
Peak #	RetTime [min]	Type	Width [min]	Area [mAU*s]	Height [mAU]	Area %
1	7.349	BV	0.1100	98.40923	14.00757	3.2177
2	7.628	VB	0.1180	2960.00024	383.90070	96.7823



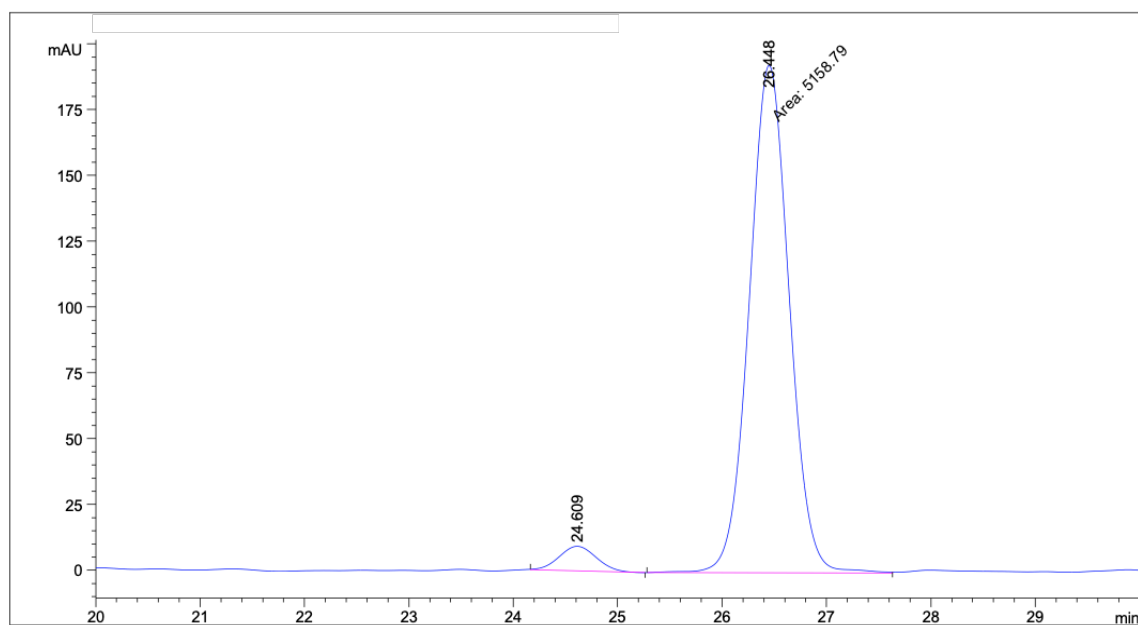
Peak #	RetTime [min]	Type	Width [min]	Area [mAU*s]	Height [mAU]	Area %
1	11.889	BV	0.2767	2.11205e4	1203.65320	49.7205
2	12.557	VB	0.2924	2.13580e4	1151.45630	50.2795



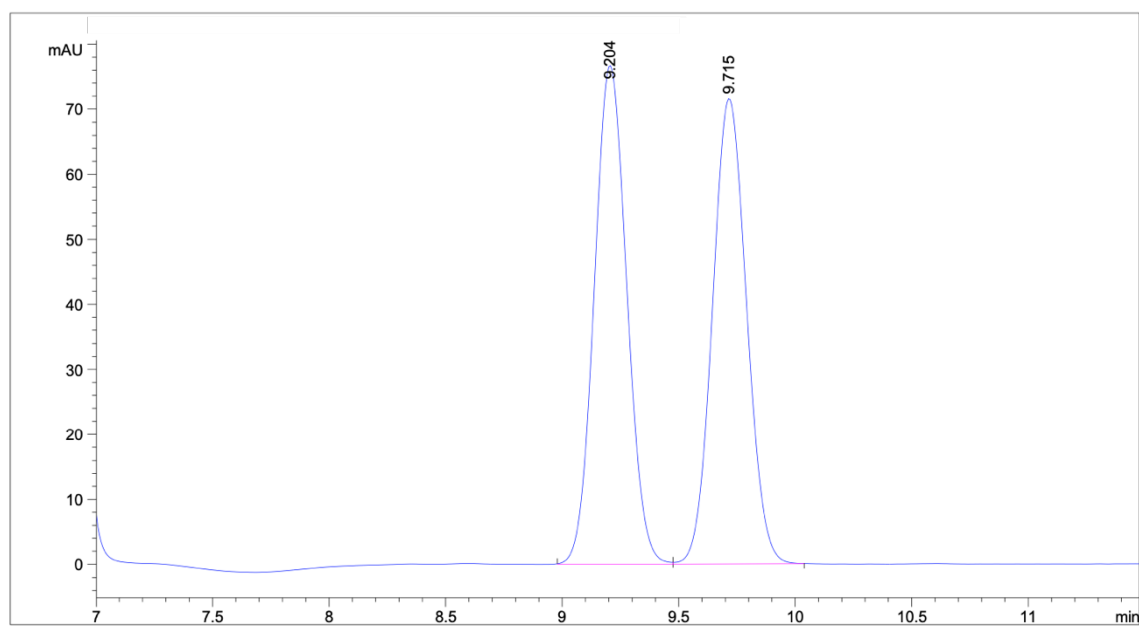
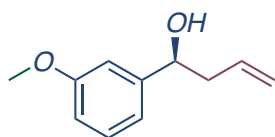
Peak #	RetTime [min]	Type	Width [min]	Area [mAU*s]	Height [mAU]	Area %
1	11.465	MM	0.2339	431.38239	30.73407	5.4659
2	12.090	MM	0.2660	7460.88330	467.50967	94.5341



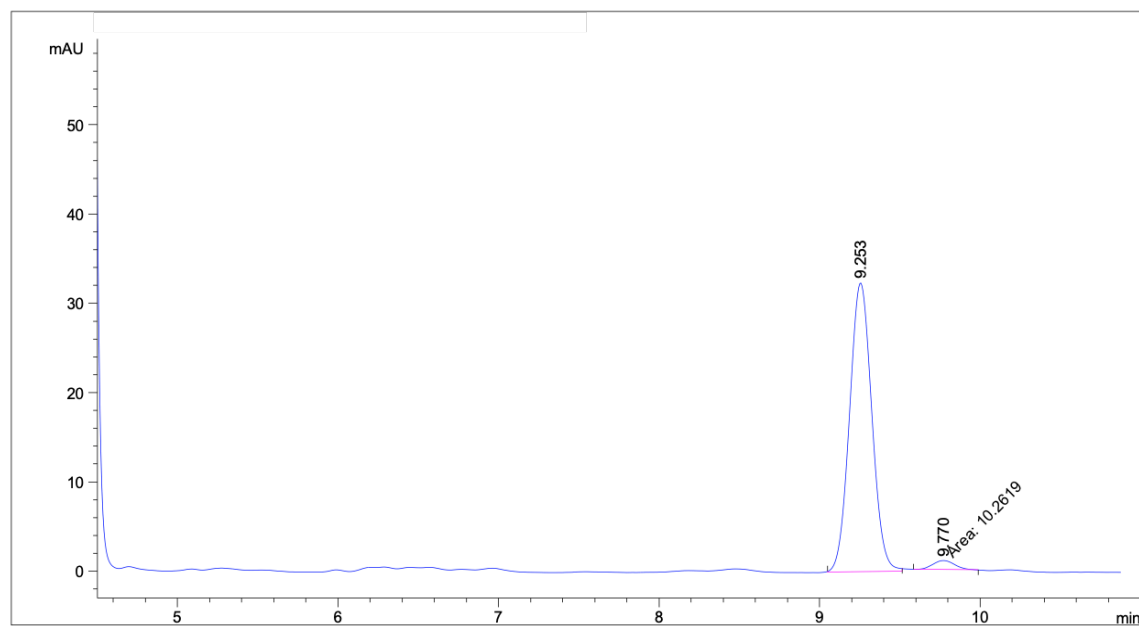
Peak #	RetTime [min]	Type	Width [min]	Area [mAU*s]	Height [mAU]	Area %
1	24.134	BB	0.3637	1.27147e4	542.05713	49.6508
2	25.931	BB	0.4208	1.28936e4	474.77478	50.3492



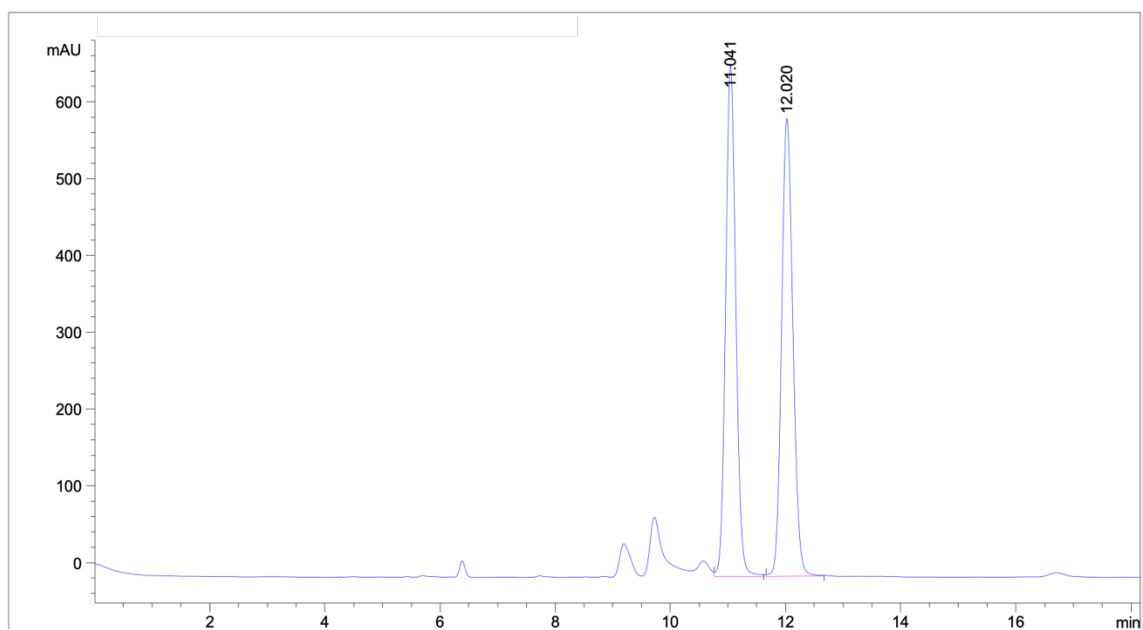
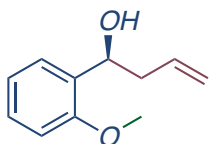
Peak #	RetTime [min]	Type	Width [min]	Area [mAU*s]	Height [mAU]	Area %
1	24.609	BB	0.3824	233.44138	9.37906	4.3292
2	26.448	MM	0.4455	5158.79248	192.97583	95.6708



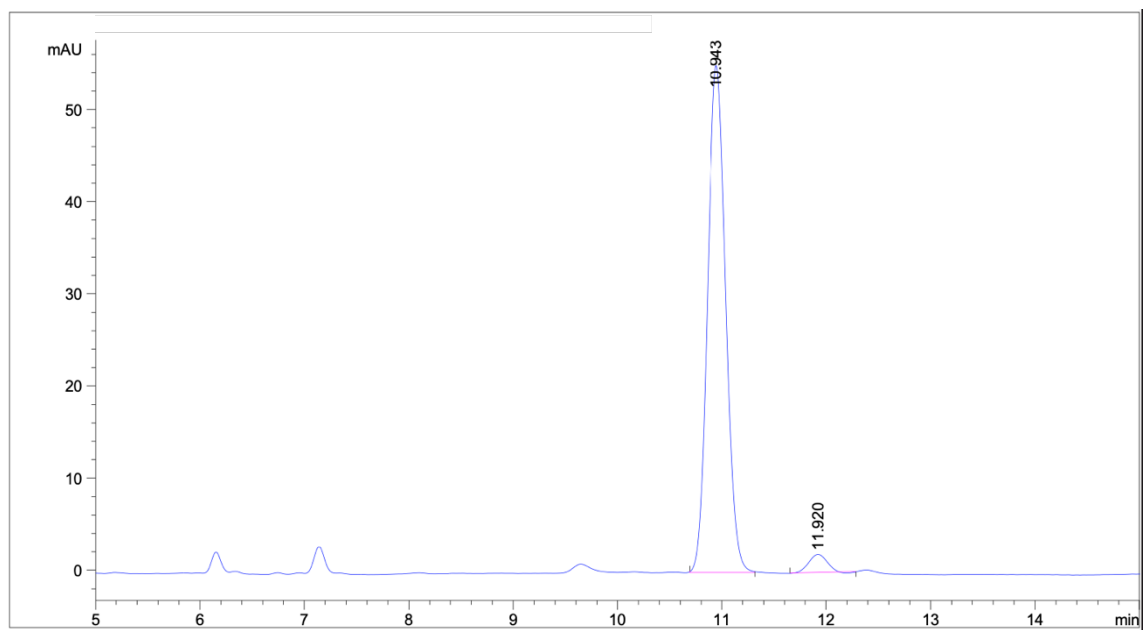
Peak #	RetTime [min]	Type	Width [min]	Area [mAU*s]	Height [mAU]	Area %
1	9.204	BV	0.1513	744.69073	76.69488	50.5318
2	9.715	VB	0.1588	729.01617	71.60784	49.4682



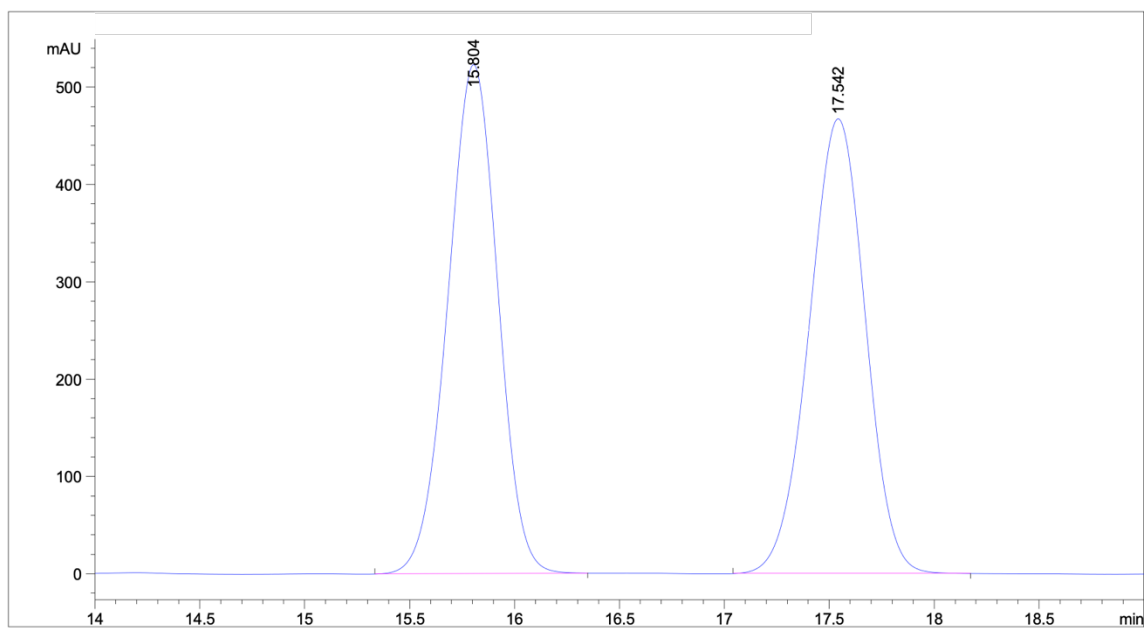
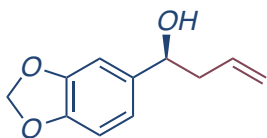
Peak #	RetTime [min]	Type	Width [min]	Area [mAU*s]	Height [mAU]	Area %
1	9.253	BB	0.1503	311.65164	32.36731	96.8122
2	9.770	MM	0.1649	10.26187	1.03703	3.1878



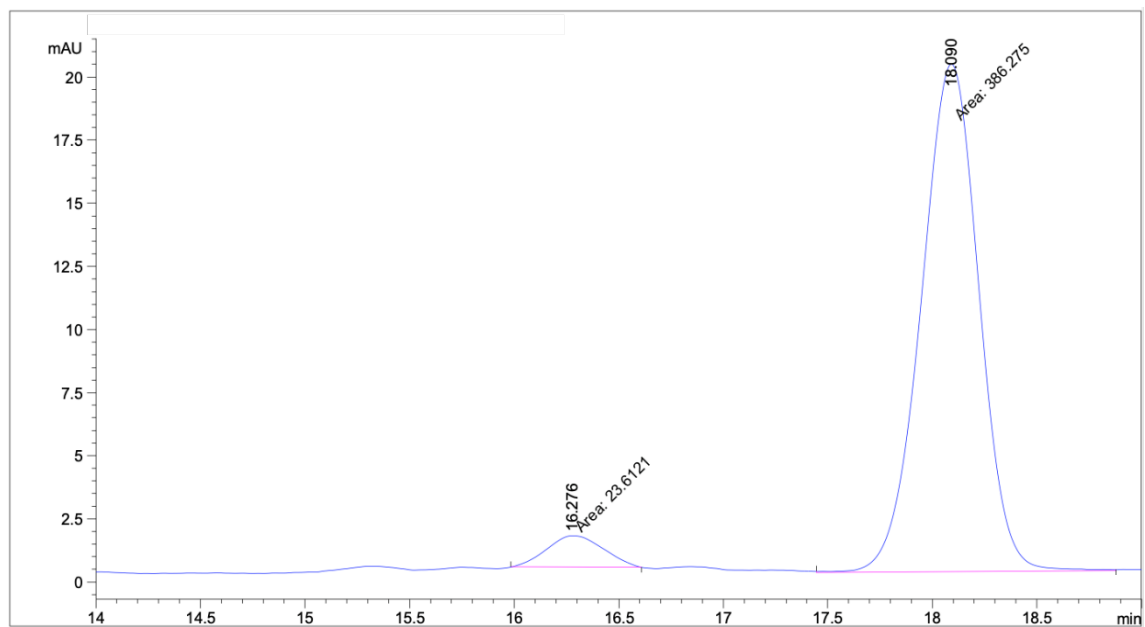
Peak #	RetTime [min]	Type	Width [min]	Area [mAU*s]	Height [mAU]	Area %
1	11.041	VB	0.1918	8201.18457	665.40497	50.0685
2	12.020	BB	0.2139	8178.75146	596.61218	49.9315



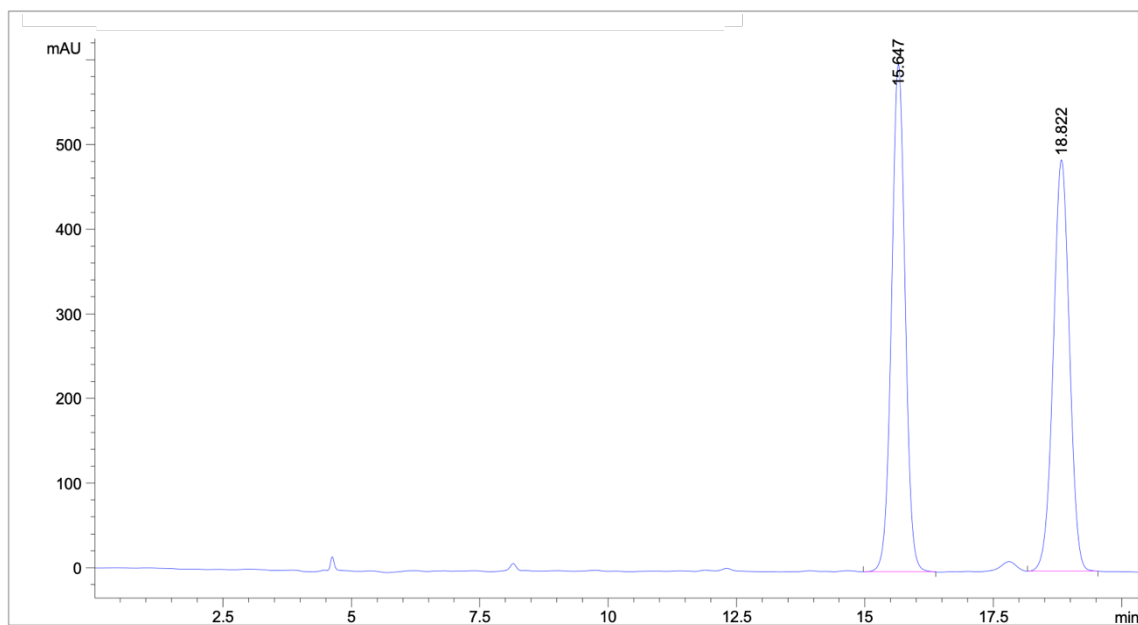
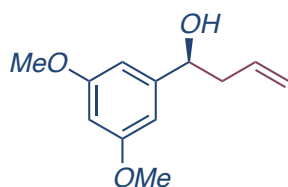
Peak #	RetTime [min]	Type	Width [min]	Area [mAU*s]	Height [mAU]	Area %
1	10.943	BB	0.1900	670.19354	55.05564	96.5114
2	11.920	BB	0.1961	24.22542	1.98835	3.4886



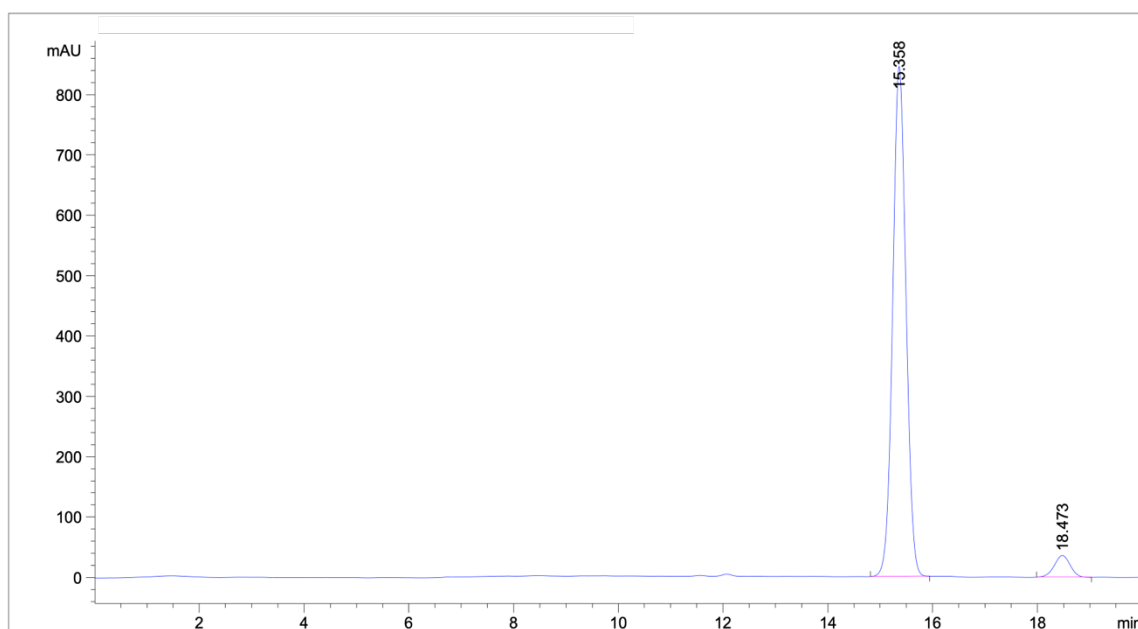
Peak #	RetTime [min]	Type	Width [min]	Area [mAU*s]	Height [mAU]	Area %
1	15.804	BB	0.2590	8656.17578	523.19885	49.8334
2	17.542	BB	0.2935	8714.06055	467.43503	50.1666



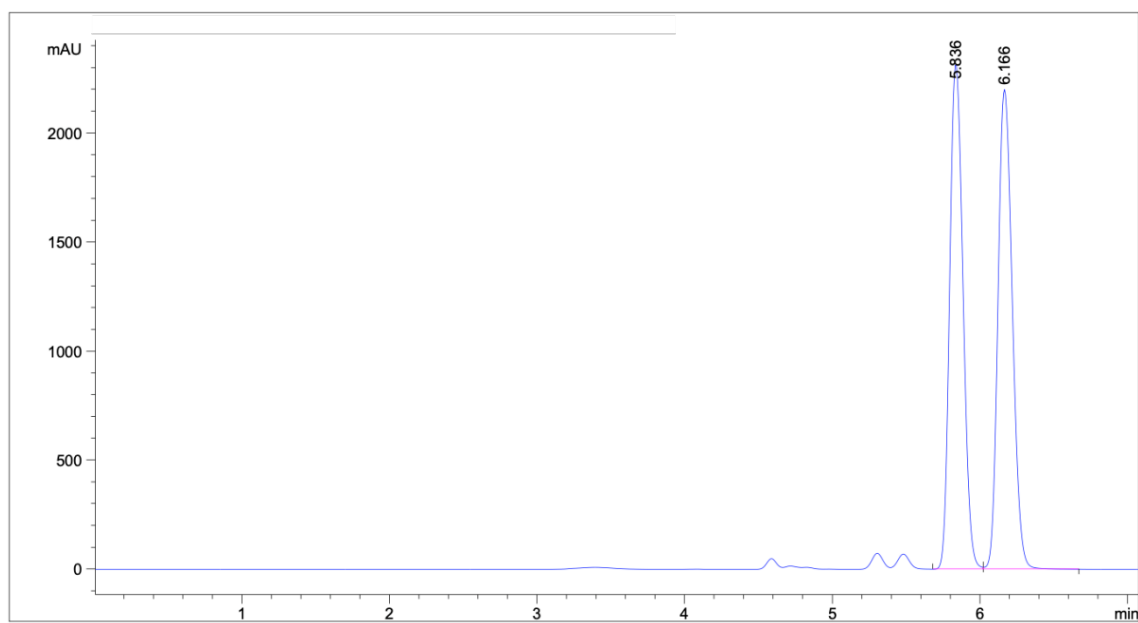
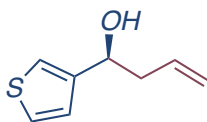
Peak #	RetTime [min]	Type	Width [min]	Area [mAU*s]	Height [mAU]	Area %
1	16.276	MM	0.3155	23.61205	1.24748	5.7606
2	18.090	MM	0.3200	386.27542	20.11740	94.2394



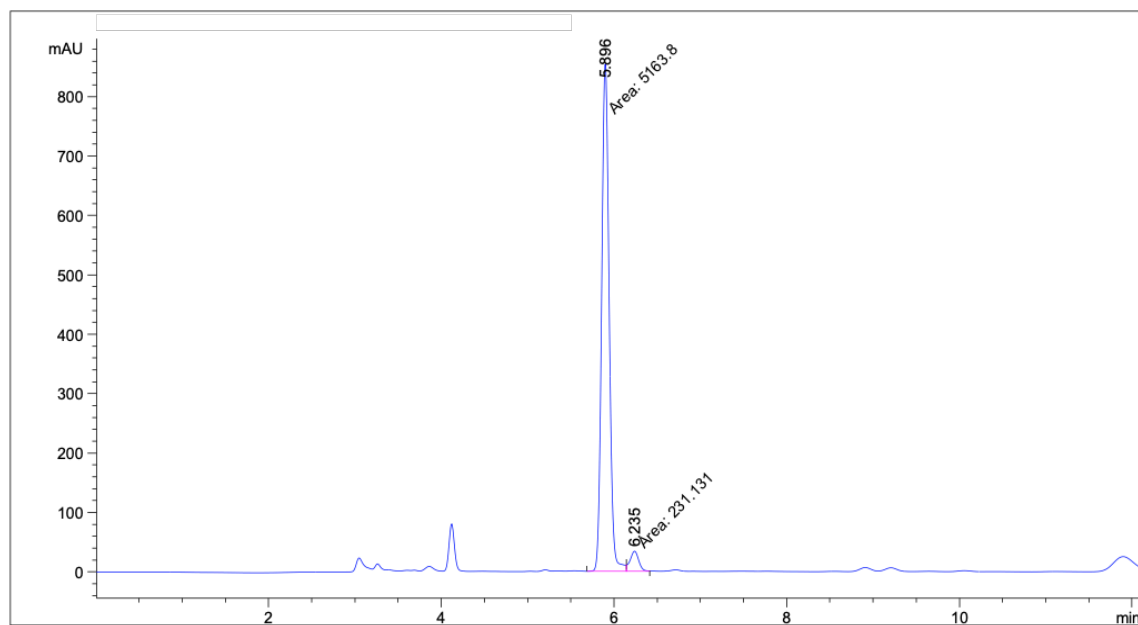
Peak #	RetTime [min]	Type	Width [min]	Area [mAU*s]	Height [mAU]	Area %
1	15.647	VB	0.2846	1.10399e4	600.23181	50.7774
2	18.822	VB	0.3426	1.07019e4	486.54633	49.2226



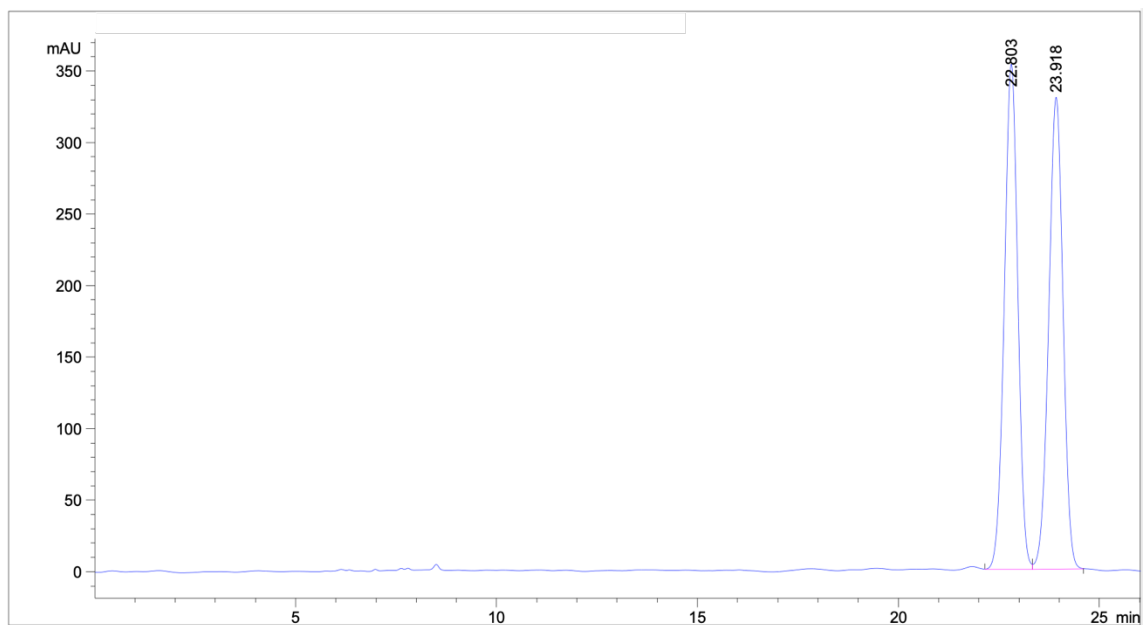
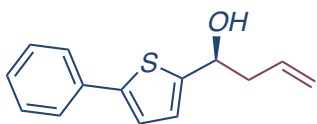
Peak #	RetTime [min]	Type	Width [min]	Area [mAU*s]	Height [mAU]	Area %
1	15.358	BB	0.2729	1.48410e4	844.87238	95.0971
2	18.473	BB	0.3296	765.15485	36.05065	4.9029



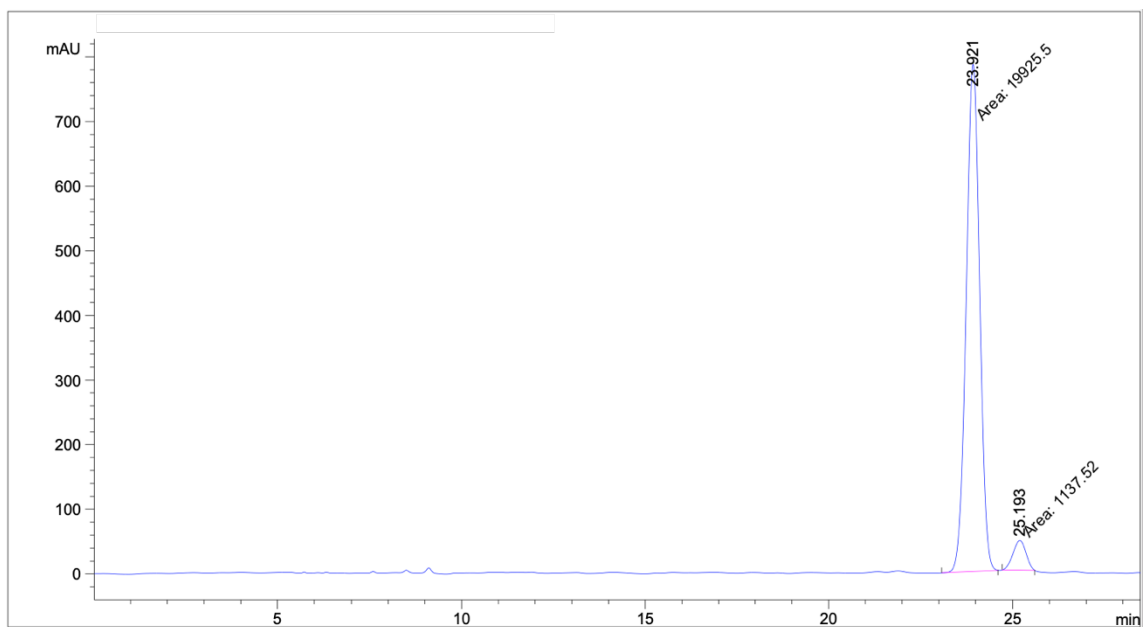
Peak #	RetTime [min]	Type	Width [min]	Area [mAU*s]	Height [mAU]	Area %
1	5.836	VV	0.0991	1.45271e4	2317.15283	49.4132
2	6.166	VB	0.1069	1.48721e4	2200.37158	50.5868



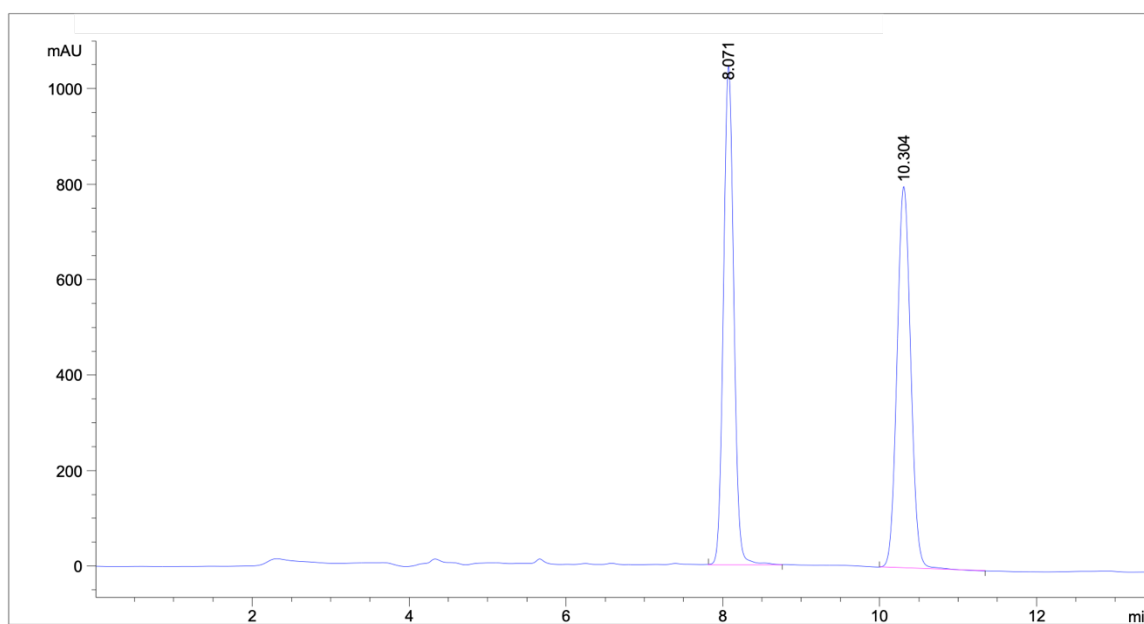
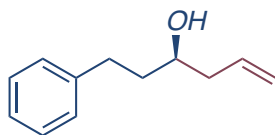
Peak #	RetTime [min]	Type	Width [min]	Area [mAU*s]	Height [mAU]	Area %
1	5.896	MF	0.1003	5163.80469	857.91492	95.7158
2	6.235	FM	0.1139	231.13107	33.83054	4.2842



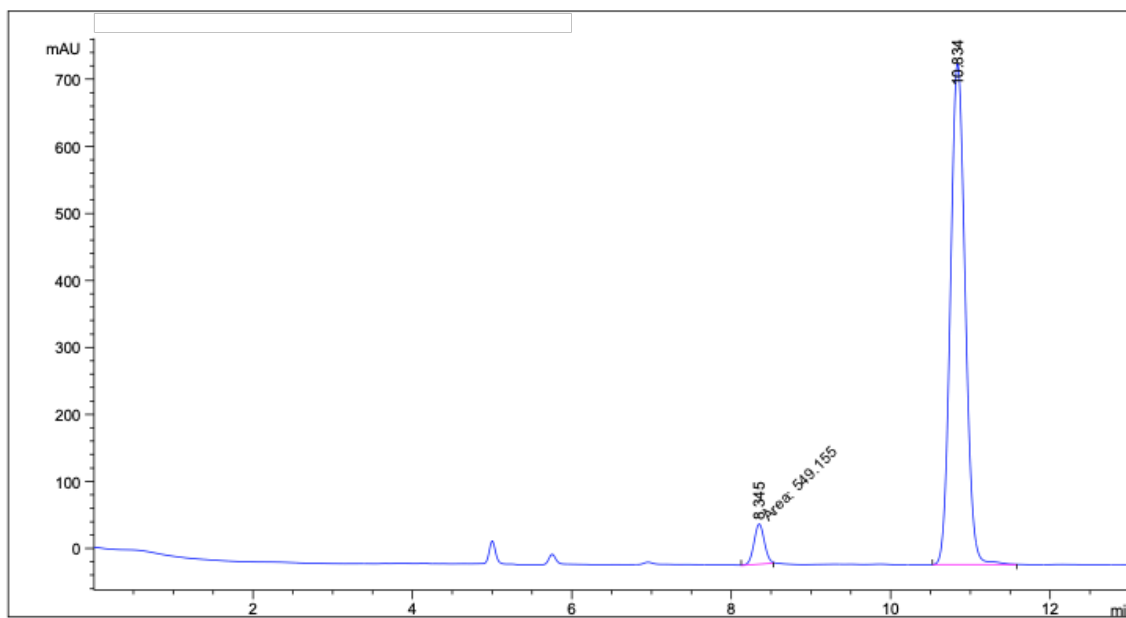
Peak #	RetTime [min]	Type	Width [min]	Area [mAU*s]	Height [mAU]	Area %
1	22.803	VV	0.3649	8265.96191	353.35672	50.2855
2	23.918	VB	0.3849	8172.09131	329.98697	49.7145



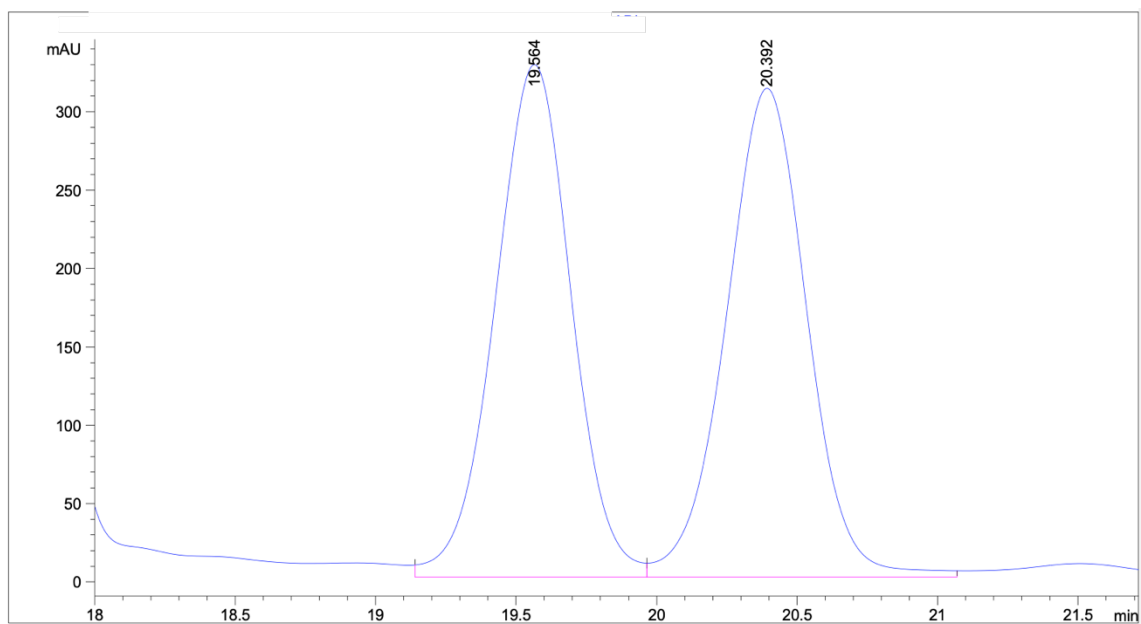
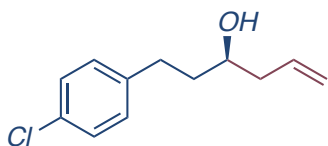
Peak #	RetTime [min]	Type	Width [min]	Area [mAU*s]	Height [mAU]	Area %
1	23.921	MM	0.4233	1.99255e4	784.62164	94.5994
2	25.193	MM	0.4110	1137.52148	46.12864	5.4006



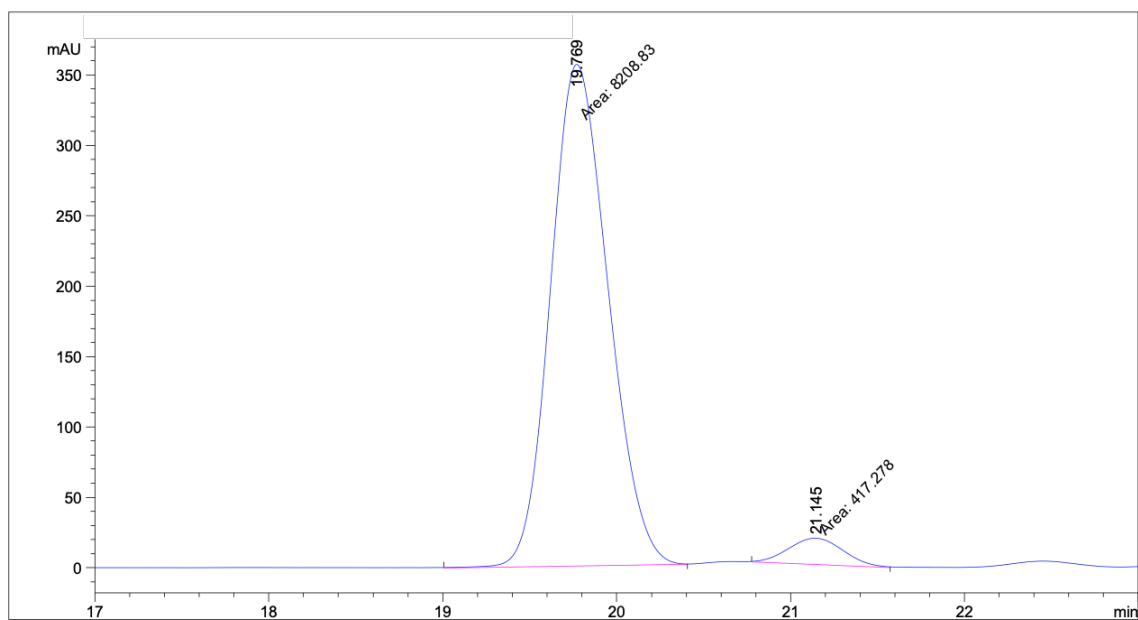
Peak #	RetTime [min]	Type	Width [min]	Area [mAU*s]	Height [mAU]	Area %
1	8.071	BB	0.1432	9599.99219	1045.14417	49.7727
2	10.304	BB	0.1894	9687.67383	799.42596	50.2273



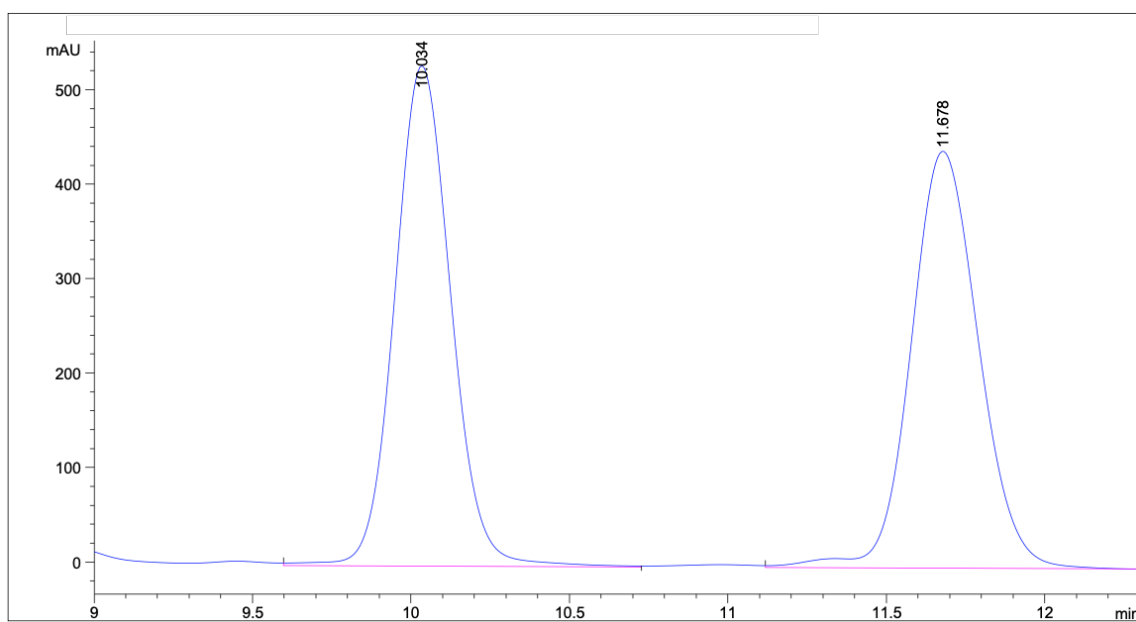
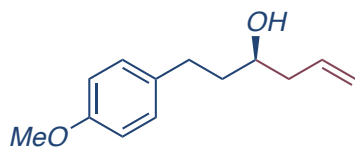
Peak #	RetTime [min]	Type	Width [min]	Area [mAU*s]	Height [mAU]	Area %
1	8.345	MM	0.1522	549.15460	60.13840	5.3969
2	10.834	BB	0.2001	9626.24805	748.20374	94.6031



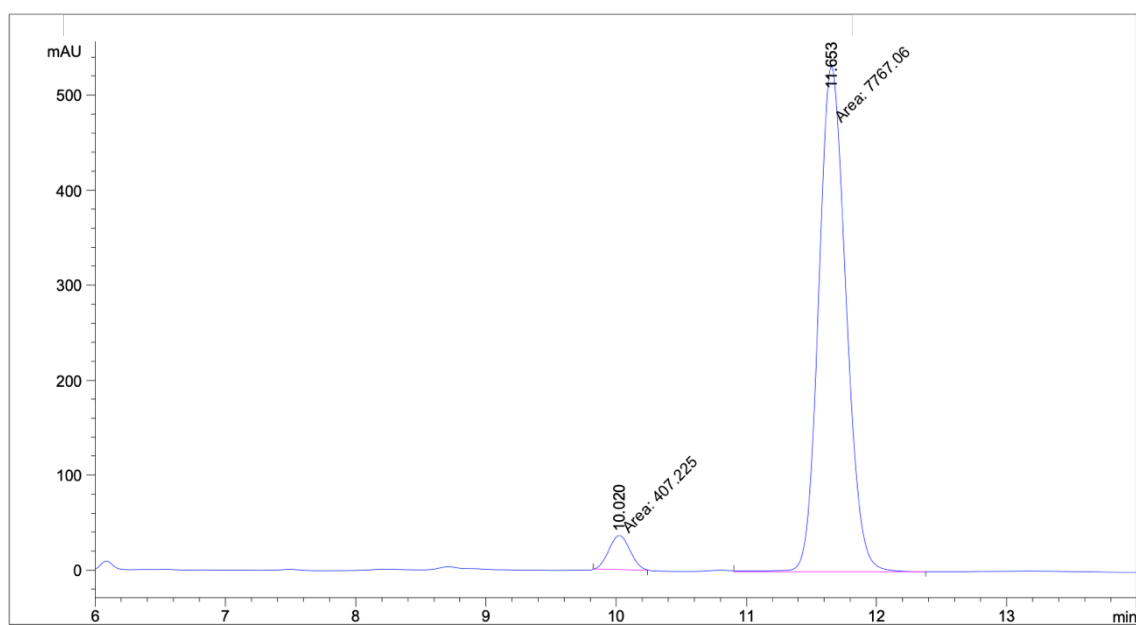
Peak #	RetTime [min]	Type	Width [min]	Area [mAU*s]	Height [mAU]	Area %
1	19.564	BV	0.2962	6174.08887	327.07098	49.6764
2	20.392	VB	0.3099	6254.52246	311.93237	50.3236



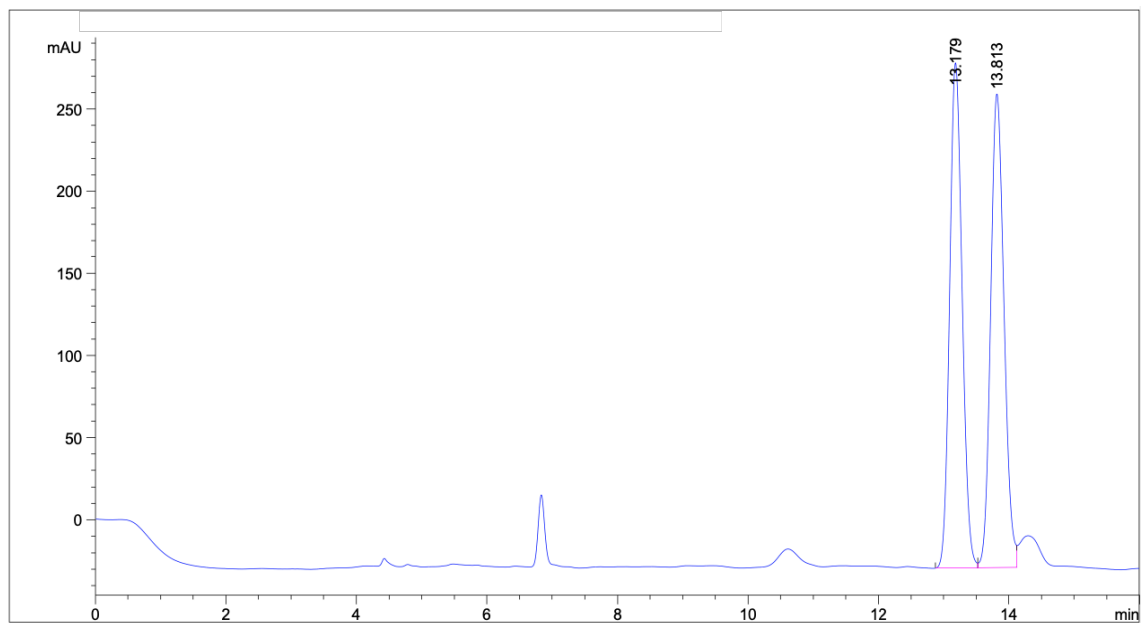
Peak #	RetTime [min]	Type	Width [min]	Area [mAU*s]	Height [mAU]	Area %
1	19.769	MM	0.3838	8208.83203	356.42542	95.1626
2	21.145	MM	0.3683	417.27771	18.88169	4.8374



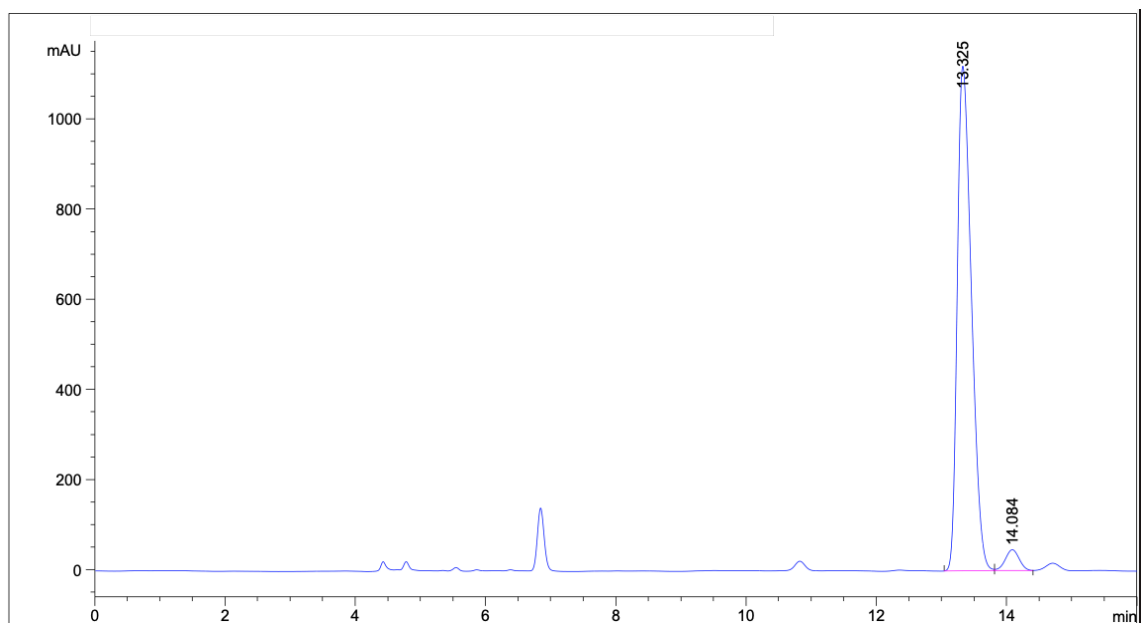
Peak #	RetTime [min]	Type	Width [min]	Area [mAU*s]	Height [mAU]	Area %
1	10.034	VB	0.1904	6562.33887	530.07117	50.0377
2	11.678	VV	0.2311	6552.46338	441.55142	49.9623



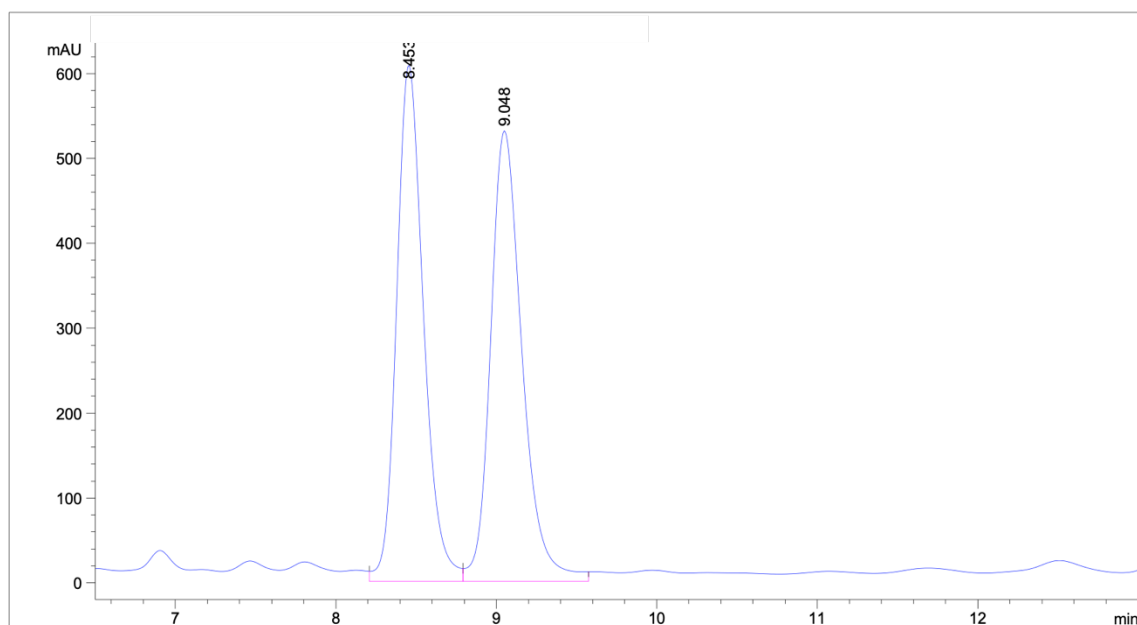
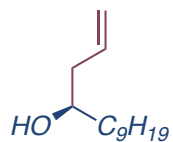
Peak #	RetTime [min]	Type	Width [min]	Area [mAU*s]	Height [mAU]	Area %
1	10.020	MM	0.1884	407.22473	36.01905	4.9818
2	11.653	MM	0.2433	7767.06055	531.98163	95.0182



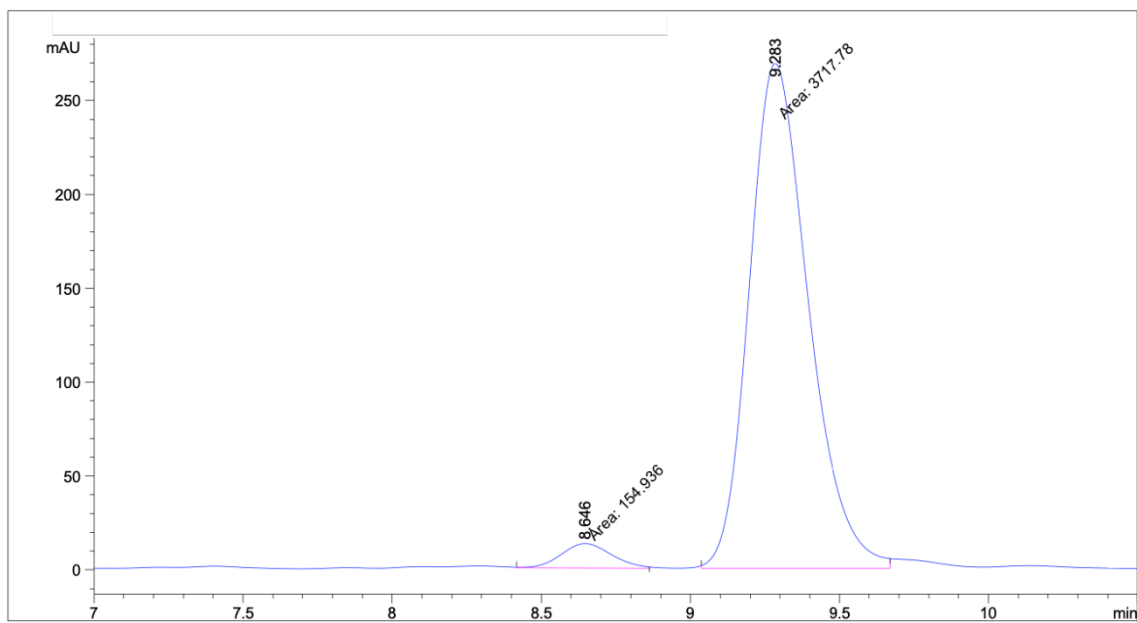
Peak #	RetTime [min]	Type	Width [min]	Area [mAU*s]	Height [mAU]	Area %
1	13.179	BV	0.2064	4069.77539	307.44882	49.7900
2	13.813	VV	0.2220	4104.10840	288.51657	50.2100



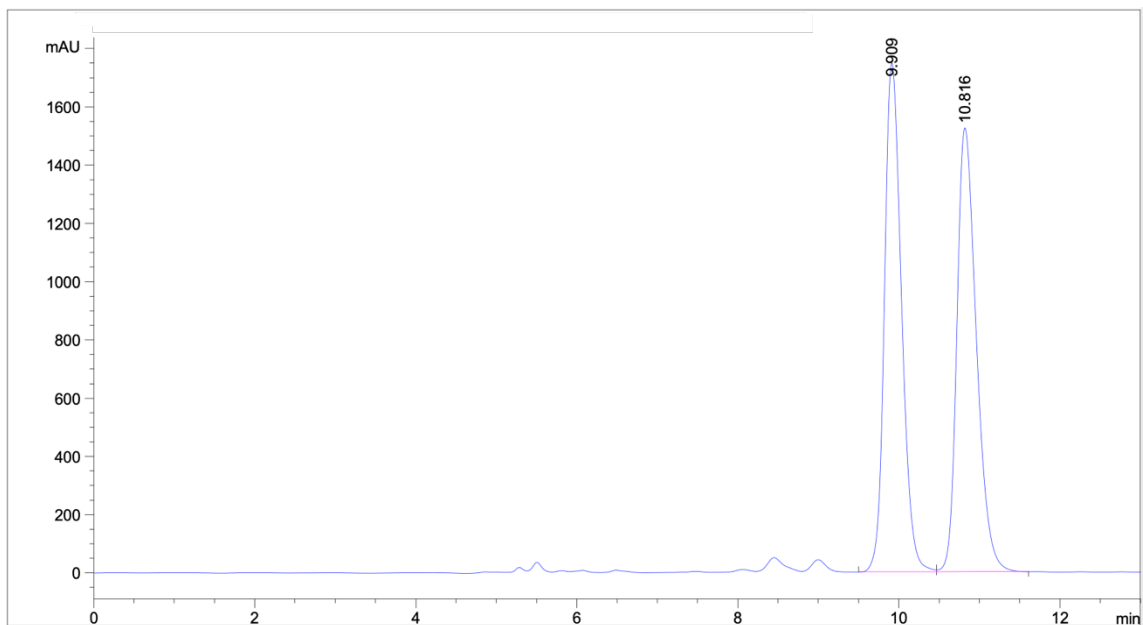
Peak #	RetTime [min]	Type	Width [min]	Area [mAU*s]	Height [mAU]	Area %
1	13.325	BV	0.2356	1.68547e4	1119.90088	95.9897
2	14.084	VV	0.2337	704.17096	46.76688	4.0103



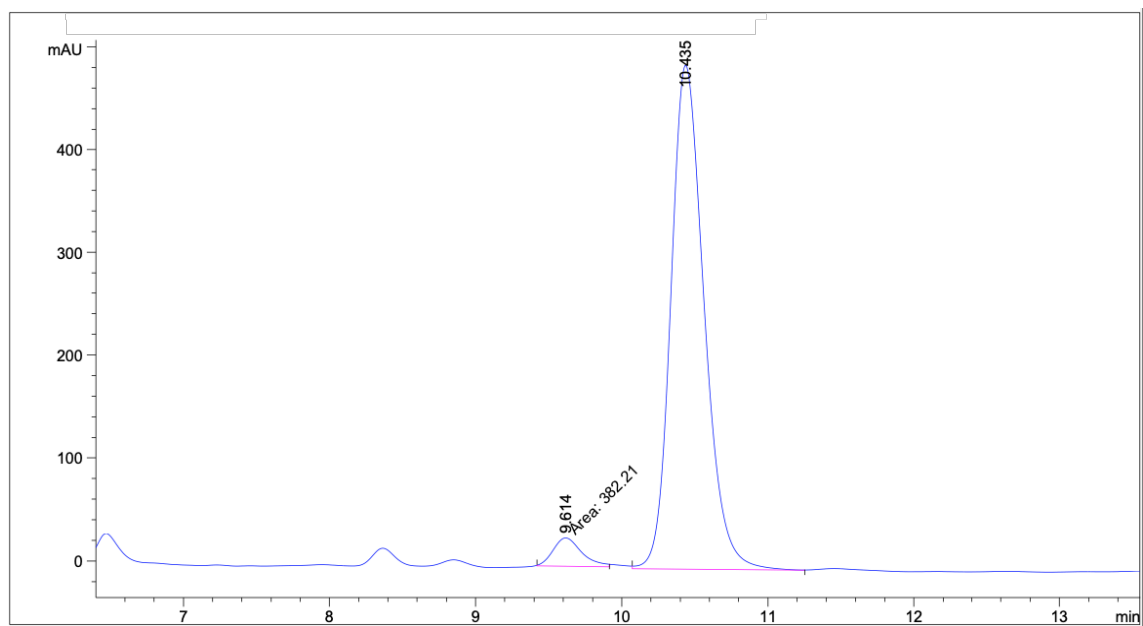
Peak #	RetTime [min]	Type	Width [min]	Area [mAU*s]	Height [mAU]	Area %
1	8.453	VV	0.1783	7101.42676	608.02545	49.4792
2	9.048	VB	0.2074	7250.91943	530.80743	50.5208



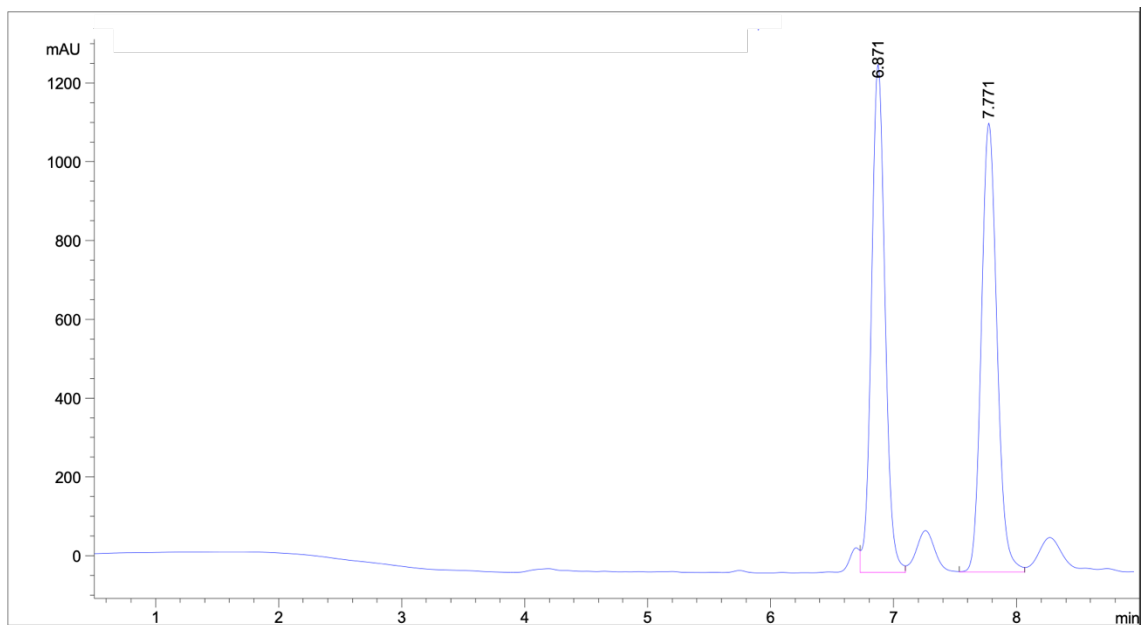
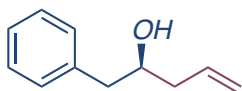
Peak #	RetTime [min]	Type	Width [min]	Area [mAU*s]	Height [mAU]	Area %
1	8.646	MM	0.1975	154.93579	13.07436	4.0007
2	9.283	MM	0.2303	3717.77661	269.05078	95.9993



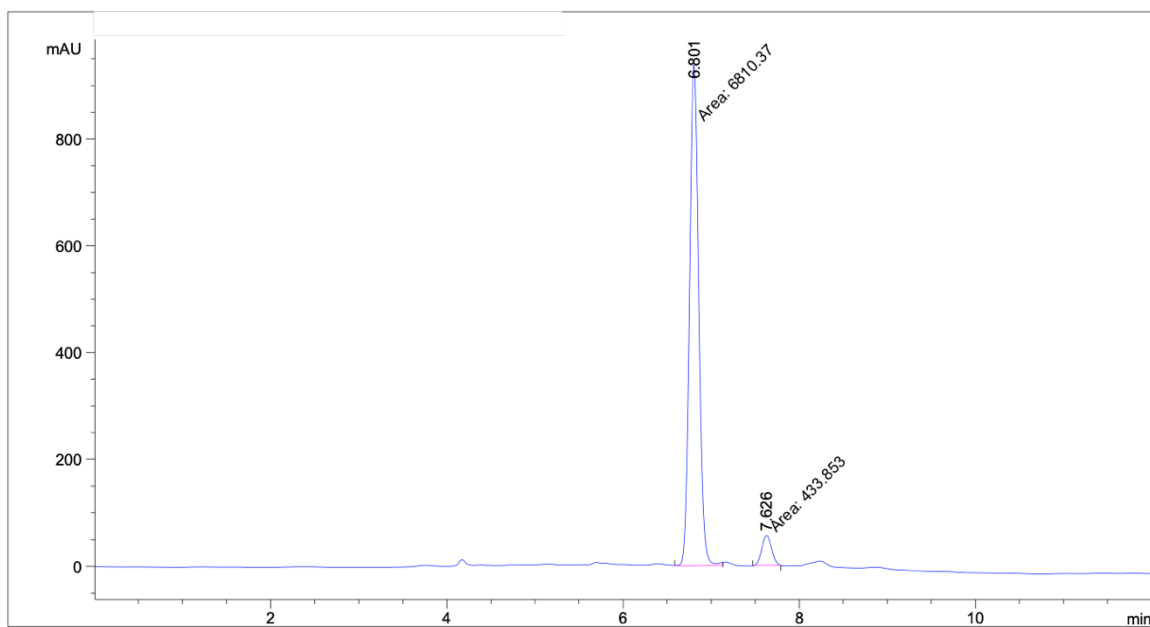
Peak #	RetTime [min]	Type	Width [min]	Area [mAU*s]	Height [mAU]	Area %
1	9.909	VV	0.2279	2.57673e4	1748.51929	50.1446
2	10.816	VB	0.2580	2.56188e4	1525.05713	49.8554



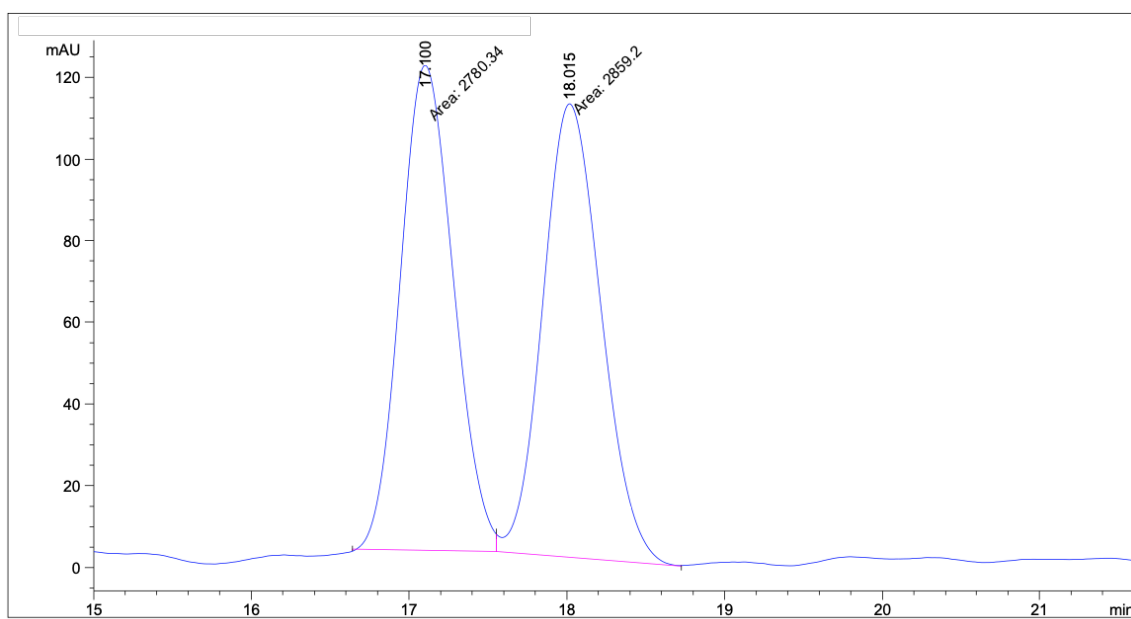
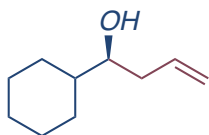
Peak #	RetTime [min]	Type	Width [min]	Area [mAU*s]	Height [mAU]	Area %
1	9.614	MM	0.2293	382.20956	27.77847	4.7018
2	10.435	VB	0.2423	7746.87305	490.27466	95.2982



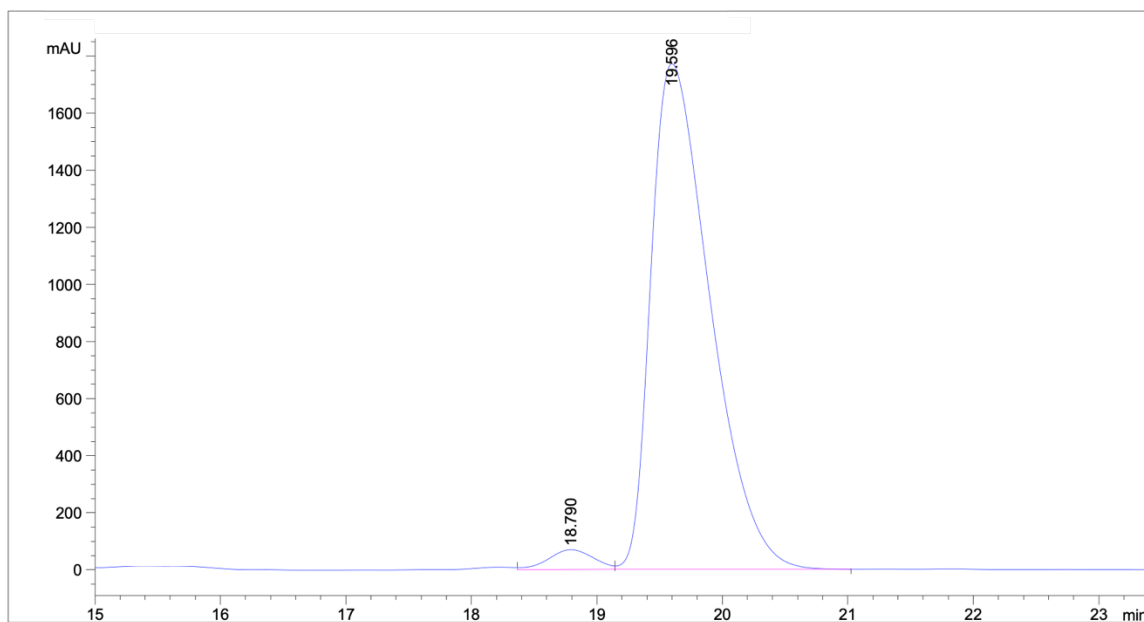
Peak #	RetTime [min]	Type	Width [min]	Area [mAU*s]	Height [mAU]	Area %
1	6.871	VV	0.1194	9876.37402	1289.58008	49.4492
2	7.771	VV	0.1373	1.00964e4	1140.25623	50.5508



Peak #	RetTime [min]	Type	Width [min]	Area [mAU*s]	Height [mAU]	Area %
1	6.801	MM	0.1208	6814.97510	940.08319	93.9621
2	7.626	MM	0.1290	437.92139	56.58780	6.0379



Peak #	RetTime [min]	Type	Width [min]	Area [mAU*s]	Height [mAU]	Area %
1	17.100	MM	0.3900	2780.34106	118.80451	49.3008
2	18.015	MM	0.4289	2859.20142	111.10230	50.6992



Peak #	RetTime [min]	Type	Width [min]	Area [mAU*s]	Height [mAU]	Area %
1	18.790	VV	0.3928	1763.36914	70.25081	2.9482
2	19.596	VB	0.5062	5.80475e4	1772.04443	97.0518